

# Proceedings of the International Meteor Conference

Egmond, the Netherlands

2–5 June, 2016



Edited by Adriana Roggemans and Paul Roggemans



# Proceedings of the International Meteor Conference

Egmond, the Netherlands

2–5 June, 2016



Edited by Adriana Roggemans and Paul Roggemans

# **Proceedings of the International Meteor Conference**

**Egmond, the Netherlands, 2–5 June 2016**

ISBN 978-2-87355-030-1

EAN 9782873550301

## **Copyright notices**

The copyright of papers submitted to the IMC Proceedings remains with the authors.

## **Production of the 2016 IMC Proceedings**

*Front cover picture:* TX 10 – the fishing boat used for the IMC excursion.

*Design IMC logo:* Uros and Dusan Bettonvil

*Typesetting:* MS Word template prepared by Vincent Perlerin.

*Editors:* Adriana Roggemans, Paul Roggemans

*Proofreaders:* Lucie Heywood, Bob Lunsford, Tony Markham, Michael O’Connell, Vincent Perlerin and Jean-Louis Rault.

*Selection of photographs and captions:* Felix Bettonvil

*Bibliographic records:* all papers are listed with the SAO/NASA Astrophysics Data System (ADS) – <http://adsabs.harvard.edu> with publication code [2016pimo.conf](http://adsabs.harvard.edu).

# Contents

Contents .....	1
Foreword	
<i>Felix Bettonvil</i> .....	6
From the editor – about the IMC Proceedings	
<i>Paul Roggemans</i> .....	8
Program of the 35 <sup>th</sup> International Meteor Conference, Egmond , 2 – 5 June, 2016.....	13
Artificial meteor test towards: On-demand meteor shower	
<i>Shinsuke Abe, Lena Okajima, Hironori Sahara, Takeo Watanabe, Yuta Nojiri</i> <i>and Tomohiko Nishizono</i> .....	17
Asteroidal meteors detected by MU radar head-echo observations	
<i>Shinsuke Abe, Johan Kero, Takuji Nakamura, Yasunori Fujiwara, Daniel Kastinen,</i> <i>Jun-ichi Watanabe and Hiroyuki Hashiguchi</i> .....	18
On the age and parent body of the daytime Arietids meteor shower	
<i>Abedin Abedin, Paul Wiegert, Petr Pokorny and Peter Brown</i> .....	19
A Monte-Carlo based extension of the Meteor Orbit and Trajectory Software (MOTS) for computations of orbital elements	
<i>Thomas Albin, Detlef Koschny, Rachel Soja, Ralf Srama and Bjoern Poppe</i> .....	20
An antenna, a radio and a microprocessor: which kinds of observation are possible in meteor radio astronomy?	
<i>Lorenzo Barbieri</i> .....	26
Accurate Geminid velocities with CHIPOLAtA	
<i>Felix Bettonvil</i> .....	31
Photographic spectra of fireballs	
<i>Jiří Borovička</i> .....	34
The 2016 Quadrantids	
<i>Brando Gaetano</i> .....	39
Recent shower outbursts detected by the Canadian Meteor Orbit Radar (CMOR)	
<i>Peter Brown</i> .....	42
The Radio Meteor Zoo: a citizen science project	
<i>Stijn Calders, Cis Verbeeck, Hervé Lamy and Antonio Martínez Picar</i> .....	46
Results from the Canadian Automated Meteor Observatory	
<i>Margaret Campbell-Brown</i> .....	50
Ablation of small Fe meteoroids – first results	
<i>David Čapek and Jiří Borovička</i> .....	53
FRIPON network status	
<i>François Colas, Brigitte Zanda, Sylvain Bouley, Jérémie Vaubaillon, Chiara Marmo, Yoan Audureau,</i> <i>Min Kyung Kwon, Jean-Louis Rault, Pierre Vernazza, Jérôme Gattacceca, Stéphane Caminade,</i> <i>Mirel Birlan, Lucie Maquet, Auriane Egal, Monica Rotaru, Laurent Jorda, Cyril Birnbaum,</i> <i>Cyril Blanpain, Adrien Malgoyre, Julien Lecubin, Alberto Cellino, Daniele Gardiol, Mario Di Martino,</i> <i>Christian Nitschelm, Jorje Camargo, M. Valenzuela, Ludovic Ferrière, Marcel Popescu and</i> <i>Damien Loizeau</i> .....	55
The dimension added by 3D scanning and 3D printing of meteorites	
<i>Sebastiaan J. de Vet</i> .....	56

Status of the Desert Fireball Network <i>Hadrien A. R. Devillepoix, Philip A. Bland, Martin C. Towner, Martin Cupák, Eleanor K. Sansom, Trent Jansen-Sturgeon, Robert M. Howie, Jonathan Paxman and Benjamin A. D. Hartig</i> .....	60
Data processing of records of meteoric echoes <i>Peter Dolinský</i> .....	63
Calibration of meteor spectra <i>Martin Dubs and Koji Maeda</i> .....	65
Investigation of meteor shower parent bodies using various metrics <i>Bogdan Alexandru Dumitru, Mirel Birlan, Alin Nedelcu and Marcel Popescu</i> .....	69
The challenge of meteor daylight observations <i>Auriane Egal, Min-Kyung Kwon, François Colas, Jérémie Vaubaillon and Chiara Marmo</i> .....	73
PRISMA, Italian network for meteors and atmospheric studies <i>Daniele Gardiol, Alberto Cellino and Mario Di Martino</i> .....	76
The evolution of ROAN 2016 - Radio surveillance of meteors and determination of reflection points through calculation of the radio path, based on times <i>Tudor Georgescu, Ana Georgescu and Cezar Lesanu</i> .....	80
Video meteor light curve analysis of Orionids and Geminids and developing a method for obtaining the absolute light curves of shower meteors from the single station data <i>Ljubica Grašić, Nikolina Milanović and Dušan Pavlović</i> .....	83
Consequences of meteoroid impacts based on atmospheric trajectory analysis <i>Maria Gritsevich</i> .....	87
Synthetic spectra of meteors <i>Meryem Guennoun, Michel-Andres Breton, Nicolas Rambaux, Jérémie Vaubaillon and Zouhair Benkhaldoun</i> .....	91
Meteoroid streams and comet disintegration <i>Ayyub Guliyev</i> .....	94
A fast meteor detection algorithm <i>Pete Gural</i> .....	96
The occurrence of interstellar particles in the vicinity of the Sun An overview – 25 years of research <i>Maria Hajdukova, jr</i> .....	105
A tale of two fireballs <i>Mike Hankey and Vincent Perlerin</i> .....	111
Results from the CAMS video network <i>Peter Jenniskens</i> .....	113
Hemispherical radiating pattern antenna design for radio meteor observation <i>Jakub Kákona</i> .....	114
Meteor trajectory estimation from radio meteor observations <i>Jakub Kákona</i> .....	117
The multi technique meteor observations in 2014 <i>Anna Kartashova, Galina Bolgova, Yuriy Rybnov, Olga Popova and Dmitry Glazachev</i> .....	120
A statistical approach to the temporal development of orbital associations <i>Daniel Kastinen and Johan Kero</i> .....	123
The role of population in tracking meteorite falls in Africa <i>Fouad Khiri, Abderrahmane Ibhi, Thierry Saint-Gerant, Mohand Medjkane and Lahcen Ouknine</i> .....	127

Height computation of a fireball <i>Detlef Koschny</i> .....	131
Simultaneous analogue and digital observations and comparison of results <i>Pavel Koten, Rostislav Štork, Petr Páta, Karel Fliegel and Stanislav Vitek</i> .....	133
Meteors and meteorites spectra <i>Jakub Koukal, Jiří Srba, Sylvie Gorková, Libor Lenža, Martin Ferus, Svatopluk Civiš, Antonín Knížek, Petr Kubelík, Tereza Kaiserová and Pavel Váňa</i> .....	137
Retrieving meteoroids trajectories using BRAMS data: preliminary simulations <i>Hervé Lamy and Cédric Tétard</i> .....	143
Easy way to estimate meteor brightness on TV frames <i>Vladislav A. Leonov and Alexander V. Bagrov</i> .....	148
Photometric stellar catalogue for TV meteor astronomy <i>Vladislav A. Leonov and Alexander V. Bagrov</i> .....	151
ROAN Remote radio meteor detection sensor <i>Cezar Eduard Lesanu</i> .....	155
Calibration of occasionally taken images using principles of perspective <i>Esko Lyttinen and Maria Gritsevich</i> .....	159
The KUT meteor radar: An educational low cost meteor observation system by radio forward scattering <i>Waleed Madkour and Masa-yuki Yamamoto</i> .....	164
Meteor spectra using high definition video camera <i>Koji Maeda and Yasunori Fujiwara</i> .....	167
Effects of meteor head plasma distribution on radar cross sections and derived meteoroid masses <i>Robert A. Marshall, Sigrid Close, Peter Brown and Yakov Dimant</i> .....	171
Numerical simulation of the BRAMS interferometer in Humain <i>Antonio Martínez Picar, Christophe Marqué, Cis Verbeek, Stijn Calders, Sylvain Ranvier, Emmanuel Gamby, Michel Anciaux, Cédric Tetard and Hervé Lamy</i> .....	175
Construction of a meteor orbit calculation system for comprehensive meteor observation <i>Satoshi Mizumoto, Waleed Madkour and Masa-yuki Yamamoto</i> .....	179
Flux density, population index, perception coefficient, and the Moon <i>Sirko Molau</i> .....	185
Current progress in the understanding of the physics of large bodies recorded by photographic and digital fireball networks <i>Manuel Moreno-Ibáñez, Maria Gritsevich, Josep Ma. Trigo-Rodríguez and Esko Lyttinen</i> .....	192
Large meteoroid's impact damage: review of available impact hazard simulators <i>Manuel Moreno-Ibáñez, Maria Gritsevich and Josep Ma. Trigo-Rodríguez</i> .....	197
Measurements of CCD optical linearity for magnitude determination during meteor observations <i>Andrey Murtazov and Alexander Efimov</i> .....	202
Astronomy through the microscope: A workshop during the opening night of the 2016 IMC <i>Gert Jan Netjes and Sebastiaan de Vet</i> .....	205
PaDe - The particle detection program <i>Theresa Ott, Esther Drolshagen, Detlef Koschny and Bjoern Poppe</i> .....	209
Evaluating video digitizer errors <i>Chris Peterson</i> .....	214
Sungrazing comets and meteoroids <i>Eduard Pittich and Nina Solovaya</i> .....	217

Werkgroep Meteoren – 70 Years and counting <i>Urijan Poerink and Sebastiaan J. de Vet</i> .....	222
Novel methods for 3D numerical simulation of meteor radar reflections <i>Jukka Rabinä, Sanna Mönkölä, Tuomo Rossi, Johannes Markkanen, Maria Gritsevich and Karri Muinonen</i> .....	227
Meteor detections at the Metsähovi Fundamental Geodetic Research Station (Finland) <i>Arttu Raja-Halli, Maria Gritsevich, Jyri Näränen, Manuel Moreno-Ibáñez, Esko Lyytinen, Jenni Virtanen, Nataliya Zubko, Jouni Peltoniemi and Markku Poutanen</i> .....	230
An attempt to explain VLF propagation perturbations associated with single meteors <i>Jean-Louis Rault and Jean-Jacques Delcourt Dr. Sc.</i> .....	235
65 years of meteor radar research at Adelaide <i>Iain M. Reid and Joel Younger</i> .....	242
Minor meteor shower activity <i>Jürgen Rendtel</i> .....	247
The radio meteor signal path from transmitter to spectrogram: an overview <i>Tom Roelandts</i> .....	250
Status of the CAMS-BeNeLux network <i>Paul Roggemans, Carl Johannink and Martin Breukers</i> .....	254
eMeteorNews: website and PDF journal <i>Paul Roggemans, Richard Kacerek, Jakub Koukal, Koen Miskotte and Roman Piffel</i> .....	261
An overview of the CILBO spectral observation program <i>Regina Rudawska, Joe Zender and Detlef Koschny</i> .....	265
ESA/ESTEC Meteor Research Group – behind the scenes <i>Regina Rudawska</i> .....	266
Meteor reporting made easy- The Fireballs in the Sky smartphone app <i>Eleanor Sansom, Jay Ridgewell, Phil Bland and Jonathan Paxman</i> .....	267
Croatian Meteor Network: Ongoing work 2015 – 2016 <i>Damir Šegon, Denis Vida, Korado Korlević and Željko Andreić</i> .....	270
Fireballs from Australian Desert Fireball Network – search for similar orbits <i>Lukáš Šhrbený, Pavel Spurný and Phil A. Bland</i> .....	275
On the accuracy of orbits from video meteor observations <i>Ivica Skokić, Damir Šegon and Goran Kurtović</i> .....	280
Collisional lifetimes of meteoroids <i>Rachel Halina Soja, G. J. Schwarzkopf, Maximilian Sommer, Jérémie Vaubaillon, Thomas Albin, Jens Rodmann, Eberhard Grün and Ralf Srama</i> .....	284
EN091214 Zdar – one of the most precisely documented meteorite fall <i>Pavel Spurny, Jiri Borovicka, Jakub Haloda, Lukas Shrbeny and Tomas Zikmund</i> .....	287
The Swedish Allsky Meteor Network: first results <i>Eric Stempels and Johan Kero</i> .....	288
No sign of the 2015 Daytime Sextantids through combined radio observations <i>Giancarlo Tomezzoli and Lorenzo Barbieri</i> .....	291
AMOS - trajectory and orbital data from SVMN and Canary Islands <i>Juraj Tóth, Leonard Kornoš, František Ďuriš, Pavol Zigo, Štefan Gajdoš, Dušan Kalmančok, Jozef Világi, Jaroslav Šimon, Marek Buček, Jaroslav Šimon, Miquel Serra-Ricart, Juan Carlos Perez, Javier Licandro, Ovidiu Vaduvescu and Jürgen Rendtel</i> .....	294

Expedition Atacama - project AMOS in Chile <i>Juraj Tóth and Stanislav Kaniansky</i> .....	295
AMOS-Spec - meteor spectra from Modra Observatory <i>Juraj Tóth, Pavol Matlovič, Regina Rudawska, Pavol Zigo and Dušan Kalmančok</i> .....	297
Rediscovery of Polish meteorites <i>Zbigniew Tymiński, Marcin Stolarz, Przemysław Żołądek, Mariusz Wiśniewski and Arkadiusz Olech</i> .....	298
A (revised) confidence index for the forecasting of meteor showers <i>Jeremie Vaubailon</i> .....	302
Software for Analysis of Visual Meteor Data: R package MetFns – Workshop report <i>Kristina Veljković</i> .....	304
Summary of the Open Session at the IMC 2016 <i>Cis Verbeeck, Megan Argo, Peter Brown, Sirko Molau, Jürgen Rendtel and Antonio Martínez Picar</i> .....	305
Open-source meteor detection software for low-cost single-board computers <i>Denis Vida, Dario Zubović, Damir Šegon, Peter Gural and Robert Cupec</i> .....	307
Big data era in meteor science <i>Dejan Vinković, Maria Gritsevich, Vladimir Srečković, Bojan Pečnik, Gyula Szabó, Victor Debattista, Petr Škoda, Ashish Mahabal, Jouni Peltoniemi, Sanna Mönkölä, Areg Mickaelian, Esa Turunen, Jakub Kákona, Jarkko Koskinen and Victor Grokhovsky</i> .....	319
Statistical approach to meteoroid shape estimation <i>Vladimír Vinnikov, Maria Gritsevich, Daria Kuznetsova, Olga Krivonosova, Dmitry Zhilenko and Leonid Turchak</i> .....	330
Catalogue of representative meteor spectra <i>Vlastimil Vojáček, Jiří Borovička, Pavel Koten, Pavel Spurný and Rostislav Štork</i> .....	333
2014 Southern $\delta$ -Aquariid observing campaign – carried out from Crete <i>Thomas Weiland</i> .....	338
Current status of Polish Fireball Network <i>Mariusz Wiśniewski, Przemysław Żołądek, Arkadiusz Olech, Zbigniew Tyminski, Maciej Maciejewski, Karol Fietkiewicz, Mariusz Gozdalski, Marcin Przemysław Gawroński, Tomasz Suchodolski, Maciej Myszkiewicz, Marcin Stolarz and Krzysztof Polakowski</i> .....	341
Space fireworks for upper atmospheric wind measurements by sounding rocket experiments <i>Masa-yuki Yamamoto</i> .....	344
Exploring the relationship between meteor parameters based on photographic data <i>Yulia Yancheva, Simona Hristova and Eva Bojurova</i> .....	348
Radar observations of the Volantids meteor shower <i>Joel Younger, Iain Reid, Damian Murphy</i> .....	352
Taurids 2015 <i>Przemysław Żołądek, Arkadiusz Olech, Mariusz Wiśniewski, Regina Rudawska, Marcin Bęben, Tomasz Krzyżanowski, Maciej Myszkiewicz, Marcin Stolarz, Marcin Gawroński, Mariusz Gozdalski, Tomasz Suchodolski, Walburga Węgrzyk and Zbigniew Tymiński</i> .....	358
International Meteor Conference 2017, Petnica, Serbia, September 21–24, 2017 <i>Dušan Pavlović, Snežana Todorović and Miroslav Živanović</i> .....	361
Participants list .....	364
Author index .....	372

# Foreword

It is always an honor to write the introduction of this meteor-specific booklet: the proceedings of the International Meteor Conference. This year, it was held in the village of Egmond (Netherlands) from June 2<sup>nd</sup> until June 5<sup>th</sup>, 2016, and organized by the Meteor Section of the Dutch Association for Astronomy and Meteorology KNVWS, on the occasion of her 70<sup>th</sup> anniversary.

This IMC was a big one, with 158 participants, making it the largest so far. That is why the memories of this conference resulted in such an extensive work: the papers of 60 oral presentations and 31 posters.

This IMC had the specialty that it was combined with Meteoroids. This professional conference took place immediately after the IMC and created an excellent opportunity to attract many professionals to the IMC and also amateurs to Meteoroids. Both did attend in large numbers, and our fear that the timing of having the conference in June, in competition with many other conferences in this busy conference month, as well as the problematic timing for students due to examinations, did not become true at all. As often, the IMC turned out to be a bowl full of energizing liquid, enabling cross fertilization between amateurs, and this year between many amateurs and professionals as well.

This time the IMC had, for the first time, a Scientific Organizing Committee (SOC), and despite it doing most of its work in the background, it helped ensure that a program that was both interesting and high quality was created. The most demanding ‘hurdle’ to be taken was how to handle the enormous amount of contributions in the limited time available. The decision was made to limit all talks to 10 minutes (plus 2 minutes for discussion) in order to allow for speaking time for all oral presenters. In addition, the SOC chose to reserve extra time on request in the evening, for those topics that benefitted from deeper discussion.

There was also another novelty: this year the conference accommodated an open session, in which questions could be asked to a panel of specialists. A report of this exciting event is included in these proceedings. Also for the first time a poster prize was handed out for the author with the best poster, as well as a photo competition, also with a nice trophy for the winner, based on selection by an ‘expert’ panel and votes. Furthermore, we actively invited participants to bring equipment along, which brought on show two new All-sky cameras of the Desert Fireball Network and a working 3D-printer for printing meteorite replicas.

Although we feel thankful that the conference was much appreciated, we did realize beforehand that due to the enormous amount of participants, we would run into physical limits. Not only did the hostel itself reach its maximum capacity, we also felt that this was also the case for the format of the conference. Luckily all went well, but some rethinking of the future conference format may be required. The many satisfaction forms that we received (more than half of the participants) will surely help.

Of course there were many aspects that were not of concern at all because they ran very smoothly. Thanks to Marc Gyssens, the registration process was no burden for us by any means. Vincent Perlerin took care of all website related issues and in the background –not visible for most of us but of enormous help- a super sophisticated database. Backstage the IMO council members were there, always open for suggestions and feedback where needed during all preparation work. A special thanks there is also for Jean Louis Rault, who offered at the last minute to take on the not easy task of giving the summary talk. And last, but not least, Paul Roggemans, who once again offered to be main editor of the(se) proceedings, and used all efforts to complete them as soon as possible.

In addition to the support from the meteor community, we got also fantastic support from the hostel staff, who did always all we asked for, and gladly accepted that we practically took over almost the entire hostel. Of course, the conference could never have been a success without the participants. Applause is deserved for how well everyone (without a single exception!) kept to the tight schedule. Very well done.

Exhausted, but satisfied, on Sunday afternoon after 3 intensive days and nights, it was also time for the LOC to leave the hostel. Each member flooded with their own intense, unforgettable memories. We all saw that the field of meteoroids – meteors – meteorites is a very exciting one, and every year more and more so. The specialization of visual observations, the initial goal of IMO in gathering these worldwide, is accompanied now by many other techniques, best maybe video, but also spectroscopy, radio, simulations, software, lab experiments. Modelling and forecasts improve year after year, and rather than making observational results less important, all these models and theory actually ask for yet more – and better – observational work. The specialism of meteors touches an ever increasing number of other disciplines:

meteorites, comets, asteroids, hazards for spacecraft. And last, but not least, technical innovations, like almost everywhere, truly become interdisciplinary.

‘Meteors’ is also a field where the contribution of amateurs still is highly appreciated. And not to be forgotten: visual work remains valuable, for the calibration of other techniques and for the continuation of the only long-term record of the monitoring of activity.

Far outside our field, the discovery of exoplanets, dust and accretion around other stars (the current big hype in astronomy) is already being linked to the dust and meteoroids in our own solar system. In the same way as the study of the sun in solar physics is relevant to stars in stellar astronomy, our own solar system is the only place in which we can currently study in detail what will be seen in the future around other stars. How exciting it is. Meteors are fun.

And IMCs are fantastic!

Of course we hope to see you all next year again.

Thanks to all!

The LOC of the IMC 2016,

*Felix, Joost, Arnold, Casper, Elise, Jos, Marc, Roy, Sebastiaan and Urijan*

*‘Organizing an IMC again was extremely exciting, but the fact to realize how vivid our field of meteors is, even more’*

Felix Bettonvil

*‘It is amazing to see how many people with such different backgrounds and cultures can be connected by a magical natural phenomenon. Being able to make possible that all these people can meet is fantastic!’*

Joost Hartman

# From the editor – about the IMC Proceedings

Paul Roggemans

Pijnboomstraat 25, 2800 Mechelen, Belgium

paul.roggemans@gmail.com

At the occasion of the 25<sup>th</sup> IMC in Roden, the Netherlands in 2006, the history of the IMCs was put in the spotlight with a dedicated presentation. Meanwhile we are 10 years later and many new faces appeared at the conference as regular participants. An update on the history of the IMCs is given. One of the first time participants at the 35<sup>th</sup> International Meteor Conference was the 1000<sup>th</sup> officially registered participant according to the final effective participants' lists since 1979. In total 1033 different individuals have participated at one or more IMCs since 1979. The 35<sup>th</sup> IMC broke a few records: the largest total number of participants, the largest number of presentations, both talks and posters and the thickest IMC Proceedings ever. The International Meteor Conference got a splendid reputation worldwide as unique event among all international meetings of amateur astronomers. As far as the author is aware of, there is no other amateur conference in any astronomy domain comparable to the IMC. Some statistics about the conference and its history are presented.

## 1 Introduction

With a record number of participants the IMC at Egmond, the Netherlands, offered plenty of time for informal chats. I was a little bit surprised to hear how few people know about the origin of the conference and its purpose. The roots of the IMC are 10 years older than the IMO and this early history has been documented before (Roggemans, 2006; Roggemans and ter Kuile, 2007). The IMO has grown out of a personal network of meteor correspondents and the early IMCs happened to be the place where correspondents could meet in person long before the IMO got founded. The journal WGN is older than the IMCs and served as journal to exchange observing reports between correspondents when the earliest IMCs were organized.

When the IMO was founded in 1988, WGN became the journal of the IMO, but the IMCs kept an independent status and never became the IMO conference. Pro's and contra's to establish a formal international meteor organization provided animated debates at each IMC until 1990. The main concern against the founding of an IMO was that any 'too large' society risked degenerating into some kind of bureaucratic institute. When IMO got created a significant group of meteor observers did not want to see 'their' IMC being taken over by IMO. As a kind of gentlemen agreement, it was decided that the IMC would keep its independent status while IMO would provide some logistic support to the event and could have its yearly General Assembly at the IMC. This explains why the IMC is being organized by a LOC and not by the IMO staff and why several of the IMC Proceedings were produced independently from IMO. After the 1990 IMC where the topic was discussed (Koschny, 1991) the discussions ceased and the IMC remained an open event without any membership requirements.

## 2 The evolution since 2006

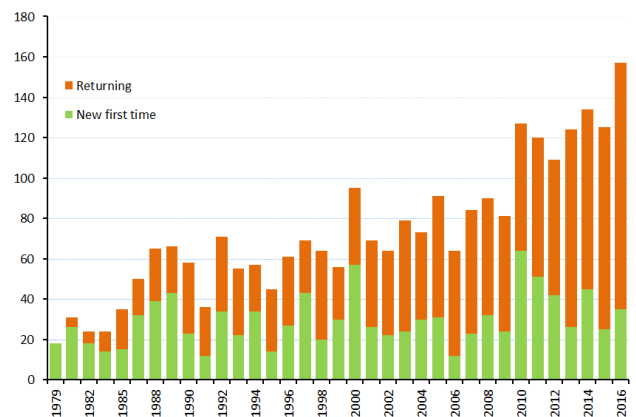
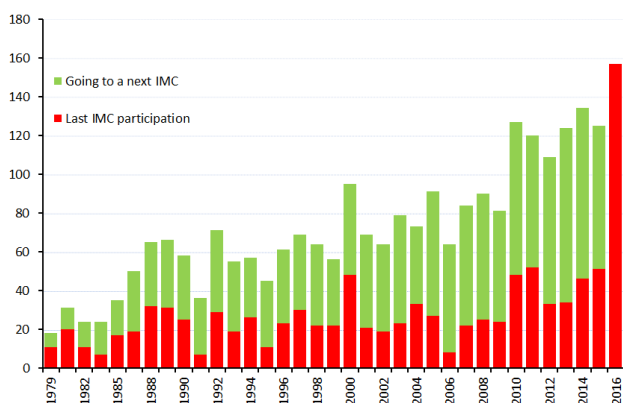


Figure 1 – The evolution of the number of registered, effectively present participants for all 35 meetings. New first time participants are marked in green, returning participants who had been at some previous IMC are marked in orange.

The history of the IMCs shows a steady growth in number of participants over a 38 year period. The first five meetings involved a rather small group with only few regular participants. Most participants were first time participants in the early years and it took a while to get a regular returning public. Figure 1 shows the evolution of the number of IMC participants, with the number of first time participants marked in green and returning participants in orange. The interest to participate remained many years very stable from 1986 till 2002, with outliers in 1991, with a rather small group due to a lack of publicity, and 2000, with many local amateurs being on the participants' list. From 2003 till 2009 a growing number of regular returning participants mark another period with more people involved than before, 2006 being an outlier due to fewer first time registrations. Since 2010 the totals were significant higher than ever before.

The success of the IMC depends on how many people experience their participation as useful and sufficient motivating to return to a next conference. *Figure 2* shows the proportion of people who quit participation after the IMC (red at bottom) and those who return at some future conference (green at top). Some people stay away for several years and do return after a long period of absence. The proportions for recent years will change as more IMCs will be organized in the future and see more people return after being absent in recent years. Some years have a remarkable large proportion of participants who quit attending IMCs after the meeting of that year. These events were known as excellent IMCs, there must be some explanation why so many did not go to next IMCs.

If we make a query to check how many first time participants never go to any next conference and how many 'regular' participants quit at each IMC, it is obvious that in 2000, 2010 and 2011 an exceptional large number of people attending just this single event had no interest in going to any future meeting. In total 646 individuals (63%) attended just a single event. Depending on the publicity and the policy of the Local IMC organizer more local amateurs take the opportunity to attend an IMC as a once in a lifetime event. These single event participants are marked in orange in *Figure 3*. The number of people who quit having attended previous IMCs is rather small (marked in red in *Figure 3*). The number of new, first time participants who return at some future meetings (green in *Figure 3*) in general is larger than the loss of 'regular' attendants who quit at a given year. As a result there is a steady growth in regular participants who had attended previous events and who continue going to future meetings (blue in *Figure 3*).



*Figure 2* – Trying to scope the interest of the participants at each IMC. The red bars represent the number of participants that never returned to any later IMC, the green bars indicate the the number of participants going to some later IMC.

There is a very obvious evolution in the international character of the IMC over 38 years. Until 1991 residents from the hosting country made up a large portion of the participants. A few peculiar years are 1993 when the IMC took place in France while interest in meteor work at that time was almost nonexistent in France. Also 2015 seduced rather few Austrian participants for the IMC in Austria. On the other hand 1994 (Bulgaria), 1997 (Serbia), 2000 (Romania), 2004 (Bulgaria) and 2011

(Romania) had remarkable many local residents participating. For Romania these two years also coincide with a rather large number of single event participants who never returned at any future meeting.

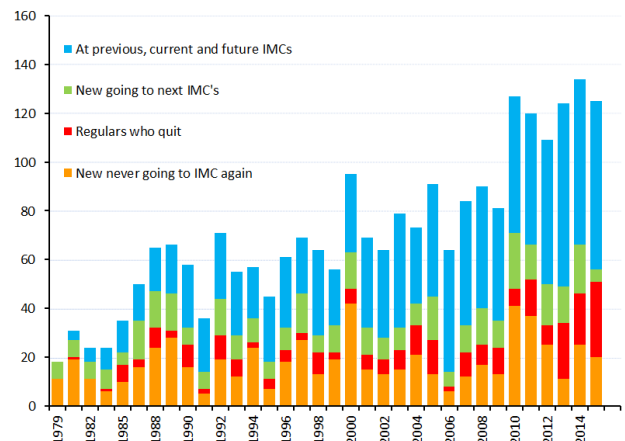


*Figure 3* – Same as *Figure 2*, but with the number of continuing participants and those who quit at a given IMC, splitted in new and returning participants (not relevant for recent years).

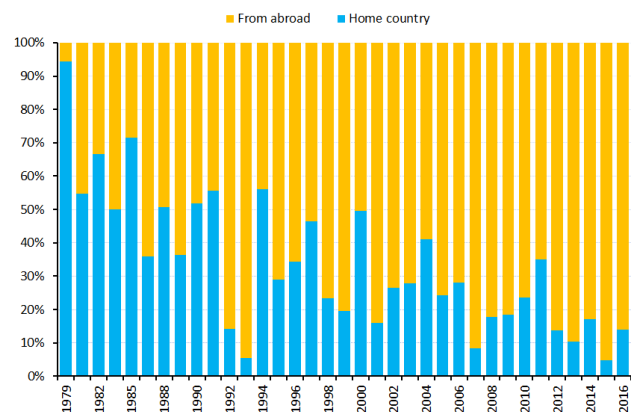


*Figure 4* – The evolution of the international composition of the IMC participants lists. Blue (bottom) indicates the percentage individuals with their domicile in the hosting country. In yellow (top) the percentage of people coming from abroad, regardless nationality but according to their legal domicile at the moment of the IMC.

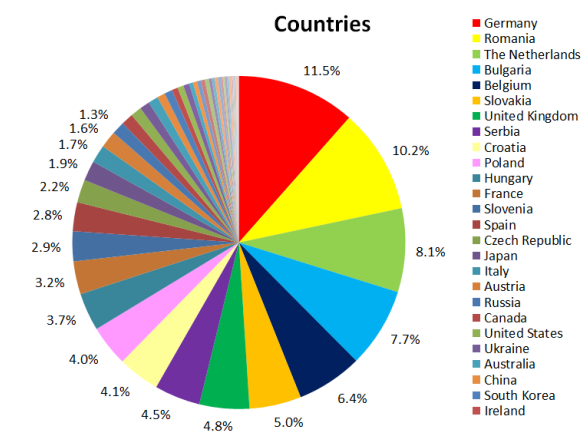


*Figure 5* – The 1033 participants of all 35 conferences came from 50 different nations on all continents. The overall distribution for 38 years of IMCs is shown with the percentages in a pie graph.

Looking at the origin of all 1033 IMC participants most

participants came from Germany which is no surprise as the first IMCs were in Germany and meteor observing has been very popular among German amateurs past 40 years. The Netherlands and Belgium were strongly involved with the IMC tradition and have a long tradition of amateur meteor observing. The large numbers of Bulgarian and Romanian participants come from two IMCs in each of these countries with a large number of local amateurs participating at these specific events, also visible in *Figure 4*.

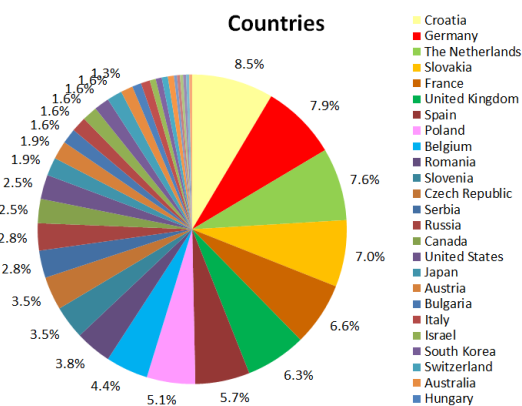


*Figure 6* – The 316 participants of the 5 last IMCs (2012–2016) according to the country where participants had their domicile during the IMC.

Of course there is an evolution in the interest in meteor astronomy which is to some extent influenced by the IMCs. Looking at more recent times, taking only past 5 years a complete different picture occurs. Croatia happens to have the strongest representation at the recent IMCs, followed by Germany and the Netherlands. The presence of British and Slovak meteor workers increased while French meteor workers made a spectacular progress in recent years. Romania, Belgium and Bulgaria were much less present at recent IMCs, Belgium because of a general decrease in interest in meteor work, Romania and especially Bulgaria as no IMC took place during past 5 years in these countries.

### 3 The role of IMC Proceedings

Except for the very first meeting in 1979 which had its Proceedings, four meetings remained undocumented without Proceedings, although the intention to make Proceedings existed, lack of time prevented a successful completion for the 1980, 1982, 1983 and 1985 Proceedings. In the early years the Meteor Seminars or Meteor Weekends like the IMC was then called, inspired rather few participants to return at a next meeting. To listen to interesting presentations is enjoyable for a dedicated meteor worker, but it remains no more than pleasant entertainment as most details are quickly forgotten once the conference is finished. Why to spend a few days, costs and efforts to attend a conference if nothing is left from all interesting presentations in a written form? At the 1986 Meteor Weekend in Belgium, the author insisted to have Proceedings again in order to assure a more stable interest for future conferences. A

Belgian amateur, Luc Vanhoeck (°1959 – †2005), volunteered to edit the 1986 Proceedings. Having complete conference Proceedings on time dramatically improved the popularity of the International Meteor Weekend after 1986. The uninterrupted availability of Proceedings had a positive effect on the interest in the conference and definitely played a major role in the current success of the IMCs.

Although that the importance to have all relevant content in Proceedings is obvious, the making of IMC Proceedings has often proved to be a challenging task that scarce off any volunteers to accept the challenge. Except for the very first (1979) Proceedings, a text editor has been used to produce the Proceedings since 1986. The advantage of any text processor is that the author can deliver his text saving the time for the editor to typewrite all content like what happened until the 1970s. Both the text editing software as the printing hardware improved a lot over past 30 years. For the first Proceedings content was still delivered on floppy disks that were sent by post services. Communication by e-mail enabled another significant improvement to submit content and to solve editorial issues. Imagine that until 1993 most of the communication about Proceedings happened with letters sent by post!

In spite of all these technical advantages the Proceedings took unreasonable long time to get ready, something that discouraged authors from making the effort to write a paper. In the early years Proceedings were ‘home made’ using some privately owned text editor and were relatively soon available. However collecting the papers has been the most difficult aspect ever since the beginning. Since poor communication was often the reason why some author failed to deliver any paper for the Proceedings, it was decided that the IMO Secretary General, having a very efficient network of contacts in the meteor world, would take care to collect all papers and to edit the IMC Proceedings. That proved to work very well as the 1993 Proceedings covered the complete content of the presentations. It was also decided to use the same style as WGN for the Proceedings which meant that these had to be prepared in LaTeX. Only very few people in IMO were able to use LaTeX and just like WGN in that time the Proceedings got a huge delay just because all edited articles had still to be converted into LaTeX code which was a time consuming job that had to be done by the WGN editors.

I collected systematically all the papers and prepared the editing work and André Knöfel took care about the LaTeX aspects. The 1994, 1995 and 1996 IMC Proceedings appeared pretty complete. When I decided to quit my mandate as IMO Secretary-General in 1998, I also quit taking care about the IMC Proceedings. André Knöfel continued as editor for the 1997 and 1998 IMC Proceedings. Without an extensive network of contacts it became impossible to collect papers for all the IMC presentations and as a result the IMC Proceedings contained only a partial coverage of all presentations. Several other editors got involved with the IMC

Proceedings. Only papers that were spontaneously submitted were included in the Proceedings and editors gave up trying to get the Proceedings more complete. To make things worse, some Proceedings appeared with huge delays such as the 2001 IMC Proceedings that appeared as late as end 2002.

The 2007 IMC Proceedings almost failed to get produced, and luckily Jürgen Rendtel took care to resume the editing work in order not to have an IMC without Proceedings. The 2007 IMC proceedings were very incomplete and appeared as late as in 2010, in the same year as the also delayed and incomplete 2008 IMC Proceedings and the more on time 2009 IMC Proceedings. The 2010 IMC in Armagh was a very successful IMC with a large number of presentations. Unfortunately only less than half of the presentations got documented in the Proceedings.

The poor performance with the IMC Proceedings made some people wondering if Proceedings were necessary at all. Incomplete and very late Proceedings made indeed very little sense while the role of the Proceedings in the success of the IMC was overlooked. The organizing of the 2011 IMC suffered from the general failure of the IMO to back up the IMC organizer. The author decided to help when too few registrations and too few lectures were announced for the 2011 IMC in Sibiu, Romania. When also no preparations were made to deal with the 2011 IMC Proceedings, the author decided to take care about the 2011 IMC Proceedings. With the experience achieved with the 1993, 1994, 1995 and 1996 IMC Proceedings, I started collecting papers. It was rather sad to see how reluctant most authors were to submit any paper. The reputation of the IMC Proceedings had got a serious blow after several years of very poor editions, with the 2007 and 2010 IMC Proceedings being the most problematic. It costed a lot of time and effort to motivate everybody to make an effort to submit a paper and to give the IMC Proceedings a last chance to prove that we could manage such publication. A strict and open editing procedure was implemented so that everybody could see the progress made with the editing work. We started in October 2011 and it took until June 2012 before the last papers were collected. Most papers were delivered in *MS Word* format and after editing the content I had to prepare the LaTeX files with a simple text editor (*Notepad*). Editing an article is time consuming, on average about 3 hours per paper. Some need just 1 hour, others need extensive rewriting and take more than 6 hours. Transferring all the content into LaTeX files, inserting all the LaTeX syntax by hand, without any LaTeX editor is a very inefficient way to work. When ready the LaTeX version had to be compiled and bugs removed to obtain a printable version. Marc Gyssens volunteered to act as co-editor and the 2011 IMC Proceedings appeared right before the 2012 IMC at La Palma, saving postage by distributing printed copies at the 2012 IMC.

Doing the 2012 and the 2013 IMC Proceedings in the same way, year after year I experienced more goodwill

among the authors to deliver a paper on time. The IMC Proceedings were taken serious again.

Still one aspect caused unjustifiable delays: the LaTeX conversion and compilation which happened to get again postponed by many months. In my opinion the usage of LaTeX in IMO and all the delay that occurred with this extraordinary time wasting LaTeX code, was an unfortunate mistake in IMO and caused a lot of damage to the organization because of the chronic delays on each and every publication. For the 2014 IMC Proceedings I decided to try out *MS Word* as 90% of all papers were delivered in Word. Vincent Perlerin offered to help with a template in Word for the IMC Proceedings. Thanks to the help and assistance of Vincent Perlerin, I managed to get the 2014 IMC Proceedings done together with Jean-Louis Rault as co-editor, in just a couple of months. In fact The 2014 IMC Proceedings were ready only a couple of months after the 2013 IMC Proceedings which had been distributed at the 2014 IMC.

A fast and efficient editing procedure generated more goodwill among all people involved and the 2015 IMC Proceedings went even smoother and faster. Although I was very keen to continue my tasks with the IMCs, I was very surprised and sadly disappointed with the initiative to cancel my task as IMC coordinator end 2015. It remained uncertain if I would do any more IMC Proceedings as dealing with the IMC Proceedings without being involved with the organizing of the IMC creates a serious handicap, not being able to anticipate on the requirements for Proceedings during the preparations for an IMC. The 2016 IMC Proceedings were expected to be exceptional in volume due to the connection with the Meteoroids conference. Felix Bettonvil involved me in the SOC and asked me if I could still take care of the 2016 IMC Proceedings. I had serious doubts because of the difficult work circumstances imposed by the IMO staff. Shortly before the IMC I decided to accept the challenge, together with my wife Adriana as co-editor.

One advice for the future: IMC papers should be submitted *before* the IMC, it is too bad to require delivery after the conference as that has nothing but disadvantages for everybody. A SOC can only function properly if it has papers at hand to consider proposed presentations.

## Acknowledgment

I thank *Felix Bettonvil* for keeping me informed about ongoing IMC matters, for his help to collect the papers from many authors and for his assistance with various other aspects. I also thank the proofreaders, *Bob Lunsford*, *Vincent Perlerin* and *Jean-Louis Rault* for their time and patience to check many papers. *Tracy Heywood*, *Tony Markham* and *Michael O'Connell* for proofreading and rewriting a number of papers. Thanks to *all the authors* for delivering their paper(s) on time and for proofreading the edited version. Last but not least I thank my wife *Adriana* who helped as co-editor to get papers in the right format and to solve specific issues with MS Word.

Table 1 – Overview of all IMC Proceedings available online. Click on the name of the Proceedings you want to consult at the *ADS Abstract Service*, then click “Send query” to see the list of available content (ADS = number of papers, PP = number of pages).

IMC Proceedings edition	Editors	ADS	PP
<a href="#">IMC Proceedings Königswinter (Bonn) - Germany, 8-10 June 1979</a>	Schmitz B., Becker H. J.	11	24
IMC Proceedings Pullach (Munich) - Germany, 21-23 November 1980	No Proceedings	-	-
IMC Proceedings Hasselt - Belgium, 26-28 February 1982	No Proceedings	-	-
IMC Proceedings Brecklenkamp - Netherlands, 13-15 May 1983	No Proceedings	-	-
IMC Proceedings Violau (Augsburg) - Germany, 22-24 February 1985	No Proceedings	-	-
<a href="#">IMC Proceedings Hingene - Belgium, 3-5 October 1986</a>	Vanhoeck L.	19	80
<a href="#">IMC Proceedings Oldenzaal - Netherlands, 25-27 March 1988</a>	Lanzing J.	24	84
<a href="#">IMC Proceedings Balatonföldvár - Hungary, 5-8 October 1989</a>	Spányi P., Tepliczky I.	24	84
<a href="#">IMC Proceedings Violau (Augsburg) - Germany, 6-9 September 1990</a>	Heinlein D., Koschny D.	26	64
<a href="#">IMC Proceedings Potsdam - Germany, 19 - 22 September 1991</a>	Rendtel J., Arlt R.	26	90
<a href="#">IMC Proceedings Smolenice - Slovakia, 2-5 July 1992</a>	Ocenas D., Zimnikoval P.	23	93
<a href="#">IMC Proceedings Puimichel - France, 23-26 September 1993</a>	Roggemans P.	35	113
<a href="#">IMC Proceedings Belogradchik - Bulgaria, 22-25 September 1994</a>	Knöfel A., Roggemans P.	19	89
<a href="#">IMC Proceedings Brandenburg - Germany, 14-17 September 1995</a>	Roggemans P., Knöfel A.	24	133
<a href="#">IMC Proceedings Apeldoorn - Netherlands, 19-22 September 1996</a>	Knöfel A., Roggemans P.	24	143
<a href="#">IMC Proceedings Petnica - Yugoslavia, 25-28 September 1997</a>	Knöfel A., McBeath A.	21	109
<a href="#">IMC Proceedings Stará Lesná - Slovakia, 20-23 August 1998</a>	Arlt R., Knöfel A.	25	117
<a href="#">IMC Proceedings Frasso Sabino - Italy, 23-26 September 1999</a>	Arlt R.	26	156
<a href="#">IMC Proceedings Pucioasa - Romania, 21-24 September 2000</a>	Arlt R., Triglav M., Trayner C.	31	132
<a href="#">IMC Proceedings Cerkno - Slovenia, 20-23 September 2001</a>	Triglav M., Knöfel A., Trayner C.	22	109
<a href="#">IMC Proceedings Frombork - Poland, 26-29 September 2002</a>	Olech A., Zloczewski K., Mularczyk K.	30	175
<a href="#">IMC Proceedings Bollmannsruh - Germany, 19-21 September 2003</a>	Triglav-Cekada M., Trayner C.	36	194
<a href="#">IMC Proceedings Varna - Bulgaria, 23-26 September 2004</a>	Triglav-Cekada M., Kac J.; McBeath A.	24	115
<a href="#">IMC Proceedings Oostmalle - Belgium, 15-18 September 2005</a>	Bastiaens L., Verbert J., Wislez J.-M., Verbeeck C.	33	195
<a href="#">IMC Proceedings Roden - Netherlands, 14-17 September 2006</a>	Bettonvil F., Kac J.	36	190
<a href="#">IMC Proceedings Barèges - France, 7-10 June 2007</a>	Rendtel J., Vaubaillon J.	20	83
<a href="#">IMC Proceedings Šachtička, Slovakia, 18-21 September 2008</a>	Kaniansky S., Zimnikoval P.	17	120
<a href="#">IMC Proceedings Poreč, Croatia, 24 - 27 September 2009</a>	Andreic Z., Kac J.	20	105
<a href="#">IMC Proceedings Armagh, Northern Ireland (UK), 16 - 19 September 2010</a>	Asher D. J., Christou A. A., Atreya P., Barentsen G.	28	106
<a href="#">IMC Proceedings Sibiu, Romania, 15 - 18 September 2011</a>	Gyssens M., Roggemans P.	47	148
<a href="#">IMC Proceedings La Palma, Spain, 20 - 23 September 2012</a>	Gyssens M., Roggemans P.	65	236
<a href="#">IMC Proceedings Poznan, Poland, 22 - 25 August 2013</a>	Gyssens M., Roggemans P., Zoladek P.	63	222
<a href="#">IMC Proceedings Giron, France, 18 - 21 September 2014</a>	Rault J.-L., Roggemans P.	58	225
<a href="#">IMC Proceedings Mistelbach, Austria, 27 - 30 August 2015</a>	Rault J.-L., Roggemans P.	62	239
<a href="#">IMC Proceedings Egmond, the Netherlands, 2 - 5 June 2016</a>	Roggemans A., Roggemans P.	100	374

## References

- Koschny D. (1991). “Preface”. In Heinlein D. and Koschny D., editors, *Proceedings of the International Meteor Conference*, Violau, Germany, 6-9 September, 2006. IMO, page iv.
- Roggemans P. (2006). “The 25<sup>th</sup> International Meteor Conference”. *WGN, Journal of the IMO*, **34**, 115–118.
- Roggemans P. and Ter Kuile C. (2007). “25 edition of the International Meteor Conference since 1979”. In Bettonvil F. and Kac J., editors, *Proceedings of the International Meteor Conference*, Roden, The Netherlands, 14-17 September, 2006. IMO, pages 129–133.

# Program of the 35<sup>th</sup> International Meteor Conference Egmond , 2–5 June, 2016

## Thursday, 2 June, 2016

14:00 – 19:00	Arrival and registration IMC participants.
19:00 – 20:00	Welcome reception & speeches.
20:00 – 21:00	Dinner.
21:00 – ...	Parallel Program. Option A - Free entertainment. Option B – Workshops.
21:00 – 21:45	Meteor Spectroscopy.
21:45 – 22:30	Microscopic view inside meteorites.

## Friday, 3 June, 2016

07:30 – 08:30	Breakfast.
08.55 - 09.00	Local announcements.
	<b>SESSION 1 – Meteor showers &amp; sporadic background I: video &amp; radio.</b> (Chair: <i>Damir Šegon</i> ).
09:00 – 09:12	<i>Peter Jenniskens</i> : “Results from the CAMS video network”.
09:12 – 09:24	<i>Joel Younger</i> : “Radar Observations of the Volantids Meteor Shower”.
09:24 – 09:36	<i>Giancarlo Tomezzoli</i> : “No sign of the 2015 Daytime Sextantids through Combined Radio Observations”.
09:36 – 09:48	<i>Paul Roggemans</i> : “Update CAMS Benelux 2015-2016”.
09:48 – 10:00	<i>Przemysław Żołqdek</i> : “Taurids 2015”.
10:00 – 10:12	<i>Ljubica Grašić</i> : “Video Meteor Light Curve Analysis of Orionids and Geminids”.
10:12 – 10:24	<i>Ivica Skokić</i> : “On the accuracy of orbits from video meteor observations”.
	<b>SESSION 2 – Meteor showers &amp; sporadic background II: visual.</b> (Chair: <i>Sirko Molau</i> ).
10:24 – 10:36	<i>Juergen Rendtel</i> : “Minor meteor shower activities”.
10:36 – 10:48	<i>Thomas Weiland</i> : “2014 Southern Delta-Aquariid Observing Campaign - carried out from Crete”.
<b>10:48 – 11:24</b>	<b>Coffee break &amp; Poster Session.</b>
	<b>SESSION 3 – Fireballs and meteorite recovery.</b> (Chair: <i>Sebastiaan de Vet</i> ).
11:24 – 11:36	<i>Pavel Spurny</i> : “EN091214 Zdar - one of the most precisely documented meteorite fall”.
11:36 – 11:48	<i>Vincent Perlerin</i> : “The tale of two fireballs”.
11:48 – 12:00	<i>Daniele Gardiol</i> : “Italian Network for Meteors and Atmospheric Studies (PRISMA)”.
12:00 – 12:12	<i>Lukas Shrbeny</i> : “Fireballs from Australian Desert Network”.
12:12 – 12:24	<i>Jiri Borovicka</i> : “Photographic spectra of fireballs”.
12:24 – 12:36	<i>Manuel Moreno-Ibáñez</i> : “Current progress in the understanding of the physics of large bolides recorded by photographic and digital fireball networks”.
12:36 – 12:48	<i>Ana Georgescu</i> : “The evolution of ROAN 2016 - Radio surveillance of meteors and determination of reflexion points through calculation of the radio path, based on times”.
12:48 – 13:00	<i>François Colas</i> : “FRIPON Network Status”.

**13:00 – 14:00 Lunch.****SESSION 4 – Observing techniques.**(Chair: *Dušan Pavlović*).

- 14:00 – 14:12 *Auriane Egal*: “The challenge of meteors daylight observations”.
- 14:12 – 14:24 *Sirko Molau*: “Flux density, population index, perception coefficient, and the Moon”.
- 14:24 – 14:36 *Pavel Koten*: “Simultaneous analogue and digital observations and comparison of results”.
- 14:36 – 14:48 *Alexander Bagrov*: “Easy way to estimate meteor brightness on TV frames”.
- 14:48 – 15:00 *Tom Roelandts*: “The radio meteor signal path from transmitter to spectrogram: an overview”.
- 15:00 – 15:12 *Lorenzo Barbieri*: “An antenna, a radio, a microprocessor: which observations in amatory meteor radio astronomy?”.

**SESSION 5 – Parent bodies, meteoroids, meteorites, planets and their relation.**(Chair: *Denis Vida*).

- 15:12 – 15:24 *Abedin Abedin*: “On the age and parent body of the daytime Arietids meteor shower”.
- 15:24 – 15:36 *Peter Brown*: “Recent Canadian Meteor Orbit Radar detected meteor shower outbursts”.

**15:36 – 16:24 Coffee break & Poster Session.****SESSION 6 – Numeric modelling.**(Chair: *Rachel Soja*).

- 16:24 – 16:36 *Daniel Kastinen*: “A statistical approach to the temporal development of orbital associations”.
- 16:36 – 16:48 *Jérémie Vaubaillon*: “A confidence index for the forecasting of the meteor showers”.
- 16:48 – 17:00 *Robert Marshall*: “Interpretation of Meteor Radar Head Echoes”.

**SESSION 7 – Atmospheric processes and phenomena**(Chair: *Jean-Louis Rault*).

- 17:00 – 17:12 *Masa-yuki Yamamoto*: “Space fireworks for upper atmospheric wind measurements by sounding rocket experiments”.
- 17:12 – 17:24 *David Čapek*: “Ablation of small Fe meteoroids”.
- 17:24 – 17:36 *Vlastimil Vojacek*: “Catalogue of meteor spectra”.
- 17:36 – 17:48 *Shinsuke Abe*: “Artificial Meteor Test towards On-demand Meteor Shower”.
- 17:48 – 18:00 *Simona Hristova*: “Exploring the relationship between meteor parameters based on a photographic data”.
- 18:00 – 18:12 *Jean-Louis Rault*: “An attempt to explain VLF propagation perturbations associated with single meteors”.

**18:12 – 19:12 Poster session with all poster authors.**

01. *Francois Colas*. “FRIPON acquisition, detection and reduction pipeline”.
02. *Eduard Pittich*. “Sungrazing comets and meteoroids”.
03. *Felix Bettonvil*. “CHIPOLAtA results”.
04. *Regina Rudawska*. “An overview of the CILBO spectral observation program”.
05. *Johan Kero*. “First results of the Swedish Allsky Meteor Network”.
06. *Zbigniew Tymiński*. “Polish Meteorites”.
07. *Rachel Soja*. “Lifetimes of meteoroids”.
08. *Peter Dolinsky*. “Data processing of records of meteoric echoes”.
09. *Gaetano Brando*. “The 2016 Quadrantids”.
10. *Juraj Toth*. “AMOS - trajectory and orbital data from SVMN and Canary Islands”.
11. *Pavel Zigo*. “AMOS-Spec - meteor spectra from Modra Observatory”.
12. *Meryem Guennoun*. “Synthetic spectra of meteors”.
13. *Maria Hajdukova*. “The occurrence of interstellar meteoroids. Overview - 25 years of research”.
14. *Paul Roggemans*. “Meteor News”.

15. *Alexander Bagrov*. “Photometric Stellar Catalogue for TV meteor Astronomy”.
16. *Ljubica Grašić*. “Video Meteor Light Curve Analysis of Orionids and Geminids”.
17. *Ibhi Abderrahmane*. “The role of population in tracking meteorite falls in Africa”.
18. *Shinsuke Abe*. “Asteroidal Meteors Detected by MU Radar Head-echo Observations”.
19. *Jakub Koukal*. “Meteors and meteorites spectra”.
20. *Sebastiaan de Vet*. “The added dimension of 3D scanning and printing of meteorites”.
21. *Antonio Martinez Picar*. “Numerical simulation of BRAMS interferometer in Humain”.
22. *Yasunori Fujiwara*. “Meteor spectra using high definition video camera in 2015”.
23. *Jakub Kákona*. “Hemispherical radiating pattern antenna design for radio meteor observation”.
24. *Maria Gritsevich*. “Novel methods for 3D numerical simulation of meteor radar reflections”.
25. *Maria Gritsevich*. “Statistical approach to meteoroid shape estimation”.
26. *Maria Gritsevich*. “Meteor detections at the Metsähovi Fundamental Geodetic Research Station (Finland)”.
27. *Tudor Georgescu*. “ROAN 2016 - Progress”.
28. *Bogdan Dumitru*. “Investigation of meteor shower parent bodies using various metrics”.
29. *Urijan Poerink*. “70 years KNVWS Werkgroep Meteoren”.
30. *Manuel Moreno-Ibáñez*. “Large meteoroids’ impact damage: review of available impact hazard simulators”.
31. *Andrey Murtazov*. “Measurements of CCD optical linearity for magnitude determination in meteor observations”.

**19:12 – 20:12****Dinner.**

20:12 – 21:12

28<sup>th</sup> IMO General Assembly.

Parallel Program.

Option A – Free entertainment.

Option B – Open session with discussion panel.

Option C - Extended-talk Session I (21:30 – 23:30).

21:30 – 22:30

*Pavel Spurny*: Recent instrumentally documented meteorite falls.

22:30 – 23:00

*Maria Gritsevich*: Calibration of occasionally taken images using principles of perspective.

23:10 – 23:30

*Maria Gritsevich*: Consequences of meteoroid impacts based on atmospheric trajectory analysis.**Saturday, 4 June 2016**

07:30 – 08:30

Breakfast.

08:55 – 09:00

Local announcements.

**SESSION 8 – Data pipelines & Software.**(Chair: *Christian Steyaert*).

09:00 – 09:12

*Thomas Albin*: “A Monte-Carlo based extension of the Meteor Orbit and Trajectory Software (MOTS) for computations of orbital elements”.

09:12 – 09:24

*Denis Vida*: “Open-source meteor detection software for low-cost single-board computers”.

09:24 – 09:36

*Pete Gural*: “A Fast Meteor Detection Algorithm”.

09:36 – 09:48

*Theresa Ott*: “PaDe - The Particle Detection Program”.

09:48 – 10:00

*Stijn Calders*: “The BRAMS Zoo, a citizen science project: current status”.

10:00 – 10:12

*Hervé Lamy*: “Automatic detection of meteor echoes in BRAMS data: towards a final decision”.**10:12 – 10:36****Coffee break & Poster Session.****SESSION 9 – Ongoing work, History & Miscellaneous.**(Chair: *Antonio Martinez Picar*).

10:36 – 10:48

*Damir Šegon*: “Croatian Meteor Network: ongoing work 2015-2016”.

10:48 – 11:00

*Juraj Toth*: “Expedition Atacama - project AMOS in Chile”.

11:00 – 11:12	<i>Regina Rudawska</i> : “ESA/ESTEC Meteor Research Group – behind the scenes”.
11:12 – 11:24	<i>Iain Reid</i> : “60 years of radio meteor studies at Adelaide University”.
11:24 – 11:36	<i>Detlef Koschny</i> : “Height computation of a fireball”.
11:36 – 11:48	<i>Eleanor Sansom</i> : “Meteor Reporting Made Easy- Fireballs in the Sky's smartphone app”.
11:48 – 12:00	<i>Maria Gritsevich</i> : “Big Data Era in Meteor Science”.
12:30	Departure for excursion to the world heritage site the Waddensee.
<b>19:00 – 20:00</b>	<b>Closing dinner.</b>
20:00 – 21:00	Parallel Program. Option A – Free entertainment.
20:00 – 20:45	Option B – Workshop: Software for analysis of visual meteor data. Option C - Extended-talk Session II (20:00 – 21:00).
20:00 – 20:20	<i>Sirko Molau</i> : “Flux density, population index, perception coefficient, and the Moon”.
20:20 – 20:40	<i>Pete Gural</i> : “A Fast Meteor Detection Algorithm”.
20:40 – 21:00	<i>Daniel Kastinen</i> : “A statistical approach to the temporal development of orbital associations”.
21:00 – ...	Last night of the IMC in the bar, free entertainment.

## Sunday, 5 June 2016

08:30 – 09:30	Breakfast.
09:55 – 10:00	Local announcements.
	<b>SESSION 5A – Parent bodies, meteoroids, meteorites, planets and their relation.</b> (Chair: <i>Denis Vida</i> ).
10:00 – 10:12	<i>Ayyub Guliyev</i> : “Meteor streams and comet disintegration”.
	<b>SESSION 10 – Instruments.</b> (Chair: <i>Pete Gural</i> ).
10:12 – 10:24	<i>Mariusz Wiśniewski</i> : “Current status of Polish Fireball Network”.
10:24 – 10:36	<i>Hadrien Devillepoix</i> : “Status of the Desert Fireball Network”.
10:36 – 10:48	<i>Chris Peterson</i> : “Evaluating video digitizer errors”.
10:48 – 11:00	<i>Martin Dubs</i> : “Calibration of meteor spectra”.
11:00 – 11:12	<i>Waleed Madkour</i> : “The KUT meteor radar: An educational low cost meteor observation system by radio forward scattering”.
11:12 – 11:24	<i>Cezar Lesanu</i> : “ROAN Remote Radio Meteor Detection Sensor”.
<b>11:24 – 12:00</b>	<b>Coffee break &amp; Poster Session.</b>
	<b>SESSION 11 – Observing techniques II.</b> (Chair: <i>Francesco Ocaña</i> ).
12:00 – 12:12	<i>Anna Kartashova</i> : “The complex meteor observations in 2014”.
12:12 – 12:24	<i>Satoshi Mizumoto</i> : “Comprehensive observation of meteors combining with infrasonic, optic and radio scattering signals”.
12:24 – 12:36	<i>Jakub Kákona</i> : “Meteor trajectory estimation from radio meteor observations”.
12:36 – 12:48	<i>Margaret Campbell-Brown</i> : “Results from the Canadian Automated Meteor Observatory”.
12:48 – 13:00	<i>Jean-Louis Rault</i> : “Conference summary”.
13:00 – 13:10	Closing of the 35 <sup>th</sup> IMC.
<b>13:10 – 14:00</b>	<b>Lunch.</b>
14:30	Departure of participants, Bus transfer to Schiphol, Bus transfer to Meteoroids 2016.

# Artificial meteor test towards On-demand meteor shower

**Shinsuke Abe, Lena Okajima, Hironori Sahara, Takeo Watanabe,  
Yuta Nojiri and Tomohiko Nishizono**

shinsuke.avell@gmail.com

An arc-heated wind tunnel is widely used for ground-based experiments to simulate environments of the planetary atmospheric entry under hypersonic and high-temperature conditions. In order to understand details of a meteor ablation such as temperature, composition ratio and fragmentation processes, the artificial meteor test was carried out using a JAXA/ISAS arc-heated wind tunnel. High-heating rate around  $30 \text{ MW/m}^2$  and High-enthalpy conditions, 10000 K arc-heated flow at velocity around 6 km/s were provided. Newly developed artificial metallic meteoroids and real meteorites such as Chelyabinsk were used for the ablation test. The data obtained by near-ultraviolet and visible spectrograph (200 and 1100nm) and high-speed camera (50  $\mu\text{s}$ ) have been examined to develop more efficient artificial meteor materials. We will test artificial meteors from a small satellite in 2018.



Sinsuke Abe (Photo Irmgard Schmidt).

# Asteroidal meteors detected by MU radar head-echo observations

Shinsuke Abe, Johan Kero, Takuji Nakamura, Yasunori Fujiwara,  
Daniel Kastinen, Jun-ichi Watanabe and Hiroyuki Hashiguchi

shinsuke.avell@gmail.com

The recent development of the technique carried out using the middle and upper atmosphere radar (MU radar) of Kyoto University at Shigaraki (34.9N, 136.1S), which is large atmospheric VHF radar with 46.5 MHz frequency, 1 MW output transmission power and 8330 m<sup>2</sup> aperture array antenna, has established very precise orbital determination from meteor head echoes. A tremendous number, more than 150000, of observed precise orbits of meteoroids by the MU radar meteor head-echo observation will shed light on new discoveries of meteoroids. Here we report some interesting features related with asteroids or distinct comets.



Wednesday evening: the LOC meets for the last time before the start, latest details are discussed. From left to right Roy Keeris, Casper ter Kuile (hidden), Arnold Tukkers, Jos Nijland, Elise Ijland, Mark Neijts, Joost Hartman and Sebastiaan de Vet.

# On the age and parent body of the daytime Arietids meteor shower

Abedin Abedin, Paul Wiegert, Petr Pokorny and Peter Brown

Dept. of Physics and Astronomy, University of Western Ontario, London, Ontario, N6A 3K7, Canada  
aabedin@uwo.ca

The daytime Arietid meteor shower is active from mid-May to late June and is among the strongest of the annual meteor showers, comparable in activity and duration to the Perseids and the Geminids. Due to the daytime nature of the shower, the Arietids have mostly been constrained by radar studies. The Arietids exhibit a long-debated discrepancy in the semi-major axis and the eccentricity of meteoroid orbits as measured by radar and optical surveys. Radar studies yield systematically lower values for the semi-major axis and eccentricity, where the origin of these discrepancies remain unclear. The proposed parent bodies of the stream include comet 96P/Machholz and more recently the Marsden's group of sun-skirting comets. In this work, we present detailed numerical modelling of the daytime Arietid meteoroid stream, with the goal to identifying the parent body and constraining the age of the stream. We use observational data from an extensive survey of the Arietids by the Canadian Meteor Orbit Radar (CMOR), in the period of 2002–2013, and several optical observations by the SonotaCo meteor network and the Cameras for All-sky Meteor Surveillance (CAMS).

Our simulations suggest that the age and observed characteristics of the daytime Arietids are consistent with cometary activity from 96P, over the past 12000 years. The sunskirting comets that presumably formed in a major comet breakup between 100 – 950 AD (Chodas and Sekanina, 2005), alone, cannot explain the observed shower characteristics of the Arietids. Thus, the Marsden sunskirters cannot be the dominant parent, though our simulations suggest that they contribute to the core of the stream.

## References

- Sekanina Z. and Chodas P. W. (2005). “Origin of the Marsden and Kracht Groups of Sunskirting Comets. I. Association with Comet 96P/Machholz and Its Interplanetary Complex”. *The Astrophysical Journal Supplement Series*, **161**, 551–586.

# A Monte-Carlo based extension of the Meteor Orbit and Trajectory Software (MOTS) for computations of orbital elements

Thomas Albin<sup>1,2</sup>, Detlef Koschny<sup>3,4</sup>, Rachel Soja<sup>1</sup>, Ralf Srama<sup>1</sup> and Bjoern Poppe<sup>2</sup>

<sup>1</sup>Institute for Space Systems, University of Stuttgart, Pfaffenwaldring 29, 70569 Stuttgart, Germany  
albin@irs.uni-stuttgart.de

<sup>2</sup>Universitaetssternwarte Oldenburg, Institute of Physics and Department of Medical Physics and Acoustics, Carl von Ossietzky University, 26129 Oldenburg, Germany

<sup>3</sup>European Space Agency, ESA/ESTEC, Keplerlaan 1, 2201 AZ Noordwijk ZH, Netherlands

<sup>4</sup>Chair of Astronautics, Technical University Munich, Boltzmannstrasse 15, 85748 Garching, Germany

The Canary Islands Long-Baseline Observatory (CILBO) is a double station meteor camera system (Koschny et al., 2013; Koschny et al., 2014) that consists of 5 cameras. The two cameras considered in this report are ICC7 and ICC9, and are installed on Tenerife and La Palma. They point to the same atmospheric volume between both islands allowing stereoscopic observation of meteors. Since its installation in 2011 and the start of operation in 2012 CILBO has detected over 15000 simultaneously observed meteors. Koschny and Diaz (2002) developed the Meteor Orbit and Trajectory Software (MOTS) to compute the trajectory of such meteors. The software uses the astrometric data from the detection software MetRec (Molau, 1998) and determines the trajectory in geodetic coordinates. This work presents a Monte-Carlo based extension of the MOTS code to compute the orbital elements of simultaneously detected meteors by CILBO.

## 1 Introduction

The Canary Islands Long-Baseline Observatory (CILBO, Koschny et al., 2013; 2014) has been in continuous operation since January 2013. One part of CILBO consists of two camera systems installed on Tenerife (ICC7) and La Palma (ICC9) that observe an overlapping area in the sky at an altitude of approximately 100 km between both islands. Meteors that cross both Field-of-Views (FOV) simultaneously are observed stereoscopically. This allows a precise reconstruction of the trajectory and orbit. *Figure 1* shows the position and pointing of the so called boresight of both CILBO cameras. The red and green skewed pyramids indicate the FOVs of ICC9 and ICC7, respectively. Additionally, an example of a stereoscopically observed meteor between both islands is shown. Each dot of the meteor represents the determined geodetic coordinates from each recorded video frame.

Based on the meteor data set of around 15000 simultaneously observed meteors, a pointing and velocity bias analysis has been completed (Albin et al., 2015a; 2015b) as well as an un-biasing of the velocity distribution and mass influx based on the ECSS model (Drolshagen et al., 2014; Ott et al., 2014; Drolshagen et al., 2015; Kretschmer et al., 2015).

The complete data recording and processing pipeline consists of miscellaneous software packages. The software *MetRec* (Molau, 1999) has been chosen for the meteor detection. Both cameras are operated with a frame

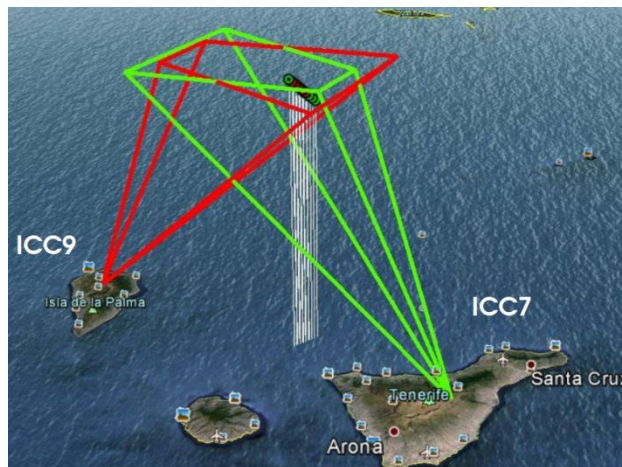


*Figure 1* – Location and camera pointing of the CILBO cameras ICC7 and ICC9 on Tenerife and La Palma, respectively. The skewed pyramids represent the field-of-views of the cameras. The data points of a recorded meteor are drawn within the overlapping observation volume.

rate of 25 fps and a video frame length of 40 ms, respectively. *MetRec* determines the photometric center of each meteor it detects on the video frames. The center's position is computed in a relative CCD coordinate system as well as in equatorial coordinates using the background stars as a reference. All information are then saved in a so-called *inf*-file. *Figure 2* shows the content of an *inf*-file. Finally, the individual video frames are saved in a stacked image for visual verification in order to exclude false detections. *Figure 3a and b* show a meteor detected simultaneously by both CILBO cameras. The meteor shows a double-peak feature and has been

```

AppearanceDate 03.05.2014
AppearanceTime 00:15:31
ReferenceStars \dev\metrec\config\20130831.ref
FrameCount 10
#   time  bright   x     y     alpha   delta   c_x   c_y   c_alpha  c_delta  use
01  31.565  ----   0.289  0.328  10.9126  27.232  ----  ----  - - - - -  - - - - -  no
02  31.605  ----   0.288  0.323  10.9053  27.186  ----  ----  - - - - -  - - - - -  no
03  31.646  ----   0.287  0.318  10.8975  27.139  ----  ----  - - - - -  - - - - -  no
04  31.686  3.2   0.287  0.314  10.8901  27.093  ----  ----   10.8913  27.098  yes
05  31.726  2.7   0.286  0.309  10.8823  27.046  ----  ----   10.8807  27.039  yes
06  31.766  3.3   0.285  0.301  10.8701  26.982  ----  ----   10.8701  26.979  yes
07  31.806  3.8   0.284  0.294  10.8589  26.916  ----  ----   10.8595  26.920  yes
08  31.846  ----   0.283  0.287  10.8477  26.850  ----  ----  - - - - -  - - - - -  no
09  31.886  ----   0.282  0.281  10.8364  26.783  ----  ----  - - - - -  - - - - -  no
10  31.926  ----   0.281  0.274  10.8257  26.716  ----  ----  - - - - -  - - - - -  no
    
```

Figure 2 – Example of an inf file. The first four rows provide the meta data (appearance time, data, reference file). The fifth row provides the table column headers for the measurement data. Column 1 is a consecutive number, column 2 lists the detection time in seconds and column 3 shows the determined brightness. In addition to the detected meteor frames, *MetRec* saves 3 frames before and after the meteor detection, for which no brightness values are given. The next four columns provide the position of the photometric center in relative CCD coordinates and in right ascension and declination. *c\_x* and *c\_y* are currently not used. *c\_alpha* and *c\_delta* are corrected astrometric right ascension and declination (by fitting the position measurements to a great circle). The last column indicates whether a meteor has been detected in the video frame.



Figure 3 – A meteor detected simultaneously by ICC7 (top) and ICC9 (bottom). The meteor appears shorter in the ICC9 image because there the radiant is closer to the camera boresight.

detected on 5 October 2013 at 05<sup>h</sup>13<sup>m</sup>59<sup>s</sup> UTC. The different lengths of the meteor and brightness are due to the flight direction and distance to the camera. Furthermore, the smaller angular velocity of the meteor on the ICC9 frames leads to less illuminated pixels

compared to ICC7. The result is that the meteor appears brighter on the ICC9 frames than on the ICC7.

For each CILBO camera individual directories contain the information for each detected meteor. A Python-based routine then checks the camera directories and identifies simultaneously detected meteor candidates. The Meteor Orbit and Trajectory Software (Koschny and Diaz, 2002) is then used to determine the trajectory for each meteor candidate in geodetic coordinates. These coordinates are shown in Figure 1 for a stereoscopically observed meteor. The geodetic information of the meteor as well as the detection time and time distance of 40 ms allows a precise trajectory reconstruction. The final positions are indicated as circles within the FOV of both cameras. An overview of the *MOTS* algorithm is shown in Section 2.

The orbit of the meteors can be computed with the geodetic trajectory information. The methods and algorithms as well as the Monte-Carlo based approach to determine the aforementioned errors are described in Section 3.

## 2 The Meteor Orbit and Trajectory Software (MOTS)

Koschny and Diaz (2002) developed the *Meteor Orbit and Trajectory Software (MOTS)* which is used in this work to compute the trajectory of a meteor in geodetic coordinates. Here a short overview of the *MOTS* algorithm is given. A complete mathematical description can be found in the corresponding paper.

Figure 4 shows the computation procedure schematics. S1 and S2 are two double-stationary meteor cameras, here ICC7 and ICC9. The meteor appears at point B and ends at the point E. Both points describe a thick black line that indicates the actual flight path of the meteor. Using the geographical coordinates of station S1 and the observation data of the meteor, a plane can be found

crossing the camera station and the flight path of the meteor.  $\vec{n}$  defines the plane normal. Hereafter, this plane is called support plane.

A directional vector can be defined with the astrometric data from the station S2 (example: vector  $(\vec{M2})$ ). The intersection point between the support plane and the defined vector from S2 can then be computed. The height and projected geographical coordinates are then computed in order to obtain final geodetic state vector of the meteor. This requires also time information.

To verify the data the same plane and vector crossing computation can be done with respect to station S2, where the astrometric data and geographical position of S2 defines the support plane.

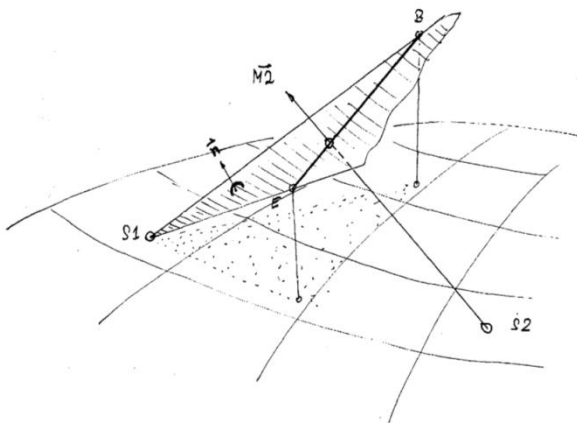


Figure 4 – Schematic diagram of the computation routine of MOTs. S1 and S2 indicate the two camera locations. The meteor is a thick black line with the starting and ending point B and E respectively.  $n$  is the normal vector of the drawn plane between meteor and S1.  $M2$  is a direction vector of a determined meteor position as seen from S2. The intersection point between  $M2$  and the plane determines a geodetic coordinates point for the meteor. From Koschny and Diaz (2002).

Albin et al. (2015b) have shown that continuously operated meteor cameras have a velocity determination bias for meteors detected on 3 frames. The velocity determination cannot use the first and last frames because the meteor appears and disappears in the frames, respectively. The following methods are applied for this work:

- Meteor on 3 frames: No suitable velocity determination. Can be used to compute the support plane.
- Meteor on 4 frames: Only one velocity value can be computed, between frame 2 and 3.
- Meteor on  $> 4$  frames: All values from the second to the second-to-last frame can be used. Depending on the total number of frames a linear, quadratic or higher polynomial fit function can be used to determine an accurate velocity function. The velocity of the meteor is then computed using the function at the initial position.

### 3 The Monte-Carlo (MC) based extension

This chapter presents the orbit code algorithm and an MC-based-extension to compute an accurate error for the orbital elements based on the astrometric accuracy.

#### Orbit Determination

The developed orbit code is based on the existing *MOTS* routines. It determines the orbital elements of a meteor in the following way. As a visual guideline, the computation steps 3 to 5 are illustrated schematically in *Figure 5*:

1. **Identification of simultaneously detected meteors:** A routine compares the inf-files in the data directories of ICC7 and ICC9 and searches for simultaneously detected meteors. Approximately 30 % of all meteors have been observed at the same time from both cameras. The identified inf-files are then loaded and sent to the *MOTS* computation routine.
2. **Trajectory determination:** The inf-files are then used to determine the trajectory of the meteor in geodetic coordinates. Two geodetic state vectors are computed with respect to each camera (see *Section 2*). The velocity of the meteor is computed if it has been recorded on at least 4 video frames. Meteors with a length of 3 frames are only used to compute the support plane.
3. **Determination of the initial state vector in an Earth-Centric coordinate system (ECCS):** The trajectory vectors and the time information are now used to generate two Cartesian state vectors  $\vec{s}_{ICC7}$  and  $\vec{s}_{ICC9}$  of the meteor in an Earth-Centric coordinate system. NASA's *SPICE* software package is used for the computation of orbital elements and other astrodynamical properties<sup>1</sup>. Furthermore, a Python wrapper needs to be used since currently no native Python support is available<sup>2</sup>.

First, the orbital elements of the two state vectors are computed in ECCS. If the determined initial meteor velocity does not exceed 11.2 km/s (escape velocity of the Earth), the corresponding eccentricity is between 0 and 1, which corresponds to a bound orbit around the Earth. The reasons for these bound meteoroids could be:

- The meteor decelerated already in the atmosphere before it was detected by CILBO.
  - The meteor was a piece of a space debris on an Earth-bound orbit.
  - The meteor was a meteoroid which has been captured by Earth following a "mini-moon" orbit with a decreasing velocity due to close encounters with Earth and friction with its exosphere.
4. **Backward propagation:** If the eccentricity is  $e \geq 1$  the corresponding meteoroid was on a para- / hyperbolic orbit in ECCS. In this case the initial state

<sup>1</sup> <http://naif.jpl.nasa.gov/naif/index.html>

<sup>2</sup> <https://github.com/AndrewAnnex/SpiceyPy>

vectors are computed backwards in time until the state vectors reaches Earth’s Sphere-of-Influence (SOI) within a certain threshold (e.g. with an accuracy of  $1^s$ , so called threshold time).

The SOI is the approximate spheroid-shaped region around a planetary body where the dominant gravitational force comes from the body. Influences and perturbations such as other planets or by the Sun can be neglected. This simplification allows a quicker trajectory computation since the orbit computation becomes a 2-body problem. The radius of a simplified spherical SOI  $r_{SOI}$  can be computed by the following equation, where  $a$  is the semi-major axis and  $m$  is the mass of the Earth.  $M$  is the mass of the Sun. This leads to a SOI radius for Earth of approximately 900000 km.

$$r_{SOI} = a \cdot \left(\frac{m}{M}\right)^{\frac{2}{5}}$$

An adaptive algorithm has been developed to compute the meteoroid’s state vector at Earth’s SOI. Initially, the backwards time steps are set to 1000 s. With an initial velocity of e.g. 30 km/s this leads to a propagation step of 30000 km. After crossing the SOI border, the propagation time is inverted and decreased by an order of magnitude until the meteoroid crosses the SOI again. This iterative approach is repeated until the threshold time is reached.

5. **Computing orbital elements in heliocentric coordinates:** After reaching Earth’s SOI the state vector is transformed to the heliocentric coordinate system in J2000 (ECLIPJ2000). This requires that the state vector of the Earth is added to the meteoroid’s one. With the final state vector the orbital elements can be computed. Additionally, further astro-dynamical properties can be computed like e.g. the radiant in an Earth-Centric Sun-Pointing coordinate system to identify sporadic background sources like e.g. the Apex- or Anti-Helion-Source.

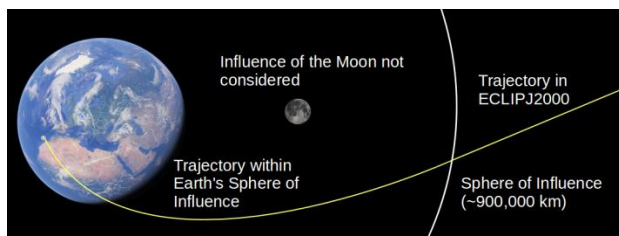


Figure 5 – Schematic overview of the computation procedure within Earth’s vicinity (graph not in scale). The initial meteor state vector is computed above the Canary Islands and computed back in time until it reaches the Sphere of Influence of Earth (SOI, approx. 900000 km). For this computation the gravity of the Moon and other celestial bodies is not considered. At the SOI the state vector of the meteoroid is transformed to a heliocentric coordinate system (ECLIPJ2000). Meteors that have a bound orbit around Earth cannot reach Earth’s SOI. In this case, the final ECLIPJ2000 transformation is not applied.

### Error propagation and computation

The described orbit determination procedure computes the orbital elements and further properties of the trajectory with respect of ICC7 and ICC9. However, it does not contain the astrometric accuracy as an input error source. Here, an MC-based approach is presented that has been developed for the described orbit determination algorithm. Figure 6a to 6d show schematically the procedure for a meteor with a length of 5 frames, projecting the MC-generated astrometric data on a support plane.

Figure 6a shows the determined astrometric data of the 5 photometric centers of the observed meteor. Due to the optical distortion and the quantization of the measurements these position values do not follow a perfect trajectory path. The white arrow indicates the flight direction of the meteor and represents the determined flight direction vector by MOTS.

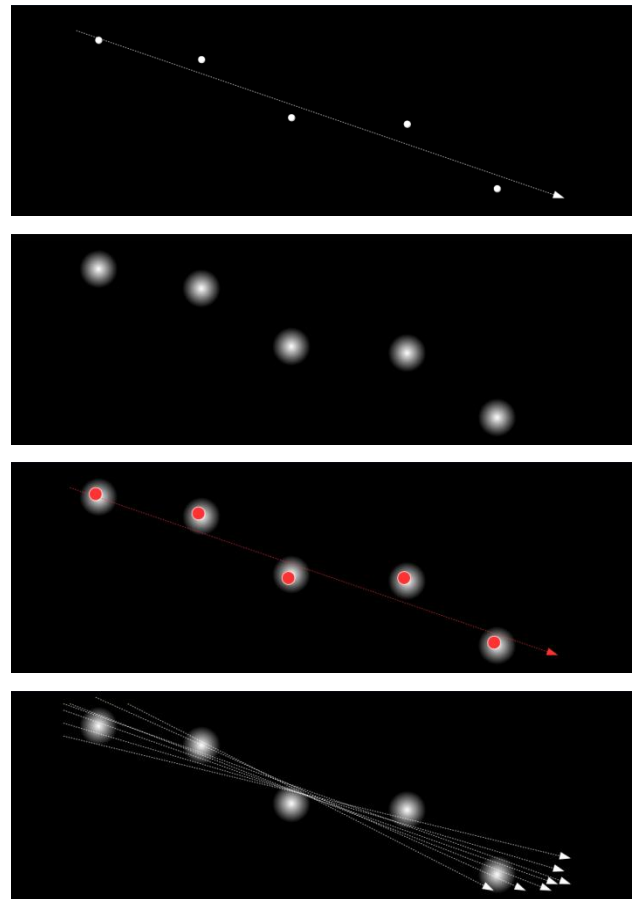


Figure 6a,b,c,d – Graphical representation of the Monte-Carlo algorithm as explained in the text.

Each observation night *MetRec* saves a log file that contains the astrometric accuracy data of each meteor observation. The accuracy is derived from the variance of the astrometric data that are fitted on a great circle. These entries are used for the extension of the existing code to a Monte\_Carlo version. The calculated astrometric positions of the meteor, (Figure 6a) are replaced by 2-D Gaussian distributions (Figure 6b). The standard deviation of the functions is the corresponding astrometric accuracy. These Gaussian distributions are assumed to represent the *Probability Density Function*

(PDF) of each determined photometric center. Since the angular distance between two right ascension values decreases for higher declinations, the Gaussian functions need to be scaled according to their corresponding declination.

A set of possible virtual observations can be generated, based on these PDFs. *Figure 6c* shows an example of a possible meteor flight path and position determination based on the measurement uncertainty. The red dots represent the newly generated photometric centers based on the Gaussian PDFs. The new flight direction path is computed, using the trajectory software *MOTS* (red arrow).

This re-sampling procedure is done several times, to generate an ensemble of possible flight direction paths (*Figure 6d*). This ensemble is then used to compute the orbital elements, using computation steps 3 to 5. To obtain sufficient statistical results the number of re-samples depends on the number of frames and the astrometric accuracy. However, a re-sampling size of at least 100 appears sufficient.

### Unbiased Descriptive Statistics

The MC approach provides a set of possible solutions. The final statistical analysis links each solution with a probability. To obtain statistical conclusions out of the resulting data set, the correct descriptive statistical parameters must be chosen. Distributions are often described by a mean and standard deviation. However, these parameters apply only for Gaussian and symmetric distributions. Since the outcome of a MC computation is unknown and likely not Gaussian or symmetric, different parameters are required. *Figure 7* shows an example of an MC-result. The distribution shows possible argument of periapsis solutions of a meteor detected at 2014-08-01T22:54:26, visualized as a histogram with evenly spaced bars. The red (dotted) and blue (solid) vertical lines indicate the mean and median (separation between lower and upper half of the distribution) respectively. The blue dashed lines show the upper and lower boundaries of the quartiles of the data (quartiles: separate the data in lowest 25 % and highest 75 % and vice versa). The plot provides information on the mean and standard deviation, median and median absolute deviation, interquartile range and the lower and upper quartile. The IQR, by definition contains 50% of the entire dataset. The *Median Absolute Deviation* (MAD) is a descriptive parameter for the scattering and variation of the data around the median and is defined by (where  $X_i$  is an element of the data array  $X$  of length  $n$ ):

$$MAD = \text{median}(|X_i - \text{median}(X_i)|)$$

Due to the skewness of the distribution the mean is shifted by about 4 % with respect to the median. Outliers do not affect the median if the total number of re-samples is large compared to the number of outliers. Since the shape of the distributions from the MC code is unknown,

we recommend using the following entries per each orbital element and further astro-dynamical calculations:

- Median;
- Median Absolute Deviation;
- Interquartile Range;
- Lower and Upper Quartile (and also additional data separations at 15 % and 85 %).

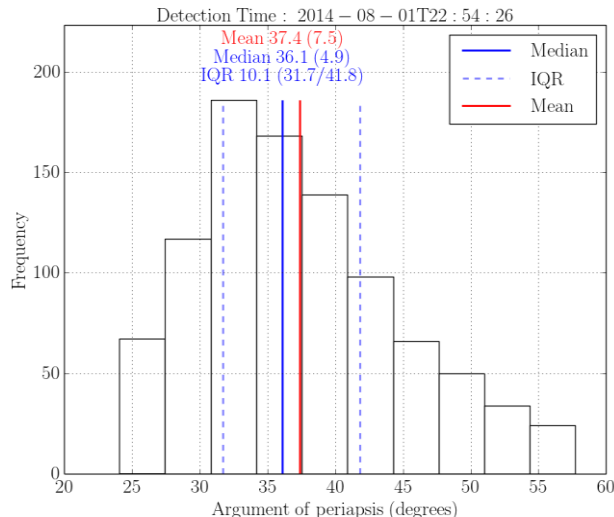


*Figure 7* – Argument of periapsis distribution (Meteor detection time: 2014-08-01T22:54:26) to visualize different descriptive statistical parameters. The dotted red and blue line show the mean and median, respectively. The blue dashed lines show the quartiles of the distribution. Above the distribution the corresponding values are shown. The standard deviation and median absolute deviation are given in parenthesis next to the mean and median values. The last row shows the width of the interquartile range, with the lower and upper quartile range given within the parenthesis. The re-sampling size is 1000.

Saving the mean and standard deviation helps to estimate the shape of the final distributions. Assuming a distribution is Gaussian shaped, the MAD scales with the standard deviation  $\sigma$  by a constant factor. The conversion is:

$$\sigma \approx 1.4826MAD$$

If the determined standard deviation and scaled MAD value are comparable, the final distribution is likely to be symmetrically shaped or even Gaussian.

Additionally, the covariance matrix between the orbital elements is saved in order to have a quantitative measure of the dependencies between each orbital element.

## 4 Conclusion

In this work we presented a Monte-Carlo based extension of the *MOTS* software. The developed algorithm considers the astrometric accuracy and previous works on the velocity determination bias, as well as un-biased descriptive statistical parameters to compute possible meteor orbit solutions.

## Reference

- Albin T., Koschny D., Drolshagen G., Soja R., Srama R. and Poppe B. (2015a). “Influence of the pointing direction and detector sensitivity variations on the detection rate of a double station meteor camera”. In Rault J.-L. and Roggemans P., editors, *Proceedings of the International Meteor Conference*, Mistelbach, Austria, 27-30 August 2015. IMO, pages 225–231.
- Albin T., Koschny D., Drolshagen G., Soja R., Srama R. and Poppe B. (2015b). “De-biasing of the velocity determination for double station meteor observations from CILBO”. In Rault J.-L. and Roggemans P., editors, *Proceedings of the International Meteor Conference*, Mistelbach, Austria, 27-30 August 2015. IMO, pages 214–219.
- Drolshagen E., Ott T., Koschny D., Drolshagen G. and Poppe B. (2014). “Meteor velocity distribution from CILBO double station video camera data”. In Rault J.-L. and Roggemans P., editors, *Proceedings of the International Meteor Conference*, Giron, France, 18-21 September 2014. IMO, pages 16–22.
- Drolshagen S., Kretschmer J., Koschny D., Drolshagen G. and Poppe B. (2015). “Mass accumulation of Earth from interplanetary dust, meteoroids, asteroids and comets”. In Rault J.-L. and Roggemans P., editors, *Proceedings of the International Meteor Conference*, Mistelbach, Austria, 27-30 August 2015. IMO, pages 220–225.
- Kretschmer J., Drolshagen S., Koschny D., Drolshagen G., Poppe B. (2015). “De-biasing CILBO meteor observational data to mass fluxes”. In Rault J.-L. and Roggemans P., editors, *Proceedings of the International Meteor Conference*, Mistelbach, Austria, 27-30 August 2015. IMO, pages 209–213.
- Koschny D. and Diaz del Rio J. (2002). “Meteor Orbit and Trajectory Software (MOTS) - Determining the Position of a Meteor with Respect to the Earth Using Data Collected with the Software MetRec”. *WGN, the Journal of the IMO*, **30**, 87–101.
- Koschny D., Bettonvil F., Licandro J., v. d. Luijt C., Mc Auliffe J., Smit H., Svedhem H., de Wit F., Witasse O. and Zender J. (2013). “A double-station meteor camera setup in the Canary Islands – CILBO”. *Geosci. Instrum. Method. Data Syst.*, **2**, 339–348.
- Koschny D., Mc Auliffe J., Bettonvil F., Drolshagen E., Licandro J., van der Luijt C., Ott T., Smit H., Svedhem H., Witasse O. and Zender J. (2014). “CILBO - Lessons learnt from a double-station meteor camera setup in the Canary Islands”. In Rault J.-L. and Roggemans P., editors, *Proceedings of the International Meteor Conference*, Giron, France, 18-21 September 2014. IMO, pages 10–15.
- Molau S. (1999). “The Meteor Detection Software MetRec”. In Arlt R. and Knoefel A., editors, *Proceedings of the International Meteor Conference*, Stara Lesna, Slovakia, 20-23 August 1998. IMO, pages 9–16.
- Ott T., Drolshagen E., Koschny D., Drolshagen G. and Poppe B. (2014). “Meteoroid flux determination using image intensified video camera data from the CILBO double station”. In Rault J.-L. and Roggemans P., editors, *Proceedings of the International Meteor Conference*, Giron, France, 18-21 September 2014. IMO, pages 23–29.

# An antenna, a radio and a microprocessor: which kinds of observation are possible in meteor radio astronomy?

Lorenzo Barbieri

<sup>1</sup>RAMBo meteor group, AAB, Associazione Astrofili Bolognesi, Bologna, Italy  
barbieriofiuco@gmail.com

Radio meteors are usually investigated by professional radars. Amateur astronomers cannot have transmitters, so usually they can only listen to sounds generated by a radio tuned to a TV or military transmitter. Until recently, this kind of observation has not produced good data. The experience of “RAMBo” (Radar Astrofilo Meteorico Bolognese) shows which data can be extracted from an amateur meteor scatter observatory and the results which can be achieved.

## 1 The meteor scatter observatory

Meteor shower observations, traditionally carried out by visual observers, have for several years also used automatically recorded images captured by TV cameras and can also be carried out using radio waves.

At an altitude of around 100 km in the upper atmosphere, the bremsstrahlung begins by the friction of meteoric particles intercepted by the Earth in its movement around the Sun. It is here that meteors appear. The bremsstrahlung by friction leads to extensive overheating of the corpuscle (ablation), the result of which is the vaporization of the material entering the atmosphere, the generation of light, and the ionization of a large number of atmospheric molecules in a radius of some meters along its trajectory. This generates a long, narrow cylinder of ionized molecules of a very short time duration (the time required for recombination of the ionized molecules) which behaves like a reflective object for radio waves, in the same way as aircraft and satellites.

“Radio meteor” observation is not affected by the presence of the Sun or Moon, or by cloud, and can thus be carried out continuously. Meteor observing via radio waves is usually achieved by “traditional” radar, which consists of a transmitter and a receiver. Normally these pieces of apparatus are spaced hundreds of kilometers apart and the antennas point towards the layers of the atmosphere around the 100 km altitude in the midway position between transmitter and receiver. The transmitted signal is directed upwards so it can only be received when a reflective object is placed along the radio electric emission optical path. When this occurs, the signal is reflected and the receiver picks up the presence of the object.

Professional radars, thanks to the fact that they transmit pulsed signals and that they use complex antenna arrays to analyze the reflected signal, are able to calculate the size, speed, direction and position of meteors at the sky. Since amateur observers cannot own transmitters, they commonly use other people’s transmitters, e.g. transmitters on VHF (Very High Frequency), possibly on

air day and night, with high power and at a great distance. They may be radio or television transmitters, or equipment installed for military aircraft and satellite control.

This situation has two great drawbacks.

Firstly, the exact technical characteristics of the transmitter and its behavior are unknown.

Secondly, the absence of multiple arrays of antennas and the lack of pulsed signals greatly reduce the capabilities of an amateur setup compared to a professional one. The experience of RAMBo (Radar Astrofilo Meteorico Bolognese) shows which data can be extracted from such observations and the results which can be achieved.

## 2 “RAMBo” set up

### The transmitter

Like other European observatories, RAMBo uses a military radar transmitter, GRAVES, that is continuously on air in VHF at great power. Located near Dijon, in France, it is built for spacecraft orbit determination.

Its transmission is directed upwards and due to the Alps, it is not receivable from Bologna directly.

Technical data:

- Frequency 143.050 MHz
- Polarization: circular
- Power = 1MW (RF)
- Irradiation = south  $\pm$  90 °
- Height oscillating in an angle of about 25 °

### The receiver setup

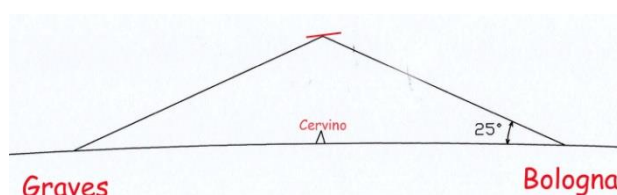


Figure 1 – Calculation of the zenithal angle of view.

The RAMBo receiving set up is composed of a Yagi directive antenna (10 elements) pointed in azimuth in the direction of the transmitter ( $300^\circ$ ), and in declination about 25 degrees above the horizon (*Figure 1 and 2*), the direction in which we have calculated the reflection point in the upper atmosphere.

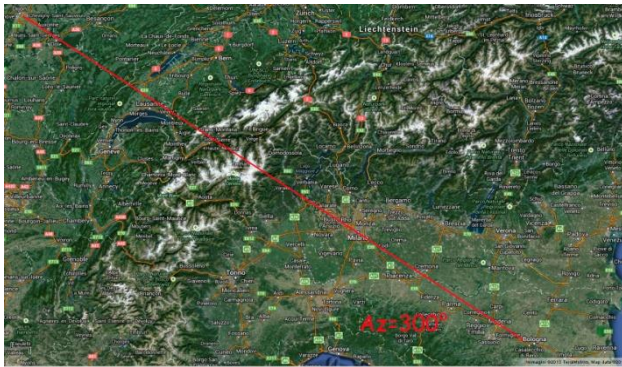


Figure 2 – Calculation of the angle of view in azimuth.

Its polarization is vertical. The choice of this polarization is based on the belief that there could be more meteors with horizontal rather than vertical traces.

Since the polarization of the transmitter is circular, and the polarization emerging from the reflection is orthogonal to the plane of reflection, we can expect a greater number of vertically polarized echoes than horizontal ones. In fact, a week of measurements specifically performed with horizontal polarization gave a two-thirds lower result compared to the vertical configuration.

Given the characteristics of the antenna (large directivity), the area of sky that should be investigated consists of an area of twenty to thirty square degrees above the Alps, roughly vertically above the Matterhorn.

The receiver is a Yaesu 897 tuned in SSB (Single Side Band) about 1000 Hz below the Graves carrier. Thanks to the SSB technique, the difference between these two frequencies means that the Graves carrier (not modulated) may be heard as a signal of frequency equal to the difference between the two frequencies. As we will see, this rate is actually affected by the Doppler Effect, both for the body speed when entering the atmosphere and for the speed of movement of the ionized cylinder due to high altitude winds.

The purpose of RAMBo is the analysis of the audio signal generated by the receiver.

### 3 Sound analysis

Sound is picked up from the direct audio output of the receiver, avoiding the potentiometer controlled headset output, and with the automatic gain control (AGC) disabled.

Normally the audio signal is a continuous rustle (chaotic noise). Over this signal we can occasionally hear three different types of sound:

- Discharge;
- Aircraft and satellites;
- Meteoric echoes.

The discharges are transient pulses: very short in time and of high amplitude, sometimes individual and sometimes in rapid sequences of variable length. These impulses, if measured and counted, represent “false positives” which will affect meteoric data.

There are a lot of causes of discharge: they may come from storms, even far away, or from ionization due to solar activity. Other causes are human activities: combustion engines in the receiver proximity, electric motors or other power transients on the power line feeding the radio receiver, such as neon lighting. These last problems can be overcome by using a power supply with a daytime battery charged by a solar panel. However, this does not completely solve the problems caused by discharges received in the antenna.

Discharges are the biggest problem of meteor scatter receivers. The RAMBo experience led to six different trials with various techniques to avoid this problem. Only the sixth attempt finally solved the problem.

Aircraft and satellite echoes are similar to those generated by meteors, but are generally of lower level, their frequency varies slowly and their duration is high. These echoes could be numerous if we receive with omnidirectional antennas and if the receiver is close to large urban areas with an airport nearby. The use of high-gain antennas (i.e. directive) solves this problem. In our case, aircraft and satellites are almost never received, and the sound level of their echoes is lower than that of meteors.

Meteors produce clear sound characterized by a frequency near 1000 Hz. This frequency, in theory, is generated by the beat between the transmitter’s carrier (in our case the Graves Tx) and the frequency of the radio receiver, tuned in at SSB 1000 Hz below the transmission carrier. The exact value of the echo frequency is not easy to predict, due to both possible instability or radio receiver tolerances, as well as to the speed of high altitude winds which propel and distort the ionization cylinder caused by the meteor’s entry into the atmosphere. Finally, the speed and direction of the meteor could also affect this frequency (Doppler Effect).

Our experience leads us to say that this variability is almost always confined inside a window of approximately 300 Hz centered on the mean frequency.

The sound analysis and data recording are both made with Arduino, the well-known low-cost microprocessor of the “Internet of Things” (IoT) through a program which we have written (*Figure 3*).

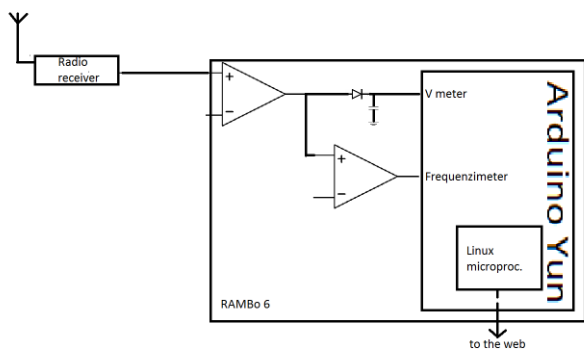


Figure 3 – Block diagram.

RAMBo 6 acts as a preamplifier for the signal coming from the radio output and then splits it into two different channels. After a further amplification, the signal is rectified and integrated. This allows Arduino to measure the received signal amplitude (Figure 4).

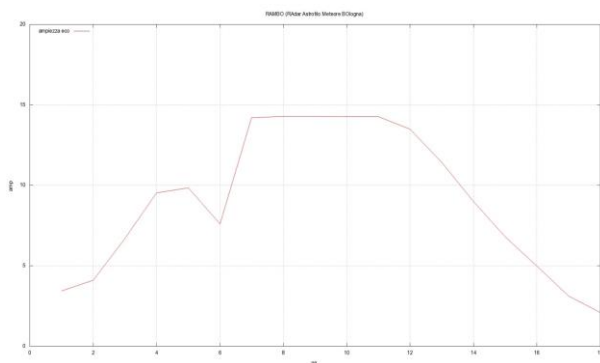


Figure 4 – An overdense meteor profile generated by “Rambo”.

In this graph we can see an overdense meteor echo analyzed by RAMBo. In Figure 5 there is another overdense meteor profile found in literature.

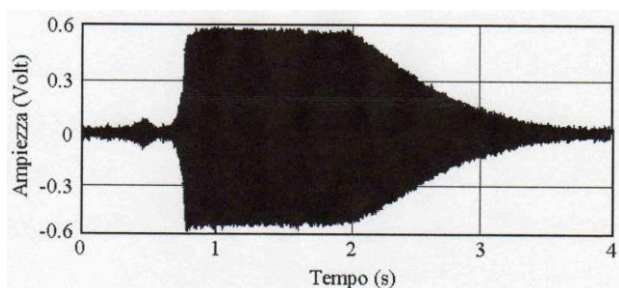


Figure 5 – An overdense meteor profile coming from a professional radar.

As can be seen, the profile is roughly the same.

At the same time, the signal is measured by using Arduino as a frequency meter. Normally, the signal of chaotic noise contains random frequencies. As soon as a meteoric echo arrives, the measured frequency tends to be confined inside a window centered about the mean frequency previously set. When this occurs, RAMBo starts counting time. At the end of this process, when the measured frequency comes back chaotic, Arduino has recorded both the echo duration (in milliseconds) and day and time of the event.

For each echo, RAMBo assigns a serial number. In addition at the zero minute of every hour, Arduino zeroes the meteor/hour count and then starts again from one.

The analysis of the rise time of the initial impulse gives us a figure that is proportional to the meteor speed coming into the atmosphere. The shorter the rise time, the faster the meteor speed, and vice versa.

## 4 The data logger

The data we now have included:

- Progressive event number;
- Hourly number;
- Date and time (UT);
- Echo length (milliseconds);
- Echo amplitude (millivolts);
- A number proportional to the rise time.

For each echo RAMBo6 creates a CSV-type (common separated values) data string containing the six listed items of information.

Every row generated by an echo is added to a log file.

Every night at 18<sup>h</sup> U.T. Arduino sends the file via internet to a cloud site, so it can be analyzed at home.

### Graphic layout

The log file is normally represented in a graphic form using math graphic software (e.g.: *gnuplot*). In this graph (Figure 6) we can see the result of a weekly recording.

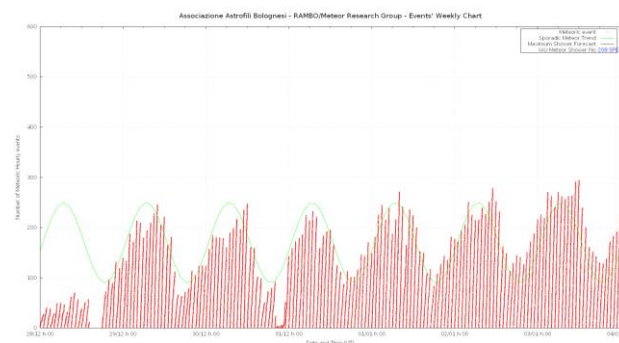


Figure 6 – A weekly “Rambo” hourly rate (HR) layout.

Each red dot represents a meteor echo; on the x-axis there is time, on the y-axis the number of events. In this manner, the height of each column represents the number of meteors per hour (hourly rate). The dot size is proportional to the echo duration logarithm.

The sinusoidal trend is clear, approximated in green, due to the diurnal variation of the apparent speed with which the Earth impacts the meteors. Day 29/12 was the first day in which Rambo6 began to run. The comparison with the previous day shows the sensitivity increase compared to the previous version (RAMBo5).

## 5 How much it costs

Here is a summary of the cost of RAMBo in Euros:

- Antenna 74;
- Cable 10;
- Connectors 5;
- Radio (2nd hand) 500;
- Sound card 40;
- Arduino Yun 68;

**Total 697**

As can be seen, a meteor scatter observatory of this kind is well within the reach of many amateur groups.

## 6 The results

Rambo 6 registers more than 2500 meteorological echoes a day, with an hourly average of about 100.

- Overdense meteors (echoes longer than 800 ms) account for about 1%, according to data in literature.
- In the days without meteor showers, we can recognize the typical sinusoidal sporadic meteor trend, with the maximum at 6 and the minimum at 18 (Local Time).
- In the case of meteor showers we can easily see the beginning time, the maximum and the end.
- We can also evaluate the shower intensity, with reference to the standard sporadic trend (Hourly Rate).

$$ZHR = \frac{\overline{HR} \cdot F \cdot r^{6.5-lm}}{\sin(hR)}$$

For this purpose we have developed a special program (in Python) for meteor shower analysis. With this program, we first subtract the average value of sporadic days immediately before and after the meteor shower containing only sporadic activity, then we adjust the hourly rate with a number proportional to the tangent of the radiant height on the horizon. We thus obtain a value very similar to the ZHR (Zenith Hourly Rate) commonly used in visual observations. An example of such processing (Figure 7) comes from the “RZHR” program, i.e. RAMBo ZHR.

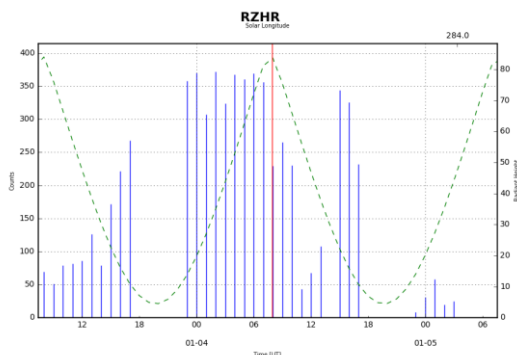


Figure 7 – An RZHR graph.

In this graph we can notice the beginning of the transit of the Earth through the Quadrantids cylinder and the Rzhr

value. We can still see that also in this case the Quadrantids have a bipolar structure, similarly to other streams (e.g. Geminids).

The dotted green line shows the radiant height on the horizon. The red line shows the moment in which the shower maximum was expected. RAMBo is thus able to indicate with great accuracy the time difference between predictions and observations.

- RAMBo also allows us to carry out a meteor mass evaluation. Since the echo duration is proportional to the meteor dimension, we can see the mass trend over time.

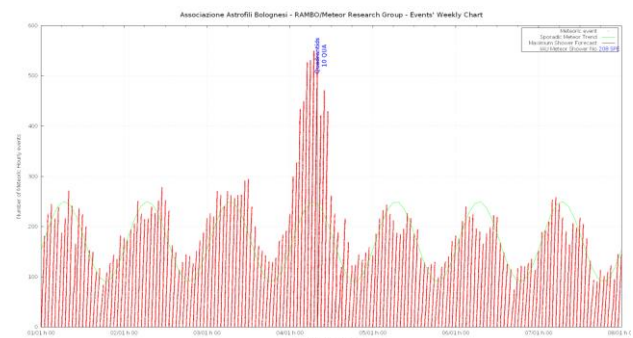


Figure 8 – The 2016 Quadrantids HR.

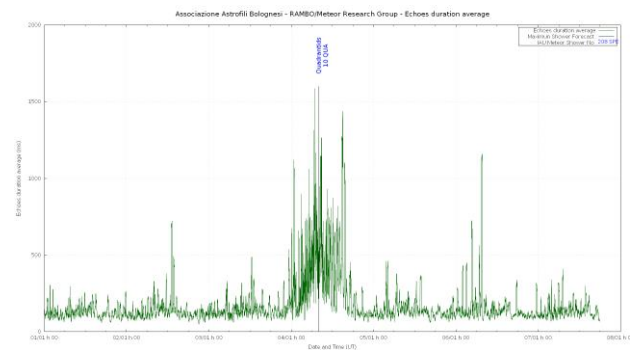


Figure 9 – The 2016 Quadrantids mass trend.

Figures 8 and 9 show the same period of time (a week). In the former we can see an activity increase in the number of echoes (hourly rate) due to the meteor shower. In the latter we note a meteor mass increase due to the echo duration average. Although the time period is the same, the two ordinate values are completely different. So the trend analogy is impressive. In the mass trend graph, the bipolar structure of the swarm is clearly visible, just as can be seen in the hourly rate graph.

## 7 Future developments

The image of the RZHR graph in the previous chapter concerning the Quadrantids swarm partially shows the shower. Most of the beginning and end of the shower is lacking. This is due to the fact that during the phenomenon the radiant was not always above the horizon.

In essence: if it is true that a meteor scatter observatory can observe night and day, with and without the Moon, in good and bad weather, it is equally true that it can

observe a meteor shower if and only if its radiant is above the horizon. It follows therefore that any observer coverage, as with any other type of observation, is partial.

Like visual or video observations, meteor radar observation should also create a global network able to achieve total coverage.

What is primarily needed is a small network of a few observers strategically placed almost  $120^\circ$  apart in the same hemisphere so as to create complete coverage for each radiant.

## 8 The “Marsadl”

### (Meteor Analyzer by Radio receiver, Sound Analyzer and Data Logger)

The RAMBo6 experience was conceived as an example of the “Internet of Things” (IoT) that simplifies the feasibility of many projects in various fields. So this leads us to propose this low-cost, simple project as an idea to set up a meteor scatter observer network. What is needed for every observer can be summarized as follows:

- 1) The existence hundreds of kilometers away of a VHF transmitter continuously *on air*, whether it is military

or television whose carrier can be tuned in amplitude modulation;

- 2) A Yagi directive antenna (from 6 to 10 elements) with a vertical polarization mount in a fairly unobstructed area, pointing in azimuth in the direction of the transmitter and with a declination pointing above the midpoint of the line between  $T_x$  and  $R_x$  at about 100 km altitude;
- 3) A receiver with good input sensitivity tuned in SSB mode 1000 Hz over the carrier (USB: Upper Side Band), with the audio output independent to the squelch and the volume potentiometer, and with automatic gain control (AGC) disabled;
- 4) An ANALOG power supply (and therefore not a switcher) able to feed all the apparatus 24 hours a day;
- 5) A network cable with web access for the data uploading.

The circuit diagram, the Arduino software and our data analysis script are available to anyone interested in this experience. The data of all those who join MARSADL will be shared, so to create a network that not only stores data but allows us all to analyze the information together.



With 157 IMC participants, the lecture room always was well filled. (Photo Casper ter Kuile).

# Accurate Geminid velocities with CHIPOIAtA

Felix Bettonvil

Sterrewacht Leiden, Universiteit Leiden, Niels Bohrweg 2, 2333 CA Leiden, the Netherlands

NOVA Optical and Infrared Instrumentation Division at ASTRON, Oude Hoogeveensedijk 4,  
7991 PD Dwingeloo, the Netherlands

KNVWS Meteor Section, the Netherlands

bettonvil@strw.leidenuniv.nl

For several years, the high-resolution photographic camera CHIPOIAtA has been used to acquire precise orbits for Geminid and Perseid meteor shower members. In this paper I analyze the first set of data obtained during the Geminids 2014.

## 1 Introduction

CHIPOIAtA (Bettonvil, 2014, 2015) is a photographic camera system that is equipped with a precise and fast chopping shutter, enabling precise measurement of the velocity of a meteor. This is the most critical parameter in the determination of its orbit, hence accurate measurement is crucial.

The camera comprises a Liquid Crystal (LC) optical chopper (Bettonvil, 2010), which periodically switches between dark and transparent state up to several hundred cycles/sec<sup>1</sup>, much faster than traditional meteor photography, and comparable with the – somewhat slower (100Hz), but more sensitive – CABERNET system as operated in the French Pyrenees area by IMCCE (Vaubailon, 2014).

High resolution orbit determination is valuable as it permits detection of fine structures in meteoroid streams and provides accurate input for meteoroid stream modelling.

This paper focuses on the reduction of obtained data, in particular the Geminids 2014. In the next Section first a brief description of the instrument setup is given.

## 2 Instrument description

CHIPOIAtA consists of two Canon 550D 18Mpxl DSLR cameras mounted on the same tripod and aligned such that one long FoV is obtained. With a relatively long focal length of 50mm a field of 18x50 deg<sup>2</sup> is formed, which is always aligned such that the long axis points to the radiant. Each camera has a built-in LC shutter, which are operated synchronously. All data is stored in jpeg format. The sensitivity is set to ISO 6400, exposure time 14s.

CHIPOIAtA is always operated in double station mode, the second station being a wider field, lower resolution system, mostly video, depending on the location of the

observations. The two stations together enable trajectory and orbit calculation.

Technical details on the instrumental setup is given in (Bettonvil, 2014, 2015).

## 3 Data

So far, 4 observing campaigns have been carried out, covering the Perseids and Geminids in 2014 and 2015. Geminids are always observed with chopper frequencies of 200Hz, Perseids -due to their higher velocity- with 300Hz. Preliminary results have already been reported earlier (Bettonvil, 2014, 2015). *Table 1* gives an overview of the collected data. So far ~66 meteors have been captured, of which ~75% were double station.

In this paper I will focus on the data of the Geminids 2014. This campaign was carried out in The Netherlands, as weather in other parts of Europe was too unstable to justify a trip elsewhere. Fortunately, the conditions in The Netherlands turned out to be rather good. Klaas Jobse (Oostkapelle), with his CAMS Benelux cameras, served as the second station (Roggemans et al., 2016).

## 4 Analysis

Depending on the brightness, trail lengths vary between ~40 and over 200 breaks, and can extend over 2500 pixels long. Bright meteors have easily measurable breaks; the weakest tend to fade out in the background noise. This noise varies from image to image and cannot be subtracted by taking dark fields.

For the analysis presented here, we focus on the three brightest captures, having (visual) brightness's of resp. +1, 0 and -2:

- December 14, 2014, 00<sup>h</sup>54<sup>m</sup>55<sup>s</sup> UT, magnitude +1
- December 13, 2014, 23<sup>h</sup>40<sup>m</sup>26<sup>s</sup> UT, magnitude 0
- December 14, 2014, 00<sup>h</sup>22<sup>m</sup>44<sup>s</sup> UT, magnitude -2

<sup>1</sup> <http://www.lc-tec.com/optical-shutter> (LC-Tec, 2015)

Table 1 – Overview of all collected data so far during Perseid and Geminid observing campaigns in 2014 and 2015. Shown are location, optics, chopper frequencies, resolution, total number of trails captured, and double station captures. The results of CABERNET (Geminids 2015) are not known yet, and as such the number of double station captures is pending.

Shower	Location	Lens	Cycl/s	Resolution	2 <sup>nd</sup> cam	# trails	# double station
Perseids 2014	Bosnia	50/F2.8	50–200 Hz	21"	none	5	none
Geminids 2014	Netherlands	2x50/F2.8	200 Hz	21"+17"	video	17	13
Perseids 2015	Croatia	2x50/F2.8	200–300 Hz	17"+17"	12M + video	13	10
Geminids 2015	France	2x50/F2.8	200 Hz	17"+17"	CABERNET*	31	?

(\*) See Vaubaillon (2014).

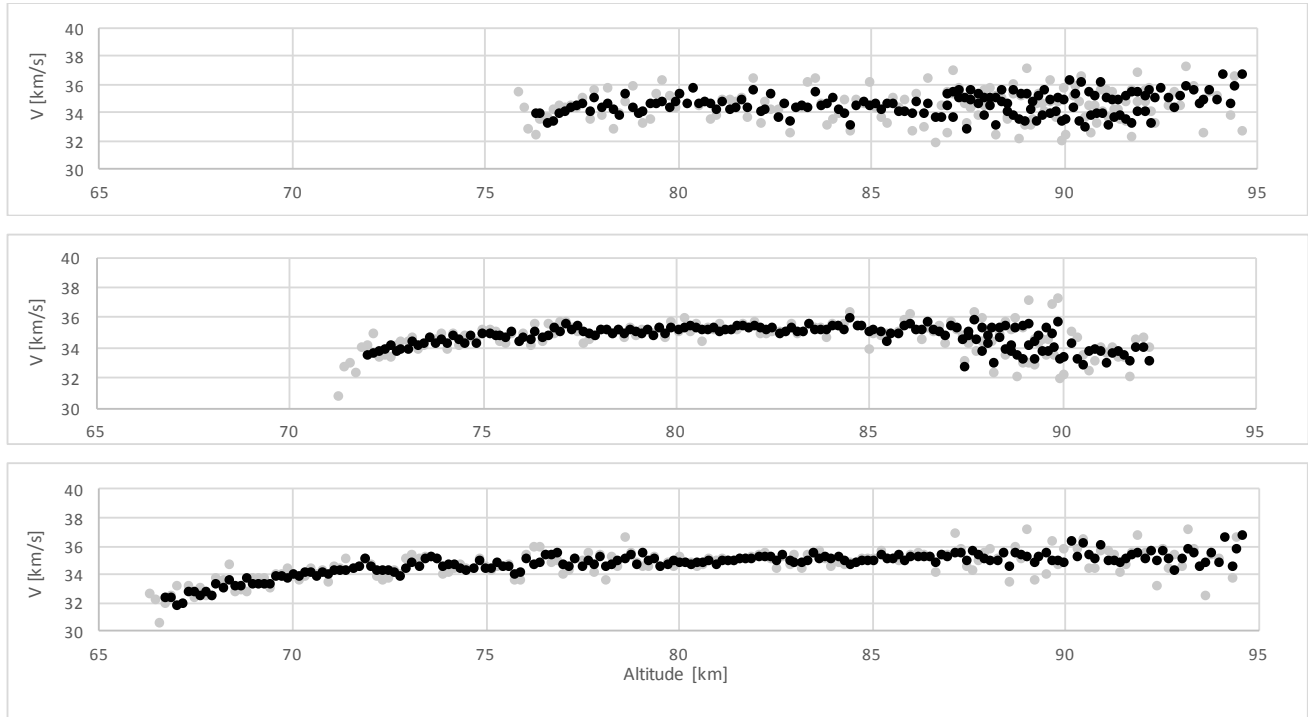


Figure 1 – Velocity profiles for all analyzed Geminids. Top: Geminid +1; Center: Geminid 0, Bottom: Geminid –2. Vertical and horizontal scale for all plots is the same. Grey dots represent a 3pt running average, black dots a 6pt running average.

The data reduction largely follows the method described in (Bettonvil, 2015). Astrometry is done with SAO Image DS9<sup>2</sup>, and both the positions of reference stars and meteor breaks measured with the help of the centroid function, which works reasonable well as both stars and meteor breaks are quasi-circular dots. The reproducibility of an individual measurement is typically in the range of 0.2 – 0.5 pxl, which depends largely on the brightness: bright dots are less affected by the background noise.

Plate reduction is carried out with own software<sup>3</sup> and, due to the lack of distortion, is straightforward. Astrometric solutions are typically precise to a couple of arc seconds.

Following the astrometry, the atmospheric trajectory is calculated, again with own software, and based on the method of intersection of planes. The line of intersection represents the meteor trajectory and finally all meteor break measurements are projected on to this line. As a

result, the length of the individual breaks in kilometers and also the velocity in km/sec become known.

## 5 Discussion

Figure 1 illustrates the measured velocity of the three analyzed Geminids. We will now look more closely at this velocity.

First of all, we can conclude that the weakest part of the trail (always the initial part) does indeed give a larger spread in velocities than the brighter parts. In addition, the +1 Geminid trail shows more variation than the brighter 0 and –2 Geminids.

The bright central parts of the 0 and –2 Geminids show stable and constant velocity.

All three meteors, but most strikingly the brightest Geminids, show a deceleration. The brighter Geminids tend, as expected, to reach lower altitudes.

From the distribution of the velocities we are able to say more about the accuracy obtained, which is illustrated in Table 2. The average velocity is computed from all data

<sup>2</sup> <http://ds9.si.edu/site/Home.html>

<sup>3</sup> Meteor35 – Software package for reduction of meteor orbits, including astrometry, atmospheric trajectory calculation and orbital elements, developed by the KNVWS Meteor Section.

in the first half of the trail (and thus the part with the evident deceleration is left out). In first order it is assumed that the velocity of this first part represents  $V_{\infty}$ . Over the entire first part the standard deviation amounts from 0.3 to 0.6 km/s per measured dot, or 1–2% of the computed velocity, which amounts to  $\sim 0.1\text{--}0.2$  pxl uncertainty per measured dot. If we assume a constant velocity, the average velocity can be determined with an accuracy better than 0.01 km/s in all cases.

Table 2 – Average apparent velocity and obtained accuracies for the three Geminids.

	+1	0	-2
Average V [km/s]	34.01	35.18	35.05
STDV [km/s]	0.63	0.32	0.41
Error avg [km/s]	0.008	0.005	0.004
Accuracy [km/s]	–	0.05	0.08

The question that then pop ups is if we are allowed to assume that the velocity in the first part is indeed constant? For this reason, the velocity in the brightest central part of the two brightest parts is analyzed a bit more closely: these parts have been split in two and for each of them the average velocity has been computed. The conclusion is clear: in both of these cases the velocity in the first part is higher than for the second half, with a difference of respectively 0.05 and 0.08 km/s for the two brightest Geminids. This allowed us to conclude that deceleration is already present in the brightest part.

## 6 Conclusions

The above results indicate that rather than averaging the first half of the trail to obtain an estimate for  $V_{\infty}$ , a fit based on a deceleration model (e.g. exponential, Gompertz or other) is required. We can conclude that the true  $V_{\infty}$  is therefore slightly higher than the average velocity computed so far until now (with an approx. amount indicated with ‘Accuracy’ in Table 2). Exact calculation of  $V_{\infty}$  is to be done and planned for the near future.

## 7 Future

Until now, Canon 550D DSLRs have been used for CHIPOIAtA. Nowadays much better cameras are available, with both higher sensitivity and lower noise, allowing for a more rapid collection of a large data sample.

## References

- Bettonvil F. (2010). “Digital All-sky cameras V: Liquid Crystal Optical Shutters”. In Andreic Z., and Kac J., editors, *Proceedings of the International Meteor Conference*, Poreč, Croatia, 24-27 September, 2009. IMO, pages 14–18.
- Bettonvil F. C. M. (2014). “High resolution photographic imaging”. In Rault J.-L. and Roggemans P., editors, *Proceedings of the International Meteor Conference*, Giron, France, 18-21 September 2014. IMO, pages 30–33.
- Bettonvil F. C. M. (2015). “High resolution orbits of Perseids and Geminids with CHIPOIAtA”. In Rault J.-L. and Roggemans P., editors, *Proceedings of the International Meteor Conference*, Mistelbach, Austria, 27-30 August 2015. IMO, pages 78–82.
- Roggemans P., Breukers M. and Johannink C. (2016). “Status of the Benelux CAMS network”. In Roggemans A. and Roggemans P., editors, *Proceedings of the International Meteor Conference*, Egmond, the Netherlands, 2-5 June 2016. Pages 254–260.
- Vaubailon J., Egal A., Clovirola A., Colas F., Bouley S., Atreya P., Reffet B. and Rudawska R. (2014). “The “CAmera for BEtter Resolution” (CABERNET): First scientific results”. In Muinonen K. et al., editors, *Proceedings Asteroids, Comets, Meteors 2014*, Helsinki, Finland, 30 June - 4 July, 2014. Page 549.

# Photographic spectra of fireballs

Jiří Borovička

Astronomical Institute of the Czech Academy of Sciences, 251 65 Ondřejov, Czech Republic

jiri.borovicka@asu.cas.cz

Two methods of spectroscopy of meteors using image intensified video cameras and classical photographic film cameras are compared. Video cameras provide large number of low resolution spectra of meteors of normal brightness, which can be used for statistical studies. Large format film cameras have been used through the history and provide high resolution spectra, which can be used to derive temperature, density and absolute abundances of various elements in the radiating plasma. The sensitivity of films is, however, low and only spectra of bright meteors (fireballs) can be studied. Examples of photographic fireball spectra are provided.

## 1 Introduction

Spectroscopy of meteors becomes increasingly popular among both amateur and professional astronomers. Nowadays, mostly low resolution video spectroscopy is being used. Meteor spectroscopy, however, has a long history in which photographic techniques using classical photographic plates and films played a major role. But photographic spectra have not only historical value. In some respects, in particular resolution, they are superior in comparison with video spectra. Classical spectrographs are still in use at the Ondřejov Observatory. In this paper I will compare both techniques and their advantages. I will also present some examples of photographic spectra. In the future, nevertheless, high resolution digital cameras will be probably fundamental for meteor spectroscopy.

## 2 Brief history of instrumental meteor spectroscopy

The first meteor spectrum was photographed by chance on June 18, 1897, during the objective prism stellar spectroscopy program performed by the Harvard College Observatory in Arequipa, Peru (Pickering, 1897a;b;c). The first systematic photographic meteor spectroscopy program was set up in Moscow (Blajko, 1907). The first spectra were obtained with objective prisms on blue sensitive emulsions. Later, panchromatic and even infrared emulsions as well as transmission diffractive gratings become available. Nevertheless, the number of obtained spectra increased only slowly and reached 122 worldwide in 1952 (Millman, 1952). The early history and the knowledge about meteor spectra around 1960 were described in Millman and McKinley (1963). At that time, large format photographic cameras with rather long focal length started to be used and detailed spectra of bright meteors containing over a hundred of emission lines were obtained (e.g. Halliday, 1961; Cepulecha, 1971; Borovička, 1993; 1994a). Of course, long term systematic observations were needed to capture a good fireball spectrum.

Later, spectra of fainter meteors were photographed by Maksutov cameras with large aperture (Harvey, 1973).

Television techniques started to be used for meteor spectroscopy as early as 1969 (Hemenway et al., 1971). Originally, it was necessary to film the TV monitor with a motion picture camera to analyze the spectra. Later it became possible to transform the video image to a hard copy. The full development of video spectroscopy started in 1990's with the advancement of computer technology. CCD spectrographs have been also occasionally used (Jenniskens, 2007).

## 3 Video spectra

An example of meteor spectrum obtained with video camera equipped with image intensifier is shown in *Figure 1*. Image intensifiers or very sensitive television cameras enable people to obtain also spectra of meteors fainter than magnitude zero. The wavelength coverage is quite wide, typically 400–900 nm, i.e. covering both visible and near infrared regions. On the other hand, the resolution of classical video signal, when digitized, is relatively low (768 x 576 pixels for PAL system). The resulting spectral resolution depends on the used lens and grating but is low in any case, typically 1 nm/pixel. The FWHM (full width at half maximum) of spectral lines in *Figure 1* is 5.8 nm, so lines spaced less than about 5.5 nm cannot be resolved.

A catalog of representative low resolution video spectra of meteors was recently published by Vojáček et al. (2015). Meteor spectra consist of a relatively faint continuum, emission atomic lines and molecular bands. Nitrogen and oxygen lines and nitrogen molecular bands are of atmospheric origin (i.e. are produced by heated atmosphere in the vicinity of the meteoroid). Atmospheric emissions are particularly prominent in fast meteors and dominate the red and infrared part of the spectrum (see *Figure 1*). To study the composition of meteoroids, meteoric lines are important. Only Mg, Na, Fe, and in some cases Ca, can be usually resolved in video spectra. Lines of  $\text{Ca}^+$ ,  $\text{Mg}^+$ ,  $\text{Si}^+$ , and H from the hot spectral component (Borovička, 1994b) are present in spectra of bright and fast meteors only.

Fortunately, the observable elements proved to be interesting and a number of meteor spectral classes could be identified by Borovička et al. (2005) when simply

plotting the Mg, Na, and Fe line intensities in a ternary diagram. This kind of analysis was repeated more recently by other authors, e.g. Madiedo (2015), Vojáček et al. (2015) or Rudawska et al. (2016). Mg represents silicates, Na the volatile part of the meteoroid, and Fe is contained in both metal and silicates (and sulfides). Ca, if observed, can be used to track the refractory part.

The advantage of video spectroscopy is its sensitivity. It can be used to study small (millimeter to centimeter) sized meteoroids, which proved to be chemically more diverse than larger bodies observed photographically. Since small meteoroids are numerous, good statistics can be obtained within reasonable period of time.

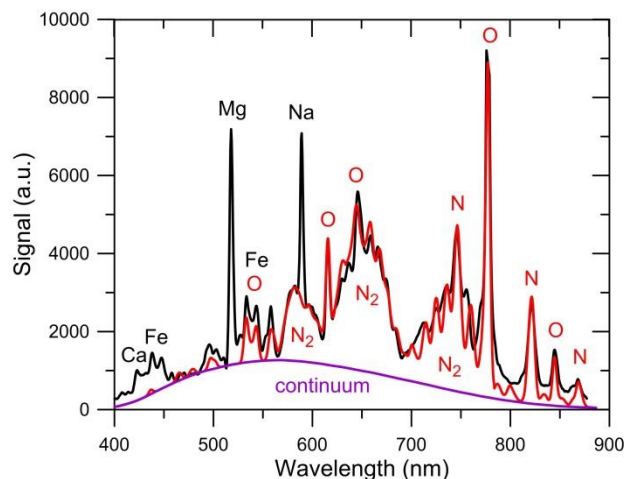


*Figure 1* – Video spectrum (SZ 1308) of a sporadic meteor of velocity 69 km/s and approximate magnitude -2 captured on November 11, 2000. Measured signal summed along the meteor path and not corrected for spectral sensitivity of the instrument is plotted as a function of wavelength (black curve). Approximate continuum level is given in violet. The estimated contribution of atmospheric emissions of N, N<sub>2</sub>, and O above the continuum level is plotted in red. Important emissions are identified; meteoric emissions in black and atmospheric emissions in red.

#### 4 Photographic spectra

Examples of two photographic spectra obtained at the Ondřejov Observatory are presented in *Figures 2 and 3*. The used spectrographs are equipped with the 4.5/360 mm Tessar lenses and blazed objective gratings with 400 and 600 grooves per mm, respectively. Whole night exposures are recorded on large format sheet film 18x24 cm (Fomapan 200 ASA) providing a field of view of 28x36°. An underpressure system is used to keep the films flat. Six spectrographs are in use in all clear moonless nights. A rotating shutter interrupts the exposure 15 times per second. The system has been used in Ondřejov since 1960 (Ceplecha and Rajchl, 1963), when it replaced older spectrographs with a smaller format, and was upgraded several times since then (e.g. prisms were replaced by gratings and glass plates, which are no longer available, were replaced by films).

The spectrum in *Figure 2* is an example of the spectrum of relatively faint (-5 mag) and slow (20 km/s) fireball. The spectrum in *Figure 3* was produced by a brighter

(-9 mag) and faster (48 km/s) fireball. Both fireballs were sporadic. The identification of 125 spectral lines in the latter spectrum was published by Mozgova et al. (2015). The resolution of the spectrum is 4.5 nm/mm. The spectrum was scanned in 14 bits by the photogrammetric scanner Ultrascan 5000 with the step of 10 μm (i.e. with resolution 2540 dpi). The typical FWHM is 0.25 nm; it is worse in the violet part of the spectrum, which is out of focus due to imperfection of the lens. On the other hand, the violet part of the second order spectrum of the Leonid spectrum S 30132 studied by Borovička (2004) was very sharp with FWHM 0.1 nm.

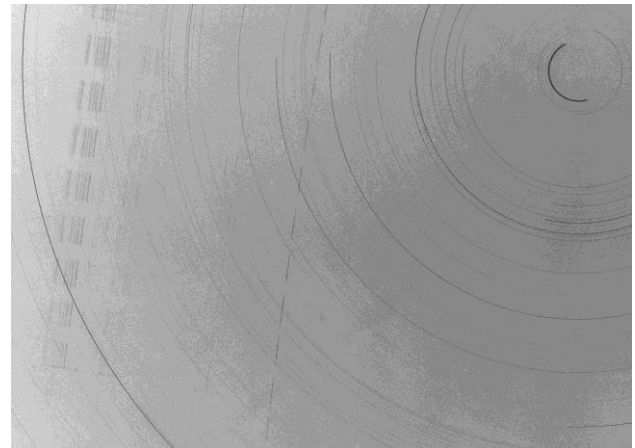


*Figure 2* – Reproduction of the photographic spectrum (plate S 38301) of a -5 magnitude sporadic fireball captured near the celestial pole on February 20, 2012. The fireball velocity was 20 km/s and maximum brightness was reached at a height of 44 km. The fireball moved from top to bottom. Wavelengths increase from left to right. The brightest line belongs to sodium.

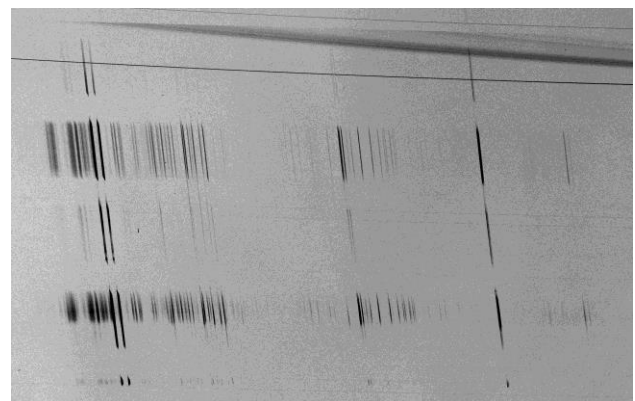


*Figure 3* – Reproduction of the first order photographic spectrum (plate S 37724) of a -9 magnitude sporadic fireball captured on August 2, 2011. The fireball velocity was 48 km/s and maximum brightness was reached at a height of 83 km. The fireball moved from top to bottom. Wavelengths increase from left to right. The brightest lines belong to ionized calcium (two lines on the left) and sodium (on the right).

A large number of spectral lines resolved in photographic spectra enable detailed analysis of the radiating region to be performed. Most spectral lines belong in almost all cases to neutral iron. Measuring intensities of a large number of Fe lines with different excitation potentials and transition probabilities makes it possible to determine plasma temperature and Fe column density (see e.g. Borovička, 2005). Lines of more elements than in video spectra can be resolved and their relative abundances can

be determined. *Figure 4* shows the magnesium triplet (seen as single line in video spectra) at 516.7–518.4 nm, numerous lines of Fe I multiplet 15 between 527–546 nm, which can be only partly resolved in video spectra, and a chromium triplet at 520.5–520.8 nm, which is usually hidden between Mg and Fe lines in video spectra. Three bright Cr lines (Cr I multiplet 1) lie at 425.4, 427.5 and 429.0 nm, respectively (*Figure 5*), but are mixed with nearby Fe lines in video spectra. The same is valid for Mn I multiplet 1 at 403.1–403.4 nm. The Ca I line at 422.7 nm is the only non-Fe line in this crowded part of the spectrum, which can be bright enough to be measured with confidence in video spectra. Very difficult is the Si I line at 390.6 nm, which is located close to Fe lines and can be resolved only in the best photographic spectra (see Borovička, 2004). It is the only silicon line in the main spectral component. There are Si II lines in the hot spectral component; this component is, nevertheless, present only in fast fireballs (Borovička, 1994b).

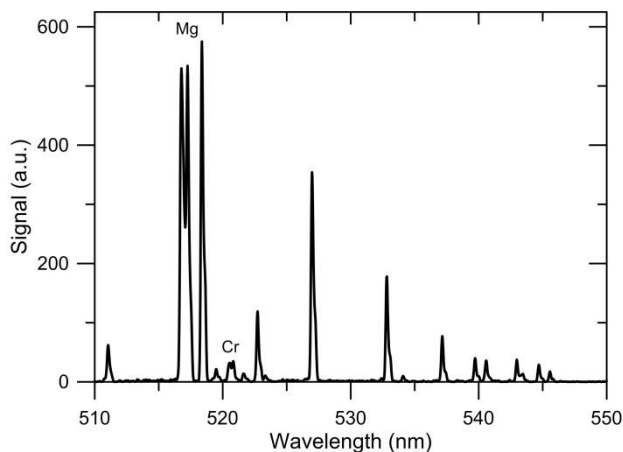


*Figure 4* – Part of the spectrum S 37724 (see *Figure 3*) at the maximum brightness containing magnesium and chromium lines. The other (non-identified) lines belong to iron.

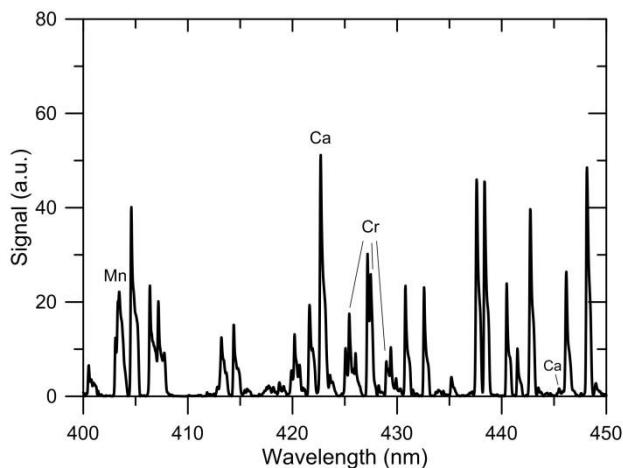


*Figure 5* – Part of the spectrum S 37724 (see *Figure 3*) at the maximum brightness containing manganese, calcium, and chromium lines. The other (non-identified) lines belong to iron.

A long term photographic program can occasionally provide unique spectra as was the case on May 7, 1991, when two spectra of the very bright Benešov superbolide were obtained in Ondřejov. The bolide had an initial velocity of 21 km/s and reached an absolute magnitude of  $-19.5$ . Four small meteorites were recovered 20 years

after the fall (Spurný et al., 2014). The meteorites were of various types, including ordinary chondrite LL3.5 with achondritic clast and H5 ordinary chondrite. The bolide spectrum was described by Borovička and Spurný (1996). *Figures 6 and 7* show part of the spectrum at the height of 57 km. Among others, lines of Ni, Ti, and Ba are present.

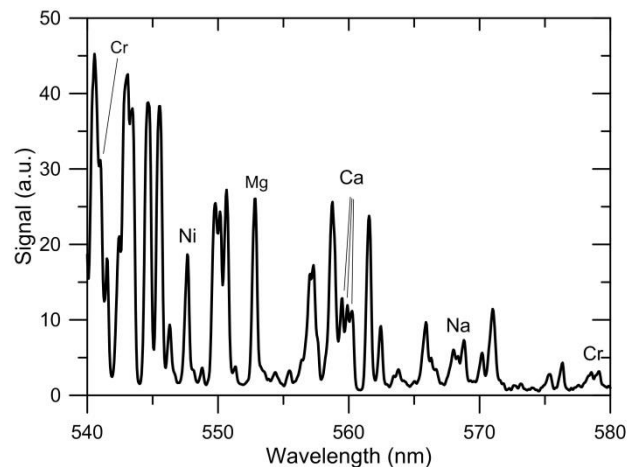


*Figure 6* – Part of the spectrum of the Benešov superbolide at a height of 57 km containing a nickel line. Some other lines are also identified; the non-identified lines belong to iron.

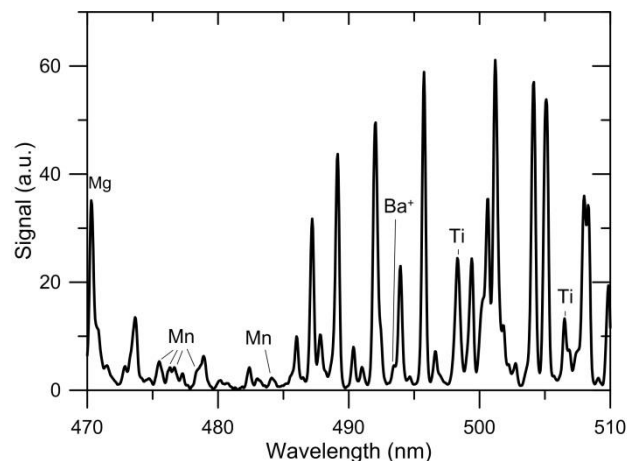


*Figure 7* – Part of the spectrum of the Benešov superbolide at a height of 57 km containing titanium lines and possibly also a line of ionized barium. Some other lines are also identified; the non-identified lines belong to iron.

High resolution photographic spectra are usually not very suited for the detection of continuous radiation and diffuse molecular bands. If the resolution is high, diffuse radiation is spread over a large area. In low resolution, on the other hand, it is concentrated into few pixels. This is the reason why the continuum and  $N_2$  bands are so prominent in video spectra. The Benešov bolide was, nevertheless, so bright that it provided the opportunity to study molecular radiation in a high resolution meteor spectrum. The beginning of the bolide clearly shows FeO radiation in the yellow and red part of the spectrum, especially in the vicinity of the sodium line (*Figure 8*). FeO can be seen in photographic spectra of slow fireballs quite regularly (see e.g. Borovička, 1994a; 2005). In Benešov, however, other oxides were also detected, namely CaO, AlO, and MgO. They are present at lower

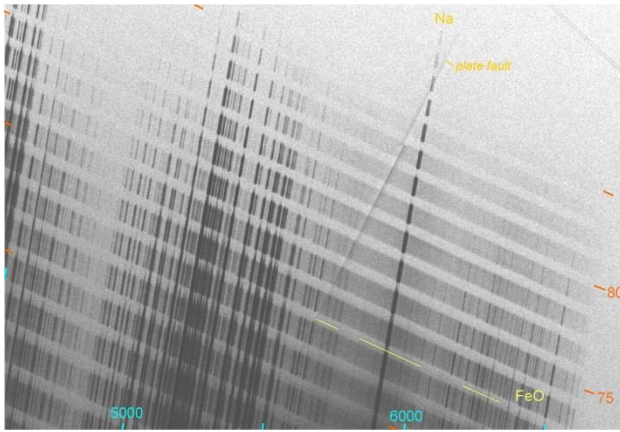


Figure 8 – Reproduction of a part of the Benešov spectrum near the beginning of the bolide. The bolide altitude in km is indicated by orange marks in the interval of 5 km. Wavelength in Å ( $1 \text{ \AA} = 0.1 \text{ nm}$ ) is indicated by cyan marks in the interval of 500 Å. Yellow lines indicate the position of three diffuse FeO bands at one particular altitude.

altitudes, especially in the wake and in the radiating cloud persisting at the position of the main flare at the height of 25 km (Borovička and Spurný, 1996). The radiating cloud spectrum is reproduced in Figure 9. In a recent paper (Borovička and Berezhnoy, 2016), we analyzed the molecular radiation in the Benešov bolide in detail, studying dependence on altitude and deriving vibrational and rotational temperatures of AlO.  $\text{N}_2$  radiation was also marginally detected as a red continuum in the bolide spectrum at heights around 50 km.  $\text{N}_2$  is a stable molecule, which can be present at temperatures around 5000 K. CN and TiO were not detected. For more details see Borovička and Berezhnoy (2016).

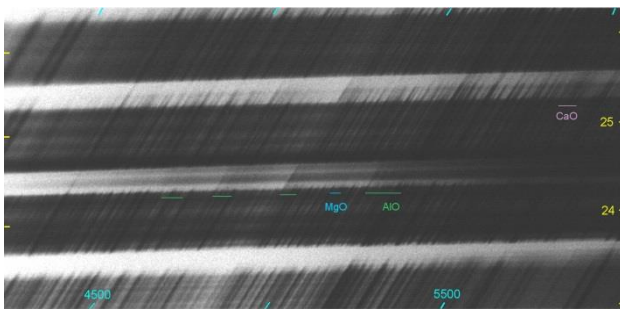


Figure 9 – Reproduction of a part of the Benešov spectrum at heights around 25 km including the radiating cloud at  $\sim 24.5$  km. The bolide altitude in km is indicated by yellow marks in the interval of 1 km. Wavelength in Å ( $1 \text{ \AA} = 0.1 \text{ nm}$ ) is indicated by cyan marks in the interval of 500 Å. The presence of the brightest molecular bands is indicated by horizontal lines: AlO in green, MgO in blue, and CaO in purple.

## 5 Conclusions

The advantage of image intensified video spectroscopy is its high sensitivity allowing to probe small (millimeter sized) meteoroids. Since video spectra are of low resolution, only few meteoric elements can be studied, namely only Mg, Na, and Fe in most cases. On the other hand, the possibility of obtaining large numbers of spectra is convenient for statistical studies. Different populations of small meteoroids with varying content of Na and Fe were revealed this way. Temporal evolution of

the spectrum can be also studied. In particular, Na sometimes behaves differently than other elements (Borovička et al., 1999).

Classical film spectroscopy has low sensitivity and only spectra of bright meteors can be obtained. Nevertheless, high resolution can be achieved and much more lines can be resolved than from video spectroscopy. Photographic spectra can be used to investigate physical conditions in the radiating plasma such as temperature and density and absolute abundances of various elements, such as Fe, Mg, Na, Ca, Cr, Mn, Al, Si, Ni or Ti (depending on the quality of the spectrum). Existing photographic archives have not been fully exploited, yet.

The advancement of digital imaging technology is, nevertheless, changing the situation described in this paper. High definition or even 4K videos provide nice spectra of resolution intermediate between analog video and film spectrographs as demonstrated at this conference by Maeda and Fujiwara (2016). The sensitivity is also intermediate between the two earlier systems. In the near future, high resolution video cameras or DSLR cameras will certainly open new chapter in the history of meteor spectroscopy.

## Acknowledgment

This work was supported by grant no. 16-00761S from GAČR and the institutional project RVO:67985815.

## References

- Blajko S. (1907). “On the spectra of two meteors”. *Astrophysical Journal*, **26**, 341–347.
- Borovička J. (1993). “A fireball spectrum analysis”. *Astronomy and Astrophysics*, **279**, 627–645.
- Borovička J. (1994a). “Line identifications in a fireball spectrum”. *Astronomy and Astrophysics Supplement Series*, **103**, 83–96.
- Borovička J. (1994b). “Two components in meteor spectra”. *Planetary and Space Science*, **42**, 145–150.
- Borovička J. (2004). “Elemental Abundances in Leonid and Perseid Meteoroids”. *Earth, Moon, and Planets*, **95**, 245–253.
- Borovička J. (2005). “Spectral Investigation of Two Asteroidal Fireballs”. *Earth, Moon, and Planets*, **97**, 279–293.
- Borovička J. and Berezhnoy A. A. (2016). “Radiation of molecules in Benešov bolide spectra”. *Icarus*, **278**, 248–265.
- Borovička J. and Spurný P. (1996). “Radiation study of two very bright terrestrial bolides and an application to the comet S-L 9 collision with Jupiter”. *Icarus*, **121**, 484–510.

- Borovička J., Stork R. and Bocek J. (1999). "First results from video spectroscopy of 1998 Leonid meteors". *Meteoritics and Planetary Science*, **34**, 987–994.
- Borovička J., Koteč P., Spurný P., Boček J. and Štork R. (2005). "A survey of meteor spectra and orbits: evidence for three populations of Na-free meteoroids". *Icarus*, **174**, 15–30.
- Ceplecha Z. (1971). "Spectral data on terminal flare and wake of double-station meteor No. 38421 (Ondřejov, April 21, 1963)". *Bulletin of the Astronomical Institutes of Czechoslovakia*, **22**, 219–304.
- Ceplecha Z. and Rajchl F. (1963). "The meteor spectrum with dispersion from 11 to 38 Å/mm". *Bulletin of the Astronomical Institutes of Czechoslovakia*, **14**, 29–48.
- Halliday I. (1961). "A Study of Spectral Line Identifications in Perseid Meteor Spectra". *Publications Dominion Observatory Ottawa*, **25**, 3–16.
- Harvey G. A. (1973). "NASA-LRC faint meteor spectra". In Hemenway C. L., Millman P. M. and Cook A. F., editors. *Evolutionary and physical properties of meteoroids*. NASA SP 319, pages 131–139.
- Hemenway C. L., Swider A. and Bowman C. (1971). "Meteor spectroscopy using an image orthicon". *Canadian Journal of Physics*, **49**, 1361–1364.
- Jenniskens P. (2007). "Quantitative meteor spectroscopy: Elemental abundances". *Advances in Space Research*, **39**, 491–512.
- Madiedo J. M. (2015). "The rho-Geminid meteoroid stream: orbits, spectroscopic data and implications for its parent body". *Monthly Notices of the Royal Astronomical Society*, **448**, 2135–2140.
- Maeda K. and Fujiwara Y. (2016). "Meteor spectra using high definition video camera in 2015". In Roggemans A. and Roggemans P., editors, *Proceedings of the International Meteor Conference*, Egmond, the Netherlands, 2-5 June 2016. Pages 167–170.
- Millman P. M. (1952). "Meteor news (Photographic meteor spectra)". *Journal of the Royal Astronomical Society of Canada*, **46**, 121–124.
- Millman P. M. and McKinley D. W. R. (1963). "Meteors". In Kuiper G. P. and Middlehursts B., editors. *The Moon Meteorites and Comets*. The University of Chicago Press, pages 674–773.
- Mozgova A. M., Borovička J., Spurný P. and Churyumov K. I. (2015). "Identification of emission lines in a meteor spectrum obtained on August 2, 2011". *Odessa Astronomical Publications*, **28**, 289–291.
- Pickering E. C. (1897a). "Spectrum of a meteor". *Harvard College Observatory Circulars*, No. 20, 1–2.
- Pickering E. C. (1897b). "Spectrum of a meteor". *Astronomische Nachrichten*, **145**, 77–78.
- Pickering E. C. (1897c). "Spectrum of a meteor". *Nature*, **57**, 101.
- Rudawska R., Tóth J., Kalmančok D., Zigo P. and Matlovič P. (2016). "Meteor spectra from AMOS video system". *Planetary and Space Science*, **123**, 25–32.
- Spurný P., Haloda J., Borovička J., Štrbený L. and Halodová P. (2014). "Reanalysis of the Benešov bolide and recovery of inhomogeneous breccia meteorites – old mystery revealed after 20 years". *Astronomy and Astrophysics*, **570**, A39.
- Vojáček V., Borovička J., Koteč P., Spurný P. and Štork R. (2015). "Catalogue of representative meteor spectra". *Astronomy and Astrophysics*, **580**, A67.

# The 2016 Quadrantids

Brando Gaetano

RAMBO/Meteor Research Group - Associazione Astrofili Bolognesi (AAB) – Bologna, Italy

brandogae@gmail.com

A report is presented on the observation of the Quadrantid shower recorded by RAMBO early January 2016. The data analysis – done by calculating the RZHR (Radar ZHR) – shows the complexity of the shower, in which the presence of multiple filaments is verified. A meteoroids mass profile is also made. Finally a comparison is made between the RAMBO radar data and the IMO visual data.

## 1 Introduction

The Quadrantid shower (10 QUA in the IAU Meteor Data Center<sup>1</sup>) is probably one of the greatest of all meteor showers that crosses the Earth's orbit each year, generating a visible increase in the number of “shooting stars” (Weiland, 2012). Its fame is lower than that for other meteor streams because of the adverse weather conditions of the first nights of the year. For this reason, radar observations take a greater importance since the radio systems are free from visibility conditions.

## 2 Quadrantids meteor shower

The shower duration is generally short - between 8.5 and 12 hours (Shelton, 1965; Hughes and Taylor, 1977; Baggaley, 1979) – and this is probably due to its very recent origin: the first sighting seems to have been around 1835. Only in 1862 there is a first document that mentions “shooting stars of January”. In 1864 Alexander Herschel identifies the radiant point near the star  $\epsilon$  Quadrantis Muralis (coordinates  $\alpha = 230^\circ$ ,  $\delta = +49^\circ$ ): the name “Quadrantids” comes from this. Since 1929, following the redefinition of the system of constellations accomplished by the International Astronomical Union, the constellation was abolished and now the radiant lies in Boötes. Some astronomers call this shower the “Bootids” (Jenniskens, 2006).

A lot has been done to find its parent body. Since 2003, the year of the discovery of the asteroid 2003 EH<sub>1</sub>, numerical simulations tend to discard a cometary origin and now it is assumed that this stream of debris may indeed have been generated by that asteroid (Porubcan and Kornos, 2005). Until now astronomers are not sure that this parent body is actually a “classically understood” asteroid or instead it is the core of an extinct comet, the C/1490 Y<sub>1</sub>.

The orbit of the Quadrantids is much tilted ( $I > 70^\circ$ ). The particles' velocity relative to the Earth (41 Km/h) is a medium value in the meteor velocity range. Different filaments were detected within this stream (Jenniskens, 2006).

## 3 The 2016 observation

For 2016 the forecast<sup>2</sup> of its peak was January, 4 at 8<sup>h</sup> 00<sup>m</sup> ( $\lambda_\odot = 283^\circ.18$ ).

The observations of the Quadrantids performed by RAMBO (Radar Astrofilo Meteorico Bolognese) - built by the Meteor Research Group<sup>3</sup> of Associazione Astrofili Bolognesi<sup>4</sup> show that the phenomenon started when the radiant is decreasing in the afternoon of January 3 (*Figure 1*). It drops to below  $10^\circ$  of altitude for six hours and then starts to rise in elevation, at about 23<sup>h</sup> UT, when the phenomenon is already in full swing. At about 6<sup>h</sup> UT on January 4, it gets at its maximum before decreasing again.

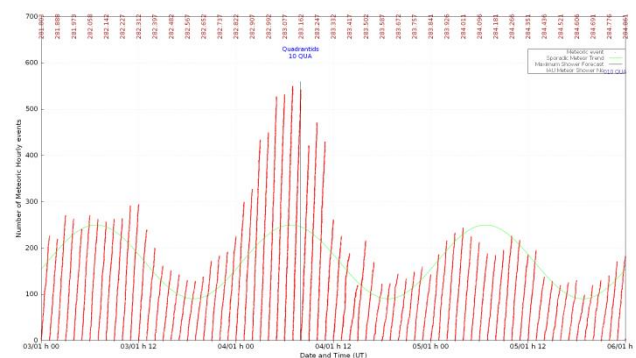


Figure 1 – 2016 Quadrantids Hourly Rate: green line represent the sporadic meteors trend.

The radiant culminates at 8<sup>h</sup> UT. Its descending elevation did not allow us to record two peaks at 9<sup>h</sup> UT and 15<sup>h</sup> UT on January 4.

## 4 Data analysis

The data analysis shows the presence of at least three filaments, two very close and one spaced of about 8 hours from the first peak.

The statistical analysis and the calculation (McKinley, 1961; Sandri, 2003) of the RZHR (*Figure 2*) – performed with RZHR3, a software program written in Python

<sup>2</sup> Data taken from the *IMO 2016 Shower Calendar*, pages 4-5.

<sup>3</sup> The RAMBO/Meteor Research Group has an email address ([rambometeorgroup@gmail.com](mailto:rambometeorgroup@gmail.com)) and a web site (<http://www.ramboms.com>) - in Italian and in English - where all the data and publication are collected.

<sup>4</sup> AAB web site: <http://www.associazioneastrofilibolognesi.com>

<sup>1</sup> IAU MDC, <http://www.ta3.sk/IAUC22DB/MDC2007/>

version 3 by the author (*Figure 7*) – highlights more effectively the hourly rate trend corrected for the height of the radiant point and for the sporadic meteors contribution.

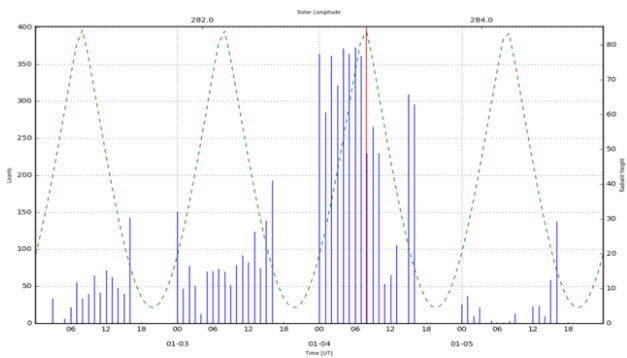


Figure 2 – Radar ZHR (RZHR): blue lines are RZHR values, the red line is the forecasted peak and the green dotted line is the radiant point position.

In addition to the hourly rate, the evidence of the stream’s complexity is illustrated by the meteoroids mass profile. *Figure 3* shows the trend of the meteor echoes duration. As the echo duration is proportional to the meteoroid mass, I can obtain an indication on the mass variation during the meteoric shower. Although the data are not related, I can see that this trend is perfectly comparable with the hourly rate profile.

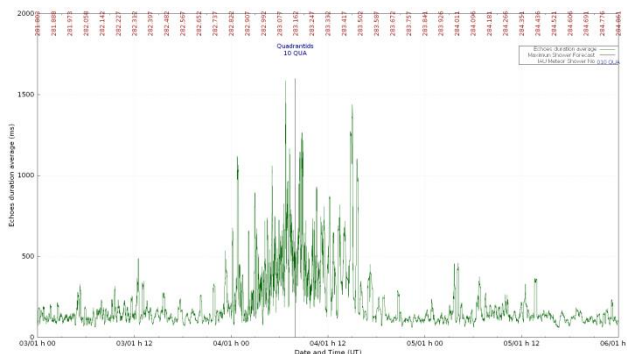


Figure 3 – Meteoroids mass variation in the echoes analysis.

I can say that the 2016 Quadrantids shower recorded by RAMBO has seen a succession of three peaks: two very close at solar longitude of 283.12 (6<sup>h</sup> 58<sup>m</sup> UT) and 283.19 (8<sup>h</sup> 37<sup>m</sup> UT) and a third at 283.45 (14<sup>h</sup> 44<sup>m</sup> UT).

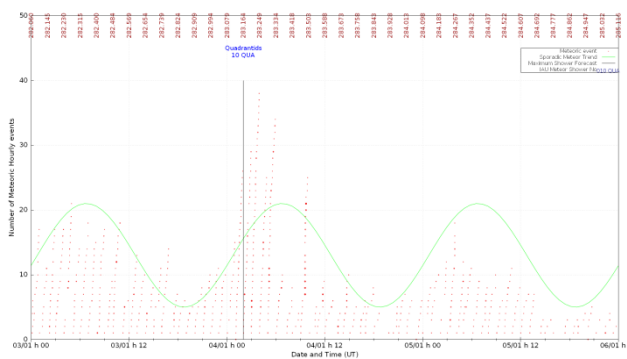


Figure 4 – 2015 Quadrantids Hourly Rate.

## 5 Data comparison

### RAMBO data

The 2015 RAMBO registration (*Figure 4*), accomplished with a less reliable version, and the RZHR calculation (*Figure 5*) shows a trend similar to those of 2016: a maximum composed of two closely spaced peaks and an extra peak about 8 hours later.

### IMO data

It may be interesting to compare RAMBO radar data with the IMO visual data.

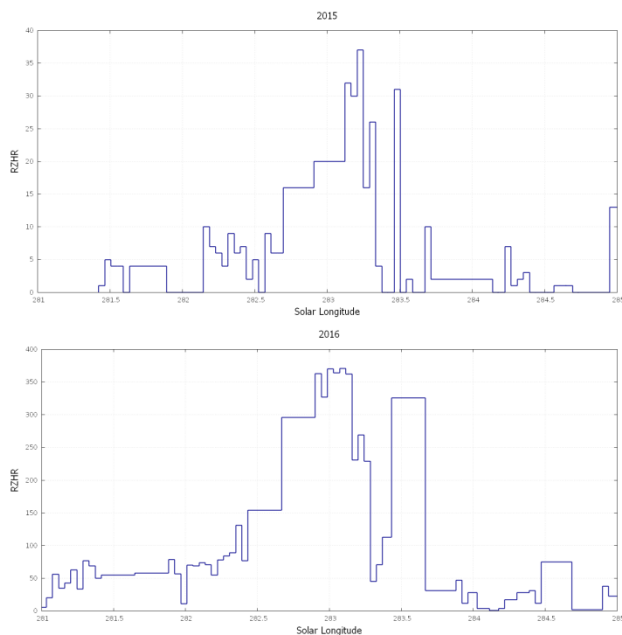
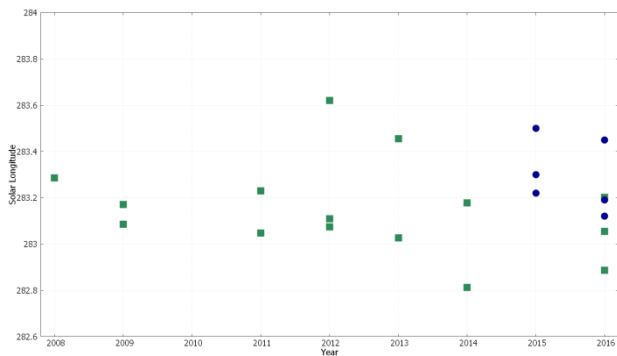


Figure 5 – 2015 (top) and 2016 (bottom) RZHR comparison.

Table 1 – Peaks of the Quadrantids from visual and radar observations.

Year	$\lambda_{\odot}$ peak	Source
2008	283.28	IMO
2009	283.08	IMO
	283.17	IMO
2011	283.23	IMO
	283.45	IMO
2012	283.07	IMO
	283.11	IMO
	283.62	IMO
2013	283.45	IMO
	283.62	IMO
2014	283.18	IMO
	283.18	IMO
2015	283.22	RAMBO
	283.30	RAMBO
	283.50	RAMBO
2016	282.88	IMO
	283.05	IMO
	283.20	IMO
	283.12	RAMBO
	283.19	RAMBO
	283.45	RAMBO

In *Table 1*, I summarize the solar longitude of the peaks observed by IMO<sup>5</sup> and by RAMBO. *Figure 6* is a graphical representation of *Table 1*. It is clear that the radio data displays the same time pattern.



*Figure 6* – Solar longitudes of the Quadrantids’ peaks in 2008–2016 from visual observations (IMO, green squares) and 2015–2016 RAMBO data (blue dots).

### 6 Future development

Looking at the IMO data represented in *Figure 6*, It looks as if a few years are not present. This may be due to unfavorable night weather conditions (widespread cloud cover, rain, snow, etc.) or the presence of light disturbances (the Moon in its various phases, light pollution). These are the limits of visual observation. On the other hand, the strength of visual observations is the possibility of observing the phenomenon on a global level.

Radar observations do not suffer from weather conditions or the presence of light pollution and they can be made throughout the day, but they need a well-built and calibrated system of registration and a subsequent statistical analysis to eliminate the part of sporadic meteors.

This is RAMBO: a system built and well calibrated that works seven days a week, twenty-four hours a day. For the moment it is limited to a single observing station (the seat of our association in Bologna) and the necessity to have the radiant point above the horizon.

These problems can be overcome if, as in visual observing, a global radio network is created. As research group, we hope for the future that other similar setups could be installed all around the world, in order to achieve a global coverage.

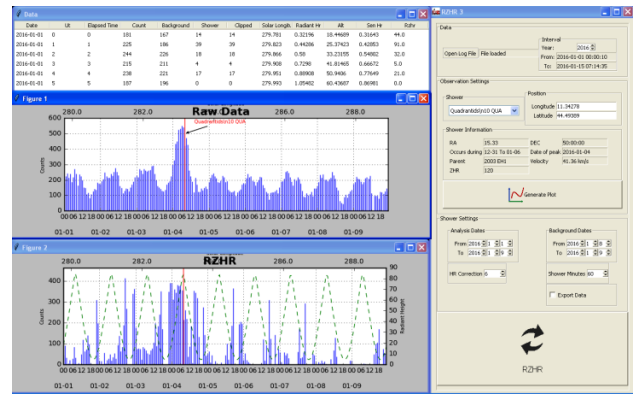


*Figure 7* – RZHR3 screenshot.

### References

Baggaley W. J. (1979). “The interpretation of overdense radio meteor echo duration characteristics”. *Bulletin of Astronomical Institutes of Czechoslovakia*, **30**, 184–189.

Hughes D. W. and Taylor I. W. (1977). “Observations of overdense Quadrantids radio meteors and the variation of the position of stream maxima with meteor magnitude”. *Monthly Notices of the Royal Astronomical Society*, **181**, 517–526.

Jenniskens P. (2006). “Meteor Showers and their Parent Comets”. *Cambridge University Press*, pages 357–376.

McKinley Q. W. R. (1961). “Meteor Science and Engineering”. *McGraw-Hill Book Company*.

Porubcan V. and Kornos L. (2005). “The Quadrantids meteor stream and 2003 EH1 V”. *Contributions Astronomical Observatory Skalnaté Pleso*, **35**, 5–16.

Sandri M. (2003). “Analisi di sciami meteorici di origine cometaria attraverso tecniche radar e visuali”. *Master Degree at Università di Padova. (In Italian)*.

Shelton J. W. (1965). “Photographic Quadrantid meteors”. *The Astronomical Journal*, **70**, 337–345.

Weiland T. (2012). “A rare opportunity: Observing the 2011 Quadrantid maximum from Austria”. *WGN, Journal of the IMO*, **40**, 171–175.

<sup>5</sup> IMO – ZHR Live Graphs, <http://www.imo.net/zhr>

# Recent shower outbursts detected by the Canadian Meteor Orbit Radar (CMOR)

Peter Brown

Dept. of Physics and Astronomy, University of Western Ontario, London, Ontario, N6A 3K7, Canada  
pbrown@uwo.ca

We present recent detections of short-duration shower outbursts as measured by the Canadian Meteor Orbit Radar (CMOR) between 2013–2016. In this interval, CMOR detected two strong shower outbursts unlinked to known showers. These included an outburst of the Kappa Cancrids (KCA – IAU 793) on January 5, 2015 and from the Gamma Lyrids (GLY – IAU 794) on February 7, 2015. Both have an orbit consistent with a Halley-type comet (HTC) or nearly isotropic-comet. Analysis of GLY activity also revealed a previously unreported annual shower, the September Ursae Majorids, (SUR – IAU 795).

## 1 Introduction

The Canadian Meteor Orbit Radar (CMOR) is a 12 kW multi-static backscatter radar operating at 29.85 MHz. Details of the system and operations are given in Jones et al. (2005) and Brown et al. (2008; 2010).

CMOR measures approximately 5000 meteoroid orbits per day. Through an automated data acquisition and analysis pipeline, all meteor echo trajectories and radiants are computed and then searched for “clumpiness” in sun-centered radiant space ( $\lambda - \lambda_0, \beta, V_g$ ) using a 3D wavelet transform to isolate probable meteor showers. The data reduction analysis procedure is described in detail in Brown et al. (2008) and Brown et al. (2010). An update to the wavelet shower detection process has been described in Pokorný et al. (2016) and this procedure is what is used in the following analysis.

## 2 CMOR outburst survey

As part of normal wavelet processing, CMOR regularly detects and identifies ~150 annual meteor showers which can be linked to those appearing in the IAU Meteor Data Center catalogue. To assess significance of shower activity in any one degree of solar longitude at any given radiant location, individual wavelet coefficients are computed and an annual time series is generated. The resulting activity-time profile provides a metric for the overdensity of radiants over any given year per day at the chosen radiant location.

*Figure 1* shows an example of this process. The xsig value (y-axis) is the number of standard deviations the wavelet coefficient in any one solar longitude bin is above the median value for the entire year. It is a proxy for relative activity. Note that for *Figure 1* all data gathered by CMOR from 2002–2016 have been stacked into a virtual year to improve signal-to-noise for annual showers.

From earlier work (Brown et al., 2010) it was found empirically that xsig values for CMOR above 3 are the minimum needed to reasonably identify “local maxima”

which may be part of true showers. In general, the majority of such weak “clumps” are still false-positives, but a string of similar radiant locations spread over time are likely to be part of a shower. As the xsig value grows, the probable existence of a shower becomes greater.

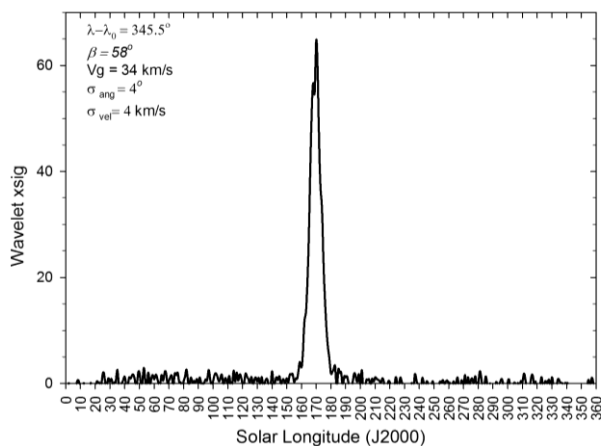


*Figure 1* – The relative strength of the wavelet coefficient in units of standard deviations above the median background throughout the year from CMOR measurements. The sun-centered radiant location and probe sizes (angular radiant and speed) are shown in the inset.

In the example of *Figure 1* it can be seen that the xsig value is in excess of 60. This is an indication of a strong shower. *Figure 2* shows a plot of all radiants measured by CMOR for  $\lambda = 171^\circ$  (the location of maximum in *Figure 1*) over all years (38720 radiants) in sun-centered coordinates. Each radiant is represented as a blue circle  $1^\circ$  in radius, a median estimate of individual radiant measurement uncertainty. Regions of higher radiant density (radiants  $\text{deg}^{-2}$ ) are shown in redder/yellow colors.

To locate meteor shower outbursts (short-lived – typically much less than a day in duration showers) we examined all CMOR wavelet maxima for each year from 2013–2016. Our search was designed to find wavelet radiant maxima not linked to any showers in the IAU catalogue. We required the xsig values to be larger than 10 and the activity to occur in no more than two solar longitude bins.

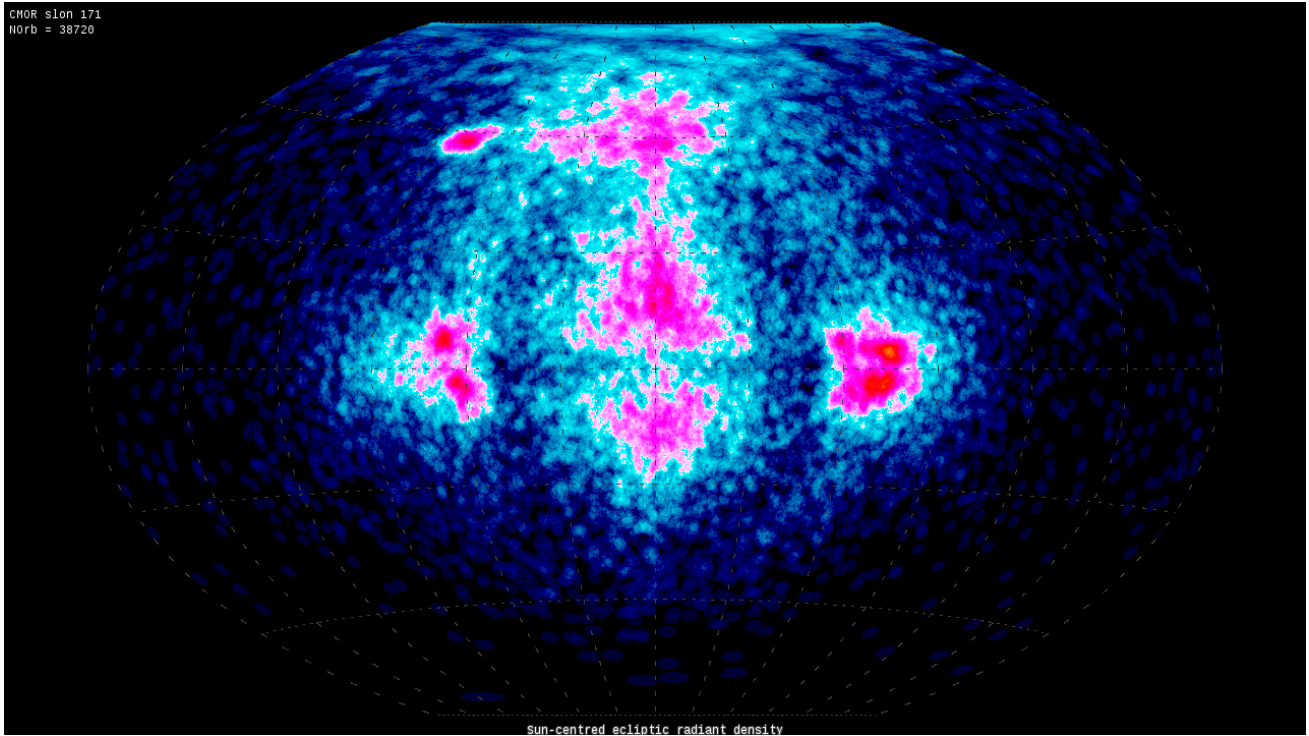


Figure 2 – The distribution of radiants measured by CMOR at  $\lambda=171^\circ$  for data stacked from all years between 2002–2015 in sun-centred ecliptic coordinates. The thick red arrow points to the radiant location corresponding to Figure 1.

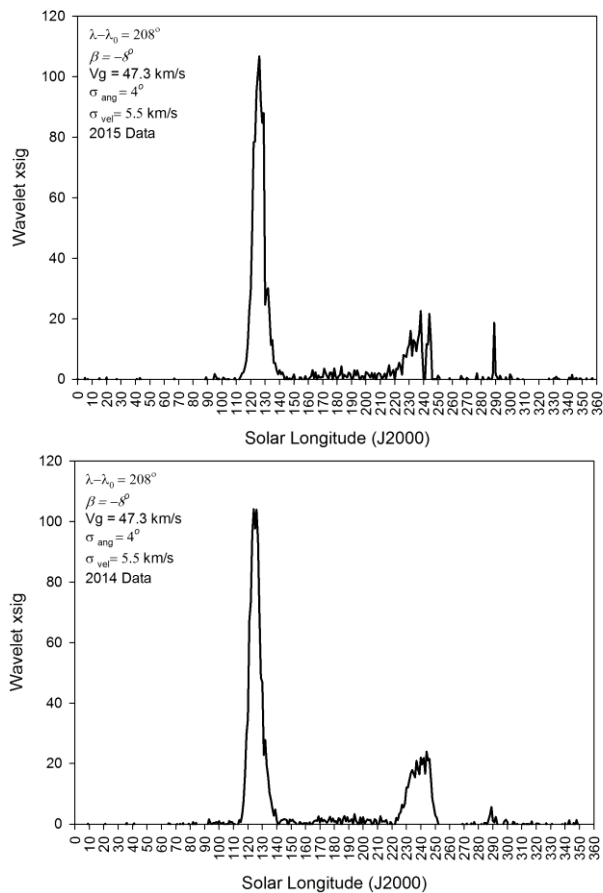


Figure 3 – The xsig value of the wavelet coefficient at the radiant coordinates shown in the figure insets for 2014 (bottom) and 2015 (top). The first peak near  $\lambda=125^\circ$  is the South Delta Aquariid (SDA) shower, while the broader activity near  $\lambda=240^\circ$  is from the November Omega Orionids (NOO). The KCA outburst is apparent at  $\lambda=289^\circ$  in 2015. Weak annual activity from the KCA is also visible in some earlier years (such as 2014), but at much lower levels than detected by CMOR in 2015.

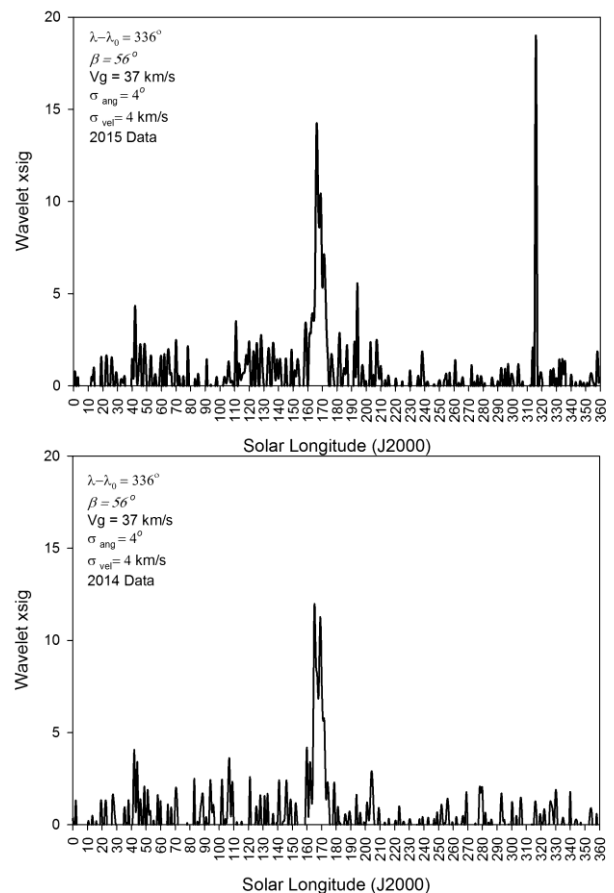


Figure 4 – The xsig value of the wavelet coefficient at the radiant coordinates shown in the figure insets for 2014 (bottom) and 2015 (top). The peak near  $\lambda=171^\circ$  is the newly recognized annual September Ursae Majorids (SUR), found during the outburst search and isolated more completely in Figure 1. The GLY outburst is apparent at  $\lambda=316^\circ$  in 2015 with an xsig of 19. No earlier evidence for this shower is visible in any year from 2002–2014 in CMOR data.

*Table 1* – Sun-centred radiant locations, geocentric speeds and orbital elements for the Kappa Cancrid outburst (Jan 9–10, 2015) and the Gamma Lyrid outburst (February 5, 2015). The number of individual CMOR orbits associated with each outburst ( $N_{\text{orb}}$ ) is also shown. All angular coordinates are J2000.0.

$\lambda-\lambda_0$	$\beta$	$V_g$ (km/s)	a (AU)	e	q (AU)	Q (AU)	i	$\omega$	$\Omega$	$N_{\text{orb}}$	Shr
208	-8	47.3	$\infty$	1.00	0.055	$\infty$	35	152.6	109.5	40	KCA
336.2	56	37	100	0.992	0.78	3000	54.6	125.7	316.5	32	GLY

*Table 2* – Sun-centred radiant locations, geocentric speeds and orbital elements for the annual September Ursae Majorid (SUR) shower. The number of individual CMOR orbits detected during all of 2002–2015 associated with the shower ( $N_{\text{orb}}$ ) is also shown. All angular coordinates are J2000.0.

$\lambda-\lambda_0$	$\beta$	$V_g$ (km/s)	a (AU)	e	q (AU)	Q (AU)	i	$\omega$	$\Omega$	$N_{\text{orb}}$	Shr
345.3	58	34	21	0.961	0.84	42	48.6	131.3	170.5	9096	SUR

### 3 Results and discussion

Using these criteria we found two outbursts over the three year survey period. Note that CMOR detected enhanced activity and/or other shower outbursts during this time (for example outburst activity from the STAs in 2015, the KCG in 2014 (Moorhead et al., 2015) and the ETA in 2013). However, all were associated with known showers and lasted more than 2 days in duration so are not included in the results from this survey.

*Table 1* summarizes radiant and mean stream orbits for these two outbursts. We do not show uncertainties in these values as the error in mean speed and radiant location for isolated single-day wavelet maxima are difficult to establish, as the wavelet transform is a non-local measure. Isolating individual orbits for each outburst we can approximately estimate uncertainties. We find a standard deviation of 1.6 km/s in speed and  $1.3^\circ$  in radiant spread for the KCA from a sample of 40 individually measured orbits. Similarly, we find an uncertainty in  $V_g$  of 2 km/s and  $2.7^\circ$  spread for the much broader shower radiant of the GLY outburst among 32 measured orbits. The corresponding xsig profiles for 2015 (and 2014 for comparison) are given in *Figures 3 and 4* respectively.

The associated orbits are typical of Halley-type comets and/ or nearly isotropic comets (NICs). However, a search of existing comet and NEOs did not find any object with a similar orbit (D-criteria  $< 0.1$ ). Hence these two outbursts may be indications of as yet-undiscovered HTC/NICs or that the original parents have disintegrated entirely.

In examining the GLY wavelet time series, an earlier recurring shower of  $\sim 2$  weeks duration peaking near  $\lambda=171^\circ$  was serendipitously detected. Manual examination of the IAU shower catalogue showed no reported shower with these characteristics, despite the strong activity in CMOR measurements. Closer examination of the CMOR shower wavelet pipeline showed that this was one of only a handful of annual

showers detected by CMOR but as yet not reported in the IAU catalogue (and not detected in the earlier CMOR surveys by Brown et al. (2010)). The associated wavelet time series and radiant plot were previously shown in *Figure 1 and 2*.

Details of the new shower (the September Ursae Majorids - SUR) are summarized in *Table 2*. As with the previously discussed two outburst showers, the SUR has an HTC/NIC-like orbit and no obvious parent. This is a common feature for showers located near the North Toroidal sporadic source (Pokorny et al., 2014). However, the SUR shows similarly strong activity each year, a long duration and broad, diffuse radiant, all indications of an old (many ka) stream.

### 4 Conclusions

Using CMOR orbital data gathered between 2013–2016 we performed a dedicated search for unlinked, brief ( $< 2$  day) shower outbursts. Our survey found two outburst showers. The first, occurring on January 9–10, 2015 (with radiant in Cancer) is now called the Kappa Cancrids (KCA). The second on February 5, 2015 (with a radiant in Lyra) is the Gamma Lyrids (GLY). Each outburst has an HTC/NIC-like orbit. Both outbursts consisted of several dozen measured radiants in regions of the sky with relatively low radiant density. The resulting wavelet excursions of the showers were more than  $10\sigma$  above the median background wavelet level at the same radiant locations recorded over the previous year.

As part of the GLY detection, an annual shower, the September Ursae Majorids (SUR), was also recognized in CMOR data with activity extending back to as early as 2002.

None of the streams has a known parent body. This demonstrates the utility of meteoroid streams for tracing either unknown or recently disintegrated HTC/NIC comets with nodes near the Earth.

## Acknowledgment

Funding for operation of CMOR is provided by the NASA Meteoroid Environment Office (MEO) through NASA co-operative agreement NNX15AC95A.

## References

- Brown P. G., Weryk R. J., Wong D. and Jones J. (2008). “A meteoroid stream survey using the Canadian Meteor Orbit Radar I. Methodology and radiant catalogue”. *Icarus*, **195**, 317–339.
- Brown P. G., Wong D. K., Weryk R. J. and Wiegert P. (2010). “A meteoroid stream survey using the Canadian Meteor Orbit Radar II: Identification of minor showers using a 3D wavelet transform”. *Icarus*, **207**, 66–81.
- Jones J., Brown P. G., Ellis K. J., Webster A., Campbell-Brown M. D., Krzemenski Z. and Weryk R. J. (2005). “The Canadian Meteor Orbit Radar: system overview and preliminary results”. *Planetary and Space Science*, **53**, 413–421.
- Moorhead A. V., Brown P. G., Spurný P., Cooke W. J. and Shrbený L. (2015). “The 2014 Kcg Meteor Outburst: Clues to a Parent Body”. *The Astronomical Journal*, **150**, id. 122, 13 pp.
- Pokorný P., Vokrouhlický D., Nesvorný D., Campbell-Brown M. D. and Brown P. G. (2014). “Dynamical Model for the Toroidal Sporadic Meteors”. *The Astrophysical Journal*, **789**, id. 25, 20 pp.
- Pokorný P., Janches D., Brown P. G. and Hormaechea J. L. (2016). “An Orbit Meteoroid Stream Survey using the Southern Argentina Agile Meteor Radar (SAAMER) based on a wavelet approach”. To be submitted.



Peter Brown: a real ambassador for the small bodies in our solar system (Photo Eva Bojurova).

# The Radio Meteor Zoo: a citizen science project

Stijn Calders<sup>1</sup>, Cis Verbeeck<sup>2</sup>, Hervé Lamy<sup>1</sup> and Antonio Martínez Picar<sup>2</sup>

<sup>1</sup>Royal Belgian Institute for Space Aeronomy

Stijn.Calders@aeronomy.be

<sup>2</sup>Royal Observatory of Belgium

Scientists from the BRAMS radio meteor network have started a citizen science project called Radio Meteor Zoo in collaboration with Zooniverse in order to identify meteor reflections in BRAMS spectrograms. First, a small-scale version of the Radio Meteor Zoo was carried out with a sample of meteor identifications in 12 spectrograms by 35 volunteers. Results are presented here and allowed us to define a method that reliably detects meteor reflections based on the identifications by the volunteers. It turns out that, if each spectrogram is inspected by 10 volunteers, hit and false detection percentages of 95% respectively 6% are expected. The Radio Meteor Zoo is online at <https://www.zooniverse.org/projects/zooniverse/radio-meteor-zoo>. Citizen scientists are kindly invited to inspect spectrograms.

## 1 Introduction

The BRAMS (Belgian RADio Meteor Stations) network consists of ~30 receiving stations spread all over the Belgian territory and a single radio transmitter installed at the Geophysical Centre of the Royal Meteorological Institute (RMI) in Dourbes (Calders et al., 2014; Lamy et al., 2015). This radio transmitter emits a sine wave with circular polarization at a frequency of 49.97 MHz and with a constant power of 150 W. At each receiving station, the signal is sampled with a frequency of 5512 Hz, providing a bandwidth of ~2.5 kHz. Data are saved as WAV (sound) files every 5 minutes. BRAMS data are usually presented as spectrograms, which provide the frequency content of the signal as a function of time. Spectrograms are built from raw data using the FFT on 16384 samples and with an overlap of 90%. Only 200 Hz of the whole bandwidth, centered on the direct signal of the transmitter, are usually shown as the majority of the meteor echoes appear there. Spectrograms are very useful because the spectral signatures of meteor echoes are very different from those due to “spurious” signals such as e.g. reflections on airplanes or broad-band interferences.

Each BRAMS receiving station is recording continuously, producing each day 288 WAV files and detecting ~ 1500–2000 meteors. This huge amount of data requires the use of automatic detection algorithms. Several attempts were made to identify meteor reflections either in raw data or in spectrograms by using automatic detection algorithms, with varying degrees of success as discussed in detail in (Calders and Lamy, 2014; Lamy et al., 2015). The automatic detection of overdense radio meteor echoes in particular remains a difficult task due to the various and complex shapes they produce in spectrograms. This problem is particularly striking during meteor showers where these types of meteor echoes are observed abundantly. In this paper, a new strategy for the identification of meteor reflections in the spectrograms is explored. Instead of detecting meteor reflections automatically by means of software, we propose to rely on the best detector which is the (trained) human eye. This is a well-established method nowadays in

observational science, known as crowdsourcing or citizen science (Lintott, 2008).

## 2 The Radio Meteor Zoo

The authors have started collaboration with the scientists at Zooniverse to use their platform to host a project called *Radio Meteor Zoo*.

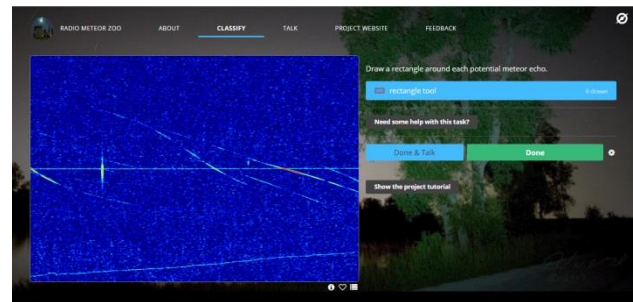


Figure 1 – The Radio Meteor Zoo website.

In order to be able to analyze the *Radio Meteor Zoo* contributions, we must be able to answer the two following important questions:

- What is the minimum number of volunteers we need to inspect a given spectrogram such that we can statistically be confident in the results?
- In a given spectrogram, how can we accurately derive the number and position of meteor echoes based on individual contributions?

In order to answer these questions, a test was performed with 12 spectrograms and 35 users.

## 3 A small-scale version of the Radio Meteor Zoo

### Description of the test data set

We used 12 spectrograms from the BRAMS receiving station in Ottignies obtained on 15 March 2015 between 0<sup>h</sup> and 1<sup>h</sup> UT. The authors carefully inspected the spectrograms together. In total 120 meteor reflections

were identified in the 12 spectrograms. These detections represent the reference dataset.

### Composition of the test group

The test group consisted of 35 volunteers with a strong physics background, and most of them are interested in meteor research but not necessarily familiar with radio observations.

### Meteor identification interface

Both the authors and the test group used the same interactive web tool to inspect the spectrograms and to identify meteor reflections. This tool is accessible online<sup>1</sup>. With this tool a user can draw a rectangle around each feature in the spectrogram that he considers to be a meteor. Once the user has identified all meteor reflections in the spectrogram, he can navigate to the next spectrogram. He can also navigate back to check his identifications in a previous spectrogram.

The coordinates of the rectangles, both in pixels coordinates and in frequency/time coordinates, are saved in a comma-separated values (CSV) file. A CSV file was created for each user.

### Training

The volunteers of the test group were asked to read first a tutorial. This tutorial explains what a spectrogram looks like and provides examples of typical signatures of meteor reflections and common distortions (like reflections on airplanes or broad-band interferences). Finally the tutorial explains what is expected from the volunteer: drawing rectangles around potential meteor echoes and how to do it correctly.

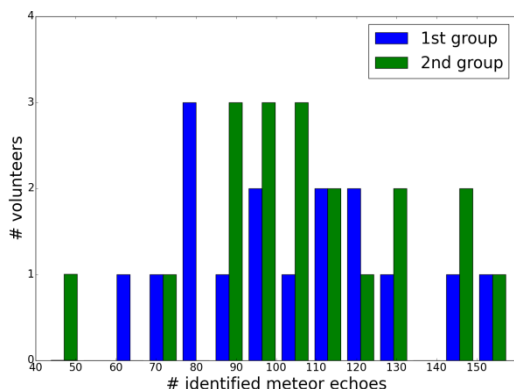


Figure 2 – Total number of meteor echoes identified by the different volunteers in the 12 spectrograms.

From the results of a first group of volunteers (16 people in the test group of 35), the authors learned that the median volunteer identified 99 meteor reflections (median absolute deviation MAD=19). This is far less than the 120 meteors that the authors had identified. The difference between the counts from the test group and the reference dataset was mostly due to the faintest meteor echoes. Therefore the tutorial was updated asking the users to draw a rectangle even when they have a doubt about a faint meteor. After all, it is easier to filter out a

false detection than to retrieve a missed meteor detection. The median volunteer of the second group identified 107 meteor reflections in the spectrograms (MAD=17). A histogram of the individual counts is given in Figure 2.

### Challenges

It was soon realized that there is a large spread on the number of meteors identified by the 35 persons. For instance, one volunteer identified 7 meteor reflections in the spectrogram in Figure 3, while another volunteer identified 17 meteor reflections, and the reference dataset yielded 15 meteor reflections.

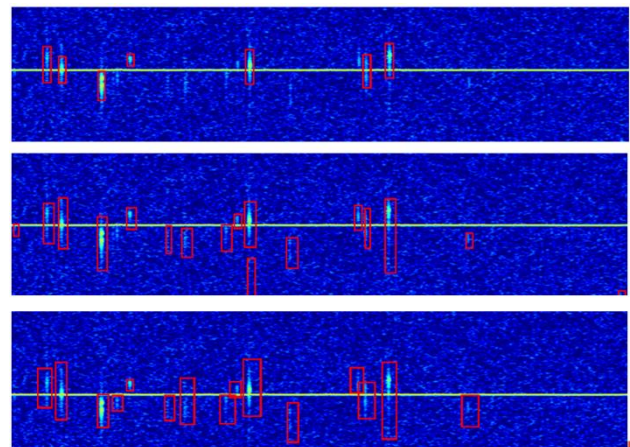


Figure 3 – Meteor reflection identifications by different volunteers in the same spectrogram. Top: volunteer 1 identifies 7 meteor reflections; middle: volunteer 2 identifies 17 meteor reflections; bottom: the reference detection identifies 15 meteor reflections.

## 4 How to interpret the *Radio Meteor Zoo* identifications?

First let us try to answer the second question from Section 2: in a given spectrogram, how can we accurately derive the number and position of meteor echoes based on individual contributions? In order to investigate this closer, we performed for every of the 12 spectrograms the following analysis for all values of  $i$  between 1 and 35.

- Create a binary version of the spectrogram called  $image_0$  which has pixel value 1 for pixels identified as a meteor pixel in the reference spectrogram, and pixel value 0 for all other pixels.
- Create a binary version of the spectrogram called  $image_1$  which has pixel value 1 for pixels which were identified as a meteor pixel by at least  $i$  volunteers, and pixel value 0 for all other pixels.
- Calculate the number  $D(i)$  of pixels for which  $image_0$  and  $image_1$  have different pixel values.

This allowed us to determine the value of  $i$  which minimizes  $D(i)$ .

It turns out that the number  $D(i)$  of pixels where “at least  $i$  volunteers” and the reference spectrogram disagree, has a minimum at  $i_{optimal} = 12$  volunteers. This means that in order to best reconstruct the reference spectrogram, we should consider as meteor pixels those pixels that have been identified as meteor pixels by at

<sup>1</sup> <http://brams.aeronomie.be/zoo>

least 12 of the 35 volunteers. The corresponding spectrogram is called the optimal identification spectrogram.

Now let us try to answer the first question of *Section 2*: what is the minimum number of volunteers we need to inspect a given spectrogram? Indeed, in the *Radio Meteor Zoo* project, it would be better to have a number of volunteers  $n$  that have to inspect a single spectrogram well below 35. For example, if 2000 spectrograms have to be investigated (corresponding to approximately one week of data for one receiving station), that would already amount to 70000 individual inspections for 35 users. So we repeated the analysis above for each number of volunteers  $n$  between 1 and 35. For every  $n$  we randomly selected 1000 combinations of  $n$  volunteers out of 35 to have a significant number of simulations without making it too CPU intensive.

*Figure 4* provides for every  $n$  the optimal number of volunteers  $i_{\text{optimal}}(n)$  which minimizes  $D(i)$ . For instance,  $i_{\text{optimal}}(35) = 12$  for  $n = 35$ , as was explained before. As expected,  $i_{\text{optimal}}(n)$  increases with  $n$ .

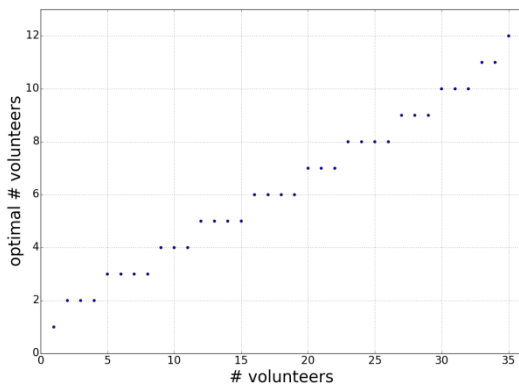


*Figure 4* – For every number of volunteers  $n$  on the x-axis, the y-axis shows the optimal number of volunteers  $i_{\text{optimal}}(n)$  that minimizes  $D(i)$ .

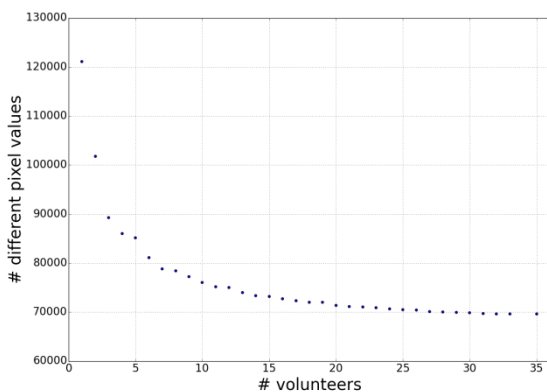


*Figure 5* – The number of pixels  $D(i)$  for which the optimal identification spectrogram for  $n$  volunteers and the reference spectrogram have different pixel values, as a function of number  $n$  of volunteers considered.

For every value of  $n$  (number of volunteers), we can now derive an optimal identification spectrogram of meteor reflections by considering a pixel as a meteor pixel if it is identified as such by at least  $i_{\text{optimal}}(n)$  volunteers. In

*Figure 5*, the number of pixels  $D(i)$  where the optimal identification spectrogram disagrees with the reference spectrogram is plotted as a function of number of volunteers  $n$ . Note that each spectrogram contains  $595 \times 864$  pixels in the 200 Hz range shown to the volunteers. For 12 spectrograms the total amount of pixels is therefore larger than  $6 \times 10^6$ . The values of  $D(i)$  shown in *Figure 5* represents thus maximum  $\sim 2\%$  of the total number of pixels in the worst case. This curve varies smoothly as a function of  $n$ , and of course has a minimal (best) value at  $n = 35$ .

*Figure 5* allows us to select a value for the number of volunteers  $n$  which is much smaller than 35 but yet still delivers accurate meteor reflection identifications. For the *Radio Meteor Zoo*, we selected  $n = 10$  volunteers per spectrogram. Indeed, using 10 volunteers instead of 35, corresponds only to an increase of 9% of  $D(i)$ , i.e. 9% more pixels with different values in the optimal identification spectrogram and in the reference spectrogram.

## 5 Results

When we apply the identification method described above on the spectrogram from *Figure 6* (with number of volunteers  $n = 12$ ), the same 15 meteors are identified as in the reference spectrogram.

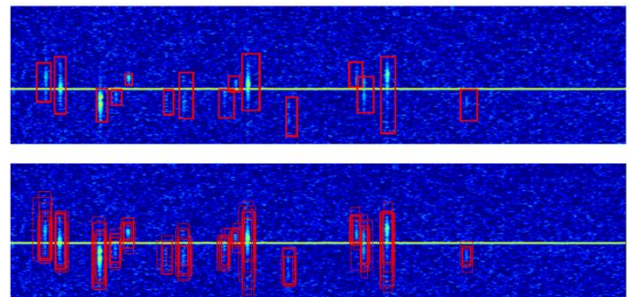


*Figure 6* – Comparison of the reference meteor spectrogram (top) and optimal identification spectrogram by the method described above with 12 volunteers (bottom). The same meteors were identified in both cases.

Until now, we have only considered meteor pixels instead of meteor reflections as a whole. To which extent does meteor reflection identification by the above method correspond to the meteor echoes in the reference dataset? In order to investigate this, we have applied a minimum bounding box algorithm to group meteor pixels into individual meteor echoes.

For every value of  $n$  between 1 and 35, 1000 random combinations of  $i_{\text{optimal}}(n)$  out of  $n$  volunteers are considered. For each combination, the number of hits (meteor reflections identified by both the reference and the proposed method) and the number of false detections (meteor reflections identified by the proposed method but not by the reference) are calculated.

In *Figure 7*, the medians of the percentage of hits and false detections over these 1000 iterations are plotted as a function of the number of volunteers  $n$ . For the *Radio*

*Meteor Zoo*, we will employ 10 volunteers per spectrogram, which amounts to a median percentage of hits of 95% and a median percentage of false detections of 6%. The median percentage of false detections is quite low because we have very few airplane echoes at night.

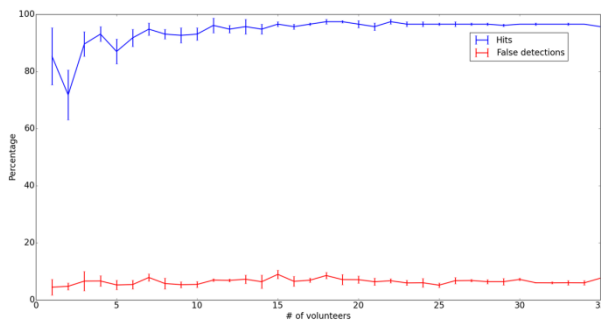


Figure 7 – Median percentage of hits and false detections of the proposed method as compared to the reference detection, as a function of number of volunteers  $n$ .

## 6 Discussion

Employing the meteor reflection identifications of 12 spectrograms by 35 volunteers, we were able to define a statistical method to identify meteor reflections. Based on  $n = 10$  volunteers inspecting each spectrogram, a median percentage of hits of 95% and a median percentage of false detections of 6% is obtained. Note that post-processing (e.g. looking at the power profile) can be invoked to analyze and reject false detections after detection.

Since the population of *Radio Meteor Zoo* volunteers may differ systematically from the population of 35 volunteers in the test (in particular with regard to their physics background), a similar test will be performed in order to validate our approach with the *Radio Meteor Zoo* volunteers.

These manual identifications will prove to be extremely useful during meteor showers because these contain many complex overdense meteor echoes. They will also be of great use to calibrate and test the pre-existing and potential new automatic detection algorithms.

We are ready to start analyzing *Radio Meteor Zoo* data. It is accessible via the following URL: <https://www.zooniverse.org/projects/zooniverse/radio-meteor-zoo>. We kindly invite all readers to help us by identifying meteor reflections and promoting this website!

## Acknowledgments

BRAMS is a project of the Royal Belgian Institute for Space Aeronomy (BIRA-IASB<sup>2</sup>) funded by the Belgian Solar - Terrestrial Centre of Excellence (STCE<sup>3</sup>). This project is carried out in collaboration with many radio amateurs from Belgium: without whose voluntary contribution we would have no observations. We thank

them for their sustained effort. The identification of radio meteors by 35 volunteers was compared with our reference detection set. They were contacted by the authors during the Meteorendag 2015 in Heesch, The Netherlands and the IMC 2015 in Mistelbach, Austria. Also some colleagues from the Royal Belgian Institute for Space Aeronomy but unfamiliar with the BRAMS project were participating. We would therefore like to thank all the participants of our test panel. Gratitude is also expressed towards the Zooniverse team for hosting the *Radio Meteor Zoo* and for their valuable advice.

## References

- Calders S., Lamy H., Gamby E. and Ranvier S. (2014). “Recent developments in the BRAMS project”. In Gyssens M., Roggemans P. and Zoladek P., editors, *Proceedings of the International Meteor Conference*, Poznan, Poland, 22-25 August 2013. IMO, pages 170–172.
- Calders S. and Lamy H. (2014). “Automatic detection of meteors in BRAMS data”. In Rault J.-L. and Roggemans P., editors, *Proceedings of the International Meteor Conference*, Giron, France, 18–21 September 2014. IMO, pages 194–196.
- Lamy H., Anciaux M., Ranvier S., Caldere S., Gamby E., Martinez Picar A. and Verbeeck C. (2015). “Recent advances in the BRAMS network”. In Rault J.-L. and Roggemans P., editors, *Proceedings of the International Meteor Conference*, Mistelbach, Austria, 27-30 August 2015. IMO, pages 171–175.
- Lintott C. J., Schawinski K., Slosar A., Land K., Bamford S., Thomas D., Raddick M. J., Nichol R. C., Szalay A., Andreescu D., Murray P. and Vandenberg J. (2008). “Galaxy Zoo: Morphologies derived from visual inspection of galaxies from the Sloan Digital Sky Survey”. *Monthly Notices of the Royal Astronomical Society*, **389**, 1179–1189.

<sup>2</sup> <http://www.aeronomy.be>

<sup>3</sup> <http://www.stce.be>

# Results from the Canadian Automated Meteor Observatory

Margaret Campbell-Brown

Department of Physics and Astronomy, University of Western Ontario, London, Canada

Margaret.campbell@uwo.ca

Some recent results from the Canadian Automated Meteor Observatory (CAMO) are presented. Comparing the begin heights and speeds of meteors between the two CAMO systems shows that the two populations, which differ by approximately an order of magnitude in mass, are quite different, with the more sensitive system recording many more slow meteors than the less sensitive system. At slow speeds for the more sensitive camera system, light curve shapes do not behave as expected, with stronger meteors having early-peaked light curves. Most meteoroids captured by the CAMO tracking system fragment in one way or another, and current ablation models are poor at predicting the nature of the fragmentation. The narrow field system is proving useful in many areas of meteor physics.

## 1 Introduction

While radio observations of meteors have the advantage of being independent of weather and daylight, there are many ways in which optical observations can provide more information about individual meteors. The errors in trajectories for multi-station meteors tend to be lower for optical than for radar meteors. Radars tend to scatter off one or a few points along the meteor trail, while optical observations can provide a more complete light curve and therefore constraints on meteor ablation. Optical observations have different observing biases than radar, and comparing speed and flux measurements in the two systems can help to determine if these are being adequately corrected.

The Canadian Automated Meteor Observatory (CAMO) consists of two sets of cameras for observing meteors optically. Here we present some of the recent work done with these systems.

## 2 The CAMO systems

### Overview

The CAMO systems are described in detail in (Weryk et al., 2013). Cameras are placed at two sites, one near Tavistock, Ontario, Canada and the other near Elginfield, Ontario, Canada. They have been in operation since 2010. The two systems operate automatically when the sky is dark, clear and moonless.

### The influx system

The first CAMO system consists of a single intensified video camera at each site. The cameras are Cooke pco.1200 CCD cameras, with 1600 by 1200 pixels and 14-bit optical depth, and run at 20 frames per second. They are lens coupled to 25 mm Gen III ITT image intensifiers with 50 mm objective lenses for a field of view of 20 degrees. The system can detect meteors as faint as +7.5 magnitude, but most of the meteors detected are around magnitude +5, since fainter meteors generally do not have enough frames to be useful.

Meteors are detected automatically, not in real time, with MeteorScan (Gural, 1997), and manually reduced.

### The tracking system

The tracking, or mirror system, is inspired by the AIM-IT system (Gural et al., 2004), which was the first instrument to track meteors in real time. It consists of two intensified video cameras at each site. All four have ImperX VGA-120L CCD cameras (640 by 480 progressively scanned pixels, 12-bit optical depth) lens coupled to 18 mm image intensifiers. One camera at each site has a 25 mm f/0.85 lens, with a field of view of 28 degrees, and runs at 80 frames per second. Meteors in this system are detected in real time using Asgard; after four frames, a predicted trajectory is calculated and used to direct light from the meteor, with a pair of orthogonal mirrors, onto the second camera. This camera has a 545 mm f/11, 80 mm refractor as an objective lens. It runs at 120 frames per second, and has a field of view of 1.5 degrees. The cameras can detect meteors down to +5 magnitude, but most of the reduced meteors area around magnitude +3.

About one in three meteors observed with the tracking system are well tracked in the narrow field camera.

## 3 Results

### Heights, speeds and sensitivity

Once the trajectories and speeds are obtained from two station meteors, one of the simplest and most useful ways to analyze the data is with a plot of begin height against speed. *Figure 1* shows these plots with more than 3000 meteors obtained with the tracking system (*Figure 1a*) and the influx system (*Figure 1b*).

Both systems show the expected trend of increasing begin height with increasing speed, and both show two approximate populations of meteoroids. More fragile or more volatile particles ablate higher at the same speed, while stronger or more refractory particles begin lower in the atmosphere. It is obvious from the plot that the influx

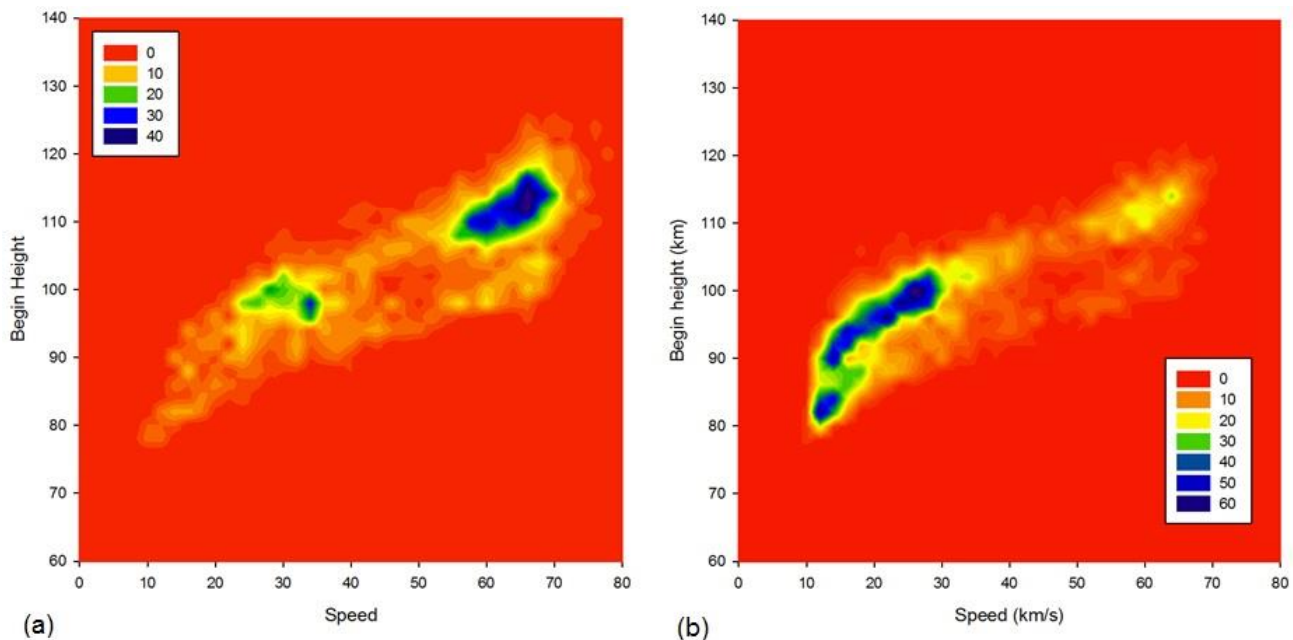


Figure 1 – Begin height vs. speed for the (a) tracking system and (b) influx system.

system sees many more slow meteors than fast ones, while the tracking system sees more fast meteors than slow ones. The reason for this is the difference in the limiting magnitudes between the two systems: the average mass at 30 km/s for the tracking system is about 1 mg, while the average for the influx system is 0.1 mg. The presence of the lowest speed, lowest begin height meteors is unexpected, and explored in Campbell-Brown (2015).

**Light curves and strengths**

The light curves of optical meteors are often used to determine the structure of meteoroids. In particular, a light curve with the peak toward the end of the curve is usually associated with a strong meteoroid, while a symmetric light curve with the peak in the middle is assumed to be produced by a weak, fragmenting meteoroid.

We can describe the shape of a light curve with the F parameter, which is the ratio of the difference between the height at peak magnitude and the end height to the difference between the begin and end heights. An F parameter less than 0.5 indicates an early-peaked light curve, and greater than 0.5 indicates a late-peaked light curve.

We can compare the F parameter to a measure of the meteoroid’s strength. The  $K_b$  parameter was developed by Ceplecha (1967) to describe the energy needed to start intensive evaporation, taking into account the speed and zenith angle. Small  $K_b$  parameters indicate fragile or volatile material, while large ones indicate strong or refractory particles. We can separate the two populations seen in the begin height / speed plots above with a  $K_b$  parameter of about 7.1.

Figure 2 shows the F parameter of meteors from the influx system as a function of speed, with the black points showing all meteors and the red triangles only the

strongest meteoroids, with  $K_b > 7.1$ . At speeds over 30 km/s, all meteors have, on average, symmetric light curves. At low speeds, however, strong meteoroids have early-peaked light curves, the opposite of what we would expect.

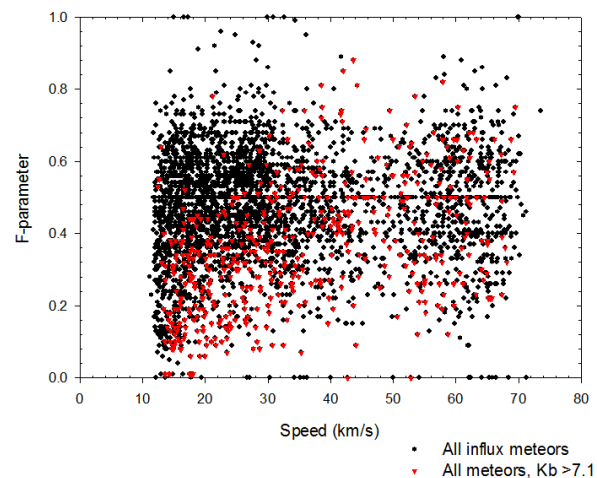


Figure 2 – Light curve skew as a function of meteor speed. The red triangles indicate the strongest meteoroids.

**Meteoroid fragmentation**

The CAMO tracking system has a resolution as high as 3 meters per pixel, though at usual ranges 5 meters per pixel is typical. This allows the system to observe fragmentation even in very faint meteors, which in lower resolution video appear not to fragment at all.

Figure 3 shows several examples of discrete and continuous fragmentation observed with the CAMO tracking system. Subasinghe et al. (2016) studied a large sample of tracking camera meteors, and found that about 85% had long tails, indicating some sort of continuous fragmentation into very small particles. Another 5% showed fragmentation into a few large pieces, and the

remainder showed almost no spread at all, implying that little or no fragmentation was taking place.

The same paper studied the connection between light curve shape and fragmentation behavior. It was found that, for fragmenting meteors, the light curves were generally symmetric, as expected. However, meteors showing very little fragmentation also had symmetric light curves: classical meteor theory suggests that their light curves should be late peaked, but this was not the case. The reason may be differential ablation of an inhomogeneous body, or small amounts of fragmentation not visible in the narrow field camera.

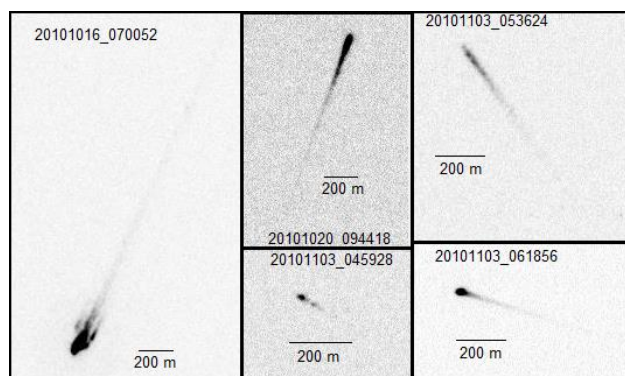


Figure 3 – Narrow field meteors observed with the CAMO tracking system.

The light emitted by fragments of meteoroids can also be used to constrain ablation models. Recently, two meteoroid ablation models (one by M. Campbell-Brown, the other by J. Borovička) were used to predict the appearance of ten meteors in the narrow field system, and both failed (Campbell-Brown et al., 2013). Both models predicted wakes which were both too long and too bright, indicating that the fragmentation models used were incorrect.

## 4 Conclusion

The difference in populations between the two CAMO systems of different sensitivities emphasizes the importance of observing meteors in different mass ranges. The origin and history of meteoroids is very different for particles of differing sizes and observations at all sizes provide interesting constraints in understanding how meteoroids formed and how their orbits evolve.

Data from the CAMO system show that light curve shape is not the simple indicator of meteoroid strength and fragmentation behavior it is sometimes assumed to be. Strong meteoroids may have symmetric or even (particularly for slow meteoroids) early-peaked light

curves, and fragmentation behavior observed in the tracking system was not predictable from the wide field light curves.

Fragmentation is known to be important in the ablation of small meteoroids, and the CAMO system confirms that about 90% of meteoroids show obvious fragmentation.

In the future, data from the CAMO optical systems will be used to investigate debiased speed distributions of the sporadic meteoroid complex, to calculate optical meteor fluxes, and to look for meteoroids on hyperbolic orbits. The very precise spatial measurements possible with the narrow field camera will help to get very precise orbits. The narrow field measurements will also provide strong constraints to ablation models, with fragmentation and deceleration both much more tightly characterized.

## Acknowledgments

CAMO was built thanks to a grant from the Canada Foundation for Innovation and support from the NASA Meteoroid Environment Office (NASA Cooperative Agreement NNX11AB76A).

## References

- Campbell-Brown M. D. (2015). “A population of small refractory meteoroids in asteroidal orbits”. *Planetary and Space Science*, **118**, 8–13.
- Campbell-Brown M. D., Borovička J., Brown P. G. and Stokan E. (2013). “High-resolution modelling of meteoroid ablation”. *Astronomy and Astrophysics*, **557**, A41.
- Gural P. (2007). “An operational autonomous meteor detector: Development issues and early results”. *WGN, Journal of the IMO*, **25**, 136–140.
- Gural P., Jenniskens P. M. and Varros G. (2007). “Results from the AIM-IT meteor tracking system”. *Earth, Moon, and Planets*, **95**, 541–552.
- Subasinghe D., Campbell-Brown M. D. and Stokan E. (2013). “Physical characteristics of faint meteors by light curve and high-resolution observations, and the implications for parent bodies”. *Monthly Notices of the Royal Astronomical Society*, **457**, 1289–1298.
- Weryk R. J., Campbell-Brown M. D., Wiegert P. A., Brown P. G., Krzeminski Z. and Musci R. (2013). “The Canadian Automated Meteor Observatory (CAMO): System overview”. *Icarus*, **225**, 614–622.

# Ablation of small Fe meteoroids – first results

David Čapek and Jiří Borovička

Astronomical institute of the Czech Academy of Sciences, Ondřejov, Czech Republic

capek@asu.cas.cz

A numerical model describing atmospheric flight of small iron meteoroids is presented. Several ablation scenarios are considered and it is discussed if these can explain a population of faint, short duration meteors with low beginning height and quick increase of brightness.

## 1 Introduction

A population of faint meteors with low velocities, low beginning heights and short duration has been described by Borovička et al. (2005) and Campbell-Brown (2015). Most of them have unusual light curves with rapid increase of brightness and maxima near the beginning of their luminous trajectory. A possible explanation is that the meteoroids are composed from iron; due to high thermal conductivity they are melted throughout before the beginning of ablation, which is then relatively rapid.

## 2 Model

We tried to check this hypothesis and developed a numerical model which considers spherical meteoroid with radial temperature field. The temperature of the meteoroid is determined from the heat diffusion equation with appropriate initial and boundary conditions. On the surface, the conservation of energy is considered – the incoming energy from the air flow is balanced by losses due to radiation, conduction and evaporation. The moving boundary between liquid and solid phase is described by Stefan's condition. The model uses thermophysical parameters for pure iron, most of which depend on temperature. Three alternative processes of ablation were studied:

### Evaporation of liquid iron

When temperature reaches 1811 K, a layer of liquid iron appears on the surface. The evaporation rate of liquid iron is computed according to the *Hertz-Knudsen* formula (also called *Langmuir* evaporation). The melting of solid iron inside the meteoroid continues. At the same time the temperature of the melt further increases until it reaches boiling temperature, which depends on dynamic pressure. The evaporation from the surface causes a decrease of the meteoroid radius. The kinetic energy of the evaporated mass is transformed into radiation.

### Liquid iron drop breakup

Liquid iron drop is subject to aerodynamic loading. If it is sufficiently intensive, the drop can deform and finally break up into many smaller droplets. This process increases the effective cross section and it would lead to a rapid increase of brightness. The condition for breakup is described by the critical *Weber* number.

### Immediate removal of liquid layer

As soon as the liquid iron appears, it is immediately removed (blown off) from the surface by air flow and its kinetic energy is transformed into radiation.

In all these cases we considered luminous efficiency to be 1 percent and the heat transfer coefficient to be equal to 1.

## 3 Results

For the comparison with the model predictions we took light curves, pre-atmospheric masses and velocities determined for eight meteors by Borovička et al. (2005).

We found that the ablation caused by evaporation of the liquid iron layer is a too slow process and it would produce much longer meteors than observed ones. The second ablation process – a breakup of liquid iron drop would take place about ten kilometers below the terminal heights of the observed meteors. In some cases it would not take place at all. This process is therefore not able to explain the observed meteors. The ablation caused by immediate removal of the layer of liquid iron would produce (in most cases) slightly shorter meteors with slightly higher beginning and terminal heights.

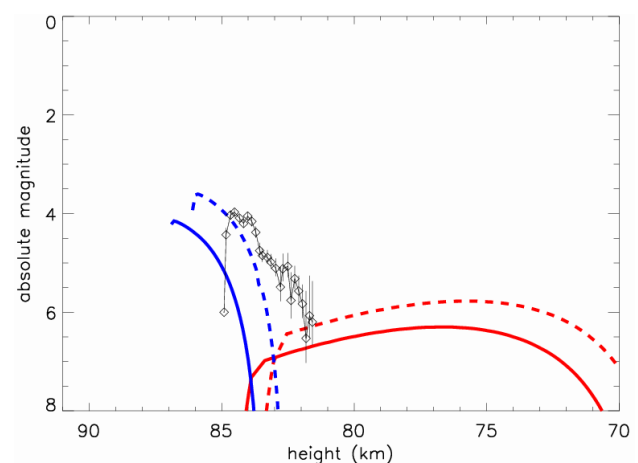


Figure 1 – Comparison of the measured light curve (black) with theoretical ones. The immediate blow off of the liquid layer would produce blue curves and the boiling of the liquid layer would produce red ones. Dashed and solid curves correspond to two different photometric masses deduced from the observation ( $3.3 \times 10^{-5}$  g and  $2.0 \times 10^{-5}$  g).

Nevertheless, the model with this process leads to results which are much more similar to the observations than in the case of the previous two ablation processes.

The model considering vaporization of the layer of liquid iron predicts light curves completely different from the observed ones as it can be seen in *Figure 1*. On the other hand, the immediate removal of the liquid iron layer produces light curves, which are more similar to the observed ones. They have rapid increase of the brightness, the maxima near the beginning height and a slower decrease.

#### 4 Conclusion

Our simple model shows that the ablation of small iron meteoroids cannot be described by the melting of the whole meteoroid volume and its consequent vaporization. Such process is too slow. The breakup of the liquid iron drop by aerodynamic loading is also inconsistent with observations since the breakup is expected at too low heights. The most probable ablation process is a fast blow

off of the melted layer forming small droplets which then ablate rapidly.

Our next research will be devoted to a more precise description of this process, the variation of model parameters and several other improvements (use of thermophysical parameters for iron-nickel alloy, taking the oxidation of the liquid into account, etc.).

#### Acknowledgment

This work was supported by GAČR grant 16-00761S.

#### References

- Borovička J., Kotešný P., Spurný P., Boček J. and Štork R. (2005). “A survey of meteor spectra and orbits: evidence for three populations of Na-free meteoroids”. *Icarus*, **174**, 15–30.
- Campbell-Brown M. (2011). “A population of small refractory meteoroids in asteroidal orbits”. *Planetary and Space Science*, **118**, 8–13.

# FRIPON network status

François Colas<sup>1</sup>, Brigitte Zanda<sup>2</sup>, Sylvain Bouley<sup>3</sup>, Jérémie Vaubillon<sup>1</sup>, Chiara Marmo<sup>3</sup>,  
Yoan Audureau<sup>3</sup>, Min Kyung Kwon<sup>1</sup>, Jean-Louis Rault<sup>7</sup>, Pierre Vernazza<sup>4</sup>, Jérôme Gattacceca<sup>5</sup>,  
Stéphane Caminade<sup>3</sup>, Mirel Birlan<sup>1</sup>, Lucie Maquet<sup>1</sup>, Auriane Egal<sup>1</sup>, Monica Rotaru<sup>6</sup>, Laurent Jorda,  
Cyril Birnbaum, Cyril Blanpain, Adrien Malgoyre, Julien Lecubin, Alberto Cellino<sup>8</sup>, Daniele Gardiol<sup>8</sup>,  
Mario Di Martino, Christian Nitschelm, Jorje Camargo, M. Valenzuela, Ludovic Ferrière,  
Marcel Popescu and Damien Loizeau

<sup>1</sup> **IMCCE, Observatoire de Paris, Paris, France**

francois.colas@imcce.fr

<sup>2</sup> **DIMPMC, Muséum National d'Histoire Naturelle, Paris, France**

Zanda@mnhn.fr

<sup>3</sup> **GEOPS, Université Paris Sud, Orsay, France**

sylvain.bouley@gmail.com

<sup>4</sup> **LAM, Institut Pytheas, Marseille, France**

pierre.vernazza@lam.fr

<sup>5</sup> **CEREGE, Institut Pytheas, Marseille, France**

gattacceca@cerege.fr

<sup>6</sup> **Universciences, Paris, France**

Monica.Rotaru@universcience.fr

<sup>7</sup> **IMO, Radio Commission**

f6agr@orange.fr

<sup>8</sup> **INAF, Osservatorio Astrofisico di Torino**

gardiol@oato.inaf.it

The FRIPON network (Fireball Recovery and Interplanetary observation Network) will be fully operational in 2016 ([www.fripon.org](http://www.fripon.org)). This “open source” project includes several new features that will be described in detail. We also discuss the opportunities for expansion outside France.

The main innovation is the connectivity of cameras enabling better efficiency for meteors detection, and the possibility of computing orbits in real time to organize an observation campaign within 24 hours.

Another innovation is the ability to daytime detections. Statistics show that there are more meteorites in late afternoon than during the rest of the day because of their low speed.

As the project has been designed from the start to handle a large number of cameras it is easy to extend it to increase its effectiveness. I will show the next extension of the network and its operation.

# The dimension added by 3D scanning and 3D printing of meteorites

Sebastiaan J. de Vet

Meteor Section, Royal Netherlands Association for Meteorology and Astronomy

Sebastiaandevet@gmail.com

An overview for the 3D photodocumentation of meteorites is presented, focussing on two 3D scanning methods in relation to 3D printing. The 3D photodocumentation of meteorites provides new ways for the digital preservation of culturally, historically or scientifically unique meteorites. It has the potential for becoming a new documentation standard of meteorites that can exist complementary to traditional photographic documentation. Notable applications include (i.) use of physical properties in dark flight-, strewn field-, or aerodynamic modelling; (ii.) collection research of meteorites curated by different museum collections, and (iii.) public dissemination of meteorite models as a resource for educational users. The possible applications provided by the additional dimension of 3D illustrate the benefits for the meteoritics community.

## 1 Introduction

The rapid technological and software developments in the ‘maker community’ have resulted in accessible means for 3D scanning and additive manufacturing, often competitive with industrial or scientific versions of similar technology. These developments also provide new means for amending scientific studies and documentation efforts of meteorites. For the meteoritics community, possible niches exist where 3D scanning and 3D printing may contribute to existing research, or even allow for new fields of science to be explored. Within the framework of this paper, I focus in particular on the digital 3D documentation and replication of objects, where the workflow itself may be broken down into three steps.

The first step involves the digitization of the object’s shape and surface texture. In this case ‘texture’ refers to the image file that is projected on the polygons of a model, rather than the small-scale topography of its surface. One approach involves projection of a light pattern to aid the digitization of an object’s shape. Examples of the method include laser scanners from a variety of commercial vendors and open source projects (i.e. using a 1D light pattern), while more advanced methods use a spatially differing light pattern (i.e. a 2D pattern) branded as ‘structured light’. This term will be used hereafter as a generic term to refer to all methods where the distortion of a separate light source is used to quantify the geometry of an object. A contrasting approach relies on photogrammetry to derive a shape model from a multitude of photographic images. This approach has been widely used in various applications, e.g. for producing digital terrain models of landscapes in geosciences. Photogrammetry can be used to render 3D models of objects when they are covered from multiple angles. Several software programs are available that can facilitate this approach for digitizing objects in 3D models.

The second step requires the processing of the model using dedicated 3D software suites. Some commercial scanning hardware comes with its own model processing software, while other freely-available software programs offer similar functionality. As these functions are indigenous and may vary between various software suites, users seeking specific details are referred to the wealth of online tutorials and work flows described by the user communities. Typically these workflows encompass steps such as the clean-up of the mesh by removing artefacts and noise, the closing of holes in the mesh, and the stitching and merging of two or more meshes. These steps allow for the fusion of the 3D scans into one single ‘watertight’ shape model of the meteorite.

The final step is *Additive Manufacturing* (AM), commonly known as ‘3D printing’, which aims at converting the digital model into a physical object. AM technology meanwhile involves many types of technologies based on extrusion, powder bed or light polymerization. As the materials portfolio has expanded rapidly the past few years, physical 3D models can now be produced using a variety of materials such as thermoplastics, polymers and ceramic powders. The innovative concept of the 3D printing approach is the additive nature of the manufacturing process, which contrasts the commonly used subtractive approach where material is removed (by e.g. drilling, milling etc.). For objects with complex organic geometries, such as meteorites, additive manufacturing offers sufficient degrees of freedom for fabrication of these types of objects. A popular method is *Fused Filament Fabrication* (FFF), also known as *Filament Deposition Modelling* (FDM), which is based on the extrusion of molten thermoplastics. This fabrication method lends itself well for the production of geometric facsimilia of meteorites. Due to the monochrome nature of the filament, models printed using FFF can only convey geometric characteristics. Other AM methods such as *Powder Bed* printing provide full-color printing capabilities and may render models into nearly photorealistic facsimilia of the

original meteorite. However, before the 3D model can be printed it has to be converted into a file format that is suitable for the printer to use, often this is the *Standard Tessellation Language* or STL file format. Subsequently this file needs to be ‘sliced’ into discrete printable layers that can be deposited by a 3D printer, using e.g. the *Fused Filament Fabrication* method. This final step in the 3D replication of a meteorite lies within reach of many, as 3D printer costs are reducing and access to 3D printing infrastructure is provided at ‘maker spaces’, via online commercial 3D printing services, or via online printing networks. In support of the workflow described above, this paper aims to (i.) qualitatively compare two different approaches to the 3D scanning of meteorites and (ii.) explore the unique potential of 3D scanning and 3D printing for the meteoritics community.

## 2 Methods and materials

For the proof of concept presented here, 3D scans and models were produced of an arbitrary meteorite; a Sayh al Uhaymir 001 meteorite that is classified as an ordinary chondrite (L5) and has been recovered from a remote desert region in Oman. Two contrasting methods for the digitization of the SaU001 were selected and compared, with user-friendliness and accessibility in mind. The first and most advanced method involves a *David 3D SLS-2* scanning system with an automated scanning platform

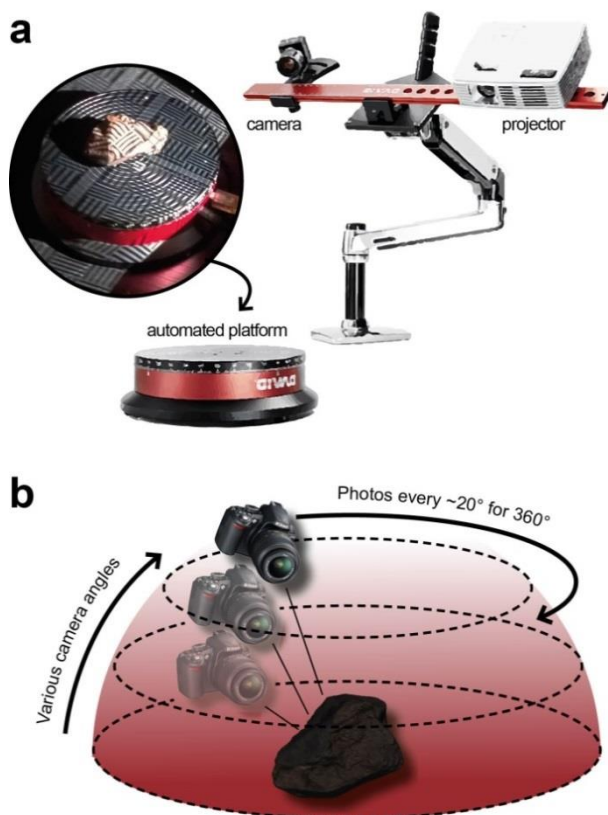


*Figure 1* – The two methods that have been compared for digitizing a SaU001 meteorite. (a) The set-up as used for scanning with the structured light approach using the David 3D SLS-2 (product images from [www.david-3d.com](http://www.david-3d.com)). In (b) the structured approach required for photographing an object when using photogrammetric software such as Autodesk’s 123D Catch.

(*Figure 1a*). This method uses a monochrome camera to measure the distortion of a light pattern projected by a projector onto an object, in order to triangulate points. Scan resolution can be as high as 0.1% of scanned object size, with a maximum of 0.06 mm, which renders an object into a high-fidelity digital model. The scanning algorithm also uses an RGB-color protocol to simultaneously obtain images in three color bands that are combined to produce a photographic texture file for draping over the shape model. Scans of the top and bottom of the SaU001 were made and semi-automatically (i.e. user-driven) merged in a manufacturer supplied software program to obtain a single shape model of the meteorite.

The second method that was evaluated did not require any special scanning hardware, other than a digital photo camera. Models were produced using Autodesk’s *123D Catch*. This freeware software program finds a photogrammetric solution of many overlapping photos to produce a 3D model of the photographed object. The accuracy of the model is dependent on parameters such as image focus, scene background and lighting conditions, and therefore requires a structured approach during photographing (*Figure 1b*). Similar to the other method, a model covering the entire shape of a meteorite requires several digital models from two or more orientations to be made, which subsequently need to be merged into one single shape model using software programs such as *MeshLab*.

## 3 Results and discussion

Digitization of the SaU001 meteorite using the two methods is shown in *Figure 2*. The 3D model comprises a surface composed of triangles (faces) that collectively form the model’s so-called ‘mesh’. The mesh’s face counts of the two models was found to differ significantly; 3954344 for structured light scanning vs. 29900 for the photogrammetric solution. This difference reflects the difference in resolution that can be achieved with each technique. In practice for 3D printing this difference may be nullified by the printing resolution (*Figure 3*). The two methods compared in this study therefore illustrate the range of options, but also the quality available to users interested in the 3D digitization of objects. Based on resolution criteria, structured light scanning offers a high-resolution approach to producing 3D models. This comes, however, at the cost of investing in the required hardware. This is contrasted by the photogrammetry approach that only requires a minimum of a photo camera, but at a tradeoff of a more extensive workflow to obtain the final 3D model. The resolution requirements of the final model and the intended application should therefore drive the method selection. For example, the 123D Catch software renders a model in arbitrary units and needs additional scaling to render a model at true size for printing (*Figure 3*), albeit that this is not a stringent requirement for e.g. online applications. The high-resolution models obtained by structured light

scanning, such as the *David 3D SLS-2* approach, may

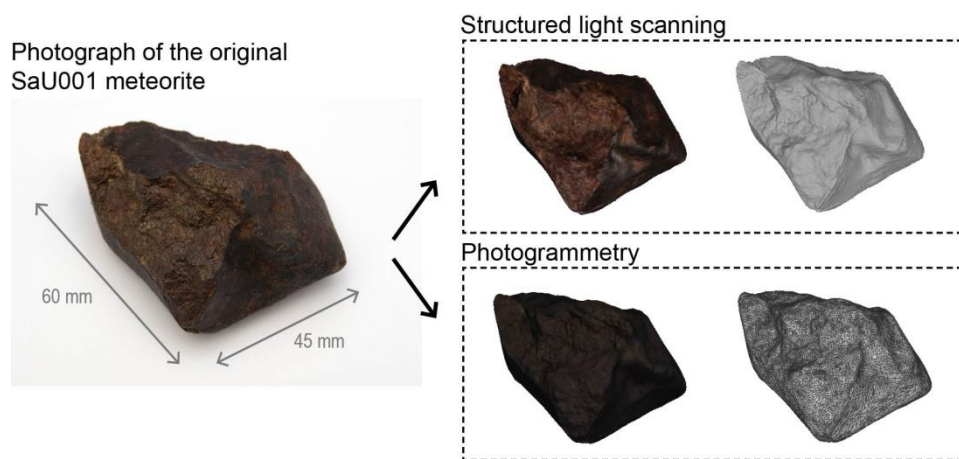


Figure 2 – Comparison of photos and digital models of the Sayh al Uhaymir 001 fragment. Each inset shows the digitized meteorite with a photographic texture file draped over the shape model, and the mesh of the model. Differences in color and mesh density are noticeable when comparing both methods. This SaU001 fragment weighs 167 grams and its dimensions are 7.5 x 5 x 3.5 cm (lwh).

better serve scientific applications when it comes to resolution and accuracy.



Figure 3 – Comparison of the SaU001 fragment with a 3D printed model. The model was manufactured using fused filament fabrication with ABS-plastic filament. Post-processing to reduce the ‘discrete’ surface of the model is possible using e.g. acetone vapor smoothing.

### 3.1 Scientific applications of 3D meteorite models

Paying attention to the limitation of the used digitization method, 3D digitization has the potential of becoming a new documentation and exchange format of meteorites, which can exist complementary to the traditional photographic documentation. 3D models offer users an unprecedented level of flexibility for rotating, zooming and studying meteorites. Standardization of 3D data is enforced by the limited range of file formats such as Alias Wave front OBJ file format<sup>1</sup> and the STL file format. These file formats make it much easier to standardize the exchange format for 3D meteorite models. Simultaneously, these formats are already supported by various software applications that allow for the embedding and display 3D models in e.g. web-based applications. One foreseeable application is the incorporation of 3D models with entries of meteorites in dedicated repositories, such as the Meteoritical Bulletin Database.

The 3D photodocumentation of meteorites also provides a way for the digital preservation of culturally, historically or scientifically unique meteorites. Studies focusing on historical applications or museum collection research may benefit from such digitization efforts. As these models preclude the need for transport of delicate fragments, the pairing of fragments can take place with the aid of 3D models in digital or 3D printed form. Similar approaches to the reunification and reassembly of objects are already employed in the study of ancient cultural artefacts included in the collections of various museums across Europe<sup>2</sup>, underlining the feasibility of this putative application.

In addition to providing a format for exchanging shape and exterior characteristics of meteorites, other object properties can be derived from 3D models. By calculating properties such as mass density, surface roughness, aerodynamic cross section, drag coefficients etc., 3D models may contribute data and addition parameters to dark flight and strewn field modelling, or provide the shape models for use as test articles in wind tunnel testing. Of equal interest is the use of 3D models in understanding the fracturing dynamics of meteorites. Like many other natural processes, meteorites often adhere to fractal relations during fracturing. Object properties can therefore provide additional data to understand fracturing dynamics of various meteorite types. Ultimately, the data that can be derived from 3D meteorite models and may support a wide range of scientific applications and foster big-data analyses of the physical features of meteorites and meteorite collections.

### 3.2 Educational potential

Educational users may also be interested in the use of 3D shape models. As blended-learning is increasing at various levels of education, models of meteorites with characteristic physical features, or cultural and historical relevance, can be widely disseminated for educational use

<sup>1</sup> <http://www.fileformat.info/format/wavefrontobj/egff.htm>

<sup>2</sup> <http://gravitate-project.eu/>

in online/digital content. It has also been recognized that learning can be enhanced when more than one sensory system is involved in the learning process, e.g. by using 3D printed objects. Facsimilia may also allow the visually impaired to use tactile cues for forming a mental image meteorites, that are otherwise too vulnerable to be handled. Public dissemination of 3D models of meteorites can therefore facilitate a wide range of educational users.

#### 4 Conclusion

Digital 3D models of meteorites can be produced in a variety of ways, all which have their benefits and disadvantages depending on the intended application. At the most accessible level in terms of hardware, photogrammetry provides a suitable way of documenting meteorites. Models are suitable for online applications and 3D printing. For higher-end applications such as

computational studies of a meteorite's shape properties, a more advanced method should be preferred. Overall, the listed benefits and applications advocating the use of 3D scanning and 3D printing, underline why the Pro-Am meteoritics community should be able to embrace the additional dimension of 3D in their work.

#### Acknowledgments

The David 3D scanning technology evaluated in this study was made possible with support of Mark Austen from *LocalMakers*, a dedicated 3D Design & 3D Printing Shop in the city Amsterdam, The Netherlands. The 3D printing of the meteorite was supported by Gert Jan Netjes.



Sebastiaan de Vet and Vincent Perlerin at the meteorite-3D-scanning-and-printing booth. (Photo Irmgard Schmidt).

# Status of the Desert Fireball Network

Hadrien A. R. Devillepoix<sup>1</sup>, Philip A. Bland<sup>1</sup>, Martin C. Towner<sup>1</sup>, Martin Cupák<sup>1</sup>,  
Eleanor K. Sansom<sup>1</sup>, Trent Jansen-Sturgeon<sup>1</sup>, Robert M. Howie<sup>2</sup>,  
Jonathan Paxman<sup>2</sup> and Benjamin A. D. Hartig<sup>2</sup>

<sup>1</sup>Dept. Applied Geology, Curtin Univ., Perth, Australia  
h.devillepoix@postgrad.curtin.edu.au

<sup>2</sup>Dept. Mechanical Engineering, Curtin Univ., Perth, Australia

A meteorite fall precisely observed from multiple locations allows us to track the object back to the region of the Solar System it came from, and sometimes link it with a parent body, providing context information that helps trace the history of the Solar System. The Desert Fireball Network (DFN) is built in arid areas of Australia: its observatories get favorable observing conditions, and meteorite recovery is eased thanks to the mostly featureless terrain. After the successful recovery of two meteorites with 4 film cameras, the DFN has now switched to a digital network, operating 51 cameras, covering 2.5 million km<sup>2</sup> of double station triangulable area. Mostly made of off-the-shelf components, the new observatories are cost effective while maintaining high imaging performance. To process the data (~70TB/month), a significant effort has been put to writing an automated reduction pipeline so that all events are reduced with little human intervention. Innovative techniques have been implemented for this purpose: machine learning algorithms for event detection, blind astrometric calibration, and particle filter simulations to estimate both physical properties and state vector of the meteoroid. On 31 December 2015, the first meteorite from the digital systems was recovered: Murrili (the 1.68 kg H5 ordinary chondrite was observed to fall on 27 November 2015). Another 11 events have been flagged as potential meteorites droppers, and are to be searched in the coming months.

## 1 Introduction

Since the 1950s, several projects have aimed to develop instruments to record meteorite falls: instruments that can both narrow down the meteorite search area, and compute the orbit the meteoroid was on before entry. The main piece of hardware required for this type of observation is a high-resolution imaging system with a very wide field-of-view. Large networks were set up in temperate areas like central Europe, the USA prairies, and Canada. Temperate areas are not ideal because of the relatively small number of clear nights, and the difficulty of spotting a meteorite in densely vegetated areas. This was the driver for starting the Desert Fireball Network (DFN) in Australia. The 4 newly installed cameras lead to the recovery of 2 meteorites in the first 5 years of operation: Bunburra Rockhole in 2007 (Bland et al., 2009) and Mason Gully in 2010 (Spurny et al., 2012). The cameras were film-based, but advances in sensor technology have made a digital equivalent smaller, cheaper, and therefore more scalable.

## 2 The network

### The instrument

The camera (Howie et al., 2016a) consists of an off-the-shelf still digital camera (36 MPixels Nikon D810), and carefully selected Samyang 8 mm f/3.5 fisheye lens, controlled by a single board PC and hard disks. A liquid crystal shutter is incorporated between the lens and the sensor, to break the fireball track and derive velocity. The shutter encodes a *de Bruijn* sequence (unique in the long exposure, precisely controlled by a GPS), which provides

absolute timing in the long exposure (Howie et al., 2016b). An internet link is provided by 3G mobile coverage, or WiFi/LAN, but the autonomous observatory can also operate completely off-the-grid, at the cost of delayed data retrieval. The system has been designed to reliably operate from a relatively small solar power installation (2 solar panels and a 120 AH battery), or on mains power when available. It takes a two-person team about 4 hours to install a whole system (such as the one shown in *Figure 1*). The autonomous observatories can run for 11 months unattended, being limited only by the advances on off-the-shelf hard drive technology.



*Figure 1* – Outback DFN observatory at Mount Ive station.

### Coverage

The Australian part of the network currently comprises of 51 cameras, which covers ~3 million km<sup>2</sup>. Apart from the small fraction of this area that falls in the ocean, the landscape is ideal for meteorite searching; the network is built around mostly arid and featureless areas.

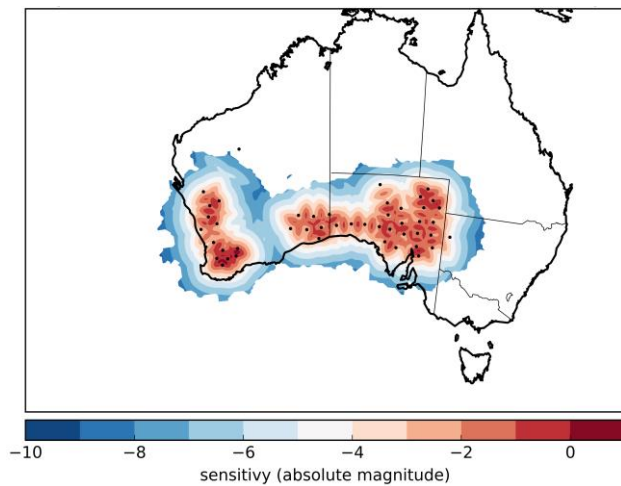


Figure 2 – DFN coverage map showing detection sensitivity.

### 3 Results



Figure 3 – The Murrili meteorite.

#### The Murrili meteorite

On November, 27<sup>th</sup>, 2015 just after sunset at 10<sup>h</sup>43<sup>m</sup>44.5<sup>s</sup> UTC, a large meteoroid entered Earth's atmosphere at 13.8 km/s over South Australia. The bolide was visible for 6.1 seconds, and slowed down to 3.83 km/s when the light went out at 18.24 km altitude. We calculated that the probable meteorite would have landed in the middle of Australia's biggest salt lake: Kati Thanda – Lake Eyre. Despite how easy spotting a meteorite on a salt lake seems, getting to the lake proved very difficult because of the extreme remoteness of the site, and the inhospitable weather conditions at this time of the year (temperatures over 45°C, tropical rains threatening to flood the lake). A reconnaissance team managed to spot a splash in the mud using a small airplane. But we were only able to safely organize a ground recovery 10 days later, after a severe rain, which had washed off the large 60 cm feature seen from the plane. On December 31<sup>st</sup>, after two days of unfruitful ground search, with the help from local aboriginal guides, our team was able to find the rock, buried 43 cm in the thick sticky clay that covers the lake. The name of the 1.68 kg H5 ordinary chondrite was chosen by the Arabana people (traditional owners of the lake): Murrili (pronounced moo-Rril-y). The low inclination close to the 3:1 resonance with Jupiter orbit is quite common for an H5 chondrite (Jenniskens, 2014):

semi-major axis = 2.62 AU, eccentricity = 0.62; inclination = 3.58°, argument of perihelion = 356.3°; longitude of the ascending node = 64.63°, perihelion distance = 0.9944 AU (J2000 equinox).

#### Large fireball orbital dataset

At its current size, the DFN yields more than 1 fireball event per night on average. Using a purposely written mostly automated pipeline, the events are systematically reduced, in order to get a mass and an orbit for each fireball. Over time, this will form a very large unbiased fireball dataset, which will yield important results about centimeter to meter scale objects – bridging the gap between dust picked up by conventional meteor networks, and NEO telescopic surveys.

### 4 Conclusions and future work

Using the conservative criteria: fireball end height < 35 km and end speed < 8 km/s (which is not a necessary nor a sufficient condition for meteorite dropping, as discussed in Brown et al., 2013), we find that 11 more events in our dataset are potential meteorite droppers. They are to be searched in the coming months.

### References

- Bland P. A., Spurny P., Towner M. C., Bevan A. W. R., Singleton A. T., Bottke W. F. Jr., Greenwood R. C., Chesley S. R., Shrubny L., Borovička J., Ceplecha Z., McClafferty T. P., Vaughan D., Benedix G. K., Deacon G., Howard K. T., Franchi L. A. and Hough R. M. (2009). "An anomalous basaltic meteorite from the innermost main belt". *Science*, **325**, 1525–1527.
- Brown P., Marchenko V., Moser D. E., Weryk R. and Cooke W. (2013). "Meteorites from meteor showers: A case study of the Taurids". *Meteoritics and Planetary Science*, **48**, 270–288.
- Howie R. M., Paxman J., Bland P. A., Towner M. C., Cupák M., Sansom E. K. and Devillepoix H. A. R. (2016a). "How to Build a Continental Scale Fireball Camera Network". In review.
- Howie R. M., Paxman J., Bland P. A., Towner M. C., Sansom E. K. and Devillepoix H. A. R. (2016b). "Sub-millisecond fireball timing for precise heliocentric orbits using de Bruijn timecodes". In review.
- Jenniskens P. (2014). "Recent documented meteorite falls, a review of meteorite – asteroid links". In Jopek T. J., Rietmeijer F. J. M., Watanabe J., Williams I. P., Mickiewicz A., editors, *Proceedings of the Astronomical Conference Meteoroids*, Poznan, Poland, Aug. 26-30, 2013. University Press in Poznan, pages 57–68.
- Spurny P., Bland P. A., Borovička J., Towner M. C., Shrubny L., Bevan A. and Vaughan D. (2012).

“The Mason Gully meteorite fall in SW Australia: Fireball trajectory, luminosity, dynamics, orbit and impact position from photographic records”. In *Asteroids Comets Meteors 2012*, Proceedings of the conference held May 16-20, 2012 in Niigata, Japan. LPI Contribution No. 1667, id.6369.



Hadrien Devillepoix.



Much interest there is in the fully robotic All sky cameras of the Australian Desert Fireball Network (DLN). Hadrien Devillepoix (white shirt, right) explains.

# Data processing of records of meteoric echoes

Peter Dolinský

Slovak Central Observatory, Hurbanovo, Slovakia

peter.dolinsky@suh.sk

The data obtained in the period from 4 November 2014 to 31 July 2014 by our receiving and recording system was statistically processed. The system records meteoric echoes from the TV transmitter Lviv 49.739583 MHz (N49.8480° E24.0369°, Ukraine) using a 4-element Yagi antenna with horizontal polarization (elevation of 0° and azimuth of 60°), receiver ICOM R-75 in the CW mode, and a computer with a recording using HROFFT v1.0.0f. The main goal was to identify weak showers in these data. Mayor or strong showers are visible without processing (referred at IMC2015, Mistelbach). To find or to identify weaker showers is more difficult. Not all echoes are meteoric echoes, but also ionospheric echoes or lightning disturbances are present.

## 1 Introduction

Reflections of radio waves from meteor trails were recorded and registered in the period from 4 November 2014 to 1 August 2015. The part from 1 December 2014 to 31 July 2015 was selected for data processing.

## 2 Description of the equipment

A 4-elements Yagi antenna horizontally polarized operating at 50 MHz was used. The antenna is oriented towards the azimuth 60° with an elevation of 0°. The conductive ground effect cannot be neglected and the beam peak of the antenna has an elevation of about 15°. The analog television transmitter Lviv at 49.739583 MHz (N49.8480° E24.0369°, Ukraine) was used as a source of electromagnetic waves. Since it is a television transmitter, one can assume a circular emission characteristic of the transmitter in the horizontal plane. The communication receiver ICOM-R75 was used to detect radio waves. It was tuned to the frequency of 49.73970 MHz with CW modulation. The difference in frequencies between the transmitter and the receiver ensured a low-frequency output in the range between 880 Hz and 940 Hz. A computer with Linux as operating system and the program HROFFT in 1.0.0f was used to register echoes.

## 3 Data processing

Data obtained by continuous registration from 1 December 2014 to 31 July 2015 were recorded by the HROFFT software. These data were converted to the RMOB format using the software HROFFTtoRMOB. RMOB data were displayed by our own software as two-dimensional chart shown in *Figure 1A*. Days are displayed at horizontal and time at vertical axis. The number of recorded echoes at 10 dB of audio output is displayed as a color map. These data were not reduced for any disturbances.

To identify short-time events in these data the 10-day “background” was used. Next formula was used to determine the background value  $BV(t)$ :

$$BV(t) = \frac{\min(HR(t - 24k_1))}{2} + \frac{\min(HT(t + 24k_2))}{2}$$

where  $k_1 = 0, 1, \dots, 5$ ,  $k_2 = 1, 2, \dots, 5$ ; HR is recorded hourly rate of echoes and min means the minimal value of these data.

$BV(t)$  is depicted on *Figure 1B* in the same way as *Figure 1A*. The pattern of  $BV(t)$  shows also strong showers with longer periods of activity.

HR(t)-data after subtraction of  $BV(t)$  is depicted on *Figure 1C*. Some short time events are emphasized, but weak, long-term showers are still invisible.

The *Figure 1D* shows the shower activity (Rendtel, 2014), with declination higher than  $-20$  deg. The period of shower activity is shown as a triangle. The first of the triangle's vertex is placed at the start of the shower activity, second at the end and third at the maximum. The day showers are depicted in the same manner, but in the opposite direction (triangles turned up down).

The obtained data set shows that showers with higher ZHR and longer activity periods are registered well, but weak or short showers are not so clear.

There is a 7-day periodicity of signal visible in the period from 15 January to 15 February. This period has an origin in disturbances and corresponds with human activity. To decrease these disturbances we lowered the frequency range in HROFFT from 1 March 2015.

Disturbances caused by the ionospheric Es layer and lightning occur during the summer period.

## 4 Conclusion

Based on the obtained data, it is possible to use this equipment to monitor the shower activity during longer periods (referred in IMC2015). Using data processing and subtracting “background” is possible to distinguish short-term effects or showers (for example Lyrids at *Figure 1C*). Also “background” (*Figure 1B*) shows stronger showers as well. It is difficult to distinguish weak, long term showers and probably it will be necessary to use a more accurate recording system (speclab instead of hrofft).

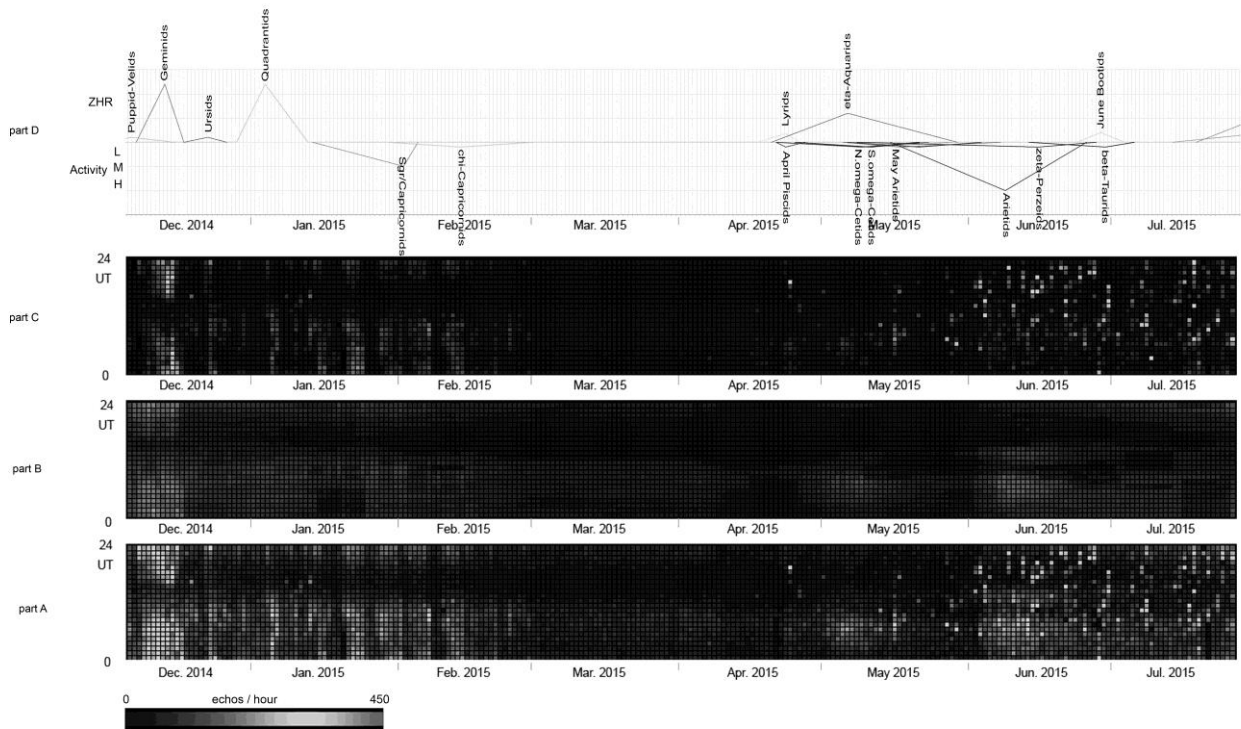


Figure 1 – Echo rates and shower activity.

## References

Rendtel J., editor (2014). Meteor Shower Workbook 2014. IMO.



Peter Dolinský, Debora Pavela and Jakub Koukal meet in the chill out corner: time for discussion.

# Calibration of meteor spectra

Martin Dubs<sup>1</sup> and Koji Maeda<sup>2</sup>

<sup>1</sup>FMA (Fachgruppe Meteorastronomie), Maienfeld, Switzerland

[martin-dubs@bluewin.ch](mailto:martin-dubs@bluewin.ch)

<sup>2</sup>Nippon Meteor Society and University of Miyazaki, Miyazaki, Japan

[mae@mrf.biglobe.ne.jp](mailto:mae@mrf.biglobe.ne.jp)

Meteor spectra give valuable information about the composition of meteors. The nonlinear dispersion of spectra together with the motion of the meteors complicates the analysis. In this presentation a simple method to calibrate spectra in wavelength and flux is presented. By an image transformation to an orthographic projection the dispersion becomes linear and the curved spectra become straight and parallel. The resulting spectra, after suitable pre-processing, can be analyzed with standard spectroscopy software.

## 1 Introduction

The widespread use of high sensitivity video cameras has led to an increased interest in meteor spectroscopy. However the calibration and analysis of spectra has been done by only a few experts, mainly because of the nonlinear dispersion of the spectra, which complicates the calibration. The appearance of meteors anywhere in the field of view and their rapid movement pose additional challenges for the analysis. Most spectra are recorded with diffraction gratings as a dispersion element. In this talk a method is described which allows to transform the nonlinear curved spectra into linear, straight spectra parallel to the main dispersion direction of the grating. All the meteor spectra images are transformed to a orthographic projection. This is done by image transformation software similar to the software used to correct lens distortion. Linear spectra with constant dispersion have the advantage that they can be stacked and processed with standard spectroscopy software used for stellar spectra.

Wavelength calibration is the main topic; however some points on intensity calibration are also highlighted. In order to achieve high numbers of meteor spectra, lenses with a wide field of view are often used. These show vignetting in the corners, which has to be corrected in addition to the correction caused by the image transformation. The angle dependence of the grating efficiency is often overlooked. The effect of atmospheric extinction should not be neglected, ideally by calibrating the spectra with close by reference stars.

## 2 Linearization of wavelength scale

As can be seen in *Figure 1*, meteor spectra show a nonlinear wavelength scale, the dispersion measured in pixel/nm varies as a function of wavelength and meteor position. This can also be seen from the grating equation (Schroeder, 1970):

$$m\lambda G = (\sin \alpha + \sin \beta) \cos \gamma \quad (1)$$

where  $m$  is the grating order,  $G$  the number of grooves/mm,  $\alpha$  the incidence angle,  $\beta$  the exit angle of the light onto the grating and  $\gamma$  the out of plane angle from the grating normal. In addition, the spectra are curved, which further complicates the analysis.

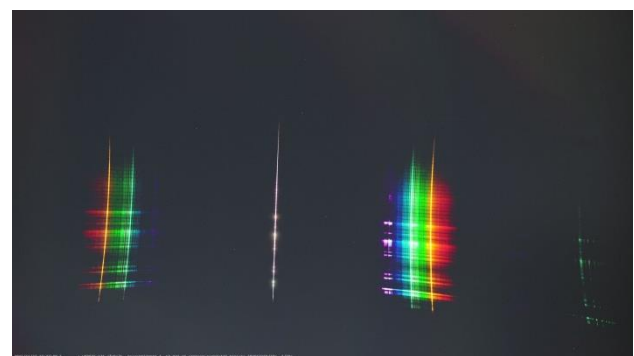


*Figure 1* – Original meteor spectrum, recorded by Koji Maeda, 20151127\_222709, Sony alpha 7S, f 24mm, grating 600L/mm.

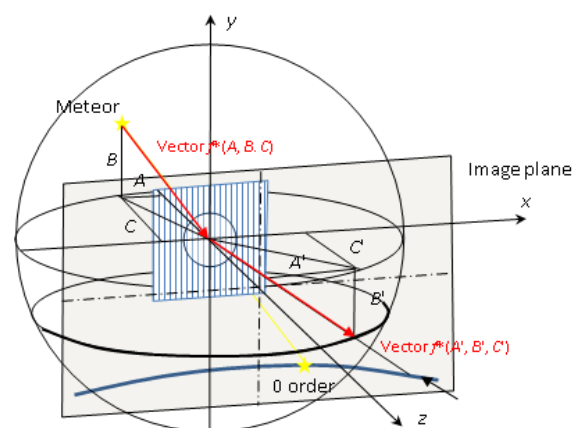


*Figure 2* – Vector components of incident and diffracted ray.

For the present discussion a different set of equations, given by Rowland (1893), is more useful. Using vector notation for the incident and diffracted ray, the following equations are obtained for the components of unit vectors:

$$A' = A + m\lambda G \quad (2)$$

$$B' = B \quad (3)$$

$$C' = \sqrt{1 - A'^2 - B'^2} \quad (4)$$

The important point is that (2) is linear in wavelength, the component  $B'$  is constant and the nonlinearity is only in (4), which is used to calculate the position of the spectrum in the CCD plane (the resulting spectrum in the CCD plane has the shape of a hyperbola).

The idea is now to transform the CCD images of the spectra and transform them to coordinates  $A'$  and  $B'$ , linear in wavelength or in other words, to transform the gnomonic projection (central perspective of a sphere onto a plane) into an orthographic projection (parallel projection of a sphere onto a plane). In this transformation the correction of lens distortion can be easily included, if the grating is oriented perpendicular to the optical axis of the lens. Details are given in Dubs and Schlatter (2015). The required transformation maps a point in the original image,  $P = (r, \varphi)$ , to a point in the radially modified image,  $P' = (r', \varphi)$ , where the coordinates are measured from the optical axis. For the transformation a polynomial equation of the following form is used:

$$r = f(r'/f + a_3(r'/f)^3 + a_5(r'/f)^5 + \dots) = r'(1 + a_3(r'/f)^2 + a_5(r'/f)^4 + \dots) \quad (5)$$

$f$  is the focal length of the lens, in the center the scale is not changed,  $a_3$  and  $a_5$  are polynomial coefficients). The coefficients are determined by recording the spectrum of a calibration light in different areas of the image and fitting the spectrum positions to the linear calculated positions by a least square fit. Fortunately this has to be done only once for each grating – lens combination. After the transformation all the spectra are parallel (a rotation has been included to make them horizontal) and the dispersion is constant everywhere in the image (which can be checked by measuring the constant separation of the negative and positive 1<sup>st</sup> order and the 2<sup>nd</sup> order of the Mg line):

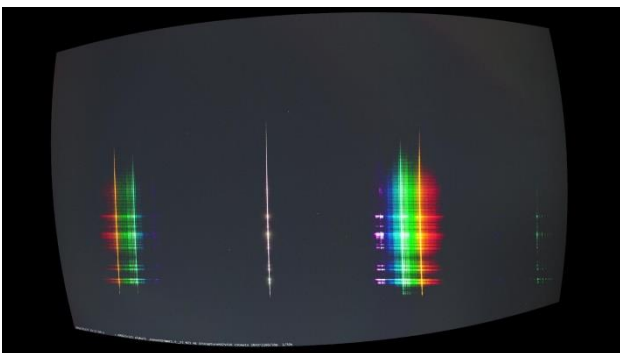


Figure 3 – Meteor spectrum of Figure 1 after image transformation and rotation.

In a color spectrum the identification of the different lines and orders is easy. The constant dispersion helps in identifying unknown lines in black and white spectra if a single line is identified, even if the zero order is missing. Wavelength differences are obtained by multiplying the separation in pixels with the known dispersion.

### 3 Processing of spectra

In order to extract a useful spectrum or a series of spectra at different times the images need some processing to remove background, correct for vignetting and align them. This is done in a similar way to the processing of stellar images, with the difference that the meteor is moving fast, so some extra step has to be taken to freeze its movement. The processing can be separated into three stages, first the preprocessing, then the image transformation and third the extraction of the spectra. It is shown for the case of video observation, for long time exposure the processing would be somewhat different.

#### Preprocessing

This consists of extracting the images from the video stream, removal of background and correcting for vignetting. Fortunately sky brightness and stars are constant over short periods, so a background image can be calculated as the average of images before the appearance of the meteor and subtracted from the meteor images.

The vignetting is particularly noticeable with wide angle lenses. A flat image can be recorded of a white screen (a foggy sky or a twilight flat serves the same purpose) without grating. Figure 4 shows an extreme example.

The background corrected images are divided by the flat image to correct for the vignetting<sup>1</sup>.

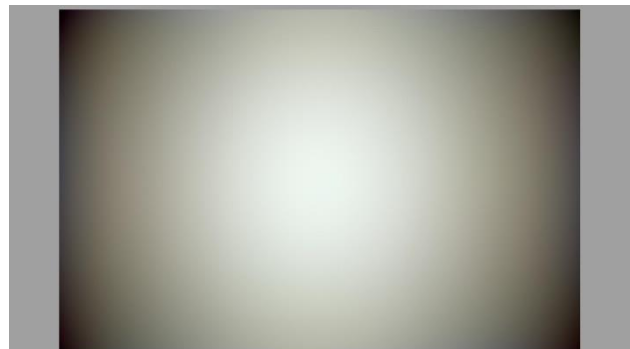


Figure 4 – Flat image of Canon EOS6d with lens Sigma 35mm, f/1.4.

#### Image transformation

The image transformation to the orthographic projection has been described above. It is done by software similar to that used for correcting lens distortion<sup>2</sup> By an additional rotation the spectra can be oriented parallel to the horizontal axis. This simplifies the extraction of the spectrum.

<sup>1</sup> An additional correction by a factor  $1/\cos(\rho)$  is necessary to take into account the change of scale from an equal projection to the orthographic projection ( $\rho = \arcsin(r'/f)$ ), in order to preserve the photon flux. This can be included in the flat correction. A different flat correction is needed without the image transformation, since a gnomonic projection also changes equal areas on the sky to different areas on the CCD. A flat correction may do more harm in that case.

<sup>2</sup> In the present work specially adapted software ImageTools by Peter Schlatter has been used.

### Extraction of spectra

After the image transformation all the spectra have a constant dispersion (the same scale in nm/pixel) and are aligned parallel. They may be shifted to a fixed position of the zero order and stacked for increase of S/N. Alternatively they can be processed image by image and displayed as a time series. The intensities of the rows containing the spectrum are added column by column. Next the pixel scale is converted to wavelength with a linear transformation, using the zero order as origin or a known line (e.g. the Na line) as a wavelength reference, in case the zero order is out of the image area. The linearity may be checked with some known other lines or higher orders.

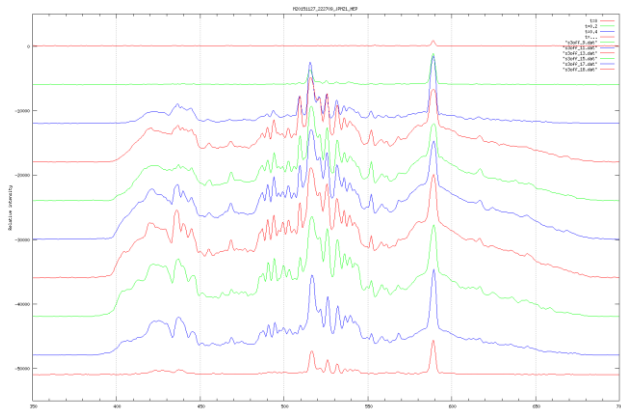


Figure 5 – Wavelength calibrated time series of spectra for the meteor of Figure 1, time interval 0.2 sec top to bottom, notice the saturation of strong lines.

## 4 Flux calibration

For many purposes this wavelength calibrated spectrum is sufficient. For a quantitative analysis of line strengths a calibration of the intensity is required. In most cases a relative calibration of intensities is sufficient. The principal factors affecting calibration are the wavelength dependence of:

- Atmospheric extinction
- Grating efficiency
- Lens transmissivity
- Sensor sensitivity or quantum efficiency

It is not possible to give a full discussion, so some points of special interest in meteor spectroscopy will be highlighted.

Atmospheric transmission follows the extinction law (Appenzeller, 2013):

$$T_a(\lambda) \approx \exp[-\tau(\lambda)/\cos(z)] \quad (6)$$

with  $\tau(\lambda)$  the optical depth of the atmosphere in the zenith.  $z$  is the zenith distance. A precise determination would require a determination of the atmospheric extinction at the time of the meteor apparition; in practice one can use a standard curve for the time of observation.

Grating efficiency curves can be obtained from the grating manufacturer. Note however that this function is

measured or calculated only for normal incidence of the light. The efficiency of a blazed grating is very sensitive to the incidence angle  $\alpha$ , as the following diagram shows for a 600 L/mm grating with a blaze angle of  $28.7^\circ$ <sup>3</sup>.

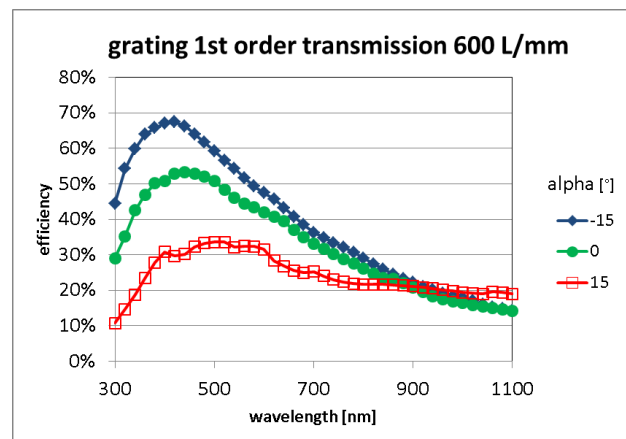


Figure 6 – Grating efficiency of a 600 L/mm grating, calculated for 1<sup>st</sup> order for different incidence angles.

For other orders the angle and wavelength dependence is even more severe, so an intensity correction is normally not done. In a standard slit spectrograph you do not have this problem, since the incident angle is fixed by the grating orientation and slit position.

The sensor sensitivity can be taken from the manufacturer datasheet, note that a factor proportional to  $\lambda$  enters for the conversion from photon number to photon energy.

The instrument response is finally calculated by multiplying all these factors. Since some of these are not precisely known (atmosphere, additional windows, lens transmission) a more practical way is to determine the instrument response by measuring a standard star and dividing its spectrum by the known spectral flux of this star. A good source for calibration spectra is e.g. the Miles database<sup>4</sup>. This can be improved by taking into account the differential atmospheric extinction with (6).

### Practical considerations

For color images with a Bayer matrix a correction with the instrument response is not advisable because of the low sensitivity at the short and long wavelength limit and the irregular shape of the response function, modified by the filter transmission of the color filters. For that reason the following example is for a Watec 902H2 ultimate camera with a 600 L/mm grating. The instrument response  $IR(\lambda)$  was determined with a reference star. Venus was in a good position in the sky at the time of the meteor.

$$IR(\lambda) = \langle I_{\text{meas}}(\lambda)/F_{\text{ref}}(\lambda) \rangle \quad (7)$$

The measured spectrum of the reference star is divided by the flux of the reference and suitably smoothed. The measured spectrum of the meteor is then flux corrected by multiplying with the IR. By carefully keeping track of

<sup>3</sup> Calculated with Gsolver V4.20b, <http://www.gsolver.com/>  
<sup>4</sup> <http://www.iac.es/proyecto/miles/>

normalization factors an absolute flux of the meteor may be calculated with the same equations.

$$Flux_{Met}(\lambda) = I_{Met}(\lambda)/IR(\lambda) \quad (8)$$

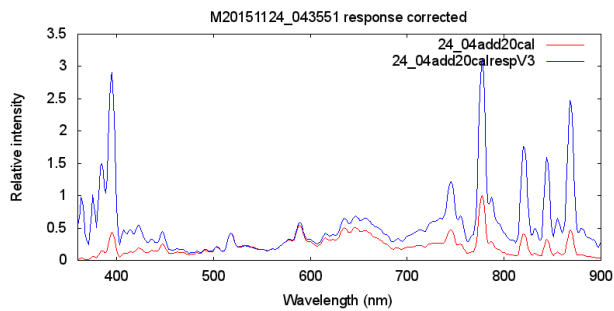


Figure 7 – Meteor spectrum recorded with a Watec902H2 ultimate, red: original, blue: instrument response corrected.

## 5 Equipment

Some words about the equipment used in these tests and the results obtained so far are useful. The first experiments were done with a video camera Watec 902H2 ultimate with a Tamron 12VG412ASIR ½", f: 4-12mm f/1.2 lens, operated at  $f \cong 7\text{mm}$ , with a Thorlabs grating with 300 grooves/mm, exchanged for a grating with 600 grooves/mm (see Figure 7). In first order this gives an inverse dispersion of 2.0 nm/pixel, which is about the minimum of usability. In addition the 8-bit readout limits the dynamic range. Unfortunately meteors do not appear with the correct intensity to make best use of this range, so they are either underexposed with a poor S/N ratio or overexposed, saturating the strong lines which make them unusable for quantitative analysis. Occasionally some video frames with the correct intensity can be used, but then much information about the temporal behavior gets lost.

The color spectra have been recorded with a Sony alpha 7s, f 24mm, or a Canon EOS6D with lens Sigma 35mm, F/1.4, both with a grating 600 grooves/mm. This records in 3 × 8-bit color mode. The larger chip size allows higher dispersion (0.62 nm/pixel for the Sony alpha at full resolution of 3840 × 2160 and 1.06 nm/pixel with the Canon at a resolution of 1920 × 1080). Unfortunately the Bayer matrix reduces the sensitivity, complicates the analysis and makes quantitative analysis unreliable. The 8-bit readout again is a limiting factor for the quantitative analysis.

A really useful camera for meteor spectroscopy should have a large chip, 12- or 16-bit monochrome readout at around 30 frames/second and an affordable price. Unfortunately these requirements are somewhat contradictory.

## 6 Conclusions

This work shows that the analysis of meteor spectra can be simplified by the transformation of the images to an orthographic projection. The resulting spectra have a constant dispersion and are parallel for any position of the meteor. They can be analyzed with standard spectroscopy

software. In the future it is planned to simplify the calibration and to streamline the processing pipeline. This may help in popularizing meteor spectroscopy in the community. At present additional stations of the FMA plan the installation of meteor spectroscopy cameras in Switzerland. Since two years the FMA operates a network of video, fireball detection, radar and seismic stations, which in combination allow a better characterization of meteors.



Figure 8 – Sony alpha7s equipped with grating 600 grooves/mm.

## Acknowledgment

Martin Dubbs thanks the FMA (Fachgruppe Meteorastronomie) for providing data and helpful discussions, in particular Peter Schlatter for his assistance with software, Roger Spinner and Jonas Schenker for the meteor database and webpage<sup>5</sup>, where the results of meteor spectroscopy are presented.

## References

- Appenzeller I. (2013). Introduction to Astronomical Spectroscopy, Cambridge University Press, 174.
- Dubs M. and Schlatter P. (2015). “A practical method for the analysis of meteor spectra”. *WGN, the Journal of the IMO*, **43**, 94–101.
- Rowland H. A. (1893). “Gratings in Theory and Practice”. *Astronomy and astrophysics / Goodsell Observatory*, **12**, 129–149.
- Schroeder D. J. (1970). “Design considerations for astronomical echelle spectrograph”. *Publications of the Astronomical Society of the Pacific*, **82**, 1253–1275.

<sup>5</sup> <http://www.meteorastronomie.ch/>

# Investigation of meteor shower parent bodies using various metrics

Bogdan Alexandru Dumitru<sup>1,2,3,4</sup>, Mirel Biran<sup>2,3</sup>,  
Alin Nedelcu<sup>3,2</sup> and Marcel Popescu<sup>3,2</sup>

<sup>1</sup>Institute of Space Science (ISS), Magurele, Romania  
bogdan.dumitru@spacescience.ro

<sup>2</sup>Paris Observatory, Paris, France  
Mirel.Birlan@imcce.fr

<sup>3</sup>Astronomical Institute of the Romanian Academy, Bucharest, Romania

<sup>4</sup>Bucharest University, Faculty of Physics, Bucharest, Romania

The present knowledge of meteor showers identifies the small bodies of our Solar System as supply sources for meteor streams. Both comets and asteroids are considered as the origin of meteor showers. The new paradigm of “active asteroids” opens up a large field of investigation regarding the relationships between asteroids and meteors. Processes like ejection and disaggregation at impacts, rotational instabilities, electrostatic repulsion, radiation pressure, dehydration stress followed by thermal fractures, sublimation of ices are sources of matter loss from asteroids.

Our objective is to find genetic relationships between asteroids and meteor showers using metrics based on orbital elements. For this objective we selected three metrics (Southworth and Hawkins, 1963; Asher et al. 1993, and Jopek, 1993, respectively), the recent MPC database and the more recent IAU meteor shower database.

From our analysis, 41 of the meteor showers have probabilities of being produced (or to be fueled) by asteroids. Our sample of asteroids contains more than 1000 objects, all of them belonging to the Near-Earth Asteroid population. The systematic approach performed, based on the physical properties of our sample, reinforced the link between asteroids and their associated meteor shower.

## 1 Introduction

The origin of meteor showers has been identified as the small bodies of the solar system, namely comets and asteroids. This concept was proposed by Kirkwood in 1861 who linked the comets to meteor showers and by Olivier in 1925 who linked the asteroids with meteor showers (Kirkwood, 1861; Olivier, 1925).

Today the relationship between comets, asteroids and meteor showers is largely accepted, thanks to discoveries of asteroids that exist as extinct comets (Weissman et al., 1989) and active asteroids (Jewitt et al., 2015).

In the case of asteroids the processes which produce meteoroids are: ejection and disaggregation at impacts, rotational instabilities, electrostatic repulsion, radiation pressure, dehydration stresses and thermal fracture, in addition to sublimation of ice (Jewitt et al., 2015). The fragments are called meteoroids, in sizes from 10 microns to 10 meters (Rubin and Grossman, 2010).

In this case, the large meteoroids, as well as asteroids and comets played an important role in the evolution of life on Earth. Such cataclysmic events undergo global regional or local effects. In the Earth Impactors Database<sup>1</sup> there are 188 confirmed impact structures.

The aim of this study is to make a sketch of common associations between asteroids and meteor showers.

## 2 Method

The most common method of measuring the degree of similarity between the orbits is the so called “D-criterion” used throughout this study.

The D-Criteria metric is used to compute similarities between two orbits (distance between the orbits). For this, the metric defines a phase space as a coordinate system in 5 dimensions, and then to each coordinate one orbital element is assigned. If  $D(A,B) < D_c$ , where  $D_c$  is a constant used as threshold, the orbits of the objects are considered similar and the objects could be associated (from the dynamical point of view).

The first metric of this criteria used in the literature was introduced by Southworth and Hawkins in 1963 ( $D_{SH}$ ), but with time other metrics appeared, introduced by Drummond in 1981 ( $D_D$ ), by Jopek in 1993 ( $D_H$ ), by Valsecchi, Jopek and Froeschle in 1999 ( $D_N$ ) (Jopek et al., 1999), by Nesvorný and Vokrouhlický in 2006 ( $D_Z$ ) (Nesvorný and Vokrouhlický, 2006), by Jopek, Rudawska and Bartczak in 2008 ( $D_B$ ) (Jopek et al., 2008), etc.

Our approach was made using three metrics, namely Southworth and Hawkins ( $D_{SH}$ ), Jopek ( $D_H$ ) and Asher, Clube and Steel ( $D_{ACS}$ , a reduced version using only three orbital elements, namely  $a$ ,  $e$ , and  $i$ ).

<sup>1</sup><http://www.passc.net/EarthImpactDatabase>

### 3 Analysis procedures

In this study we use the databases from the IAU Minor Planet Center (over 700000 asteroids in February 2016) and the IAU Meteor Data Center (over 100 established meteor showers in February 2016).

The number of associated asteroids is highly dependent on the selection threshold. Each metric requires a different threshold, because the method of computation will produce different statistical distances (Table 1 in Jopek (1993)).

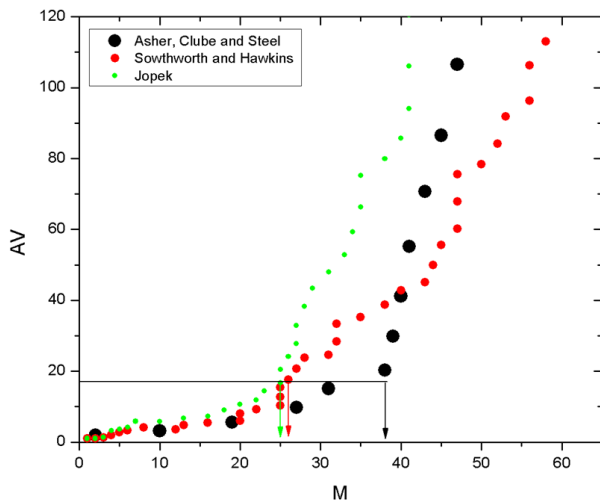


Figure 1 – Threshold selection in terms of medium association objects per meteor shower vs associated meteor showers. We observe that metrics have an ascending behaviour after a certain number of meteor showers, but the average number of associations at the ascending behaviour is the same. The arrows are indicators for the changes in slopes.

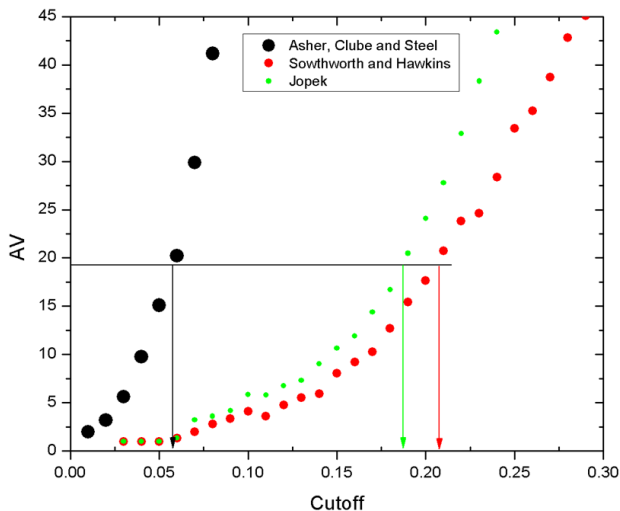


Figure 2 – Representation of the average association objects per meteor shower vs the D-criterion cutoff. We select the cutoff for each metric at the point where all metrics dramatically change the slopes (Figure 1). The arrows in the figure indicate the selected cutoff value.

Our approach is to look for a global parameter which could characterize all the population of meteor showers. For this reason we define a parameter after the formula:

$$AV=N/M$$

where  $N$  is the total number of asteroids associated with a given metric, and  $M$  is the number of meteor showers which could be produced by these asteroids.

$AV$  is a dimensionless number with no physical meaning. It represents just a way to qualify the evolution of the clustering. We investigate its evolution over the three metrics. Thus Figure 1 shows the evolution of this parameter for all three metrics. Globally for a value of  $AV$  around 17 we observed an important change in the slopes for the three metrics. The choice of our method was tuned to this empirical parameter in order to establish the threshold for the metrics as well as the cutoff value.

The  $AV$  value will be used to find the cutoff of each metric as presented in Figure 2. The cutoff values were of 0.06 for  $D_{ACS}$ , 0.21 for  $D_{SH}$ , and 0.19 for  $D_H$ .

### 4 Results

We identified 1086 asteroids as being associated with 41 meteor showers. 22 of the meteor showers are associated by each of the three metrics, 5 meteor showers are associated by two metrics (3 by  $D_{ACS}$  and  $D_{SH}$ , 2 by  $D_{SH}$  and  $D_H$ ) and 14 meteor showers are associated by one single metric (one by  $D_H$  and 13 by  $D_{ACS}$ ). The results are plotted in Figure 3.

All the associated objects are Near-Earth Asteroids (NEA). 62.42% of the associated asteroids have Apollo orbits, followed by Amor type orbits with 37.21% and the rest have Aten orbits. From those objects 17.28% are Potential Hazardous Asteroids (Figure 4).

Our simulation did reproduce some already established associations, including:

- 3200 *Phaethon* associated with the *Geminid meteor shower*. In our simulation we obtained the same conclusion with a high probability,  $D_{ACS} = 0.02$ ,  $D_{SH} = 0.03$  and  $D_H = 0.04$ .
- 2005 *UD* associated with *Daytime Sextantid meteor shower*. In our case this asteroid was associated with the same meteor shower, but with medium probability,  $D_{SH} = 0.18$  and  $D_H = 0.16$  and  $D_{ACS} = 0.70$  being over the cutoff.

Our simulation also revealed some puzzling results regarding previously published associations, including:

- The association between 2002 *EV11* and the *Daytime  $\kappa$  Aquariids*, all metrics are larger than the selected cutoff,  $D_{ACS} = 0.23$ ,  $D_{SH} = 0.24$ ,  $D_H = 0.26$ .
- 2004 *TG10* associated with *Daytime  $\beta$  Taurids*. Here we have again different results. In the simulation the asteroid 2004 TG10 was associated at medium probability with the Daytime  $\beta$  Taurids,  $D_{SH} = 0.14$ ,  $D_H = 0.15$ ,  $D_{ACS} = 0.20$  (over cutoff) and with high probability to the Northern Taurids,  $D_{ACS} = 0.05$ ,  $D_{SH} = 0.12$  and  $D_H = 0.13$ .

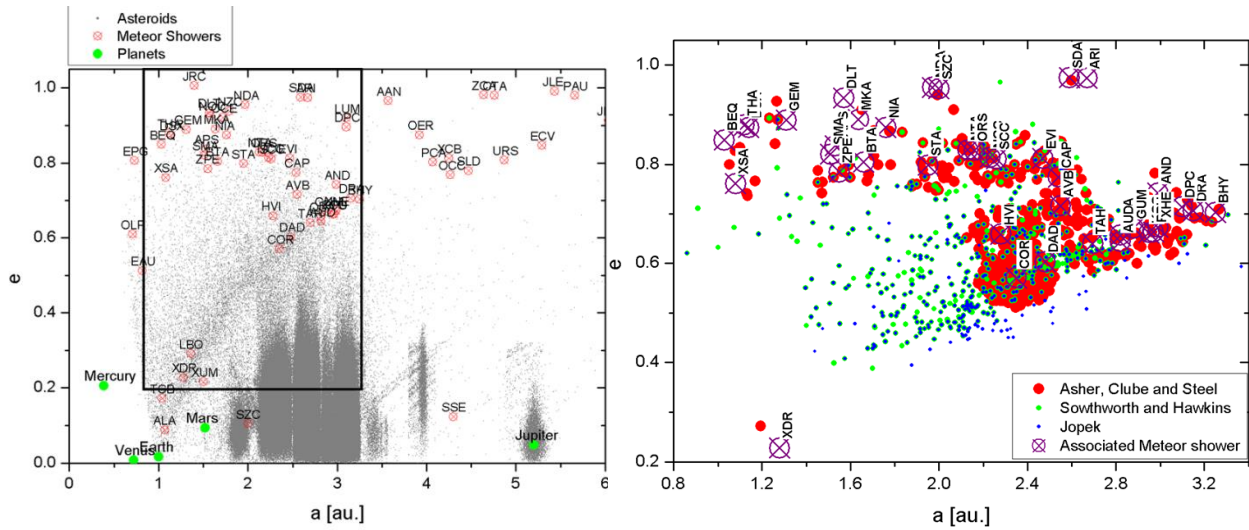


Figure 3 – The position of associated asteroids in the Solar System, in a diagram of eccentricity vs semi-major axis. At left we have all objects from the IAU Minor Planet Center (all asteroids – grey), all established meteor showers (red) and planets from Mercury to Jupiter (green). In the second diagram we show all associated objects by all used metrics, with  $D_{ACS}$  in red,  $D_{SH}$  in green and  $D_H$  in blue and the meteor showers that the asteroids were associated with in violet.

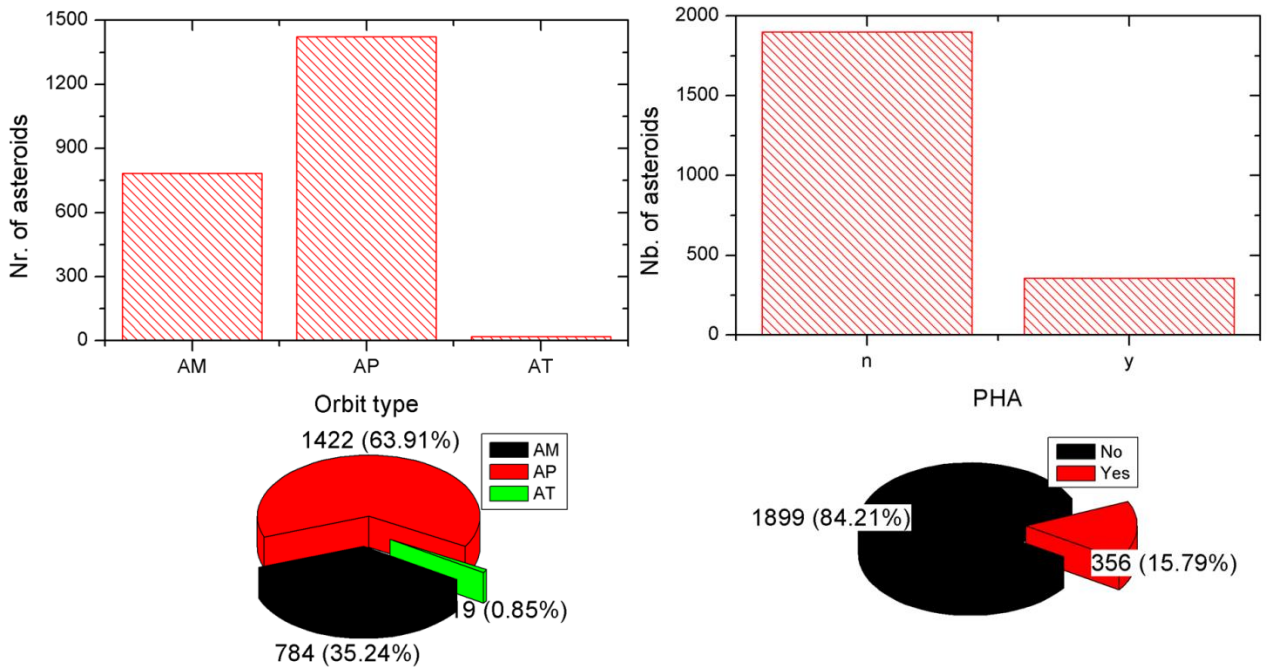


Figure 4 – Asteroid orbital types and the hazardous asteroids. On the left we show the orbital types of the associated asteroids orbital type. All objects have Near-Earth Orbits. On the right we show the PHA asteroids. From the association we found 17.28% with PHA flag.

For the associated asteroids, a systematic search in the European Asteroid Research Node (EARN) database<sup>2</sup> was carried out for the physical parameters. Of our sample of 1086 NEAs, 72 asteroids exhibit spectra in visible and near-infrared, 61 asteroids have an associated taxonomic class, 82 asteroids have a value for the albedo, and 57 asteroids have a rotation period.

7% of the selected NEAs have a computed albedo (Figure 5). Low albedo asteroids (less than 0.1) are objects which are usually associated with primitive asteroids (C, D or P taxonomic classes).

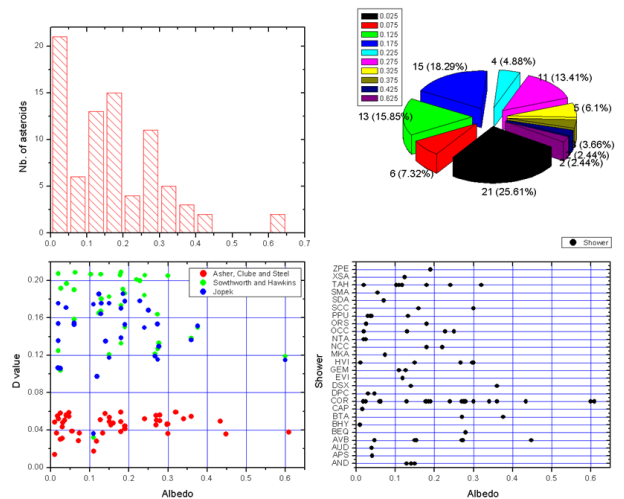
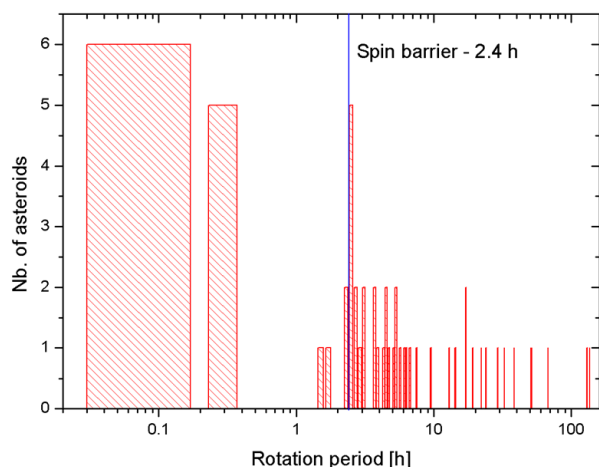


Figure 5 – Statistics on albedo found in literature.

<sup>2</sup> <http://earn.dlr.de>

Rotation periods have been computed for 57 objects of our sample. Such studies are important as this is a factor in fragmentation and dust production from a possible parent body for meteoroids. Indeed, for the asteroids larger than 200 meters, a spin value of 2.4 hours (Pravec et al., 2007) was defined to distinguish between “rubble-piles” and monolithic NEAs. This value is also known as the “spin barrier” value. The histogram of asteroids with known rotation periods is shown in *Figure 6*. Approximately 30% of objects exhibit rotation periods shorter than the spin barrier value.



*Figure 6* – Histogram of asteroids with known rotation periods. The axis is shown with a logarithmic scale.

## 5 Conclusion

An investigation of the most recent database of asteroids was performed using three different metrics. 1086 asteroids were selected during the clustering procedure. Our simulation can reproduce some of the previously published associations in the literature; but some of the published data are puzzling. A small number of objects of our selected asteroids have known physical parameters in the EARN-database. A systematic approach to observe the selected NEAs in order to derive their physical parameters has now been undertaken.

## References

- Asher D. J., Clube S. V. M. and Steel D. I. (1993). “Asteroids in the Taurid Complex”. *Monthly Notices of the Royal Astronomical Society*, **264**, 93–105.
- Drummond J. D. (1981). “A test of comet and meteor shower associations”. *Icarus*, **45**, 545–553.
- Jewitt D., Hsieh H. and Agarwal J. (2015). “The Active Asteroids”. In Michel P., DeMeo F. E. and Bottke W. F., editors, *Asteroids IV*. University of Arizona Press, Tucson, pages 221–241.
- Jopek T. J. (1993). “Remarks on the Meteor Orbital Similarity D-Criterion”. *Icarus*, **106**, 603–607.
- Jopek T. J., Valsecchi G. B. and Froeschle Cl. (1999). “Meteoroid stream identification: a new approach - II. Application to 865 photographic meteor orbits”. *Monthly Notices of the Royal Astronomical Society*, **304**, 751–758.
- Jopek T. J., Rudawska R. and Bartczak P. (2008). “Meteoroid Stream Searching: The Use of the Vectorial Elements”. *Earth, Moon, and Planets*, **102**, 73–78.
- Kirkwood D. (1861). “Cometary astronomy”. *Danville Quarterly Review*, **1**, 614–638.
- Nesvorný D. and Vokrouhlický D. (2006). “New Candidates for Recent Asteroid Breakups”. *The Astronomical Journal*, **132**, 1950–1958.
- Olivier C. P. (1925). “Meteors”. The Williams and Willkins Company, Baltimore.
- Pravec P., Harris A. W. and Warner B. D. (2007). “NEA rotations and binaries”. In Valsecchi G. B., Vokrouhlický D. and Milani A., editors, *Near Earth Objects, our Celestial Neighbors: Opportunity and Risk*, Proceedings IAU Symposium 236. Cambridge University Press, pages 167–176.
- Rubin A. E. and Grossman J. N. (2010). “Meteorite and meteoroid: New comprehensive definitions”. *Meteoritics and Planetary Science*, **45**, 114–122.
- Southworth R. R. and Hawkins G. S. (1963). “Statistics of meteor streams”. *Smithsonian Contributions to Astrophysics*, **7**, 261–286.
- Weissman P. R., A’Hearn M. F., McFadden L. A. and Rickman H. (1989). “Evolution of comets into asteroids”. In Binzel R. P., Gehrels T. and Matthews M. S., editors, *Asteroids II*; Proceedings of the Conference, Tucson, AZ, Mar. 8-11, 1988 (A90-27001 10-91). Tucson, AZ, University of Arizona Press, pages 880–920.

# The challenge of meteor daylight observations

Auriane Egal<sup>1</sup>, Min-Kyung Kwon<sup>1</sup>,  
François Colas<sup>1</sup>, Jérémie Vaubaillon<sup>1</sup> and Chiara Marmo<sup>2</sup>

<sup>1</sup>IMCCE, Observatoire de Paris, 77 av. Denfert-Rochereau, 75014 Paris, France

auriane.egal@obspm.fr, kwon.minkyung@obspm.fr,  
francois.colas@obspm.fr, jeremie.vaubaillon@obspm.fr

<sup>2</sup>GEOPS (Géosciences Paris Sud), Université Paris Sud, 91405 Orsay Cedex, France

chiara.marmo@u-psud.fr

One of the goals of the FRIPON network is to perform the daylight detection of fireballs. If the cameras used are adapted to these observations, the reduction method still needs to be improved in order to reduce the high number of false detections. To deeply check the daylight reduction software, the FRIPON team is looking for observations of fireballs and atmospheric reentries during the day. For this purpose, the team has organized in emergency (in less than 10 days) an observation campaign of the reentry of the WT1190F space debris in November 2015. Although the bad weather conditions have hampered the success of the mission, it remains a great example of the value of the collaboration between scientists and amateurs, without whom this challenge wouldn't have been overcome.

## 1 Introduction

Daytime meteor showers can be detected by different camera networks dedicated to their observation. The radiants of these showers are located close to the Sun's position, and it is therefore possible to briefly observe meteors early in the morning or late in the evening. Such optical observations of daytime meteors have been conducted for example for the daytime Arietids (171 ARI) or the daytime Sextantids (221 DSX) (Rendtel, 2014). However, none of the meteor networks currently at work have already performed daylight observation of fireballs. Events like the Chelyabinsk fall in 2013 are usually recorded by undedicated surveillance cameras or mobile phones. Since half of the asteroids impacts occur during the day, it would be highly beneficial to use camera networks dedicated to the daylight observations of fireballs.

## 2 Daylight detections with FRIPON

### The FRIPON network

With more than 60 operational cameras among the hundred installed, the FRIPON network provides multiple detections of meteors during the clear nights. In a few months and with good weather, the coverage of the network will allow the detection of any bright fireball crossing the French sky at night. The reduction pipeline for nighttime observations is almost achieved and provides satisfactory results. That is why the next objective of the FRIPON project is now investigated: the daylight detection of fireballs. As many recent numerical cameras, the gain and exposure duration of each camera can be set to provide unsaturated images of the sky; there is then no major obstacle to the daylight acquisition. The main problem comes from the detection method. During the day and depending on the weather, a huge number of false detections is currently recorded by a single camera. The reflections of the sun on rain drops, the snow or dust

on the lens can be associated to a moving bright source by the software. In this situation, the number of false alarms for a given camera can exceed the hundred per day. An example of such false detections is given in *Figure 1*. The current version of the *Freeture* software (Audureau et al., 2014) only retains the pixels with intensity above a defined threshold (set in function of the background value). If a difference between the clusters of bright pixels from two consecutive frames is noticed, the images are stored and a message is sent to the users to warn about a possible detection.

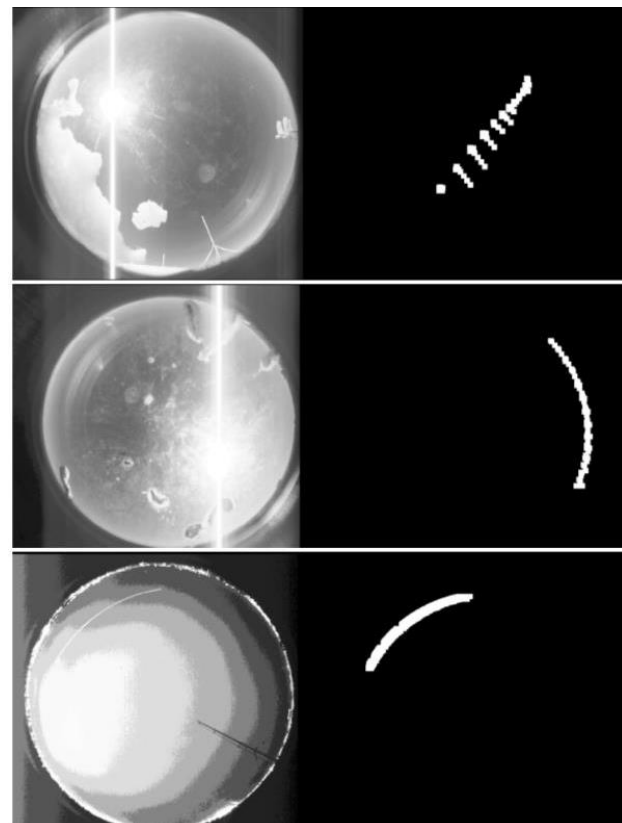


*Figure 1* – Example of false detections recorded by FRIPON. On the left: images provided by the cameras. On the right: bright pixels above the threshold in intensity.

## Towards a solution

The huge variety of shapes, velocity and intensity levels of the events prevent too easily suppress the false detections. The best way to reduce the number of false alarms will then be to use one of the strengths of the FRIPON network: the interconnection. Indeed, if a camera records an event, other detections are checked in the data of all the other cameras of the network for the corresponding time. If another camera has also recorded an event, then the user is alerted. It will be easy to modify this process to only warn the user if an event has been recorded by at least three (or more) cameras during the day. This should highly decrease the number of false detections, since the weather conditions are usually variable for three different locations of the stations. The possibility of filtering the events depending on the shape or the velocity is also investigated.

To develop a reliable detection algorithm, it would be necessary to own several images of daytime fireballs. Currently, the FRIPON network does not possess enough data to test the daylight detection software. The 24<sup>th</sup> of June 2015 at 12<sup>h</sup>40<sup>m</sup> UT, two witnesses in the south of France have reported observations of a bright fireball to the IMO. At the same time, the Pic du Midi station was recording photographic images for test purposes. At the time of the event, a bright trail crossing the sun was recorded by the camera; this trail is not present in the other images taken a few minutes before or after (cf. *Figure 2*, first image). This case may be the first daylight fireball detected by FRIPON; unfortunately, as no video of the fireball was recorded, we have no certainty about the nature of this trail.

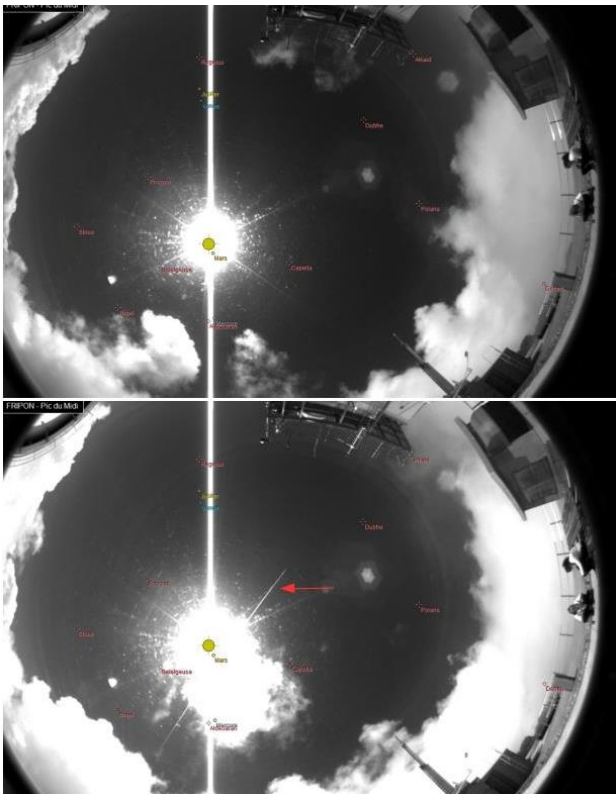


*Figure 2* – Bottom: photographic record of a potential daylight fireball recorded by the Pic du Midi station, 24/06/2015, 12<sup>h</sup>40<sup>m</sup> UT. Top: image of the same FOV taken a few minutes before.

A perfect solution to test the complete daylight reduction process of FRIPON would be to observe an atmospheric reentry during the day. Indeed, the reentry of well-observed space debris or asteroids would offer an exceptional occasion to test the software detection of the cameras, as well as the orbit computation and the fragmentation modeling of the object. Although quite rare, these events have an indisputable scientific value. That is why the FRIPON team was very interested by the atmospheric reentry of the space debris WT1190F, the 13<sup>th</sup> of November 2015.

## The observation campaign of the WT1190F reentry

WT1190F was a man-made object that impacted the Earth over the Indian Ocean near the Sri Lankan coasts in November 2015. The debris was predicted to enter into the atmosphere during the day, at 06<sup>h</sup>18<sup>m</sup> UT, with an initial velocity of 10.61 km/s and an entry angle of about 20°. The estimated trajectory of WT1190F is illustrated at *Figure 3*. Because of the geometrical configuration of the trajectory, the reentry allowed a double-station observation from the shore. This offered the opportunity of a precise determination of the fragmentation altitude and increased the interest of observing the phenomenon.

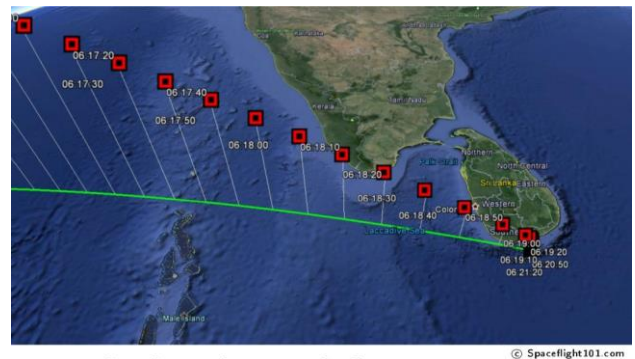


*Figure 3* – Reentry trajectory of WT1190F.

A FRIPON campaign was set up in emergency (in less than ten days) to observe the reentry of WT1190F. Despite of the lack of local contacts in the country, the bad weather forecast and the little experience of the observers, two stations at a distance of 100 km from each other were successfully installed at Sri Lanka in a record time. Two IMCCE members (A. Egal and M-K. Kwon) reached the south of Sri Lanka just a few days after deciding to observe the reentry, with a FRIPON camera and two Watec cameras (one for the trajectory and the other one for spectroscopic purposes) for each station. The equipment was limited by the weight allowed for cabin luggage. Thanks to the help of amateurs, the two observers managed to install the stations safely and in time for the reentry, despite many difficulties encountered in the country. Unfortunately, and regardless of all the efforts put in this campaign, the bad weather conditions have hampered any ground-based observations. The only available images of the reentry were provided by an airborne campaign organized by a SETI-IAC (Jenniskens et al., 2016) team. This mission remains however a perfect example of the value of the

collaboration between scientists and amateurs, without whom this challenge wouldn't have been overcome.

### 3 Conclusion

The daylight detection of fireballs with FRIPON is currently hampered by the massive number of false detections caused by the reflections of the sun on external elements (rain drops, ice, dust, etc.). The comparison of the detections recorded by more than three cameras during the day can be easily performed by the FRIPON network and should highly decrease the number of false alarms. However, it would be very useful to obtain daylight detections to deeply check the detection method and to improve its performance. In order to record some of these images, an observation campaign of the atmospheric reentry of the WT1190F debris was set up in less than 10 days. Thanks to the help of local contacts in Sri Lanka established at this occasion, two observers were able to successfully set up two distant observation stations at the opposite part of the world, with very bad initial conditions, and in a few days only. Despite of the weather which prevented the success of this mission, it was a great technical challenge that highlighted the importance of the collaboration between scientists and amateurs.

### Acknowledgment

We thank Danushka Subath, Subath Amadarasa, Manjula Srinath, Charindu Jayasanka and Nalin Samarasinha very much for their support and their precious help during the installation of the stations.

### References

- Audureau Y., Marmo C., Bouley S., Kwon M.-K., Colas F., Vaubaillon J., Birlan M., Zanda B., Vernazza P., Caminade S. and Gatteccaca J. (2014). "FreeTure, A Free software to capTure meteors for FRIPON". In Rault J.-L., and Roggemans P., editors, *Proceedings of the International Meteor Conference*, Giron, France, 18–21 September 2014. IMO, pages 39–41.
- Colas F., Zanda B., Vaubaillon J., Bouley S., Marmo C., Audureau Y., Kwon M. K., Rault J.-L., Caminade S., Vernazza P., Gattacceca J., Birlan M., Maquet L., Egal A., Rotaru M., Birnbaum C., Cochard F. and Thizy O. (2015). "French fireball network FRIPON". In Rault J.-L. and Roggemans P., editors, *Proceedings of the International Meteor Conference*, Mistelbach, Austria, 27-30 August 2015. IMO, pages 37–40.
- Jenniskens P., Duckworth H. and Grigsby B. (2012). "Daytime Arietids and Marsden sunskirters (ARI, IAU #171)". *WGN, Journal of the IMO*, **40**, 98–100.
- Jenniskens P., Albers J., Koop M. W., Odeh M. S., Al-Noimy K., Al-Remeithi K., Al Hasmi K., Dantowitz R. F., Gasdia F., Löhle S., Zander F., Hermann T., Farnocchia D., Chesley S. R., Chodas P. W., Park R. S., Giorgini J. D., Gray W. J., Robertson D. K. and Lips T. (2016). "Airborne Observations of an Asteroid Entry for High Fidelity Modeling: Space Debris Object WT1190F". *AIAA Science and Technology Forum and Exposition (SciTech 2016)*, 4-8 Jan. 2016, San Diego, CA. 11 pages.
- Rendtel J. (2014). "Daytime meteor showers". In Rault J.-L. and Roggemans P., editors, *Proceedings of the International Meteor Conference*, Giron, France, 18-21 September 2014. IMO, pages 93–97.

# PRISMA

## Italian network for meteors and atmospheric studies

Daniele Gardiol, Alberto Cellino and Mario Di Martino

INAF – Osservatorio Astrofisico di Torino, Pino Torinese, Italia

gardiol@oato.inaf.it

The aim of the PRISMA project is to develop the Italian participation in a network of European observing facilities whose primary targets are bright meteors (the so-called bolides and fireballs) and the recovery of meteorites. Several all-sky cameras have been recently installed in France (FRIPON project), and we propose to do the same in Italy, interconnecting the Italian network with the French one. Such a network is of great interest for the studies of interplanetary bodies and the dynamical and physical evolution of the population of small bodies of the Solar System and for the studies of collected meteorites. Those eventually recovered will be classified and investigated from the petrologic, genetic and evolutionary points of view, analyzed for their spectral characteristics and compared with known asteroids. The possibility to measure the radioactivity of samples shortly after the fall using gamma-ray spectrometers available in the Osservatorio Astrofisico di Torino laboratories, will allow us to reveal the presence of short-lived cosmogenic radioisotopes. PRISMA is also very suitable for the purposes of atmospheric studies. This includes the statistics of cloud coverage and lightning frequencies, as well as the comparison of the optical depth measured using satellites and PRISMA cameras.

### 1 Scientific motivations

#### PRISMA for meteor studies

Meteorites represent samples of Solar System bodies naturally brought to our labs from a variety of different locations. Dynamical studies suggest that most meteorites come from the asteroid main belt, rather than from the closer population of so-called near-Earth asteroids, as commonly believed (Burbine, 2002). However, it is difficult to conclusively identify possible links between some individual asteroids and some meteorite classes. It is therefore important to develop ground-based observations of meteor phenomena to improve our capability of deriving accurate orbits of the small bodies impacting our planet, to monitor a statistically sufficient number of events to study their origin and possibly to recover “fresh” meteorites. The currently open scientific problems for which we can expect to get some important answers from an extensive work of detection of fireballs and recovery of freshly fallen meteorites include the following questions:

- Where do meteorites come from?
- How many parent bodies of known meteorites can we surely identify?
- Can we better understand the mechanisms of delivery from the asteroid main belt?
- What is the abundance of water possibly delivered to the Earth by different classes of asteroids?
- Are there new classes of meteorites that we have not yet discovered?

The latter question is not academic. Actually, many meteorites presently in our collections are “finds” (as opposed to “falls”), *i.e.* meteorites found a significant amount of time after their fall, often weathered having

been exposed to terrestrial alteration, which makes them scientifically less valuable. A way to reliably determine the source regions of meteorites is to witness the falls when they occur. For this purpose, the same event should be detected simultaneously from different directions, in order to be able to derive at the same time the original heliocentric orbit of the impactor and the site of fall of possible meteorites produced by the event. This has been the goal inspiring many observation networks, such as the European Fireball Network in middle-Europe, the NASA All-sky Fireball Network<sup>1</sup> in the USA, and a similar one in Australia<sup>2</sup>. In this context a new generation of detectors optimized for the studies of bright meteors and the establishment of a much wider network of automatic observing stations, with a grid spacing of 60–100 km, operating 24 hours per day, can allow us to obtain a major improvement. The French community (Colas, 2012; Colas 2014) has recently accomplished the first steps forward to start this enterprise (FRIPON, Fireball Recovery and Inter Planetary matter Observation Network)<sup>3</sup>. Doing the same in Italy would give a decisive contribution to a full European network.

#### PRISMA for atmospheric studies

The inherently multi-disciplinary nature of the project makes it appealing to a wide scientific community. In the field of atmospheric science, cloudiness forecasting is a challenge for numerical models. To validate current numerical models of cloud cover it is essential to compare simulations with large amounts of measurements. Data detected by all-sky cameras are useful for this and other branches of atmospheric physics (Arbizu-Barrena, 2015). In this respect PRISMA is

<sup>1</sup> <http://fireballs.ndc.nasa.gov>

<sup>2</sup> <http://fireballsintthesky.com.au>

<sup>3</sup> <http://www.fripon.org>

complementary to traditional weather ground networks, such as the ones operated by Agenzia Regionale Per l’Ambiente (ARPA), Local Governments and other Institutions. The continuous sky monitoring by PRISMA can provide much additional information on the status of the atmosphere, including also statistics of lightning. Finally, the sky’s polarization is sensitive to the aerosol properties in the sky and it is an ideal complementary measurement device in combination with aerosol optical depth measurements.



Figure 1 – Meteorite falls and finds on Italian soil since the beginning of times.

## 2 Project description

### Project description

The project consists of the installation of a network of fireball detectors. We plan to use the same typology of detectors adopted in France in the framework of the FRIPON project, which started operations in early 2016. These detectors are cutting edge technology. The goal of PRISMA is to develop a full Italian network, suitably covering the national territory. The planned camera grid distribution will make it possible to derive the orbital paths of the impactors with an accuracy of the order of 200 meters. The first nodes of the grid will be hosted in North-Western Italy, to be easily interconnected with the FRIPON network. The fireball detectors have a 100% duty cycle, as bright fireballs can be detected even in daytime. The cameras operate at the wavelengths of visible light, with an estimated visual magnitude limit as faint as  $m_v = 2-3$ . Each camera is connected to the internet, and will acquire data at a maximum frequency of 30 frames per second, with recording starting in case of detection of a bright moving source, according to triggering conditions defined by the automatic software of data processing. Every 10 minutes the camera takes a longer single exposure for astrometric calibration and other purposes, including public outreach and further scientific processing, such as for atmosphere studies. Detections and long exposures are automatically

transmitted to the data processing center where they are saved and stored.

Table 1 – Meteorite falls and finds on Italian soil.

Name	Region	Year	
Albareto	Emilia-Romagna	1766	Fall
Alessandria	Piemonte	1860	Fall
Alfianello	Lombardia	1883	Fall
Assisi	Umbria	1886	Fall
Bagnone	Toscana	1904	Find
Barbianello	Lombardia	1960	Find
Barcis	Friuli V.G.	1950	Find
Borgo S.Donino	Emilia-Romagna	1808	Fall
Castel Berardenga	Toscana	1791	Fall
Castenaso	Emilia-Romagna	2003	Find
Castiglione d. Lago	Umbria	1970	Find
Castrovillari	Calabria	1583	Fall
Cereseto	Piemonte	1840	Fall
Collescipoli	Umbria	1890	Fall
Fermo	Marche	1996	Fall
Girgenti	Sicilia	1853	Fall
Lago Valscura	Piemonte	1995	Find
Masua	Sardegna	1967	Find
Messina	Sicilia	1955	Fall
Mineo	Sicilia	1826	Fall
Monte Milone	Marche	1846	Fall
Motta dei Conti	Piemonte	1868	Fall
Narni	Umbria	921	Fall
Noventa Vicentina	Veneto	1971	Fall
Orvinio	Lazio	1872	Fall
Patti	Sicilia	1922	Fall
Piancaldoli	Toscana	1968	Fall
Renazzo	Emilia-Romagna	1824	Fall
Rivolta de’ Bassi	Lombardia	1491	Fall
San Michele	Marche	2002	Fall
Siena	Toscana	1794	Fall
Sinnai	Sardegna	1956	Fall
Tessera	Veneto	2000	Fall
Torino	Piemonte	1988	Fall
Trenzano	Lombardia	1856	Fall
Vago	Veneto	1668	Fall
Valdinizza	Lombardia	1903	Fall
Valdinoce	Emilia-Romagna	1496	Fall
Vigarano	Emilia-Romagna	1910	Fall

### Expected rates

Over Italy we can expect to have about 1 bright meteor every 48 hours. Among these events, according to current estimates (Halliday, 1996), we can expect, in a country as extended as Italy, the recovery rate of meteorites to be somewhere between 2 and 10 per year, these numbers depending critically on whether the corresponding

fireball is seen or not. The actual recovery fraction has been very low in the past (see *Table 1* for a complete list of confirmed Italian meteorites, including the very recent confirmation of Castiglione del Lago, and *Figure 1* for a geographical distribution), only less than 40 meteorites have been recovered (and among them only 32 are falls) since the beginning of times. The proposed fireball network is expected to produce a significant improvement.

### Sites choice

The choice of the sites hosting the network nodes will be done taking into account the strong community of Italian amateur astronomers that operate several small observing stations located in very convenient locations, and our intention to deeply involve secondary schools. This is an excellent opportunity for several amateur teams and schools to work and collaborate with professional researchers following the citizen science and audience engagement philosophies. *Figure 2* shows a preliminary assessment of possible candidate sites in Northern Italy.

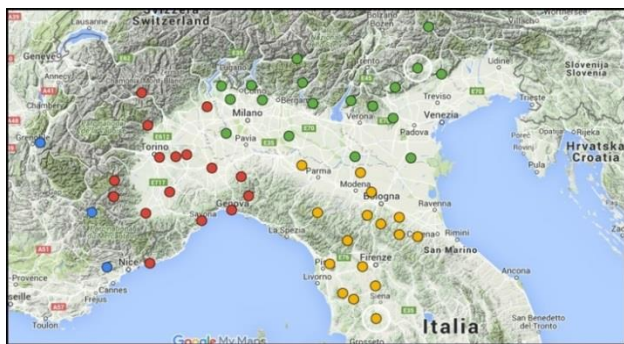


*Figure 2* – Candidate sites for node deployment in Northern Italy. On the left the three FRIPON cameras already operating in France.

### Participating institutes

PRISMA is a project of the Italian National Institute for Astrophysics (INAF), led by INAF-Osservatorio Astrofisico di Torino. Other INAF participating structures are: INAF-Osservatorio Astrofisico di Catania, INAF-Osservatorio Astronomico di Trieste, INAF-Osservatorio Astronomico di Bologna, INAF-Istituto di Radio Astronomia (with the Medicina and Noto sites), INAF-Osservatorio Astronomico di Padova and INAF-IAPS in Rome. Collaborations include regional observatories such as Osservatorio Regionale della Valle d'Aosta<sup>4</sup> (OAVdA) and Osservatorio Polifunzionale del Chianti (OPC, Florence)<sup>5</sup>, as well as several amateur astronomer groups, some of which are already part of small meteor tracking networks. For the atmospheric studies we rely on the Italian Meteorological Society<sup>6</sup> and on the Agenzia Regionale per l'Ambiente<sup>7</sup>, the former being in particular interested in improving the meteorological data on five historical monitoring stations for which long time historical data record exist. Strong collaboration is also under development with universities,

in particular Università di Torino, Università di Firenze and Università di Padova, and with the Consiglio Nazionale delle Ricerche (CNR)<sup>8</sup>. We are developing our outreach activities in contact with Infini.to (Museum of Astronomy and Space – Planetarium of Torino)<sup>9</sup> and with Museo Regionale di Scienze Naturali<sup>10</sup> and Museo Craveri<sup>11</sup>, located in Piedmont, and with Parco Astronomico delle Madonie (Sicily), that soon will begin the activities. *Figure 3* shows the geographical distribution of the currently involved institutes.

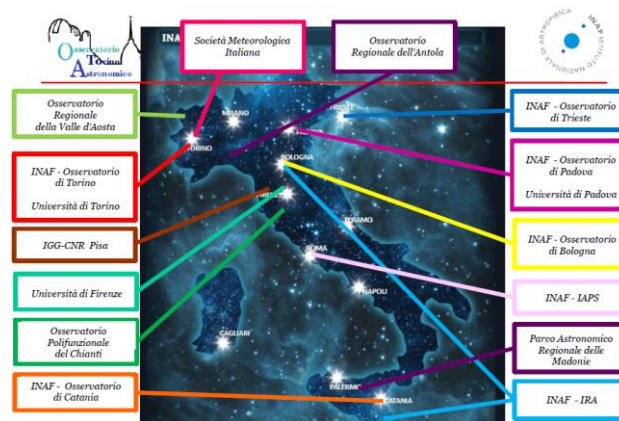


*Figure 3* – Geographical distribution of the PRISMA participating institutes.

### Strategy for network funding and deployment

We are currently looking for funds to realize the project. The natural funder for a scientific project is the Italian Ministry for Education, University and Research (MIUR)<sup>12</sup>, that operates in several ways. The PRIN (Progetti di Ricerca di Interesse Nazionale) is a call that is issued usually once a year, for which we already submit a proposal. Another interesting call is PLS (Piano Lauree Scientifiche)<sup>13</sup>, an educational program which aim is to increase the number of undergraduate students choosing scientific studies in Universities, such as Mathematics or Physics, that should be issued in late summer. A second channel is represented by private bank foundations, as most of them are interested to support scientific research (although mainly in the medical area) and, more interesting for us, educational activities in schools. The bigger bank foundations operate at regional or super-regional level, the smaller ones instead focus their activities in a small territory such as the neighborhood of a single city. Therefore, following this second channel, it is very unlikely to get the entire network funded. We are currently proposing to bank foundations to support regional sub-networks or even single nodes, following a modular approach for the network implementation, so that the smaller sub-networks can be later on integrated to form a whole Italian network.

<sup>8</sup> <http://www.cnr.it>

<sup>9</sup> <http://www.planetarioditorino.it>

<sup>10</sup> <http://www.mrsntorino.it>

<sup>11</sup> <http://www.museocraveri.it>

<sup>12</sup> <http://www.istruzione.it>

<sup>13</sup> <https://laureescientifiche.miur.it>

<sup>4</sup> <http://www.oavda.it>

<sup>5</sup> <http://www.osservatoriodelchianti.it>

<sup>6</sup> <http://www.nimbus.it>

<sup>7</sup> <http://www.arpa.piemonte.gov.it>

### Meteorites analysis facilities

At INAF- Osservatorio Astrofisico di Torino Monte dei Cappuccini laboratory we perform gamma spectrum analysis of meteorite samples (Colombetti, 2013). The HyperPure Germanium detector (see *Figure 4*) allows determining very low emission rates of cosmogenic radioisotopes. A second detector, a NaI scintillator, is used to work in coincidence in order to suppress unwanted signal and noise. Analysis of very recently fallen meteorites (few days) is able to determine the activity of short-lived cosmogenic isotopes, as it was done for the Torino meteorite (Bhandari, 1988). The University of Firenze runs a laboratory for Electronic Microscopy and Micro Analysis (MEMA)<sup>14</sup> where meteorite samples are normally classified after chemical analysis with a Scanning Electron Microscope (SEM) using the Energy Distribution Spectrometry (EDS) technique.



*Figure 4* – A detail of the detector of the Monte dei Cappuccini laboratories in Torino.

### 3 Conclusion

We are just at the beginning of the project, we have already installed a FRIPON camera on the rooftop of our Observatory in Pino Torinese and started acquisition. Currently this camera is connected to the French network, but if we succeed in getting the required funds we will start deploying the Italian network. A web site<sup>15</sup> dedicated to the project is under construction but already accessible.

### References

- Arbizu-Barrena C., Pozo-Vázquez D., Ruiz-Arias J. A. and Tovar-Pescador J. (2015). “Macroscopic cloud properties in the WRF NWP model: an assessment using sky camera and ceilometer data”. *Journal of Geophysical Research: Atmospheres*, **120**, 297–312.
- Bhandari N., Bonino G., Callegari E. and Cini Castagnoli G. (1988). “The Torino Meteorite:

Classification and Cosmogenic Effects”. *Meteoritics*, **23**, 258.

- Burbine T. H., McCoy T. J., Meibom A., Gladman B. and Keil K. (2002). “Meteoritic Parent Bodies: Their Number and Identification”. In Bottke Jr. W. F., Cellino A., Paolicchi P. and Binzel R. P., editors, *Asteroids III*. University of Arizona Press, Tucson, pages 653–667.
- Colas F., Zanda B., Vernazza P., Vaubaillon J., Bouley S., Gattacceca J., Baratoux D., Birlan M., Courne de C., Fieni C., Hutzler A., Jambon A., Maquet L., Mousis O., Rochette P., Strajnic J. and Vachier F. (2012). “(FRIPON) Fireball Recovery and Interplanetary Matter Observation Network”. In *Proceeding of the conference on Asteroids, Comets, Meteors*, Niigata, Japan, 16-20 May 2012. LPI contribution No. 1667, id.6426.
- Colas F., Zanda B., Bouley S., Vaubaillon J., Vernazza P., Gattacceca J., Marmo C., Audureau Y., Kwon M. K., Maquet L., Rault J.-L., Birlan M., Egal A., Rotaru M., Birnbaum C., Cochard F. and Thizy O. (2014). “The FRIPON and Vigie-Ciel networks”. In Rault J.L. and Roggemans P., editors, *Proceeding of the International Meteor Conference*, Giron, France, 18-21 September 2014. IMO, pages 34–38.
- Colombetti P., Taricco C., Bhandari N., Sinha N., Di Martino M., Cora A. and Vivaldo G. (2013). “Low  $\gamma$  activity measurement of meteorites using HPGe-NaI detector system”. *Nuclear Instr. And Methods in Physics Research A*, **718**, 140–142.
- Halliday I., Griffin A. A. and Blackwell A. T. (1996). “Detailed data for 259 fireballs from the Canadian camera network and inferences concerning the influx of large meteoroids”. *Meteoritics and Planetary Science*, **31**, 185–217.

<sup>14</sup> <http://www.mema.unifi.it>

<sup>15</sup> <http://prissma.oato.inaf.it>

# The evolution of ROAN 2016 - Radio surveillance of meteors and determination of reflection points through calculation of the radio path, based on times

Tudor Georgescu<sup>1</sup>, Ana Georgescu<sup>2</sup> and Cezar Lesanu<sup>3</sup>

<sup>1</sup>Elcos Proiect ltd, str. Blandesti nr.24C, sect. 4 Bucuresti, Romania  
teo@elcospro.ro

<sup>2</sup>ICHB, Sos. Mihai Bravu Nr.428 Sec. 3,Bucuresti, Romania

<sup>3</sup>Faculty of Electrical Engineering and Computer Science, Stefan cel Mare University of Suceava, Romania

The article presents the activity calendar describing the steps until the finalization of the Allsky project in December 2016. It presents also the new developed technology for detection and localization of meteors' ionic traces, which is based on information time-stamped on the radio carrier.

The year 2016 is the final one for our project, during which our target is the creation of 25 integrated stations (radio and video, Allsky MK3 type) and to install the ROAN radio beacon. Its location will be the operation base initially, before being moved to an eastern spot, near the Ukrainian border.

The novelty of it all is brought by the newly patented technology of time-stamping.

## 1 Introduction

Our effort to join the community of meteor observers is called Romanian Allsky Network (ROAN) and it was conceived as a research and development project for 2012–2016 (Georgescu et al., 2014; 2015).

The main objective of this project is to formalize a technical solution (Allsky) for a coherent, automated, multisensory national network, 24/24h operating time, for detecting and tracking meteors. This research and development project is led by *Elcos Project ltd* and the consortium includes teams from the “Politehnica” University of Bucharest, the National Research and Development in Optoelectronics Institute, and the Romanian Space Agency.

Three steps are scheduled for the network implementation of ROAN. In the initial phase, the network will have only one layer, formed exclusively of experimental sensors from the main locations. As the project evolves, some of them will be replaced and transferred, based on custody documents, to legal persons or persons that are interested in hosting the sensors (astroclubs, amateur astronomers, schools, universities, planetariums, etc.).

Together with the manufactured and traded sensors from the last phase of the project, the sheltered ones will form the second layer (calibrated sensors, but outside the normal control of the project team). Finally, the third step consists in implementing the sensors received from different sources installed in Romania, which are not calibrated, but can provide data in the format accepted by the main server, and remain online long periods of time.

The locations of main sensors are chosen following several criteria such as the number of clear nights per year, following a systematic study of climatology and

nebulosity; studies concerning this subject were published recently, and the light and radio pollution situation over Romania. The sensors will be placed to avoid human settlements or proximity of radio and light sources. The second criterion is the presence of a 3G/4G/Wimax network for sending data to the main server. The sensors from the secondary network can be installed in inhabited areas and under the direct supervision of enthusiasts or organizations interested in astronomy. The third touchstone involves the possibility of obtaining authorizations from the local agencies and the land's legal owner in order to install the system.

After finalizing the project at end of 2016, the management and finance of ROAN will be transferred to a non-governmental organization – The Romanian Society for Astronomy, without any charges to this organization.

## 2 Technical solution

The technical solution, formalized under the acronym Allsky, is conceived as being a complex of components containing both optical and radio detectors, electronics and power supply, as well as the capability of transferring data in real-time once the detection occurs (*Figure 1*). The technical solution for the optical part is ready – a brand new digital camera with global shutter. Unlike the 2015 version, the block diagram of the standard model has added changes, besides the old CCD camera.

A problem of primordial importance for the Fish Eye lenses mounted on the analog CCTV cameras is that the resolution of the classic CCD sensors is too low; the addition of the FullHD resolution CMOS sensors raises the number of pixels and thus the precision of measurement. Our team has opted for a digital sensor mainly because it provides high resolution, the alternative

being to use multiple cameras at each location, each of them covering a sector of the sky.

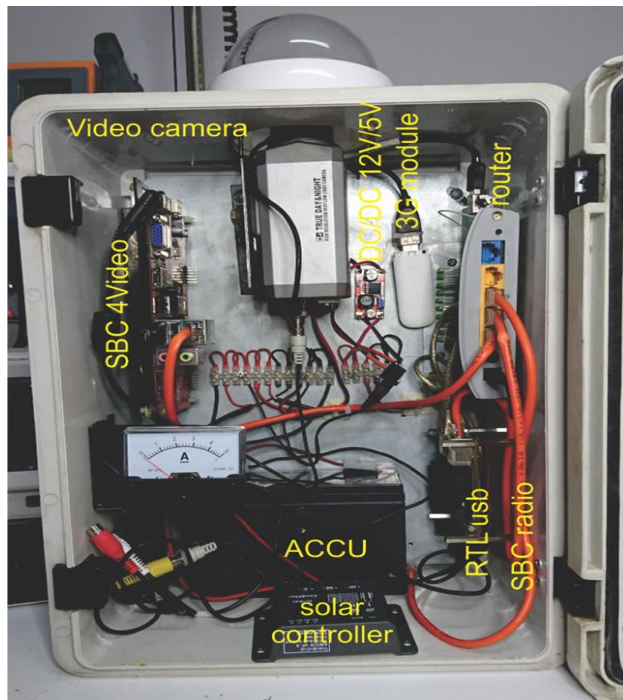


Figure 1 – Picture of the technical solution as a prototype. The dome for optical observation is on the top of this picture, while the names different components are highlighted with yellow.

Thus, we obtain a better solid angle/number of pixels ratio and we maintain a high sensibility, but with huge costs. Within the Allsky project there were 16 types of CCD sensors tested, together with respective systems, to which we add 5 other types of CMOS-global shutter sensors and 2 CMOS with progressive scanning sensors (but with a DSP specialized in elimination deficiencies for the rapid movement of the sensor). These cameras (23 of them) will form, together with the 12 other Allsky-CMOS global shutter MK3, the calibrated camera network that will be installed in the field at the end of the project.



Figure 2 – The cheap polycarbonate transparent domes – as the dome on the left side in this pictures – change their optical properties into a relative short period of time. An upgrade was made for the systems developed at the beginning of Allsky project.

Part of the stations used in the incipient stage of the project have been repaired and upgraded to 2016 standards. We needed to change the polycarbonate

domes, because after only 3 years in use, they started showing aging signs (Figure 2).

In order to optically calibrate all the Allsky stations, we use an instrument that we developed throughout the project and that will be improved in 2016 by adding a new command and control interface for testing/calibrating operations (Georgescu et al., 2015).

### 3 Radio detection new paradigm in ROAN

Initially, the Allsky project included a single radio beacon which would have sent a single time reference. After further analysis, this aspect has been reconsidered through the relocation of radio beacon 1 to the operational base of ROAN in Daia, Romania and the installment of a second radio beacon at a distance of over 425 km from the first one, close to the eastern border of Romanian and the EU. Finally, ROAN will operate two separate radio beacons in a border frequency between 10–30 kHz, so that both can also be received simultaneously by receivers with a relative narrow band.

The system transmits continuously a modulated signal in phase, to ensure the maximum efficient energy. The signal is made up of units of 1000 ms, 950 of which are sync pulses and 50 are info pulses – beacon ID and timestamp.

Modulating the phase of the 50MHz allows minimum quanta of 50 kS/s, but for our initial needs and the use of an RTL-SDR system and a minimal Single board computer (SBC) we prefer to start with only 1000 pulses/s (Figure 3).

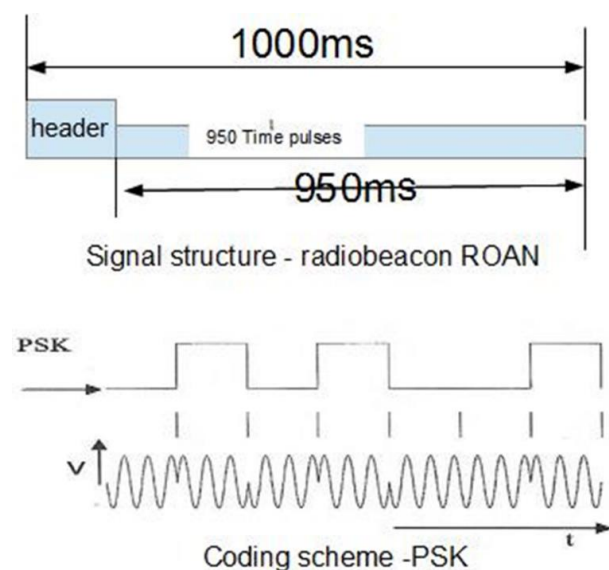


Figure 3 – Pulse and modulated signal of a radio beacon, timestamped by a local GPS.

The received signal is timestamped with a Pulse per second (PPS) type signal from the local GPS. We have two time information entries that allow us to roughly

calculate the path of the wave, from emission to the reflection point and then the receiver.

To eliminate the delays of the emitter modulator, it will be calibrated so to hide lateness during the final processing segment, it being constant and thus easy to eliminate through software.

For measuring the precise position of the radio echo, a simple scheme is presented in *Figure 4*.

The points to be recorded are designed by  $R_1 - R_4$  and are considered as collinear.

We note  $C_1 - C_4$  the distances between receivers and beacons.

The procedure will compute  $P_1 - P_4$  after measuring the distances  $A_i$  and  $B_i$  with  $i = 1$  to 4.

$$P_1 = A_1 + B_1$$

$$P_2 = A_2 + B_2$$

$$P_3 = A_3 + B_3$$

$$P_4 = A_4 + B_4$$

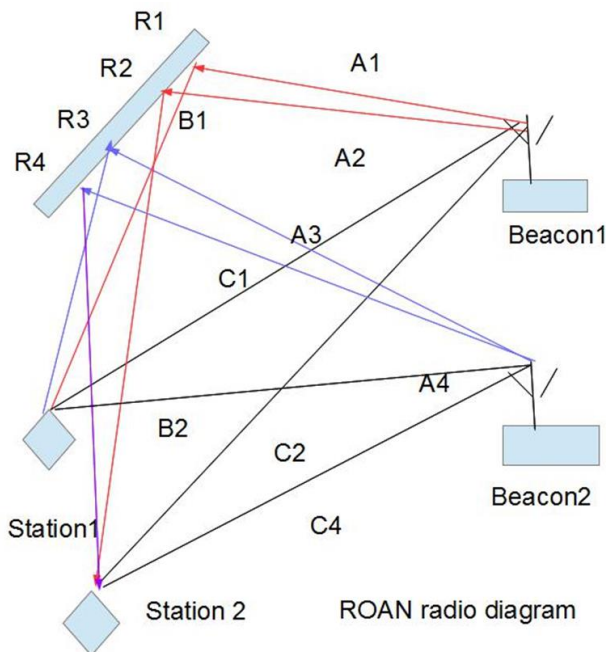


*Figure 4* – Scheme of the upgraded radio detection diagram in the frame of Allsky system.

This solution works only if the network has a good density of receiving stations around the radio beacon.

For the efficient testing of a low-cost solution, we will use in an experimental regime a vertical antenna and the pure continuous wave (CW) way of working (Lesanu, 2016). After finalizing the *Phase Shift Key* (PSK) type modulation system (expected to be operational by September 1<sup>st</sup>, 2016), this antenna will be replaced with a ‘turnstile’ type one.

The major advantage of a solution with two radio beacons is the efficient increase in meteor detection; it also especially allows the entire community in Central and Eastern Europe to make use of eastern signal sources in the maximum efficiency band for meteor detection (approx. 50 MHz).

Right now, ROAN already has an emitter, designed to emit 1 kw CW 24/7, type *italab MD 1000 BX50*. The request for the authorization of this power was turned down (excessive power) by the Romanian authorities – the current request is for a power of 500 W CW, the entire system having a considerable power reserve. The system’s stability is ensured by a *Rohde Schwarz* signal generator, piloted by a GPS receiver through the 10 MHz port (precision better than 0.5 mHz from nominal value).

The GPS receiver allows the extraction of time data as UTC and modulation in phase of the base system (PSK-) so that the reception of it by any ROAN station, or its equivalent, can calculate the length of the radio wave’s path, based on the time difference between the two events. PSK has been chosen as the preferred modulation method because of the maximum power saving, thus sending maximum energy to the receiver and the demodulation for the reception is relatively simple.

Processing of the location data is done on the central ROAN server, based on the data received from as many affiliated ROAN stations as possible. There, the correlation between radio and video data occurs, as well as the estimated meteor trajectories.

## References

- Georgescu T., Georgescu A., Ghită I., Potlog S., Lesanu C., Birlan M., Savastru D., Banică C.-K. and Drăgăsanu C. (2013). “Romanian ALLSKY Network - a systematic approach for meteor detection”. In Gyssens M., Roggemans P. and Zoladek P., editors, *Proceedings of the International Meteor Conference*, Poznan, Poland, 22-25 August 2013. IMO, pages 40–43.
- Georgescu T., Georgescu A., Pancu F., Birlan M., Savastru D., Banica C. K. and Dragasanu C. (2015). “ROAN: A calibration unit for a meteor camera”. In Rault J.-L. and Roggemans P., editors, *Proceedings of the International Meteor Conference*, Mistelbach, Austria, 27-30 August 2015. IMO, pages 98–100.
- Lesanu C. E. (2016). “ROAN Remote radio meteor detection sensor”. In Roggemans A. and Roggemans P., editors, *Proceedings of the International Meteor Conference*, Egmond, Netherlands, 02-05 June 2016. Pages 155–158.

# Video meteor light curve analysis of Orionids and Geminids and developing a method for obtaining the absolute light curves of shower meteors from the single station data

Ljubica Grašić, Nikolina Milanović and Dušan Pavlović

Petnica Meteor Group, Petnica Science Center, Valjevo, Serbia

grasicljubica@gmail.com, nikolinamilanovic@gmail.com,  
dusan.pavlovic@gmail.com

We developed a method for obtaining the absolute light curves of the shower meteors from single station video data. We found that even though the height of a meteor atmospheric trajectory obtained by using this method may have a large error, the absolute light curve shape is preserved. We used our method to calculate the  $F$  parameters of the Orionid and Geminid light curves. The light curves were obtained from the single station video data by the instrument with a limiting sensitivity of  $3.5^m$ . We found that for our sample of the light curves the zenith distance of meteor radiant does not affect the  $F$  parameter for either of the two showers. The value of  $F$  parameter of the Orionids obtained in this paper matches the values obtained by other authors, whilst for the Geminids it is significantly different.

## 1 Introduction

Meteoroids, small bodies of our Solar system, mostly originate from comets and asteroids. They may produce light during their interaction with the Earth's atmosphere. Although they are mostly disintegrated before reaching the ground, studying the processes which are occurring during the interaction can provide some insights into their composition and structure. Understanding the structure of a meteoroid has a great importance in meteor astronomy. For instance, it is a necessary parameter for accurate estimation of the meteoroid mass. Analysis of the meteor light curves (luminous intensity as a function of height) has been used as a valuable technique when it comes to investigating meteoroid structure, and also for testing models and theories about meteoroids and processes which cause the phenomena observed in Earth's atmosphere (e.g. Fleming et al., 1993; Campbell et al., 1999; Murray et al., 2000).

The classical theory of meteors shows good agreement with the photographic data of bright meteors (e.g. Ceplecha et al., 1998). The theory describes a meteoroid as a single body of uniform density and composition. This model predicts that the point of maximum brightness of a meteor is skewed toward the end of its luminous trajectory. Therefore the light curves of such meteors should be asymmetrical.

On the other hand, for fainter meteors the dustball model (formulated by Hawkes and Jones, 1975) shows better agreement with the image intensified video data (e.g. Campbell-Brown and Koschny, 2004). In this case meteoroids are assumed to be composed out of elementary grains coupled together by another more volatile substance. Light is produced only by ablation of the grains. Meteoroids causing such meteors are believed

to be mostly cometary in origin. This model predicts that the maximum brightness point of such meteors occurs approximately at the middle of their luminous trajectories. Therefore the light curves of such meteors are nearly symmetrical.

The shape of a meteor light curve can be quantitatively described by the so-called  $F$  parameter (introduced by Fleming et al., 1993). Fleming et al. (1993) found that the light curves of most sporadic meteors used in the analysis are nearly symmetrical. Campbell et al. (1999) fitted the light curves with a parabola rotated about the point of maximum luminous intensity and also found that the Perseid as well as the Leonid light curves are nearly symmetrical with no significant difference between the showers. Koten et al. (2004) found that the maximum brightness point of the Geminid light curves is skewed to the right more than it is for the light curves of the other four showers they analyzed.

The absolute light curve of a meteor can be acquired if the meteor was observed from at least two stations. It represents the absolute luminous intensity as a function of height, which can be determined with sufficient accuracy by triangulation procedures (e.g. Hawkes et al., 1992).

The number of meteors recorded from two or more stations is generally smaller than the number of meteors recorded from a single station. In this paper we provide a method for determining the absolute light curve shape of a shower meteor using only data acquired from one station. This provides a larger sample of the shower meteor light curves which can play a big role in determining some properties of the specific groups of meteor light curves with statistical methods (e.g. determining the  $F$  parameter for a particular shower). We have applied this method on large samples of video data of Orionids and Geminids, provided by SonotaCo, in

order to calculate the  $F$  parameters for those showers. Also, we studied the  $F$  parameter dependence on the zenith distance of radiant for each of those meteor showers.

## 2 Meteor light curves

### $F$ parameter

A meteor light curve shape can be described by the set of  $F$  parameters (Fleming et al., 1993):

$$F_i = \frac{H_B(M_{max} - i \cdot \Delta M) - H(M_{max})}{H_B(M_{max} - i \cdot \Delta M) - H_E(M_{max} - i \cdot \Delta M)} \quad (1)$$

where  $H(M_{max})$  is the height of the meteoroid at the point of maximum meteor brightness,  $H_B(M_{max} - i \cdot \Delta M)$  and  $H_E(M_{max} - i \cdot \Delta M)$  are the heights where the meteor brightness is  $M_{max} - i \cdot \Delta M$  ( $i \in \{1, 2, \dots, n\}$ ) before and after the maximum brightness point, respectively. Number  $n$  can be arbitrarily chosen (we have used value  $n = 10$ ). Value of  $\Delta M$  is calculated using the expression  $\Delta M = \frac{M_{max} - \max\{M_B, M_E\}}{n}$ , where  $M_B$  and  $M_E$  are absolute magnitudes at the beginning and ending point of the meteor light curve. Most authors have used just the average value of the above set of  $F$  parameters to quantify the shape of a meteor light curve, and the same approach is used in this paper.

If the maximum brightness point is skewed toward the beginning of the light curve, then  $F < 0.5$  and if it is skewed toward the ending of the light curve, then  $F > 0.5$ .

Meteoroids described by the classical single body theory produce light curves with the average value of the  $F$  parameter about 0.7, and for the ones described by the dustball model  $F \approx 0.5$  (Koten et al., 2004). Therefore the larger value of the  $F$  parameter can indicate that a meteoroid is less fragile (as the light curve of the corresponding meteor is more similar to the one predicted by the classical theory) and vice versa.

### A method for obtaining light curves from single station video data

In this paper we have used video data acquired from an instrument with a limiting sensitivity of about  $3.5^m$  and with a frame rate of 30 fps which were provided by SonotaCo. The video data were acquired and processed using *UFO Capture* and *UFO Analyzer* software. The processed data of the recorded meteor were converted into an XML file which contains information about the camera's position, properties, time and date of the recording, etc. It also contains horizontal and equatorial coordinates of the meteor and its apparent luminosity for each frame, information about the duration of the meteor, its angular velocity, the shower it originates from, etc.

In order to calculate the  $F$  parameters from the XML files we have written a Python 3 code. The code processes all XML files which contain the previously mentioned

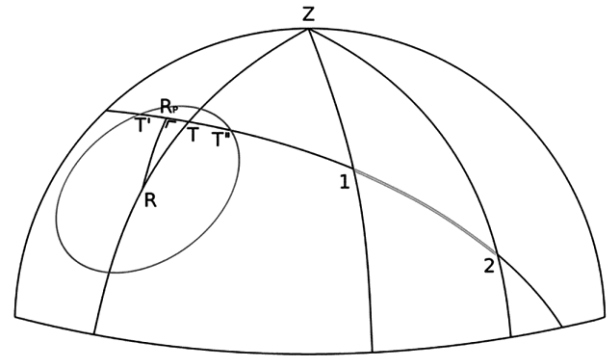


Figure 1 – Illustration of the method for obtaining light curves from single station data:  $R$  – common radiant of the meteor shower,  $R_p$  – its projection on the great circle which contains the beginning (1) and the ending (2) point of the meteor,  $T'$  and  $T''$  – the possible extreme positions of the actual meteor radiant (when  $R_p$  is shifted along the great circle by  $2^\circ$ )

information about meteors belonging to the specific showers. We imported the average meteoroid velocities of those showers, and the equatorial coordinates of shower radiants for every day during the period of its activity in the code. Radiant coordinates for every fifth day during the activity period of those showers were acquired from the IMO website<sup>1</sup>. Linear interpolation was applied in order to obtain its coordinates for every day in between.

We have constructed a great circle on the celestial sphere which contains the beginning and the ending point of the meteor's projection on the celestial sphere (Figure 1). Then we projected the radiant of the corresponding shower ( $R$ ) on that circle, since a shower radiant is an area on the celestial sphere and not a single point. Using the previously calculated meteor radiant ( $R_p$ ), the meteor's duration, the average velocity of the matching shower, and the horizontal coordinates of the beginning and ending points, we find the Cartesian coordinates of the meteor's atmospheric trajectory.

Finally we have obtained the absolute light curve (absolute brightness of the meteor as a function of height) by converting the meteor's apparent brightness to a distance of 100 km for each frame and then performing linear interpolation in order to obtain a continuous curve.

We have applied the 1–2–1 nearest neighbor smoothing in order to obtain a larger number of smooth light curves, but even after that procedure we had to discard over 70% of our sample as the light curves were still not smooth enough and therefore we could not calculate their  $F$  parameters.

### Testing the method

As previously mentioned, the radiant of the shower does not have to be the radiant of a particular meteor belonging to the shower. We used a projection of the shower radiant on the meteor's path on the celestial sphere ( $R_p$  in Figure 1) as the radiant of a meteor in order to calculate the position of its atmospheric trajectory.

<sup>1</sup> <http://www.imo.net/>

Since the shower radiant is an area on the celestial sphere, it is possible that actual radiant of a meteor is shifted by a few degrees along its trajectory relative to the one we have obtained (*Figure 1*). Therefore we have performed trajectory calculation using the meteor radiants shifted by  $2^\circ$  (marked as T' and T'' on *Figure 1*) to see how it affects the obtained meteoroid heights. We found that the beginning and the ending heights can change by up to  $30\text{ km}$  when the meteor radiant shifting is performed in both directions relative to the one we have obtained ( $R_p$ ). However, we have calculated the  $F$  parameters for the light curves obtained by shifting the meteor radiant and established that it affects the change in the  $F$  parameter at the third decimal point.

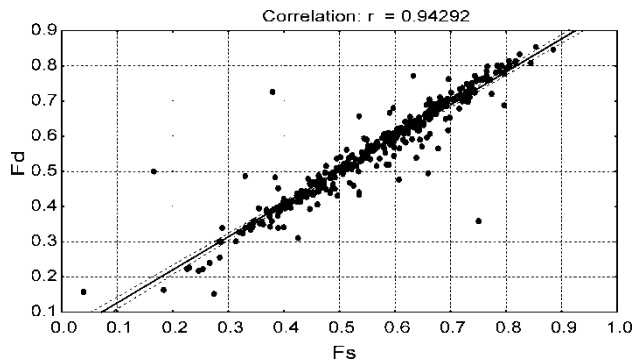


*Figure 2* –  $F$  values for two types of luminous trajectory determination:  $F_s$  – single station approach,  $F_d$  – standard paralactic (double station) approach.

If a meteor is recorded from two or more stations, it is possible to find the Cartesian coordinates of the meteoroid's atmospheric trajectory by the standard triangulation techniques. When recordings of the meteor from two stations are processed using *UFO Analyzer*, its atmospheric trajectory can be obtained by using the *UFO Orbit* software. We have compared the  $F$  parameters of the light curves obtained using our method (single station

data) with those we have obtained using the atmospheric trajectories calculated with *UFO Orbit* (double station data) for the same meteors. We found no statistically significant difference. Also, the correlation factor between  $F$  parameters obtained in these two different ways for our sample of 351 meteors recorded from two stations is  $r = 0.94242$  (*Figure 2*).

### 3 Results

We have calculated the  $F$  parameters for our samples of Orionid and Geminid meteors recorded from two stations (by using data processed with *UFO Orbit*). We divided the sample of Orionids into two categories with equal number of meteors: the first one containing the meteors with lower radiant and the other one containing meteors with higher radiant. We have done the same with our sample of Geminids. We found no statistically significant difference between the  $F$  parameters of these two groups for both showers. We have also created two groups from the double station sample of Orionids by taking one sixth of meteors with the highest radiant and one sixth with the lowest radiant. We found no statistically significant difference between the  $F$  parameters of meteors in these two groups (*Table 1*). Since we have established that for the double station sample of Orionids and Geminids the zenith distance of a meteor does not affect the value of its  $F$  parameter in a statistically significant way, we have calculated the  $F$  parameters of the whole sample of meteors using only the single station data (by applying our method) for both showers. For Orionids we obtained  $F = 0.548 \pm 0.006$  and for Geminids  $F = 0.511 \pm 0.03$ . We found a statistically significant difference in the  $F$  parameters of our samples of Orionids and Geminids by using only single station data. We have also calculated the  $F$  parameters of the samples of Orionids and Geminids recorded from two stations (by using *UFO*

*Table 1* – Results for the mean  $F$  parameter and its standard error for meteors of the same shower with higher ( $F_1$ ) and lower ( $F_2$ ) radiant, and t-statistics for compared groups.

Compared groups	N	$F_1$	$F_2$	t	$t_{0.05}$
Orionids – high vs. low radiant	157	$0.558 \pm 0.012$	$0.563 \pm 0.012$	0.3719	1.9679
Orionids – highest vs. lowest radiant	51	$0.58 \pm 0.03$	$0.58 \pm 0.02$	0.3139	1.9842
Geminids – high vs. low radiant	18	$0.53 \pm 0.04$	$0.55 \pm 0.04$	0.2140	2.0311

$N$  is the number of meteors in each group used in the analysis,  $t$  is the t-value obtained by comparing the two groups,  $t_{0.05}$  is the critical t-value for a significance level  $p = 0.05$ . The sample of all absolute light curves is obtained from double station data by standard triangulation techniques.

*Table 2* – Results for the mean  $F$  parameter and its standard error for Orionids ( $F_O$ ) and Geminids ( $F_G$ ), and the t-statistics for the two showers.

Approach for determining luminous trajectory	$N_O$	$F_O$	$N_G$	$F_G$	t	$t_{0.05}$
From single station data	845	$0.548 \pm 0.006$	244	$0.511 \pm 0.011$	3.2711*	1.6489
From double station data	315	$0.561 \pm 0.008$	36	$0.54 \pm 0.03$	0.8128	2.0181

We used the same notation as in *Table 1*. A statistically significant difference is marked with \*.

Orbit). In this case for the Orionids we obtained  $F = 0.561 \pm 0.008$  and for the Geminids  $F = 0.54 \pm 0.03$  and we found no statistically significant difference between the  $F$  parameters of the two showers (Table 2).

## 4 Conclusion

We have developed a method to obtain the absolute light curves of meteors by using only information which can be acquired from single station video data of a shower meteor. We have tested the method by comparing the  $F$  parameters obtained by using our method with the values obtained using the double station video data of the same meteors.

We found that for our samples of Orionid and Geminid meteors the zenith distance of the radiant does not affect the value of the  $F$  parameter. We have calculated the  $F$  parameters of Orionids and Geminids using the method we have developed and found a statistically significant difference between the  $F$  parameters of these two showers. Yet, the obtained  $F$  parameter of Orionids is larger than the one of Geminids which is in contradiction with the model predictions. The obtained value of the  $F$  parameter of the Orionids ( $F = 0.548 \pm 0.006$ ) matches the value obtained by Koten et al. (2004),  $F = 0.545 \pm 0.012$  but the value of the  $F$  parameter of the Geminids ( $F = 0.511 \pm 0.03$ ) significantly differs from the one obtained in the same paper ( $F = 0.583 \pm 0.016$ ). A possible reason for the difference is that we have applied our analysis on the data acquired by an instrument with much lower limiting sensitivity ( $3.5^m$ ) then the one used by Koten et al. (2004) –  $5.5^m$ . In order to test this hypotheses we would need to apply our method for obtaining the  $F$  parameters of light curves acquired by an instrument with higher limiting sensitivity (e.g.  $5.5^m$ ). Also we could calculate the  $F$  parameter of the part of the light curve with a meteor brightness larger than  $3.5^m$  and compare it to the  $F$  parameter of the whole light curve. This should be done especially for the Geminids as the  $F$  parameter of the Geminids obtained in this paper differs significantly from the values obtained by other authors.

## Acknowledgment

We are grateful to SonotaCo for providing us with video data information, their patience, and cooperation. We would like to express our gratitude to Vladimir Lukić and Branislav Savić for useful ideas and suggestions. Thanks to Viktor Kerkez for helping us with the adaptation of the Python 3 code for operating on computers used by SonotaCo.

## References

- Campbell M., Hawkes R. L. and Babcock D. (1999). “Light curves of shower meteors: implications for physical structure”. In Baggaley W. J. and Porubcan V., editors, *Meteoroids 1998 Proceedings of the International Conference*, Tatranska Lomnica, Slovakia, August 17-21, 1998. Astronomical Institute of the Slovak Academy of Sciences, pages 363–366.
- Campbell-Brown M. D. and Koschny D. (2004). “Model of the ablation of faint meteors”. *Astronomy and Astrophysics*, **418**, 751–758.
- Ceplecha Z., Borovička J. and Elford W. G. (1998). “Meteor Phenomena and Bodies”. *Space Science Reviews*, **84**, 327-471.
- Fleming F. E. B., Hawkes R. L. and Jones J. (1993). “Light curves of faint television meteors”. In Štohl J. and Williams I. P., editors, *Meteoroids and their parent bodies, Proceedings of the International Astronomical Symposium*, Smolenice, Slovakia, July 6-12, 1992. Astronomical Institute, Slovak Academy of Sciences, pages 261–264.
- Hawkes R. L., Mason K. I., Fleming D. E. B. and Stultz C. T. (1992). “Analysis procedures for two station television meteors”. In Ocanas D. and Zimnikoval P., editors, *Proceedings of the International Meteor Conference 1992*, Smolenice, Slovakia, 2-5 July 1992. IMO, pages 28–43.
- Hawkes R. L. and Jones J. (1975). “A quantitative model for the ablation of dustball meteors”. *Monthly Notices of the Royal Astronomical Society*, **173**, 339–356.
- Koten P., Borovička J., Spurný P., Betlem H. and Evans S. (2004). “Atmospheric trajectories and light curves of shower meteors”. *Astronomy and Astrophysics*, **428**, 683–690.
- Murray I. S., Beech M., Taylor M. J., Jenniskens P. and Hawkes R. L. (2000). “Comparison of 1998 and 1999 Leonid light curve morphology and meteoroid structure”. *Earth, Moon, and Planets*, **82–83**, 351–367.

# Consequences of meteoroid impacts based on atmospheric trajectory analysis

Maria Gritsevich<sup>1,2,3,4</sup>

<sup>1</sup>Finnish Geospatial Research Institute, Department of Geodesy and Geodynamics, FI-02431 Masala, Finland  
maria.gritsevich@nls.fi

<sup>2</sup>Ural Federal University, Institute of Physics and Technology, 620002 Ekaterinburg, Russia

<sup>3</sup>Dorodnicyn Computing Centre, Federal Research Center “Computer Science and Control” of the Russian Academy of Sciences, 119333 Moscow, Russia

<sup>4</sup>Moscow State University of Geodesy and Cartography (MIIGAiK), Extraterrestrial Laboratory (MExLab), Gorokhovskiy per. 4, 105064 Moscow, Russia

Using dimensionless expressions, which involve the pre-atmospheric meteoroid parameters, we have built physically based parametrization to describe the changes in mass, height, velocity and luminosity of the object along its atmospheric path. The developed model is suitable to estimate a number of crucial unknown values including the shape change coefficient, ablation rate, and surviving meteorite mass. Besides the model description, we demonstrate its application using the wide range of observational data from meteorite-producing fireballs appearing annually to larger scale impacts. In particular, this approach enabled us to recently recover the Annama meteorite which was observed from 3 stations of the Finnish Fireball Network on 19 April 2014.

## 1 Introduction

One of the important steps in the prediction of an impact threat to Earth raised by potentially hazardous asteroids is the understanding and modeling of the processes accompanying the object’s entry into the terrestrial atmosphere. Such knowledge enables characterization, simulation and classification of possible impact consequences. For observed meteor events the reconstructed atmospheric trajectory is the key to deriving the pre-impact meteoroid’s orbit in the Solar System on the one hand (e.g. Dmitriev et al., 2015), while on the other hand, it is also a requirement for dark flight simulations which enable us to follow any surviving meteorite fragments all the way down to the ground (Gritsevich et al., 2014a).

Interestingly, out of a total over 50000 meteorites currently known to science, only about 25 were recorded instrumentally with the potential to derive their atmospheric trajectories and pre-impact Solar System orbits. The same is true for the observations of meteors, which bring thousands of new registrations per month to existing databases, but rarely, if not exceptionally, do they add to the meteorite recovery records. Thus, these unique cases deserve a thorough examination by different techniques – not only to ensure that we are able to match the model with the observations, but also to enable the best possible interpretation scenario and facilitate the robust extraction of key characteristics of a meteoroid based on the available data.

## 2 A solution to the inverse problem of matching the atmospheric trajectory

The change in main fragment’s mass and height can be approximated as functions of velocity using the following dependencies (Gritsevich, 2007; 2009):

$$m = \exp(\beta(1 - v^2)/(\mu - 1)) \quad (1)$$

$$y = \ln(2\alpha) + \beta - \ln(\bar{E}i(\beta) - \bar{E}i(\beta v^2)) \quad (2)$$

Detailed naming conventions and basic definitions for all variables and parameters used, and the description of the special function  $\bar{E}i(x)$  is provided e.g. in (Gritsevich, 2009; Gritsevich and Koschny, 2011; Bouquet et al., 2014; Lyytinen and Gritsevich, 2016). We provide a brief summary also in the *Appendix* to this paper. As a rule, we use capital letters for the dimensional variables (e.g.  $M$  for the mass in kg) and small letters for the dimensionless variables (e.g.  $m$  for the mass ranging between 0 and 1, referring to the mass  $M$  normalized by its pre-atmospheric value  $M_e$ ). The equations (1) – (2) rely on three dimensionless quantities  $\alpha$ ,  $\beta$ , and  $\mu$ , which are unique for the subgroup of meteor events with similar aerodynamic and friability properties. These parameters are introduced within a dimensional analysis concept (Stulov, 1997).

The ballistic coefficient,  $\alpha$ , describes the drag properties of the meteoroid. It is proportional to the mass of the atmospheric column a meteoroid has to penetrate to reach the ground, to the pre-atmospheric meteoroid mass,  $M_e$ .

The parameter  $\beta$  corresponds to the mass loss rate and can also be linked to the ablation coefficient.

The shape change coefficient,  $\mu$ , may be estimated through light curve analysis (Gritsevich and Koschny, 2011; Bouquet et al., 2014). It reflects the meteoroid's rotation rate and it takes into account the changes in the meteoroid's shape along its trajectory.

The inverse problem of finding the  $(\alpha, \beta)$  pair, that corresponds to the particular case, can be solved by the least-squares method by matching Equation (2) to the set of  $(y_i, v_i)$  values obtained at  $n$  trajectory points along the observed visual path of the fireball, as previously described in (Gritsevich, 2008; 2009) where this method was also applied to a number of observations. Moreno-Ibáñez et al. (2015) provide a grounded justification of the method by calculating terminal height values and comparing them to the observations. In addition, it is possible to use the method with appropriate modifications under condition of an arbitrary atmosphere model (Lyytinen and Gritsevich, 2016).

### 3 General statistics and possible impact consequences

The model is used to estimate a number of crucial unknown values based on meteor observations, including the pre-atmospheric mass, ablation rate, and surviving meteorite mass. It is also applicable in the prediction of the terminal height of the luminous portion of flight and therefore, the duration of the fireball (Moreno-Ibáñez et al., 2016a). We also demonstrate application of the model using the wide range of observational data from meteorite-producing fireballs appearing annually (such as the Annama, Košice and Neuschwanstein fireballs) to larger scale impacts (such as the Chelyabinsk, Sikhote-Alin and Tunguska events). We show that the proposed physical parametrization is adequate to classify the possible consequences of meteoroid impacts. In the  $(\ln \alpha, \ln \beta)$  plane the obtained results evidently group together (i) larger events, resulting in crater formation, (ii) meteorite-producing fireballs, and (iii) fully ablated meteor events with no surviving terminal mass. These results support corresponding criteria derived in analytical way (Gritsevich et al., 2012; 2013). In particular, it is easy to explain why no craters and no meteorites were found in case of Tunguska.

This approach enabled us to reliably identify and promptly recover the Annama meteorite fall which was observed from 3 stations of the Finnish Fireball Network on 19 April 2014 (Gritsevich et al., 2014a,b; Trigo-Rodriguez et al., 2015; Kohout et al., 2015; Lyytinen and Gritsevich, 2016). *Figure 1ab* partly demonstrates our results using the large statistical data samples available from the Prairie Network (USA) and the *Meteorite Observation and Recovery Project* (MORP, Canada), see also (Turchak and Gritsevich, 2014; Moreno-Ibáñez et al., 2016b) for more data points and relevant conclusions.

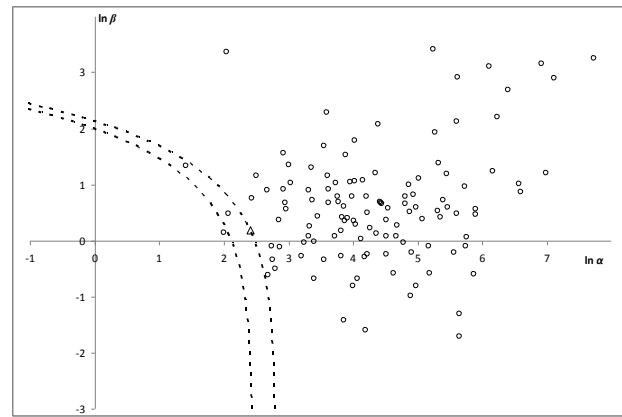


Figure 1a – Distribution of the derived  $\alpha$  and  $\beta$  parameters for the Prairie Network fireballs.  $\Delta$  - Lost City meteorite. See also Moreno-Ibáñez et al. 2016b for relevant details.

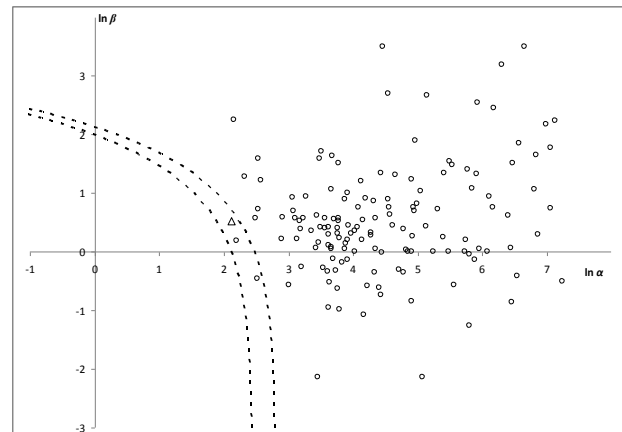


Figure 1b – Distribution of the derived  $\alpha$  and  $\beta$  parameters for the MORP fireballs.  $\Delta$  - Innisfree meteorite. See also Moreno-Ibáñez et al. 2016b for relevant details.

#### Appendix A: List of symbols

$\alpha$	= ballistic coefficient
$\beta$	= mass loss parameter
$\gamma$	= slope between horizon and the trajectory
$\rho_0$	= gas density at sea level
$\rho_a$	= gas density
$\rho_m$	= meteoroid bulk density
$A$	= shape factor of meteoroid
$A_e$	= pre-entry shape factor of meteoroid
$c_d$	= drag coefficient
$c_h$	= heat-transfer coefficient
$h$	= height
$H^*$	= effective destruction enthalpy
$h_0$	= scale height
$M$	= meteoroid mass
$M_e$	= pre-entry meteoroid mass
$n$	= number of considered points along the trajectory
$S$	= middle section area of meteoroid
$S_e$	= pre-entry middle section area of meteoroid
$t$	= time
$V$	= velocity
$V_e$	= pre-entry velocity
$\mu$	= shape change coefficient

**Appendix B: Dimensionless quantities**

$$y = h/h_0$$

$$v = V/V_e$$

$$m = M/M_e$$

$$A_e = \frac{S_e \rho_m^{2/3}}{M_e^{2/3}}$$

$$\alpha = 0.5c_d \frac{\rho_0 h_0 S_e}{M_e \sin \gamma}$$

$$\beta = 0.5(1 - \mu) \frac{c_h V_e^2}{c_d H^*}$$

$$\mu = \log_m \frac{S}{S_e}$$

$$\Delta = \bar{\text{Ei}}(\beta) - \bar{\text{Ei}}(\beta v^2)$$

$$\Delta_i = \bar{\text{Ei}}(\beta) - \bar{\text{Ei}}(\beta v_i^2) = -2 \ln v_i + \sum_{k=1}^{\infty} \frac{\beta^k}{k \cdot k!} (1 - v_i^{2k})$$

$$(\Delta_i)'_{\beta} = \sum_{k=1}^{\infty} \frac{\beta^{k-1}}{k!} (1 - v_i^{2k})$$

$$(\Delta_i)''_{\beta} = \sum_{k=2}^{\infty} \frac{\beta^{k-2}}{(k-2)! \cdot k} (1 - v_i^{2k})$$

**Appendix C: Special mathematical function  $\bar{\text{Ei}}(x)$**

The exponential integral  $\bar{\text{Ei}}(x)$ , which is defined for real nonzero values of  $x$  as:

$$\bar{\text{Ei}}(x) = \int_{-\infty}^x \frac{e^z dz}{z}.$$

The integral has to be understood in terms of the Cauchy principal value, due to the singularity in the integrand at zero.

Integrating the Taylor series for function  $e^{-z}/z$ , and extracting the logarithmic singularity, we can derive the following series representation for  $\bar{\text{Ei}}(x)$  for real values of  $x$  (see e.g. (Abramovitz and Stegun, 1972)):

$$\bar{\text{Ei}}(x) = c + \ln x + \sum_{n=1}^{\infty} \frac{x^n}{n \cdot n!}, x > 0,$$

where  $c$  is the Euler–Mascheroni constant (also called Euler’s constant). It is defined as the limiting difference between the harmonic series and the natural logarithm:

$$c = \lim_{n \rightarrow \infty} \left( \sum_{k=1}^n \frac{1}{k} - \ln n \right) \approx 0.5772.$$

**Acknowledgments**

The author warmly thanks many colleagues for their valuable support. The integration of the described methods into the software “Meteor Toolkit” (Dmitriev et al., 2015) was carried out at MIIGAiK and supported by the Russian Science Foundation project “Study of

fundamental geodetic parameters and relief of planets and satellites”, No. 14-22-00197.

**References**

Abramovitz M. and Stegun I. A. (Eds.) (1972). “Handbook of Mathematical Functions with Formulas, Graphs, and Mathematical Tables”. New York, Dover Publications.

Bouquet A., Baratoux D., Vaubaillon J., Gritsevich M. I., Mimoun D., Mousis O. and Bouley S. (2014). “Simulation of the capabilities of an orbiter for monitoring the entry of interplanetary matter into the terrestrial atmosphere”. *Planetary and Space Science*, **103**, 238–249.

Dmitriev V., Lupovka V. and Gritsevich M. (2015). “Orbit determination based on meteor observations using numerical integration of equations of motion”. *Planetary and Space Science*, **117**, 223–235.

Gritsevich M. I. (2007). “Approximation of the Observed Motion of Bolides by the Analytical Solution of the Equations of Meteor Physics”. *Solar System Research*, **41**, 509–514.

Gritsevich M. I. (2008). “The Pribram, Lost City, Innisfree, and Neuschwanstein Falls: An analysis of the Atmospheric Trajectories”. *Solar System Research*, **42**, 372–390.

Gritsevich M. I. (2009). “Determination of Parameters of Meteor Bodies Based on Flight Observational Data”. *Advances in Space Research*, **44**, 323–334.

Gritsevich M. and Koschny D. (2011). “Constraining the luminous efficiency of meteors”. *Icarus*, **212**, 877–884.

Gritsevich M. I., Stulov V. P. and Turchak L. I. (2012). “Consequences for Collisions of Natural Cosmic Bodies with the Earth Atmosphere and Surface”. *Cosmic Research*, **50**, 56–64.

Gritsevich M. I., Stulov V. P. and Turchak L. I. (2013). “Formation of Large Craters on the Earth as a Result of Impacts of Natural Cosmic Bodies”. *Doklady Physics*, **58**, 37–39.

Gritsevich M., Lyytinen E., Moilanen J., Kohout T., Dmitriev V., Lupovka V., Midtskogen V., Kruglikov N., Ischenko A., Yakovlev G., Grokhovsky V., Haloda J., Halodova P., Peltoniemi J., Aikkila A., Taavitsainen A., Lauanne J., Pekkola M., Kokko P., Lahtinen P. and Larionov M. (2014a). “First meteorite recovery based on observations by the Finnish Fireball Network”. In Rault J.-L. and Roggemans P., editors, *Proceedings of the International Meteor Conference*, Giron, France, 18-21 September 2014. IMO, pages 162–169.

- Gritsevich M., Lyytinen E., Kohout T., Moilanen J., Midtskogen S., Kruglikov N., Ischenko A., Yakovlev G., Grokhovsky V., Haloda J., Halodova P., Lupovka V., Dmitriev V., Peltoniemi J., Aikkila A., Taavitsainen A., Lauanne J., Pekkola M., Kokko P. and Lahtinen P. (2014b). “Analysis of the bright fireball over Kola peninsula on April 19, 2014 followed by successful meteorite recovery campaign”. *Meteoritics and Planetary Science*, **49**, 77th Annual Meeting of the Meteoritical Society, held September 7-12, 2014 in Casablanca, Morocco. LPI Contribution No. 1800, id.5369.
- Kohout T., Gritsevich M., Lyytinen E., Moilanen J., Trigo-Rodríguez J. M., Kruglikov N., Ishchenko A., Yakovlev G., Grokhovsky V., Haloda J., Halodova P., Meier M. M. M., Laubenstein M., Dimitrev V. and Lupovka V. (2015). “Annama H5 Meteorite Fall: Orbit, Trajectory, Recovery, Petrology, Noble Gases, and Cosmogenic Radionuclides”. *Meteoritics and Planetary Science*, **50**, MetSoc 2015 special issue, # 5209.
- Lyytinen E. and Gritsevich M. (2016). “Implications of the atmospheric density profile in the processing of fireball observations”. *Planetary and Space Science*, **120**, 35–42.
- Moreno-Ibáñez M., Gritsevich M. and Trigo-Rodríguez J. M. (2015). “New methodology to determine the terminal height of a fireball”. *Icarus*, **250**, 544–552.
- Moreno-Ibáñez M., Gritsevich M. and Trigo-Rodríguez J. M. (2016a). “Measuring the terminal heights of bolides to understand the atmospheric flight of large asteroidal fragments”. In Trigo-Rodríguez J. M., Gritsevich M. and Palme H., editors, “*Assessment and Mitigation of Asteroid Impact Hazards*”. Springer, NY, in print.
- Moreno-Ibáñez M., Gritsevich M., Trigo-Rodríguez J. M. and Lyytinen E. (2016b). “Current progress in the understanding of the physics of large bodies recorded by photographic and digital fireball networks”. In Roggemans A. and Roggemans P., editors, *Proceedings of the International Meteor Conference*, Egmond, the Netherlands, 2-5 June 2016. Pages 192–196.
- Stulov V. P. (1997). “Interactions of space bodies with atmospheres of planets”. *Applied Mechanics Reviews*, **50**, 671–688.
- Trigo-Rodríguez J. M., Lyytinen E., Gritsevich M., Moreno-Ibáñez M., Bottke W. F., Williams I., Lupovka V., Dmitriev V., Kohout T. and Grokhovsky V. (2015). “Orbit and dynamic origin of the recently recovered Annama's H5 chondrite”. *Monthly Notices of the Royal Astronomical Society*, **449**, 2119–2127.
- Turchak L. I. and Gritsevich M. I. (2014). “Meteoroids Interaction with the Earth Atmosphere”. *Journal of Theoretical and Applied Mechanics*, **44**, 15–28.

# Synthetic spectra of meteors

Meryem Guennoun<sup>1</sup>, Michel-Andres Breton<sup>3</sup>, Nicolas Rambaux<sup>3</sup>,  
J r mie Vaubaillon<sup>3</sup> and Zouhair Benkhaldoun<sup>1,2</sup>

<sup>1</sup> LPHEA Laboratoire de Physique des Hautes  nergies et Astrophysique, Department of Physics,  
Faculty of Sciences Semlalia, BP: 2390, Marrakech, Morocco  
meryem.guennoun@ced.uca.ma

<sup>2</sup> Oukaimeden Observatory, LPHEA, Facult  des Sciences Semlalia, Cadi Ayyad University, Morocco  
zouhair@uca.ma

<sup>3</sup> Institut de M canique C leste et de Calcul des Eph m rides, UMR8028,  
77 Avenue Denfert Rochereau, 75 014, Paris, France  
michel-andres.breton@obspm.fr, nicolas.rambaux@imcce.fr  
jeremie.vaubaillon@obspm.fr

Synthetic meteor spectra provide information which help to identify the different types of meteorites resulting from a meteor. They also help anticipate what an instrument might observe in a given range of wavelengths. We developed a program that computes synthetic spectra of meteorites for which we know the chemical formula, in the case of plasma in local equilibrium. Three different examples are presented here.

## 1 Introduction

A good quality photograph of a meteor spectrum includes information about the meteor phenomenon. Inspection of the spectral lines that are present gives clues as to the meteor’s composition.

Synthetic spectra of meteors serve to identify spectral lines that haven’t been observed. They help identify types of meteorite resulting from a meteor and help anticipate what an instrument could observe in a given range of wavelengths.

We developed a program `Synthetic.f90` that, given the chemical formula of a meteorite, can compute synthetic spectra.

## 2 The program

### First Step: `SpectrumV3.f90`

In the case of a cool plasma in quasi-local thermodynamic equilibrium, the intensity of a spectral line is:

$$I_{ij} = g_i g_0 E_{ij} A_{ij} e^{-\frac{E_{i0}}{k \cdot T}}$$

where  $E_{ij}$  is the energy level difference between  $i$  and  $j$  of the transition and  $E_{i0}$  is the energy of the upper state.  $A_{ij}$  is the atomic transition probability for spontaneous emission and  $g_i$  is the electric degeneracy factor (Jenniskens et al., 2002). The values of these arguments are taken from the Harvard-Smithsonian center for Astrophysics Kurucz Atomic Line Database (Kurucz and Bell, 1995).

In this step, we considered a wavelengths range of (200,1700) nm and we computed the spectral line intensities for : FeI, FeII, MgI, MgII, Cl, HI, OI, SiI, SI,

KI, CaI, NaI, CII, AlI, CuI, MnI and NiI. For this, we used a FWHM of 1.5 nm.

By convention, MgI is the neutral atom, MgII is the atom ionized once, MgIII is the atom ionized twice.

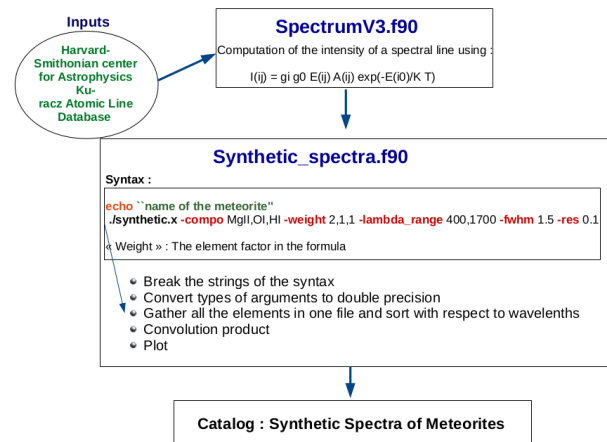


Figure 1 – Schematic overview procedure.

### Second Step : `Synthetic_spectra.f90`

If we know the atomic composition of a meteorite (Table 1), the weights of the elements and the wavelength range we want, we can compute the synthetic spectra. Syntax:

- echo “name of meteorite (X1<sub>n1</sub> X2<sub>n2</sub> X3<sub>n3</sub>)”
- synthetic\_spectra.x
- compo X1,X2,X3,
- weight n1,n2,n3,
- lambda\_range 200,1700
- fhwm 1.5
- res 0.5

The program breaks the strings containing the composition, weights, etc. and recovers each argument before the decimal point until each string is finished. It

then, it converts types of arguments to double precision when needed. After that, the program sorts the line intensities with respect to wavelengths. The last step is to perform the convolution product to have a Gaussian profile instead of discrete lines.

Table 1 – Examples of meteorites with their chemical formula (Zanda, 2014).

Mineralogic group	Pure pole	Chemical formulae
Serpentine	Chrysolite	$Mg_3Si_2O_5(OH)_4$
Amphibole	Anthophyllite	$Mg_7Si_8O_{22}(OH)_2$
Pyroxene	Hedenbergite	$(CaFe)Si_2O_6$
Sulfates	Gypsum	$CaSO_4 \cdot 2H_2O$
Carbonates	Calcite	$CaCO_3$
Oxides	Magnetite	$Fe_3O_4$
Sulphides	Pentlandite	$(FeNi_9)S_8$

### 3 Results

Here are three different examples of synthetic spectra. They are plotted on a logarithmic scale.

### 4 Conclusion

In this program, we compute the spectral line intensity of atoms in the case of a cool plasma with a typical excitation temperature of 4000 K, this plasma is in quasi-local thermodynamic equilibrium. In future studies, we will allow for variations in the plasma (absorption, temperature, etc.) and will also compute the spectral line intensity of molecules.

### References

- Jenniskens P., Tedesco E., Murthy J., Laux C. O. and Price S. (2002). “Space-borne ultraviolet 251-384 nm spectroscopy of a meteor during the 1997 Leonid shower”. *Meteoritics and Planetary Science*, **37**, 1071–1078.
- Kurucz R. and Bell B. (1995). “Atomic Line Data”. CD-ROM No. 23. Cambridge, Mass.: Smithsonian Astrophysical Observatory, 1995.
- Zanda B. (2014). “Les météorites d’hier, science de demain”. *Le Règne Minéral* magazine N°4.

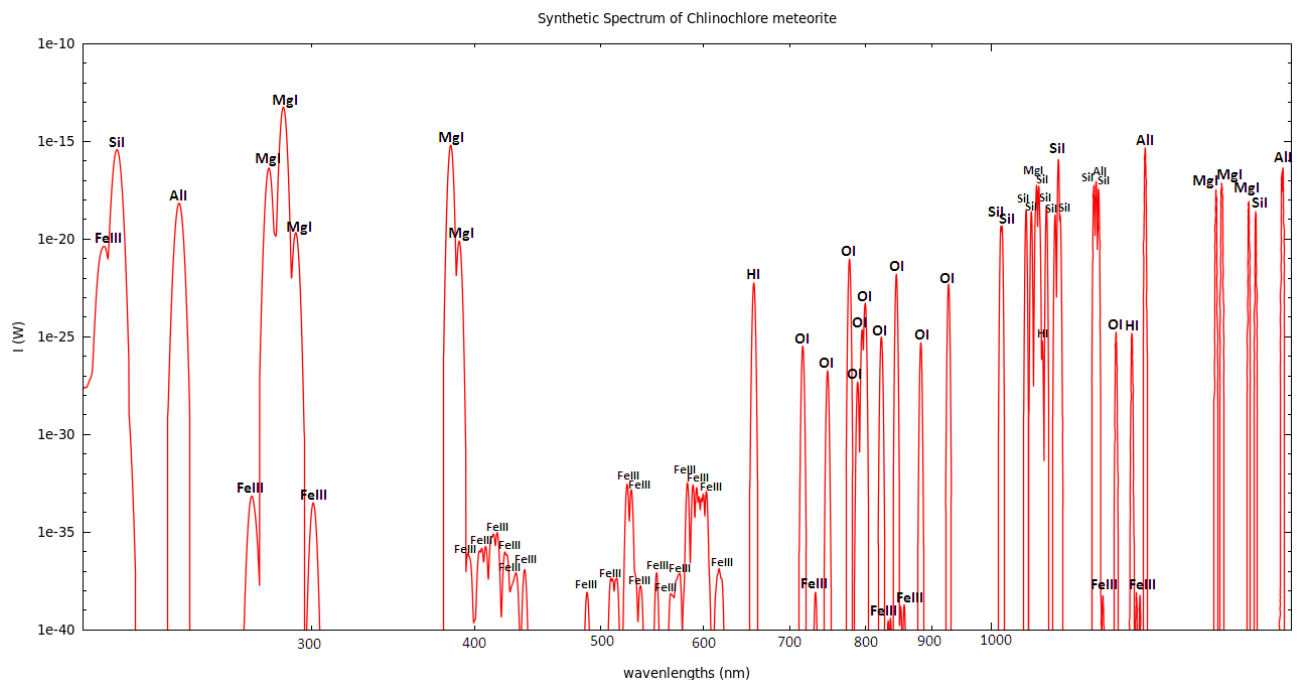


Figure 2 – Example 1: The first example is “Clinocllore” meteorite, with a chemical formula:  $(Mg,Fe^{2+})_5 Al (Si_3Al) O_{10} (OH)_8$ .

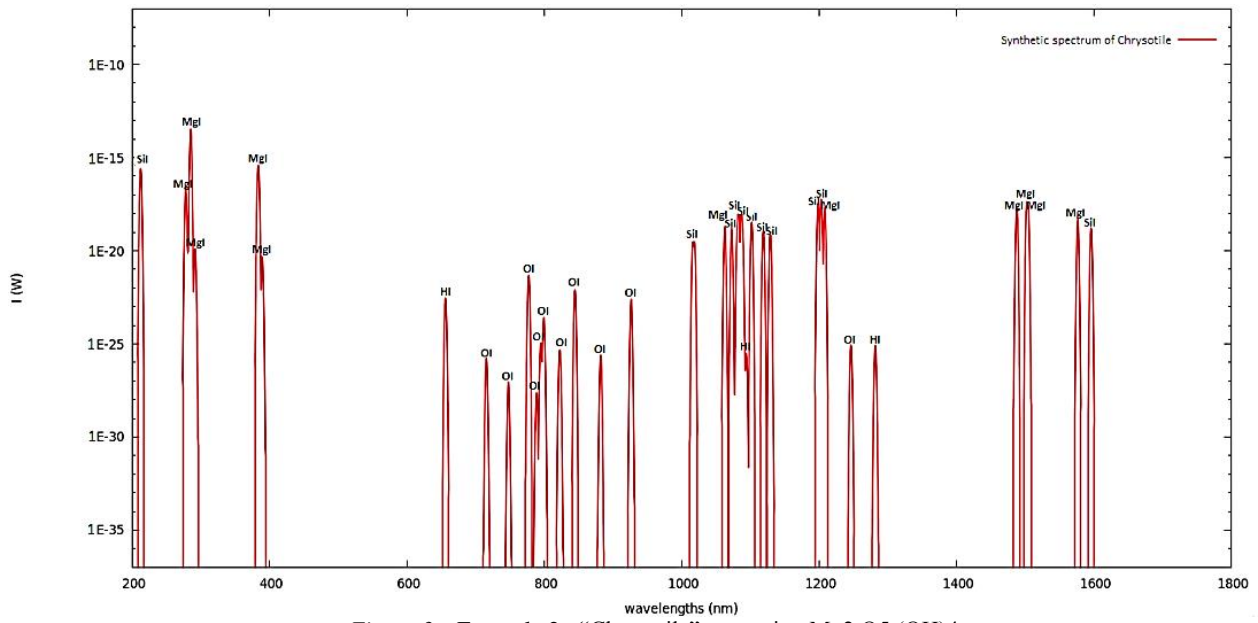


Figure 3 – Example 2 : “Chrysotile” meteorite:  $Mg_2 O_5 (OH)_4$ .

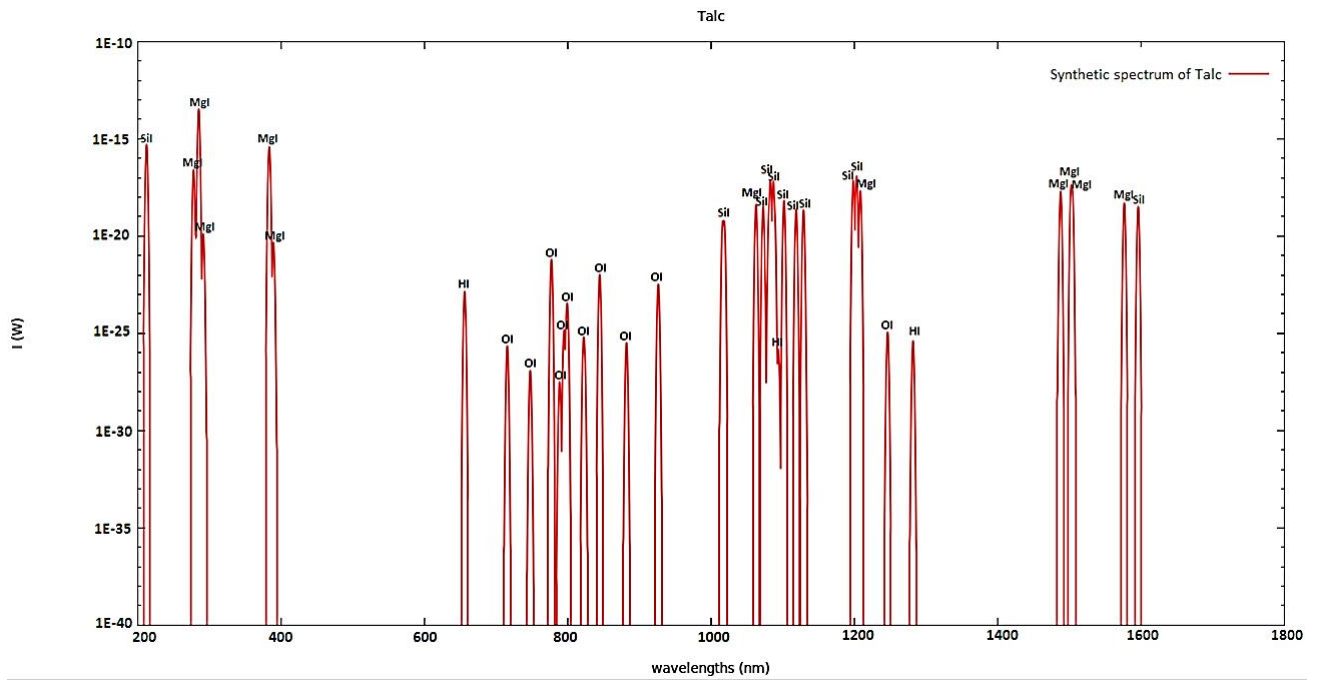


Figure 4 – Example 3 : “Talc”  $Mg_3 Si_4 O_{10} (OH)_2$ .

# Meteoroid streams and comet disintegration

Ayyub Guliyev

Shamakhy Astrophysical Observatory, Azerbaijan

guliyevayyub@gmail.com

The results of the statistical analysis of the dynamic parameters of 114 comets that have undergone nuclear splitting are presented in the article. The list of the objects contains: comets that have split in the period of the observation; data of twin-comets; lost comets with designation D; comets with large-scale structure in the coma. We will describe these comets as “splitted”. Some aspects of the following hypothesis are studied: disintegration of comet nuclei happens as the result of their collision with meteoroid streams. For the verification of this hypothesis, the position of splitted comet orbits relatively to 125 meteor streams from Kronk’s list is analyzed. It was found that the total number of comet orbit nodes located close to the meteor stream planes (for the distances up to 0.1 AU) is  $N = 1041$ . It is shown that if these comets are replaced by randomly selected different comets,  $N$  will be reduced by a factor of approximately three.

## 1 Introduction

The splitting of cometary nuclei into secondary fragments is very interesting and common fact. According to the modern convention, the cause of this phenomenon can be tidal influence of the Sun, gravitational influence of giant planets, and irregular sublimation on the surface of the comet nucleus, their rotation instability, changes of the sector structure of the magnetic field, etc.

Another possible mechanism for comet splitting has been proposed by the author of this article (Guliyev, 2010). According to this mechanism, splitting occurs due to the passage of comet nuclei through meteoroid streams and the impacts received during collisions with meteoroids. Based on some of the arguments, we suggest that the family of well-known short -perihelion comets of Kreutz, Meyer, Kracht, Marsden, etc. have formed in this way. In this paper we will consider some kinematic and statistical aspects of this idea for comets with perihelion distance  $q > 0.1$  a.u.

## 2 Objects and purpose of the study

In the first stage of our study, we tried to make a list of comets that have split or have been seen to disintegrate. Our list includes 114 comets. 26 of them are periodic, 15-disappeared and 73 long-period comets. To compile this list, data from the catalogue by Marsden and Williams (2008), selected MPEC issues for the period 2008–2015, the dissertation of Ibadinov (1998), articles of Boehnhardt (2005), Guliyev and Nabiyeu (2006) have been used. Comparative analysis of the orbits of the elements shows that this group has no significant difference from the total population of comets.

The purpose of this investigation is to analyze the distribution of disintegrated comets orbits relative to the orbital planes of 125 known meteor streams, the data of which are contained in the catalog of Kronk (2014). We will try to prove that the number of nodes of the orbits of splitting comets in the vicinity of some meteoroid streams is much higher than the natural background level. This level will be determined after the test calculations.

## 3 Research methodology

We specifically solve two tasks in this work: the number of nodes of cometary orbits near each of the selected streams will be determined and the existence of an excess of comet orbit nodes near the orbits of meteor streams will be demonstrated.

The first task is solved in the following way. We calculate the orbital elements for each studied comet relative to the plane of the orbit of each selected meteor stream. The start point in the calculation of the angular elements of the comet’s orbit is the accepted value of the ascending node of the selected stream orbit. After that heliocentric distances for the near and distant nodes of the cometary orbits are calculated using the formula:

$$r_c = \frac{a_c(1 - e_c^2)}{1 \pm e_c \cos \omega'} \quad (1)$$

where  $a_c$  and  $e_c$  are the semi-major axis and eccentricity of the orbit of the comet, and  $\omega'$  is the argument of perihelion in a new counting system. The heliocentric distance  $r_s$  to the stream in the direction of nearest node of the comet’s orbit is determined by the formula

$$r_s = \frac{a_s(1 - e_s^2)}{1 + e_s \cos(\omega_s + \Omega')} \quad (2)$$

If the comet’s corresponding orbit node is more distant, then  $r_s$  can be calculated using the following formula

$$r_s = \frac{a_s(1 - e_s^2)}{1 + e_s \cos(\omega_s + \Omega' + 180^\circ)} \quad (3)$$

In (2–3),  $e_s$ , and  $\omega_s$  are the orbital elements of the selected stream, and  $\Omega'$  is the angular value of the node of the comet orbit in the plane of the stream’s orbit. In the next step we introduce into the analysis a value of  $\Delta$ :

$$\Delta = |r_c - r_s|$$

The definition of the parameters  $r_c$ ,  $r_s$  and  $\Delta$  is shown in *Figure 1*. We will try to prove that the number of nodes

Table 1 – Frequency of crossings for the distances  $\Delta < 0.1$  for three groups of comets.

Interval of frequency	0–3	4–6	7–9	10–12	13–15	>15	Total
Frequency for 114 split comets	12	113	340	284	275	19	1043
Frequency for last 114 LPC	129	180	70	0	0	0	379
Frequency for last 114 PC	116	133	30	12	0	0	291

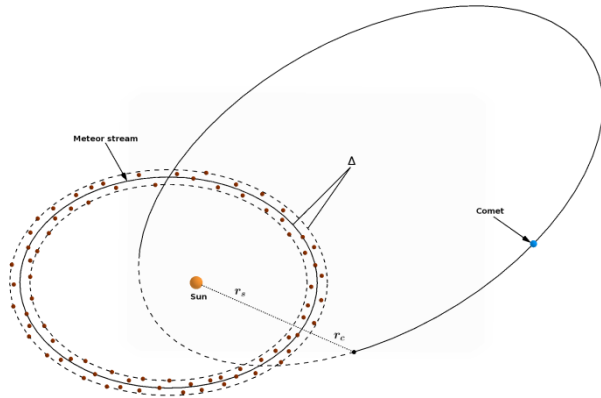


Figure 1 – Specification of the comet and meteor stream parameters.

of comets located within a  $\Delta$  surrounding meteor streams is above average. A similar task for the study of comet outbursts was solved in the article (Guliyev et al., 2013).

#### 4 Results of calculations

Investigation of complex consisting  $114 \times 125 = 14250$  values of the parameter  $\Delta$  can allow an estimate to be made for the possible involvement of meteoric streams in the splitting of comet nuclei. Calculations show that 1041 of them correspond to the distance  $\Delta = 0.1$  a.u. of the orbits under consideration for the streams from the list of Kronk (2014).

In order to estimate of the significance of the number  $N = 1041$  we use following method. The 114 comets undergoing nuclear splitting are replaced with other ones and calculations using formulas (1–3) are carried out. Finally results for the two groups of comets are compared.

However, the selection method for the comparison group should be unbiased. For this group, we use the 114 long-period comets discovered up to 2016 and the same number of latest periodic comets discovered up to 2016.

The above calculation algorithm was applied to each group of comets and meteor streams for the further comparison. Results of calculations for the  $\Delta < 0.1$  AU are presented in the Table 1.

As the table shows, the total frequency passing of comets undergoing nuclear splitting through the interval  $\Delta < 0.1$  AU is almost three times higher than the value for the other two groups of comets. This can be considered to be supportive of the studied hypothesis.

Another, more exact demonstration of the significance of the value  $N = 1041$  will be reported in our next article (Guliyev, 2016).

#### 5 Conclusion

We have established that disintegrated comets have a significant property: the frequency with which they cross known meteor streams is much more than for other comets. This leads to the conclusion that one of the possible causes of the fragmentation of cometary nuclei is their encounter with meteoroid streams. This explanation does not contradict other hypotheses regarding cometary splitting.

#### References

- Guliyev A. S. (2010). “Origin of short-perihelion comets”. Baku, Publ. Comp. Elm, 151.
- Guliyev A. S. and Nabiyev Sh. A. (2006). “Twin comets”. *Azerbaijani Astr.J.*, **1**, 5–9.
- Ibadinov X. I. (1998). “Disintegration of comet nucleus”. Dissertation., Moscow, 296 pages.
- Boehnhardt H. (2005). “Comet splitting – observations and model scenarios”. *Earths, Moon, and Planets*, **89**. 91–115.
- Kronk Gary W. (2014). “Meteor Showers”. Springer, 350 pages.
- Guliyev A. S., Kokhirova G. I. and Poladova U. D. (2014). “Comet outbursts and the meteor showers”. In Jopek T. J., Rietmeijer F. J. M., Watanabe J. and Williams I. P., editors, *Meteoroids 2013*, Proceedings of the Astronomical Conference held at A.M. University, Poznan, Poland, Aug. 26-30, 2013. A.M. University Press, 2014, pages 263–265.
- Marsden B. G. and Williams G. V. (2008). “Catalogue of Cometary Orbits”. 17<sup>th</sup> edition. Cambridge.SAO, 207 pages.
- Guliyev A. S. (2016). “Collision with meteoroids as one of possible causes of cometary nucleus splitting”. Proceedings of the conference *Meteoroids 2016*, in press.

# A fast meteor detection algorithm

Pete Gural

Gural Software Development, 351 Samantha Drive, Sterling, Virginia, USA 20164

`peter.s.gural@leidos.com`

A low latency meteor detection algorithm for use with fast steering mirrors had been previously developed to track and telescopically follow meteors in real-time (Gural, 2007). It has been rewritten as a generic clustering and tracking software module for meteor detection that meets both the demanding throughput requirements of a Raspberry Pi while also maintaining a high probability of detection. The software interface is generalized to work with various forms of front-end video pre-processing approaches and provides a rich product set of parameterized line detection metrics. Discussion will include the Maximum Temporal Pixel (MTP) compression technique as a fast thresholding option for feeding the detection module, the detection algorithm trade for maximum processing throughput, details on the clustering and tracking methodology, processing products, performance metrics, and a general interface description.

## 1 Introduction

One may wonder, why do we need to develop yet another meteor detection algorithm given the various software applications available? The answer derives from the rapid pace of technological advancement in algorithms, processing boards, focal planes, and multi-camera configurations with their continuing decreasing cost to entry. Up until recently, the last remaining large component in terms of cost and physical size footprint was the PC, which given the advent of the *Raspberry Pi*, completes the downward spiral of outfitting a meteor station on the cheap and as an extremely compact unit (Zubovic et al., 2015). We now have available low cost components for CCTV lenses, low-light cameras, capture dongles, and image processing chips.

However, there are some considerations one has to deal with. In the case of the *Raspberry Pi (RPI)*, there is a trade-off of lower computing throughput on a small board-level computer versus using a modern desktop processor. The *RPI* is currently about 20 times slower for about 30 times cheaper cost. In addition, the use of HD focal plane sensors will become prevalent in meteor work in the near future with their starting price point now at US\$300. However, the number of pixels to process for HD cameras relative to standard PAL and NTSC, will increase by approximately six times with the consequent increase in computing load. Large format cameras of  $1K \times 1K$  and  $4K \times 4K$  pixels are also being used in meteor astronomy, the latter representing an additional factor of four increase in pixel count. And lastly, due to the low cost of both sensors and multi-channel capture boards, multi-camera units feeding a site's single PC will become much more common. Thus many of the existing meteor detection applications will have a hard time keeping up with the demanding processing load despite having access to multi-core processors. Secondly, the existing software may not be thread safe for multi-processor configurations, nor operate with more than a single video channel feeding the system. One could wait for Moore's law to catch up to deal with the processing

load on a board-level computer. Instead it was thought this may be a good time to revisit the detection algorithm portion of the video meteor processing chain, since it had been first tackled in the 1990's (Molau, 1993; Molau and Arlt, 1997; Gural, 1995; Gural, 1997; Molau and Gural, 2005). Have there been algorithmic advances that could help speed up the entire meteor detection process and also maintain a high probability of detection, short of reverting to less portable FPGAs or custom GPU code?

While considering this aspect of the investigation, it was also felt that a generic stand-alone detection engine should be made available to the meteor community. This would be unlike the situation today with the detection functionality generally embedded in a larger application and inaccessible to other developers. So several requirements were considered as the new detection module was designed and implemented:

- It should have a simple interface that could be easily plugged into any processing work flow;
- Commonly used language that is efficient in processing (*ANSI C*);
- Callable modules that could be embedded in other languages (*Python, Java, Matlab*, etc.);
- Can handle both interleave or progressive scan imagery;
- Supports all imagery data types (unsigned char, short, long, float, double);
- Thread safe for multi-processor environments;
- Well documented, open source, and distributable;
- Fast, robust, with high probability of detection (Pd) for meteors;

In general, meteor image processing comes in a variety of functional work flows depending on the collection mode of the sensing system (all-sky, moderate field-of-view, telescopic, video frame rates, long integration times on large format sensors, daylight, intensified, gated, spectral, etc.). These can all be broken down into the four main steps of meteor image processing. The functional options for each step are as follows (Gural, 2008; Gural, 2011):

- Pre-processing: Capture, Cleanup, Dark removal, Flat fielding, Hot pixel masking/removal;
- Clutter removal: Frame differencing, Mean removal, Whitening, Spatial filter, Thresholding;
- Detection: Hough transform,  $5 \times 5$  kernel, Phase coded disk, Blob detection, Matched filter;
- Post-processing: False alarm mitigation, Signal and noise metrics, Detection reporting

The developer is usually free to choose the functional sub-option or combination thereof, at each stage of the work flow, by tuning it towards the nature of the collection system's imagery stream. However, for this development, rather than try to write a generic "end-to-end" software application to handle all work flow situations one may encounter, or alternatively one tuned specifically to a unique imaging system configuration, it was felt that building a fast but generic core detection module was the most critical need. Thus the user would need to provide the front end processing to feed data to the detection engine after thresholding, and the detection module would pass back the detections before false alarm mitigation is performed by the user application. This allows each unique imaging system to be optimally tuned for pre-processing and clutter removal, followed by post-processing and reporting. The detection module can then be focused on speed and Pd, less focused on false alarms, and be agnostic to front and back end processing. This design decision flowed down the requirement for a very simple and generic interface to and from the detection module.

Please note that one detection algorithm will not be the best solution in all cases. Unlike Lord of the Rings, one algorithm does not rule them all. For example, a very sensitive camera may perform faint meteor detection optimally with a matched filter detector which does not involve a per frame thresholding operation. Alternatively, a telescopic camera system may benefit from using a line detection algorithm. The clustering approach to be described later could potentially concatenate centroids per frame in that latter scenario. This paper will concentrate on standard FOV sized meteor video systems that are the most prevalent in use and where meteors appear as moving blobs or moderate length line segments (< 32 pixels) with SNR of 3 or higher.

Given this scenario of developing compact and portable processing components, the remainder of the paper covers three modules of the meteor image processing work flow. The first part will discuss an implicit fast thresholding scheme based on the CAMS compression algorithm, pointing out a feature not recognized until recently. The second and third parts will describe the fast detection module itself which is based on a low-latency clustering algorithm and multi-frame tracking algorithm.

## 2 Fast thresholding algorithm

The Cameras for All-sky Meteor Surveillance (CAMS) software employ a unique compression technique

extended from one used in the SkyPatrol software<sup>1</sup> (Vornhusen, 2003). The algorithm is described in (Jenniskens et al., 2011; Gural and Segon, 2012) and consists of taking a sequence of 256 image frames and forming four component images for an effective compression ratio of 64:1. Each of the four components represents the processing of each pixel in a spatially independent way, by obtaining temporal statistics across frames. One image is the maximum value in time of each pixel, a second is the frame number of the maximum pixel, the third is the temporal mean excluding the maximum pixel, and the fourth is the temporal standard deviation also excluding the maximum pixel contribution. The advantages are the ability to store an entire night's video from multiple cameras on a single hard drive yet still be able to do good astrometry, photometry, whitening, and an ability to reconstruct the propagating meteor sequence. The disadvantage occurs when there is a very bright meteor whose image blooming covers the same pixel in adjacent frames. In that case the meteor in the reconstructed frame has a speckle-like appearance from the special maximum frame number algorithm for same valued pixels (distributes noise evenly in time). In general however, this is not an issue for over 99% of meteors captured in video.

What was realized quite recently is that when one reconstructs the frame-by-frame sequence after MTP compression, that a single image looks just like an exceedance pixel map AFTER thresholding a classic meteor image (e.g. by taking an image, subtract a running mean, divide by a running standard deviation, and threshold above a user defined factor to identify exceedance pixels). The appearance as visualized in *Figure 1* shows sparsely populated background noise distributed across the focal plane and a linear segment or blob of closely adjacent exceedance pixels at the location of the meteor. Thus it was realized that the process of MTP compression effectively thresholds the pixels and we have a map of those exceedances on a per frame basis as a natural by-product of the compression!

So for example in CAMS processing, rather than use the existing method of reconstructing the image sequence and sending pairs to the *MeteorScan* detection module for differencing and thresholding, one could just pass exceedance pixel locations directly into a detection module using the compressed data content. However, there was one other attribute of the compression that was also discovered. Those compression based exceedance pixels actually represent a moderately high effective threshold factor times the pixel's standard deviation (over the mean). A *Matlab* simulation was built to examine this property and it was discovered that for 256 frame compression, the effective threshold is  $2.8 \sigma$  and the factor varies with the number of frames used in the compression (see *Figure 2*). In contrast, *MeteorScan* nominally runs at  $1.4 \sigma$  on raw difference frames (so effectively  $2 \sigma$  because of the noise amplification from

<sup>1</sup> <http://www.jostjahn.de/metsoft.html>, under 'SkyPatrol'

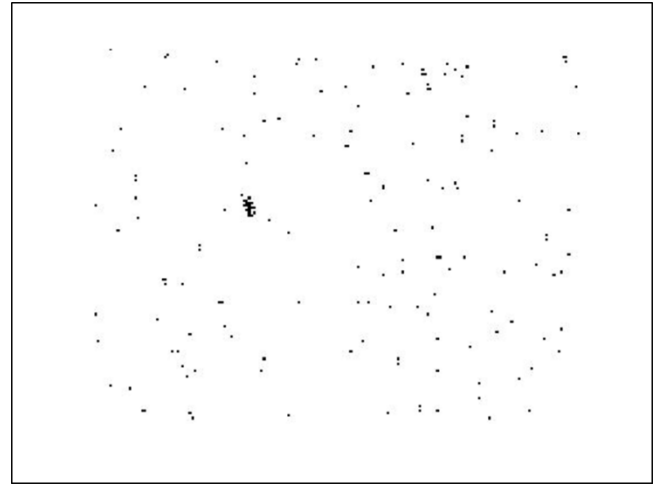
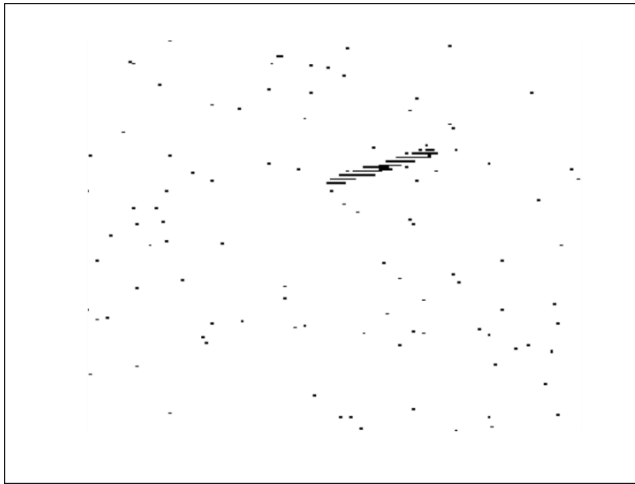


Figure 1 – Single reconstructed frame after MTP compression that looks like a classic threshold exceedance mapping of significant value pixels for a given frame. A fast meteor streak (left panel) and slow meteor blob (right panel) are images courtesy CMN Rovinj, Croatia and CAMS mid-Atlantic, USA.

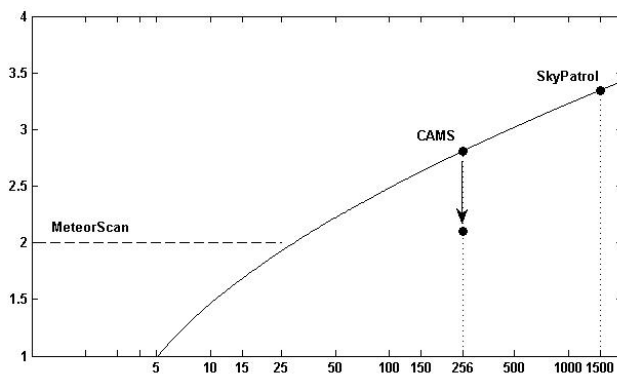


Figure 2 – Effective threshold levels of the SkyPatrol software, MeteorScan, and the MTP compression method as a function of total frame count. CAMS MTP compression on 256 frames has an effective threshold of  $2.8 \sigma$  but when using the four highest pixels rather than just the maximum value, this drops to  $2.1 \sigma$ .

the difference operation). But those meteors close to the noise limit usually result in poor track centroids. The CAMS team felt that high quality meteor centroids are desirable for orbit estimation, and having higher SNR per frame was a worthwhile advantage arising from the effective higher threshold.

A study was done to try compression algorithm modifications to lower the effective threshold. The most effective one was to keep track of the four highest pixel values temporally, along with their frame numbers of the maximums. The four values could also be used to provide a more robust mean and standard deviation, by excluding the four highest values in their respective computations (this helps eliminate ghosting in the mean from very bright meteor contamination). The effective compression-based threshold when saving the four highest values is reduced to  $2.1 \sigma$  with only a 30% increase in compression runtime to a total of 2 milliseconds per NTSC frame on a desktop PC. But this comes at a cost of 3x more storage needed per multi-frame sequence when retaining all video from the night. For a situation in which all processing is done in real-time on an in-situ processor and there is no need to store the compressed video information (unless a meteor is detected), this is a very viable approach to get a lower effective threshold out of the compression

algorithm and suits itself nicely to a *Raspberry Pi* target processor.

An operations count comparison of various thresholding work flows were compared to show how the compression algorithm is a much more efficient processing technique. In *Table 1* is a breakdown of the required image processing steps and integer operations counts for various methods that lead to a thresholding operation. One could:

- Track a running mean and running threshold with a first order response filter;
- Use difference frames to remove stationary objects with its associated increase by root-two in noise level and track a zero-mean running threshold;
- Compute the mean and threshold for a limited number of frames;
- Use the *MTP* compression and optionally compute the mean and standard deviation for later processing.

If using the compressed maximum pixel and associated frame number as a reference point, the next closest performing method is four times slower. Thus the compression algorithm is a very efficient thresholding approach and also provides an exceedance list which is the primary input source for the detection algorithm to be described in the next section. It also builds the compression products by ingesting one frame at a time, thus not requiring all frames present in memory at once. This is a huge advantage in the case of large format pixel count cameras.

Thus the compression algorithm is a very fast method for finding exceedance pixels, but one should be aware that it is not optimal. To perform down to the noise limit of the imagery, one really needs to directly estimate and remove the stationary background, whiten the image via second order noise statistical estimation, and operate with a lower effective threshold. For a situation in which processing throughput is the driving factor, this compression approach to thresholding is a highly recommended alternative to current techniques and should be satisfactory in most situations the meteoritic community encounters.

Table 1 – Image processing algorithms leading to a thresholded exceedance list with their associated total integer operations count. Actual implementation runtimes of each method may not be exactly proportional to the ops count in the rightmost column, due to coding and compiler efficiencies, but are representative of relative performance.

Running Mean & Threshold	Update $\langle X \rangle$ - 1 <sup>st</sup> order response	$4 N^2$	
	Update $T$ - 1 <sup>st</sup> order response	$7 N^2$	$12 N^2$
	$X > T$	$1 N^2$	
Difference Frames $\langle X \rangle = 0$ but $s \times \sqrt{2}$	$d =  X(t+2) - X(t+1) $	$1 N^2$	
	Update $T$ - 1 <sup>st</sup> order response	$4 N^2$	$5.5 N^2$
	$ d  > T$	$\frac{1}{2} N^2$	
Block of Frames Mean & Threshold	$\sum X \rightarrow \langle X \rangle$	$1 N^2$	
	$\sum X^2 \rightarrow \sigma$	$2 N^2$	$4 N^2$
	$X > T = \langle X \rangle + k \sigma$	$1 N^2$	
Maximum Pixel	Max Temporal Pixel	$1.1 N^2$	$1.1 N^2$
Maximum Pixel w/ Mean & Sigma	Max Temporal Pixel	$1.1 N^2$	
	$\sum X \rightarrow \langle X \rangle$	$1 N^2$	$4.1 N^2$
	$\sum X^2 \rightarrow \sigma$	$2 N^2$	

### 3 Meteor detection algorithm considerations

The pursuit of implementing a fast meteor detection algorithm arose from work being done by the Croatian Meteor Network to embed a *Raspberry Pi* processor right in the camera box enclosure (Zubović, 2015). Since the *RPi* operates with a throughput equivalent to a desktop PC from circa 2000, essentially 20 x slower per core than a modern day desktop, it was thought an efficient detection algorithm would be worth developing relative to the existing software deriving from that era. In 2000, it was common practice for meteor software to throttle back processing just to keep up with the real-time data rate from a single video stream. *MetRec* would aggregate pixels in  $2 \times 2$  blocks so there were four times fewer to process and *MeteorScan* would randomly drop exceedance pixels sent to the Hough transform to dynamically adjust to just below the maximum processing load of the CPU. On today’s desktop PCs these techniques are no longer used, but it didn’t seem prudent to revert back to those methods.

So the first task was to examine existing meteor detection algorithms as embedded in various meteor software packages and look for an efficient algorithm. Note that “embedded” is a key word here since in most cases the detection functionality could not be easily extracted from the software package nor it may not have been distributable as source code. But what is of interest here is the algorithm descriptions and runtime implications of the methods used. The meteor detection software options and basic functionality are as follows (not all inclusive):

- *MeteorScan* – Frame differences adjacent-in-time image pairs, tracks a threshold based on a factor times the difference-frame running standard deviation, thresholds for exceedances that are then Hough transformed using localized exceedance pixel pairs, tracks noise in Hough space and thresholds looking for peaks, and performs a matched filter on each hypothesized line from the peak parameters to mitigate false alarms (Gural, 1999). The detection modules are separable from the *MeteorScan* code but involve global variables and thus not thread safe for multi-core processors. Also despite a highly efficient implementation within *MeteorScan*, the pixel pair Hough transform is still a computationally expensive processing approach.
- *MetRec* – Subtracts a running mean from each image and divides by the running noise variance to whiten the data. A series of eight  $5 \times 5$  orientation kernels are convolved with the resultant image searching for peak signals that are fed a motion tracker/detector (Molau and Gural, 2005). As seen in Table 1, even a running mean and variance can be a costly operation, let alone the kernel convolution operation applied eight times across the whitened image. This again seemed an expensive image processing approach for implementation on a *RPi*, plus there was the unavailability of the core detection functions as a separable code base.
- *UFOfapture* – Applies a  $5 \times 5$  spatial filter with frame differencing that is then masked and thresholded. The source code has not been made available and the details of the algorithm are not published. The types of operations are similar to



binary exceedance pattern). The row and column centroid constitutes the “measurement” of a cluster of pixels in a given frame. A first pass cluster detection criteria is checked that employs a user specified threshold (typically 0 dB) on the ratio of the integrated signal-squared to the noise variance. Various additional metrics are retained such as signal and noise energy, detection statistics, various pixel counts, and line related parameters.

## 5 Tracking algorithm for multi-frame detection

Given a set of cluster detections in a single frame, one still needs to detect a “propagating” object in a sequence of frames to reliably declare a linearly moving meteor was found. Thus a tracker is used to combine cluster measurements from multiple frames and build up the full meteor motion. At this stage of the processing, the runtime costs are very minimal, as most of the heavy lifting has already been done by the cell level clustering of the previous step. The tracker chosen is a Kalman filter approximation often used in radar systems and referred to as an alpha-beta tracker (Blair, 1992). It is a two-state (position and velocity) predictor/corrector approach that avoids the need for a detailed state model or covariance as in a full-up Kalman filter. It assumes the object is moving close to a constant angular velocity, but can adjust to deviations from that model such as the small deceleration seen in some meteors. This was done by initially employing a least squares filter followed by a mean squared filter to handle small changes. The alpha-beta update equations below use a set of alpha and beta coefficients that adapt with measurement number until the 7<sup>th</sup> measurement, at which point the coefficients remain constant. As a linear motion tracker in the two focal plane dimensions, the algorithm essentially stitches together a sequence of track-associated cluster measurements in time.

$$X_{\text{pred}}(k+1) = X_{\text{corr}}(k) + V(k)(T_{\text{meas}} - T_{\text{lastupdate}}) \quad (1)$$

$$X_{\text{corr}}(k+1) = X_{\text{pred}}(k) + \alpha [X_{\text{meas}} - X_{\text{pred}}(k+1)] \quad (2)$$

$$V(k+1) = V(k) + \frac{\beta [X_{\text{meas}} - X_{\text{pred}}(k+1)]}{T_{\text{meas}} - T_{\text{lastupdate}}} \quad (3)$$

$$\alpha = \frac{2(2k+1)}{k(k+1)}; \beta = \frac{6}{k(k+1)};$$

$$\text{for } k = 1, 2, 3, \dots, 7, \text{ then fixed} \quad (4)$$

Initial conditions:

$$X_{\text{corr}} = X_{\text{pred}} = X_{\text{meas}}; V = 0; \text{ for } k=1 \quad (5)$$

After the first detection, a given tracklet resides in a “spinup” state until a user specified n-of-m detections have been obtained. At that point the tracklet is declared “firm” and has met the criteria for final track reporting once the tracklet is “closed” at a later point in time. If subsequent frames have a user specified number of missed detection measurements associated with this given

tracklet, then the tracklet is declared “troubled” but maintained and coasted forward in time. Either a new detection that meets the n-of-m criteria pulls the tracklet status back to “firm” or after too many have been missed, the tracklet then gets “closed”. The user extracts the closed track information and only then is the tracklet released back to the system. The tracker as implemented performs these functions on multiple tracks across multiple frames. It is agnostic to whether measurements are fed on a per-field (interleaved) or per-frame (progressive scan) basis, but the tracker expects an update call at the field or frame cadence of the imaging system to maintain an evenly spaced history of detected/dropped measurements for track status revision across all tracklets.

## 6 Performance and availability

The combined runtime performance of the hierarchical clustering and alpha-beta tracking was nearly 40 times faster than the existing CAMS detection processing approach of feeding *MeteorScan* with image pairs from reconstructed frame sequences. The timing was 0.04 seconds versus 1.7 seconds per 8.5 seconds (256 frames) of NTSC video respectively. In addition, on the CAMS data sets in which both algorithms have been applied to perform a side-by-side comparison, the same number of meteors was detected by both algorithms to within 0.5%. With the initial implementation and tests successful, this has been deployed to CAMS stations in California, Virginia, and BeNeLux for beta testing with excellent success thus far. Cloud false alarms have been found to be higher, but re-tuning of the cloud mitigation parameter thresholds for the new algorithm is a work in progress.

The software has been written in *ANSI C* and is well documented with inline comments and an extensive header section describing each module’s calling sequence and usage. It also has well defined and simple interfaces. The software modules are exportable worldwide to anyone who wishes to integrate the compression, clustering and/or tracking modules into their meteor image processing streams. One of the attributes of the software is that it also provides a rich set of data products from the various modules, many of which can be used in post-processing false alarm mitigation.

For the clustering module on a per frame basis, the following products are available:

- Time, row, and column centroid measurements where time is user specified (e.g. field or frame number or absolute Julian date/time);
- Integrated signal, integrated variance, and  $10 \log_{10}(\text{signal}^2 / \text{variance})$ ;
- Number of exceedance pixels, saturated pixels, total in the region of interest;
- Entropy measure, PCD orientation angle and line width, Hueckel line orientation angle.

For the tracking module on a per track (multi-frame) basis, the following products are available:

- Historical set of the cluster attributes listed immediately above for all measurements in the track;
- Multi-frame integrated SNR and BNR (exceedance count to total pixel count);
- Multi-frame average entropy and average PCD angle;
- Metrics for non-linearity and evenness of spacing between measurements.

Some near term planned upgrades include the following:

- Cloud and aircraft mitigation optimization;
- Matched filter metric across multiple frames for the tracker;
- Detect long streaks by stitching clusters before tracking (telescopic scenario);
- Integrate into the CMN Raspberry Pi project;
- $2 \times 2$  raw image aggregation as a potential SNR booster.

## 7 Interface discussion

This section covers the high level input interface requirements for each of the modules discussed. The headers and in-line code comments are the ultimate source of details on the exact formats on both ingest and output products. This discussion is simply to describe what each module expects and how that might define the means by which a developer uses these functions. An example set of function calls are listed in the appendix.

The MTP compression module ingests a series of frames, one at a time in sequential temporal order. There is a single initialization call near your program's start to define common settings for the duration of the processing. As currently implemented, the imagery data type expected is 8-bit unsigned integers, but could be easily adapted to other data types. In interleave mode, the full frames are expected to be passed to the compressor and not pass the individual fields (the clustering module will sort out fields in its processing stage if the data was interleaved). A frame number and image array are all that is input per call. The compressed four array product is generated after the last of the number of specified frames is reached and the arrays reset on the call to the next first frame in a block of frames (based on modulus calculation of the frame number).

The clustering module also has a single initialization call at program start-up. The subsequent calls to the clustering module functions are at the frame cadence for both interleaved and progressive scan cameras (the clustering module will form even and odd field or full-frame centroids appropriately). The data passed into the clustering module is an exceedance location vector as a pointer offset from the first pixel in the internal storage array along with the total exceedance pixel count for that frame. The compression module provides this exceedance list as a natural by-product.

The tracking module has a single initialization call at program start. Each subsequent call to the tracking

module occurs after the clustering calls to feed cluster detections to the tracker and associate with any existing tracks or form new tracks. The interface of the tracker ingest is compatible with the cluster measurements output and should be called even if there were no detections for that frame. After each frame is processed, the user needs to check for any closed tracks for extraction and storage/reporting.

## References

- Blair W. D. (1992). "Fixed-gain, two-stage estimators for tracking maneuvering targets". Naval Surface Warfare Center, Dahlgren Division 1992 Technical Report 297 (NSWCDD/TR-92/297), 1–68.
- Gural P. (1995). "Applying state-of-the-art video and computer technology to meteor astronomy". *WGN, Journal of the IMO*, **23**, 228–235.
- Gural P. (1997). "An operational autonomous meteor detector: Development issues and early results". *WGN, Journal of the IMO*, **25**, 136–140.
- Gural P. (1999). "MeteorScan Documentation and User's Guide". Sterling VA, USA.
- Gural P., Jenniskens P. and Varros G. (2004). "Results from the AIM-IT Meteor Tracking System". *Earth, Moon, and Planets*, **95**, 541–552.
- Gural P. (2008). "Algorithms and Software for Meteor Detection". *Earth, Moon, and Planets*, **102**, 269–275.
- Gural P. (2011). "From MeteorScan to FTP: A Variety of Meteor Detection Software Packages and Approaches". *Meteor Video Observations and Analysis NASA Workshop: Pisgah Astronomical Research Institute*, August 4-5, 2011 Organized by the NASA Meteoroid Environment Office.
- Gural P. and Šegon D. (2012). "A new meteor detection processing approach for observations collected by the Croatian Meteor Network (CMN)". *WGN, Journal of the IMO*, **37**, 28–32.
- Jenniskens P., Gural P., Dynneson L., Grigsby B., Newman K., Borden M., Koop M. and Holman D. (2011). "CAMS: Cameras for Allsky Meteor Surveillance to establish minor meteor showers". *Icarus*, **216**, 40–61.
- Molau S. (1993). "MOVIE: Meteor Observation with Video Equipment". In Roggemans P., editor, *Proceedings of the International Meteor Conference*, Puimichel, France, 23-26 September 1993. IMO, pages 71–75.
- Molau S. and Arlt R. (1997). "Meteor shower radiant positions and structures as determined from single



```

//      ClusteringDetector      - Called after the centroid refinement for all the cluster
//                               peaks to estimate various additional attributes such
//                               as the squared signal over variance detector, entropy,
//                               orientation, and per frame/field threshold detections.
//
//      TrackingAllMeasurements - Called for each frame/field's measurements collection for
//                               the given frame/field time to associate measurements
//                               with tracks and propagate ALL active tracks forward
//                               to the current time. For interleaved collected frames
//                               this would entail two calls. One for the odd field
//                               and a second for the even field measurements (or
//                               vice versa of even then odd, depending on sensor and
//                               capture card interleave mode/timing). The field centroid
//                               measurements will be time tagged by the actual respective
//                               "field" times passed as a separate argument.
//
//      while( TrackingSaver( trackers, &track ) == 1 ) { do stuff with "track" }
//
//                               - Called to identify any CLOSED tracks, one at a time,
//                               extract them from the trackers structure, and give
//                               the user an opportunity to perform final track
//                               refinement, false alarm reduction, and reporting.
//                               Each track that is extracted is released back
//                               into the new track pool (with a NOTRACK status).
//
//      "Post-processing"      - Back end processes to perform multi-frame tracking,
//                               track refinement, false alarm reduction, and reporting.
//
//                               IMPORTANT NOTE: The clustering codes are working on a
//                               frame or field pair and are thus agnostic
//                               to the absolute time of each measurement,
//                               so the post-processing functions is where
//                               the assignment of a time is made to each
//                               interleaved or progressive scan measurement.
//
//      ---- End of frame loop -----
//
//      ClusteringFreeMemory    - Call once at the end to free cluster memory
//      TrackingFreeMemory      - Call once at the end to free tracker memory
//
//
//      End of user program ...
//=====

```

# The occurrence of interstellar particles in the vicinity of the Sun

## An overview – 25 years of research

Maria Hajdukova jr.

Astronomical Institute of the Slovak Academy of sciences, Bratislava, Slovakia

astromia@savba.sk

Using different observational techniques, research into interstellar particles produced controversial results concerning their occurrence in the vicinity of the Sun. The proportion of possible interstellar particles to interplanetary ones was found to be much higher for small particles obtained from cosmic dust detectors in comparison with results of photographic, video and radar meteors. This might be partly caused by different mass distributions of interstellar and interplanetary particles, and by different physical processes leading to each population. However, in the range of larger meteoroid particles, the vast majority of hyperbolic orbits were found to be as a consequence of measurement errors. We present here an overview of studies related to interstellar particles showing their flux as a function of their mass and distance from the Sun.

### 1 Introduction

The interaction of our solar system with the interstellar medium, due to the Sun's motion relative to the local interstellar cloud (LIC), should lead to the presence of interstellar particles (ISP), or, at least, to interstellar dust grains. The search for them, provoked by the high presence of hyperbolic orbits among detected meteors, became more intensive shortly after Ulysses was launched in 1990. Using different observational techniques, research into ISP produced controversial results concerning their occurrence in the vicinity of the Sun.

### 2 ISP in interplanetary medium

The influx of the ISP depends on both their mass and distance from the Sun. The dynamics of the ISP is influenced, except for gravitation, by strongly size-dependent solar radiation pressure and Lorentz forces (Mann, 2010). As expected, the proportion of possible interstellar particles to interplanetary ones was reported to be much higher for small particles obtained from cosmic dust detectors in comparison with the results of radar, photographic and video meteors in the range of larger meteoroid particles. However, it was a surprise that the flux of interstellar dust grains from the Ulysses and Galileo detectors beyond 3 AU was reported to dominate above the interplanetary dust (Gruen, 1993; Gruen et al., 1994; 1995; Baguhl et al., 1994). The authors argued for the interstellar origin of the dust based on three criteria: their retrograde trajectories, their high impact speed and their independence from the ecliptic latitude (Krueger et al., 1999 a, b; Gruen and Landgraf, 2000). The latter is possible because of the high inclination of the interplanetary trajectory of Ulysses; however, the retrograde Halley-type comets' particles and other populations of interplanetary particles also contribute to the vertical structure of the dust. The ISD flux at larger distances (about 10 AU) is suggested to be even larger

than the fluxes measured by Ulysses at distances up to 5 AU according to a recent study based on the Cassini's cosmic dust analyzer (Altobelli et al., 2016). On the other hand, dust detected at 1 AU by the Wind/WAVES instrument is highly dominated by particles on bound trajectories, rather than dust with hyperbolic orbits (Malaspina et al., 2014; 2015).

In general, to distinguish the detected interstellar particles, and to separate them, from interplanetary ones is a big challenge, which requires high accuracy data and a proper error analysis. It is impossible to detect a hyperbolic excess of a heliocentric velocity which is of the same order as the uncertainty in the velocity measurement (Wiegert, 2015). Regarding larger particles ( $m > 10^{-8}$  kg), the vast majority of hyperbolic orbits in the meteor databases was found to be as a consequence of measurement errors (Hajdukova, 1994; 2008). An overview of studies related to ISP within the last 25 years is shown in *Figure 1*.

### 3 The direction of the ISP arrivals

The Earth-based observation did not show any concentrations of ISP radiants to the Sun's apex or the Galactic plane, nor any distributions following the motion of interstellar material (Hajdukova, 1994; 2011; Musci et al., 2012), as expected for interstellar meteoroids.

The grain population detected by Ulysses and Galileo enters the solar system from the same direction as the helium atoms that originate from the gas phase of the LIC (Landgraf et al., 2000). However, in 2005, a shift in the dust flow direction was observed by Ulysses, most likely caused by Lorentz force in the inner heliosphere (Starken et al., 2012; 2015); even so, an extra filtering mechanism is needed to fit the data. The dust data are not related to the radar data detected by AMOR (Baggaley, 2007), which are believed to arrive from the southern ecliptic hemisphere (Landgraf et al., 2000).

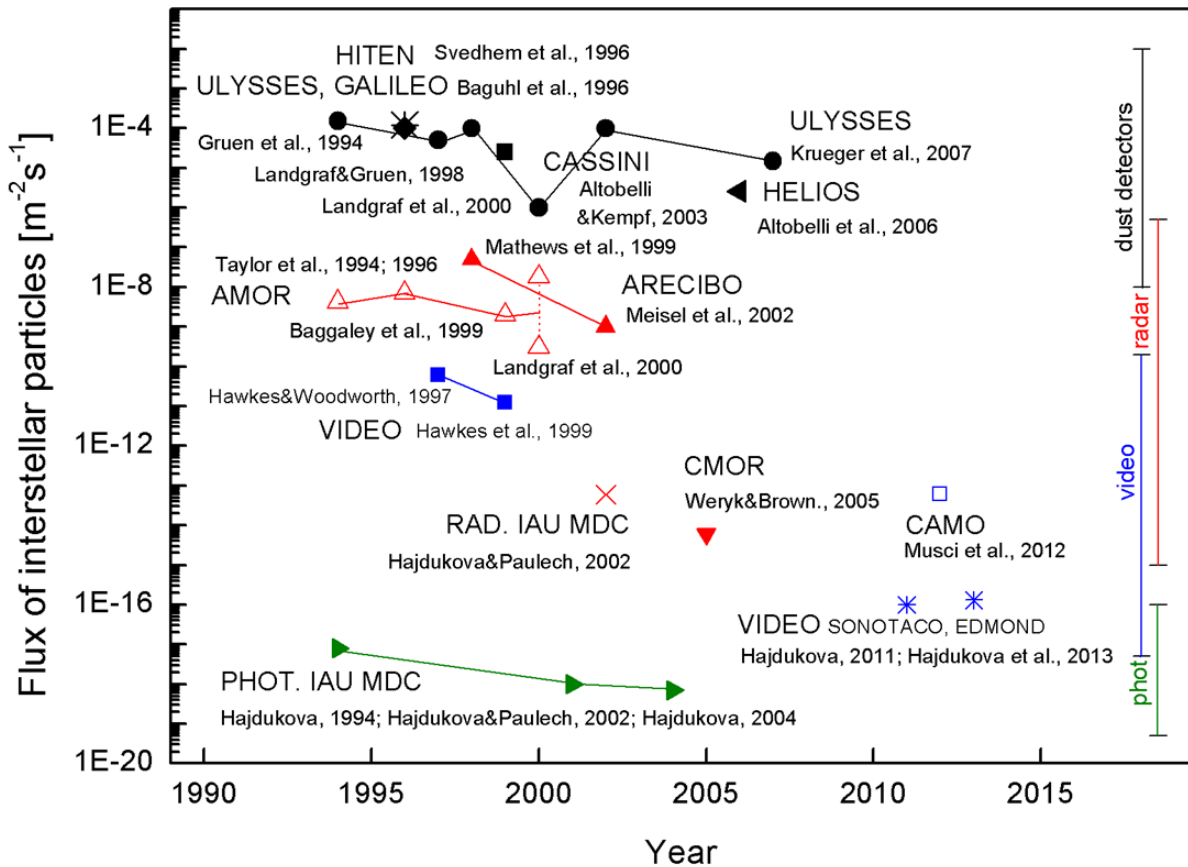


Figure 1 – Overview of the ISP flux as reported by various authors within the last 25 years. (The year does not necessarily mean the time of measuring, but rather the year of publication.)

#### 4 The flux of the ISP related to their masses

Figure 2 shows the flux of ISP along the mass range corresponding to various observation techniques, in comparison with the flux of interplanetary particles. For large particles, the flux of ISP is more than three orders of magnitude lower than the flux of interplanetary ones. The interstellar dust particles, as mentioned above, represent more than 50 percent of all of the dust population. The bulk of their mass distribution is located around  $3 \times 10^{-16}$  kg (Landgraf et al., 2000), which is a slightly higher value than expected from the size distribution of interstellar grains derived from optical observation by Mathis et al. (1997). Specifically, there is a lack of dust grains with masses from  $1 \times 10^{-17}$  to  $3 \times 10^{-16}$  kg that were intercepted under 4 AU (Landgraf et al., 2003; Krueger et al., 2015) in the Ulysses data.

As seen in Figure 2, the mass distribution of the measured ISP shows a drop-off at small masses ( $m < 10^{-17}$  kg), explained by filtering at the heliospheric boundary due to the Lorentz force keeping small charged grains out of the heliosphere (Baguhl, 1994; 1995; Kimura and Mann, 1998). However, according to Linde and Gombosi (2000), it alone does not explain the above-mentioned deficit in the spacecraft data. Therefore, an additional filtering mechanism at work inside the interplanetary medium was searched for. Landgraf et al. (1999) demonstrated the influence of a strong solar radiation pressure, deflecting small grains, the strength of

which is expected to increase with decreasing distances to the Sun (Altobelli et al., 2003).

However, the question could also be, whether the in-situ measurement uncertainties could not have shifted a part of the interplanetary particle population to the ISP population, and hence be responsible for the discrepancy between the optical and dust detector measurements.

In the mass range of  $10^{-10} - 10^{-7}$  kg, detection of interstellar meteoroids with extremely high velocities was reported on the basis of observations from the Advanced Meteor Orbit radar (AMOR) (Baggaley et al, 1993; Baggaley, 1999; Taylor et al., 1994). Nevertheless, a reexamination of the methods for the meteor velocity determination used in the AMOR project lead to the conclusion that the sets of highly hyperbolic velocities in the range of  $100 - 500 \text{ km s}^{-1}$  cannot be accepted (Hajduk, 2001). Therefore, also the conclusions based on these highly hyperbolic orbits, especially those concerning interstellar sources of high velocity meteors, derived from AMOR system, needs some revision.

Detections of interstellar meteors using the Arecibo radar were reported by Mathews et al. (1999) and Meisel et al. (2002). Owing to large uncertainties in the velocities, their results also remain controversial (Musci et al., 2012). The uncertainties in meteor radar data and the problem of hyperbolic meteors were studied also by *Kolomijets (2015)* analyzing Kharkiv data from the Meteor Automatic Radar System.

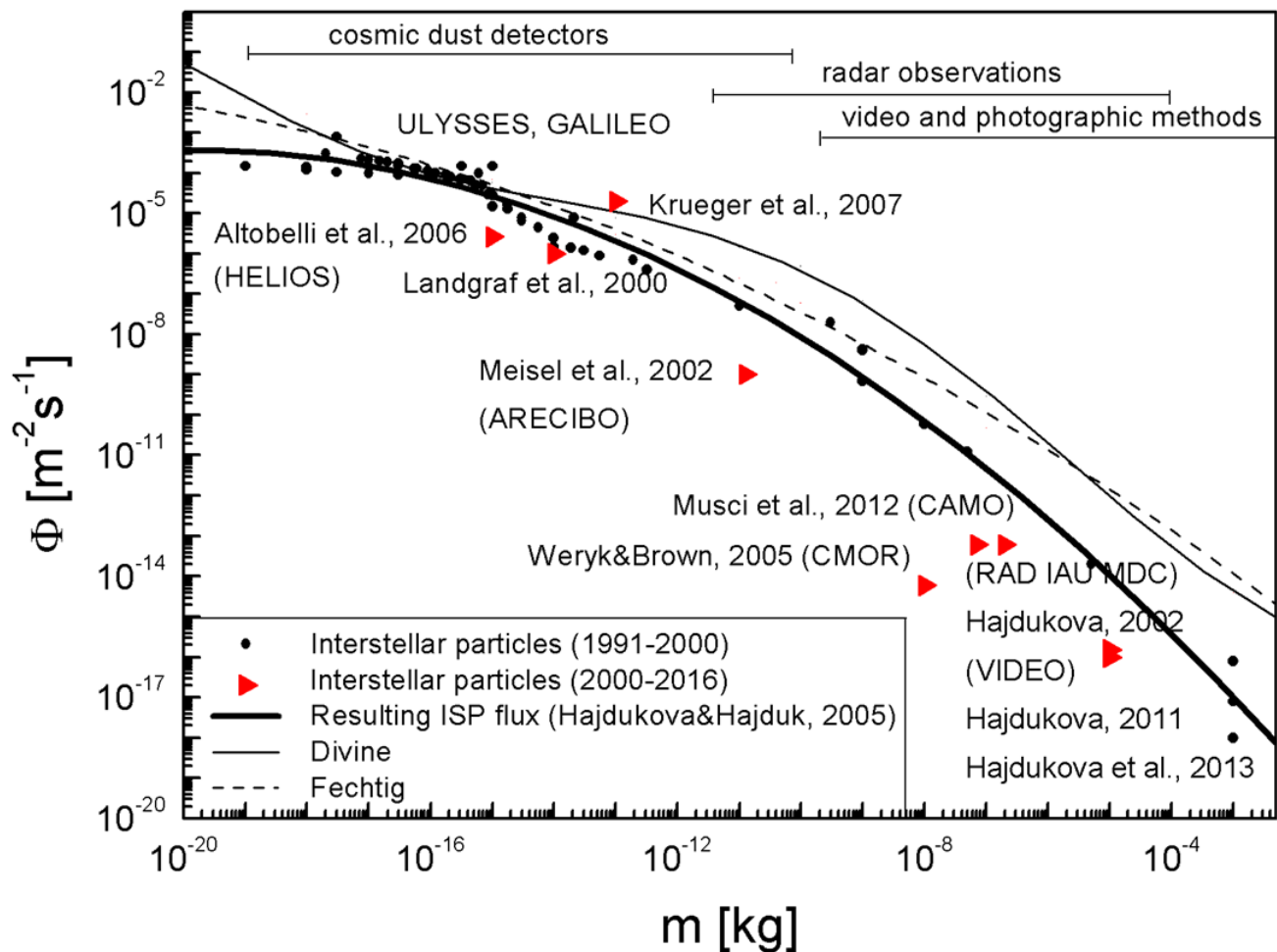


Figure 2 – ISP flux  $\Phi$  obtained from observations with different techniques shows an increasing proportion of the ISP towards smaller masses, which might be caused by different mass distributions of interstellar and interplanetary particles. The resulting ISP flux (Hajdukova and Hajduk, 2005) is compared with the older flux models of interplanetary particles suggested by Fechtig (1973) and Divine (1993). To match spacecraft dust measurements, new models were developed (Staubach et al., 2001; Dikarev et al., 2002) that consider the population on hyperbolic orbits for dust particles, which is predicted to disappear for larger masses.

Weryk and Brown (2005), analyzing radar meteors with masses  $> 10^{-8}$  kg, detected by the Canadian Meteor Orbit Radar (CMOR), determined a lower limit on the ISP flux which corresponded to their proportion of only 0.0008% of all the observed radar echoes.

An analysis of the radar data of the IAU Meteor Data Center (Lindblad, 2003), with a limiting mass of  $10^{-7}$  kg, made by Hajdukova and Paulech (2002, 2007), showed that the vast majority of hyperbolic orbits was clearly caused by errors, mostly in the velocity determination, shifting a part of the data through the parabolic limit.

Hyperbolic meteors obtained by video detector technique were reported by Hawkes and Woodworth (1997 a, b), Hawkes et al. (1999) and Guliyev and Nabiyeu (2015). The Canadian Automated Meteor Observatory (CAMO) data were searched for ISP by Musci et al. (2012), who found no clear evidence of interstellar meteoroids with a limiting mass of  $m > 2 \times 10^{-7}$  kg, and also concluded that their few identified hyperbolic meteors were most likely the result of measurement errors. The flux of the ISP obtained from the SonotaCo video catalogue (SonotaCo, 2009) was found to be close to zero (Hajdukova, 2011).

Photographic meteor orbits were analyzed by Hajdukova (1994), who set the frequency upper limit for hyperbolic meteors of a possible interstellar origin as 0.002% for the meteors with masses  $m > 10^{-3}$  kg from the most precise Harvard catalogs of the IAU Meteor Data Center (Lindblad et al., 2005).

## 5 The variability of the ISP flux

Regarding the question of an actual variability of the ISP flux into the solar system, long-term observations are needed. The interstellar dust flow in the interplanetary medium was monitored by Ulysses over 15 years. The flux of the small grains was found to exhibit temporal variations (Krueger and Gruen, 2009). The reason for the drop between the years 1997 and 2000 (Figure 3) was attributed to increased filtering of small grains by the solar wind-driven interplanetary magnetic field during solar minimum conditions (Landgraf et al., 2000; Strub et al., 2015). The flux of larger grains, detected by Cassini and Galileo (Altabelli et al., 2003), are not affected by the solar wind and their flux is approximately constant.

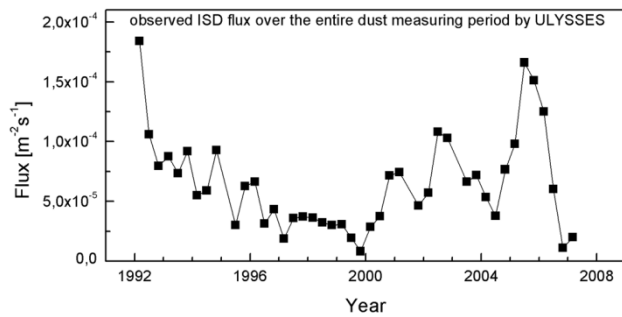


Figure 3 – Temporal variation of the interstellar dust flux due to an interaction with the heliosphere and/or due to the solar cycle (Starken et al., 2015). Data are taken from Strub et al., 2015.

## 6 Summary

The problem of hyperbolic or interstellar particles detected by Earth-based and space-born observation has led to many searches, the main results of which are presented in this paper.

The substantial question is how many interstellar particles we should register in comparison with those belonging to the interplanetary medium. The proportion of possible interstellar particles to interplanetary ones was reported to be much higher for small particles obtained from cosmic dust detectors in comparison with the results of radar, photographic and video meteors in the range of larger meteoroid particles.

The studies based on the in-situ dust detections undoubtedly report identification of interstellar dust grains flowing through the heliosphere, which originate from the local interstellar cloud. The flux of interstellar dust grains outside about 3 AU was reported to dominate above the interplanetary dust (e.g. Gruen et al., 1993; Krueger et al., 2015; Altobelli et al., 2016).

The hyperbolic velocities observed at Earth are most likely a consequence of observational and measurement errors, mostly in the velocity. Other sources which can produce the hyperbolicity of a meteor orbit, including planetary perturbations, are negligible in comparison (e.g. Hajdukova et al., 2014 a, b).

## Acknowledgment

The work is supported by Slovak grants APVV-0517-12 and VEGA 1/0225/14.

## References

Altobelli N., Kempf S., Landgraf M., Srama R., Dikarev V., Krueger H., Moragas-Klostermeyer G. and Gruen E. (2003). “Cassini between Venus and Earth: detection of interstellar dust”. *Journal of Geophysical Research*, **108**, A10, 8032.

Altobelli N., Moissl R., Krüger H., Landgraf M. and Grün E. (2004). “Influence of wall impacts on the Ulysses dust detector on understanding the

interstellar dust flux”. *Planetary and Space Science*, **52**, 1287–1295.

Altobelli N., Gruen E. and Landgraf M. (2006). “A new look into the Helios dust experiment data: presence of interstellar dust inside the Earth’s orbit”. *Astronomy and Astrophysics*, **448**, 243–252.

Altobelli N., Postberg F., Fiege K., Trieloff M., Kimura H., Sterken V. J., Hsu H.-W., Hillier J., Khawaja N., Moragas-Klostermeyer G., Blum J., Burton M., Srama R., Kempf S. and Gruen E. (2016). “Cassini detects interstellar dust grains”. *Science*, **352**, Issue 6283, 312–318.

Baggaley W. J., Taylor A. D. and Steel D. I. (1993). “The influx of meteoroids with hyperbolic heliocentric orbits”. In Stohl J. and Williams I. P., editors, *Meteoroids and their Parent Bodies*, Proceedings of the International Astronomical Symposium held at Smolenice, Slovakia, July 6-12, 1992, Bratislava. Astronomical Institute, Slovak Academy of Sciences, pages 53–56.

Baggaley W. J. (1999). “Interstellar Particle Component measured by AMOR”. In Baggaley W. J. and Porubcan V., editors, *Meteoroids 1998*, Proceedings of the International Conference held at Tatranska Lomnica, Slovakia, August 17-21, 1998. Astronomical Institute of the Slovak Academy of Sciences, pages 265–273.

Baggaley W. J., Marsh S. H. and Close S. (2007). “Interstellar meteoroids”. *Journal of Geophysical Research*, **105**, A5, 10 353–10 361.

Baguhl M., Gruen E., Hamilton D. P., Linkert G., Riemann R. and Staubach P. (1994). “The flux of interstellar dust observed by Ulysses and Galileo”. *Space Science Reviews*, **72**, 471–476.

Baguhl M., Hamilton D. P., Gruen E., Dermott S. F., Fichtig H., Hanner M. S., Kissel J., Lindblad D., Linkert B. A., Linkert G., Mann I., McDonnell J. A. M., Morfill G. E., Polansky C., Riemann R., Schwehm G., Staubach P. and Zook H. A. (1995). “Dust measurements at high ecliptic latitudes”. *Science*, **268**, 1016–1019.

Baguhl M., Grün E. and Landgraf M. (1996). “In situ measurements of interstellar dust with Ulysses and Galileo space probes”. *Space Science Reviews*, **78**, 165–172.

Divine N. (1993). “Five populations of interplanetary meteoroids”. *Journal of geophysical research*, **E9**, 17 029–17 048.

Dikarev V., Jehn R. and Gruen E. (2002). “Towards a new model of the interplanetary meteoroid environment”. *Advances in Space Research*, **29**, 1171–1175.

- Fechtig H. (1973). "Cosmic dust in the atmosphere and in the interplanetary space". *Evolutionary and physical properties of meteoroids, NASA SP*, **319**, 209–220.
- Gruen E. (1993). "Dust detection from space vehicles". In Stohl J. and Williams I. P., editors, *Meteoroids and their Parent Bodies*, Proceedings of the International Astronomical Symposium held at Smolenice, Slovakia, July 6-12, 1992, Bratislava. Astronomical Institute, Slovak Academy of Sciences, pages 349–356.
- Gruen E., Gustafson B. A., Mann I., Baguhl M., Morfill G. E., Staubach P., Taylor A. and Zook H. A. (1994). "Interstellar dust in the heliosphere". *Astronomy and Astrophysics*, **286**, 915–924.
- Gruen E., Baguhl M., Hamilton D. P., Kissel J., Linkert D., Linkert G. and Riemann R. (1995). "Reduction of Galileo and Ulysses dust data". *Planetary and Space Science*, **43**, 941–951.
- Gruen E. and Landgraf M. (2000). "Collisional consequences of big interstellar grains". *Journal of geophysical research*, **105**, 10 403–10 410.
- Guliyev A. and Nabiyev S. (2015). "The features of sporadic hyperbolic meteors observed by television techniques in the period of 2007–2009". *Planetary and Space Science*, **118**, 107–111.
- Hajduk A. (2001). "On the very high velocity meteors". In Warmbein B., editor, *Proceedings of the Meteoroids 2001 Conference*, 6 - 10 August 2001, Kiruna, Sweden. ESA SP-495, Noordwijk. ESA Publications, pages 557–559.
- Hajdukova M. Jr. (1994). "On the frequency of interstellar meteoroids". *Astronomy and Astrophysics*, **288**, 330–334.
- Hajdukova M. Jr. (2004). "Highly hyperbolic orbits in the IAU MDC photographic data". *Acta Astron. et Geophys. Univ. Comenianae*, **XXV**, 25–30.
- Hajdukova M. Jr. (2008). "Meteors in IAU MDC on hyperbolic orbits". *Earth, Moon, and Planets*, **102**, 67–71.
- Hajdukova M. Jr. and Hajduk A. (2006). "The mass distribution of interstellar and interplanetary particles". *Contributions Astronomical Observatory Skalnaté Pleso*, **36**, 15–26.
- Hajdukova M. Jr., Kornos L. and Toth J. (2014). "Frequency of hyperbolic and interstellar meteors". *Meteoritics and Planetary Science*, **49**, 1–6.
- Hajdukova M. Jr. and Paulech T. (2002). "Interstellar and interplanetary meteoroid flux from updated IAU MDC data". In Warmbein B., editor, *Proceedings of Asteroids, Comets, Meteors - ACM 2002*. International Conference, 29 July - 2 August 2002, Berlin, Germany. ESA SP-500. Noordwijk, Netherlands. ESA Publications Division, pages 173–176.
- Hawkes R. L. and Woodworth S. C. (1997a). "Do some meteorites come from interstellar space?". *Journal Royal Astronomical Society Canada*, **91**, 68–73.
- Hawkes R. L. and Woodworth S. C. (1997b). "Optical detection of two meteoroids from interstellar space". *Journal Royal Astronomical Society Canada*, **91**, 218–219.
- Hawkes R. L., Close T. and Woodworth S. C. (1999). "Meteoroids from outside the solar system". In Baggaley W. J. and Porubcan V., editors, *Meteoroids 1998*, Proceedings of the International Conference held at Tatranska Lomnica, Slovakia, August 17-21, 1998. Astronomical Institute of the Slovak Academy of Sciences, pages 257–264.
- Kimura H. and Mann I. (1999). "Filtering of the interstellar dust flow near the heliopause: the importance of secondary electron emission for the grain charging". *Earth Planets Space*, **51**, 1223–1232.
- Kolomiyets S. V. (2015). "Uncertainties in MARS Meteor Orbit Radar Data". *Journal of Atmospheric and Solar-Terrestrial Physics*, **124**, 21–29.
- Krüger H., Grün E., Hamilton D. P., Baguhl M., Dermott S., Fechtig H., Gustafson B. A., Hanner M. S., Horányi M., Kissel J., Lindblad B. A., Linkert D., Linkert G., Mann I., McDonnell J. A. M., Morfill G. E., Polanskey C., Riemann R., Schwehm G., Srama R. and Zook H. A. (1999 a). "Three years of Galileo dust data: II. 1993 – 1995". *Planetary and Space Science*, **47**, 85–106
- Krüger H., Grün E., Landgraf M., Baguhl M., Dermott S., Fechtig H., Gustafson B. A., Hamilton D. P., Hanner M. S., Horányi M., Kissel J., Lindblad B. A., Linkert D., Linkert G., Mann I., McDonnell J. A. M., Morfill G. E., Polanskey C., Schwehm G., Srama R. and Zook H. A. (1999 b). "Three years of Ulysses dust data: 1993 to 1995". *Planetary and Space Science*, **47**, 363–383.
- Krueger H., Strub P., Sterken V. J. and Grün E. (2015). "Sixteen years of Ulysses interstellar dust measurements in the solar system. I. Mass distribution and gas-to-dust mass ratio". *The Astrophysical Journal*, **812**, id 139, 16 pages.
- Landgraf M. and Grün E. (1998). "In situ measurements of interstellar dust". *Lecture Notes in Physics*, **506**. In Breitschwerdt D., Freyberg M. J. and Truemper

- J., editors, *The Local Bubble and Beyond. Lyman-Spitzer Colloquium, Proceedings of the IAU Colloquium No. 166*, held in Garching, Germany, 21-25 April, 1997, XXVII. Springer-Verlag Berlin Heidelberg New, pages 381–384.
- Landgraf M., Baggaley W. J. and Gruen E. (2000). “Aspects of the mass distribution of interstellar dust grains in the solar system from in situ measurements”. *Journal of geophysical research*, **105**, 10 343–10 352.
- Landgraf M., Krueger H., Altobelli N. and Gruen E. (2003). “Penetration of the heliosphere by the interstellar dust stream during solarmaximum”. *Journal of geophysical research*, **108**, A10, 8030.
- Lindblad B. A. (2003). Private communication.
- Lindblad B. A., Neslusan L., Porubcan V. and Svoren J. (2004). “IAU Meteor Database of photographic orbits - version 2003”. *Earth, Moon, and Planets*, **93**, 249–260.
- Linde T. J. and Gombosi T. I. (2000). “Interstellar dust filtration at the heliospheric interface”. *Journal of Geophysical Research*, **105**, 10411.
- Mann I. (2010). “Interstellar dust in the solar system”. *Annual Review of Astronomy and Astrophysics*, **48**, 173–203.
- Mathews J. D., Meisel D. D., Janches D., Getman V. S. and Zhou Q. H. (1999). “Possible origins of low inclination antapex micrometeors observed using the Arecibo UHF radar”. In Baggaley W. J. and Porubcan V., editors, *Meteoroids 1998*, Proceedings of the International Conference held at Tatranska Lomnica, Slovakia, August 17-21, 1998. Astronomical Institute of the Slovak Academy of Sciences, pages 79–82.
- Mathis J. S., Rumpl W. and Nordsieck K. H. (1977). “The size distribution of interstellar grains”. *The Astrophysical Journal*, **217**, 425–433.
- Meisel D. D., Janches D. and Mathews J. D. (2002). “The size distribution of Arecibo interstellar particles and its implications”. *The Astrophysical Journal*, **579**, 895–904.
- Musci R., Weryk R. J., Brown P., Campbell-Brown M. D. and Wiegert P. (2012). “An optical survey for millimetersized interstellar meteoroids”. *The Astrophysical Journal*, **745**, 161–166.
- Staubach P., Gruen E. and Matney M. J. (2001). “Synthesis of Observation”. In Grün E., Gustafson Bo. A. S., Dermott S. and Fechtig H., editors, *Interplanetary Dust*. Springer Berlin Heidelberg, pages 347–384.
- Sterken V. J., Altobelli N., Kempf S., Schwehm G., Srama R. and Gruen E. (2012). “The flow of interstellar dust into the solar system”. *Astronomy and Astrophysics*, **538**, A102.
- Sterken V. J., Strub P., Krueger H., von Steiger R. and Frisch P. (2015). “Sixteen years of Ulysses interstellar dust measurements in the solar system. III. Simulations and data unveil new insights into local interstellar dust”. *The Astrophysical Journal*, **812**, 141.
- Strub P., Krueger H. and Sterken V. J. (2015). “Sixteen years of Ulysses interstellar dust measurements in the solar system. II. Fluctuations in the dust flow from the data”. *The Astrophysical Journal*, **812**, 140.
- Sveden H. (1996). “Detection of possible interstellar particles by the HITEN Spacecraft”. In Gustafson Bo A. S. and Hanner M. S., editors, *Physics; chemistry; and dynamics of interplanetary dust*. Astronomical Society of the Pacific Conference Series; Proceedings of the 150th colloquium of the International Astronomical Union held in Gainesville; Florida; USA; 14-18 August 1995. San Francisco: Astronomical Society of the Pacific, **104**, 27–30.
- Taylor A. D., Baggaley W. J., Bennett R. G. T. and Steel D. I. (1994). “Radar measurements of very high velocity meteors with AMOR”. *Planetary and Space Science*, **42**, 135–140.
- Taylor A. D., Baggaley W. J. and Steel D. (1996). “Discovery of interstellar dust entering the Earth's atmosphere”. *Nature*, **380**, 323–325.
- Weryk R. J. and Brown P. (2004). “A search for interstellar meteoroids using the Canadian meteor orbit radar (CMOR)”. *Earth, Moon, and Planets*, **95**, 221–227.
- Wiegert P. A. (2011). “Preliminary Results on the Gravitational Slingshot Effect and the Population of Hyperbolic Meteoroids at Earth”. In Cooke W. J., Moser D. E. and Janches D., editors, *Proceedings of the Meteoroids 2010 Conference* held in Breckenridge, Colorado, USA, May 24–28, 2010. Pages 106–113.

# A tale of two fireballs

Mike Hankey and Vincent Perlerin

American Meteor Society, USA

mike.hankey@gmail.com, vperlerin@gmail.com

In this article, we briefly present two daytime fireball events that occurred in late winter of 2016. One event occurred in the United States and one in France. Both events generated 100s of eyewitness reports via the IMO/AMS online fireball report and had the signs of meteorite dropping fireballs. The prospects for meteorite hunting were positive enough that expeditions to recover fragments from both events took place. The US effort resulted in the recovery of 6 meteorite fragments. The French event has yet to produce any meteorite finds. Here in we discuss some details of each event, the efforts undertaken to estimate the respective strewn fields and the fieldwork that followed.

## 1 Introduction

Two daytime fireballs occurred in late winter of 2016 over the US and over France. The first one occurred over Northern Florida (Osceola) on Jan 24<sup>th</sup>, 2016 at 15<sup>h</sup>27<sup>m</sup> UTC. This event generated 134 witness reports<sup>1</sup> via the IMO/AMS online fireball report (Hankey et al., 2013). The second event occurred over Northeast France on February 25<sup>th</sup>, 2016 at 10<sup>h</sup>30<sup>m</sup> UTC and was reported by 342 witnesses<sup>2</sup>. Witnesses of both events described delayed sonic booms shortly after each event, indicating the fireballs reached the lower atmosphere and suggesting meteorites made it to the ground.

## 2 US fireball: radar data and witness reports

Dr. Marc Fries detected the Osceola meteorite fall on numerous NEXRAD Doppler Radar<sup>3</sup> stations a few hours after the event and before the witness reports were processed on the American Meteor Society website. Upon finding the returns, Dr. Fries notified Mike Hankey and asked him to create the event and compute the trajectory (Figure 1). Upon completion and review, Dr. Fries noted the AMS witness trajectory intersected the location of the meteorite cloud perfectly. Inspired in part by Dr. Fries resounding confidence that meteorites were on the ground in Florida, Hankey embarked on a recovery expedition a few days later.

Currently, meteorite recovery using Doppler weather has only been possible in the United States due to the open nature and distribution of the NEXRAD data set. When meteorite clouds in Doppler are found following witnessed falls, the precise location of the strewnfields are indicated by virtue of the return alone. For the purposes of meteorite recovery, trajectory reconstruction and dark flight models are not required. This was the case in Florida and meteorites were recovered on the second day of hunting before any video trajectories or dark flight were modeled. Only one picture and one video of the

Osceola fireball emerged following the event and using these Rob Matson modeled a 3D Trajectory and a dark flight model (Figure 2).

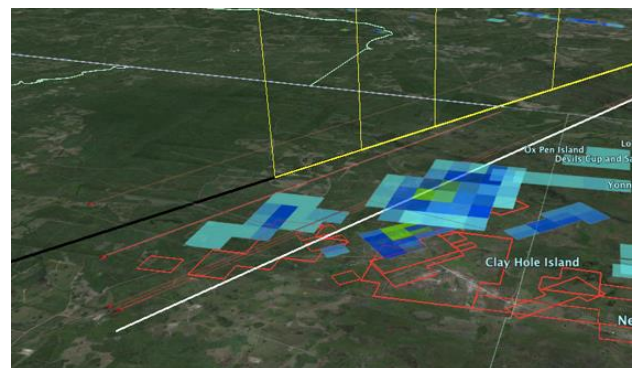


Figure 1 – Osceola Meteorite Fall Trajectory and NEXRAD RADAR, Credit AMS and Rob Matson.

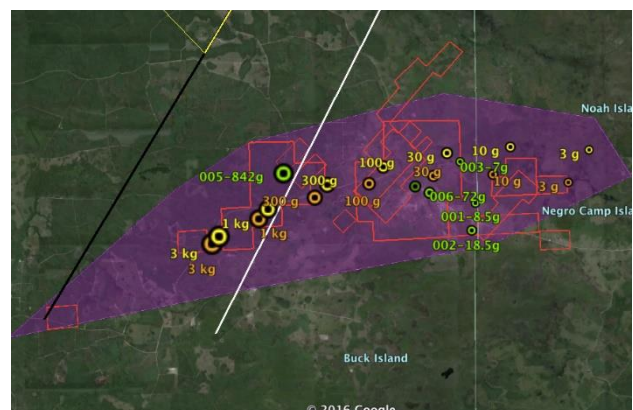


Figure 2 – Osceola Meteorite Fall Video Trajectory, Witness Trajectory, Dark Flight Model, Radar Returns and Meteorite Finds. Credit Rob Matson and American Meteor Society.

## 3 French fireball: photos and witness reports

The French fireball investigation has been conducted mainly by Tioga Gulon from REFORME (Réseau Français d'Observation de Météores). No video of the French event has been found so far and the French camera network FRIPON (Colas et al., 2015) was not working for daytime detection at this time. In addition to the 342 witness reports, three photos of the event have

<sup>1</sup> [www.amsmeteors.org/members/imo\\_view/event/2016/266](http://www.amsmeteors.org/members/imo_view/event/2016/266)

<sup>2</sup> [www.amsmeteors.org/members/imo\\_view/event/2016/732](http://www.amsmeteors.org/members/imo_view/event/2016/732)

<sup>3</sup> [www.intellicast.com/National/Nexrad/](http://www.intellicast.com/National/Nexrad/)

been used to redefine the witness-generated trajectory obtained by Vincent Perlerin from the online reports. Two of these photos were taken a few seconds to minutes after the event. They both show the trail of the fireball. Only one photo shows the fireball itself (*Figure 3*).



*Figure 3* – Three Photos of the French Event. a) Credit: P. Haydont – trail enhancement by T. Gulon b) Credit: Y. Blanchard c) Credit: A. Acer - trail enhancement by T. Gulon.

After interviewing the authors of the photos, Tioga Gulon measured some of the visible elements of the photos to estimate the trajectory from a Plane-Intersection computation. Karl Antier from REFORME managed to get wind information at the time of event. The result estimated trajectory was pretty close to the optimized witness-generated trajectory but the end points of both results were more than 3 miles apart. This can be explained by the fact that most of the witnesses that were on the West side of the fireball trajectory were hundreds of kilometers away from the event: most of the West side was cloudy as the time of the event (*Figure 4*).

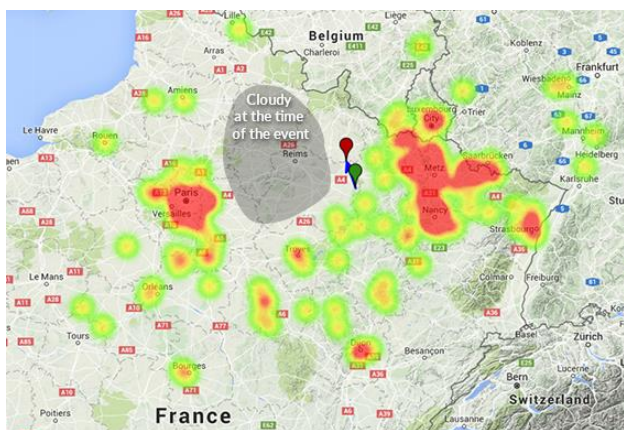


*Figure 4* – Location of the French Fireball witnesses and witness-generated trajectory.

After a couple of dozens of hours of search, no meteorite has been found for this event so far.

## 4 Conclusion

Meteorites are the rarest material on Earth for a good reason – they are extremely difficult to find. Efforts to recover freshly fallen meteorites from new candidate falls while difficult are worthwhile. The beauty of the NEXRAD system in the USA is that it is monitoring the lowest parts of the atmosphere. When meteorites appear at these low altitudes, the impact of wind and other forces displacing the meteorites before they hit the ground is almost non-existent. Even when these near perfect conditions exist, recovery is still extremely difficult and finds can take days, weeks or longer. Inspired from the talk, several IMO members have embarked on the investigation into obtaining radar data for their countries from the proper government agencies. If these files are saved by the government and can be accessed by the public then European Radar Meteorite Recovery should be possible.

## Acknowledgment

The authors wish to thank Marc Fries and Rob Matson for their assistance in finding and analyzing the NEXRAD radar data, inspection of video and trajectory reconstruction work and investigation and analysis of seismic data for the US Fireball. The authors also wish to thank Tioga Gulon and Karl Antier from REFORME for their work on the French Fireball study.

## References

- Colas F., Zanda B., Bouley S., Vaubaillon J., Marmo C., Audureau Y., Kwon M. K., Rault J.-L., Caminade S., Vernazza P., Gattacceca J., Birlan M., Maquet L., Egal A., Rotaru M., Gruson-Daniel Y., Birnbaum C., Cochard F. and Thizy O. (2015). “FRIPON, the French fireball network”. *Proceedings of European Planetary Science Congress 2015*, Nantes, France, 27 September - 2 October, 2015. Online at <http://meetingorganizer.copernicus.org/EPSC2015> id. EPSC2015-800.
- Hankey M., Perlerin V., Lundsford R. and Meisel D. (2014). “American Meteor Society online fireball report”. In Gyssens M., Roggemans P. and Zoladek P., editors, *Proceedings of the International Meteor Conference*, Poznan, Poland, 22-25 August 2013. IMO, pages 115–119.

# Results from the CAMS video network

Peter Jenniskens

SETI Institute, 189 Bernardo Ave., Mountain View, CA 94043, USA

Petrus.M.Jenniskens@nasa.gov

A status report is given on results from the CAMS meteoroid orbit and meteoroid spectroscopy survey. The survey detected some 230 meteor showers and shower components throughout the year. 70 of these are already in the IAU list of Established Meteor Showers, after 26 were verified by CAMS. An additional 55 previously known showers in need of confirmation were also validated. 19 new shower components were identified that are still in need of validation. 86 new showers were discovered, 54 of which were also found present in the SonotaCo meteoroid orbit database. There are ongoing efforts to expand the CAMS survey to sites spread in latitude and longitude.



Peter Jenniskens. (Photo Adriana Roggemans).

# Hemispherical radiating pattern antenna design for radio meteor observation

Jakub Kákona

Universal Scientific Technologies s r.o., Soběslav, Czech Republic

Czech Technical University, Prague, Czech Republic

kakonjak@fel.cvut.cz

A highly directional pattern antenna is usually used for radio meteor observations, but these types of antennas became impractical in cases where we have multiple transmitters spread around a reception station. In that situation the hemispherical sensitivity of the antenna is more important than directional antenna gain. We present a hemispherical radiation pattern antenna design which could be modified for almost any observational frequency reflective by a meteor trail. The symmetry of the radiation pattern of such antenna allows an easy construction of antenna arrays which could be used for the angular measurement of received signals.

## 1 Introduction

Historically, highly directional antenna designs such as Yagi were used for meteor observations (Maegawa et al., 1999). This approach was the simplest one due to the low sensitivity of receivers and easy mitigation of possible signal interference from other transmitters<sup>1</sup>.

However, if we want to build a multi-static SDR based radar network, we need a different antenna design which meets the following requirements:

- All-sky sensitivity;
- Stable parameters over the hemisphere (polarization, gain);
- Attenuation of signals from very low elevations (terrestrial noise);
- Capability of the antenna array construction;
- Robust maintenance-free design.

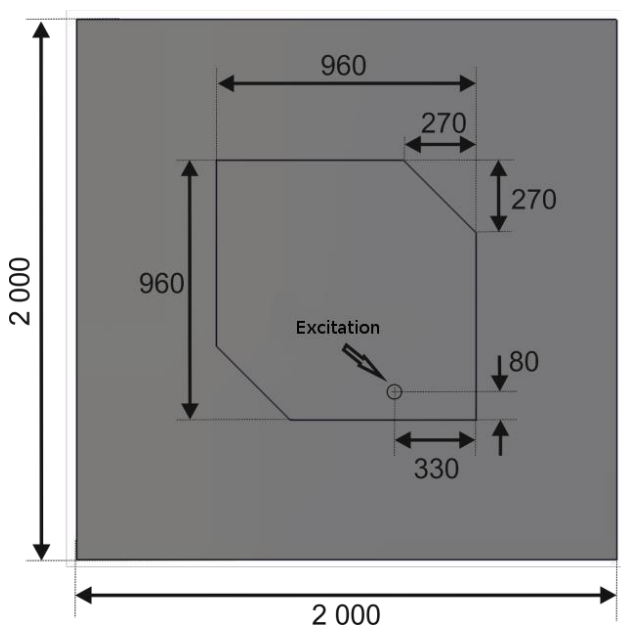


Figure 1 – Simplified drawing of a patch antenna design.

Two types of satellite communication antennas were tested: a patch antenna designed from a wire-mesh and a short-circuited quadrifilar helix.

## 2 Patch antenna design

The Patch antenna was initially examined due to expectation of a simple construction and manufacturing. The antenna was experimentally constructed from wire mesh with a square grid of about 10mm. This grid was chosen as a compromise between the antenna quality (surface conductivity) and the possibility of icing on the antenna's wire surfaces.

Preliminary tests and optimization were performed using the antenna numerical model. The result of the model was the antenna geometry (Figure 1) and the expected antenna radiation pattern (Figure 2).

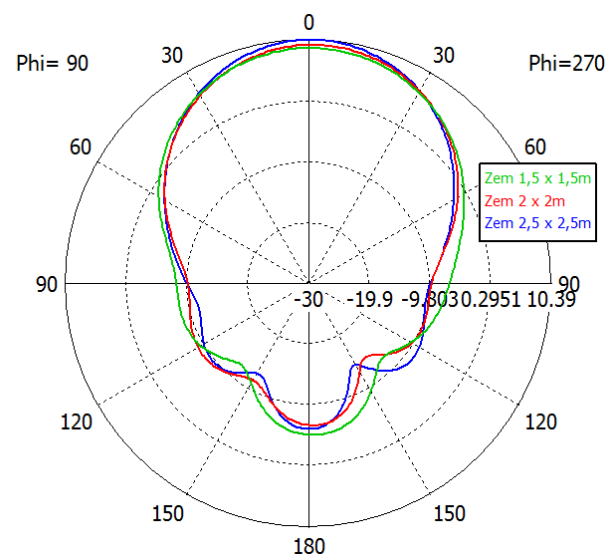


Figure 2 – Expected radiation pattern (vertical plane) of the patch antenna with a given size of reflector.

The real prototype of the antenna was made according to the computer model. A separation of two antennae patches were made by PVC water pipes which were cut to the proper length. Small perpendicular notches were

<sup>1</sup> <http://www.imo.net/radio/practical/antenna>

created on both ends to fix the wire mesh in place. The resulting antenna construction is shown in *Figure 3*.



*Figure 3* – Implemented form of the patch antenna mounted on an observatory roof.

Unfortunately, after the antenna’s construction and verification it was found that the antenna is very sensitive to deformation of patch base element and for the position of the central elevated element. Additionally, the central element must be a precise square to achieve a circular polarization. If these conditions are not satisfied the antenna has multiple resonances at different frequencies and easily affected the circular polarization and therefore could not be used. Therefore multiple metal sheets which allow tuning must be added to the central patch element. But the tuning will not be stable in time due to possible deformations of the antenna caused by environment or visiting animals.

### 3 Short-circuited quadrifilar helix

Another antenna type was proposed to overcome the issues of the previous antenna design experiment. A short-circuited quadrifilar helix (SC-QHA) is a variant of a well-known self-phased quadrifilar helix antenna (SP-QHA) (*Figure 4*). But unlike the SP-QHA type, the SC-QHA has a narrower bandwidth which depends primarily on a bandwidth of a phasing network. Therefore the antenna could be more efficient for narrow band signals like meteor reflections. The antenna was numerically modeled in *NEC2++* software. The source code of the model is published on Github<sup>2</sup>. The antenna radiation



*Figure 4* – Implemented form of a quadrifilar helix mounted on a metal base.

pattern models are shown in *Figure 5* and impedance characteristics are shown in *Figure 6*.

The real antenna prototype was made of “soft copper piping” with an outer diameter of the pipe of 18mm. It was twisted into a helix with a diameter of 390 mm and a height of 312 mm. Every helix arm was fed by a coaxial phasing network with  $\pi/2$  phase increment; the phase shift was generated by different lengths of RG58 cable. The  $\pi/2$  length is supposed to be 295 mm.

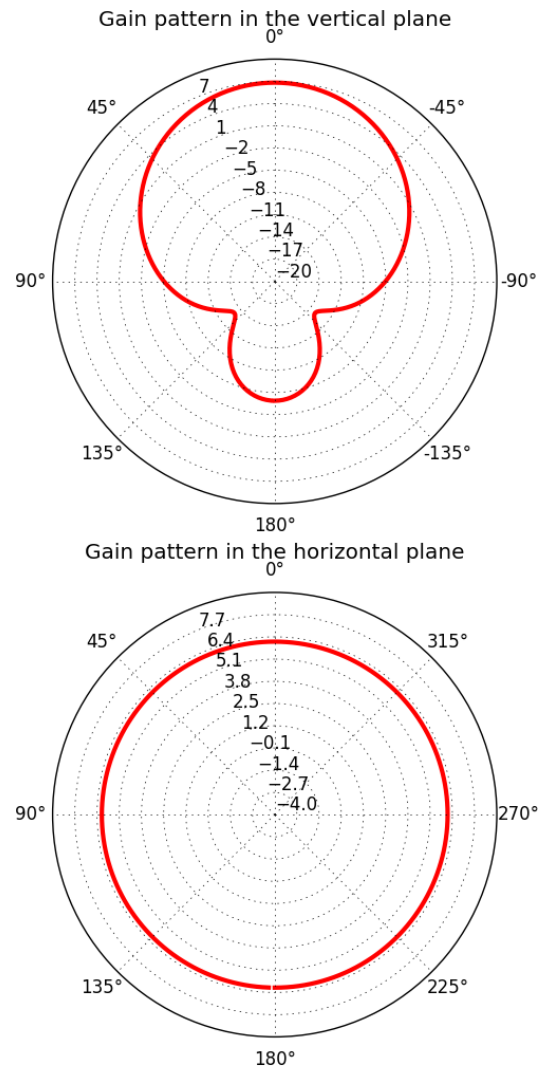


*Figure 5* – Expected radiation patterns of the quadrifilar helix antenna.

Unfortunately the resulting antenna resonance was at 161.5 MHz as is shown in *Figure 7*. This design frequency error is probably caused by temperature instability of the coaxial cable parameters. The frequency resonance measurement was made by a reflection bridge with a spectrum analyzer equipped with a tracking generator. The measurement was done on direct sunlight with temperatures around 60° C, but the coaxial cable parameters are specified for 25° C temperature conditions. Therefore the velocity factor of the coaxial cable could be different than the expected value in the calculation of the coaxial cable lengths in a phasing network.

<sup>2</sup> <https://github.com/bolidozor/NEC-models>

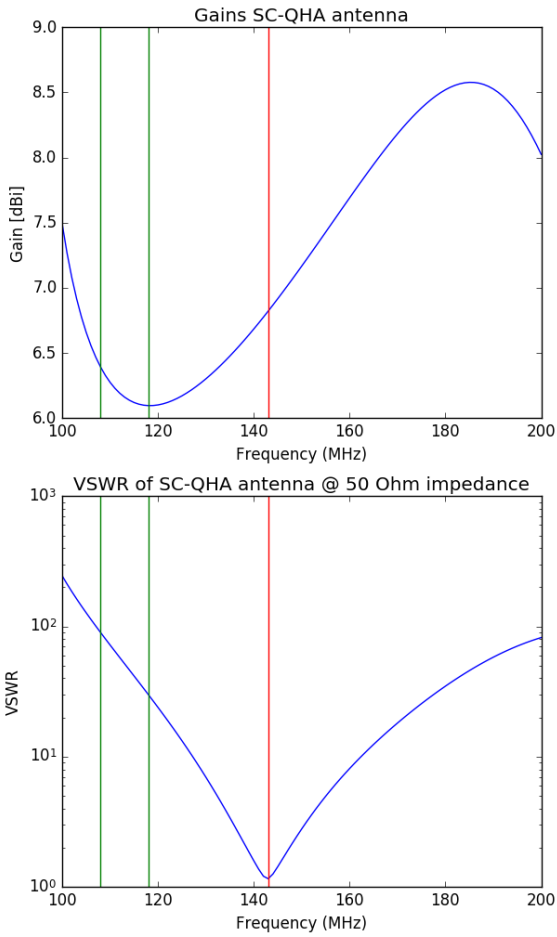


Figure 6 – Expected gain and impedance match of the quadrifilar helix antenna. Red vertical line indicates the GRAVES carrier frequency.

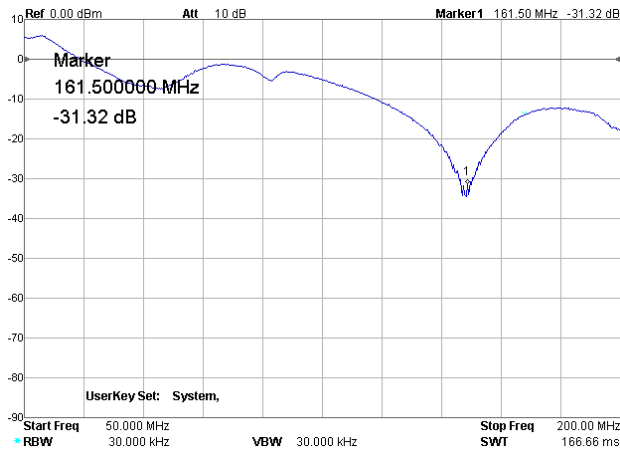


Figure 7 – Measured reflection (impedance match) of the quadrifilar helix antenna.

### 4 Conclusion

Both patch and QHA antennas were examined as potential candidates for multi-static observation networks. Unfortunately, the patch antenna was found too much demanding for manufacturing labor and the antenna parameters were unstable, therefore, it is considered insufficient for widespread use at the Bolidozor stations. The QHA antenna seems to be a better option but the implemented prototype shows a resonance of almost 20 MHz above the designed frequency. The precise reason for this error must be further explored.

### Acknowledgment

The project was supported by funds provided by the Czech Institute of Informatics, Robotics and Cybernetics (CIIRC).

### References

Maegawa K. (1999). “HRO: A New Forward-Scatter Observation Method Using a Ham-Band Beacon”. *WGN, Journal of the IMO*, 27, 64–72.

# Meteor trajectory estimation from radio meteor observations

Jakub Kákona

Universal Scientific Technologies s r.o., Soběslav, Czech Republic

Czech Technical University, Prague, Czech Republic

kakonjak@fel.cvut.cz

Radio meteor observation techniques are generally accepted as meteor counting methods useful mainly for meteor flux detection. Due to the technical progress in radio engineering and electronics a construction of a radio meteor detection network with software defined receivers has become possible. These receivers could be precisely time synchronized and could obtain data which provide us with more information than just the meteor count. We present a technique which is able to compute a meteor trajectory from the data recorded by multiple radio stations.

## 1 Introduction

Several meteor trajectory estimation attempts were made in the past several years. Two main methods emerged based on the forward scattering radio detection principle. The first one is based on rotation ellipsoids calculation (Maintoux et al., 2014) and the second method is based on Doppler shift measurements caused by a head echo reflection phenomenon of meteors (Steyaert et al., 2010).

The trajectory estimation method based on the “head-echo” Doppler shift seems to be the most promising estimation method according to our experiments.

However, a successful trajectory estimation from radio signal must meet several criteria:

- Meteor head-echo reflection has to be recorded by multiple stations (at least 3);
- Head-echo Doppler frequencies must be precisely known;
- Precise time must be known for each measured Doppler data point.

## 2 Meteor head-echo signal

If the meteoroid enters the atmosphere with hypersonic speed a shock wave is created on the front of the meteoroid (*Figure 1*). The shock wave contains plasma which is capable to reflect radio waves. The reflection is possible on higher frequencies than the reflection caused by a meteor trail due to higher density of plasma in the shock wave. However, the surface of a head-echo shock wave with a usable plasma density has a quite small area, usually only a few square meters. Therefore, we need to use a shorter wavelength to observe meteors compared to wavelengths commonly used in traditional meteor observation techniques. Using a VHF beacon, such as the GRAVES transmitter, has the advantage of causing the majority of meteor reflections to have the head-echo signal signature (*Figure 2*). Head-echo signal can be distinguished easily from meteor trail reflection signal as it has a strong Doppler shift caused by the fast movement of a shock-wave in front of a meteoroid. The Doppler

shift always begins on higher frequencies than in the case of the meteor trail reflection. It reflects a basic principle – the meteoroid always travels from the top layers of the atmosphere down to the bottom ones.

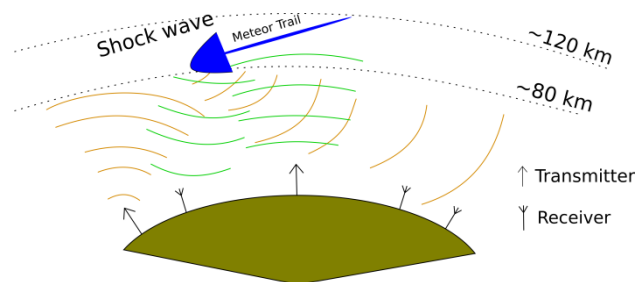


Figure 1 – Head-echo signal formation.

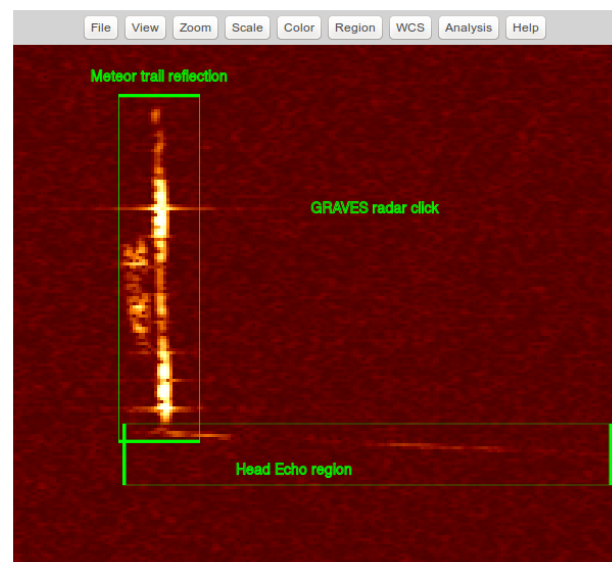


Figure 2 – Typical meteor reflection signal. Vertical axis corresponds to time (the latest sample on top). Horizontal axis corresponds to signal frequency ( the lowest frequency on left).

## 3 Trajectory estimation principle

The Doppler footprint of a meteor is specific for each station and each observed meteor. The signal difference between stations is shown in *Figure 3*. Head-echo differs only in time shift between stations and the time/frequency

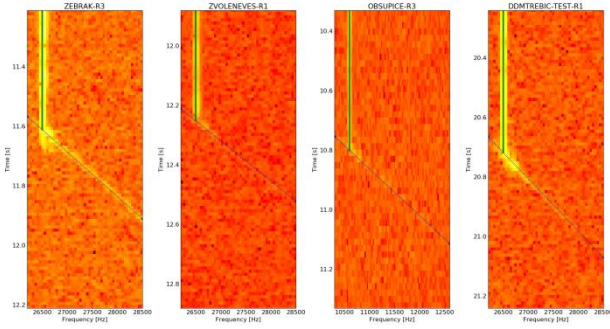


Figure 3 – Example of radio signal recorded from the same meteor at multiple stations.

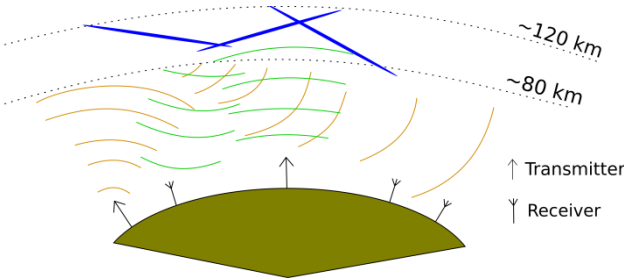


Figure 4 – Multiple possible meteor vectors generated as possible candidates.

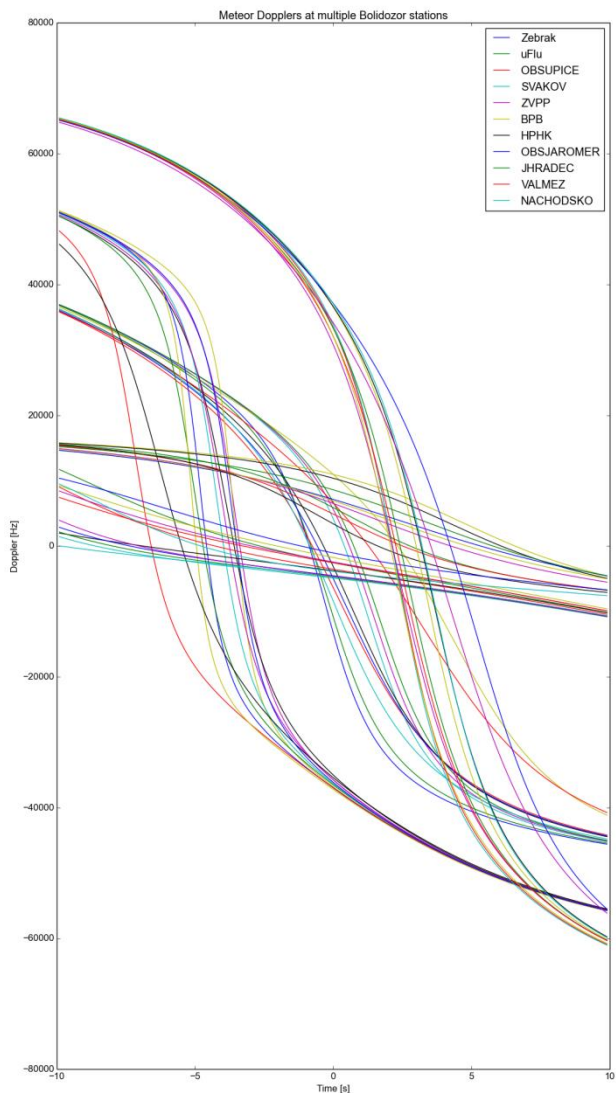


Figure 5 – Head-echo Dopplers generated by a model from several meteor trajectories.

slope of the Doppler shifted signal. Therefore the trajectory estimation task consists of finding a meteor trajectory which fits the best to the measured time differences and head-echo signal slope.

We created a simple signal modeling tool which takes the meteor vector coordinates and calculates the meteor head-echo signature. Then the trajectory estimation process proceeds with finding the input parameters of the model which gives a signal which is similar to the measured signal. Several gradient and evolutionary algorithms were tested for that task. But the general principle is to generate many possible meteor candidates in known boundaries and selecting the one, which fits the best (Figure 4).

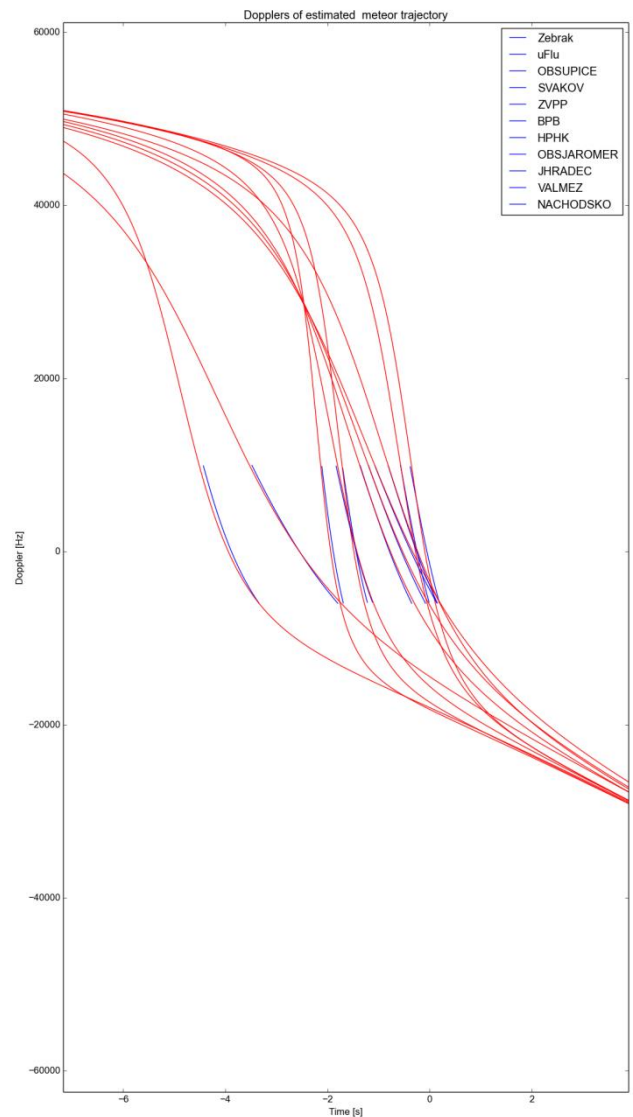


Figure 6 – Example of model parameters well fitted to the measured data points. Measured data are blue lines in the center of the image. The model output are the red lines fitted on the measured data.

The main problems of this method are optimization algorithm robustness, signal model precision and measured data accuracy. The optimization problem is nonlinear and usually ill-conditioned. Therefore the numerical solving presents a computationally difficult problem which takes hours of running on a generic

computer to find a satisfactory result. The quality of the result could be easily verified by overlapping the measured data points with the signal model output. One example of well fitted meteor data is shown in *Figure 6*.

The result of this model fitting is the most probable meteor vector in the atmosphere.

The source codes for the above-mentioned experiment are published at the Bolidozor's github<sup>1</sup> which gives further details on the algorithm and its test results.

## 4 Conclusion

A described meteor trajectory estimation algorithm was preliminary tested on several radio meteor detection events. However, further development verification and automation of the method is needed. Verification of the method with optical and radio coincident events is the nearest goal in the future development.

## References

- Maintoux J.-J., Azarian S., Maintoux J. and Rible F. (2014). "RETRAM recognition and trajectories of meteors". In Rault J.-L. and Roggemans P., editors, *Proceedings of the International Meteor Conference*, Giron, France, 18-21 September 2014. IMO, pages 211–214.
- Steyaert C., Verbelen F. and VVS Beacon Observers (2010). "Meteor Trajectory from Multiple Station Head Echo Doppler Observations". *WGN, Journal of the IMO*, **38**, 123–129.

---

<sup>1</sup> <https://github.com/bolidozor>

# The multi technique meteor observations in 2014

Anna Kartashova<sup>1</sup>, Galina Bolgova<sup>1</sup>, Yuriy Rybnov<sup>2</sup>,  
Olga Popova<sup>2</sup> and Dmitry Glazachev<sup>2</sup>

<sup>1</sup>Institute of Astronomy of the Russian Academy of Sciences, Moscow, Russia

<sup>2</sup>Institute for Dynamics of Geospheres Russian Academy of Sciences, Moscow, Russia  
akartashova@inasan.ru

Test multi technique (optical and acoustical) meteor observations were organized by the Institute Astronomy RAS (INASAN) and the Institute for Dynamics of Geospheres RAS (IDG RAS) in 2014. The goal of our multi technique meteor monitoring is to collect basic meteor observations and to study the formation and propagation of pressure pulses which are formed due to the interaction of meteoroids with the atmosphere.

## 1 Introduction

The interaction of meteor particles with the atmosphere produces the optical (actually meteors) and infrasound emission. Most meteor particles do not reach the surface of the Earth, their properties (mass, size, density, etc.) are estimated based on the observational data under different assumptions. The details of meteor-atmosphere interaction are poorly known, the parameters of meteor particles are determined with large uncertainty. Simultaneous registration of meteors by different techniques provides the possibility to refine both the meteor parameters and models of particle interactions with the atmosphere (Silber and Brown, 2014; Silber et al., 2015).

Test multi technique (optical and acoustical) meteor observations were organized by the Institute Astronomy RAS and the Institute for Dynamics of Geospheres RAS in 2014. The goal of testing multi technique observations was to check the possibility of continuous combined (optical and acoustical) meteor monitoring.

## 2 Optical meteor observations

Since 2011 INASAN has been conducting the meteor observations from two stations: Zvenigorod observatory INASAN and ISTR station (Kartashova, 2015; Kartashova and Bolgova, 2015). In the beginning the

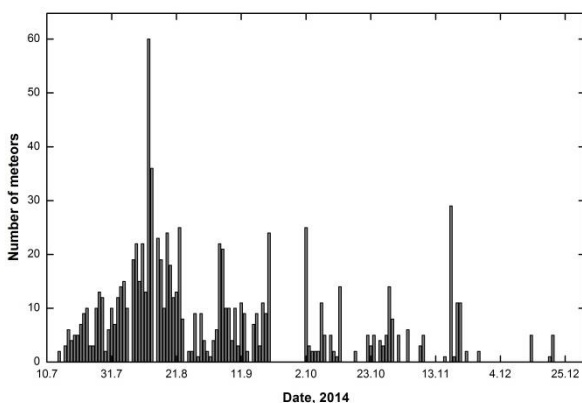


Figure 1 – The distribution of the number of meteors detected at the ZO INASAN in 2014.

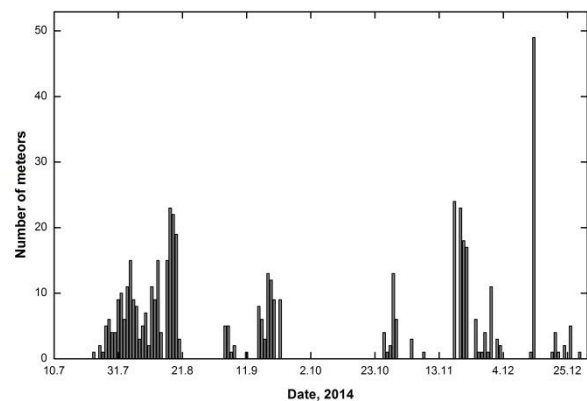


Figure 2 – The distribution of the number of meteors detected at the GPhO Mikhnevo in 2014.

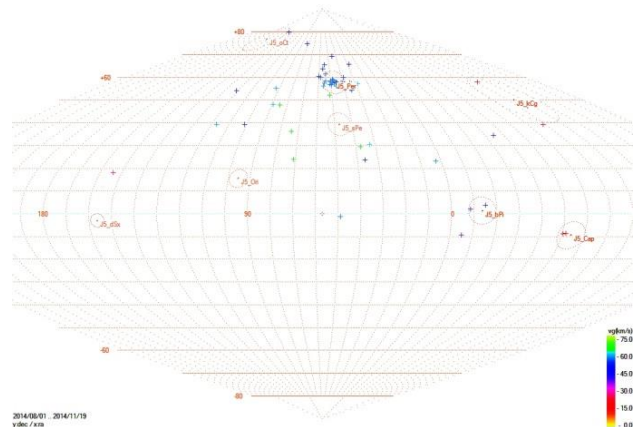


Figure 3 – The distribution of meteor radiants by observations in 2014.

meteor observations were performed from the Geophysical observatory Mikhnevo IDG RAS in 2014.

The distance between the stations (the ZO INASAN and GPhO Mikhnevo IDG RAS) is 104 km. The distribution of the number of meteors detected at the ZO INASAN and GPhO Mikhnevo from July to December in 2014 is shown on *Figures 1 and 2*.

67 double-station meteors were obtained at these stations in 2014. The radiant positions, geocentric velocity, heights and orbit parameters were calculated for all

double-station meteors. The distribution of radiant positions is presented on the *Figure 3*.

Most of the meteors detected at both stations in this period of time were Perseids.

### 3 Acoustical meteor observations

Continuous monitoring of infrasound is carried out by the IDG RAS at two sites (Geophysical observatory Mikhnevo and the main building of the Institute for Dynamics of Geospheres RAS). The registration of pressure variations is carried out by infrasound stations. The microbarometers used (*Figure 4, Table 1*) allow one to register the pressure changes from 0.02 Pa to 200 Pa in the frequency band of 0.001 – 20 Hz. Three pressure sensors arranged in a triangle with a base of  $\approx 100\text{m}$  in the IDG RAS are used to track infrasound fluctuations.



*Figure 4* – The microbarometer MB-03.

*Table 1* – The parameters of the microbarometer MB-03.

Parameters	
The pressure measuring range	0.05÷200 Pa
Band registration	0.001÷20 Hz

The time of arrival of the acoustic signal from the meteoroid to the registration point is estimated, taking into account the stratification of the atmosphere and the velocity/direction of the wind. The time interval of  $\pm 1$  min of the estimated arrival time was selected for a more detailed search. A special algorithm for the signal analysis is used (*singular spectrum analysis*). The analyzed 3-dimensional time series (consisting of signals from three detectors) are filtered and divided into overlapping blocks, each of which was the maximum eigenvalue of the spectral matrix. The signal was indicated as detected in the block in which the maximum eigenvalue exceeds a certain prescribed level. The block duration and bandwidth are chosen depending on the expected origin of the signal.

The direction to the source of the signal is determined for each pair of bases. The final direction is defined as the weighted average of these directions. The average velocity of the signal at arrival and corresponding

velocity and direction uncertainties are determined simultaneously. If the obtained direction is in agreement with the estimated arrival time, then the signal is considered as appropriate.

### 4 The results

Possible infrasound signals were detected for two meteors (*Figures 5 and 6*).

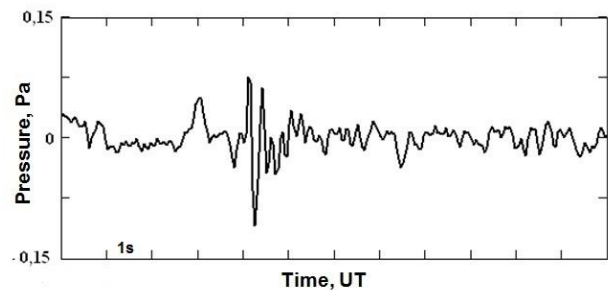


*Figure 5* – The detected signal of the “20140803\_220009” meteor detected by IDG RAS.

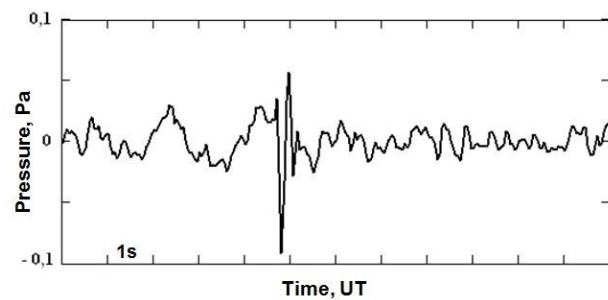


*Figure 6* – The detected signal of the “20140804\_223531” meteor detected by IDG RAS.

These meteors were detected simultaneously by two optical stations.

The parameters of these meteors were calculated from optical double-station observations (*Table 2*).

Unfortunately, the infrasound measurements were obtained only from one station, so there was no possibility to confirm the relation between these signals and the optical meteor registrations, it is only possible to suspect their interrelation (based on the timing and the position of the observations).

### 5 Conclusion

The test meteor observations in 2014 confirmed the possibility to carry out multi technique observations at a few locations. In the future the optical meteor observations will be carried out at five stations in 2016 (ZO INASAN, “Istra” station, GPhO Mikhnevo, RSU and the “Sazhnevo” station). Simultaneously infrasound meteor observations will be carried out by three stations (IDG RAS, GPhO Mikhnevo, ZO INASAN) (*Figure 7*).

The coordinates of the source (the meteor) on the Earth’s surface (the hypocenter) will be calculated by infrasound

Table 2 – The parameters of “20140803\_220009” and “20140804\_223531” meteors.

Name	$M_a$	$\alpha_R$ °	$\delta_R$ °	$V_g$ km/s	$H_b$ km	$H_e$ km	a a.u.	q a.u.	e	$\omega$ °	$\Omega$ °	incl °
20140803_220009	0.45	2.39	23.19	60.52	103	91.31	7.9	0.5	0.94	272.2	131.2	133.79
20140804_223531	-0.67	33.24	57.2	58.34	108.57	89.92	26	0.9	0.96	156.8	132.2	110.19

observations from two stations using the intersection of the directions on the source. The multi technique meteor observations will provide the possibility to obtain different parameters of meteoroids, including their masses.

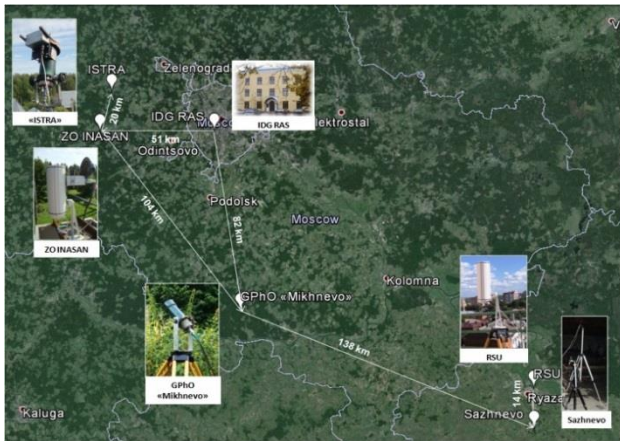


Figure 7 – Locations of television meteor stations in Russia.

## Acknowledgment

We would like to thank Dr. A.V. Bagrov for his help with the observations. The work was partially supported by Program № 7 of the fundamental research of the

Presidium of RAS “Experimental and theoretical research of Solar system and planetary systems of stars. Transient and explosive processes in astrophysics”.

## References

- Kartashova A. (2013). “Television meteor observations in INASAN”. In Gyssens M. and Roggemans P., editors, *Proceedings of the International Meteor Conference, September 20-23, 2012, La Palma, Canary, Spain*. IMO, pages 174–177.
- Kartashova A. P. and Bolgova G. T. (2015). “TV observations of the Perseid meteor shower in 2012-2013”. *Planetary and Space Science*, **118**, 120–126.
- Silber E. A. and Brown P. G. (2014). “Optical Observations of Meteors Generating Infrasound – I: Acoustic Signal Identification and Phenomenology”. *Journal of Atmospheric and Solar-Terrestrial Physics*, **119**, 116–128.
- Silber E., Brown P. and Krzeminski Z. (2015). “Optical observations of meteors generating infrasound – II Weak Shock Theory and Validation”. *Journal of Geophysical Research*, **120**, 413–428.

# A statistical approach to the temporal development of orbital associations

Daniel Kastinen<sup>1,2</sup> and Johan Kero<sup>2</sup>

<sup>1</sup>Department of Computer Science, Electrical and Space Engineering,  
Luleå University of Technology, Sweden  
dankas-1@student.ltu.se

<sup>2</sup>Swedish Institute of Space Physics (IRF), Kiruna, Sweden  
kero@irf.se

We have performed preliminary studies on the use of a Monte-Carlo based statistical toolbox for small body solar system dynamics to find trends in the temporal development of orbital associations. As a part of this preliminary study four different similarity functions were implemented and applied to the 21P/Giacobini-Zinner meteoroid stream, and resulting simulated meteor showers. The simulations indicate that the temporal behavior of orbital element distributions in the meteoroid stream and the meteor shower differ on century size time scales. The configuration of the meteor shower remains compact for a long time and dissipates an order of magnitude slower than the stream. The main effect driving the shower dissipation is shown to be the addition of new trails to the stream.

## 1 Introduction

A lot of problems in astrophysics and celestial mechanics can be traced back to the comparison of objects, or collections of objects, and the resulting associations that are made. Often, this process involves creating some sort of similarity or dissimilarity measure, like the commonly known D-criterion first developed by Southworth and Hawkins (1963). Sometimes, this measure can be an actual representation of distance, i.e. a metric. More often, however, it represents a subjective view of similarity. Using such a measure, a set of objects can be examined for patterns.

Most common types of association analysis for meteor measurements that we are aware of are the density function analysis, the wavelet transform, and cluster analysis. Another common method is to manually look at the data. The density function method will bin the space looking for regions of bins with high frequencies of meteors. However, to avoid manual selection, it is often needed to use a critical threshold where one can say that the density is large enough to imply the presence of a pattern. Sometimes this threshold can be derived by long term continuous observations, while this may not always be the case. The same principle applies for the wavelet analysis, with the difference that the specific pattern of the mother wavelet is searched for in addition to an increase in meteor count. Lastly, the cluster analysis approach involves choosing a critical distance, or threshold, at which a connection is made. If two objects are within this threshold they are connected to each other. After a connection has been made, there are several ways to merge the clusters. However, whatever method is used the clusters that are formed depend on the size of the critical threshold. Thus, all these methods rely on knowledge of either the background, i.e. the sporadic meteor complex and measurement uncertainties, or of the critical threshold needed for the shower to be selected.

In a straightforward and integrable system one can use models to exactly propose what restrictions to apply to the data in order to associate elements. If, however, the system is either chaotic or the amount of variables is so large that it appears impossible to predict a definite evolution of the system, statistics and approximations have to be applied. When considering meteoroids or meteors, the reliability of an association heavily depends on applied assumptions of, e.g. the correct value for the critical threshold (Kastinen et al., 2014). This is one of the main reasons we have chosen to apply a statistical approach to the problem, in order to start investigating the general statistics related to meteoroid streams.

We here present some of the first results from applying a new software toolbox that we are developing. The intention is to improve orbital association methods, such as those used for identifying meteor shower members in observational data by choice of method and calibration using simulations rather than *ad hoc* assumptions.

## 2 Software

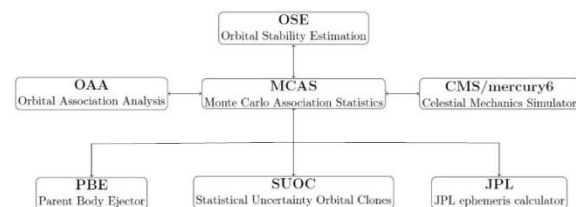


Figure 1 – Overview of the software toolbox modules.

One of the most challenging tasks when creating new software is broad functionality without losing usability. To maximize the functionality of all the developed software we have chosen to proceed in a modular fashion as illustrated in Figure 1. Every significant self-contained part of the analysis and simulation is packaged into an independent module. One module acts as a master

program, the Monte Carlo Association Statistics (MCAS) module, which has the ability to call several other independent modules. The modules can run independently of the master program or in unison. The user can therefore link modules in different orders, choose to distribute data between modules in different ways, and tailor case studies in a powerful fashion.

Not to restrict ourselves to a specific method in our preliminary set of simulations, we have chosen to calculate an orbital association distance matrix at each time step, defined as:

$$D_{nm} = D(O_n, O_m), \quad (1)$$

where  $O_n = \{a_n, e_n, i_n, \omega_n, \Omega_n\}$  are the orbital elements of the meteoroid labeled  $n$ . All the functions we have applied are symmetric  $D(O_n, O_m) = D(O_m, O_n)$ , and follow the coincidence axiom:

$$D(O_n, O_m) = 0 \Leftrightarrow O_n = O_m$$

Thus, this matrix has a zero diagonal and is symmetric, which means that it is only necessary to consider the upper triangular part of the matrix. In other words, if we have  $N$  objects, the indices will range from  $1 \leq n < N$  while  $n < m \leq N$ . This will provide a list of all unique inter-meteoroid orbital similarities in the stream at each time step.

In equation (1) the function  $D$  may represent any of several different similarity functions. Here we present results from an investigation using four different similarity functions. Two of these are D-criteria;  $D_{SH}$  (Southworth and Hawkins, 1963) and  $D_D$  (Drummond, 1980). The other two are the metrics of the Kepler space;  $\rho^2$  (Kholshchevnikov and Vassiliev, 2004) and  $\varphi_1$  (Kholshchevnikov, 2004).

A detailed description of the software is presented in Kastinen (2016).

### 3 Simulation

The results presented here is a subset of an extensive dust trail simulation of 21P/Giacobini-Zinner, a comet which is recognized as the parent body of the October Draconids meteor shower. Its short orbital period of six years and perihelion distance very close to that of the Earth has led to extensive observations and an early connection between the comet and its meteor shower on Earth. These properties make the produced dust stream an ideal candidate for causing strong meteor outbursts on Earth. As such, it is also an ideal candidate for a first case study performed with the new software toolbox. In the simulation cometary material was ejected between 1866 and 1972 and propagated until the year 2020. Due to limitations in computing power, we only performed the stream dissipation calculation on the dust trail formed during the 1900 passage. Each of the perihelion passages where sampled with 50 clones of 21P/Giacobini-Zinner, each clone ejecting  $\sim 8000$  test particles with individual weights indicating the amount of meteoroids it

represented. The weights and ejection speeds were calculated using the cometary ejection model outlined by Hughes (2000). The clones were generated by assuming a multidimensional Gaussian distribution of the orbital elements based on observational uncertainties provided by the JPL small body database<sup>1</sup>. A detailed description of the simulation is reported by Kastinen (2016).

## 4 Results

As the amount of inter-meteoroid distances scales as  $\mathcal{O}(N^2)$  we have reduced the data by taking the mean and standard deviation of the distance matrix defined in equation (1) at each time step. The results for the distance matrices calculated at each time step for the dust trail formed in 1900 is presented in Figure 2. This curve is the mean dissipation curve calculated by averaging all of the dissipation time series produced by the 50 clones of 21P/Giacobini-Zinner to account for variations due to initial condition uncertainties.

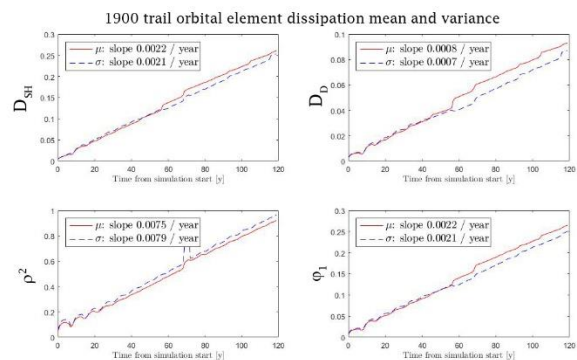


Figure 2 – Temporal evolution of the 1900 trail dissipation.

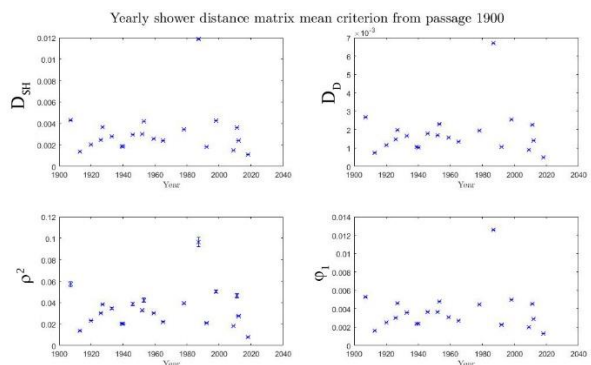


Figure 3 – Temporal evolution of the dissipation within the meteor showers caused by the 1900 trail.

Figure 3 shows the same mean and standard deviation calculation of the distance matrices, when applied on the meteoroids that encountered the Earth during specific years, separately. Here, the error bars are the standard deviation of the distance matrix. We have chosen not to connect the yearly points in the graph as not all years contain meteor showers.

<sup>1</sup> <http://ssd.jpl.nasa.gov/sbdb.cgi>

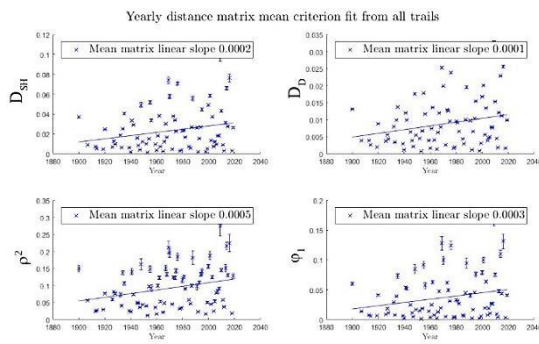


Figure 4 – Temporal evolution of the dissipation within the meteor showers caused by all the simulated trails.

Since the amount of particles that encounters the Earth is significantly smaller than the amount that is ejected during sublimation, we could perform the same calculation as shown in Figure 3 but including all the simulated dust trails without extensively increased computing time. The resulting graph is presented in Figure 4, where we have also included the linear regression fit to emphasize the trend of increased dissipation. As there are more dust trails and test particles included than in Figure 3, the number of years where showers are present is larger.

## 5 Discussion

To conclude the results, for the 21P/Giacobini-Zinner stream on the time scale of around 100 years:

- Given just one dust trail:
  - The stream dissipates linearly.
  - The shower remains at constant density.
- Given the entire stream:
  - The complete shower disperses with time due to addition of trails.
  - This dissipation of the shower is much slower than the dissipation of the stream.
  - The dust trail configuration is more complex and cannot be adequately described by simple means and standard deviations.

We can also find some general scale differences, as the linear trend in Figure 4 is an order of magnitude less than the trend in Figure 2. Also, the almost absent trend in Figure 3 is situated at around two orders of magnitude less than the total dissipation after 100 years shown in Figure 2. These considerations can be translated into practical use when considering questions such as:

- If the stream has dissipated over large sections of orbital element space, can there still be concentrated meteor showers on Earth?
- What are the main effects causing this behavior and can they be used for a classification of meteoroid streams?
- How should a meteor shower selection be calibrated in observational data?
- Which similarity functions and analysis methods excel in which scenarios, and where do they fail?

We believe that performing these kinds of simulations is a good starting point to begin answering these questions.

One of the strengths of inferring properties from simulations such as this is that all possible scenarios within the assumed initial uncertainties are considered. Thus one can assume that the general statistical trends will better represent reality. However, this is also the main weakness as many of the subtle trends in a specific scenario are lost. There is a middle ground where one can pick and choose scenarios based on some criterion to bring out specific characteristics and this is something that should be considered in the future.

From examining the results described here we can conclude that there can be compact outbursts of the October Draconids even if the trail has dissipated as a whole over large sections of the solar system. We can also use such simulations to begin inferring the maximum age of the detected meteoroids and we can start considering at what point the dust trail should be considered a part of the sporadic complex. As the transition from stream to sporadic membership is smooth and a threshold is subjective, one may use simulation such as this one to justify the choice.

The collection of many case studies like this, together with sporadic modeling, can begin to clarify such concepts and general statistical properties of the meteoroid complex. We intend to use the models and preliminary results from the previous work presented by Kastinen et al. (2014) to find such properties of the meteoroid complex and will attempt to validate and reproduce statistics that are found in observations.

## References

Drummond J. D. (1980). “On the meteor/comet orbital discriminant D”. *Proceedings of the Southwest Regional Conference for Astronomy and Astrophysics*, **5**, 83–86.

Hughes D. W (2000). “On the velocity of large cometary dust particles”. *Planetary Space Science*, **48**, 1–7.

Kastinen D., Kero J. and Nakamura T. (2014). “Meteor shower analysis using a Hausdorff metrization function”. In Muinonen K. et al., editors, *Asteroids, Comets, Meteors 2014*. Proceedings of the conference held 30 June - 4 July, 2014 in Helsinki, Finland. Page 253.

Kastinen D. (2016). “Meteors and celestial dynamics: association and numerical analysis”. *Master thesis (in press)*, Luleå University of Technology.

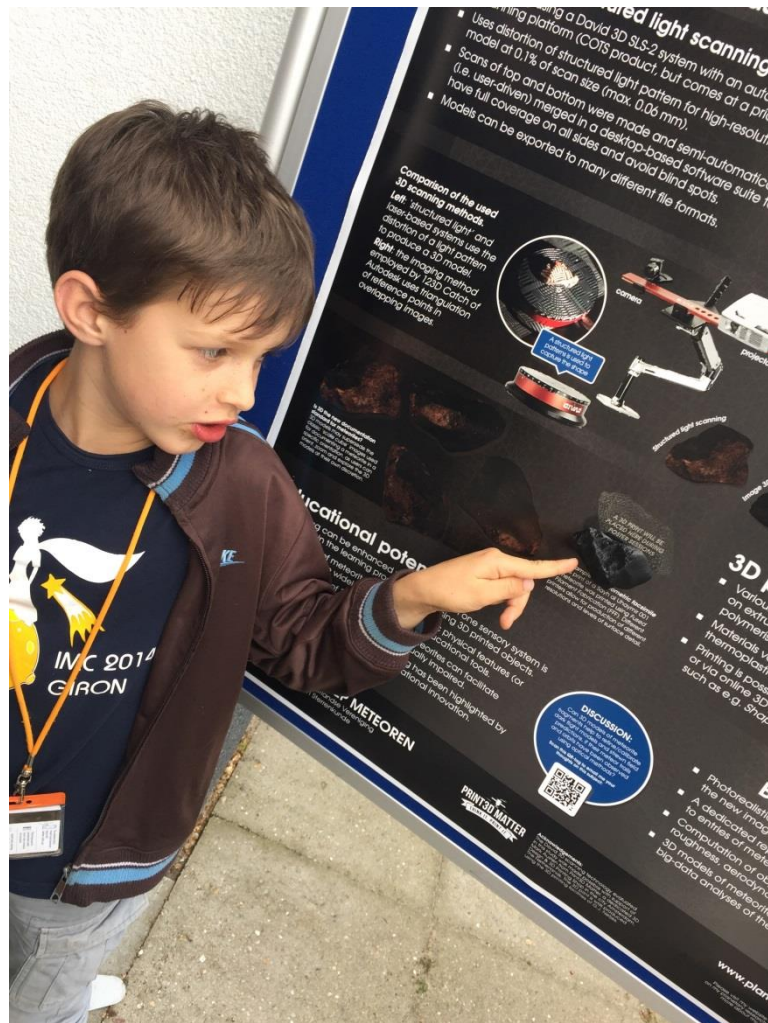
Kholshevnikov K. V. and Vassiliev N. N. (2004). “Natural metrics in the spaces of elliptic orbits”. *Celestial Mechanics and Dynamical Astronomy*, **89**, 119–125.

Kholshchevnikov K. V. (2008). “Metric spaces of Keplerian orbits”. *Celestial Mechanics and Dynamical Astronomy*, **100**, 169–179.

Southworth R. B. and Hawkins G. S. (1963). “Statistics of meteor streams”. *Smithsonian Contributions to Astrophysics*, **7**, 261–285.



Daniel Kastinen.



Uroš Bettonvil discovers a 3D printed meteorite.

# The role of population in tracking meteorite falls in Africa

Fouad Khiri<sup>1,2</sup>, Abderrahmane Ibhi<sup>1</sup>, Thierry Saint-Gerant<sup>3</sup>,  
Mohand Medjkane<sup>3</sup> and Lahcen Ouknine<sup>1</sup>

<sup>1</sup> Geoheritage and Geomaterials Laboratory, University Ibn Zohr, Agadir, Morocco  
a.ibhi@uiz.ac.ma

<sup>2</sup> Regional Center of Trades of Education and Training, Inzegane, Agadir, Morocco  
fkhiri2009@gmail.com

<sup>3</sup> Identité et différenciation des espaces, de l'environnement et des sociétés (IDEES), Université de Caen  
thierry.saint-gerand@unicaen.fr

The 158 African meteorite falls recorded during the period 1801 to 2014, account for more than 12.3% of all meteorite falls known from the world. Their rate is variable in time and in space. The number of falls continues to grow since 1860. They are concentrated in countries which exhibit large population (mainly rural population) with an uniform distribution. Generally, the number of falls follows the increase of the population density (coefficient of correlation  $r = 0.98$ ). The colonial phenomenon, the education of population in this field, the population lifestyle and the rural exodus, are also factors among others which could explain the variability of the recovery of meteorite falls in Africa. In this note, we try by a statistical study, to examine the role of the African population in tracking meteorite falls on this continent.

## 1 Introduction

Meteorites are rocky fragments coming from space and which have an extremely old formation ages (4.55 Ga). So, it constitutes a great source of information about the history of the solar system. For this, their collection is important for scientific study, especially the observed meteorites falls (meteorite seen to fall and subsequently collected), which offer fresh materiel. Based on photographic data of fireballs from a network of 60 cameras operational in western Canada for nine years, Halliday et al. (1984) calculated that some 5800 meteorites with masses of at least 100 grams may be deposited annually on the Earth's land surface. However, on average, only five to six meteorites have been seen to fall annually throughout the world and recovered over the two last centuries (Graham et al., 1985).

According to the "Meteorite Nomenclature Committee of the Meteoritical Society"<sup>1</sup>, 158 meteorite falls have been recorded during the period 1801 to 2014 in Africa. This number accounts for more than 12.3% of all meteorite falls known from the world. Some of these meteorites have great scientific and cultural value, as the Martian observed falls "Nakhla" and "Tissint" (Ibhi, 2013; Ibhi et al., 2013; Treiman, 2003). In this very populous continent (1.138 billion inhabitants in 2014), the rate of meteorite falls is variable in time and in space (Khiri et al., 2015). In this note, we try by a statistical study, to examine the role of the African population in tracking meteorite falls and to explain the variable distribution of these fragments in this continent.

## 2 Results and discussion

In Africa, the meteorite fall recovery rate, during these past 214 years, is 0.74 falls per year on average (or approximately one fall recovery per 1.35-year time interval, or equivalently, 0.023 falls per year per 106 km<sup>2</sup>).

Figure 1 illustrates the cumulative number of meteorite falls since 1800. It reveals varied temporal distribution. The falls spreading rate has increased from 3 falls only in the continent during the period 1800–1860, to 23 falls between 1860 and 1920, and 132 falls during the period 1920–2014.

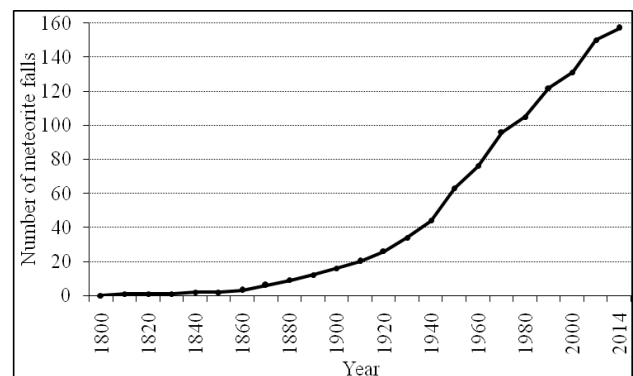


Figure 1 – The cumulative number of meteorite falls recorded in Africa.

Moreover, the  $\frac{1}{3}$  of African countries (19) has not yet recorded meteorite falls, others account 1 to 22 falls.

The cumulative number of African meteorite falls and the African population density since 1950 are shown in Figure 2. Generally, there is a net correlation between the fall rate and the population density in this continent

<sup>1</sup> <http://www.lpi.usra.edu/meteor>

(coefficient of correlation  $r = 0.98$ ). In the 64-year time interval from 1950 to 2014, the African population density increased by 500% and ninety five African meteorite falls were recorded, i.e., an increasing of 250%. The meteorite fall rate roughly varies linearly with the time varying population density in the period 1950–1990. Between 1990 and 2014 we note a deficiency of falls observed. Some 95 meteorite falls might have reasonably been expected especially in the last 24 years. It would appear, therefore, that the fall observed rate is related to the increasing of population density among others.

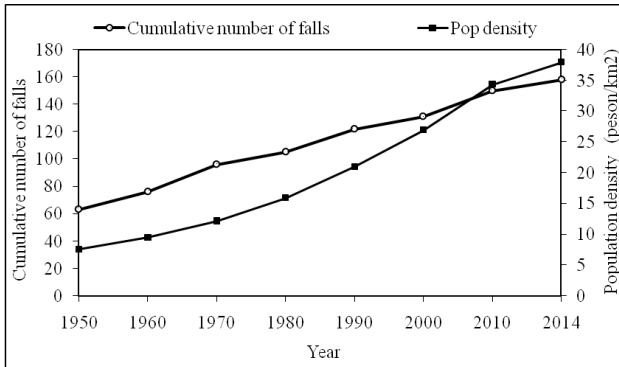


Figure 2 – The cumulative number of meteorite falls recorded and population density (people per square kilometer) in Africa from 1950 to 2014.

The projection of African meteorite coordinates (using ArcGIS 10.2.2 application) according to the population density (Figure 3) shows that more than 52% (82) of the African meteorite falls have been recovered from East and Southern Africa, and 40% from North-Western Africa. The bulk (22 ; 15 ; 11 ; 11) of these coming from South Africa, Nigeria, Morocco and Sudan respectively. It's clear that the regions with high and medium population densified (the North of Morocco, Algeria and Tunisia, Nigeria (163 people per km<sup>2</sup>), Rwanda (372 people per km<sup>2</sup>), Burundi (319 people per km<sup>2</sup>), the South-East of South Africa, has recorded the most meteorite falls. However, the western part of the Sahara desert recorded meteorite falls despite their low population density (less than five persons per km<sup>2</sup>). However, this region appears to be much less empty if we calculate the population density per km of roads or trails, some significant population densities appear along the roads (until 600 inhab. per km<sup>2</sup>) with some cities of more than 10000 inhabitants (Tamanrasset, Arak, Reggane in Algeria) (SWAQ, 2015). Most of the people living in the Sahara today villages or they are nomads who move from region to region throughout the desert.

According to the continent or to their countries, the rate of meteorite falls increases with the population density. However, the population is very unevenly distributed in Africa. Some populous countries such as Libya and Egypt present less than 2 falls with population condensed on the north or on the banks of the Nile respectively. The uneven distribution of population (concentrated in part of the country) would make it difficult for the falls to be discovered. This confirms that the uniformed distribution of the inhabitants is an essential factor for the spreading

rate of meteorite falls. Rasmussen (1991) and Wickman and Palmer (1979) have mentioned that the distribution of human populations affects the probability of meteorite recognition and recovery.

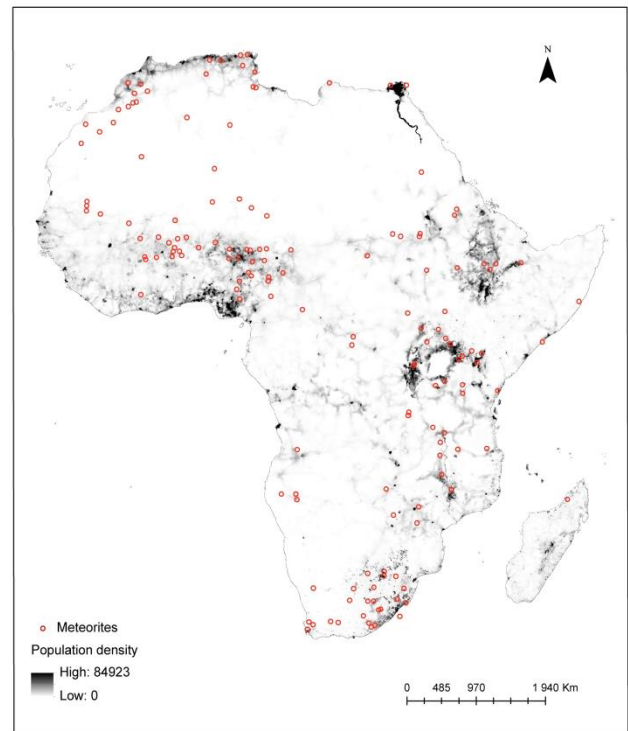


Figure 3 – Geographical distribution of African meteorite falls according to population density.

More, we have used the time of observing meteorite falls available for 52 African falls in order to calculate the percentage of meteorite fallen during the day and those observed at night. This calculation shows that 75% of these meteorite falls (39 of the 52 falls) had been observed at daytime. This result can be related to the presence of human being out of their houses during the day. If we consider that the flux of meteorite falls is the same during the day and night, therefore the same number (39) might have been observed at night, but this number does not exceed one third (13 falls). Then, 67% of meteorite falls at night would not been seen when they fall.

According to the African countries, we have opposed the number of falls to the total population, rural population and to urban population. This calculation shows that the rate of meteorite falls is more correlated with rural population ( $r = 0.69$ ) than with the total population ( $r = 0.62$ ) and urban population ( $r = 0.44$ ). The lifestyle of rural population, including nomads (who have developed a true know in favor of meteorites observing and collecting) and who live far from the contemporary modern world: their night light is the moon or the small fire; they are constantly in touch with nature, concerned about what is around them in heaven as on Earth. So they can look for falls of meteorites and testify. While in cities people have their eyes fixed on their television, computer and tablet. They live entirely inside houses and are

therefore occupied assailed by all kinds of artificial lighting sources to the point that although meteorites fall, nobody notices them!

Moreover, the fall recovery rate has apparently not increased with increasing population density since 1990. This could be linked to the migration population to the cities: the average rural population has decreased from 66.6% in 1990 to 57% in 2014 in Algeria, from 48% to 29% in South Africa, from 48% to 35% in Morocco, 73% to 52% in Nigeria.

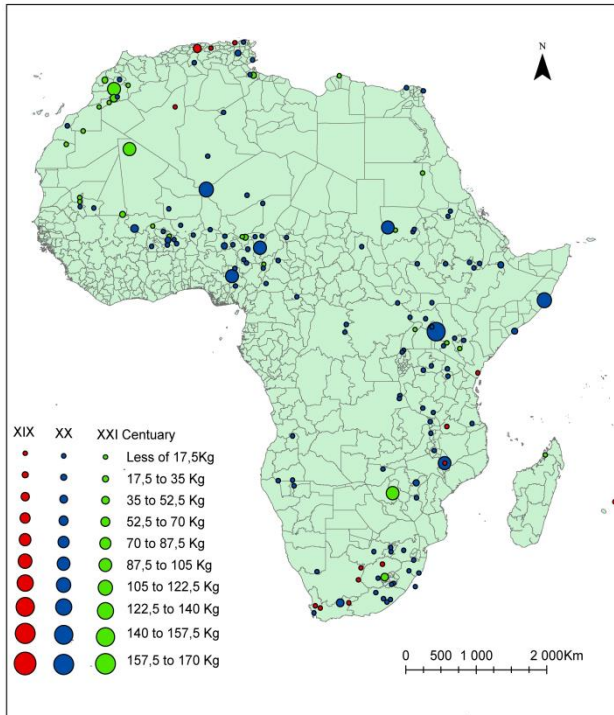


Figure 4 – Distribution of African meteorite falls according to the century of their fall.

Figure 4 shows the distribution of African meteorite falls according to the century of their fall. The fall rate was low in the 19<sup>th</sup> century (14 falls). This rate is timed into 10 during the 20<sup>th</sup> century with 115 meteorite falls recorded. Then, 28 meteorites have been seen and recorded during the period 2000–2014.

In the following, we try to confront the variation of the fall number with the evolution of the population density at the level of the African continent. In 1700 Africa had counted 100 million inhabitants i.e., 17% of the world population. In 1900, it still had 100 million (6% of the world population). During these two centuries, there has been a real demographic recession: the effects of the slave trade (35 million departed from Africa as slaves), the European colonial penetration and internal wars had depopulated this continent (Louise and Diop, 1985). This decrease of the population could be a factor among others which explain the low rate of recorded falls during the 19<sup>th</sup> century in Africa.

The low rate of the period 1800–1860 can be also correlated to the lack of culture and education about meteorites: since ancient times and in many African countries, the passage of such objects remains linked to

false beliefs such as the death of somebody or the passage of the devil.

The small increase recorded in the period 1860–1920 can be linked to the entrance of European countries that began in 1860 in Algeria and South Africa. Indeed, Figure 4 shows that Algeria and South Africa are among the first countries that had recorded meteorite falls in the 19<sup>th</sup> century. We noticed that the most successful African countries in terms of recovery of meteorite falls were colonized by Great Britain (South Africa; Nigeria and Sudan) and France (Morocco; Mauritania, Algeria and Tunisia). More, the first falls observed in most of the African countries have on subsequent dates those of their colonization (for example: Algeria in 1865, Malawi in 1899, etc.). These two occupant countries experienced meteorite falls since the beginning of 17<sup>th</sup> century and many falls were observed and collected during the 19<sup>th</sup> century. Dodd (1986) had noted that France was the country in which the scientific importance of meteorites was first recognized around 1800. The colonization was accentuated in 1885 and was widespread in 1914 in parallel with the demographic growth (from 8 to 35 per km<sup>2</sup> in the period 1950–2014), that could explain the increase of the meteorite fall rate in the 20<sup>th</sup> century and the beginning of the 21<sup>st</sup> century. It's apparent that the colonial phenomenon had a cultural impact on the meteorite education. Dodd (1986) and Bevan (1992) had recognized that historical and educational factors have also contributed to the recovery of meteorites. This period 1920–2014 was so productive also by dint of the interest given to the exploration of space and the increase of researchers' teams who are interested in meteorites. Beech (2003) suggests that to recover more meteorites we need both an educated and inspired public, as well as an active team of field researchers.

### 3 Conclusion

In Africa, the observing and collecting of meteorite falls appears to be related to the population and its uniform distribution. More, this rate is well correlated with the largest proportion (60%) of African rural population. The lifestyle of this population, including nomads (constantly in touch with nature) and their education and supervision in the field of meteorites are in favor of meteorites observing and collecting. The historical and educational factors have also contributed to the recovery of African meteorites. Although the colonization contributed to the decrease of the population in the 19<sup>th</sup> century, it had a cultural impact which is behind the increase of meteorite falls during the 20<sup>th</sup> century. Despite this, the fall rate is low.

In order to increase the observed falls number, we need to install surveillance cameras of celestial stones in some African countries, just like in some European countries. 100 all-sky cameras have been installed at the end of 2015 in the program FRIPON (Fireball Recovery and Interplanetary Observation Network) to cover all the French territory to collect a large number of meteorites

with an accurate orbit determination (François et al, 2015).

## References

- Beech M. (2003). "Canadian fireball rates and meteorite falls-declining returns?". *Meteorites Magazine*, **9**, 3–9.
- Bevan A. W. R. (1992). "Australian meteorites". *Records of the Australian Museum*, Supplement **15**: 1–27.
- Colas F., Zanda B., Vaubaillon J., Bouley S., Marmo C., Audureau Y., Kwon M. K., Rault J.-L., Caminade S., Vernazza P., Gattacceca J., Birlan M., Maquet L., Egal A., Rotaru M., Birnbaum C., Cochard F. and Thizy O. (2015). "French fireball network FRIPON". In Rault J.-L. and Roggemans P., editors, *Proceedings of the International Meteor Conference*, Mistelbach, Austria, 27-30 August 2015. IMO, pages 37–40.
- Dodd R. T. (1986). "Thunderstones and shooting stars: the meaning of meteorites". Harvard University Press, Cambridge, Massachusetts and London, England. 196 pages.
- Graham A. L., Bevan A. W. R. and Hutchison R. (1985). "The catalogue of meteorites". 4<sup>th</sup> edition, Trustees of the British Museum (National History), London.
- Halliday I., Alan T. B. and Arthur A. G. (1984). "The Frequency of Meteorite Falls on the Earth". *Science*, **223**, 1405–1407.
- Ibhi A. (2013). "New Mars meteorite fall in Morocco: final strewn field". *International Letters of Chemistry, Physics and Astronomy*, **11**, 20–25.
- Ibhi A., Nachit H. and Abia El. H. (2013). "Tissint Meteorite: New Mars Meteorite fall in Morocco". *J. Mater. Environ. Sci.*, **4**, 293–298.
- Khiri F. and Ibhi A. (2015). "African meteorites falls: some statistics". *European Planetary Science Congress 2015*, **10** # 80.
- Louise M. and Diop M. (1985). "Essai d'évaluation de la population de l'Afrique Noire aux XVe et XVIe siècles". **40**, 855–884.
- Rasmussen K. L. (1991). "Historical accretionary events from 700 BC to AD 1850-A 1050 year periodicity". *Quarterly Journal of the Royal Astronomical Society*, **31**, 95–108.
- SWAQ (Sahel and West Africa Club). January 2015. Population density in the Sahara. (14).
- Treiman A. H. (2003). "The Nakhla Martian meteorite is a cumulate igneous rock. Comment on Glass-bearing inclusions in Nakhla (SNC meteorite) augite". *Mineralogy and Petrology*, **77**, 271–277.
- Wickman F. E. and Palmer C. D. (1979). "A study of meteorite falls". In *Indian Academy of Sciences Proceedings Section*, **88**. Pages 247–272.

# Height computation of a fireball

Detlef Koschny

European Space Agency, Noordwijk, the Netherlands  
Lehrstuhl für Raumfahrttechnik, TU Munich, Germany  
detlef@koschny.de

This article describes the first height computation of a bright fireball which the author performed in 1977.

## 1 Introduction

My family moved into the Munich area in Southern Germany in the year 1974. Just a few months earlier I became interested in astronomy, and quickly found some friends in my new school who shared my interest. One of our common activities was to follow talks at the public observatory of Munich, the *Volkssternwarte München*. In 1975 we heard a talk by Hans Georg Schmidt about visual observations of meteors. We were fascinated by the idea of doing interesting sky observations without the need for a telescope and decided to try this ourselves. It took another year and a half until August 1977 when Roland Egger, Franz Hauswirth and myself met in the house of my grandmother in Pfarrkirchen in lower Bavaria – the place where I was born. In this rural area the sky was dark and seeing the Milky Way was normal. We spent four nights outside to observe the Perseid meteor shower. I remember that we were not really prepared, no sleeping bags only a thin blanket... I was freezing and the humidity was high. We were observing from a hill which we dubbed 'Dreikreuzsberg' since three large wooden crosses towered over us during our observations, see *Figure 1*. Fog hampered our observations and all in all we only saw a bit over 100 meteors in a few hours over the four nights.

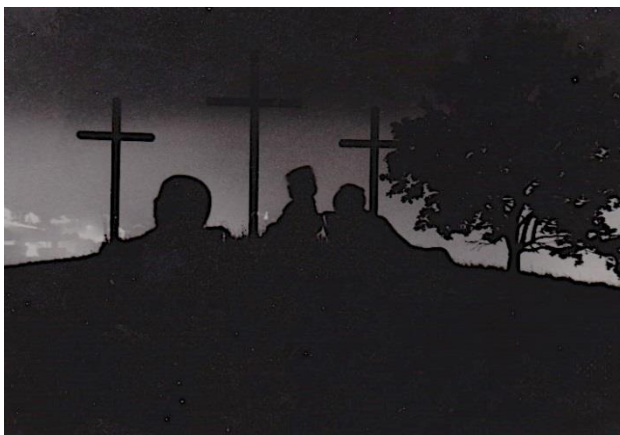


Figure 1 – Three meteor observers in August 1977 next to the three crosses of the Dreikreuzsberg.

## 2 The observations

A summary of the observations can be found in our report, the introduction of which is shown in *Figure 2*. An English translation would read roughly like this:

*“Observations and conditions – 11/12 August: The first night on the ‘three-cross hill’. It was spooky. The hill indeed has three crosses on top. The fog climbed up the hill like a huge amoeba, swallowing everything which gets into its way. Also there was a ‘beam of darkness’ – just like the beam from car headlights, only dark instead of bright. Still, we were able to observe until around 01:30, then the amoeba swallowed us and we had to pack up. 13/14 August: Starting around 20:00 high fog came up. When it was still there around midnight we gave up. We saw only one meteor in 3 hours L...”*

### 1. Beobachtungen und Bedingungen

11./12. 8.

Die erste Nacht auf dem "Dreikreuzsberg"! Es war sehr gespenstisch, denn der Berg, genauer gesagt Hügel, trägt seinen Namen zu Recht: auf ihm stehen wirklich drei Kreuze. Aber nicht nur deswegen war es so gespenstisch, sondern auch wegen des Nebels, der um unseren Hügel kroch wie eine riesige Amöbe, die alles verschlingt, was sich ihr in den Weg stellt. Oder auch wegen eines geheimnisvollen Dunkelstrahls, der wie das Licht eines Autoscheinwerfers den Nebel durchdrang, nur eben mit dem Unterschied, daß er dunkel war. Trotzdem konnten wir bis etwa 01h30m beobachten, dann aber schloß sich der Nebel über uns, und wir mußten das Feld räumen.

13./14. 8.

Ab etwa 20h00m zog starke hochnebelartige Bewölkung auf. Als diese sich um Mitternacht noch nicht versogen hatte, gab das Team die Beobachtung auf. Trauriges Ergebnis: Eine Schnuppe in drei Stunden!

14./15. 8.

Bereits um 23h00m, als wir mit den Beobachtungen begannen, war der Horizont vernebelt (Brunnenschachtphänomen!). Um Mitternacht aber schlug der Wettergott erbarmungslos zu und vereitelte jede weitere Beobachtung.

15./16. 8.

Diese Nacht war wohl vom Wetter her die günstigste. Das trotzdem nur so wenig Meteoriten gesichtet wurden, liegt wohl an der starken Übermüdung der Beobachter. Interessant war, zu beobachten, wie die Perseiden langsam von anderen Strömen abgelöst wurden.

Figure 2 – Introduction of our observing log. For an English translation at least of the beginning, see the text.

In the night 15/16 August a very bright fireball showed up behind my back. None of us were facing into that direction, but I do remember that my first thought was “who is taking photographs with a flashlight at this time in the night?”. We all turned to see the fireball, and recorded that it “... appeared exactly in the west, at a zenith distance of 40 degrees”.

Besides this fantastic experience we enjoyed not only the observations but also the hospitality of my grandmother and spent a few nice days together. From that time on we regularly went out to perform visual meteor observations for many years. Of course we shared our experiences with H. G. Schmidt when back at the *Volkssternwarte München*. He remembered that they had also seen the bright fireball.

We were 15 years old and after that Perseid season started with 7<sup>th</sup> grade in high school. In December I had one of the key experiences in my life: In math class the teacher explained the sine and cosine function to us – see *Figure 3* for a copy of my notes, which I still have at home. I immediately realized that with these functions and the combined observations of our group and those from the *Volkssternwarte München* it would be possible to compute the height of the fireball. Hans-Georg checked their observing log – they had seen the fireball directly towards the North direction. They had been observing from the Sudelfeld in the Alps Mountains. I sketched the viewing directions into a map, see *Figure 4*.

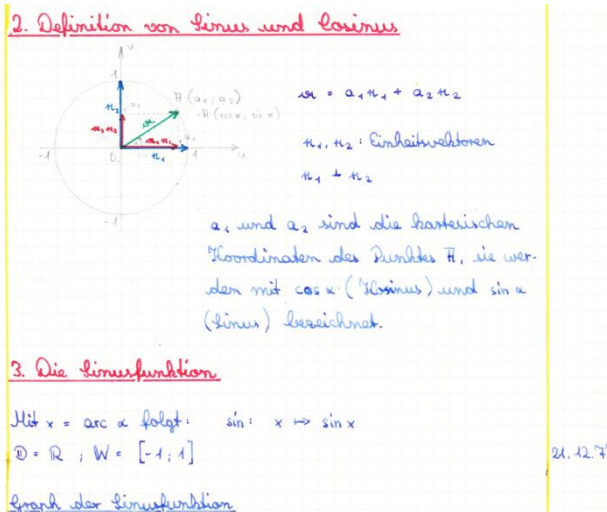


Figure 3 – Copy of the author’s notes from his math course on 21 Dec 1977.

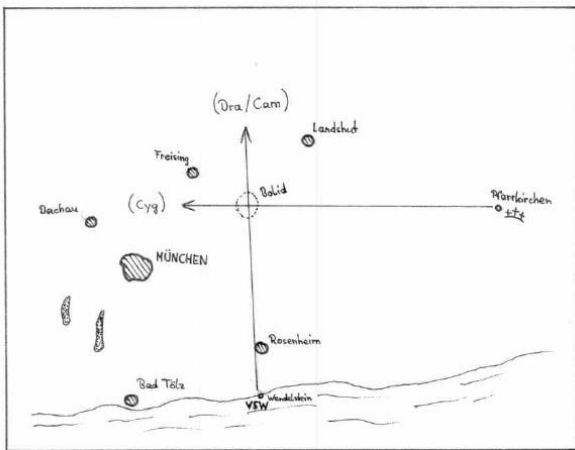


Figure 4 – Observing geometry of the fireball. ‘VSW’ indicates the location of the Volkssternwarte München; we were observing from Pfarrkirchen.

The fireball entered the Earth’s atmosphere about half way between Munich and Ingolstadt. From the plot the

distance between the fireball and us could be taken from a map. Applying the cosine function now gives the height, see *Figure 5*.

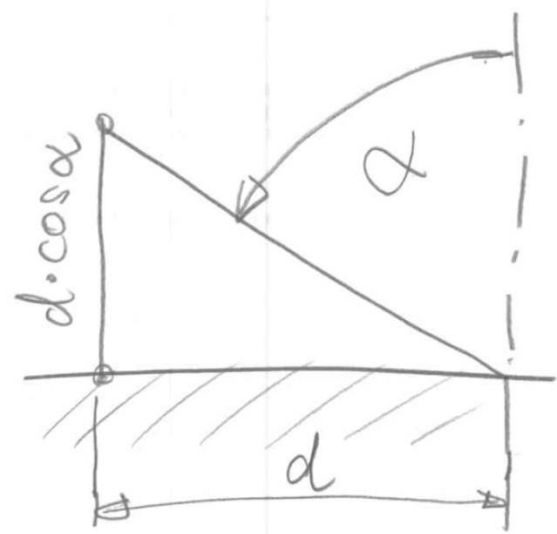


Figure 5 – From the distance  $d$  and the zenith angle  $\alpha$  the height of the fireball can be computed via  $d \cdot \cos(\alpha)$ .

The result was documented in our report from the observation, see *Figure 6*. It says “... the height was between 30 and 50 km”. In one of the hardcopies of the report this was corrected by hand to 81 km though.

7. Der Bolid 26-15./16.

Leider liegen nur ungenaue Angaben über dieses Objekt vor, da er in einer von uns nicht besetzten Gegend fiel. Unsere Aufmerksamkeit erregte er dadurch, daß er mit mehreren Explosionen die Landschaft wie eine defekte Blitzlichtlampe ausleuchtete. Der Bolid fiel genau im Westen bei einer Zenitdistanz von 40 Grad. Durch Vergleich mit den Aufzeichnungen der Volkssternwarte München, die den Boliden vom Wildalpjoch aus in den Sternbildern Draco-Camelopardis sahen, konnte ich den Fallort bestimmen: ungefähr in der Mitte zwischen München und Landshut. Die Aufleuchtzeit lag zwischen 30 und 50 km.

Figure 6 – Extract from the observing report, describing the result of the fireball computation.

Using *Google Earth* I find a distance between our observing location and the plotted fireball position of 75 km. Computing  $75 \text{ km} \cdot \cos(40^\circ)$  results in 57 km. Thus it seems that neither ‘30-50 km’ nor ‘81 km’ were correct. Still, I remember this experience well and now, almost 40 years later, I am still observing meteors, normally on my computer screen, imaged by cameras operating automatically in the Canary Islands. And we have software available to compute the trajectory of a meteoroid to a few tens of meters accuracy... But I will never forget the experience of sitting outside at night and the impressiveness of a bright fireball like the one we witnessed in August 1977.

# Simultaneous analogue and digital observations and comparison of results

Pavel Koten<sup>1</sup>, Rostislav Štork<sup>1</sup>, Petr Páta<sup>2</sup>, Karel Fliegel<sup>2</sup> and Stanislav Vítek<sup>2</sup>

<sup>1</sup>Astronomical Institute of ASCR, Ondřejov, Czech Republic  
koten@asu.cas.cz

<sup>2</sup>Faculty of Electrical Engineering, Czech Technical University, Prague, Czech Republic

Double station observations using analogue video cameras are carried out at the Ondřejov observatory since 1998. Recently new digital cameras MAIA were developed and introduced. Both systems are based on the same type of image intensifier. To evaluate the enhanced properties of the new cameras several simultaneous campaigns with both systems were accomplished.

## 1 Introduction

The video cameras with image intensifiers are used for the double station observations of the meteors and meteor showers. They are usually deployed at two astronomical observatories – Ondřejov and Kunžak. The distance between them is 92.5 km, the azimuth of the southern station is 340°. The analogue cameras were in operation since 1998. The new digital camera systems MAIA equipped with the same image intensifiers were developed in recent years (Fliegel et al., 2009; Koten et al., 2011) and deployed on both stations, too. New detection software (*dMAIA*) as well as the software for measuring of the video records (*MAIAMetPho*) were also developed.

To evaluate the capabilities of the new observational systems, we carried out several simultaneous campaigns with both analogue and digital cameras employed. The same meteors detected by both camera systems were identified, measured and the results are compared in this paper.

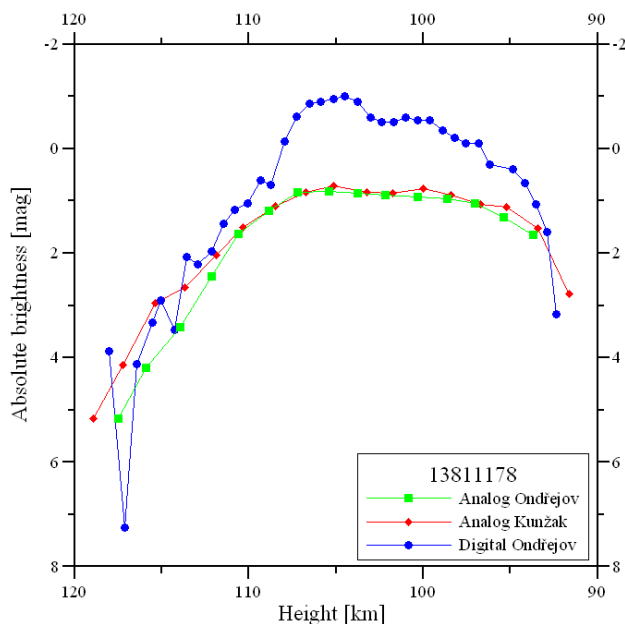


Figure 1 – Light curves of meteor 13811178.

## 2 Observations, data processing

The analogue observations were carried out by the instrumentation already described in recent papers (e.g. Koten et al., 2007). Both analogue and digital systems are based on a *Mullard XX1332* image intensifiers and 50mm lenses. The comparison of the system properties is summarized in *Table 1*.

The observational campaigns of the Lyrid, Perseid and Taurid meteor showers were planned in such a configuration which allowed employing both cameras of one system and at least one camera of the second system. Therefore at least three cameras were in use during each campaign.

Table 1 – Comparison of both observing systems.

	Analogue system	Digital system
Camera	S-VHS	JAI GigE Vision
Resolution [px]	768 x 576	776 x 582
Scanning	Interlaced	Progressive
Max. frame rate [s <sup>-1</sup> ]	25	61.25
Max. bit depth [bits]	8	10
Field-of-view	45°	52°
Limiting stellar magnitude	+6.5	+8.0

The analogue records were searched using the *MetRec* software (Molau, 1999). It was run several times with different parameter setting. On the other hand the digital observations were processed using the new detection software *dMAIA*, which is processing the data just once before the records are deleted. The comparison of the detection efficiency, which was done for the Perseid campaign, shows that the new software is able to detect about 72% of the meteors detected by *MetRec*. There were usually also meteors recorded and detected by the new system but not by the old one.

### 3 Properties of both systems

#### Photometry of meteors

One of the most important properties, which we are interested in, is the brightness of the meteors. Of course, we require to get the same values of the brightness for the same meteor observed by different cameras.

Since the new system provides us with two more bits of depth, we expected improved photometrical measurements especially for the brighter meteors. Moreover the frame rate 61 vs. 25 fps results in a better coverage of the meteor light curve.

Already first results showed that the light curves provided by both observational systems are indeed comparable, what results in similar values of the photometric masses of the meteors.

This is not fully valid for the brighter meteors such as *Figure 1* shows. Although a certain correction is already applied on the analogue data to suppress the effect of the overexposure, we can clearly see that this is not sufficient. The record obtained by the digital camera is not saturated (blue line). While the photometric mass obtained by the analogue cameras is about  $8 \cdot 10^{-3}$  g, the digital record resulted in the value of  $4 \cdot 10^{-2}$  g. The comparison of the data for more meteors shows that the difference can reach up to 1 order of mass for the brightest meteors. This is a very important fact, since the photometric mass is often used in different kinds of the analyses. The distribution of the beginning heights of the meteors in relation with their photometric masses is an example. *Figure 2* shows how some points are shifted to the right in such a plot in the case of the Lyrid meteor shower.

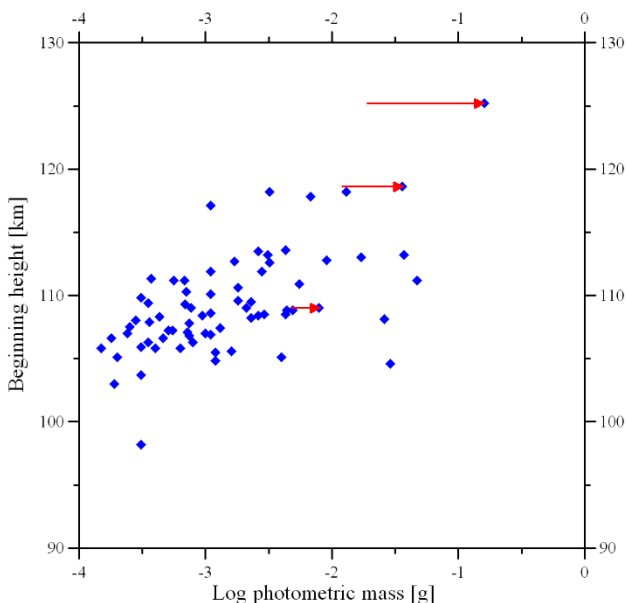


Figure 2 – Shift of the beginning height distribution.

#### Heights of meteors

Another important characteristic of the meteor is the range of heights, especially the beginning heights. Since the digital cameras provide us with records of higher

quality and lower noise, one would expect that the meteors will be recorded earlier i.e. at the higher heights. On the other hand the higher frame rate means shorter exposure time and therefore lower sensitivity to fainter meteors as well as to the very initial phase of the meteors.

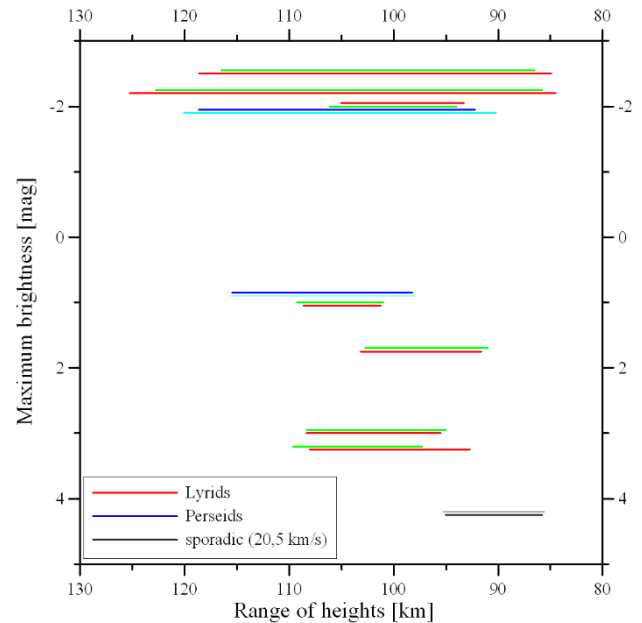


Figure 3 – Range of heights of meteors.

*Figure 3* shows the range between the beginning and terminal heights for several meteors including the Lyrids, Perseids and also one sporadic case. There are two lines for each meteor – the bottom one shows the range recorded by the analogue cameras, whereas the upper line shows the range obtained by the digital ones. It seems that very faint points at the beginning or end of the meteor can be missed by the digital camera. Nevertheless the differences are very small and typically both systems record meteors at similar heights.

#### Atmospheric trajectories

When introducing a new observation system, one would expect the precision of the meteor trajectory and orbit determination to be the same or even better than the same characteristics obtained by a previous camera system. The simultaneous observations using both systems showed that such a requirement is fulfilled in our case. A typical deviation on individual measured points from the averaged meteor trajectory is up to 100 m in the case of the video observations. New data show that also the new digital system is providing us with such a precision of the recorded data.

#### Deceleration of the meteors

As an additional scientific bonus the simultaneous campaigns provided us also with the opportunity to compare models of the Lyrid meteors. Several of the recorded cases exhibit deceleration during their atmospheric passage. Therefore it was possible to apply the erosion model of the meteoroids developed by Borovička et al. (2007). The model allowed us to determine the grain composition of the meteoroids.

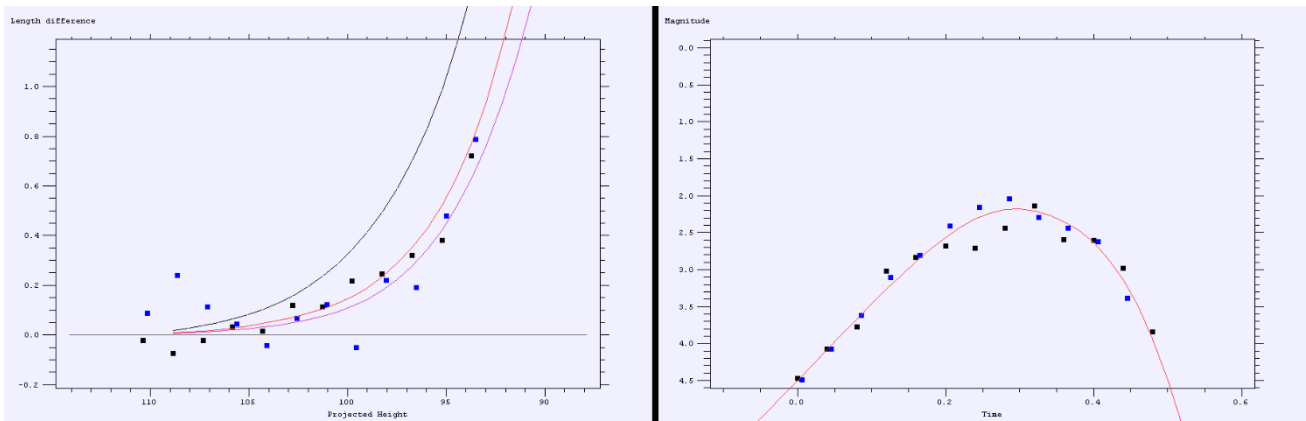


Figure 4 – Deceleration and light curve of meteor 04421047 recorded by two analogue cameras.

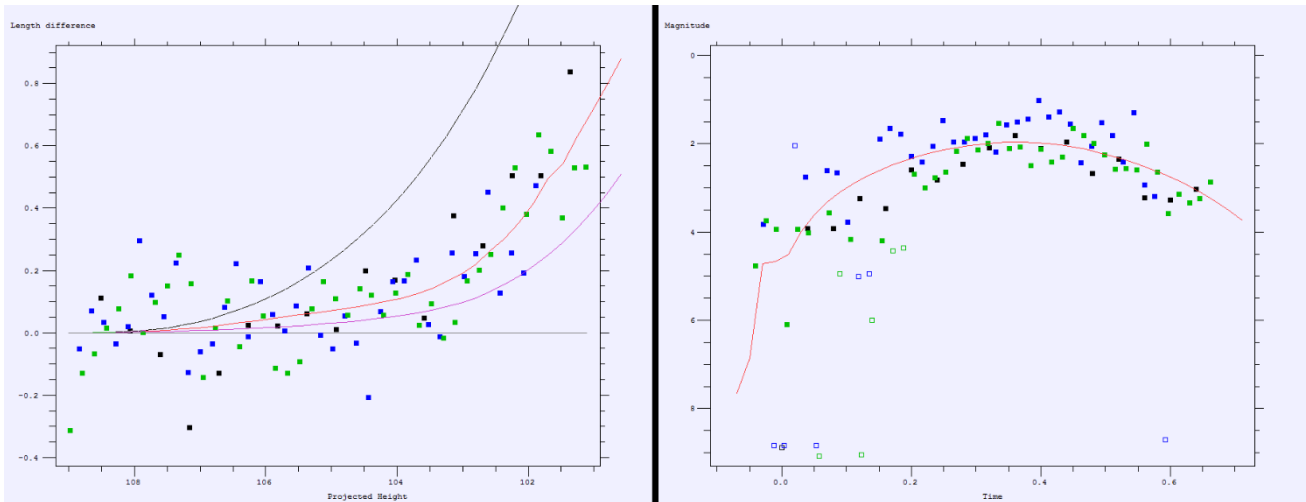


Figure 5 – Deceleration and light curve of meteor 15422005 recorded by two digital and one analogue cameras.

Table 2 shows the basic properties of two meteoroids. First one catalogued as the meteor number 04421047 was observed only by the analogue systems during the dedicated Lyrid campaign in 2004. As Figure 4 shows, the model results in a good fit of both the deceleration and the light curves. Nevertheless only small number of points is available for the modelling.

Table 2 – Composition of the meteoroids.

	04421047	15422005
Initial mass [g]	$3.4 \times 10^{-3}$	$7 \times 10^{-3}$
Range of grain masses [g]	$8 \times 10^{-8}$ to $1.6 \times 10^{-7}$	$8 \times 10^{-8}$ to $1.5 \times 10^{-7}$
Number of grains	~ 25000	~ 55000
Grain distribution index	1.7	2.0

Meteor number 15422005 is another case. It was detected during the simultaneous analogue – digital campaign. The number of points entering the model is significantly higher. Again, good fits were obtained for this meteor as Figure 5 shows.

## 4 Conclusion

A simultaneous double station meteor observing using both analogue and digital cameras was carried out for several meteor showers. The obtained data show that the new observing systems, which are fully automatic contrary to the older ones, provide us with data of comparable or even better quality.

Two more bits of the signal depth are significant in the case of bright meteors since the signal is not saturated and the more realistic values of the meteor brightness and then also of the photometric mass are obtained. Moreover higher frame rate brings more data for the modelling of the meteoroid structure. The atmospheric trajectory precision is comparable for both systems as well as the range of the meteor heights. On the other hand the digital systems sometimes miss faint points at the beginning or at the end of the luminous trajectory or even the faintest meteors due to shorter exposure time.

## Acknowledgment

This work was supported by grant number 14-25251S from the Grant Agency of the Czech Republic and the Czech institutional project RVO: 67985815.

## References

- Borovička J., Spurný P. and Koten P. (2007). “Atmospheric deceleration and light curves of Draconid meteors and implications for the structure of cometary dust”. *Astronomy and Astrophysics*, **473**, 661–672.
- Fliegel K., Páta P., Vítek S. and Koten P. (2010). “Meteor automatic imager and analyser: system design and its parameters”. *Applications of Digital Image Processing XXXIII*, Proceedings of SPIE, 7798, id. 77982B.
- Koten P., Borovička J., Spurný P. and Štork R. (2007). “Optical observations of enhanced activity of the 2005 Draconid meteor shower”. *Astronomy and Astrophysics*, **466**, 729–735.
- Koten P., Fliegel K., Vítek S. and Páta P. (2011). “Automatic video system for continuous monitoring of the meteor activity”. *Earth, Moon, and Planets*, **108**, 69–76.
- Molau S. (1999). “The Meteor Detection Software METREC”. In Arlt R. and Knöfel A., editors, *Proceedings of the International Meteor Conference*, Stará Lesná, Slovakia, 20–23 August 1998. IMO, pages 9–16.



Due to the nice weather, the poster session could take place outside. (Photo Casper ter Kuile).

# Meteors and meteorites spectra

Jakub Koukal<sup>1,2</sup>, Jiří Srba<sup>1,2</sup>, Sylvie Gorková<sup>1,2</sup>, Libor Lenža<sup>1</sup>, Martin Ferus<sup>3</sup>, Svatopluk Civiš<sup>3</sup>, Antonín Knížek<sup>3</sup>, Petr Kubelík<sup>3</sup>, Tereza Kaiserová<sup>3</sup> and Pavel Váňa<sup>3</sup>

<sup>1</sup>Valašské Meziříčí Observatory, Vsetínská 78, 75701 Valašské Meziříčí, Czech Republic  
j.koukal@post.cz, sgorkova@astrovm.cz, jsrba@astrovm.cz

<sup>2</sup>SMPH, Society for Interplanetary Matter, Kraví hora 522/2, 61600 Brno, Czech Republic

<sup>3</sup>J. Heyrovský Institute of Physical Chemistry, Academy of Sciences of the Czech Republic,  
Dolejškova 3, 18223 Prague 8, Czech Republic  
martin.ferus@jh-inst.cas.cz, svatopluk.civis@jh-inst.cas.cz

The main goal of our meteor spectroscopy project is to better understand the physical and chemical properties of meteoroids. Astrometric and spectral observations of real meteors are obtained via spectroscopic CCD video systems. Processed meteor data are inserted to the EDMOND database (European viDeo MeteOr Network Database) together with spectral information. The fully analyzed atmospheric trajectory, orbit and also spectra of a Leonid meteor/meteoroid captured in November 2015 are presented as an example. At the same time, our target is the systematization of spectroscopic emission lines for the comparative analysis of meteor spectra. Meteoroid plasma was simulated in a laboratory by laser ablation of meteorites samples using an (ArF) excimer laser and the LIDB (Laser Induced Dielectric Breakdown) in a low pressure atmosphere and various gases. The induced plasma emissions were simultaneously observed with the Echelle Spectrograph and the same CCD video spectral camera as used for real meteor registration. Measurements and analysis results for few selected meteorite samples are presented and discussed.

## 1 Introduction

Main goal in the meteors spectroscopy is to better understand the physical and chemical properties of meteoroids by using simultaneous video and spectral observations of meteors compared with meteoritic material laboratory spectra. Spectral observations of meteors are now obtained via fixed (at Valašské Meziříčí Observatory) and mobile spectroscopic CCTV systems. All records of meteors and processing data (orbital elements, speed of deceleration, etc.) are inserted to the EDMOND database (European viDeo MeteOr Network Database) together with spectral information (Kornoš et al., 2014). Another very valuable source of the physical and chemical properties of meteoroids are spectra taken by BRAMON (BRAZilian Meteor Observation Network). This network covers the southern hemisphere and is a source of information about the little-known southern hemisphere meteor showers.

Simultaneously, our target is the systematization of spectroscopic emission lines for the comparative analysis of meteor spectra. The solids will be irradiated using excimer and PALS lasers (Na, Ti, Mg, Al, Si, Fe, and Ca), their simple binary oxides, sulfides, minerals and real sample of meteorites. The LIDB (laser-induced dielectric breakdown) in a gas media representing the atmospheres (O<sub>2</sub>, N<sub>2</sub>, Ar and CO<sub>2</sub>) will also be spectroscopically characterized. These spectra will be recorded in situ on the discharges and excimer laser ablations using a Fourier time resolved high resolution spectrometer Bruker, a high resolution Echelle spectrograph LLA and a CCD spectrograph Ocean Optics. Complying data will allow for not only

qualitative determinations of the impacting body composition but also the assignment of spectral lines for products from the meteorite alterations and plasma interactions in atmosphere.

## 2 Equipment and data reduction

Spectrographs use a highly sensitive CCD video camera VE 6047 EF/OSD (spectrograph VM\_N) and CMOS video cameras QHY5L-IIIM (spectrographs VM\_NW and VM\_SW). The VE 6047 EF/OSD camera is equipped with a 1/3" CCD chip Sony ICX 673AKA with an effective resolution of 720 × 576 px, resolution of the VM\_N spectrograph is 30,4 Å/px (Koukal et al, 2015). The QHY5LII-M camera is equipped with a 1/3" CMOS chip Aptina MT9M034 with an effective resolution of 1280 × 960 px. The field of view is 80° × 60° (spectrograph VM\_SW) and 89° × 67° (spectrograph VM\_NW), these systems use fast Tamron megapixel lenses (f/1.0) with a variable focal length (3 – 8 mm). FOV and resolution of the CMOS chip enables the use of holographic diffraction grating with a density of 1000 lines/mm. In this configuration the spectrograph reaches a stellar limiting magnitude of +4.5<sup>m</sup>, the faintest recorded meteors then have a relative magnitude of up to +2.0<sup>m</sup>. The magnitude of meteors with measurable spectrum has to be at least –2.0<sup>m</sup>.

The detection of meteors is done by UFOCapture software<sup>1</sup>, and for the astrometric and photometric processing UFOAnalyzer software<sup>2</sup> (SonotaCo, 2009) is used. The resulting video is divided into individual

<sup>1</sup><http://sonotaco.com/soft/UFO2/help/english/index.html>

<sup>2</sup>[http://sonotaco.com/soft/download/UA2Manual\\_EN.pdf](http://sonotaco.com/soft/download/UA2Manual_EN.pdf)

images (frames), every image is subsequently a dark frame and flat field corrected with frames captured by the cameras VE 6047 EF/OSD and QHY5LII-M. Orbits of meteoroids in the solar system are calculated using the software UFOOrbit<sup>3</sup> (SonotaCo, 2009). The deceleration is derived from this software as an exponential fit of the actual speed of the meteor for each frame. Spectrograph calibration in the x-axis (wavelength) was performed using a calibration neon lamp. Calibration was performed as non-linear, using 6 multiplets of neon emission lines at wavelengths between 5852 and 7032 Å. The resulting basic spectrograph resolution was determined from 5 independent measurements at 9.7 Å/px (spectrograph VM\_SW) and 10.8 Å/px (spectrograph VM\_NW). The calibration of the emission line intensity (y-axis) was performed using a diagram of relative sensitivity CMOS Aptina MT9M034 at a wavelength between 3500 and 9000 Å (Figure 1). For the identification of the emission wavelengths of the individual elements the revised tables were used (Moore, 1972).

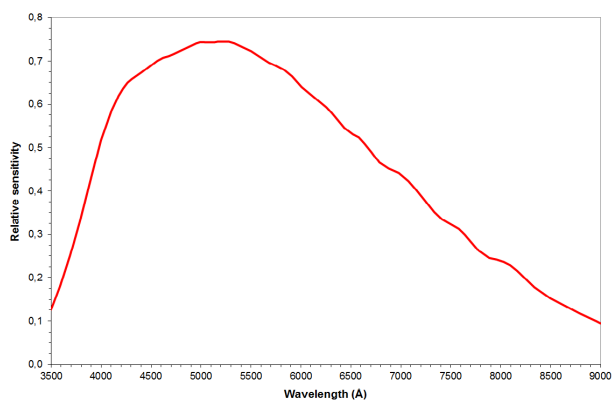


Figure 1 – Relative spectral sensitivity of CMOS chip Aptina MT9M034.

### 3 Comparative experiments with LIBS

The meteoroid plasma was simulated in our laboratory by a laser ablation of meteorites samples using a Lambda Physik (ArF) excimer laser. Comparative experiments with atmospheric gases have been performed using a Laser Induced Breakdown in gases and electric discharges. The emission spectra of plasma were simultaneously observed with the Echelle Spectrograph and the astronomical camera (Figure 2, 3 and 8).

The laser emits ~10- ns pulses on a wavelength of 193 nm and an energy of 200 mJ. The Laser beam was focused using a calcium fluoride lens (focal length of 50 mm) on a solid target (a sample of a meteorite) attached on the XYZ rotation stage. The system is placed in a vacuum interaction chamber equipped with a collimator connected directly with a high resolution Echelle Spectrograph (ESA 4000, LLA Instruments GmbH, Germany). The spectrograph allows simultaneous measurement of complex spectra within the entire 200 – 780 nm UV / VIS – region with an effective resolution ranging from 0.005 nm (200 nm) to 0.019 nm (780 nm).

In our measurement, the spectrograph was set to trigger a 500 ns laser pulse and to start the measurement with a delay of 4 μs with a gate open for 5 μs with the accumulation of 3500 counts and 30 accumulations of the signal. The positive column discharge was maintained by a high-voltage transistor switch applied between the stainless steel anode and the grounded cathode of the discharge tube (25 cm long with an inner diameter of 12 mm). The air plasma was cooled by water in the outer jacket of the cell. The voltage drop across the discharge was 1200 V, and the current was 250 mA.

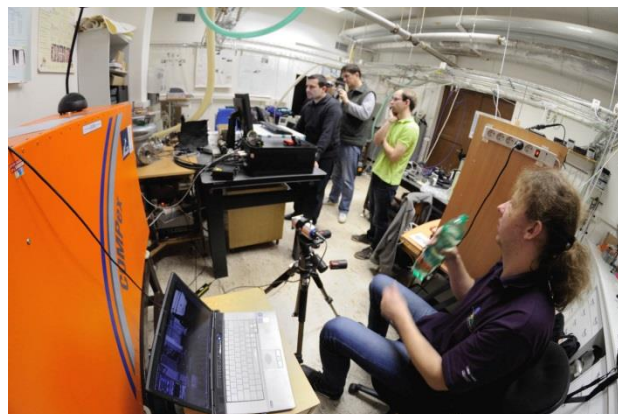


Figure 2 – Comparative spectroscopy in the laboratory of the J. Heyrovsky Institute of Physical Chemistry (the Czech Academy of Sciences) – the Echelle ESA 4000 high resolution spectrograph and the astronomical spectrograph QHY5LII-M.

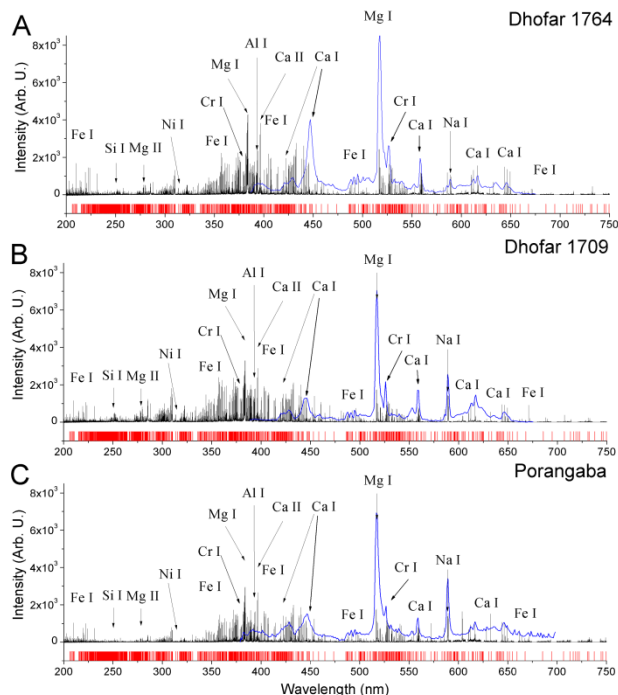


Figure 3 – Global survey on ablation emission spectra of all three samples of meteorites with assignment of the most prominent lines. The spectrum is also filled with a large number of Fe lines. Their positions are marked by red sticks below. In the figure, the spectrum recorded by the meteor spectrographic camera is imprinted in blue.

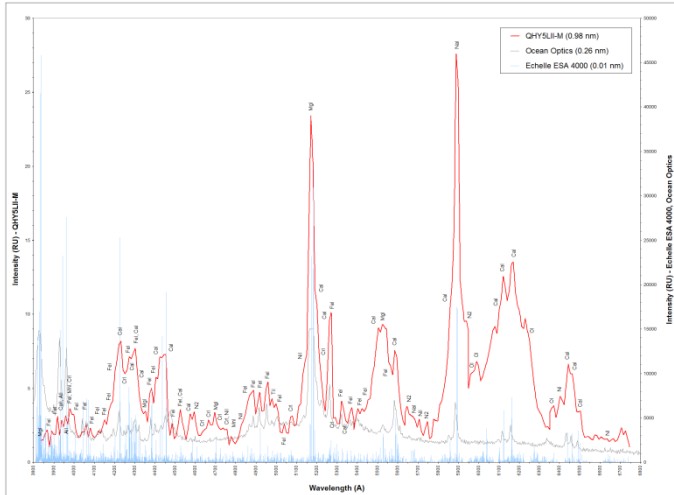
First of all, high resolution spectra of ablation plasma measured by Echelle spectrograph have been processed by the Calibration Free Method. The positions of the most prominent lines are depicted in Figure 3.

<sup>3</sup> [http://sonotaco.com/soft/UO2/UO21Manual\\_EN.pdf](http://sonotaco.com/soft/UO2/UO21Manual_EN.pdf)



Sample	Electron temperature (eV)	Electron density (cm <sup>-3</sup> )	Fe/Mg	Na/Mg	Ca/Mg	Mg	Si/Mg	Al/Mg	Cr/Mg	Ni/Mg
A Dhofar 1764	7172	3.18 x 10 <sup>16</sup>	1.22	0.003	0.11	1.00	0.82	0.19	0.02	0.06
B Dhofar 1709	6541	3.03 x 10 <sup>16</sup>	1.83	0.020	0.17	1.00	1.15	0.34	0.05	0.09
C Porangaba	6731	2.84 x 10 <sup>16</sup>	1.54	0.030	0.18	1.00	1.60	0.22	0.05	0.01

Figure 7 – Elemental abundances in all three samples of meteorites estimated using CF-LIBS technique.



Element	λ, Å	Peak	Multiplet	Element	λ, Å	Peak	Multiplet	Element	λ, Å	Peak	Multiplet	Element	λ, Å	Peak	Multiplet
Mg	3832	1	3	Fe	4358	23	42	Fe	5056	42	216	Ca	8507	87	47
	3838	1	3	Ca	4319	21	5	Fe	5042	44	36	Ca	8500	86	1
Fe	3856	2	4	Mg	4352	22	14	Ni	5073	45	8	Fe	5995	98	1
	3860	2	4		4355	22	13	Ca	5137	46	48		5928	28	
	3866	2	4	Fe	4364	23	41	Ni	5197	2	2		5932	28	
Fe	3889	3	45	Fe	4405	24	41	Mg	5173	47	2	Ni	5940	99	28
	3900	3	4		4425	24	4		5184	47	2		5941	28	
	3903	3	45	Ca	4435	25	4	Ca	5189	48	48		5950	23	
Ca	3923	4	4		4436	25	4	Cr	5206	48	7	Cr	5959	70	23
Ca	3924	5	1	Ca	4455	25	4	Cr	5209	48	7	Cr	5965	71	44
Al	3944	1	1		4456	25	4		5202	22	22	Ca	6103	72	3
Al	3952	5	1	Fe	4462	27	2	Ca	5206	50	22	Ca	6122	73	3
Fe	3978	7	72	Ca	4527	28	38	Fe	5270	51	15	Ca	6162	74	3
Ni	3980	7	33	Fe	4529	28	38	Cr	5206	52	16		6164	74	3
Cr	3989	3	388	Cr	4579	23	23	Fe	5204	53	53	Ca	6257	75	3
Fe	4005	8	43	Ca	4581	29	23	Fe	5228	53	15	Cr	6262	75	50
Fe	4046	9	43		4586	29	23	Ca	5250	54	33	Cr	6306	76	60
Fe	4054	10	43	Ni	4607	30	5	Fe	5267	55	1488		6374	78	58
Fe	4072	11	43	Cr	4632	31	171	Ca	5486	56	16	Ca	6439	77	18
Fe	4132	12	43	Cr	4666	32	99	Fe	5425	57	15	Ca	6443	78	18
Fe	4164	13	43	Mg	4703	33	11	Fe	5447	58	15		6464	78	18
Fe	4182	14	354	Cr	4723	34	292	Ca	5513	59	48	Ca	6509	79	18
Fe	4187	14	102	Cr	4724	34	145	Mg	5528	60	9	Ni	6537	80	20
Fe	4189	152	102	Cr	4756	35	145	Fe	5570	61	688				
Fe	4202	15	42	Ni	4757	35	98		5580	61	21				
Ca	4207	16	2	Mg	4763	36	16		5580	61	21				
Cr	4224	17	1	Ni	4831	37	111	Ca	5584	62	21				
Fe	4272	18	42	Fe	4859	38	318		5598	62	21				
Ca	4283	19	5	Fe	4879	39	318		5603	62	21				
Ca	4289	19	5	Fe	4891	39	318	Ni	5607	63	3				
Fe	4289	192	102	Fe	4921	40	318	Ni	5603	64	6				
Ca	4303	20	5	Fe	4958	41	318	Ni	5710	65	46				
Ca	4308	20	5	Fe	4981	42	38	Ni	5747	66	9				

Figure 8 – The ablation emission spectrum of the Jiddat al Harasis meteorite (JAH 815) – the comparative measurement from the three sources. The measurement was performed using an Echelle ESA 4000 high resolution spectrograph, a CCD spectrograph Ocean Optics and an astronomical spectrograph QHY5LII-M with diffraction grating. The identified emission lines in the spectrum of the meteorite JAH 815 are listed in the table on the right.

### 4 Observations and results

Bolide 20151119\_034504 (#013 LEO). The 2<sup>nd</sup> order is obvious in the recorded spectrum as well as the spectrum of the persistent trail (Figure 9).



Figure 9 – Combined spectrum image of bolide 20151119\_034504 - spectrograph VM\_NW.

Overall 9 video frames of the bolide with 1<sup>st</sup> order spectrum were analyzed (spectrograph VM\_NW) and a time resolved evolution of emission in the range from 3500 to 9000 Å was examined (Figure 10).

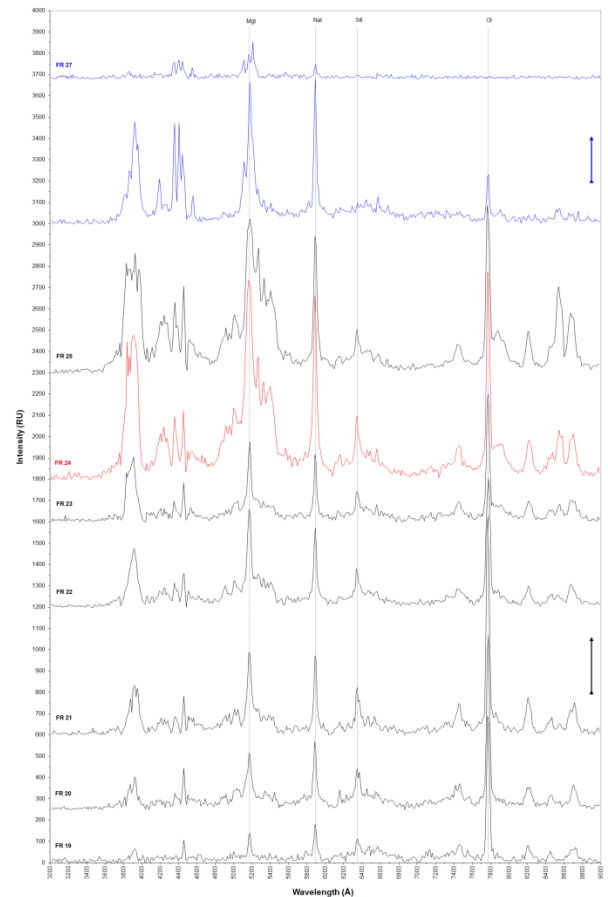


Figure 10 – Uncalibrated evolution of meteor spectrum in selected frames – 1<sup>st</sup> order, spectrum of the persistent trail is marked with blue, frame with the strongest emissions is marked with red.

Except of the dominant emissions of MgI-2, NaI-1 and CaII-1, the FeI-15 (5270, 5328 and 5405 Å) multiplet, MgI (3, 13 and 14 multiplets), CrI (1), CaI (4), FeI (318), and SiII (2) in combination with the emission line of the atmospheric elements (NI, OI, N<sub>2</sub> – 1<sup>st</sup> positive) identified in the 1<sup>st</sup> order (Figure 11, 12).

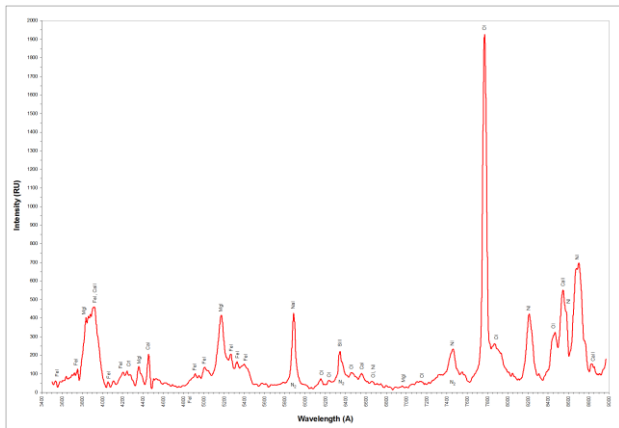


Figure 11 – Calibrated spectrum of bolide 20151119\_034504 (1<sup>st</sup> order) in the range from 3500 to 9000 Å.

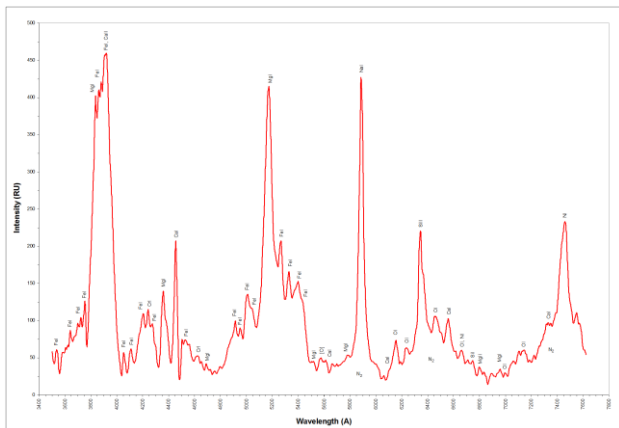


Figure 12 – Calibrated spectrum of bolide 20151119\_034504 (1<sup>st</sup> order) in the range from 3500 to 7700 Å.

To calculation of the atmospheric path of the bolide and the orbit of the meteoroid in the Solar system the recordings from the stations Otokovice, Zlín and Valašské Meziříčí (camera N) have been used. The projection of the beginning of the atmospheric path was located at coordinates N50.571° E17.603° near the village of Goszczowice (PL), the height of the bolide at this time was 126.6 kilometers above the Earth’s surface. The end of the projection of the atmospheric path was located at coordinates N50.805° E17.292° near the village of Brylów (PL), the height of the bolide at this time was 74.7 kilometers above the Earth’s surface, the bolide reached an absolute brightness of -8.6<sup>m</sup> (Figure 13).

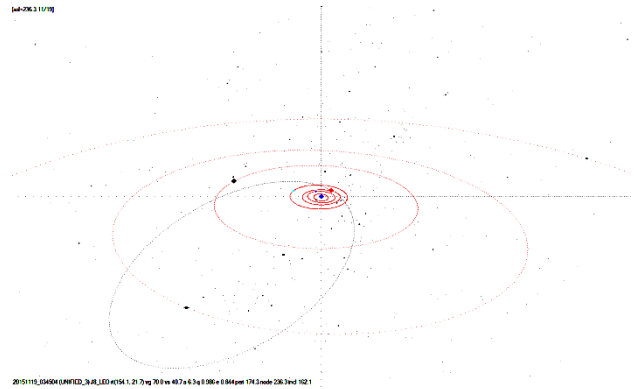


Figure 13 – Orbit of bolide 20151119\_034504 (#013 LEO).

## 5 Summary and conclusion

The Observatory in Valašské Meziříčí has been successfully employed in the European Video Meteor Network (EDMONd), which consists of 265 CCD cameras across Europe. The main goal of this network is the determination of meteoroid trajectories. Additionally, we increase the scientific quality of the data by upgrading our EDMOND stations by spectrographs. For instance, recently (April 30, 2016), there are 74 spectra in the EDMOND database, of which 63 were recorded using spectroscopic systems in Valašské Meziříčí and 11 with mobile spectrographs (Figure 14, 15).

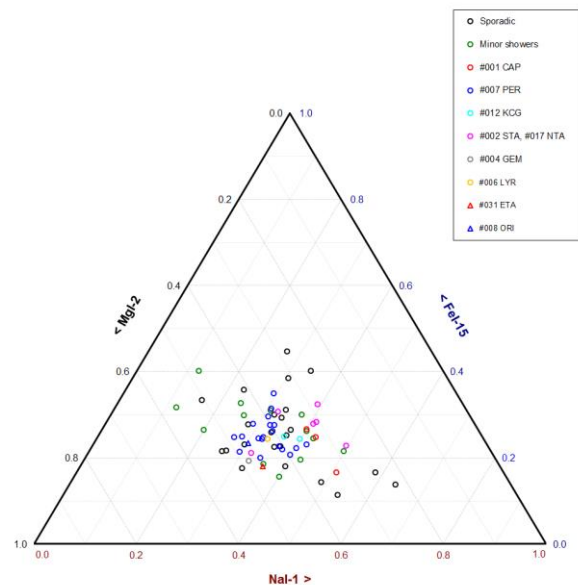


Figure 14 – Position of the parent shower of meteoroids in the ternary graph of the Mg I (2), Na I (1), and Fe I (15) multiplet relative intensities. Every shower is represented with a different symbol.

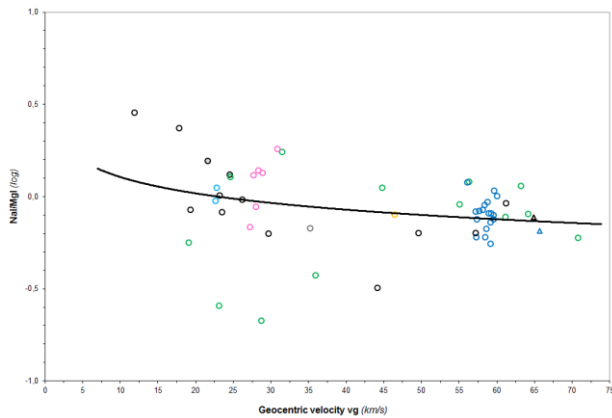


Figure 15 – Intensity ratio of the Na/Mg lines in meteor spectra as a function of the geocentric velocity.

Within the frame of the EDMOND database a new section of meteor spectra is gradually arising, which contains the combined observations taken with a mobile spectrograph in 2013, and observations collected since 2014 with spectrographs in Valašské Meziříčí. In the database there are also 19 meteor spectra (April 30, 2016) from BRAMON, which were recorded using the same spectroscopic system as the mobile spectrograph (Watec 902H2 Ultimate, diffraction grating 500 lines/mm).

## Acknowledgment

The research has been funded by the Program of regional cooperation of the Czech Academy of Sciences, grant no. R200401521.

## References

- Kornoš L., Koukal J., Píffl R. and Tóth J. (2014). “EDMOND Meteor Database.” In Gyssens M. and Roggemans P., editors, *Proceedings of the International Meteor Conference*, Poznań, Poland, August 22-25, 2013. IMO, pages 23–25.
- Koukal J., Gorková S., Srba J., Ferus M., Civiš S. and Di Pietro C. A. (2015). “Meteor Spectra in the EDMOND database”. In Rault J.-L. and Roggemans P., editors, *Proceedings of the International Meteor Conference*, Mistelbach, Austria, Aug. 27-30, 2015. IMO, pages 149–154.
- Moore Ch. E. (1972). “A Multiplet Table of Astrophysical Interest – Revised Edition”. NSRDS-NBS 40, U.S. Nat. Bur. Stand., reprint of NBS Technical note 36 (PB151395).
- SonotaCo (2009). “A meteor shower catalog based on video observations in 2007-2008”. *WGN, Journal of the IMO*, **37**, 55–62.



Matej Korec and Jakub Koukal.

# Retrieving meteoroids trajectories using BRAMS data: preliminary simulations

Hervé Lamy and Cédric Tétard

Space Physics, Royal Belgian Institute for Space Aeronomy, Brussels, Belgium

Herve.lamy@aeronomie.be, cedric.tetard@aeronomie.be

One of the main goals of the BRAMS project is to retrieve meteoroids trajectories from multi-station observations. In this paper a large number of meteoroid trajectories are simulated and several criteria are discussed to select trajectories compatible with multi-station observations. The criteria are the altitude of the specular reflection points, the minimum power detectable at a given station, and the time delays observed between appearances of meteor echoes at each receiving station. Finally, future improvements of these simulations are considered.

## 1 Introduction

BRAMS (Belgian RAdio Meteor Stations) is a radio network located in Belgium using forward scatter measurements to detect and characterize meteoroids. It consists in one dedicated transmitter located in Dourbes in the south of Belgium and approximately 30 receiving stations spread all over the Belgian territory (see *Figure 1*). The transmitter emits a circularly polarized continuous wave (CW) at a frequency of 49.97 MHz and with a power of 150W. All receiving stations use the same material (including a 3 elements Yagi antenna) and are synchronized using GPS clocks. More details can be found in e.g. (Lamy et al., 2015).

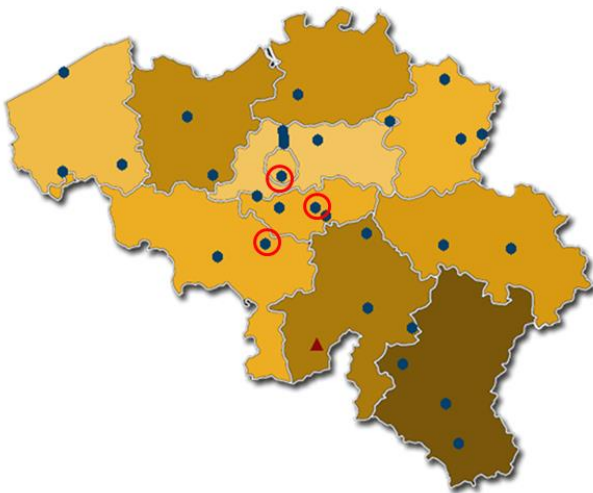


*Figure 1* – Map of the BRAMS network in 2016. The transmitter is located in Dourbes and is represented by the red triangle. All the blue dots are the BRAMS receiving stations. The three red circles indicate the positions of the Uccle, Ottignies and Senefve receiving stations.

## 2 Finding the specular reflection point on a given meteoroid trajectory

The BRAMS receiving stations mostly detect specular reflections on meteor trails, meaning the power essentially comes from one point of the trail / meteoroid trajectory  $L$ . Mathematically the reflection point  $p$  must be the point along  $L$  which is tangential to an ellipsoid  $E$

whose foci are located at the positions of the transmitter  $T$  and the particular receiving station  $R$  detecting the meteor echo (see *Figure 2*).

When the meteoroid trajectory is known, finding the location of the specular reflection point is an analytical problem. This was described in (Nedeljkovic, 2006). The principle is briefly reminded here.

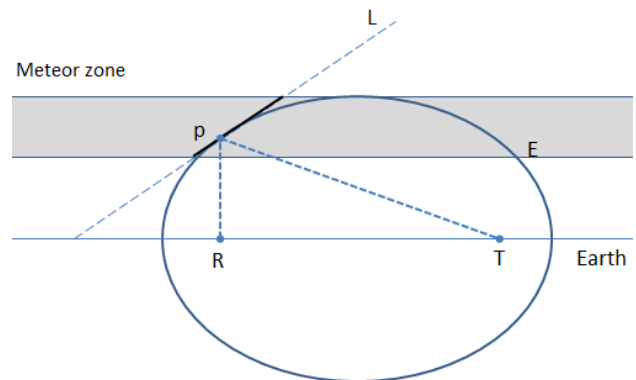


*Figure 2* – schematic of the specular reflection of the radio wave off the meteor trail  $L$ .  $p$  is the tangential point.  $E$  is the ellipsoid tangential to  $L$ , with foci located at the transmitter position  $T$  and receiver position  $R$ . The grey zone represents the meteor zone where enough ionization in the meteor trail occurs.

Let us assume that the ellipsoid equation is given by

$$\frac{x^2}{a^2} + \frac{y^2}{b^2} + \frac{z^2}{b^2} = 1 \tag{1}$$

where  $a$  and  $b$  are respectively the semi-major and semi-minor axes, and that the equation of the meteoroid trajectory, assumed to be a straight line, passes through 2 points  $(x_1, y_1, z_1)$  and  $(x_2, y_2, z_2)$ ,

$$\frac{x-x_2}{x_1-x_2} = \frac{y-y_2}{y_1-y_2} = \frac{z-z_2}{z_1-z_2} \tag{2}$$

The intersection points of this line and the ellipsoid can simply be obtained by expressing e.g.  $y$  and  $z$  as functions of  $x$  in (2) and inject these expressions into (1). This provides a second order equation in  $x$

$$Ex^2 + Fx + G = 0 \tag{3}$$

for which there could be 0, 1 or 2 solutions depending on whether the discriminant  $F^2 - 4EG$  is respectively negative, zero or positive. To find the tangential point, the discriminant must be equal to zero, which provides a first analytical expression where the only two unknowns are  $a$  and  $b$ . A second expression linking  $a$  and  $b$  is the focus equation

$$f^2 = a^2 - b^2 \quad (4)$$

where  $f$  is the focus of the ellipse, equal to the distance between  $T$  and  $R$ . Solving these two equations for the two unknowns  $a$  and  $b$  provides the characteristics of the ellipsoid from which the  $x$  coordinate of the tangential point can be obtained via (3). Similar equations will give  $y$  and  $z$  coordinates.

### 3 An attempt to retrieve a meteoroid trajectory from multi-station observations

Solving the direct problem described in the previous section is straightforward. The inverse problem, which requires finding a meteoroid trajectory tangent to a set of  $n$  ellipsoids with a common focus  $T$  and various second focuses corresponding to the positions of the  $n$  receiving stations detecting the same meteor, is much more challenging. Here we investigate an idea similar to that proposed by (Nedeljkovic, 2006) to generate a large number of possible meteoroid trajectories and select only those tangential to a given number of ellipsoids. As shown below, a number of additional criteria must be used in order to select only a few possible trajectories.

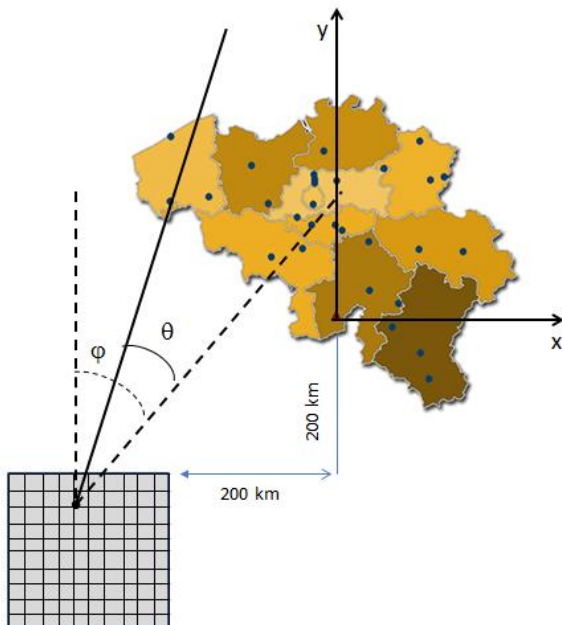


Figure 3 – Illustration to show how the  $\sim 10^6$  meteoroid trajectories are simulated. The grid on the left hand side contains the 121 “starting” points of the trajectories and their directions are given by the azimuth angle  $\phi$  and elevation angle  $\theta$ . The point at the top right corner of the grid is located at a distance of -200 km in both directions N-S and E-W (respectively along  $y$  and  $x$  axes).

In the following simulations, a Cartesian coordinate system is used with the center being located at the transmitter site  $T$  in Dourbes, with  $x$  and  $y$  axes being directed along E-W and N-S directions, and axis  $z$  being vertical. Trajectories are simulated using a point and a direction described by an elevation angle  $\theta$  and an azimuth angle  $\phi$  (see Figure 3).  $\phi$  is measured from the north direction and counted positively toward the east. Both angles vary between  $0^\circ$  and  $90^\circ$  with steps of  $1^\circ$  in order to ensure that trajectories are passing above Belgium. The point is chosen as the (theoretical) intersecting point of the trajectory with the  $x$ - $y$  plane. In order to generate trajectories with meteor trails in the adequate altitude range over Belgium, these points are chosen on a grid with distances along  $x$  and  $y$  axes varying between -200 and -400 km with steps of 20 km (see Figure 3). A grid of 121 points was placed southwest of Belgium, favoring trajectories coming from the north-east quadrant. Similar grids could be used for the other quadrants. In total,  $121 \times 91 \times 91 \sim 10^6$  trajectories are simulated. For each one, the position of the specular reflection point and the characteristics of the ellipsoid  $a$  and  $b$  can be calculated for each combination  $T$ - $R_1$ ,  $T$ - $R_2$ , ... where  $R_1$ ,  $R_2$  are the different receiving stations.

In the following simulations, 3 BRAMS stations are considered: Uccle (U), Senefte (S) and Ottignies (O). These stations are rather close to each other (distances between them in the range from 20 to 32 km) and also more or less located to the north-west direction with regard to the transmitter (see Figure 1). This maximizes the chances for all stations to detect the same meteors.

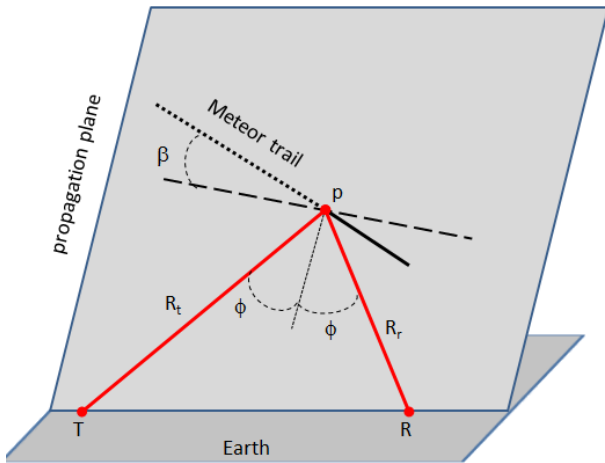
The first selection criterion is that the altitude of the reflection point must be located within the meteor zone. If this altitude is too high, the atmosphere is too tenuous and the impact of the meteoroid with the atmospheric molecules and atoms does not produce enough ionization to reflect the radio wave. If the point is located at a too low altitude, the meteoroid will be fully burnt before this point is created. In Table 1, the meteor zone is taken between 95 and 110 km, which is a reasonable range for the underdense meteor echoes considered in this study.

Table 1 – Number of remaining trajectories using the altitude criterion. Three stations are considered: U = Uccle, O = Ottignies and S = Senefte.  $z_p$  is the altitude of the specular reflection points.

	$95 < z_p < 110$ km
U	65631
O	65344
S	67870
U & O	61186
O & S	57003
U & O & S	54734

For individual stations, less than 7% of the simulated trajectories remain, with comparable numbers, which is expected since the distances of the three stations and their

directions to the transmitter are very similar. If the lower boundary is changed to 90 km, 86486 possible trajectories remain for Uccle (instead of 65631). When multi-station observations are considered, the 2 or 3 specular reflection points must all fall within the selected altitude range. This stronger criterion should reject more simulated trajectories. However, as can be seen in *Table 1*, the number of remaining trajectories does not decrease drastically when receiving stations O and S are added to station U, possibly again because the geometry T-R is rather similar for all three stations. Additional information is therefore needed to select fewer trajectories.



*Figure 4* – Geometry of the forward scatter problem. The dashed line is the projection of the meteoroid trajectory in the propagation plane. The scattering angle  $2\phi$  is divided in two equal parts by the perpendicular (dotted line) to this projection.

A possible second criterion is based on the minimum power that can be measured at the receiving station. This depends on the sensitivity of the receiving chain and of the local noise background, and hence should be slightly different at each station. However, for this study, a typical value of  $10^{-17}$  watt is chosen as minimum detectable power, which is valid for most BRAMS stations<sup>1</sup>. To compute the peak power received at each station, the classical formula of (McKinley, 1961), valid for underdense meteor echoes and extended to the forward scatter case, is used:

$$P_{peak} = \frac{P_t G_t G_r \lambda^3 r_e^2 \alpha^2 \sin^2 \gamma}{16\pi^2 R_t R_r (R_r + R_t) (1 - \sin^2 \phi \cos^2 \beta)} \quad (5)$$

In this equation,  $P_t$  is the transmitted power (=150 watts),  $G_t$  and  $G_r$  the gains of the transmitting and receiving antennas,  $\lambda$  is the wavelength ( $\sim 6$ m),  $r_e$  is the classical Bohr radius ( $\sim 5.29 \times 10^{-11}$  m),  $\alpha$  is the electron line density,  $\gamma$  is the angle between the electric vector of the incident wave and the line of sight to the receiver

<sup>1</sup>The BRAMS calibrator (Lamy et al., 2015), which emits a signal with a constant power of  $10^{-16}$  watt (-130 dBm) in a very narrow bandwidth ( $\sim 1$  Hz), appears well above the noise level in the spectrograms. This supports the choice of a value 10dB below this level as the minimum detectable power.

(polarization),  $R_t$  and  $R_r$  are the distances between the specular reflection point  $p$  and respectively the transmitter  $T$  and the receiver  $R$ ,  $\phi$  is half of the scattering angle, and  $\beta$  is the inclination of the meteor trajectory with respect to the propagation plane of the wave (see *Figure 4*). Formula (5) also assumes an infinitely thin meteor trail where all electrons are distributed along a straight line.

For each simulated trajectory and each pair T-R, the position of the reflection point can be calculated, and therefore all the geometrical parameters from the denominator in (5) can be computed. The remaining parameters in the numerator are the antenna gains, the polarization and the electron line density. For the antenna gains, the patterns simulated in (Martinez Picar et al., 2014) are used in the directions from T and R to the specular reflection point. The polarization of the incoming wave can only be measured with crossed Yagi antennas and only two BRAMS stations are currently equipped with such antennas. A statistical study of the polarization of meteor echoes will be carried out soon. Meanwhile a reasonable value of  $\gamma = 45^\circ$  is assumed here, i.e.  $\sin^2 \gamma = 0.5$ . This means that only half of the power is received by single Yagi antennas. The only remaining unknown in (5) is the electron line density  $\alpha$  which depends in a complex way on the speed  $v$  and the initial mass  $m$  of the meteoroid.

In order to apply the power criterion to a single receiving station, a first possibility is to assume a typical range of  $\alpha$  values, valid for underdense meteors, at each reflection point of the 65631 remaining trajectories (after application of the altitude criterion). 30 values of  $\alpha$  between  $10^{12}$  and  $3 \times 10^{13} \text{ m}^{-1}$  with step  $\Delta\alpha = 10^{12} \text{ m}^{-1}$  are considered. *Figure 5* shows how many trajectories remain for the station Uccle for each value of  $\alpha$ .

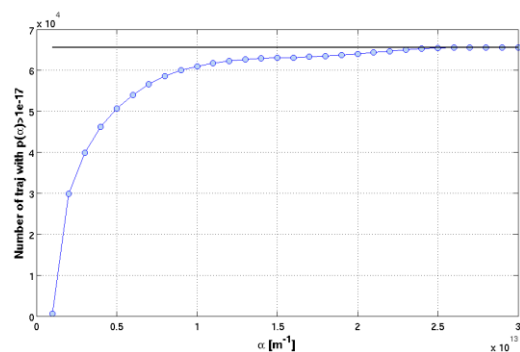


*Figure 5* – Number of remaining trajectories for the station Uccle as a function of the line density  $\alpha$  at the reflection points. The straight line is the number of remaining trajectories after application of the altitude criterion (65631).

For values of  $\alpha \geq 2.5 \times 10^{13} \text{ m}^{-1}$ , all meteor echoes will be detected no matter the location of the reflection point. When  $\alpha$  decreases, the number of remaining trajectories decreases as well, owing to the larger distances of some of the reflection points to both the transmitter and the receiver. Indeed low values of the electron line density at distant reflection points will produce fainter meteor

echoes below the power threshold. For  $\alpha = 10^{12} \text{ m}^{-1}$ , only  $\sim 600$  trajectories remain possible. This study also provides an estimate of the minimum detectable value of  $\alpha$  for the station Uccle and is  $\sim 0.9 \times 10^{12} \text{ m}^{-1}$ .

Conversely, for each 65631 trajectories, the minimum value of the electron line density,  $\alpha_{\min}$ , providing a signal of power equal to  $10^{-17}$  watt at Uccle, can be calculated. The distribution of  $\alpha_{\min}$  values as a function of the total distance travelled by the radio wave from transmitter  $T$  to reflection point  $p$  and finally to receiver  $R$ , is plotted in *Figure 6*.

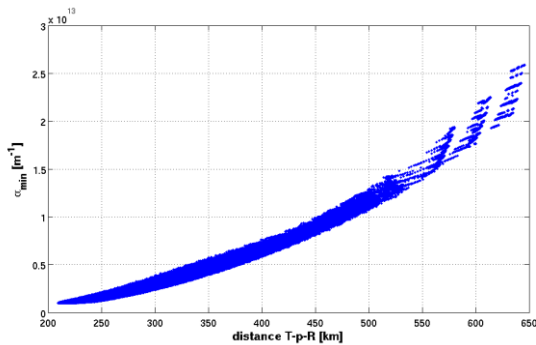


*Figure 6* – Distribution of  $\alpha_{\min}$  for the 65631 remaining trajectories for Uccle, as a function of the distance travelled by the radio wave.

As expected,  $\alpha_{\min}$  increases with the distance travelled by the radio wave, meaning that more ionization is needed to produce a similarly weak echo, when this distance increases.

In order to apply the power criterion to multiple stations, a distribution of  $\alpha$  along the trajectory should be known. A simple analytical and empirical formula, such as e.g. formula (10) from (Belkovich and Verbeeck, 2005) could be used but this is beyond the scope of this paper.

A third criterion that can be used is the time delay  $\Delta t_{12}$  between the start of meteor echoes observed at two (out of three) receiving stations  $R_1$  and  $R_2$ . Indeed, because of the specular character of the radio wave reflection, for a given meteoroid trajectory, a station  $R$  starts detecting a measurable signal when ionization has been created at the corresponding specular reflection point. Hence, for each trajectory remaining after the altitude criterion, time delays between two stations  $R_1$  and  $R_2$  can be computed as the distance between their respective reflection points divided by the speed of the meteoroid (assuming no deceleration). A priori, the meteoroid speed  $v$  is unknown and should be assumed.

*Figure 7* shows the time delays computed for the 3 stations U, O, and S for  $v = 20 \text{ km/s}$  and for the remaining 54734 trajectories. A reference station has to be chosen such that a time delay is counted positive if the reflection point of the other station is created after that of the reference, and negative otherwise. When included in the computation of the time delays, Uccle is the reference, otherwise Ottignies is. Since simulated trajectories are coming from the north-east quadrant and

going to the south-west direction, and since Seneffe is located south of the other two stations (see *Figure 1*), time delays between S and either U or O are expected to be positive and this is indeed the case in *Figure 7*. Time delays between U and O can be positive or negative.

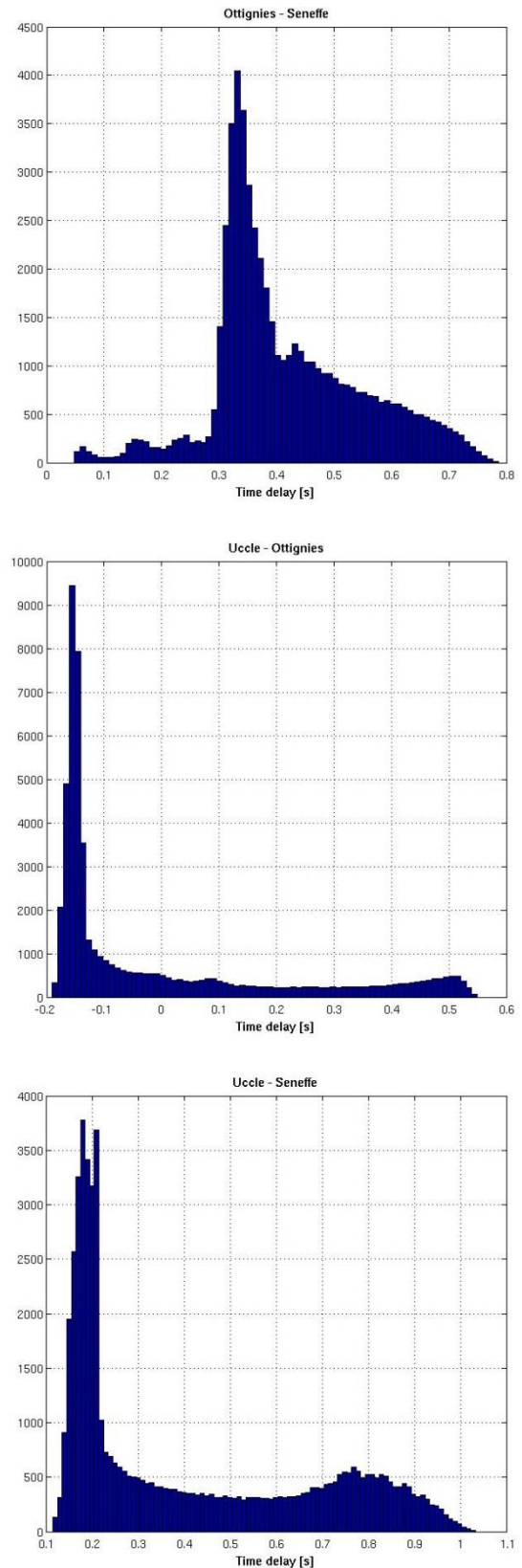


*Figure 7* – Time delays between stations U, S and O for the trajectories with altitude of reflection points between 95 and 110 km and for a meteoroid speed of 20 km/s. Width of the bins is 0.01 sec.

In practice, time delays should be measured from real data and selected among these three sets of values in order to constrain the trajectory of the meteoroid. This is possible since BRAMS receiving stations are synchronized using GPS clocks. The difficulty is to define accurately the start of the meteor echo at each station.

#### 4 Discussions and conclusion

Since the CW signal sent by the BRAMS transmitter does not contain any type of modulation, the distance traveled by the wave is not available for stations detecting meteor echoes. Hence, in the most general case, 6 receiving stations must detect the same meteor in order to solve for the 6 unknowns (3 coordinates of a point, 2 angles for a direction and the meteoroid speed  $v$ ) and to retrieve the meteoroid trajectory. In this paper, we have first carried out simulations to test the geometrical approach proposed by (Nedeljkovic, 2006). Only results with 3 BRAMS stations, geometrically close to each other, were presented. Next, simulations will be carried out with up to 6 stations although, based on experience using BRAMS data, it is rather hard to find meteor echoes detected by at least 6 stations.

The reason might lie in the sensitivity of the various receiving stations, which is why an additional criterion based on a minimum detectable power was considered, assuming strictly underdense meteor echoes and electrons distributed along a straight line. Since the electron line density  $\alpha$  at the specular reflection point is a priori unknown, a range of typical values for underdense meteors had to be assumed. Because of this limitation, this power criterion cannot be used in practice to solve the problem of the meteoroid trajectory but it is useful to estimate the minimum value  $\alpha_{\min}$  detectable by a given receiving station. Also, if the trajectory and speed are available from e.g. optical observations, then the power criterion can be used to check if a given station will be able to detect a meteor echo or not. However, it is questionable if even the faintest detected optical meteors would still produce underdense meteor echoes. Another formula could be used for overdense meteor echoes instead, such as e.g. the classical one from (Mc Kinley, 1961) where the power  $P \sim \alpha^{1/2}$ , but due to the longer lifetime of the trail and the strong shear winds in the meteor zone, the validity of this formula is doubtful. In any case, a comparison between optical and radio observations with the BRAMS network would be highly valuable.

Finally a third criterion based on time delays of the meteor echoes observed at different receiving stations was also briefly discussed. Tests using real data will be carried out soon in order to check if only a very low number of trajectories can be selected. Of course for this comparison with real data, simulations of trajectories from all four quadrants should be made as real meteoroids can come from any direction.

These simulations will also be used with the interferometric station in Humain (Lamy, 2015), which has the advantage of providing the direction of arrival of the meteor echo. This will strongly reduce the number of possible trajectories.

During meteor showers, the position of the radiant at a given time is known. In our simulations, this would fix the values of  $\theta$  and  $\varphi$ . In this case, results of the simulations can also be compared to those predicted by the observability function method proposed by (Verbeek, 1997) for underdense meteor echoes.

#### Acknowledgment

The BRAMS network is a project from the Royal Belgian Institute for Space Aeronomy and funded by the Solar-Terrestrial Center of Excellence (STCE). It is a very active collaboration between professionals and amateurs, the latter hosting most of the BRAMS receiving stations. The authors would like to thank them for their constant support. C. Tétard is funded by the Belgian Science Policy via the Brain-Be project BR/143/A2/METRO.

#### References

- Belkovich O. I. and Verbeek C. (2006). “The physics of meteoroid ablation and the formation of ionized meteor trails”. In Verbeek C. and Wislez J.-M., editors, *Proceedings of the Radio Meteor School*, Oostmalle, Belgium, 10-14 September 2005. IMO, pages 21–16.
- Lamy H., Anciaux M., Ranvier S., Calders S., Gamby E., Martinez Picar A. and Verbeek C. (2015). “Recent advances in the BRAMS network”. In Rault J.-L. and Roggemans P., editors, *Proceedings of the International Meteor Conference*, Mistelbach, Austria, 27-30 August 2015. IMO, pages 171–175.
- Martinez Picar A., Ranvier S., Anciaux M. and Lamy H. (2014). “Modelling and calibration of BRAMS antenna systems”. In Rault J.-L. and Roggemans P., editors, *Proceedings of the International Meteor Conference*, Giron, France, 18-21 September 2014. IMO, pages 201–206.
- McKinley D. W. R. (1961). “Meteor science and engineering”. McGraw-Hill Book Company New-York U.S.A.
- Nedeljkovic S. (2006). “Meteor forward scattering at multiple frequencies”. In Verbeek C. and Wislez J.-M., editors, *Proceedings of the Radio Meteor School*, Oostmalle, Belgium, 10-14 September 2005. IMO, pages 108–116.
- Verbeek C. (1997). “Calculating the sensitivity of a forward scatter setup for underdense meteor showers”. *Proceedings of the International Meteor Conference*, Apeldoorn, the Netherlands, 19-22 September 1996. IMO, pages 122–132.

# Easy way to estimate meteor brightness on TV frames

Vladislav A. Leonov and Alexander V. Bagrov

Institute of Astronomy of Russian Academy of Science

leonov@inasan.ru; abrgrov@inasan.ru

The traditional method of the meteor brightness measurements claims that the meteor brightness is equal to the stellar magnitude of a star that looks like a meteor in the brightest point of its track. This rule was convenient for the comparison of meteor observations by different observers and for the analysis of the brightness distributions of meteors from observed showers. This traditional method suffers from systematic errors, particularly those that arise from using stellar brightness measured in specific spectral wave bands different from the observer's ones, but mainly due to neglecting the influence of the meteor angular velocity on the real meteor brightness. To get a proper estimate of the meteor brightness that is a measure of the ground meteor illumination in the non-systematic units, an observer must take into account that the effective exposition of a meteor image in any resolution element of its track is a few times shorter than the corresponding exposition of a star image in the same frame. We propose a very simple method for improved estimations of meteor brightness by applying a correction to the meteor stellar magnitude obtained within the traditional framework.

## 1 Introduction

For many decades meteor observers had a tradition to measure meteor stellar magnitudes by simple comparison of the visual brightness of stars and meteors (Roggemans, 1989; Lunsford, 2009). The traditional method of the meteor brightness measurements claims that the meteor brightness is equal to the stellar magnitude of a star that looks like a meteor in the brightest point of its track. The obtained brightness has to be adjusted to the “standard” 100 km distance for a proper comparison of meteors that have been observed at different distances. This rule was convenient for the comparison of meteor observations by different observers and for the analysis of the brightness distributions of meteors from observed showers (Molau, 1995; Hawkes and Jones, 1986). This “meteor brightness” is only a “slang” unit, because it does not refer to the ground meteor illumination measured in the standard stellar magnitude units. The matter is that the astronomical stellar magnitudes are carefully measured for catalogued stars in special wide- or narrow spectral bands (as B, V, R, and others) with a careful correction for sensitivity of a used light sensor to different wavelengths (Sterken and Manfroid, 1992). This astronomical approach is suitable for studies of stars because they have black body radiation spectra. Once the correct temperature of a star is known within its spectral class, one can determine its ground illumination in energetic units by measuring its brightness in the bands B, V and R. On the other hand, brightness measured in any band in stellar magnitudes ( $m_V$ ,  $m_B$  and so on) gives ground illumination of a light source in non-systematic units, though reducible to the systematic ones.

Contrary to this, meteor observations are usually performed in a whole waveband, where the light sensor is sensitive. So the referred brightness of the background stars are not the same as the catalogued values in narrower bands. To use the background stars as a photometric standard, one should have their brightness in the real observation waveband. We proposed in (Leonov

and Bagrov, 2016) such a catalogue, especially prepared for meteor TV observers that use WATEC902H cameras without color filters.

Meteors are observed as fast moving light sources, thus the real exposition of a meteor image in any element of its track differs from the exposure time of background stars in the same frame. When someone compares visible brightness of a meteor track and stars, they compare the brightness of both in equal resolution elements and do not take into account the number of resolution elements in a single track of a meteor in the frame. Very often, meteor observers believe that they observe faint meteors at a similar magnitude as background stars, while the real brightness of a registered meteor is few times larger.

## 2 Brightness of meteor images

The light flux of a meteor during a frame exposition disperses over its whole track that may be longer or shorter depending on the meteor angular velocity, focal length of the camera lens and the angular camera resolution. In the same frame images of stars look like spots of various sizes. Normally the brighter stars are larger than the weaker ones. But when an observer tries to compare meteor images of similar brightness, they have to compare images of similar widths  $d$ . So a meteor image differs from the stellar ones only by length. Evidently, when the meteor length is  $l$ , it is  $l/d$  times longer than its diameter; it means that the meteor has to be  $l/d$  times brighter than a similarly looking star. Hence the proper brightness of a meteor in stellar magnitudes will be  $2.5lg(l/d)$  brighter than the stellar magnitude of a reference star of similar brightness. The correction factor  $2.5lg(l/d)$  depends only on the relative length of the meteor track, so it may be estimated as a function of the  $l/d$  ratio and tabulated. Taking into account that the estimates of meteor brightness are reported in whole numbers, we present below a table of the necessary correction factor  $2.5lg(l/d)$  values:

Table 1 – Meteor magnitude correction factors.

$l/d$	2.5	6	16	40
$\Delta m$	1	2	3	4

In visual observations human eyes are used as light sensors, and in most cases they are identical in the spectral band limits as well as in the angular resolution power. So the relative estimate of the meteor brightness by different observers will be nearly equal. And for the relative characterization of meteors from the same meteor shower (when the meteors have nearly the same angular velocities) such brightness estimates are good, though they have systematic errors. But this brightness measurement is not sufficient for the calculation of the light energy emitted by a meteor particle in the Earth atmosphere. To eliminate these systematic errors one has to know the meteor angular velocity relative to the angular resolution of a human eye.

A human eye is able to resolve about 16 frames per second. When it looks at a star, it is collecting light in 0.06 sec segments. But fast moving meteors illuminate every eye resolution element in a shorter time. The angular resolution of a human eye is  $\sim 1-2'$ , which means that a meteor with an angular velocity of 5 deg/sec illuminates nearly 250 resolution elements in a second, and therefore the effective exposition of a meteor in a resolution element is 40 times shorter. To produce an equal sense of visual brightness with a star, the meteor must be 4 magnitudes brighter than the star. So to get proper stellar magnitudes of meteors, visual observers have to be skillful enough to estimate angular velocities of meteors. This is a difficult task for astronomers using video technology, let alone amateurs using traditional visual methods of meteor stellar magnitude estimations. It is necessary to remember that these estimations cannot be used for photometric investigations.

### 3 Looking at TV frames

Meteor video registrations are rows of frames with images of background stars and a meteor track. All these images have equal exposition, were they interlacing or progressive. So it is easy to estimate the correction parameter  $l/d$  in any frame. There might be various images of a meteor track. An example (taken with extremely sensitive camera FAVOR (Karpov et al., 2004)) is presented in *Figure 1*. This track is homogeneously bright, so it may be compared with a star image of the same width (upper one to the right of the meteor in this frame). The length of this meteor track is nearly 2.5 times its width, so the correction coefficient for this image is  $-1$  magnitude. Thus the meteor is in fact one stellar magnitude brighter than the star it looks like.

When a meteor track has a trail (*Figure 2*), an observer has to estimate only the track length without the trail. As one can see in *Figure 2*, its  $l/d \approx 5$  at homogeneous

brightness, so the real stellar magnitude of the meteor is 2m brighter than that of its neighboring stars.

Often the meteor brightness varies along its track. In that case the standard rule of brightness estimation relies to the maximal brightness. So the width of the track has to be measured at the brightest point of the track to estimate its  $l/d$ . *Figure 3* presents this kind of meteor track. In any case the length of the track is determined by the meteor velocity independently of its brightness, so in order to estimate the meteor parameter  $l/d$  in the brightest point of its track we should take  $l/d \approx 10$  for the case on *Figure 3*. It means that the meteor is 2.5 magnitudes brighter than a star of similar brightness.

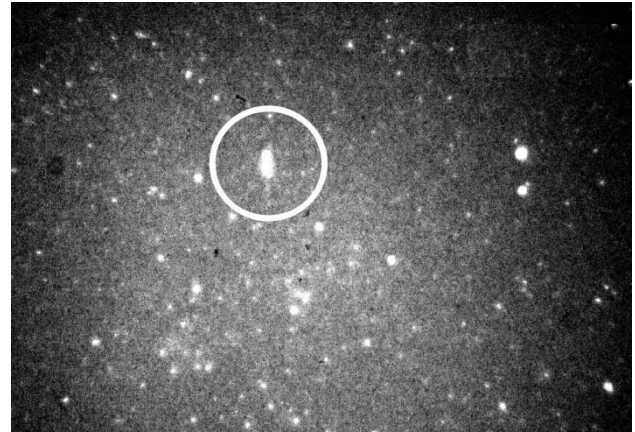


Figure 1 – Low velocity meteor track with  $l/d \approx 2.5$  taken with camera FAVOR (Karpov et al., 2004).

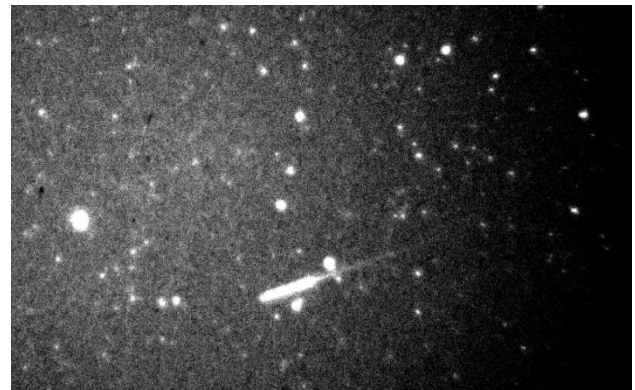


Figure 2 – Meteor track with  $l/d \approx 5$  (without trail).

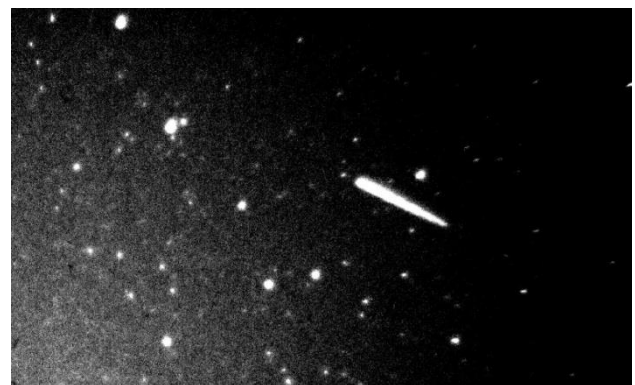


Figure 3 – Meteor track with variable brightness along it. As its  $l/d \approx 10$ , the correction coefficient for this meteor is 2.5 magnitude.

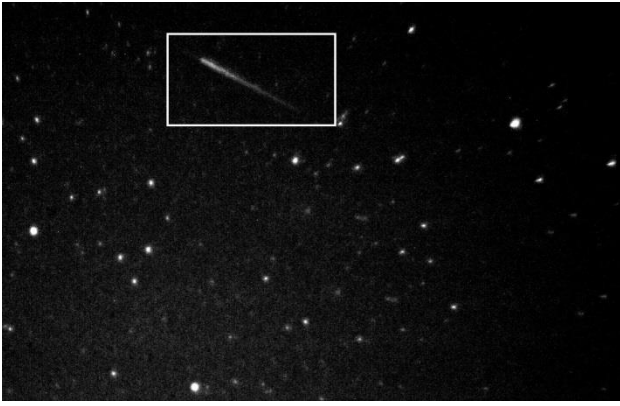


Figure 4 – A relatively weak meteor which maximal brightness seems to be only 3 magnitudes brighter than the weakest background stars. But as its  $l/d \approx 16$ , its real magnitude is 3m brighter.

Meteors with large angular velocities produce tracks with  $l/d \approx 16$  and even longer. One such image is presented in Figure 4. The maximal brightness of this meteor is 3m more than the one of a comparatively bright background star. But if a meteor track is homogeneously bright along its length, its relative length would be about 40, and its real stellar magnitude will be 5m brighter than the limiting magnitude in the frame. Evidently, it means that no meteor with brightness equal to the limiting star magnitude can be registered by TV cameras.

#### 4 Telescopic meteor observations

Using binoculars or a telescope, an observer achieves a deeper limiting magnitude of visible stars than with a naked eye. This advantage also comes with an increase in eye angular resolution. Thus the meteor angular velocity will increase by a factor of telescope magnification. Though the limiting magnitude of background stars increases, the detectable brightness of meteors remains the same. Some growth of meteor limiting magnitude may be noted only for very low-speed meteors. While some meteors have low speeds near to their radiant, they are really very rare. Observations of such meteors cannot provide representative data for analysis, so they are of limited use.

#### 5 Conclusion

A very simple method of correcting estimates of meteor brightness described here may be used for a preliminary analysis of TV meteor registrations. An observer only has to roughly estimate the relative length of a meteor track in a chosen frame with the meteor's maximal brightness and to apply a tabulated correction to the value of meteor magnitude obtained by the traditional method. The results should then be refined by using a special photometric

catalogue of reference stars, prepared for visual-to-near infrared waveband of the WATEC cameras sensitivity.

The limiting magnitude of meteors as shown here cannot coincide with the limiting magnitude of background stars, and meteors of a brightness equal to the limiting star magnitude cannot be observed.

#### Acknowledgment

The reported study was partially funded by Presidium RAS according to the 2015 research program № 9.

#### References

- Hawkes R. L. and Jones J. (1986). "Electro-optical Meteor Observation Techniques and Results". *Quarterly Journal of the Royal Astronomical Society*, **27**, 569–589.
- Karpov S., Bad'in D., Beskin G., Biryukov A., Bondar S., Chuntunov G., Debur V., Ivanov E., Katkova E., Plokhotnichenko V., Pozanenko A., Zolotukhin I., Hurley K., Palazzi E., Masetti N., Pian E., Nicastrò L., Bartolini C., Guarnieri A., Nanny D., Piccioni A., Brosch N., Eichler D., Shearer A., Golden A., Redfern M., Atteia J.-L. and Boer M. (2004). "FAVOR (FAst Variability Optical Registration) – two telescope complex for detection and investigation of short optical transients". *Astronomische Nachrichten*, **325**, 6–8, 677.
- Leonov V. A. and Bagrov A. V. (2016). "Photometric Stellar Catalogue for TV meteor Astronomy". In Roggemans A. and Roggemans P., editors, *Proceedings of the International Meteor Conference*, Egmond, the Netherlands, 2-5 June 2016. Pages 151–154.
- Lunsford R. (2009). "Meteors and how to observe them". Springer, Science + Business Media, LLC. 192 pages.
- Molau S. (1995). "Systematic Errors on visual Meteor Brightness Estimates". *WGN, Journal of the IMO*, **23**, 225–228.
- Roggemans P. (1989). "Handbook for Visual Meteor Observations". Sky Publishing Corp., Cambridge, Mass., USA.
- Sterken C. and Manfroid J. (1992). "Astronomical Photometry: A Guide". Kluwer Academic Publishers.

# Photometric stellar catalogue for TV meteor astronomy

Vladislav A. Leonov and Alexander V. Bagrov

Institute of Astronomy of Russian Academy of Science

leonov@inasan.ru; abrgrov@inasan.ru

Photometry for ordinary astrophysics was carefully developed for its own purposes. As stars radiation is very similar to the blackbody radiation, astronomers measure star illumination in wide or narrow calibrated spectral bands. This is enough for star photometry with precise accuracy and for measuring their light flux in these bands in energetic units. Meteors are moving objects and do not allow collection of more photons then they emit. So meteor observers use the whole spectral band that can be covered by sensitivity of their light sensors. This is why measurements of stellar magnitudes of background stars by these sensors are not the same as catalogued star brightness in standard photometric spectral bands. Here we present a special photometric catalogue of 93 bright non-variable stars of the northern hemisphere, that can be used by meteor observers of standard background whose brightness are calculated in energetic units as well as in non-systematic stellar magnitudes in spectral wavelength of the WATEC 902 sensitivity.

## 1 Introduction

Long ago Hipparcos introduced the stellar brightness scale for visual astronomical observations. Modern astronomers use opto-electronic sensors that can count photons but have variable sensitivity depended on wavelength. Photometrists agreed to make their observations in some alternatively determined wavelength bands and sensor sensitivities. Since 1953 astronomers used the photometric system (U, B, V) which was first proposed by Johnson and Morgan (1953). In most cases astrophysics use well-calibrated middle-band or narrow-band photometrical systems (*Figure 1*). As different stars in these bands have different brightness, photometrists measure stellar magnitudes in each band (say, B, V, R) and characterize stars be differences (B-V), (V-R) and so on. One can easily calculate light flux energy of a star in any spectral band having its magnitude as well as calculate its total light flux by signatures (B-V) and (V-R).

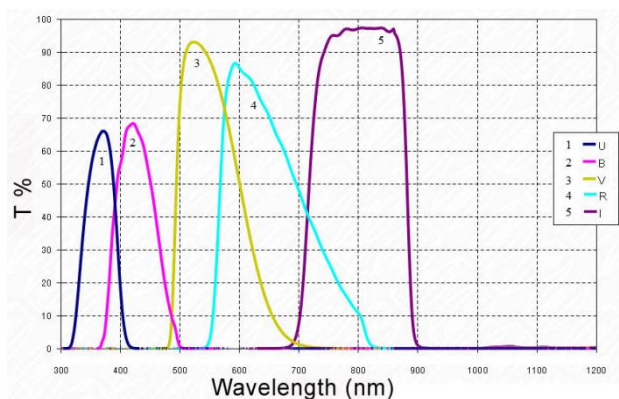


Figure 1 – Spectral bands mostly used in stellar photometry.

Meteor observers always use “integral” light, i.e. they capture every photon from a meteor and use no filters.

One cannot estimate the light flux from a meteor in energy units by simple comparison of signals from meteor and stars even in one frame. But it may be done having a special photometric catalogue of star magnitude

in the used spectral band with references to the true energy fluxes in the band.

## 2 Meteor TV sensors

Every light sensor has its own spectral sensitivity that depends on a light wavelength  $\lambda$ . There are many TV cameras that meteor observers use (Rendtel and Arlt, 2009). One of the most popular of them is the high sensitive CCD cameras WATEC LCL 902 or its successors. These cameras have the ICX429ALL sensor for which the sensitivity curve is presented on *Figure 2*<sup>1</sup>.

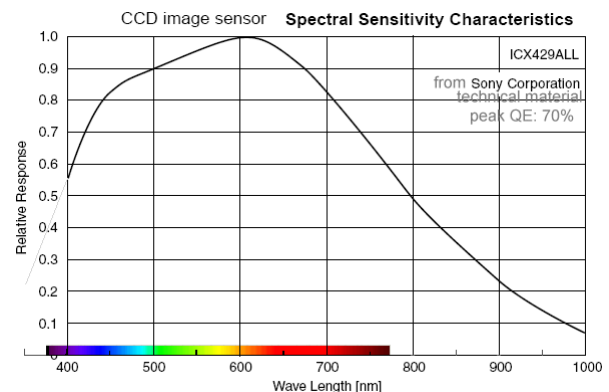


Figure 2 – Spectral sensitivity of WATEC LCL 902<sup>1</sup>.

The output (registered) signal in a light wavelength  $\lambda$  depends on the input light flux  $I(\lambda)$  of the source, transmission of the lens  $T(\lambda)$  and sensitivity of the light registration  $Q(\lambda)$ :

$$S(\lambda) = I(\lambda) \cdot T(\lambda) \cdot Q(\lambda)$$

A wide-angle high resolution lens consists of many components, some of them being aspherical. Such lenses do not have 100% transparency. *Figure 3* shows the transparency dependency on wavelength for the very popular lens Computar HG0608AFCS-HSP on its optical axis<sup>2</sup>. With increased viewing angle its transparency

<sup>1</sup> <http://datasheet.seekic.com/PdfFile/ICX/ICX429ALL.pdf>  
<sup>2</sup> <http://www.cctv-catalog.ru/catalog/f0n0s0p0pos196a.htm>

decreases. There is no necessity to pre-calculate a lens transparency for every point of its field of view, because if the observer will calibrate the TV pictures by stars across the measured image, the lens transparency will be the same for images of an object and a star. So the lens transparency will act on limiting magnitude, but may be neglected for photometric calibrations. This is why we can declare  $T(\lambda) = 1$  for a relative calculation of the output light signals from stars. The total output signal is the integral:

$$S = \int_{\lambda} S(\lambda) \cdot d\lambda = \int_{\lambda} I(\lambda) \cdot Q(\lambda) \cdot d\lambda$$

As meteor observers use input optics for visible light, it is possible to adopt the limits of the camera sensitivity as 322.5 to 757.5 nm. Outside of these limits, both star brightness and camera sensitivity are low and can form less than 5% of the output signal.

### 3 Basic conception of a special photometric catalogue of bright stars for meteor photometry

To provide meteor observers with the true brightness of background stars as they are seen by WATEC cameras, we calculate the ground illumination by some bright stars within the limits of camera sensitivity.

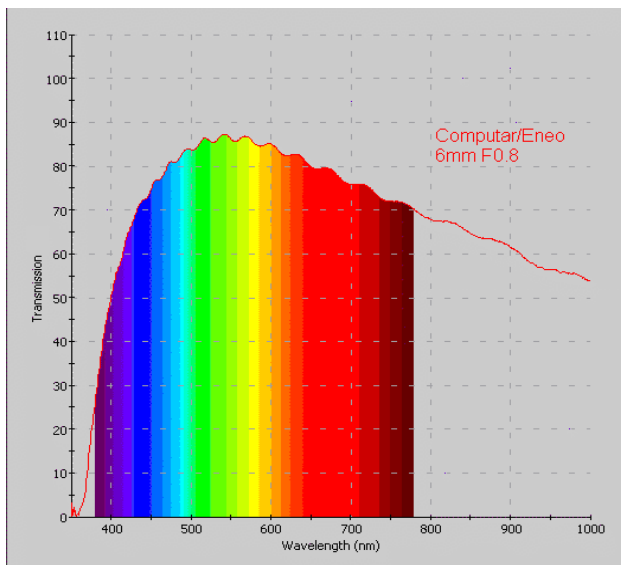


Figure 3 – Transmission dependence on wavelength for the Computar HG0608AFCS-HSP lens.

Meteor TV-cameras with frame ratio 25 to 30 fr/s can register stars brighter than 4m in the V-band. So for the first version of our catalogue we selected 93 non-variable bright stars of the northern hemisphere from the *Stellar Spectrophotometric Catalogue* by Kharitonov et al., 1988<sup>3</sup>. Their spectral brightness was measured with 2.5 nm steps, so we estimated  $Q(\lambda)$  with the same steps from Figure 2 to calculate  $S$  as a sum of multiplications  $I(\lambda) \cdot Q(\lambda)$  over the whole spectral band.

All data was calculated as integral from multiplication of the spectral sensitivity of the ICX429ALL sensor and the spectral energy distribution for each star for 25-angstrom wavelength bands. The presented Photometric Catalogue covers northern hemisphere stars with brightness above  $m_v = 4.0^m$ . As meteors are shining at the very upper atmosphere, their optical observations are done through the same atmosphere as referred stars, so the calculated meteor luminance will be obtained directly in extra-atmospheric energy units.

Table 1 presents the celestial coordinates (RA, DE) and the names of 93 stars of the northern hemisphere, their spectral classes Sp, visual magnitudes  $m_v$  and the relative magnitudes in the WATEC sensitivity spectral band. The last column contains energy luminance by stars in energetic units  $\text{erg}/(\text{cm}^2 \cdot \text{s})$ .

### Acknowledgment

The reported study was partially funded by Presidium RAS according to the 2015 research program № 9.

### References

- Johnson H. L. and Morgan W. W. (1953). “Fundamental Stellar Photometry for Standards of Spectral Type on the Revised System of the Yerkes Spectral Atlas”. *Astrophysical Journal*, **117**, 313–352.
- Kharitonov A. V., Tereshchenko V. M. and Knyazeva L. N. (1988). “Spectral-photometric stellar catalogue”. Alma-Ata, Nauka publ. (*in Russian*).
- Rendtel J. and Arlt R. (editors) (2009). Handbook for meteor observers. International Meteor Organization.

<sup>3</sup> <http://cdsarc.u-strasbg.fr/viz-bin/Cat?cat=III%2F202&target=readme&>

Table 1– Special photometric catalogue of bright stars for meteor photometry.

	Name		RA		DE		$V_{\text{mag}}$	$V_{\text{watec}}$	Sp	E erg/(cm <sup>2</sup> ·s)
	<i>Letter</i>	<i>Const.</i>	<i>h</i>	<i>m</i>	<i>d</i>	<i>m</i>				
1	$\beta$	Cas	0	9	59	9	2.27	2.38	F2III-IV	2.15
2	$\zeta$	Cas	0	36	53	53	3.66	3.47	B2IV	0.79
3	$\alpha$	Cas	0	40	56	32	2.23	2.50	K0IIIa	1.93
4	$\eta$	Cas	0	48	57	49	3.44	3.57	G0V+dM0	0.72
5	$\gamma$	Cas	0	56	60	43	2.47	2.01	B0IVe	3.02
6	$\mu$	And	0	56	38	29	3.87	3.95	A5V	0.51
7	$\beta$	And	1	9	35	37	2.06	2.25	M0IIIa	2.42
8	$\delta$	Cas	1	25	60	14	2.68	2.74	A5III-IV	1.55
9	$\alpha$	Umi	2	31	89	15	2.02	2.17	F7:Ib-II	2.60
10	51	And	1	37	48	37	3.57	3.84	K3III	0.56
11	$\varepsilon$	Cas	1	54	63	40	3.38	3.20	B3III	1.01
12	50	Cas	2	3	72	25	3.98	3.94	A2V	0.51
13	$\gamma$	And	2	3	42	19	2.10	2.31	K3IIb/B8V+A0V	2.29
14	$\beta$	Tri	2	9	34	59	3.00	3.09	A5III	1.12
15	$\eta$	Per	2	50	55	53	3.76	3.93	M3Ib-IIa	0.52
16	$\tau$	Per	2	54	52	45	3.95	4.13	G4III+A4V	0.43
17	$\gamma$	Per	3	4	53	30	2.93	3.05	G8III+A2V	1.16
18	$\rho$	Per	3	5	38	50	3.39	3.32	M4II	0.91
19	$\kappa$	Per	3	9	44	51	3.80	4.00	K0III	0.49
20	$\alpha$	Per	3	24	49	51	1.80	1.92	F5Ib	3.29
21	$\delta$	Per	3	42	47	47	3.01	2.84	B5III	1.41
22	$\nu$	Per	3	45	42	34	3.77	3.91	F5II	0.53
23	$\varepsilon$	Per	3	57	40	0	2.89	2.53	B0.5V+A2V	1.88
24	$\zeta$	Aur	5	2	41	4	3.75	3.87	K4II+B8V	0.55
25	$\eta$	Aur	5	6	41	14	3.17	2.97	B3V	1.25
26	$\alpha$	Aur	5	16	46	0	0.08	0.25	G5III+G0III	15.28
27	$\nu$	Aur	5	51	39	8	3.97	4.22	K0III	0.40
28	$\delta$	Aur	5	59	54	17	3.72	3.99	K0III	0.49
29	$\beta$	Aur	5	59	44	56	1.90	1.87	A2IV	3.43
30	$\theta$	Aur	5	59	37	12	2.62	2.53	A0p	1.87
31	$\omicron$	Uma	8	30	60	43	3.36	3.59	G5III	0.71
32	$\iota$	Uma	8	59	48	2	3.14	3.22	A7IV	0.99
33	$\kappa$	Uma	9	3	47	9	3.60	3.53	A1Vn	0.75
34	38	Lyn	9	18	36	48	3.82	3.85	A3V	0.56
35	$\alpha$	Lyn	9	21	34	23	3.13	3.37	K7IIIab	0.87
36	23	Uma	9	31	63	3	3.67	3.76	F0IV	0.61
37	$\theta$	Uma	9	32	51	41	3.17	3.30	F6IV	0.92
38	$\upsilon$	Uma	9	51	59	2	3.80	3.90	F2IV	0.54
39	$\lambda$	Uma	10	17	42	54	3.45	3.44	A2IV	0.81
40	$\mu$	Uma	10	22	41	29	3.05	3.22	M0III	0.99
41	$\beta$	Uma	11	1	56	22	2.37	2.38	A1V	2.14
42	$\alpha$	Uma	11	3	61	45	1.79	2.07	K0IIIa	2.85
43	$\psi$	Uma	11	9	44	29	3.01	3.27	K1III	0.95
44	$\lambda$	Dra	11	31	69	19	3.84	3.96	M0III	0.50
45	$\chi$	Uma	11	46	47	46	3.71	3.95	K2III	0.51
46	$\gamma$	Uma	11	53	53	41	2.44	2.48	A0Ve	1.97
47	$\delta$	Uma	12	15	57	1	3.31	3.36	A3V	0.88

	Name		RA		DE		$V_{\text{mag}}$	$V_{\text{watec}}$	Sp	E erg/(cm <sup>2</sup> ·s)
	<i>Letter</i>	<i>Const.</i>	<i>h</i>	<i>m</i>	<i>d</i>	<i>m</i>				
48	$\kappa$	Dra	12	33	69	47	3.87	3.75	B6IIIpe	0.61
49	$\varepsilon$	Uma	12	54	55	57	1.77	1.80	A0p	3.68
50	$\alpha$	CVn	12	56	38	19	2.90	2.79	A0p	1.48
51	$\zeta$	Uma	13	23	54	55	2.27	2.23	A1Vp	2.46
52	$\zeta$	Uma	13	23	54	55	3.95	3.99	A1m	0.49
53	$\eta$	Uma	13	47	49	18	1.86	1.68	B3V	4.08
54	$\alpha$	Dra	14	4	64	22	3.65	3.64	A0III	0.67
55	$\gamma$	Boo	14	32	38	18	3.03	3.14	A7III	1.07
56	$\beta$	Umi	14	50	74	9	2.08	2.33	K4III	2.25
57	$\beta$	Boo	15	1	40	23	3.50	3.76	G8IIIa:	0.60
58	$\gamma$	Umi	15	20	71	50	3.05	3.10	A3II-III	1.11
59	$\iota$	Dra	15	24	58	57	3.29	3.56	K2III	0.72
60	$\tau$	Her	16	19	46	18	3.89	3.77	B5IV	0.60
61	$\eta$	Dra	16	23	61	30	2.74	2.96	G8IIIab	1.26
62	$\eta$	Her	16	42	38	55	3.53	3.70	G8III	0.64
63	$\zeta$	Dra	17	8	65	42	3.17	3.03	B6III	1.18
64	$\pi$	Her	17	15	36	48	3.16	3.39	K3IIab	0.85
65	$\beta$	Dra	17	30	52	18	2.79	3.06	G2Ia-IIa	1.15
66	$\iota$	Her	17	39	46	0	3.80	3.59	B3IV	0.71
67	$\xi$	Dra	17	53	56	52	3.75	3.97	K2III	0.50
68	$\theta$	Her	17	56	37	15	3.86	4.10	K1II	0.44
69	$\gamma$	Dra	17	56	51	29	2.23	2.40	K5III	2.12
70	$\chi$	Dra	18	20	72	44	3.57	3.68	F7V	0.65
71	$\alpha$	Lyr	18	36	38	46	0.03	0.03	A0Va	18.74
72	$\delta$	Dra	19	12	67	39	3.07	3.30	G9III	0.92
73	$\kappa$	Cyg	19	17	53	22	3.77	4.01	G9III	0.48
74	$\iota$	Cyg	19	29	51	43	3.79	3.85	A5Vn	0.56
75	$\delta$	Cyg	19	44	45	7	2.87	2.86	B9.5IV+F1V	1.39
76	$\varepsilon$	Dra	19	48	70	16	3.83	4.04	G7III	0.47
77	$\eta$	Cyg	19	56	35	5	3.89	4.15	K0III	0.42
78	31	Cyg	20	13	46	44	3.79	3.95	K2II+B3V	0.51
79	32	Cyg	20	15	47	42	3.98	4.14	K3Ib+B3V	0.43
80	$\gamma$	Cyg	20	22	40	15	2.20	2.39	F8Ib	2.13
81	$\alpha$	Cyg	20	41	45	16	1.25	1.25	A2Iae	6.12
82	$\eta$	Cep	20	45	61	49	3.43	3.65	K0IV	0.67
83	$\nu$	Cyg	20	57	41	10	3.94	3.93	A1Vn	0.52
84	$\xi$	Cyg	21	4	43	55	3.72	3.90	K4-5IB	0.53
85	$\tau$	Cyg	21	14	38	2	3.72	3.83	F2IV	0.57
86	$\alpha$	Cep	21	18	62	35	2.44	2.52	A7V	1.90
87	$\beta$	Cep	21	28	70	33	3.23	2.92	B1IV	1.30
88	$\zeta$	Cep	22	10	58	12	3.35	3.64	K1.5Ib	0.67
89	$\alpha$	Lac	22	31	50	16	3.77	3.76	A1V	0.61
90	$\iota$	Cep	22	49	66	12	3.52	3.80	K0III	0.58
91	o	And	23	1	42	19	3.62	3.52	B6IIIpe+A2p	0.75
92	$\lambda$	And	23	37	46	27	3.82	4.01	G8III-IV	0.48
93	$\gamma$	Cep	23	39	77	37	3.21	3.46	K1III-IV	0.79

# ROAN Remote radio meteor detection sensor

Cezar Eduard Lesanu

Integrated Center for research, development and innovation in Advanced Materials,  
Nanotechnologies, and Distributed Systems for fabrication and control

MANSiD, Stefan cel Mare University, Suceava, Romania

cezar1@usv.ro

Only few meteor enthusiasts across the world today, approaches systematically the radio meteor detection technique, one of the reasons being the difficulty to build and install proper permanent antennas, especially when low-VHF frequency opportunity transmitters are used as illuminators. Other reasons were in the past the relatively high cost of the entire system, receivers and computers, and not ultimately the high power consumption of the system in a 24/7 operation, when using regular personal computers. The situation changed in the recent years with the advent of the low cost software defined radio SDR receivers and low consumption/cost single board computers SBC. A commercial off-the-shelf hardware based remote radio meteor detection sensor is presented.

## 1 Introduction

In the radio meteor detection field, there are various technical aspects that make this observation technique less used by amateurs, only few radio detection stations being present online in continuous operation. The radio hardware setup choice, antenna and receiver, the overall cost of the equipment and the power consumption in a 24/7 operation, adds to the lack of knowledge in the field of radio electronics.

During the time, several radio meteor detection networks emerged, making use of commercial off-the-shelf (COTS) or dedicated hardware defined radio receivers (HRD) and, later on, software defined radio receivers (SDR) (Lesanu, 2011; Sufitchi, 2015). These networks make use of dedicated radio beacons or opportunity transmitters (such as GRAVES Radar).

Table 1 – Radio Meteor Detection Networks

Network	Receiver	f [MHz]
AMRO-NET	Dedicated HDR (HRO)	53.750
BRAMS	COTS HDR	49.970/49.990
BOLIDOZOR	Dedicated SDR (QSD)	143.050
FRIPON	COTS SDR (FCD Pro+)	143.050
ROAN	COTS SDR (RTL-SDR)	TBD (~50MHz)

A commercial off-the-shelf (COTS) hardware based remote radio meteor detection sensor, developed for the Romanian ALLSKY Network ROAN (Georgescu, 2013), operating in the six meter band (~50MHz), is presented.

## 2 System overview

### System architecture

The radio meteor detection sensor comprises the same components already known: antenna, receiver and the processing unit (computer). Unlike the classical setup, the radio subsystem is installed remote from the processing

unit, the data being streamed between the two via internet TCP/IP (Figure 1).

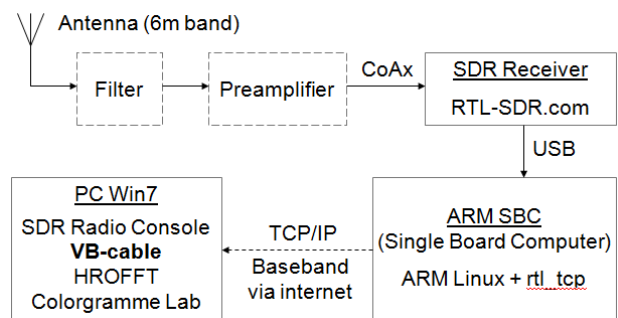


Figure 1 – Radio meteor sensor architecture.

The signal from antenna is applied, after filtering, to an optional preamplifier in order to improve the overall sensitivity of the system. The radio receiver chosen is an improved version of the well-known, mass produced, USB software defined radio receiver dongle RTL-SDR, designed especially for DAB/DVB-T reception. The radio sensor streams the baseband signal from the receiver to the processing server via internet (TCP/IP), by means of an ARM single board computer (SBC).

### Antenna

The most challenging technical aspect is the setup of a proper receiving antenna: building, tuning and installation issues. Several goals were imposed when the antenna design was chosen.

An omnidirectional radiation pattern was desirable in order to be able to implement a multi-transmitter / multi-frequency reception concept. In the same time, an antenna design with a favorable radiation lobe at medium elevation angles was called for, having in mind the use of radio beacons situated at low and medium ranges. In addition, the simplicity of building, tuning and installing the antenna, were other goals searched for.

It is well known that by increasing the length of an end fed radiator with multiples of half wavelengths, the main lobe of radiation approaches the direction of the radiator. The gain increases in the same time with the number of the half wavelength segments.

In *Figure 2*, a comparison between the far field radiations patterns in the vertical plane of several vertical radiators with various lengths, placed over the ground, is presented.

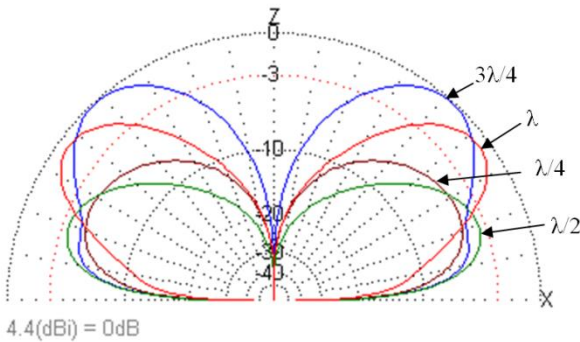


Figure 2 – Vertical antennas far field radiation patterns.

One can note that the radiation pattern of a three quarter wavelength  $3\lambda/4$  vertical antenna, fulfills the requirements imposed and has been chosen for further analysis. The geometry of a  $3\lambda/4$  vertical antenna, with the current distribution plotted, fitted with four respectively with one radial, is shown in *Figure 3*.

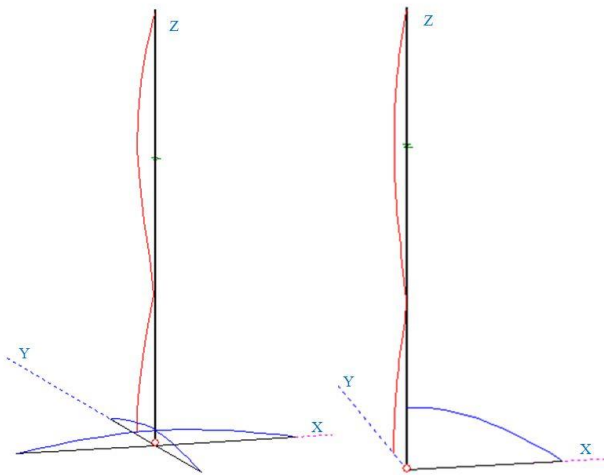


Figure 3 – The geometry of a  $3\lambda/4$  vertical antenna with four radials (left) and one radial (right).

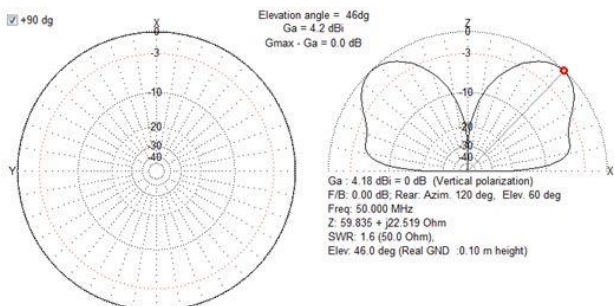


Figure 4 –  $3\lambda/4$  vertical antenna with four radials far field plot: horizontal field (left), vertical field (right).

The far field radiation patterns in both vertical and horizontal plane of a  $3\lambda/4$  vertical antenna with four radials is shown in the *Figure 4*.

The simulations of a  $3\lambda/4$  vertical antenna with only one radial, shows that some directivity can be obtained, making it even simpler to build and tune (*Figure 5*).

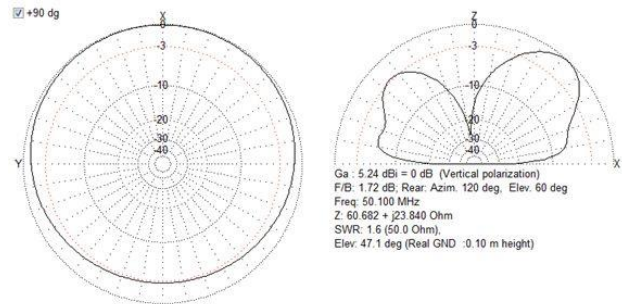


Figure 5 –  $3\lambda/4$  vertical antenna with one radial far field plot: horizontal field (left), vertical field (right).

Both these antenna designs have the advantages of being end-fed and having intrinsic low impedance, close to 50 ohms, making them easy to feed with common coaxial cables. The end fed design allows a light structure to be used as antenna pole. When installed close to the ground, beside the easy installation and maintenance, the lightning protection is also ensured, considering that higher and protected structures are in the area. The antenna simulations were made using MMANA-GAL software.

A prototype of a  $3\lambda/4$  wire vertical antenna with one radial was built, using a fiberglass pole as support. The antenna was tuned using a Rig Expert AA200 antenna analyzer, the measurements of the standing wave ratio SWR, impedance Z, the resistive R and reactive X components being depicted in *Figure 6*.

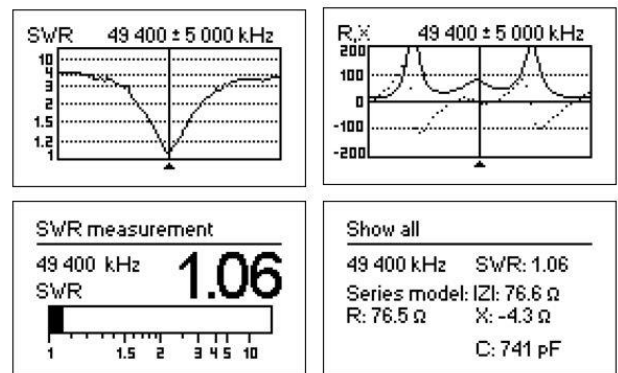


Figure 6 –  $3\lambda/4$  prototype wire vertical antenna with one radial measurements.

The antenna prototype was designed for 75 ohms impedance in order to match the impedance of the transmission line and receiver used for the radio meteor sensor.

**Transmission lines and connectors**

Even the fact that the receiver can be mounted directly at the base of the antenna in a waterproof box, in some

practical situations it is necessary to place the receiver at some distance from the antenna. For that, some sort of transmission line must be used. A tri-shield RG6 type coaxial cable, designed for use in CATV/broadband, was chosen due to its good price/performance ratio. These cables have 75 Ω impedance, which fits the declared impedance of the RTL-SDR receivers. It should be noted that the impedance mismatch between 50 Ω and 75 Ω, introduces less than 0.2dB attenuation of the signal.

In the whole RF chain, F-type connectors and adapters were used. Despite their very simple design, the F-type connectors have very good performance being in the same type very easy to mount, with no soldering and no special crimping tools needed. A wide range of connectors and adapters are available.

**Filters and preamplifiers**

Unless the radio receiver is placed in a radio-electric quiet region, a RF filter must be used. The spectrum scanning, in the area where the radio meteor sensor was installed, showed that the wide frequency modulation WFM broadcast stations, constitute the most powerful sources of interference.

One easy way to reduce the WFM signals is to use a coaxial stub notch filter (Leech, 2012). This type of filter consists in a piece of coaxial cable, λ/4 in length at the frequency of interest, shorted at one end, that is placed in parallel to the input of the preamplifier/receiver (Figure 7).

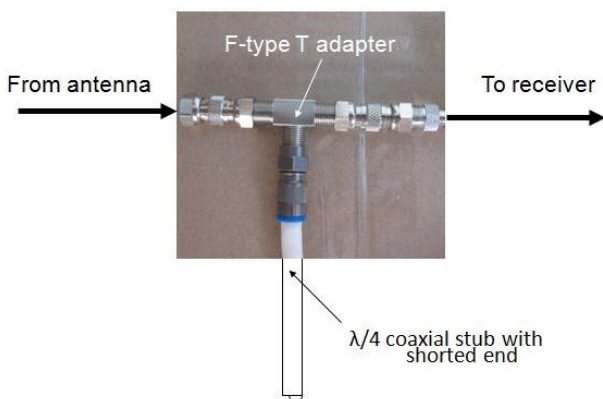


Figure 7 – Coaxial stub notch filter.

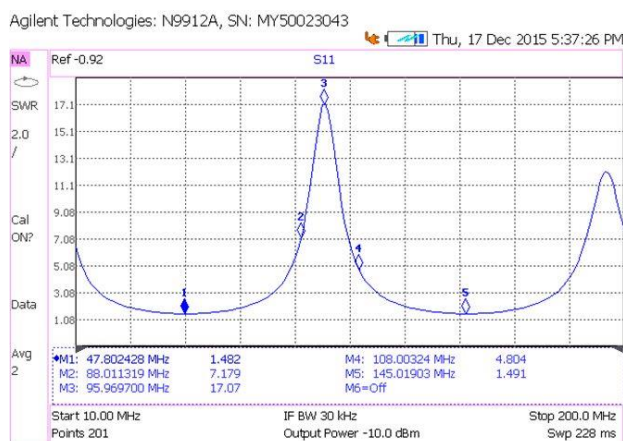


Figure 8 – WFM Coaxial stub notch filter measurements.

This type of filter, which has the shortened end to the ground, provides also electrostatic discharge (ESD) protection. The tuning of a prototype CoAx notch filter was made with a cable and antenna analyzer Agilent N9912A (Figure 8).

Other front-end parameters (i.e. receiving input parameters) that are of interest are the sensitivity (signal to noise ratio SNR) and the linearity (resilience to intermodulation – third order intercept point IP3). These parameters can be improved by inserting a RF preamplifier which has better performance than the receiver itself. Preamplifiers designed for DVB-T (Digital Video Broadcast – Terrestrial) broadcast, have parameters that cover the required needs. A measure of the sensitivity of a radio reception system is the noise figure (NF). According to the literature (Fisk, 2008), the minimum necessary NF for space applications, on the frequencies of interest, is depicted in the Table 2.

Table 2 – Acceptable noise figure (NF) for space applications.

Frequency [MHz]	Noise figure NF [dB]
50	5
144	1

An example is the broadband in-line amplifier DVB-T Wentronic 67237, which has the following parameters: gain = 18 dB, frequency range = 5-2300 MHz, Noise figure NF < 5dB, power supply 5 – 18V / 40mA. As a „rule of thumb”, the higher is the current consumption the higher is the dynamic range / the resilience to intermodulations (IP3).

**Radio receiver**

The chosen radio receiver is an improved version of the renowned RTL SDR software defined radio receiver USB dongle, which was originally designed for the DAB/DVB-T broadcast reception. This improved RTL-SDR receiver (Figure 9), compared to the original release, has a second generation RF tuner (Rafael Micro R820T2) with improved sensitivity and a 1ppm (parts per million) thermo-compensated crystal oscillator, for better frequency stability.

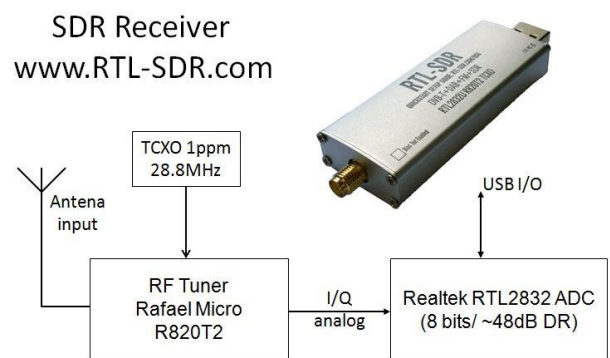


Figure 9 – RTL-SDR receiver block diagram.

As a plus, this improved version from www.RTL-SDR.com, has implemented a bias-T circuit for DC power of a RF preamplifier via the coaxial cable and a

direct sampling input pads that, as we discovered, can be used as a TIME STAMP INPUT (*Figure 10*). The unit has shielded metal casing and a silicon pad for heat transfer (better cooling = better sensitivity). The only drawback of this SDR receiver is the use of the same Realtek RTL2832 analog to digital converter (ADC), which has a resolution of only 8 bits (theoretical dynamic range of 48dB). The minimum baseband of the RTL-SDR receiver, that can be transferred via USB, is 250 kHz.

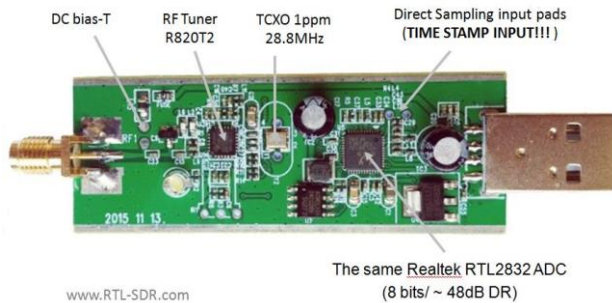


Figure 10 – www.RTL-SDR.com SDR receiver.

### Single Board Computer and Server

The baseband I/Q (In phase/Quadrature) signal, from the software defined radio receiver RTL-SDR, is transferred to the remote processing server via an ARM single board computer (SBC). A Marsboard A10 SBC, with 1GHz clock frequency and 1GB of RAM was used, running an ARMHF Ubuntu Linux release and the `rtl_tcp` application that streams the baseband I/Q signal to the server via TCP/IP.

At the other end of the internet connection, a classical meteor detection software setup was used for testing this remote radio detection sensor. A server, based on a Win7 PC, runs a suite of software applications. The SDR Console software demodulates the baseband signal and controls the RTL-SDR receiver via internet. The HROFFT1.0.0 software counts the meteor echoes. The virtual cable VB-cable software allows, under Win7, the audio streaming between the radio control software and the meteor count software. The results are posted online, on the RMOB website, using the *Colorgramme RMOB Lab v 2.9*.

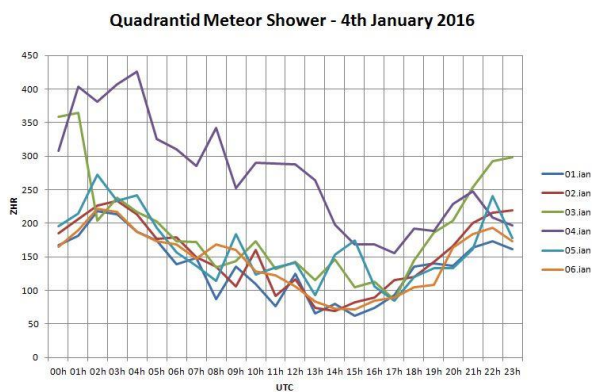


Figure 11 – Preliminary test results – ZHR for the Quadrantids Meteor Shower 2016.

### 3 Conclusion

A commercial off-the-shelf (COTS) hardware based remote radio meteor detection sensor, operating in the low VHF frequency range (around 50MHz), was tested.

Preliminary test results, using an east European band I analog TV transmitter as illuminator of opportunity, are shown in *Figure 11*.

The accent of this study was put on the RF (radio frequency) components. Further receiving tests, using the ROAN radio meteor beacon as illuminator, are in view.

### Acknowledgment

This work was supported by the project “Integrated Center for research, development and innovation in Advanced Materials, Nanotechnologies, and Distributed Systems for fabrication and control – MANSiD”, Contract No. 671/09.04.2015, Sectoral Operational Program for Increase of the Economic Competitiveness co-funded from the European Regional Development Fund and the Romanian Ministry of Education, Research and Innovation Agency through PNCDI 2 Program research contracts 205/2012.

### References

- Fisk J. R. (2008). “Receiver noise figure sensitivity and dynamic range - what the numbers mean”. From Ham Radio Magazine October 1975. Repaginated and edited by Perry Sandeen Sept. 2008.
- Georgescu T., Georgescu A., Ghită I., Potlog S., Lesanu C., Birlan M., Savastru D., Baniță C.-K. and Drăgăsanu C. (2013). “Romanian ALLSKY Network - a systematic approach for meteor detection”. In Gyssens M., Roggemans P. and Zoladek P., editors, *Proceedings of the International Meteor Conference*, Poznan, Poland, 22-25 August 2013. IMO, pages 40–43.
- Leech M. (2012). “Forward-scatter meteor detection using Gnu Radio + RTL-SDR devices”. Science Radio Laboratories.
- Lesanu C. and Dragoiu A. (2011). “SDR - radio meteor affordable approach”. In Gyssens M. and Roggemans P., editors, *Proceedings of the International Meteor Conference*, Sibiu, Romania, 15-18 September, 2011. IMO, page 81.
- Sufitchi C. (2015). “Detecting meteor radio echoes using the RTL/SDR USB dongle”. Society of Amateur Radio Astronomers (SARA) Conference 2015.

# Calibration of occasionally taken images using principles of perspective

Esko Lyytinen<sup>1</sup> and Maria Gritsevich<sup>1,2,3</sup>

<sup>1</sup>Finnish Fireball Network, Helsinki, Finland

esko.lyytinen@jippii.fi

<sup>2</sup>Finnish Geospatial Research Institute (FGI), Masala, Finland

firstname.lastname@nls.fi

<sup>3</sup>Institute of Physics and Technology, Ural Federal University, Ekaterinburg, Russia

gritsevich@list.ru

Recent years brought a large number of observational data of fireballs accidentally captured by dash-type cameras. In addition to directly measured azimuth-directions from satellite images, direct lines and their perspective properties can be used for the calibration of the camera.

We have updated our calibration program taking this into account and we discuss the methods in this paper and we apply them to a recent case of a fireball seen in Thailand (September 7, 2015).

## 1 Introduction

Reliable calibration of an unknown camera images is a difficult challenge.

The techniques of meteor camera calibrations go back at least to the work done by Cepelcha (1987) and Borovička et al. (1995). Our calibration method is based on the evaluation of similar parameters. The differences between the approaches concern mainly the radial correcting terms. However, the selection of the characteristic parameters is not of significant importance to use the described principles. But there may be some advantages in the radial correction technique that we have implemented.

It is very helpful that in many cases the satellite images like Google-images can be used to help the process. One can hopefully locate the camera accurately in such an image and measure directions to some characteristic objects also seen in the image.

In this study we suggest that such directions from satellite images can be used and are highly recommended. In addition to this, there may be visible buildings or other useful objects in the field of view of a camera. We have already quite a good experience in using building edges etc. that are expected to be actually vertical. In particular, an accurate calibration was done to enable the trajectory reconstruction in the spectacular cases of the Annama and Chelyabinsk (Gritsevich et al., 2013; 2014; Trigo-Rodríguez et al., 2015; Dmitriev et al., 2015; Lyytinen and Gritsevich, 2016). In case the horizon is clearly visible in the distance, this can be used as well.

We have been updating our calibration program to use some features of projective geometry. An introduction to these principles is the main topic of this study.

In a building the roof edge and windows up- or down-edge lines can be assumed to be actually horizontal. Measuring these with enough reference points gives information on the imaging geometry. And two or more of such lines of the actual identical direction will also define one point at the actual horizon. And if there is a corner of a building visible, assumed mutually being at the right angle position, this will help to provide information on the image scale. Vertical lines in the image can help to define in principle the zenith. The fireball apparent track, if visible for enough length at the sky, is helpful for the imaging geometry. Likewise any straight line of any direction can be used.

Our first test according to these ideas with the updated program proved to be more successful than what was anticipated. There has been a previous calibration with only some vertical lines and some google-image directions and one assumed horizon point in use. We made a test in which only one actually measured azimuth direction was used and all the rest had been measured from the lines as discussed above. We could derive the imaging geometry as well as the location of the assumed imaging symmetry point. The resulting focal length in image-pixels differed by only about 1% from the previous calibration with the directions measured from the Google-images.

## 2 Principles and methods

We assume an imaging model with the next properties:

- There is a symmetrical point in the image that can have a coordinate offset from the actual image center;
- The image scale is given by means of the focal length in image pixels;
- The scaling can be different in X and Y directions and this is defined by means of the factor X/Y. A

value smaller than 1.0 means that things in the image are stretched longer in the height direction. The mentioned focal length is for Y-pixels.

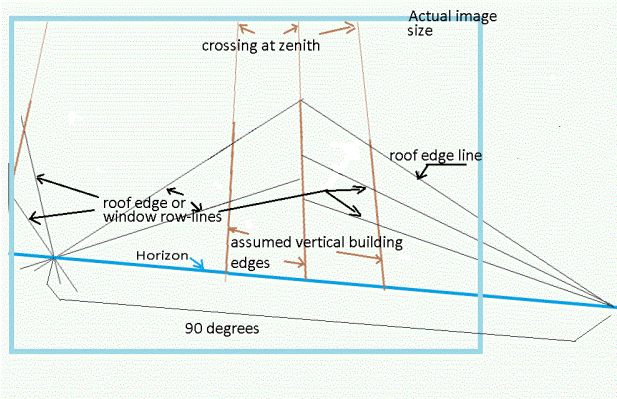


Figure 1 – Some main principles can be best described with gnomonic projection. The same ideas can be applied with calculations in other projections too.

- The azimuthal and elevation directions of the symmetric point are required parameters as well as the camera tilt angle or with other words the rotation along the axis in this direction.
- The radial distance from the image center is given with a rational formula. We have a special formula for this, which has the property that this is assumed to give good results even with a single correcting term for most cameras. According to our experience, this formula leads to close to the best achievable solution for unknown video cameras in most cases.

This formula is a weighted average of the equidistant and gnomonic projections.

Of course, other types of correcting terms can be applied. Because of the typically scarce data for calibrations, it is desirable that the number of parameters to be derived is as small as possible. Many correcting factors would allow a better model of course, but the lack of enough data for a calibration would lead to a less precise model and/or not to a unique solution.

### 3 Our radial correcting term

Here, we give the details of our radial correcting term:

- Assume the focal length to be  $f$  pixels (to simplify, assume the X/Y ratio is 1.0);
- In an equidistant projection the angle from the symmetry point is (in radians)  $R_e = \frac{r}{f}$ , where  $r$  is the image point distance from the symmetry point;
- In a gnomonic projection the angle would be  $R_g = \text{atan} \frac{r}{f}$ ;
- The weighted average of this is  $R = W \cdot R_e + (1 - W) \cdot R_g$ , where  $W$  is the weight, which is one of our parameters being used. We call this  $W$  the “radial correction parameter”;
- If  $W = 0$ , then the case is a gnomonic projection;

- If  $W = 1$ , then it is an equidistant projection;
- In wide-field cameras  $W$  quite typically is larger than 1;
- An inverse solution to the problem is more time-consuming than one with weighted averaging. In this case we use a few (fixed number) iteration;
- This approach seems to give a quite good result for most cameras with only this single correcting term. In an all-sky camera, usually more terms are needed to resolve the geometry, but this entire general approach is probably not applicable for all-sky cameras.

We assume that in the image to be calibrated there are some buildings and that in these buildings some “lines” can be assumed to be vertical and some other lines to be horizontal. For example building wall corners are vertical and roof edges and window rows are horizontal. In Figure 1 some such lines can be seen.

In the case of the gnomonic projection, all the vertical lines would cross at the zenith (or nadir), even though this is typically outside the image.

Lines different from the horizontal direction, which are commonly in the same direction will cross the horizon at the same point and thus define a horizon point. If there are more than one such defined horizon points, then the horizon in the image will get defined.

The horizon in combination with the zenith defines the image scale.

This can have the simplification that the X/Y ratio is 1.0 and also the symmetry point is in the image center.

If there are horizon-defining lines as described above, associated with the same building corner, one can assume that the directions of these horizon points are separated by 90 degrees. This can also help to define the image scale.

If there is not enough data, then one may need to assume the X/Y ratio to be 1.0, as was done in this case at the first stage, (or whatever would look most reasonable) and the offsets can be put as zero too.

### 4 The spherical trigonometry formula

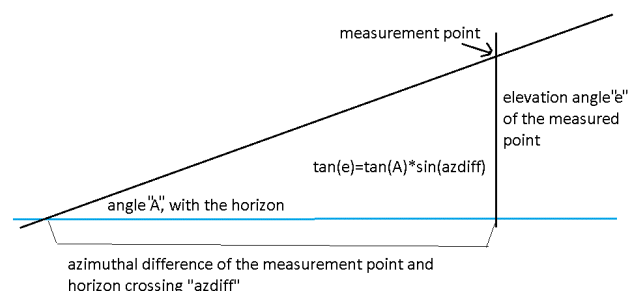


Figure 2 – The blue line defines the horizon. Spherical arcs are drawn as straight lines.

Figure 2 explains the spherical trigonometry that we use. The image also contains the formula. The formula gives the equations that need to be fulfilled as well as to be possible. A least squares solution is applied for the parameters.

We have the measured point connected with a spherical arc and a horizon point. The horizon point is typically unknown in the image and the azimuth direction of this point may be unknown or in some cases previously known. The elevation angle of the measurement point is unknown as well as its azimuth direction. The angle  $A$  between the direction and the horizon is unknown.

A single line requires three different points to be of any use in the calibration. One of these may be the horizon point, but in mostly this is not the case.

If there is another straight line that is actually known to be connected (for example on the same wall of a building) to the same horizon point then two points on one of the lines are sufficient to obtain useful information, but it is desirable to have more points. At least some, hopefully more than one, of the used lines must have more than two points to get defined. (A theoretical example where this may not be needed would be several actually known azimuth directions.) It is desirable that several of the lines have at least three points.

In our calculations, we use the formula as given. This formula calculates the elevation angle  $e$ . But using lines from other frames that are actually vertical but not as such in the calibrated frame, the  $\tan(A)$  has a very large value (with  $A$  close to 90 deg). The iterative solution converges very slowly because it does not effectively treat the required minor changes tested in  $A$ . The angle  $A$  is priority unknown and may change position relatively to 90 degrees.

However, we got a solution for this. In future calculations it might be better to calculate the azimuth difference instead of the elevation angle  $e$  in the actually used formula.

## 5 Our example, Thailand 2015 Sept 7

The model was implemented in a MS Excel and the solution is achieved by means of the Excel solver add-in, similarly to the *fb\_entry* program (Lyytinen and Gritsevich, 2013).

We will show the results with as example a fireball reported from Thailand. This was a major daylight fireball which was captured in several videos such as like car dash cameras. This fireball was also listed with the list of released satellite-based data of fireballs with a total energy of 3.9 kt.<sup>1</sup>

We have located a few of the observing sites and calibrated the videos. Unfortunately most of these were

taken from roughly the same direction in the vicinity of Bangkok. The fireball occurred at a distance of almost 200 km from Bangkok.

Our purpose in this study is not to give a more general treatment of the atmospheric entry. There may be some later publications on this event dealing with all its peculiarities. However, it is worth mentioning that we also have used some seismic data for sonic boom timings which were very useful in the analysis. The video for the calibration is from Bangkok and can be seen online<sup>2,3</sup>.

In this study we calibrate one of the frames of this video with the techniques described above and compare the result with an earlier calibration with more actual directions derived from google-images. The earlier ‘main’ calibration was made for a different frame for which the exact camera location was identified with a better precision, but in which the fireball itself was not visible.



Figure 3 – This is the frame that we calibrated in this study and in this picture the fireball is seen at about its brightest. The measured points for calibration are marked with black dots and the resulting horizon is marked by a red line with barely visible red triangles, at 5 degrees spacing in azimuth. There may still be a more complete analysis of the fireball which tries to combine the advantages of both calibrations.

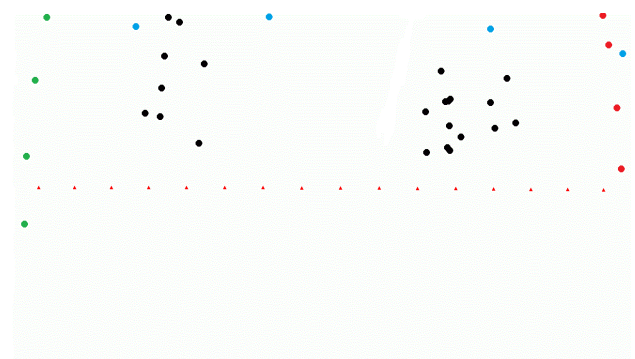


Figure 4 – In this image the dots of Figure 3 are displayed without the image background. This figure also contains the points from three different frames (shown correspondingly with different colors).

In this case, at the first stage we have used only “lines” from the calibration image itself. However one can also take lines from other frames of the same video. This assumes that the camera direction can freely change in

<sup>1</sup> <http://neo.jpl.nasa.gov/fireballs/>

<sup>2</sup> <https://www.youtube.com/watch?v=Ku5wYb5nNkQ>

<sup>3</sup> [https://www.youtube.com/watch?v=PFN\\_PZ4vj3I](https://www.youtube.com/watch?v=PFN_PZ4vj3I)

between these frames but the imaging geometry of the camera remains fixed. For example, if one takes an actually vertical line, in this approach it cannot be assumed as vertical.

We selected three different frames for this. One has the included line close to the left edge and another close to the right edge and the third has a line at the upper edge.

The main calibration frame is shown in *Figure 3* and in this figure the measured points of this frame are marked with black dots. The derived horizon is marked with red triangles at 5 degrees spacing, a red line was drawn through these points. This almost passes through the center of the image (and the symmetry point), therefore it is practically straight.

*Figure 4* also contains the points from the other frames marked with different colors. This figure is without the frame image background. In this figure the derived horizon differs in principle slightly from that of *Figure 3*.

During the first stage, the symmetry point offsets were also derived but the quality of these was not good – e.g. it would be comparable to the assumption that the symmetry point is at the image center.

After adding also the measurements from the three different frames, the offset point gets very well determined. And it appears that also the radial correction can be further improved by adding an additional correction of the fifth power to this.

When using this, then also the parameter value  $W$  would slightly change and even the best matching value of the focal length would very slightly change. At this stage we assume that the calibration geometry for the “distortions” is almost as well derived as in a star calibration. However the actual direction and even the focal length (image scale) are not as accurate. This result is expected to be quite good for the fireball measurements. The entry modeling of the fireball is not treated further in detail in this paper.

As results, we get the following data for the  $1280 \times 720$ -size frame image.

- Focal length = 914.7 pixels (assumed to be the same in horizontal and vertical directions);
- The X/Y pixel ratio was assumed to be 1.0;
- Symmetry point offsets (pixels from image center): X = 0.0 (increases towards the right from the center) and Y = 7.9;
- Symmetry point azimuth direction: 282.6 (degrees), Elevation = -0.60 (degrees);
- Camera tilt-angle = -0.7 (degrees) (negative means camera was rotated counter-clockwise, the image rotated clockwise);
- $W = 1.243$

A fifth power radial correction brings a point near the side (middle) edge by about 2 pixels towards the center.

Without these corrections most of the discrepancies would be compensated by the different values of focal length and  $W$  that are derived.

There are 35 measured points in the solution. The positions were manually assumed at sub-pixel accuracy. The largest residual is 0.5 pixels and the RMS value is about 0.2 pixels.

## Acknowledgments

The analysis of the Thailand case was done in collaboration with Passakorn Pananout, Thailand and Robert D. Matson, USA. We got a lot of help from them with the video-links and also for searching the actual video sites from the Google-images.

We also thank the URSA, Finnish Fireball Network and all the members of this network for the many earlier fireball examples that have been very essential in the development of our calibration tools.

## References

- Borovička J., Spurný P. and Kecklíková J. (1995). “A new positional astrometric method for all-sky cameras”. *Astronomy and Astrophysics Supplement*, **112**, 173–178.
- Cepelcha Z. (1987). “Geometric, dynamic, orbital and photometric data on meteoroids from photographic fireball networks”. *Bulletin Astronomical Institutes of Czechoslovakia*, **38**, 222–234.
- Dmitriev V., Lupovka V. and Gritsevich M. (2015). “Orbit determination based on meteor observations using numerical integration of equations of motion”. *Planetary and Space Science*, **117**, 223–235.
- Gritsevich M., Lyytinen E., Grokhovsky V. I., Vinnikov V., Kohout T. and Lupovka V. (2013). “Orbit, Trajectory, and Recovery of Chelyabinsk Meteorite”. *Meteoritics and Planetary Science*, **48**, 76th Annual Meeting of the Meteoritical Society, held July 29-August 7, 2013 in Edmonton, Canada. Published in Meteoritics and Planetary Science Supplement, id.5228.
- Gritsevich M., Lyytinen E., Moilanen J., Kohout T., Dmitriev V., Lupovka V., Midtskogen V., Kruglikov N., Ischenko A., Yakovlev G., Grokhovsky V., Haloda J., Halodova P., Peltoniemi J., Aikkila A., Taavitsainen A., Lauanne J., Pekkola M., Kokko P., Lahtinen P. and Larionov M. (2014). “First meteorite recovery based on observations by the Finnish Fireball Network”. In Rault J.-L. and Roggemans P., editors, *Proceedings of the International Meteor Conference*, Giron, France, 18-21 September 2014. IMO, pages 162–169.

Lyytinen E. and Gritsevich M. (2013). “A flexible fireball entry track calculation program”. In Gyssens M. and Roggemans P., editors, *Proceedings of the International Meteor Conference*, September 20–23, 2012, La Palma, Canary, Spain. IMO, pages 155–167.

Lyytinen E. and Gritsevich M. (2016). “Implications of the atmospheric density profile in the processing of fireball observations”. *Planetary and Space Science*, **120**, 35–42.

Trigo-Rodríguez J. M., Lyytinen E., Gritsevich M., Moreno-Ibáñez M., Bottke W. F., Williams I., Lupovka V., Dmitriev V., Kohout T. and Grokhovsky V. (2015). “Orbit and dynamic origin of the recently recovered Annama’s H5 chondrite”. *Monthly Notices of the Royal Astronomical Society*, **449**, 2119–2127. <http://dx.doi.org/10.1093/mnras/stv378>



Korado Korlevic, Christian Steyaert, Peter Jenniskens and Hervé Lamy. (Photo Casper ter Kuile).

# The KUT meteor radar: An educational low cost meteor observation system by radio forward scattering

Waleed Madkour and Masa-yuki Yamamoto

Kochi University of Technology, Kochi, Japan

186006f@gs.kochi-tech.ac.jp

yamamoto.masa-yuki@kochi-tech.ac.jp

The Kochi University of Technology (KUT) meteor radar is an educational low cost observation system built at Kochi, Japan by successive graduate students since 2004. The system takes advantage of the continuous VHF-band beacon signal emitted from Fukui National College of Technology (FNCT) for scientific usage all over Japan by receiving the forward scattered signals. The system uses the classical forward scattering setup similar to the setup described by the international meteor organization (IMO), gradually developed from the most basic single antenna setup to the multi-site meteor path determination setup. The primary objective is to automate the observation of the meteor parameters continuously to provide amounts of data sufficient for statistical analysis. The developed software system automates the observation of the astronomical meteor parameters such as meteor direction, velocity and trajectory. Also, automated counting of meteor echoes and their durations are used to observe mesospheric ozone concentration by analyzing the duration distribution of different meteor showers. The meteor parameters observed and the methodology used for each are briefly summarized.

## 1 Introduction

Radio observation of meteors can be a rich source of information on the deep space components and mesospheric conditions for professionals, as well as a live experience for amateurs interested in listening to space continuously. Professional observers usually use satellites or large ground radar systems of high cost to detect the largest amount of meteor records possible. On the other hand, amateurs use the low cost classical basic setups to observe meteor echoes as a hobby. In between them there exist researchers at low budget institutes trying to use the classical setups for educational and scientific purpose such as the KUT meteor radar system. The KUT meteor observation system utilizes the forward scattering of the continuous 50 W, 53.75 MHz radio signals transmitted from the FNCT at a distance of 340 km from KUT (Maegawa, 1999). The structure of the KUT meteor observation system is detailed in Madkour et al. (2016a). In order to collect sufficient data for research purpose, it was necessary to automate the observation process by developing software applications locally. The observed meteor parameters and the methodology used at KUT are briefly summarized in this paper.

## 2 Astronomical meteor observations

Since 2004, the KUT system has gradually developed from the basic setup configuration to an interferometric direction finding configuration, then finally to a multi-site meteor path determination setup. The primary target is to develop a mechanism for determining the origin of every meteor echo. The observed parameters are summarized in the following subsections:

### Meteor echo counts and durations

Using the HROFFT (Ham-band Radio meteor Observation Fast Fourier Transform) spectrum images

generated every 10 minutes, meteor echo counts and durations are automatically scanned and recorded by image processing software of “Meteor Echo Counter” (MEC). The details of MEC software operation are explained by Noguchi and Yamamoto (2008).

### Meteor echo directions

The 5 antennas setup is used to determine meteor echo directions through interferometric analysis. The developed software applications HRO\_IF\_V2 and HRO\_IF\_VIEW are used to automate direction finding of every meteor echo (e.g. *Figure 1 and Figure 2*). The direction (azimuth and elevation) information was observed with higher accuracy for meteor echoes with duration longer than 3 seconds (Madkour et al. 2016a). Meteor echo direction is the basic element required towards trajectory and velocity determination.

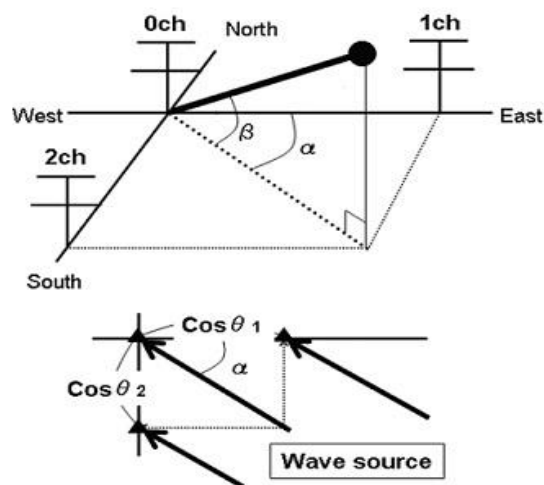


Figure 1 – Direction finding by interferometric analysis.

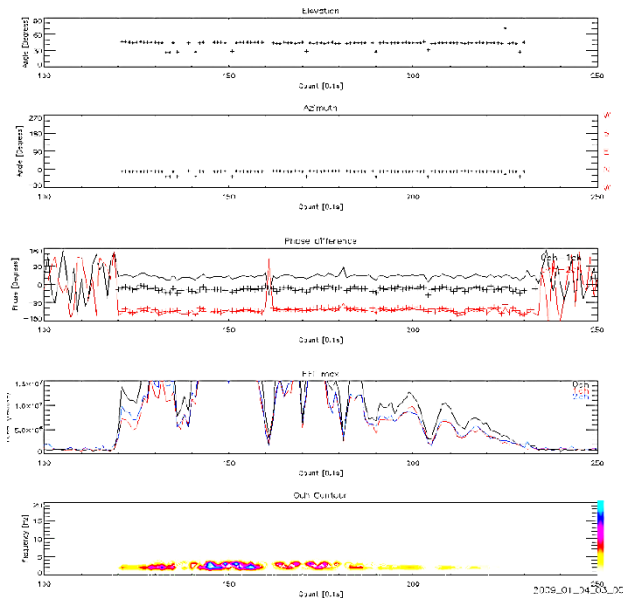


Figure 2 – HRO\_IF\_VIEW graphical interface for meteor echo directions.

**Meteor echo trajectory and velocity**

In 2012, two remote sites were added at a distance of around 15 km from KUT to enable observing the meteor trajectories and velocities (Figure 3). Based on the meteor echo direction analysis and using the detection time differences between the three receiving points, meteor trajectories and velocities are calculated. As the remote sites are single antenna stations, certain assumptions were used to perform the analysis such as the assumption of a vertical angle between the received signal at central site and the meteor trajectory.

The software HRO\_TRA was developed to automate trajectory and velocity observation for undersense meteor echoes only because of the determined signal profile of this type with impulsive rise at the beginning of each echo. Another software is currently under development for velocity determination for meteor showers with known radiant points. The method is presented in details in a separate proceedings.

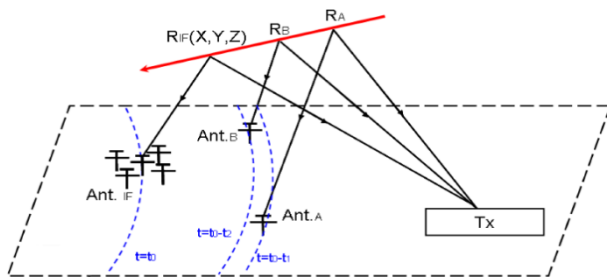


Figure 3 – Meteor trajectory determination using multiple receiving sites with an interferometer.

**Meteor echo absolute power**

The received signals intensity are relatively levelled on the HROFFT spectrum at 13 levels from 0 to 12 on a varying noise floor, however, the absolute power level is not obtained. A calibration device was developed by adding a signal generation (SG) to generate a reference scale simulated signal in descending step function for a

short time every 10 minutes to be used for meteor echo absolute power measurements (Figure 4).

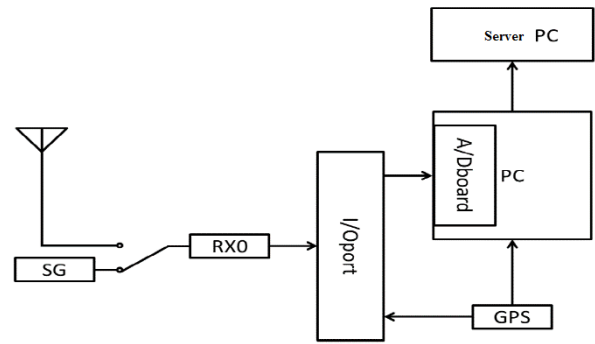


Figure 4 – Addition of calibration SG device for absolute power measurement.

**Meteor trail density**

Having the absolute power measured, it is possible to calculate the meteor trail plasma density using the forward scattering radar power equation. A software application HRO\_IF\_LV was developed to calculate the absolute power and meteor trail plasma density and generate a daily text file of combined results. The absolute power and density measurements were temporarily performed during the period from 2012 to 2013 and is currently on hold.

**Meteor heights**

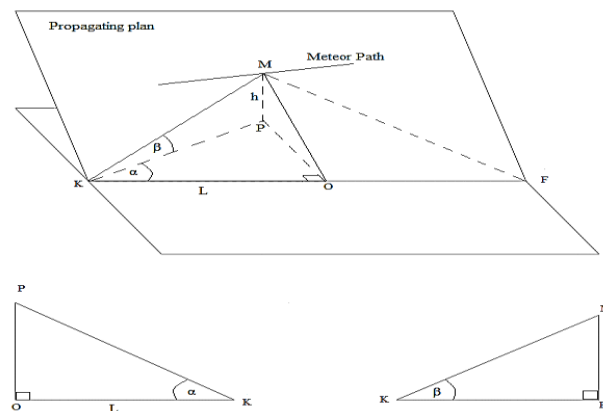


Figure 5 – Height estimation from forward scattered signals geometry (after Madkour and Yamamoto, 2016b).

Meteor height determination is currently under development in KUT. Using the direction-finding system and the geometry of the forward scattering signals (Figure 5), the meteor heights can be obtained using the relation:

$$h = L \cdot \tan \beta \sec \alpha \tag{1}$$

where  $h$ ,  $\beta$  and  $\alpha$  are as shown in Figure 4.

The missing parameter  $L$  requires the determination of the meteor position. This can be achieved by upgrading one of the remote sites to an interferometric setup or adding a code in the transmitting signal for range determination.

### 3 Mesospheric observations

#### Mesospheric ozone concentration

The ozone concentration observation is based on the method proposed by Jones et al. (1990), where the cumulative duration distribution of overdense meteor echoes is analyzed using the HROFFT and MEC softwares. Grouping of meteor echoes in terms of meteor shower echoes, day/night echoes or different season echoes could reflect the mesospheric ozone density level by observing the knee position on the distribution for each group. In *Figure 6*, the duration distribution of the Perseids overdense meteor echoes over 10 years at KUT is shown. The knee duration position of the Perseids differed from that of the Geminids by around 30 seconds which can be indicative about the ozone concentration impact on both showers (Madkour and Yamamoto, 2016b). The characteristics of each shower such as the average meteor heights and velocities need to be considered for comprehensive observation results. The vertical ozone concentration profile could be reached by using height information obtained after completion of the method explained above under *Section 2*.

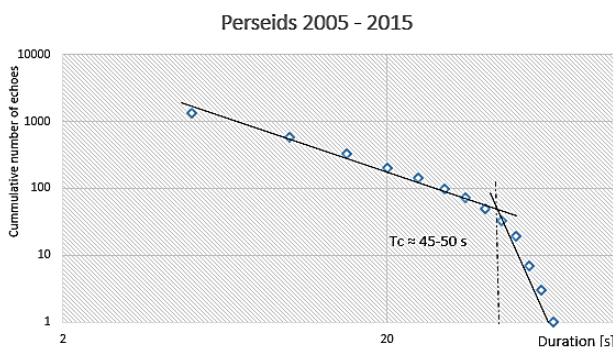


*Figure 6* – Cumulative duration distribution of the Perseids meteor shower during 10 years (after Madkour and Yamamoto, 2016b).

#### Solar cycle activity

As a further step on using the duration distribution analysis, the decrease of the ozone concentration by increasing solar activity level and vice versa could allow indirect observation of the 11-year solar cycle activity. This can be achieved by observing the knee curves of meteor showers annually along 11 years. Currently there were not enough data records in KUT to perform a full 11-years analysis. As a preliminary analysis, we have compared the Geminid meteor shower duration distribution during 2 years at half-cycle points in 2006 and 2011 which showed 2~3 seconds difference (Madkour and Yamamoto, 2016b).

### 4 Meteor burst communication (MBC)

A new research area was branched at KUT meteor studies to make practical use of the information obtained by scientific technical research. The data communication through meteors could have various applications in uncovered areas such as deserts and maritime at lower

cost than the satellite telecom option. As a primary objective, the automatic transfer of observation data at the 2 remote sites to the central site at the KUT campus will be tested.

### 5 Summary

The KUT meteor radar attempts to observe the following astronomical meteor parameters automatically:

- Meteor echo counts and duration.
- Meteor echo direction.
- Meteor trajectory and velocity under certain assumptions.
- Meteor echo absolute power (currently on hold).
- Meteor trail plasma density (currently on hold).
- Meteor heights (under development).

Basic mesospheric observations are performed using the duration distribution analysis methods such as mesospheric ozone concentration and its dependence on the 11-years solar cycle activity. Large amounts of data among different events are still required to improve the results. Finally, a practical use of meteor studies is targeted at KUT through the launching of MBC low cost telecom research activities in 2016.

### Acknowledgment

The authors are grateful to previous/current graduate students at KUT since 2004 who participated in the development of the KUT radio meteor observation system.

### References

- Jones J., McIntosh B. A. and Simek M. (1990). "Ozone and the duration of overdense radio meteors". *Journal of Atmospheric and Terrestrial Physics*, **52**, 253–258.
- Madkour W., Yamamoto M.-Y., Kakinami Y. and Mizumoto S. (2016a). "A low cost meteor observation system using radio forward scattering and the interferometry technique". *Experimental Astronomy*, **41**, 243–257.
- Madkour W. and Yamamoto M.-Y. (2016b). "Mesospheric observations by a forward scattering radar basic setup". *Astrophysics and Space Science*, **361**, article 247. DOI10.1007/s10509-016-2832-y.
- Maegawa K. (1999). "Hro: A new forward-scatter observation method using Ham-band beacon". *WGN, Journal of the IMO*, **27**, 64–72.
- Noguchi K. and Yamamoto M.-Y. (2008). "Development of an automatic echo-counting program for HROFFT spectrogram". *Earth, Moon, and Planets*, **102**, 323–329.

# Meteor spectra using high definition video camera

Koji Maeda<sup>1,2</sup> and Yasunori Fujiwara<sup>1,3</sup>

<sup>1</sup> Nippon Meteor Society (NMS)

<sup>2</sup> University of Miyazaki, Miyazai, Japan  
t0b153u@cc.miyazaki-u.ac.jp

<sup>3</sup> SOKENDAI / National Institute of Polar Research, Tachikawa, Tokyo, Japan  
fujiwara.yasunori@nipr.ac.jp

We have carried out observations of meteor spectra using high-definition video camera systems in Japan and we present the first results using this system. The camera,  $\alpha 7s$  (Sony) had a 35mm full- frame high sensitive CMOS sensor and could capture high definition video. It was equipped with a 24mm–50mm lens and 300–600 grooves/mm grating. The detection of spectra was done by the UFOCaptureHD2 software (SonotaCo). The limiting magnitude for a meteor spectrum was around magnitude 0. We obtained more than three hundred meteor spectra within partial spectra during one year. The classification according to the main element (Mg, Na, Fe) abundances of meteors resulted in 91% of classifiable meteor belonging to the main stream type.

## 1 Introduction

Meteor spectral observation is one of the important techniques in meteor studies (Vojáček et al., 2015). We have the following research objectives:

- Spectral classification of sporadic and shower meteors;
- Statistical distribution of spectra for shower meteors;
- Statistical distribution of the relation between the meteor spectra and the orbits for sporadic meteors.

We need an unprecedented number of spectra for these studies. The technique of meteor spectral observation progressed recently. We set up new equipment for a high-sensitive and high definition video observing system. In this paper we present the first results of the meteor spectra obtained within the recent year.

## 2 Observation

We selected the camera,  $\alpha 7s$  (Sony) which has a 35mm full frame, high sensitive CMOS sensor which can



Figure 2 – Photo of the Osaka site. Sony alpha 7s, f50 mm, grating 300 G/mm (right) and a Watec WAT-902H2U, f8 mm (left).



Figure 1 – Photo of the Miyazaki site. Sony alpha 7s, f24mm, grating 600 G/mm.

Table 1 – Observational systems at Miyazaki and Osaka.

Site	Miyazaki, Japan	Osaka, Japan
	131.42E, 31.83 N, 13m	135.48 E, 34.74N, 10m
Observer	K. Maeda	Y. Fujiwara
Camera	Sony alpha 7s (normal)	SONY alpha 7s (remove the IR cut filter)
Video mode	4K (3840 x 2160), 30p	HD (1920 x 1080), 60p
Lens	Canon FD24mm F 1.4L (sometimes FD 50mm F 1.4)	Canon FD 50mm F1.4
Grating	600 grooves/mm UV, Edmund opt.	300 grooves/mm VIS, Edmund opt.
Software	UFOCapture HD2 V4.10 UFO Analyzer V2.42	UFOCapture HD2 V4.10 UFOAnalyzer V2.42 UFO Orbit V2.34
Observing wavelength	400–660 nm	about 400–800nm
Observation type	Single station	Multi station

capture high definition video, 4K or HD format. A transparent grating was placed in front of the objective lens. The video meteor images were captured by the *UFOCaptureHD* software<sup>1</sup>. The details of the equipment are shown in *Table 1*. The observed limiting magnitude for meteor spectra was around mag. 0 for the meteors. The look of the system at the Miyazaki and the Osaka sites are shown in *Figure 1 and 2*, respectively. The Miyazaki site and the Osaka site observed independently. The cameras in both sites were not fixed because a housing for the cameras had not yet been prepared.

### 3 Results

The summary of the results for the Miyazaki site is shown in *Table 2*. The site began the observations in July 2015 during clear nights even with moon light. 488 spectra were recorded in 10 months. The brightness of the meteors and the shower associations were evaluated by the *UFOAnalyzer* software. All captured still spectral images of 2015 can be seen and downloaded from the SonotaCo Network Japan Forum<sup>2</sup>.

*Table 2* – Results of Miyazaki site.

Year	Month	Number of Spectra	Shower	Number of sporadics
2015	July to Dec.	362	STA, NTA, PER, ORI, GEM, etc.	160
2016	Jan. to Apr.	126	QUA LYR	111
Total	10	488	217	271

The summary of the results at the Osaka site is shown in *Table 3*. The site began the observations in Dec. 2015. One direct camera (WAT-902h2U, f 8mm) and one spectral camera ( $\alpha 7s$ ) have been operated. The orbits of the captured meteor with spectra were computed from SonotaCo meteor database<sup>3</sup>, where each meteor was individually measured by the *UFOAnalyzer* software. The *UFOOrbit* software was used for the orbit computation. The orbits for 63 meteors out of a total of 96 detections (66 %) were obtained.

*Table 3* – Results of Osaka site.

Year	Month	Obs. Night	Number of meteors	Number of Spectra	Number of Orbits
2015	Dec.	8	55	37	25
	Jan.	4	24	15	11
	Feb.	7	22	19	8
2016	Mar.	4	12	9	5
	Apr.	5	13	10	9
	May	4	11	6	5
Total	6	32	137	96	63

### 4 Spectral classification of meteors

The three typical meteor spectral lines (Mg, Na and Fe) were easy to identify by the color of the line and the length from the 0<sup>th</sup> order line. The intensity ratio of Mg and Na was evaluated by the naked eye and the *BASS* software<sup>4</sup>. The intensity of the lines has not been calibrated yet by the spectral sensitivity of the CMOS sensor and grating. The classification was based on the Mg-Na-Fe ternary diagram (Borovička et al., 2005). First, when only one spectral line was seen, spectra were classified as *um* or *un* type where *um* shows only the Mg line and *un* shows the Na line. Second, when a bunch of lines around 510 – 550 nm was clearly seen, this was attributed to the Fe type spectrum. Finally, the remaining spectra are classified from N0 to N7, according to the intensity ratio of the Na / (Mg+Na) value. The summary of the codes and the ratio are shown in *Table 4* and the code is drawn in *Figure 3* in blue characters to compare the classification with Borovička et al. (2005). The typical N3 and N7 spectra are shown in *Figure 4 and 5* respectively.

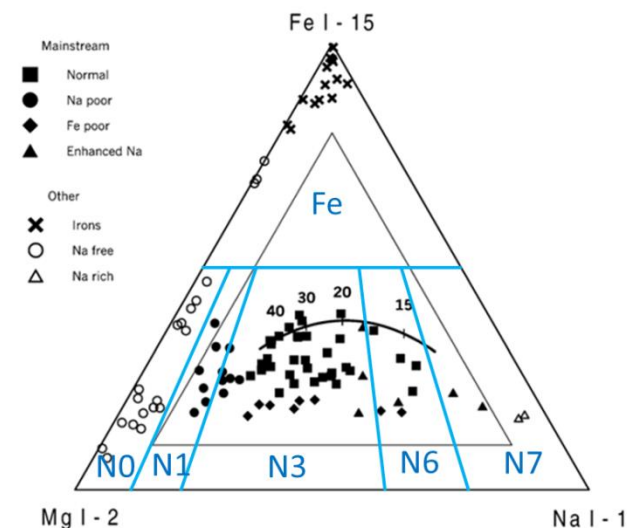


*Figure 3* – Spectral classification (N0 - N7 and Fe) based on Mg-Na-Fe diagram quoted from Borovička et al. (2005).

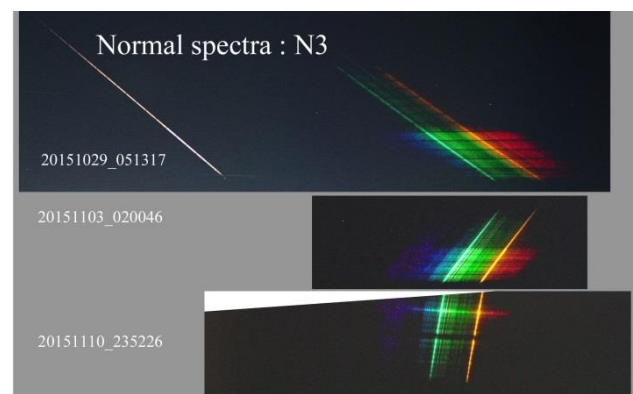


*Figure 4* – N3 type meteor spectra captured at the Miyazaki site.

<sup>1</sup> <http://sonotaco.com/>

<sup>2</sup> <http://sonotaco.jp/forum/viewtopic.php?t=3650>

<sup>3</sup> <http://sonotaco.jp/forum/viewforum.php?f=15>

<sup>4</sup> Basic Astronomical Spectroscopy Software, <https://uk.groups.yahoo.com/neo/groups/astrobodger/info>

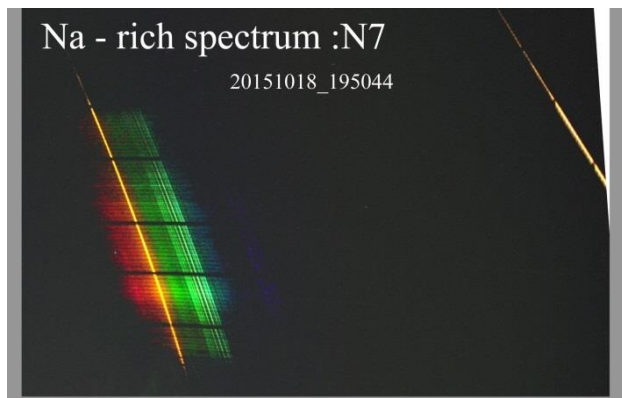


Figure 5 – N7 type meteor spectrum captured at the Miyazaki site.

The results of the classification of the 2015 data at the Miyazaki site are shown at the right side part of Table 4. 30 % of all spectra had only one spectral line. The ratio of 72% of classifiable spectra was of the main stream type. The Na free and Na rich types were less than 4%.

Table 4 – Results of spectral classification of this work in 2015. These results were used at the Miyazaki site.

Classification			2015		
Cod.	Na/(Mg+Na)	Characterization	Num	%	%
Fe	-	Iron rich	13	3.6	5.2
N0	<10%	Na free	6	1.7	2.4
N1	10-20%	Na poor	38	10.5	15.3
N3	20-60%	Main-stream Normal	179	49.4	71.9
N6	60-75%	Enhanced Na	9	2.5	3.6
N7	>75%	Na rich	8	2.2	3.2
Sub-total			253	69.9	100
um		Faint Mg line only	84	23.2	
un		Faint Na line only	21	5.8	
u		unknown	4	1.1	
Tot.			362	100	

## 5 Iron Meteoroids

### 5.1 Spectrum

The Fe type spectra, accounting for 5% shown in Figure 6, is interesting for the characteristic shape of the spectral image. The bottom image of Figure 6 is a mag. -2 meteor captured by a 50 mm lens. The first order spectrum was saturated but fortunately the 2<sup>nd</sup> order could be obtained. The spectral chart of the meteors in Figure 6 are shown in Figure 7. The wavelengths were calibrated using four Fe lines<sup>5</sup> (516.75, 522.72, 526.95, 532.80 nm). The spectral shapes agree well with each other. The emission wavelength of MgI excites 516.73, 517.27 and 518.36 nm (Cheng et al., 2011). In our case MgI at 518.36 nm could

not be observed in the Fe type spectrum. Then Mg did not emit in the Fe type meteor.

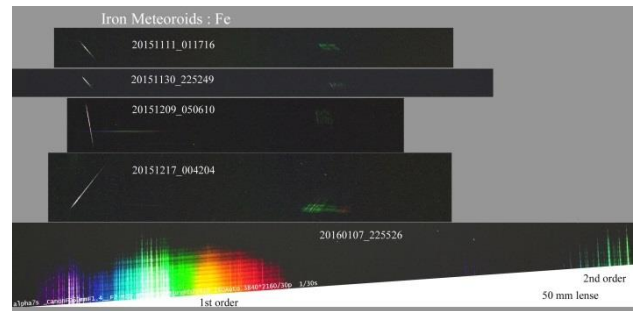


Figure 6 – Fe type meteor spectra captured at the Miyazaki site.

A full width at half maximum (FWHM) of a normal spectra (24 mm lens, 1<sup>st</sup> order spectrum) is 2.3 nm while in the special case (50 mm lens, 2<sup>nd</sup> order spectrum) this is 0.7 nm. We can count 28 spectral lines in the range of 500 – 550 nm. The resolution is very high in the 4K video observation.

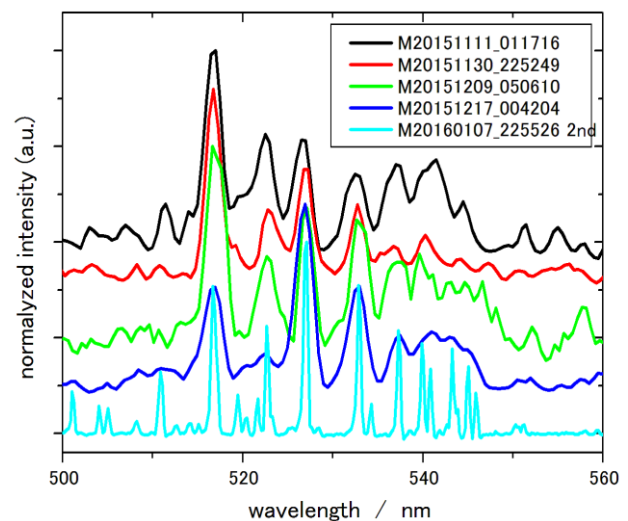


Figure 7 – Video spectra of Fe type meteors.

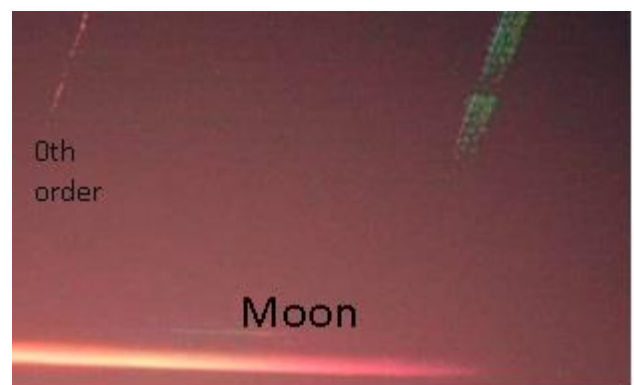


Figure 8 – Video spectrum of Fe type meteor captured at the Osaka site.

### 5.2 Orbit

Figure 8 shows the video spectrum of a Fe type meteor captured at 18<sup>h</sup>49<sup>m</sup>29<sup>s</sup> UT on January 3, 2016 at the Osaka site. The trajectory and orbital data are presented as follows:

- *Geocentric radiant:*  $\alpha = 153.3^\circ$ ,  $\delta = +9.6^\circ$   
 $v_g = 20.3 \text{ km s}^{-1}$ ;

<sup>5</sup>Chronological Scientific Tables 2011, edited National Astronomical Observatory of Japan, 439.

- *Maximum absolute brightness:* +0.7 mag.;
- *Beginning height:* 84.4 km, *ending height:* 78.6 km;
- *Heliocentric orbit* (J2000.0):  $a = 0.6$ ,  $q = 0.116$ ,  $e = 0.809$ ,  $\omega = 346.8^\circ$ ,  $\Omega = 282.6^\circ$ ,  $i = 0.7^\circ$ .

## 6 Spectrum and orbit

Figure 9 shows the video spectrum of a December Monocerotid captured at 15<sup>h</sup>55<sup>m</sup>20<sup>s</sup> UT on Dec. 18, 2015 at the Osaka site. The trajectory and orbital data are presented as follows:

- *Geocentric radiant:*  $\alpha = 106.2^\circ$ ,  $\delta = +7.0^\circ$   
 $v_g = 38.5 \text{ km s}^{-1}$ ;
- *Maximum absolute brightness:* -2.7;
- *Beginning height:* 104.4 km, *ending height:* 83.1 km;
- *Heliocentric orbit* (J2000.0):  $a = 4.9$ ,  $q = 0.226$ ,  $e = 0.954$ ,  $\omega = 125.3^\circ$ ,  $\Omega = 86.2^\circ$ ,  $i = 30.8^\circ$ .



Figure 9 – Video spectrum of Dec. MON captured at the Osaka site.

Figure 10 shows the video spectrum of a sporadic meteor captured at 12<sup>h</sup>13<sup>m</sup>46<sup>s</sup> UT on Dec. 30, 2015 at the Osaka site. The trajectory and orbital data are presented as follows:

- *Geocentric radiant:*  $\alpha = 85.3^\circ$ ,  $\delta = +5.4^\circ$   
 $v_g = 18.8 \text{ km s}^{-1}$ ;
- *Maximum absolute brightness:* -1.8 mag.;
- *Beginning height:* 90.2 km, *ending height:* 72.2 km;
- *Maximum brightness height:* 79 km;
- A persistent emission of Na remained around the maximum brightness point;
- *Heliocentric orbit* (J2000.0):  $a = 3.1$ ,  $q = 0.753$ ,  $e = 0.756$ ,  $\omega = 62.9^\circ$ ,  $\Omega = 98.2^\circ$ ,  $i = 9.6^\circ$ .

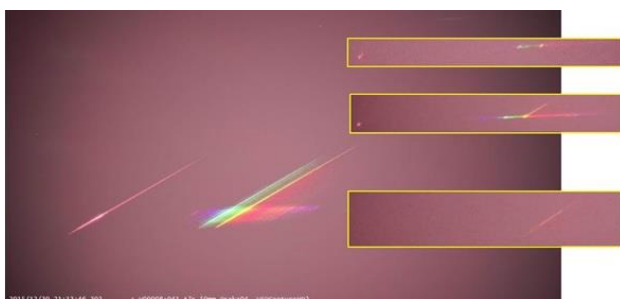


Figure 10 – Video spectrum of a sporadic meteor captured at the Osaka site. Three insets are flame images of the spectrum.

## 7 Conclusions

We obtained meteor spectra using high-sensitive and high-definition video cameras. Our video systems can obtain spectra of meteors brighter than magnitude 0. The FWHM of the spectral peak was about 2.3 nm in a typical condition. Our system had a potential to obtain about 500 spectra per year under good conditions. 90 % of the classifiable spectra belonged to the main stream type spectrum. We could obtain meteor spectra with their heliocentric orbit for more than 60 meteors in a half year of time.

## Acknowledgment

We thank Shinsuke Abe for providing his camera and grating. We also thank the following observers of the SonotaCo network for their reports which are essential for the determination of the meteor orbits: Masayoshi Ueda, Sadao Okamoto, Naoya Saito, T. Masuzawa, Hiroshi Kawakami and Junichi Yokomichi. We acknowledge SonotaCo and Ken Sugawara for numerous helpful advices in setting up our 4K and FHD video observations and the analyzing of meteor spectra.

## References

- Borovička J., Koten P., Spurný P., Boček J. and Štork R. (2005). “A survey of meteor spectra and orbits: evidence for three populations of Na-free meteoroids”. *Icarus*, **174**, 15–30.
- Cheng S. and Cheng S, (2011). “Meteor spectral observation with DSLR, normal lens and prism”. *WGN, Journal of the IMO*, **39**, 39–46.
- Vojáček V., Borovička J., Koten P., Spurný P. and Štork R. (2015). “Catalogue of representative meteor spectra”. *Astronomy and Astrophysics*, **580**, A67, 31 pages.

# Effects of meteor head plasma distribution on radar cross sections and derived meteoroid masses

Robert A. Marshall<sup>1</sup>, Sigrid Close<sup>2</sup>,  
Peter Brown<sup>3</sup> and Yakov Dimant<sup>4</sup>

<sup>1</sup>Aerospace Engineering Sciences, University of Colorado Boulder, Boulder, Colorado, USA  
robert.marshall@colorado.edu

<sup>2</sup>Aeronautics and Astronautics, Stanford University, Stanford, California, USA  
sigridc@stanford.edu

<sup>3</sup>Physics and Astronomy, University of Western Ontario, London, Ontario, Canada  
pbrown@uwo.ca

<sup>4</sup>Center for Space Physics, Boston University, Boston, Massachusetts, USA  
dimant@bu.edu

We present calculations that relate meteor head echo radar cross sections to the meteor head plasma distribution. We use a forward model of radar scattering from meteor plasma using a finite-difference time-domain (FDTD) model of the electromagnetic wave interaction with the plasma. This model computes the meteor head RCS for a given meteor plasma distribution, specified with a peak plasma density and a characteristic size. We then relate measured RCS values to the input size and density parameters to better characterize the meteor plasma. We present simulation results that show that the RCS is directly related to the overdense meteor area; that is, the cross-section area of the meteor inside which the plasma frequency exceeds the radar frequency. This provides a direct estimate of the meteor plasma size from a given RCS measurement. Next we investigate the effect of the assumed plasma distribution. We study the RCS resulting from Gaussian, parabolic exponential and  $1/r^2$  distributions. Comparing the different calculated RCS from these different distributions to three-frequency head echo data from the CMOR radar, we show that the  $1/r^2$  distribution provides the best fit to the data. However, given uncertainties in the data, we cannot conclude that any distribution is the most valid. In addition, we show that the choice of distribution assumed can alter the resulting line density  $q$  by an order of magnitude for the same data.

## 1 Introduction

The problem of determining the meteoroid mass flux input to Earth's atmosphere has persisted for decades (Plane, 2012); two orders of magnitude separate the high and low ends of the commonly-cited estimates. These differences arise due to different observational methods, but also due to a large number of uncertainties in assumed parameters for each method.

We focus herein on estimates derived from meteor head echoes observed with high-power, large-aperture (HPLA) and standard meteor radars. Meteor head plasma and radar cross section (RCS) are regularly detected by these ground-based radars. However, because of the plasma nature of the meteor head, the relationship between the measured RCS and the meteor plasma parameters is not straightforward. Close et al. (2004) and others relate the meteor head RCS to the electron line density  $q$  in the meteor, and then relate the line density to the meteoroid mass as

$$qv\mu = \beta \frac{dm}{dt}$$

In order to extract meteoroid masses, the velocity  $v$  must be measured, and the mean molecular mass  $\mu$  is assumed. The ionization potential  $\beta$  is summarized by Campbell-Brown et al., (2012) as a function of velocity, but is also a

function of composition and is only reasonably well known; understanding of the ionization potential is an area of ongoing research. The line density  $q$  is thus left to be determined. In this work, we use a Finite-Difference Time-Domain (FDTD) model (Marshall and Close, 2015) to evaluate the line density  $q$  from a set of meteor observations using the three-frequency Canadian Meteor Orbit Radar (CMOR) (Jones et al., 2005). In the next two sections we describe the FDTD model application and the meteor radar data. In *Section 4* we present extracted parameter results and determine the most likely meteor plasma density distributions based on least-squares fits to the data.

Note that the evaluation of meteoroid mass in the equation above requires integration of the line density  $q$  over the duration of the meteor. In the analysis that follows, we only have single-point observations of RCS and thus  $q$ , and cannot integrate to derive the mass of the parent meteoroids.

## 2 Meteor plasma model

We use the FDTD model of Marshall and Close (2015) to model the relationship between the meteor plasma distribution and the radar cross section (RCS). *Figure 1* shows RCS values computed using the FDTD model with a Gaussian plasma distribution, for a range of peak

plasma frequencies and three different meteor sizes. Solid lines show FDTD results, and dots show validating calculations using the method of moments code WIPL-D (Kolundzija et al., 2000). As expected, we find that the RCS is monotonic with both peak plasma density and meteor size.

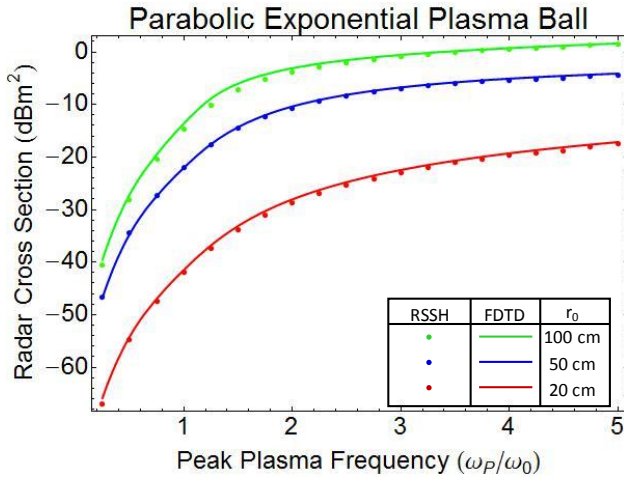


Figure 1 – RCS computed using FDTD model (solid lines) and using a method of moments solution (dots), for a range of plasma frequencies and three different meteor sizes.

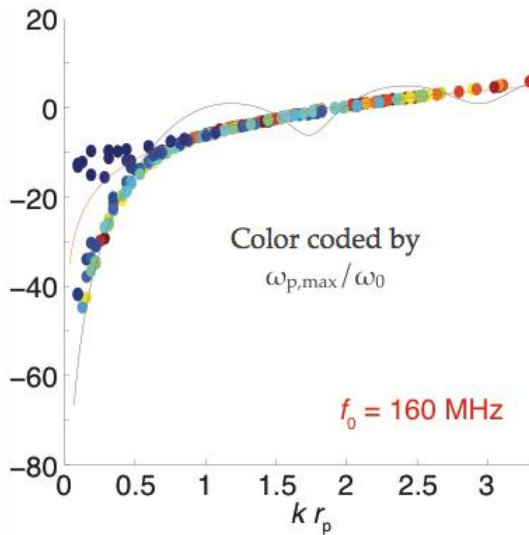


Figure 2 – Meteor head echo RCS versus overdense area,  $r_p$ , normalized by radar wavelength. We find that for  $kr_p > 0.7$ , the RCS is given by  $\pi r_p^2$ .

We wish to find a relationship that describes the meteor RCS as a function of a single parameter that can be used to infer the line density  $q$  and thus meteoroid mass. We find that the RCS is a direct, monotonic function of the meteor “overdense area”  $A_{OD} = \pi r_p^2$ , where  $r_p$  is the radius where the meteor becomes overdense, i.e. the plasma frequency exceeds the radar frequency. This result is shown in Figure 2, where we plot the meteor RCS versus  $kr_p$ , where  $k$  is the radar wavenumber. We find that for  $kr_p \gtrsim 0.7$  (equivalently,  $r_p \gtrsim 0.1\lambda$ ), the RCS is given by the overdense area, while for lower values of  $kr_p$ , the RCS is given by the Rayleigh scattering condition and the RCS is proportional to  $r_p^6$ . The outliers in Figure 2 (the dark blue points at top left) are those where the meteor plasma is just barely overdense, and the

FDTD model does not resolve the overdense area well, i.e. the area is given by just a few grid points.

This observation provides a valuable tool that can be applied to multi-frequency radar head echo data. If we assume the meteor head plasma is overdense at some radius for all frequencies, each frequency-RCS data pair can be translated to an electron density-radius pair. The radar frequency corresponds to a plasma frequency, which translates to electron density, at a radius given by the RCS value using the overdense analysis above. With two or more frequencies, we thus have two or more data points, to which we can fit a distribution.

### 3 CMOR radar observations

We apply the FDTD overdense area analysis to a dataset of 14 meteor head echoes observed by the Canadian Meteor Orbit Radar (CMOR). The CMOR radar transmits and receives simultaneously at 17.45, 29.85, and 38.15 MHz. Each of the meteor head echoes analyzed herein had particularly large RCS values, in some cases as high as 30 dBsm or higher at the lowest frequencies. As such, these may be among the outliers of meteor head echoes, and it remains to be seen if this analysis will apply equally well to the more common, small head echoes observed by HPLA radars.

### 4 Meteor head plasma distributions

Applying the overdense area analysis to the CMOR observations, we fit distributions to the three-point radius-plasma density pairs for each meteor. In order to discern the best fit distribution, we have fit Gaussian, parabolic exponential,  $1/r$ ,  $1/r^2$ , and exponential distributions, given by the equations below:

$$n_e(r) = n_{e0} \exp\left(-\frac{r^2}{r_0^2}\right)$$

$$n_e(r) = n_{e0} \frac{2e^{\pi r/r_0}}{e^{2\pi r/r_0} + 1}$$

$$n_e(r) = n_{e0} \frac{1}{1 + r/r_0}$$

$$n_e(r) = n_{e0} e^{-r/r_0}$$

$$n_e(r) = n_{e0} \frac{1}{1 + (r/r_0)^2}$$

In each of these equations,  $n_{e0}$  is the peak electron density, and  $r_0$  is a radius parameter; however the radius parameter is not the same for each. For example, in the Gaussian and exponential distributions,  $r_0$  is where the density is reduced to  $1/e$  of its peak, while in the  $1/r$  and  $1/r^2$  distributions,  $r_0$  is where the density is reduced to  $1/2$  of its peak.

Figure 3, panels (a)—(d) and (h) shows fits to the meteor observations using these distributions. Panels (e) and (f) show the extracted radius and peak density parameters

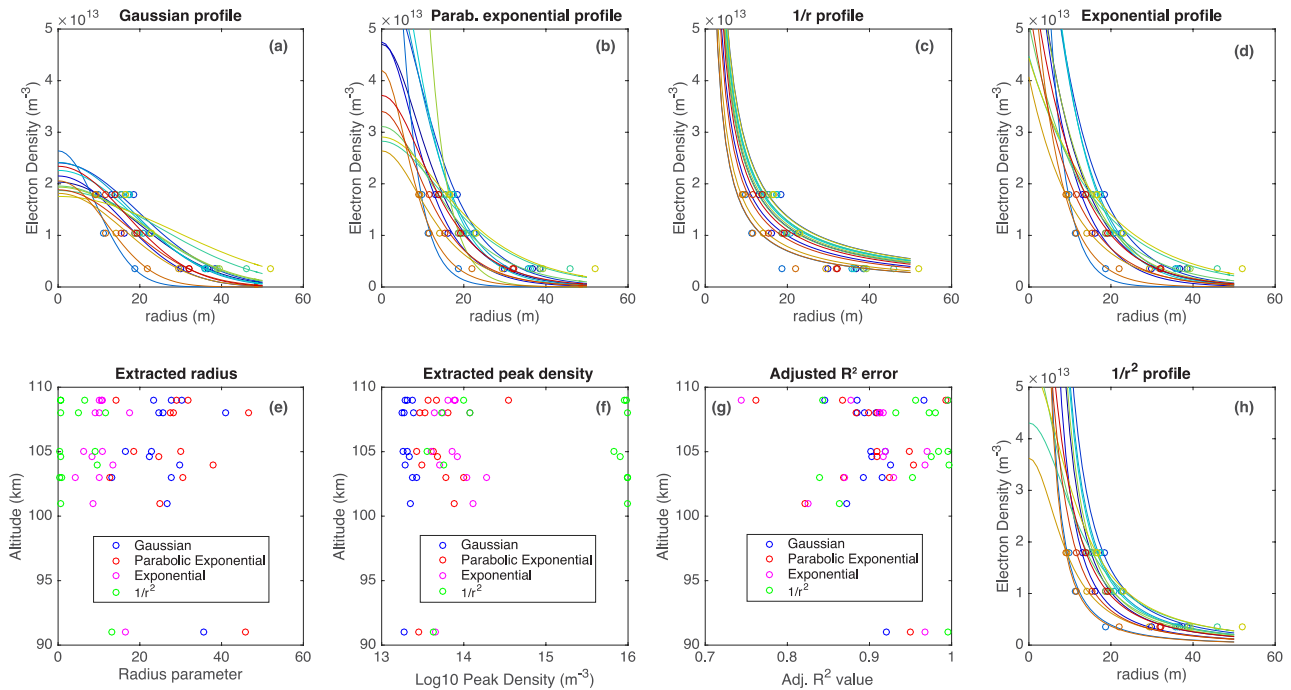


Figure 3 – Profile fits to CMOR radar RCS data and extracted parameters. Panels (a)-(d) and (h): fits to CMOR observations using different profiles. Panels (e) and (f): extracted meteor head radius parameter and peak densities. Panel (g): Adjusted R-squared error for each fit.

from these fits, and panel (g) shows the adjusted  $R^2$  error from each fit. The latter three values are plotted versus the altitude of the meteor observation, for the purpose of looking for altitude trends; however, no altitude trends are obvious from these data. Note that the radius and peak density for the  $1/r$  fit are not shown as they would fall off the range of these plots. We observe that most of the distributions give similar results, except the  $1/r^2$  distribution, which yields much smaller radii and larger peak densities. The  $1/r^2$  distribution also yields the best fits, as measured by adjusted  $R^2$ .

Next, given these distributions and fitted parameters, we can integrate the distribution using the following equation to obtain the meteor head line density  $q$ :

$$q = \frac{1}{N} \sum_{r=0}^{r=N} n_e(r) \pi r^2$$

where in the equation above the electron density is summed over discrete radial shells. Figure 4 plots the resulting line densities for each meteor, for each distribution above. The most important observation from these results is that the line density depends strongly on the choice of distribution. While the Gaussian and parabolic exponential distributions yield line densities within about 10% of each other on average (blue and red circles), the  $1/r^2$  distribution yields line densities about  $\frac{1}{4}$  those (green circles). The exponential distribution (pink circles) is somewhere in between, about  $\frac{1}{2}$  the values of the Gaussian and parabolic exponential.

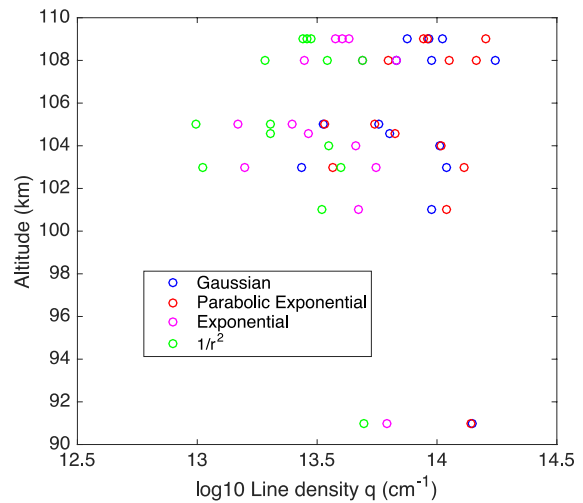


Figure 4 – Extracted instantaneous line density  $q$  for CMOR meteor data, using overdense area analysis.

## 5 Discussion and conclusions

Previous analyses of meteor head echoes have used Gaussian or parabolic exponential distributions. These results suggest that a) the  $1/r^2$  distribution may be the most likely distribution in the meteor head plasma, and b) the resulting line density  $q$  may be considerably lower than previously determined. That result flows down to the meteoroid mass, which is roughly proportional to the line density.

These conclusions are tentative, however, and need to be evaluated with further data. First, the CMOR dataset used here include only 14 meteor head echoes. Second, these are particularly large head echo RCS values, which may be outliers compared to more typical, small meteors.

Third, we recognize that we are fitting two-parameter distributions to three data values for each event. While three data points allows an estimate of the fit quality, it is not robust. This is unlikely to be improved upon – more data points for each meteor would require more radar frequencies – but more meteor observations would provide a better statistical dataset.

## Acknowledgment

This work was supported in part by NASA grant NNX15AJ86G from the Meteoroid Environment Office.

## References

- Campbell-Brown M. D., Kero J., Szasz C., Pellinen-Wannberg A. and Weryk R. J. (2012). “Photometric and ionization masses of meteors with simultaneous EISCAT UHF radar and intensified video observations”. *Journal of Geophysical Research: Space Physics*, **117**, A9, A09323.
- Close S., Oppenheim M., Hunt S. and Coster A. (2004). “A technique for calculating meteor plasma density and meteoroid mass from radar head echo scattering”. *Icarus*, **168**, 43–52.
- Jones J., Brown P., Ellis K. J., Webster A. R., Campbell-Brown M., Krzeminski Z. and Weryk R. J. (2005). “The Canadian Meteor Orbit Radar: system overview and preliminary results”. *Planetary and Space Science*, **53**, 413–421.
- Kolundzija B. M., Ognjanovic J. S. and Sarkar T. (2000). “WIPL-D: Electromagnetic Modeling of Composite Metallic and Dielectric Structures: Software and User's Manual”. Artech House.
- Marshall R. A. and Close S. (2015). “An FDTD model of scattering from meteor head plasma”. *Journal of Geophysical Research: Space Physics*, **120**, 5931–5942.
- Plane J. M. C. (2012). “Cosmic dust in the earth's atmosphere”. *Chem. Soc. Rev.*, **41**, 6507–6518.



Joost Hartman, Sebastiaan de Vet and Gert-Jan Netjes. (Photo Casper ter Kuile).

# Numerical simulation of the BRAMS interferometer in Humain

Antonio Martínez Picar<sup>1</sup>, Christophe Marqué<sup>1</sup>, Cis Verbeeck<sup>1</sup>,  
Stijn Calders<sup>2</sup>, Sylvain Ranvier<sup>2</sup>, Emmanuel Gamby<sup>2</sup>,  
Michel Anciaux<sup>2</sup>, Cédric Tetard<sup>2</sup> and Hervé Lamy<sup>2</sup>

<sup>1</sup>Solar–Terrestrial Centre of Excellence — Royal Observatory of Belgium, Brussels, Belgium  
antonio.martinez@observatory.be

<sup>2</sup>Royal Belgian Institute for Space Aeronomy, Brussels, Belgium  
herve.lamy@aeronomy.be

The Royal Belgian Institute for Space Aeronomy (BISA) operates a network for radio meteor studies based in Belgium. One of the receiving stations is located in the Humain Radio-Astronomy Station (HuRAS) and consists of an array of five 3-element Yagi antennas. In this paper the results of detailed numerical simulations are presented in order to obtain a first approach for the direction finding capability of this interferometer.

## 1 Introduction

The Belgian RADio Meteor Stations (BRAMS) is a point–multipoint network with dozens of radio receiving stations spread all over Belgium recording – under a fairly continuous regime – reflections off meteor trails of a signal generated by a dedicated transmitter located at Dourbes Geophysical Centre, which emits a pure sine wave at a frequency of 49.97 MHz with a constant power of 150 W (Calders and Lamy, 2012). *Figure 1* shows a picture of the beacon’s radiating system, consisting of a turnstile antenna and a metallic grid underneath acting as a reflector.

The physical principle, known as forward scattering, states that the ionization trail produced by a meteoroid entering the Earth’s atmosphere (meteor) can reflect a radio wave. Any receiver tuned to the transmitter’s frequency, in principle, is capable of detecting that signal, also known as meteor echo. Please note that transmitter and receiver are not located in the same place (McKinley, 1961).

Most of the stations are basic receiving systems consisting of a single 3-element Yagi antenna (see *Figure 2*), a single receiver (*ICOM IC-R75*), an amplitude and frequency calibrator (developed at BISA), a GPS clock, a sound card and a PC.



*Figure 1* – BRAMS beacon radiating system in Dourbes, Belgium.

In order to obtain reliable information of meteoroids and meteoroid streams, among other parameters, it is important to know the performance of the antenna system regarding the many possible incoming directions of the meteor echo. This three dimensions (3D) map of the antenna performance is known as *Antenna Directional Pattern*. However, this value depends on many factors (antenna geometry, relative position of the antenna and nearby objects/facilities, ground characteristics, etc.) and usually getting reliable figures represents a challenge. Numerical simulations are increasingly being applied successfully, using different methods.



*Figure 2* – Typical 3-element Yagi antenna of a BRAMS basic receiving system.

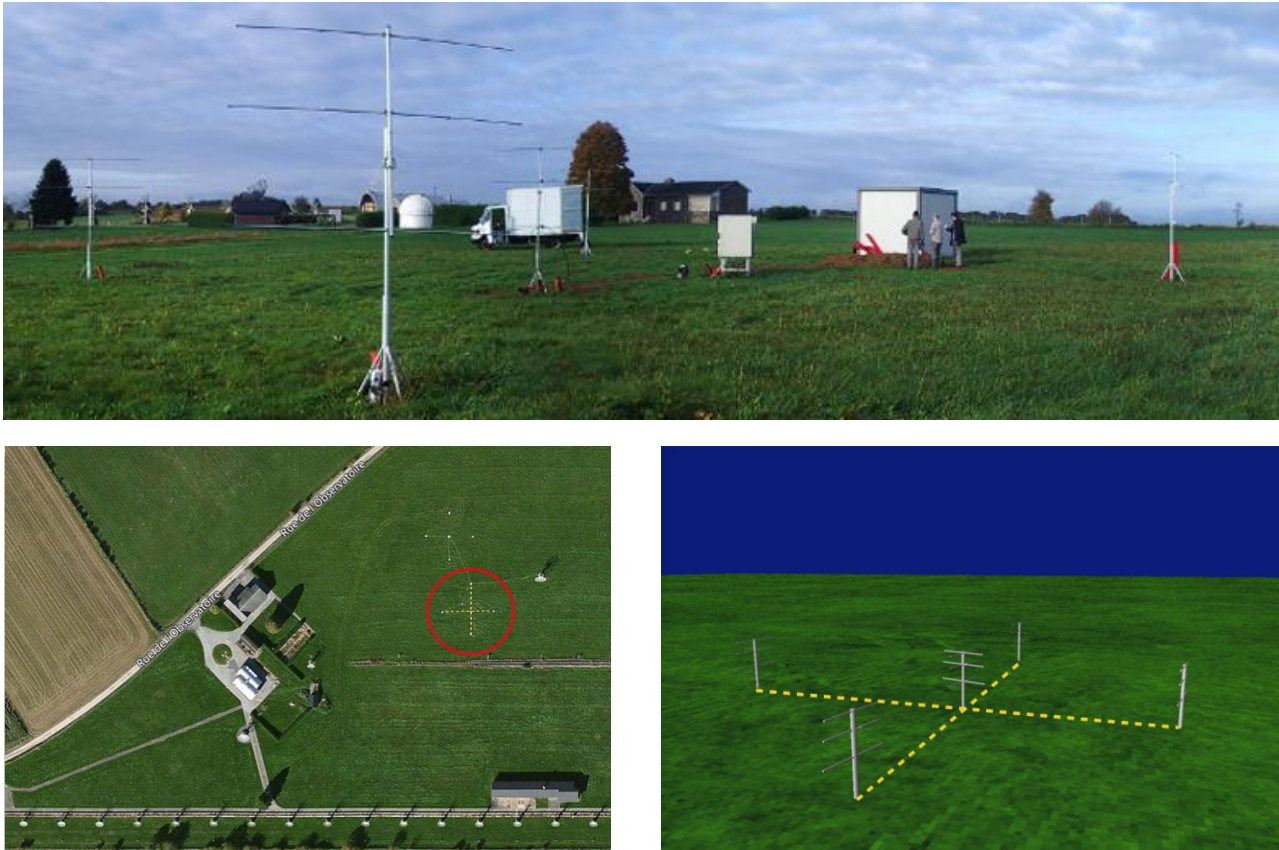


Figure 3 – The BRAMS interferometer in HuRAS (Top: General view of the site at HuRAS; bottom-left: Location of the array antennas at HuRAS; bottom-right: Visualization of a computer-based modelling of the array).

## 2 BRAMS Interferometer

The Solar Physics department of the Royal Observatory of Belgium (ROB) maintains and operates a solar radio astronomy station in Humain (south of Belgium), which also hosts the BRAMS interferometer system. The array, inspired by the work of Jones et al. (1998) comprises five 3-elements Yagi type (standard BRAMS) antennas which allow applying interferometric techniques over the data recorded by the receivers attached to each antenna. This technique permits measuring the direction of the radio meteor reflections, which will aid retrieval of individual meteoroid trajectories.

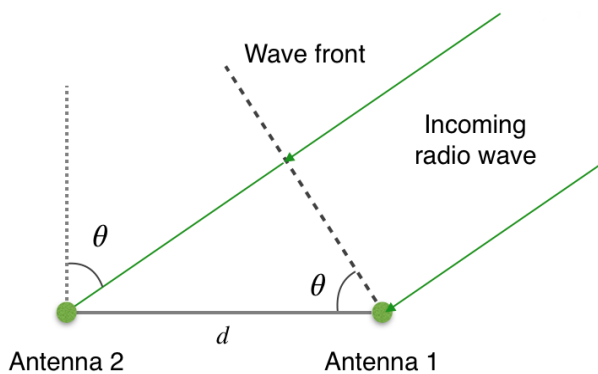


Figure 4 – Principles of two-element interferometer.

The direction finding problem can be defined in time delay measurement. Figure 4 shows the basic geometry. The principle is that a plane wave arriving at an angle is received by one antenna earlier than the other due to the difference in path length.

If the distance between two antennas is denoted by  $d$  and the speed of light  $c = 299792458$  m/s then the time delay  $\tau$  between the signals in both antennas is

$$\tau = \frac{d \cdot \sin \theta}{c} \quad (1)$$

where  $\theta$  is the Angle of Arrival (AoA). It is possible to obtain the directional information from the spatial position of the lines or surfaces of equal phase.

In order to solve the AoA determination problem, it is necessary to measure the time delays and from these an angle can be inferred. The arrangement of the BRAMS interferometer in HuRAS is inspired on Jones et al.'s (1998) work, consisting of two orthogonal three-element linear interferometers with a common central element which allow performing angular measurements in 3D.

Each BRAMS antenna at this location has its own radiation pattern (Martínez Picar et al., 2014), but under the direction-finding operation, the interferometer works as a unit, so the directional pattern of the whole array is needed in order to understand appropriately the level of the received signal.

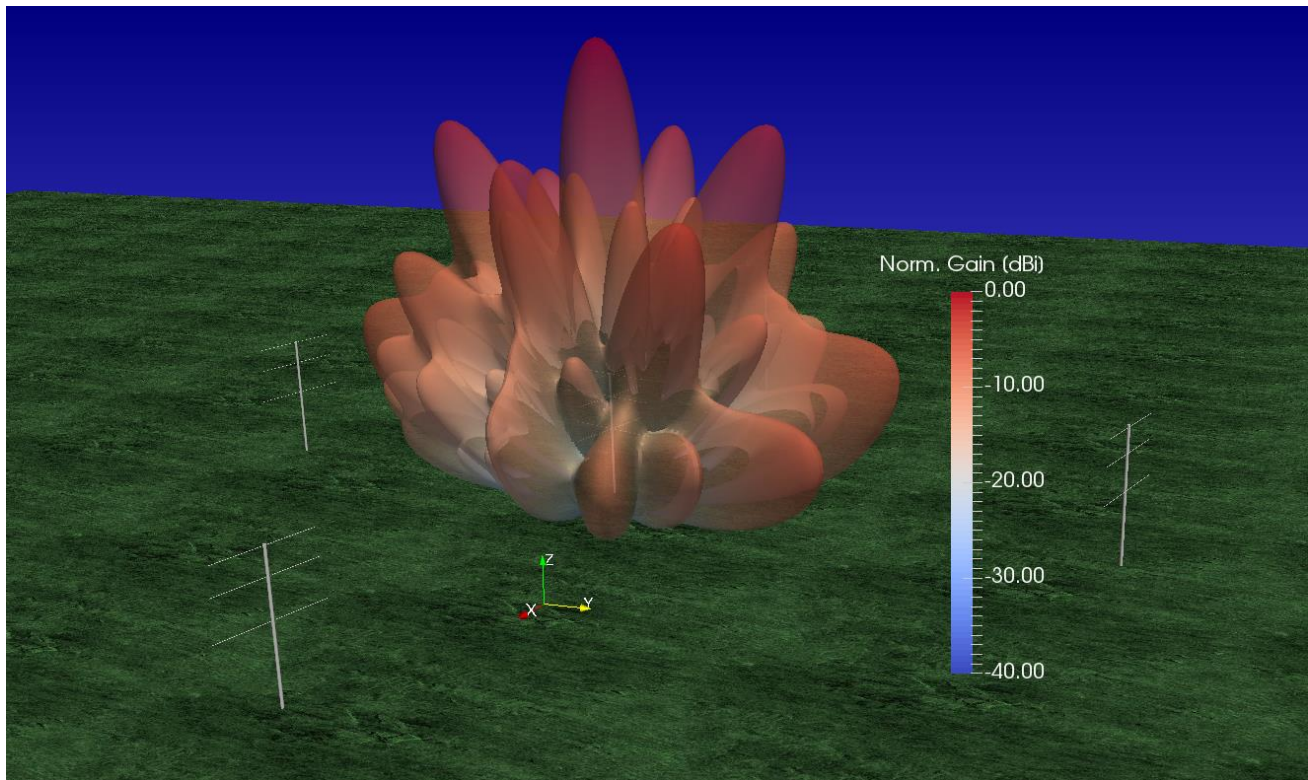


Figure 5 – Visualization of the (antenna) array pattern obtained by numerical simulation of the BRAMS interferometer in Humain. The gain is normalized to the maximum value ( $G_{max} = 14$  dBi).

The use of interferometers, however, has its problems. In order to measure the AoA unambiguously over the visible hemisphere down to low elevation angles, the antennas of a two-element interferometer must be separated by no more than half a wavelength ( $\lambda/2$ ) if nothing else than time (or phase) is used. On the other hand, the mutual coupling between adjacent closely spaced antennas is an important consideration which can lead to errors in the measurements. These mutual coupling effects diminish as the spacing is increased, i.e., as the mutual impedance decreases. It is necessary to take this effect into account in order to obtain a reliable (antenna) array pattern.

### Array modelling

In order to obtain the directional pattern of the BRAMS interferometer, the initial approach of modelling the full array was adopted using *Numerical Electromagnetics Code* (NEC), which is a software package based on the *Method of Moments* (MoM) technique for analyzing the electromagnetic response of an arbitrary structure (Burke and Poggio, 1983). *NEC2++* (Molteni, 2014), the software's version used in this work, is capable of dealing with ground effects and intrinsically takes into account any possible mutual coupling between the antennas.

## 3 Numerical simulation

Detailed models of the antennas were prepared including the conductivity of their elements as well as their *gamma match*, a physical device available in the antenna used for matching the unbalanced characteristic impedance of the coaxial feedline to the much lower balanced impedance of the antenna. Additionally, terrain characteristics

(relative permittivity  $\epsilon$ , and conductivity  $\sigma$ ) were also taken into account in the model.

The receivers of the interferometer are synchronized, which means that – initially – the feeders (excitation point of each antenna) must be kept aligned for simulation purposes. The result is shown in the gain-normalized visualization of Figure 5. A total directional pattern with very complex features is observed.

Summarizing the main characteristics:

- Main lobe pointing to the zenith with a *maximum gain of  $G_{max} = 14$  dBi*;
- Presence of *many secondary lobes* in  $\sim 65^\circ$  elevation with only 1 to 2 dB difference below the maximum;
- Existence of *several nulls* of 10 to 15 dB below the maximum in many directions ( $\sim 80^\circ$ ,  $\sim 60^\circ$ ,  $\sim 45^\circ$ ,  $\sim 35^\circ$ , ...).

All these findings point to the fact that, if no phase manipulation is applied to the signals registered by the different receivers, the array will have *preferred observing directions in the sky*. If phase delay techniques are in place, the directional pattern must be computed again taking this into account.

## 4 Future work

The numerical simulation results are a good approach for the antenna performance characterization. Nevertheless, in order to use the most precise and reliable values, the real array directional pattern must be measured on-site. The *Radio Antenna Measurement Onsite* (RAMON) system (Martinez Picar et al., 2015) is currently fully

operational and it will be used to perform those measurements carefully.

## References

- Burke G. J. and Poggio A. J. (1981). “Numerical Electromagnetics Code (NEC) – Method of Moments, Part I: Program Description – Theory”. Lawrence Livermore National Laboratory.
- Calders S. and Lamy H. (2012). “BRAMS: status of the network and preliminary results”. In Gyssens M. and Roggemans P., editors, *Proceedings of the International Meteor Conference*, Sibiu, 15–18 September 2011. IMO, pages 73–76.
- Jones J., Webster A. R. and Hocking W. K. (1998). “An improved interferometer design for use with meteor radars”. *Radio Science*, **33**, 55–65.
- Martínez Picar A., Ranvier S., Anciaux M. and Lamy H. (2014). “Modeling and calibration of BRAMS antenna systems”. In Rault J.-L. and Roggemans P., editors, *Proceedings of the International Meteor Conference*, Giron, 18–21 September 2014. IMO, pages 201–206.
- Martínez Picar A., Marqué C., Anciaux M. and Lamy H. (2015). “Directional pattern measurement of the BRAMS beacon antenna system”. In Rault J.-L. and Roggemans P., editors, *Proceedings of the International Meteor Conference*, Mistelbach, Austria, 27–30 August 2015. IMO, pages 177–179.
- McKinley D. W. R. (1961). *Meteor Science*. New York: McGraw-Hill.
- Molteno T. C. A. (2014). “NEC2++: An NEC-2 compatible Numerical Electromagnetics Code”. *Electronics Technical Reports* No. 2014-3, ISSN 1172-496X, October 2014.



Two prizes were to be awarded this IMC: a prize for the best poster (won by Antonio Martínez Picar) and one for the nicest photograph of the photo contest (won by Koji Maede).

# Construction of a meteor orbit calculation system for comprehensive meteor observation

Satoshi Mizumoto, Waleed Madkour and Masa-yuki Yamamoto

Kochi University of Technology  
s.mizumoto0918@gmail.com

At Kochi University of Technology (KUT), the development of an HRO (Ham-band Radio meteor Observation) - Interferometer (IF) was started in 2003, and we realized the meteor orbit calculation system by multiple-site radio observation with GPS time-keeping combining with the 5 channel (5ch) HRO-IF in 2012. Here, we introduce a future plan of comprehensive meteor observation by Radio, Optical and Infrasound observation.

## 1 Introduction

Comets release dusts of about several micrometer to several cm in diameter. The dust going around along the cometary dust trail will be gradually deviating from the original cometary dust trail due to perturbation effects by gravitational forces of planets such as Jupiter or Saturn and begin to distribute in the Solar System. When the Earth approaches the cometary dust trail, the dust enters into the atmosphere of the Earth, collides intensely with the atmospheric particles and they are vaporized at high temperature. Upper atmospheric species and the vaporized dust ingredients emit light and heat, being observed at this occasion as a meteor.

A forward scattering meteor radar using 53.750 MHz VHF (Very High Frequency) continuous radio wave (CW) for observation of meteor shower activities has been operated at KUT since 2003. There are few groups observing constantly the activities of meteors in other Japanese research organizations. The Kyoto University, Research Institute for Sustainable Humanosphere (RISH) has a large-scale MU radar (Middle and Upper atmospheric radar). The radar can detect meteor shower activity in detail by a high-power backscattering method, using the same location as transmitting and receiving station (Kero et al., 2012). However, its observation period has limitation, i.e., the MU radar cannot always perform observation of the meteors because observation time is occupied by the observation of other atmospheric phenomenon than the meteors.

Each meteor shower has many parameters that are not yet elucidated, such as the period of appearance, activity level, mass size, mass distribution, etc. A meteorite and a huge meteor event, so-called a bolide, may produce sound signal at the time of its atmospheric plunge. The meteor can be seen as a large fireball flying in the atmosphere at a supersonic speed then, we sometimes can hear bass (shock wave) sound a few minutes afterward. Infrasound (lower sounds less than human audible 20 Hz frequency) is generated in the sky at the same time of generating the strong shock wave. It arrives at the Earth's surface at the speed of sound and is observed by using high sensitivity infrasound sensors (Le Pichon et al.,

2013) (*Figure 1*). Moreover, we can catch the infrasound caused by an explosion in the sky as well as by meteorite droppings on the Earth's surface propagating from the source in the atmosphere. It is considered that the infrasound can be generated by many kinds of explosive events such as launches of rockets (Kaschak et al., 1970), nuclear bomb tests and huge chemical explosions (Christie and Campus, 2009), reentry of satellites or large space debris (Yamamoto et al., 2011), explosion of volcanos (Johnson et al., 2004), Tsunamis (Arai et al., 2011), landslides and thunders.

In June 2010, an infrasound signal was observed in the Australian Woomera desert area when the Japanese asteroid space-probe "Hayabusa" returned to the Earth at the corresponding time of atmospheric plunge (Yamamoto et al., 2011). The data (arrival time, direction, shock pressure) of the shock wave taken during the artificial reentry are very important as basic estimation of the mass of a meteor which is not correctly provided by electromagnetic observation for tiny particles (Brown et al., 2013).

In addition, huge datasets of meteors and fireballs have been archived from naked-eye observations in history, and the optical observation using high-sensitivity cameras has been developed as an important precise observation technique. As for the data provided by radio observation and infrasound sensors, it is necessary to check with the optical observations as calibration datasets to improve their reliability because the distinction of each meteor phenomenon under the influence of the environmental radio/sound noises at each observation site is difficult. We can confirm the optic imaging data by checking afterward by our naked-eye or automatic image processing, and it could be an important element to prove that the data we detected by radio and infrasound observation were real signals of meteors and fireballs exactly at the time of each phenomenon. On the other hand, observation of electromagnetic waves and infrasound has a statistical advantage of continuous operation under rainy weather condition and even in daytime. Here we introduce a design of a comprehensive meteor observation system by using three kinds of observations: infrasound, radio wave and optics.

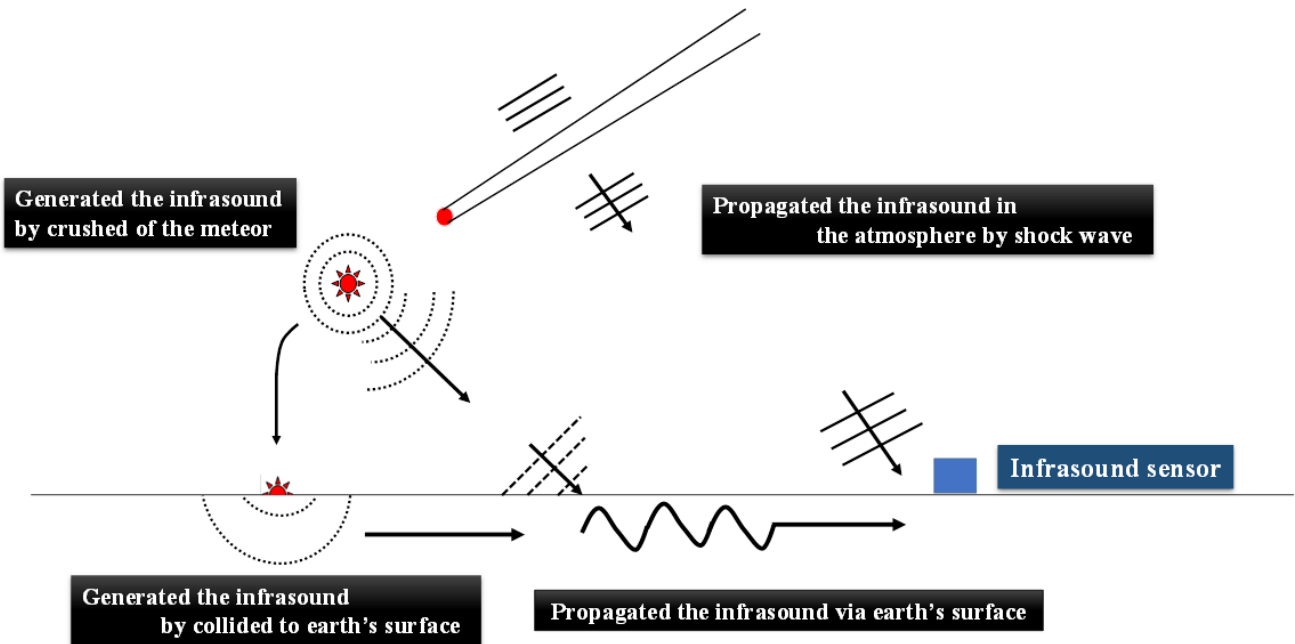


Figure 1 – The infrasound caused by the meteor.

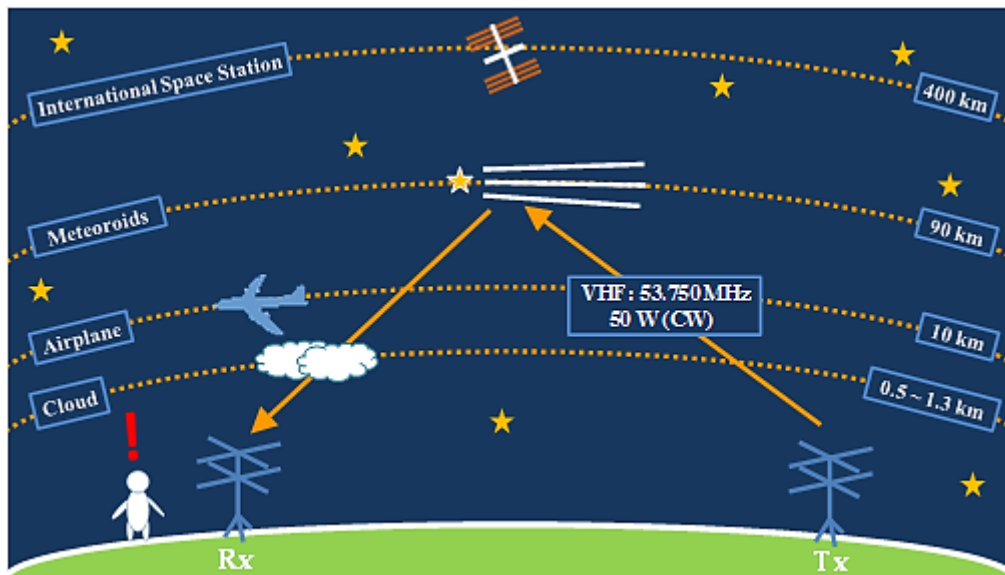


Figure 2 – The forward scattering method meteor radio observation system conceptual diagram.

## 2 Meteor radio observation

When a dust particle enters into the upper atmosphere, it emits light there, at the same time microscopically, atmospheric molecular species and meteoric origin ones are ionized and become plasma particles, separated into plus ions and free electrons. At this moment, a slim columnar high-density plasma pillar is formed for a short time, along the meteor trajectory. To have an idea of a scale of length, we would like one to imagine the length of a runway on the airport for several times. The ionized pillar has a property to scatter radio waves of a frequency less than a certain uniformity depending on the plasma density (plasma frequency). The HRO (Ham-band Radio meteor Observation) is an observation method using the density characteristics of meteor plasma. The radio observation of meteors uses such meteor plasma as a scattering media in the sky (Figure 2). The radio meteor observing using ham-band radio waves (HRO) was

established in Japan at the peak period of the Leonid meteor shower activity during 1998 – 2002 with its 33 years revolution cycle. Amateur meteor observers and ham operators spread all over Japan focus on meteor astronomy mainly since the “*Meteor radio observation manual*” (Nakamura, 2002) introduced the observing details of HRO. The HRO is a method usually receiving the VHF beacon wave of 53.750 MHz in the amateur radio band, using a transmitter of 50 W power located at the National Institute of Technology, Fukui College at Sabae, Fukui prefecture with 24/7 continuous operation. Thereby, we can observe the meteor without being influenced by bad weather and daylight (Maegawa, 1999). The VHF wave can propagate only in a prospect range, like FM radio broadcasting waves (76 MHz to 90 MHz in Japan). We cannot receive it at the observation point so far from the distant place from the transmission station due to attenuation by mountains and/or buildings. However, the transmitted waves can be detected at the

receiving station once it is scattered on an ionized meteor plasma pillar. Using this characteristic of the forward scattering method, we have been operating the HRO radio observation at KUT (Figure 2).

There are not many groups doing meteor radio observing at Japanese research institutes. By the meteor radio wave observation of the backscattering method with the above-mentioned MU radar, they can obtain in short time very accurate meteor parameters by its 1 MW high-power transmission with a composed radar system from many antenna groups. But, the available operation time of the MU-radar is limited only to campaign periods, thus the detection of meteor echoes for an occasional sporadic meteor bursts is almost impossible. The Western Ontario University developed the *Canadian Meteor Orbit Radar* (CMOR) which produced many statistical studies recently. The CMOR team established two receiver stations just near the neighborhood (6.2 and 8.1 km) of the CMOR back-scatter transmitting and receiving site, and quasi-backscattering multi-site observing has been carried out to receive meteor-scattered radio waves by five antennas, like the KUT system (Jones and Webster, 1992) as well as the two remote sites. Currently, the only research group observing continuously meteor activity by a 5 channel interferometer (5ch HRO-IF) with forward scattering method is KUT in Japan.

### 3 The state of meteor radio observing at KUT

We started a basic development of the HRO meteor radio observing in 2003 at KUT, and developed the 3ch HRO-IF system which was improved to the current 5ch HRO-IF system in 2005, starting continuous meteor observing (Horiuchi, 2005; Okamoto, 2005). Namely, in the previous 3ch HRO-IF, there was a large measurement error in the arrival angle calculated from phase differences especially in the case of lower elevation angles, thus the accuracy of the observations was limited only when the elevation angle was larger than 45°. In order to solve this problem, we developed the 5ch HRO-IF (Figure 3) (Noguchi, 2009).

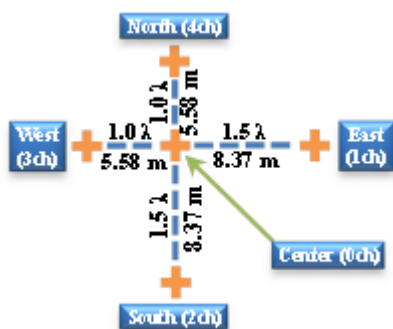


Figure 3 – KUT 5-ch HRO-IF.

We can calculate the phase difference of  $0.5\lambda$  ( $\lambda$ : wavelength) baseline length from (Ant.0–Ant.1) – (Ant.0–Ant.3), and calculate the phase difference of  $2.5\lambda$  baseline length from (Ant.0–Ant.1) + (Ant.0–Ant.3). In

the  $0.5\lambda$  baseline, the arrival angle is derived from a single phase difference (one-to-one correspondence), but the calculation error of the arrival angle with respect to the measurement error of the phase difference will be larger (Figure 4 left). On the other hand, in the case of a  $2.5\lambda$  baseline, an arbitrary of  $2\pi$  phase shift exists with 5 solutions, but the error on the arrival angle with respect to the measurement error of the phase difference becomes small (Figure 4 right). Thus, in a combination of three antennas arranged in one straight line as shown in Figure 3, an accurate arrival angle can be obtained. So, if we arranged two more antennas (Ant.2, Ant.4) along the perpendicular line, we can know the true angle in 3D space (azimuth and elevation).

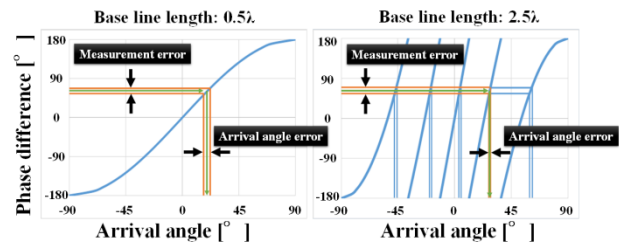


Figure 4 – Relation between the phase difference and arrival angle by 5ch HRO-IF.

After successfully and stable automatic observing with the 5ch HRO-IF, we have operated for approximately two years with an improved measurement accuracy of the arrival angle. Furthermore, we can plot the meteor appearance position on a map assuming 90 km as the appearance altitude of the meteor, and show them on a web page in quasi real time (Noguchi, 2009). The automatic meteor observing system has been performed continuously since January 2009 but was suspended in March 2012 due to the lack of man power. In 2014, we repaired the KUT 5ch HRO-IF, and restarted the radio observations since then. In 2014, we successfully observed two periodical meteor showers occasionally, the Camelopardalis and the Phoenicids, as well as the major meteor showers Daytime Arietids, Leonids, Geminids and Quadrantids. Currently, we rebuilt the 5ch HRO-IF system, and we are constructing a multi-site observing system. We built two observation sites adding on to the 5ch HRO-IF, hereby we can obtain at almost the same time meteor echo data at the three independent sites, thus we can calculate a meteor trajectory angle and meteor velocity by using slight time difference among each other. Therefore, we can judge for each echo if it is originating from seasonal meteor showers or from the sporadic background as well as to compare the datasets with the optical and radio observations. For the newly added two sites, each site has the same antenna as an element of the 5ch HRO-IF.

We are using wave extraction software for meteor observing in exact timing (Yamasaki, 2012). This software generates a receiving intensity trend in 1 ms accuracy with the usually operated spectrum analysis result of receiving a signal at a 0.1 s resolution for each

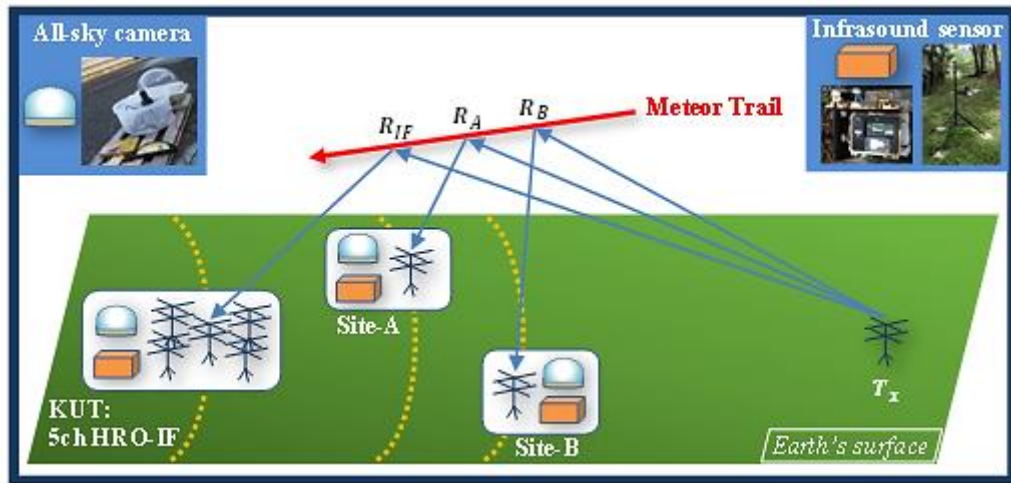


Figure 5 – Comprehensive meteor observation plan at KUT.

10 minutes observing bin. Here we have to obtain high-accuracy time differences for the calculation of the meteor trajectory angle and velocity from the multi-site observation. It is generally known that the meteor velocity on the Earth is about 40 km/s on average depending on its Kepler velocity around the Sun

Thus, we have to take a distance between *5ch HRO-IF* and the other two remote sites of over a 10 km scale. When we do not observe a meteor simultaneously by multi-site observation, the *5ch-interferometer* software analyzes the receiving signal with a 0.1 s time frame, and calculates the meteor appearance time, azimuth and elevation parameters. When we successfully observe a meteor simultaneously by multi-site observing at all three sites, we launch the wave extraction software and analyze the receiving signal by a 1 ms time resolution for all observation stations. Afterwards, we can calculate the meteor trajectory angle and velocity by each time difference if we assume a meteor shower radiant. In 2011, we observed the Geminid meteor shower and calculated the meteor parameters shown above. Later, we compared the radio observing data with optical observing data, and confirmed the precision of the radio measurement (Yamasaki, 2012). In this time, we can obtain an angular difference result with an error range within about 3 degrees. However, during the trial of 2011 for a short time, we got only one example of simultaneous meteor data. Therefore, we have to collect much more simultaneously observed data of meteors by continuous operation of both radio and optical systems.

#### 4 Toward the first collecting of a meteorite in Japan by comprehensive meteor observation

We propose a comprehensive meteor observing system consisting of radio, optical and infrasound observing methods as a future plan. By using the comprehensive observing method, we will be able to obtain many meteor parameters, expecting many advantages (Figure 5).

The Western Ontario University observes meteors using an all-sky camera system at the Southern part of Ontario (the Southern Ontario Meteor Network), the above-mentioned CMOR and the Elgin field infrasound array at the same time (Wayne et al., 2008). If an observed meteor was a meteoroid of  $-2$  absolute magnitude or brighter (even in case of a meteor less than 10 cm in diameter), infrasound of detectable amplitude was reported by the Western Ontario University meteor observing network. Furthermore, they found that at least one meteor per month produced infrasound in their observing region (Wayne et al., 2008). Energy and size estimations of the Chelyabinsk meteorite in 2012 as well as the artificial reentry of the “Hayabudsu” capsule were carried out as useful examples of infrasound signal calibrations (Yamamoto et al., 2011; Brown et al., 2013).

We observed the Geminid meteor shower at around 3<sup>h</sup>00<sup>m</sup> LT on December 15, 2015 by multi-site radio observing. At that time, we obtained about 100 meteor data per single hour by our system. Then, we could calculate the meteor trajectory angle and velocity for 9 examples. Additionally, we judged the origin of each meteor using the actual data, a Geminid meteor or a sporadic meteor, with the result shown in Figure 6, as example.



Figure 6 – Relation of meteor trajectory angle and radiant point (Three pins are observation sites. Yellow: Otoyo-town, Green: KUT, Red: Geisei-town).

In KUT, we observed meteors by optical and radio observing for three weeks during January into February 2009. We got 43 meteor examples simultaneously observed by two observing methods during this period (Noguchi, 2009). We calibrated the radio observing results with the optical ones for examples with a duration time over 4 s and with the maximum signal intensity of 13 among a scale of all 13 levels. Then we concluded that a rate of 80% of correspondence (16/20) was obtained for the meteor appearance time, azimuth and elevation (Noguchi, 2009). As the optical observation could be affected by the influence of light pollution as well as bad weather at the observing site, it cannot always be used for meteor observing. However, the Japanese optical observing network coverage is very wide and many amateur people observed a lot continuously with their emotional motivation. If one site could not observe the meteor due to bad weather, the other observing site may cover it. The cases of fireball-class meteors are observed simultaneously with a high probability, deriving meteor trajectory, brightness, velocity and altitude, calculated at the Forum of Sonotaco Network, Japan<sup>1</sup> (SonotaCo, 2009).

The reliability goes up for each meteor data if we get many meteor parameters simultaneously when performing the comprehensive meteor observing like the Western Ontario University's comprehensive meteor observing with seven all-sky camera observation sites, the CMOR radio facility and an infrasound observation array (Wayne et al., 2008). In KUT, we will build three optical observing sites and three infrasound observing sites with multi-site forward-scatter radio observing sites for future comprehensive meteor observing. The infrasound observing is expected to detect a total power of meteors with the energy estimation of the fireball-class meteors. However, influences such as wind turbulence are significant, making it difficult to identify the infrasound meteor origin only by using one observing site. Thus, we have to install as many observing sites as we can. We can identify an origin of the infrasound, if we can observe at least from 3 observing sites at the same time. It is the same as with radio observing. If we have a sensor array, the investigation to verify the origin becomes easy. When a fireball-class meteor encounters the Earth, and if we succeed in the simultaneous observation by the methods in the three ways as explained above, we know the meteor size and trajectory parameter in detail by each observation method. We will be able to obtain the information necessary to know the origin and the evolution of the solar system from the metal composition ratio of the meteorite if we can recover meteorites on the ground. In addition, we become able to check the precision of each given meteor parameter from each observation method. Furthermore, we can know "Where did the meteor come from in the solar system?" Using these results as a clue for the meteor phenomenon elucidation, we would like to achieve the collection of the

meteorites after having various parameters of each meteor measured by the three kinds of observing techniques which is still not accomplished in Japan at the same time and in the same region.

Dust from the comets carry a key clue for knowing the origin of the solar system from far space to the Earth. Currently, the elucidation of many meteor phenomena and the studies on the origin of the solar system are still an open discussion. If we succeed in collecting a meteorite by comprehensive meteor observing, we can move one big step forward. Although each meteor particle is very small, we would like to build a sensor network for the comprehensive meteor observing technique, and observe meteors continuously as long as possible to make more statistical studies in order to know a part of the grand histories of the universe.

## Acknowledgment

We are grateful to the Midorino-tokeidai owners and the Geisei Astronomical Observatory for their help in our experiment.

## References

- Arai N., Iwakuni M., Watada S., Imanishi Y., Murayama T. and Nogami M. (2011). "Atmospheric boundary waves excited by the tsunami generation related to the 2011 great Tohoku-Oki earthquake". *Geophysical Research Letters*, **38**, L00G18, doi:10.1029/2011GL049146.
- Brown P. G., Assink J. D., Astiz L., Blaauw R., Boslough M. B., Borovicka J., Brachet N., Brown D., Campbell-Brown M., Ceranna L., Cooke W., de Groot-Hedlin C., Drob D. P., Edwards W., Evers L. G., Garces M., Gill J., Hedlin M., Kingery A., Mialle P., Moser D. E., Saffer A., Silber E., Smets P., Spalding R. E., Spurny P., Tagliaferri E., Uren D., Weryk R. J., Whitaker R. and Krzeminski Z. (2013). "A 500-kiloton over Chelyabinsk and an enhanced hazard from small impactors". *Nature*, **503**, 238–241.
- Christie D. R. and Campus P. (2009). "The IMS Infrasound Network: Design and Establishment of Infrasound Stations". In Le Pichon A., Blanc E. and Hauchecorne A., editors, *Infrasound Monitoring for Atmospheric Studies*, Springer Science, pages 29–75, doi: 10.1007/978-1-4020-9508-5\_2.
- Horiuchi H. (2005). "Basic development of interferometer system in radio meteor observation". Bachelor thesis, Kochi University of Technology (*in Japanese*).
- Johnson J. B., Aster R. C. and Kyle P. R. (2004). "Volcanic eruptions observed with infrasound". *Geophysical Research Letters*, **31**, L14604, doi: 10.1029/2004GL020020.

<sup>1</sup> SonotaCo (2004): SonotaCo Network Japan, <http://sonotaco.jp/> (2015-02-02).

- Jones J. and Webster A. R. (1992). "Forward-Scatter Radio-Meteor Studies". In Lunar and Planetary Inst., *Asteroids, Comets, Meteors 1991*, Held June 24-28, 1991, in Flagstaff, AZ. ISBN: 0-942862-07-04, pages 273–276.
- Kaschak G., Donn W. L. and Fehr U. (1970). "Long-Range Infrasonics from Rockets". *Acoustical Society of America*, **48**, 12–20, doi: 10.1121/1.1912102.
- Kero J., Szasz C., Nakamura T., Meisel D. D., Ueda M., Fujiwara Y., Terasawa T., Nishimura K. and Watanabe J. (2012). "The 2009-2010 MU radar head echo observation programme for sporadic and shower meteors: radiant densities and diurnal rates". *Monthly Notices of the Royal Astronomical Society*, **425**, 135–146.
- Le Pichon A., Ceranna L., Pilger C., Mialle P., Brown D., Herry P. and Brachet N. (2013). "The 2013 Russian fireball largest ever detected by CTBTO infrasound sensors". *Geophysical Research Letters*, **40**, 3732–3737, doi:10.1002/grl.50619.
- Maegawa K. (1999). "HRO: A New Forward-Scatter Observation Method Using a Ham-Band Beacon". *WGN, Journal of the IMO*, **27**, 64–72.
- Nakamura T. (editor) (2002). "Radio meteor observation guidebook". RMO editing committee, CQ Publishing Co., Ltd. 175 pages (*in Japanese*).
- Noguchi K. (2009). "High-accuracy direction findings of meteors and development of an automatic meteor observation system by 5-channel radio interferometer". Master thesis, Kochi University of Technology (*in Japanese*).
- Okamoto G. (2005). "Basic development of interferometer system in radio meteor observation". Bachelor thesis, Kochi University of Technology (*in Japanese*).
- SonotaCo (2009). "A meteor shower catalog based on video observations in 2007-2008". *WGN, Journal of the IMO*, **37**, 55–62.
- Yamamoto M.-Y., Ishihara Y., Hiramatsu Y., Kitamura K., Ueda M., Shiba Y., Furumoto M. and Fujita K. (2011). "Detection of Acoustic/Infrasonic/Seismic Waves Generated by Hypersonic Re-Entry of the HAYABUSA Capsule and Fragmented Parts of the Spacecraft". *Publications of the Astronomical Society of Japan*, **63**, 971–978.
- Wayne E. E., Brown P. G., Weryk R. J. and ReVelle D. O. (2008). "Infrasonic Observations of Meteoroids: Preliminary Results from a Coordinated Optical-radar-infrasound Observing Campaign". *Earth, Moon, and Planets*, **102**, 221–229, DOI: 10.1007/s11038-007-9154-6.
- Yamasaki T. (2012). "Improvement of the KUT radio meteor observation system and development of meteor trajectory measurement method based on 5-channels interferometer and multi-site observation". Master thesis, Kochi University of Technology (*in Japanese*).

# Flux density, population index, perception coefficient, and the Moon

Sirko Molau

Abenstalstr. 13b, 84072 Seysdorf, Germany  
sirko@molau.de

While analyzing sporadic meteors recorded by the IMO Video Meteor Network in the first half of 2015 we found systematic variations of the flux density and population index correlating with the lunar phase. At times of Full Moon, the measured flux density is 15% smaller than average, and at New Moon 15% higher. Likewise, the measured population index is 10% larger than the average at New Moon, and 10% smaller at Full Moon. While searching for the root cause of this systematic bias we analyzed two parameters in detail. If a perception coefficient is calculated and applied to each camera, the scatter in flux density can be reduced by 40% and the population index shows fewer outliers. However, the correlation with the lunar phase remains unaltered. Another parameter in question is the *NoiseLevel* segmentation threshold, which is applied when segmenting a background image for stellar limiting magnitude calculation. It could be shown that this threshold did not converge to a stable solution in the previous implementation of *MetRec*. An improved procedure is proposed, analyzed and implemented. Whether this solves the lunar phase correlation can only be answered when sufficient observations with the new software version are collected.

## 1 Introduction

The scientific focus of the IMO Video Meteor Network (Molau, 2001) has shifted at the end of the last decade. Originally the primary goal was to collect a sufficient amount of meteors to determine base meteor shower properties like the radiant position, radiant drift, activity interval and peak time. We also conducted automated searches for known and new meteor showers and confirmed the detection of meteor showers by other teams. Thanks to the large data set of over a million single station meteors, we were highly successful in this respect (Molau, 2013).

Starting from 2010 the *MetRec* software could automatically determine the limiting magnitude in the field of view, which opened new perspectives in meteor shower research. At first we could determine meteor shower flux densities, and later also population indices (Molau, 2014). With these values we are able to

determine other important characteristics of meteoroid streams like the overall particle density, the particle size distribution and fine structures like dust trails.

After five years of measuring flux densities we can conclude, that looking from a high level perspective we can distinguish between “well-behaved” and “erratic” meteor showers. “Well-behaved” showers present effectively the same activity profile every year, so that the segments of the individual years form a smooth overall profile. A fine example are the Lyrids (*Figure 1*). “Erratic” showers, on the other hand, show every year a different activity profile – either with respect to the peak time or to the activity level. The Quadrantids are an example for the latter category (*Figure 2*).

Even though “well-behaved” showers confirm the consistency of the flux density determination, it is worthwhile to check the quality of the result and look for

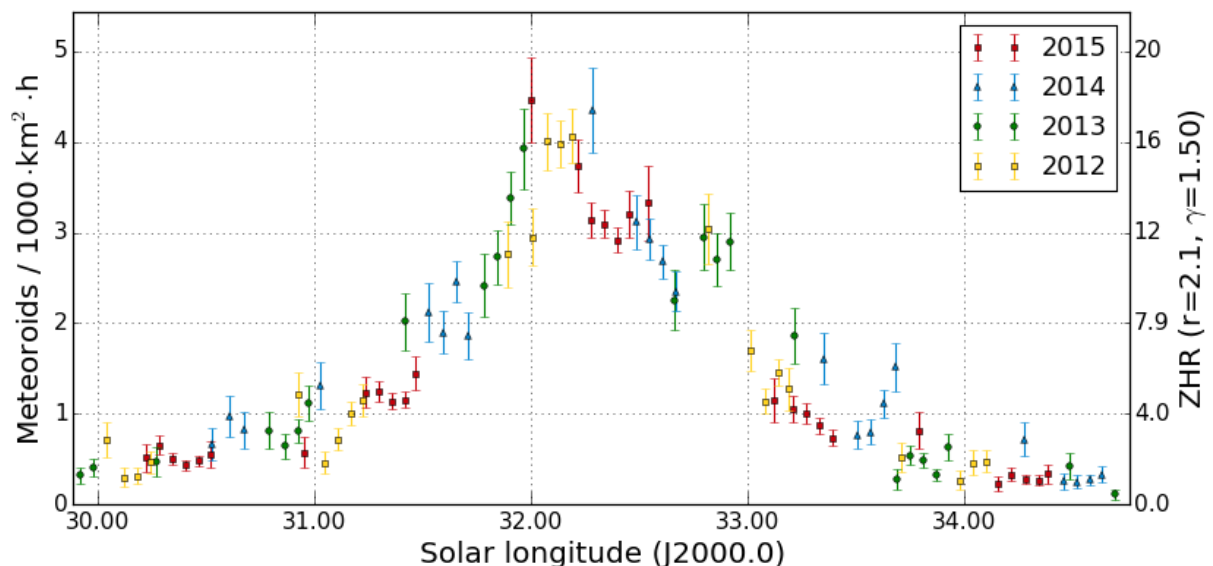


Figure 1 – Activity profile of the Lyrids, obtained from IMO Network video observations 2012–2015.

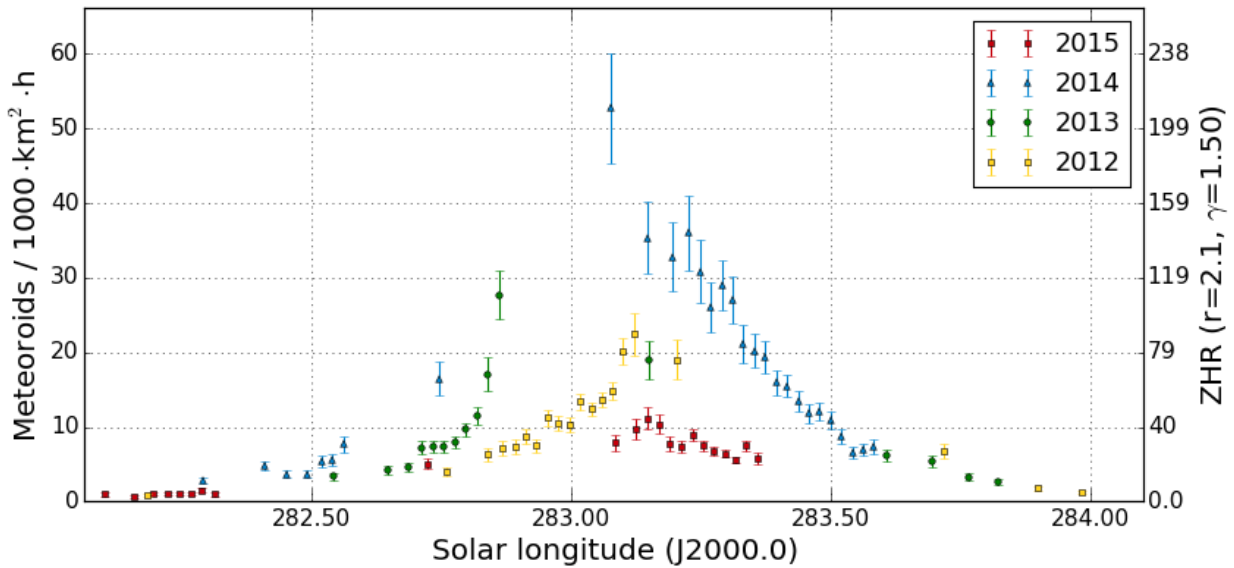


Figure 2 – Activity profile of the Quadrantids, obtained from IMO Network video observations 2012–2015.

possible systematic error sources. For this reason, we analyzed in detail the sporadic meteors in the IMO network data of the first half of 2015. Under the assumption, that both the sporadic flux density and the sporadic population index are about constant in the first half of a year (at least over shorter time scales of days to weeks) and that there is no dilution by major meteor showers, we took this data set as reference and checked for the short- and long-term variations.

## 2 Correlation with the lunar phase

On the first glimpse, the flux density shows some random scatter around the average value of 20, but also some long term trend is visible (Figure 3). If a sliding five-days mean is applied to remove scatter, the trend becomes very clean (Figure 4): The flux density follows some sine-shaped pattern which is correlated with the lunar phase. At times of Full Moon the flux density is about 15% higher than average and at New Moon about 15% lower.

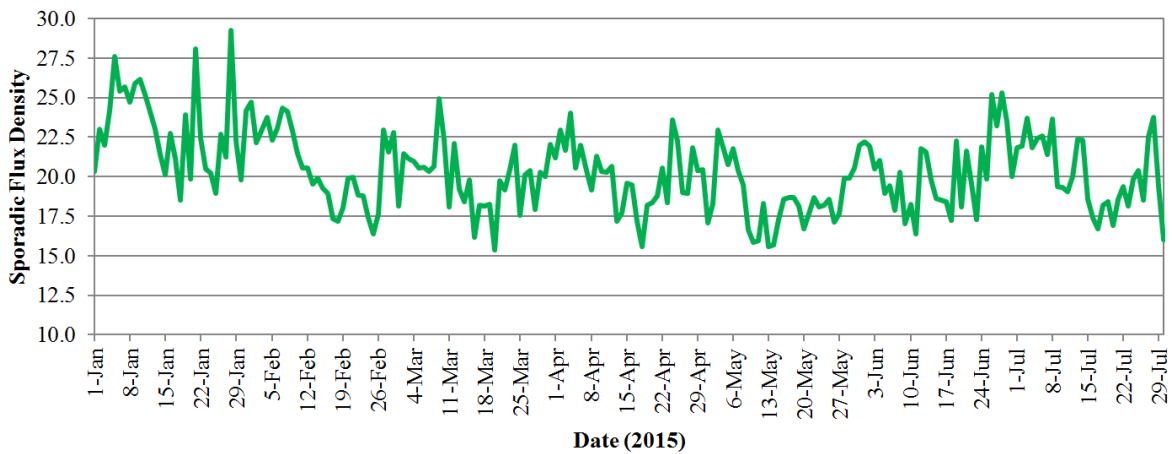


Figure 3 – Sporadic flux density in the first half of 2015, obtained from IMO network data.

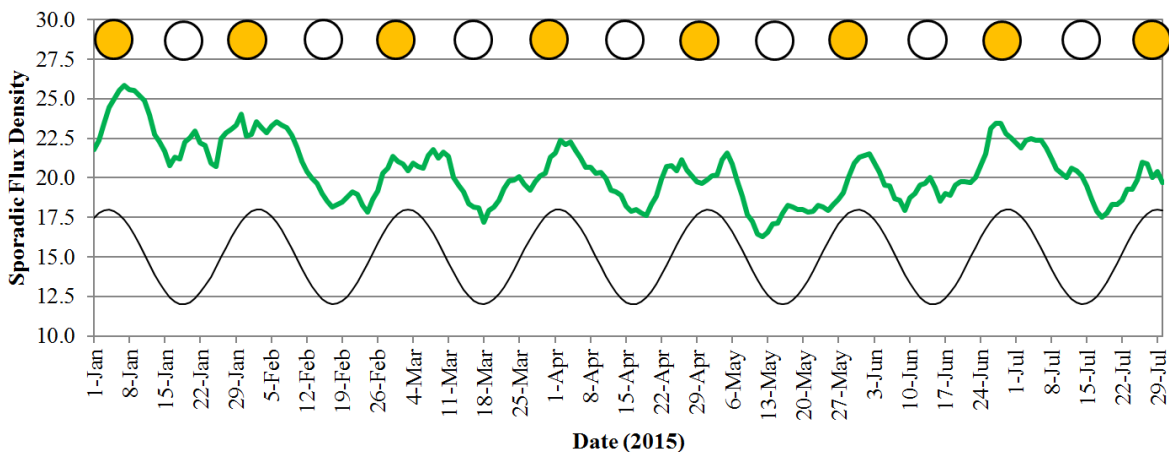


Figure 4 – Sporadic flux density in the first half of 2015, smoothed by a five-days sliding mean. The times of Full and New Moon and a sine curve representing the lunar phases are shown as well.

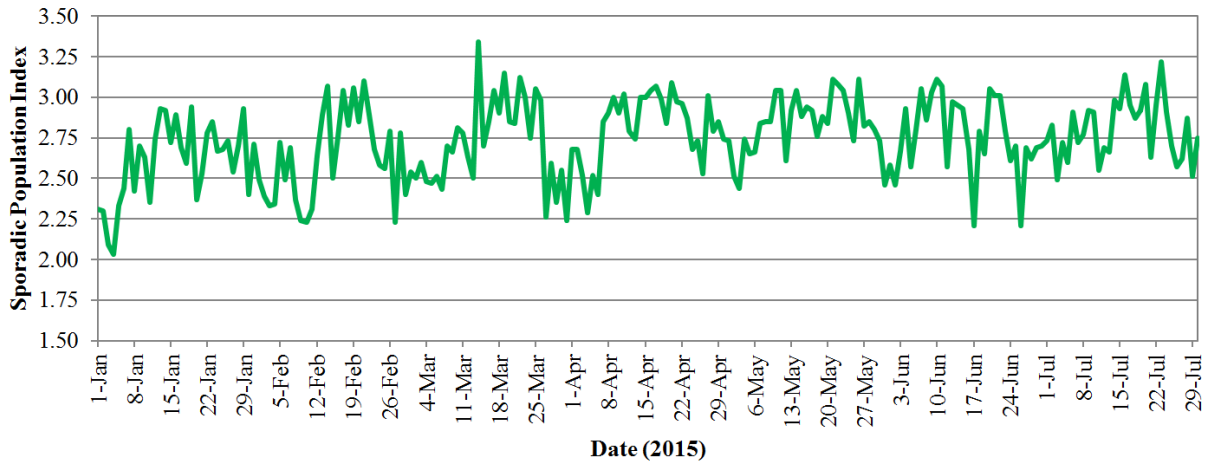


Figure 5 – Sporadic population index in the first half of 2015, obtained from IMO network data.

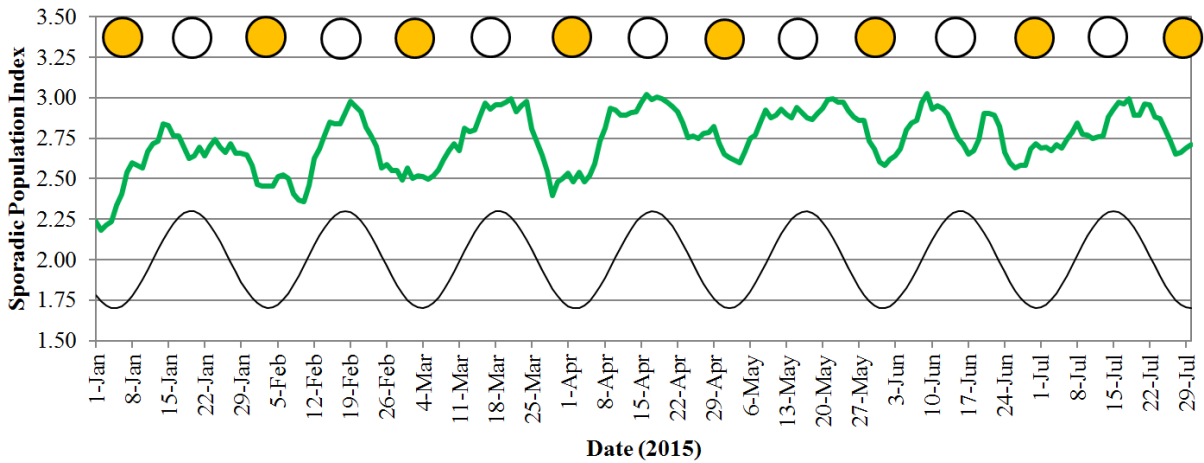


Figure 6 – Sporadic population index in the first half of 2015, smoothed by a five-days sliding mean. The times of Full and New Moon and a sine curve representing the lunar phases are shown as well.

The same effect can be observed for the population index (Figure 5): If the graph is smoothed with a five-days sliding mean, a sine-shaped profile with peak values about 10% above the average at New Moon and about 10% below the average at Full Moon is obtained (Figure 6).

So there must be some systematic bias in the calculation of the flux density and population indices.

### 3 Discussion

The limiting magnitude is the most delicate parameter in the determination of the flux density and population index. All other parameters (meteor count, collection area, observing time) can be determined easily from video data. Since the cyclic variations are correlated with the lunar phase (Figure 7), it can be assumed that they are caused by different night sky illumination, which would be directly linked to the limiting magnitude determination. However, a simple dependency can be ruled out. If, for example, the limiting magnitude of the more powerful cameras would be systematically over- or underestimated, this would result in a constant shift in flux density and population index, but it would not change with the lunar phase. In fact, both the limiting magnitude for stars and the meteor detection is based on the same principle. They determine the faintest object which is barely above the noise level. So if the

background brightness or the noise level changes, both the stellar limiting magnitude and the meteor detection should be affected in the same way and systematic deviations should cancel each other out.

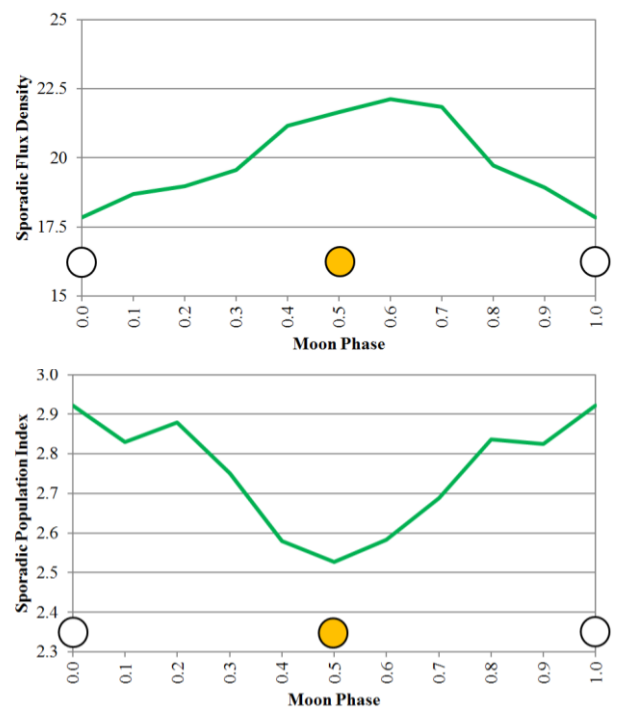


Figure 7 – Dependency of the sporadic flux density (top) and population index (bottom) from the lunar phase.

Let's consider some facts about the limiting magnitude and population index calculation:

- Lower flux densities at New and higher flux densities at Full Moon imply that either the limiting magnitude under dark skies is generally overestimated or the limiting magnitude under poor skies is generally underestimated or both.
- Higher r-values at New and lower r-values at Full Moon imply that the difference in limiting magnitude between powerful and weak cameras under dark skies is underestimated or under poor skies is overestimated or both.
- Generally speaking, the limiting magnitude calculation should be more precise under clear skies, for powerful cameras and for cameras with small field of view, because more stars can be identified in these cases and the field of view is more uniform.

Beside possible algorithmic shortcomings, the observed correlation with the lunar phase could also be caused by technical or physical properties of the camera, like automatic adaptation of camera gain or integration time with changing background brightness, or non-linear response of CCD chips at low light levels. There are indeed observations which hint on such technical or physical reasons:

- Contrary to human observers, video cameras sometimes perform better under light polluted than under real dark skies. An explanation could be that the CCD pixel requires some minimum illumination before it creates a measurable signal and reaches the linear response regime.
- We observed that some cameras report a consistently increasing limiting magnitude at dusk and dawn when the background is getting bright and the limiting magnitude should break down (Figure 8).

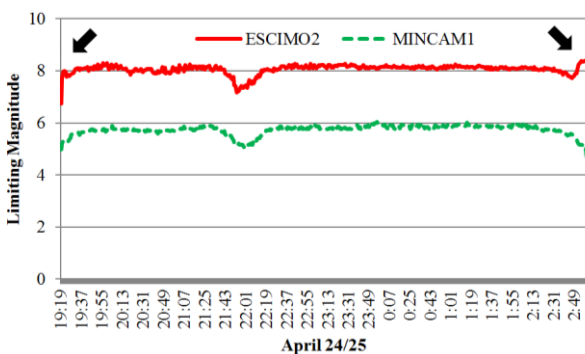


Figure 8 – Stellar limiting magnitude of MINCAM1 and ESCIMO2 in the course of one April night in 2015. Whereas the limiting magnitude of MINCAM1 breaks down at dusk and dawn as expected, it increased temporarily for ESCIMO2.

### 4 Perception coefficient

The perception coefficient is a well-known concept in visual observation (Koschack and Rendtel 1990). Two observers may have the same stellar limiting magnitude, but one of them reports regularly higher meteor counts than the other. The reason is that the observers perform

different in detecting faint stationary (stars) and moving (meteor) objects. Such an effect would in theory not be expected for video cameras, because all relevant parameters are determined in the same fashion over all cameras, and also the meteor detection routine is identical. Still, when the mean flux density for each camera is plotted for the first half of 2015, we find significant deviations (Figure 9, top). The different perception coefficient can be interpreted and corrected as a camera-specific fixed offset to the determined stellar limiting magnitude (Figure 9, bottom).

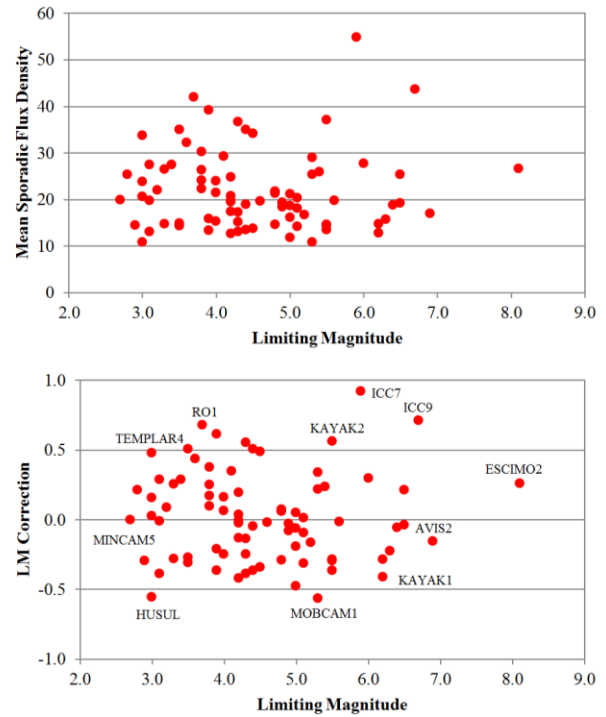


Figure 9 – Mean sporadic flux density (top) and the perception coefficient expressed as limiting magnitude correction (bottom) for individual cameras of the IMO Network between January and July 2015.

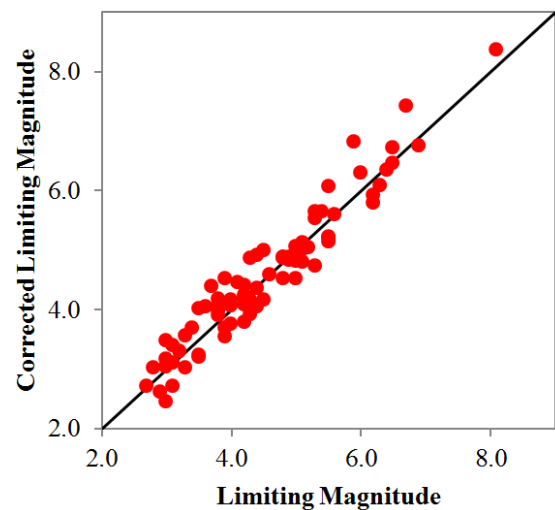


Figure 10 – Dependency of the perception coefficient (i.e. the corrected stellar limiting magnitude) from the absolute stellar limiting magnitude of a camera.

The offset is independent of the absolute limiting magnitude of the camera (Figure 10) and it has a positive effect when applied to the video data. The scatter in the

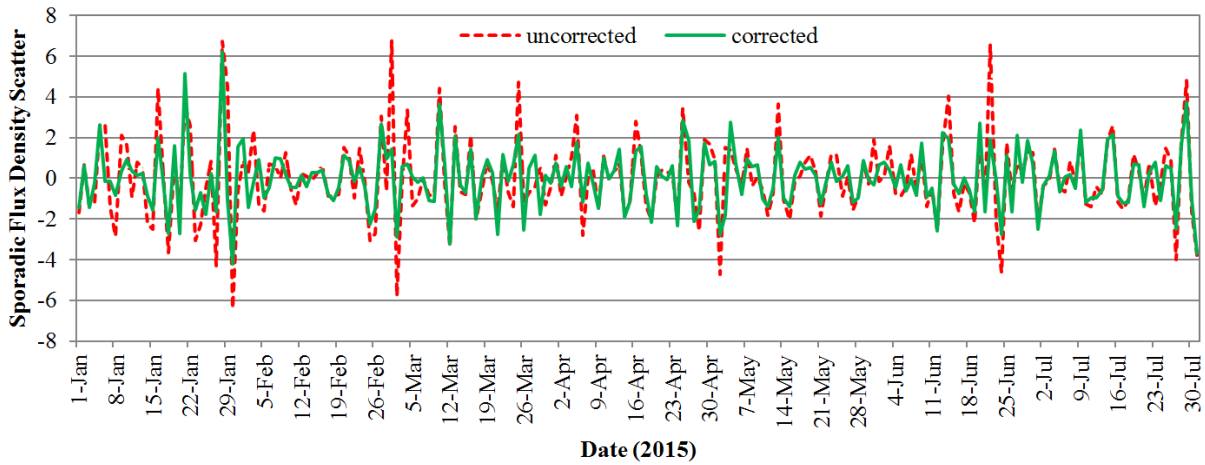


Figure 11 – Sporadic flux density in the first half of 2015 with and without perception coefficient correction.

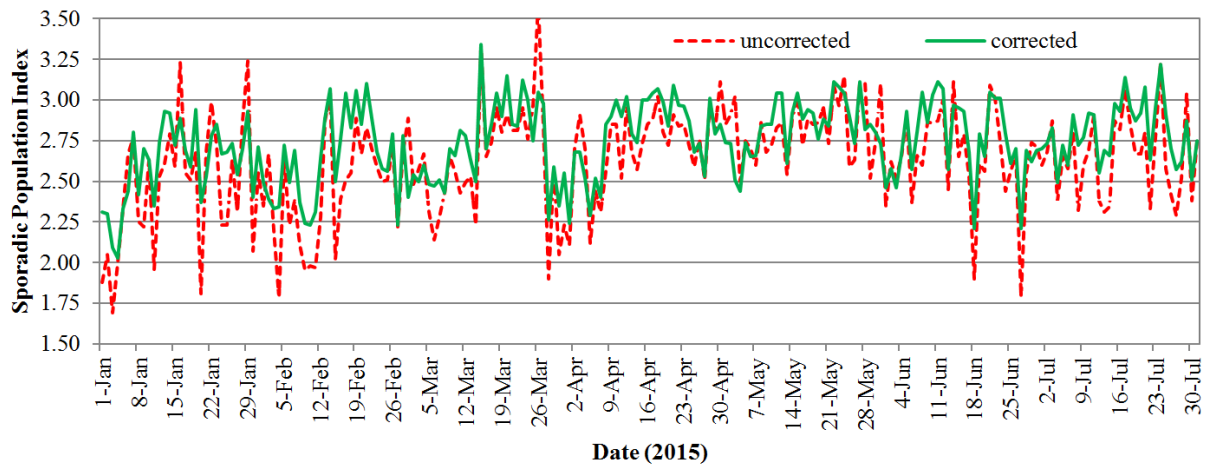


Figure 12 – Sporadic population index in the first half of 2015 with and without perception coefficient correction.

sporadic flux density is reduced by 40% (Figure 11) and the population index profile shows a minor shift towards higher r-values and a reduced number of outliers (Figure 12).

However, the lunar phase correlation cannot be explained or removed by introducing a perception coefficient for video cameras.

### 5 NoiseLevel

The *NoiseLevel* is a specific threshold in the meteor detection routine. Most if not all meteor detection software will have this parameter in one or the other way (in *MetRec* it is called “*NoiseLevel*”), but a systematic shift of this threshold has no impact on astrometry or photometry. However, it plays a vital role in the limiting magnitude and thereby also the flux density and population index calculation.

So what is this threshold used for? When stars are to be identified in the field of view, an averaged background image (Figure 13) is pre-processed in some way (e.g. by a high-pass filter) and then a threshold is applied to differentiate between stars and background noise. This *NoiseLevel* parameter determines how many objects are

segmented. The lower the threshold, the more objects are isolated and the larger is the number of identified stars later on. When the parameter is increased, fewer noise pixels become visible, but also fewer real stars (Figure 14). Since the limiting magnitude is derived from the number of identified stars (similar to star field count in visual observation), this segmentation threshold has a direct impact on the calculated stellar limiting magnitude.

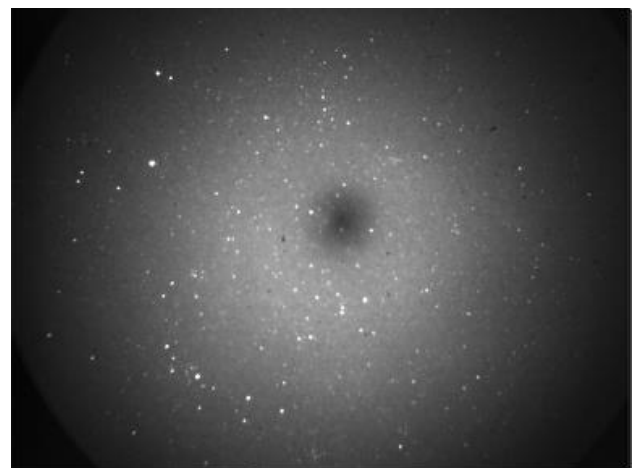


Figure 13 – An averaged background image is the basis for the stellar limiting magnitude calculation.

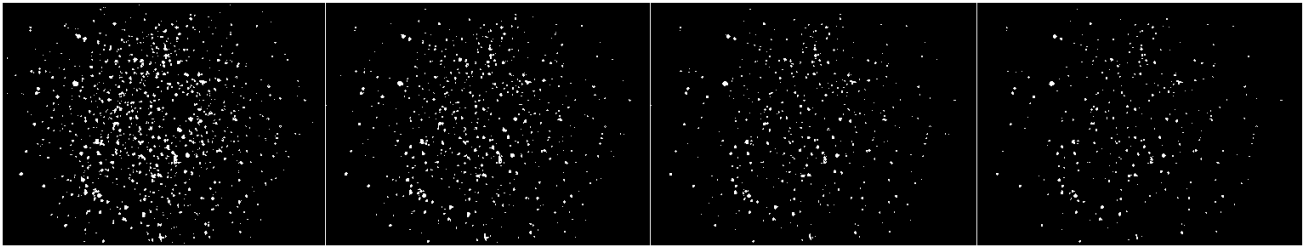


Figure 14 – Depending on the segmentation threshold (which increases from left to right), fewer and fewer objects are segmented for star identification.

The segmentation threshold cannot be fixed, because it depends on the variance per pixel and varies from camera to camera, from night to night and sometimes even within one night. So the threshold has to be adapted dynamically according to some optimization criterion. In practice, the number of false detections in the segmented image is used as criterion, i.e. the *NoiseLevel* parameter is adapted in an iterative fashion (every minute) such, that a defined number of false detections (i.e. pixels that cannot be identified as stars) are visible in the segmented background image. Hot pixels are removed from the list beforehand.

Originally the target number of false detection was correlated to the number of identified stars, i.e. the more stars were identified, the more false detections were allowed. However, it turned out that this empirical choice was a bad one, because for different start values the *NoiseLevel* parameter converged to different residual values resp. limiting magnitudes. That was demonstrated with a 15 minutes test video which was analyzed by *MetRec* several times with different settings (Figure 15). In fact, the uncertainty in stellar limiting magnitude after 15 minutes was still of the order of 0.5 mag.

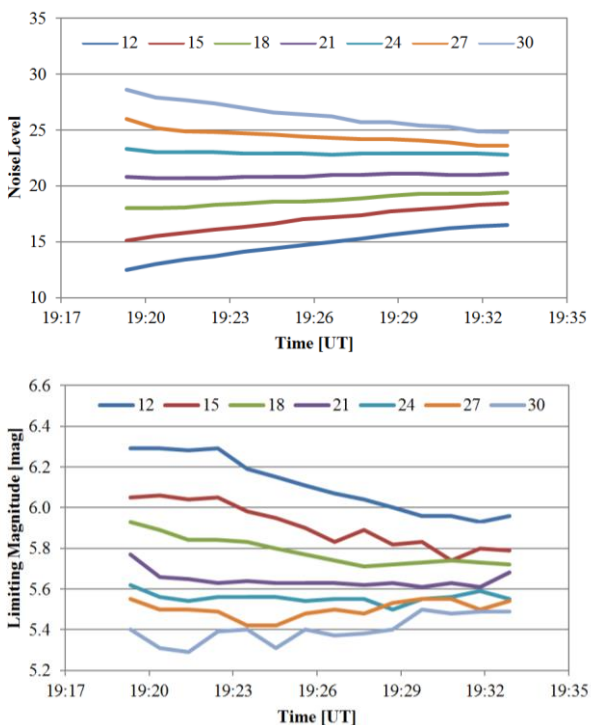


Figure 15 – Conversion of the *NoiseLevel* segmentation threshold (top) and the corresponding stellar limiting magnitude (bottom) for different *NoiseLevel* start values.

Better test results were achieved when the target number of false detection was fixed. In order to account for different sizes of field of view (*PAL* vs. *NTSC*, cameras with and without obstruction), the target number of false detections was fixed as 0.04% of the overall number of active pixels. That clearly improved the convergence of the *NoiseLevel* segmentation threshold, but the limiting magnitude still varied by about 0.2 mag after 15 minutes (Figure 16).

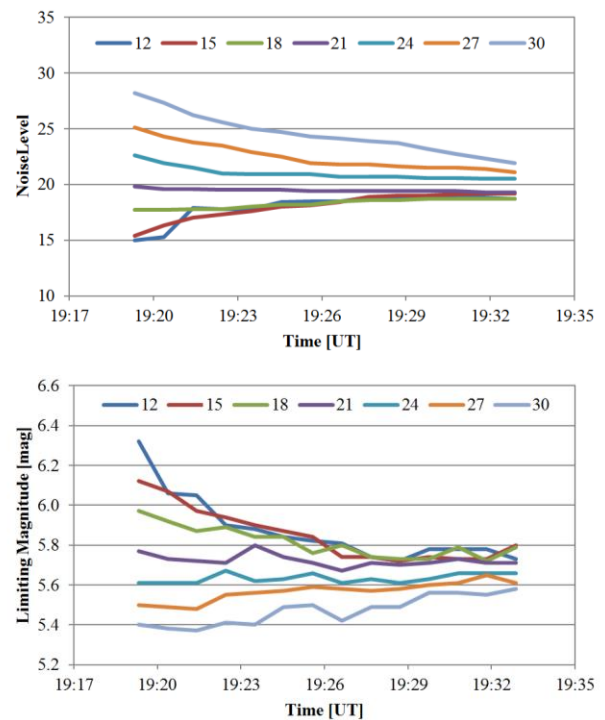


Figure 16 – Conversion of the *NoiseLevel* segmentation threshold (top) and the corresponding stellar limiting magnitude (bottom) with a fixed target percentage of false detections.

The reason is that the update function (Figure 17, top) for the iterative adaptation of the *NoiseLevel* threshold had to be quite shallow near the target number of false detections. That is, when the measured number of false detection was close to the target value, the *NoiseLevel* parameter was adapted by only a very small amount. That is necessary to prevent oscillations of the *NoiseLevel* segmentation threshold, which had been observed in the past.

To circumvent this problem, the update function was made asymmetric now (Figure 17, bottom). If the number of false detection is too small, the *NoiseLevel* parameter will be adapted by a large amount in a linear fashion. In

the opposite direction, the same smooth update function is applied as before. Oscillations cannot occur in this configuration, because a possible over-correction would take place in only one direction.

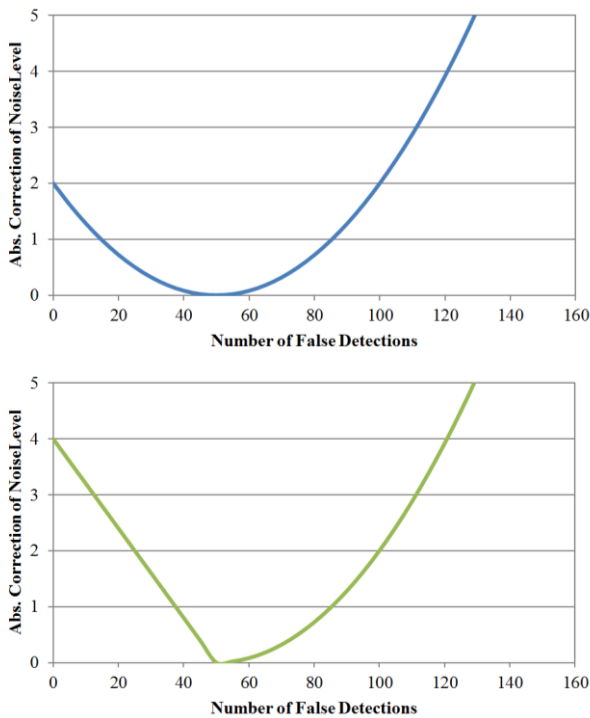


Figure 17 – Absolute value of the update function of the *NoiseLevel* parameter depending on the measured number of false detection. In this example the target value is 50. At the top the original symmetric update function is shown, at the bottom the new asymmetric function.

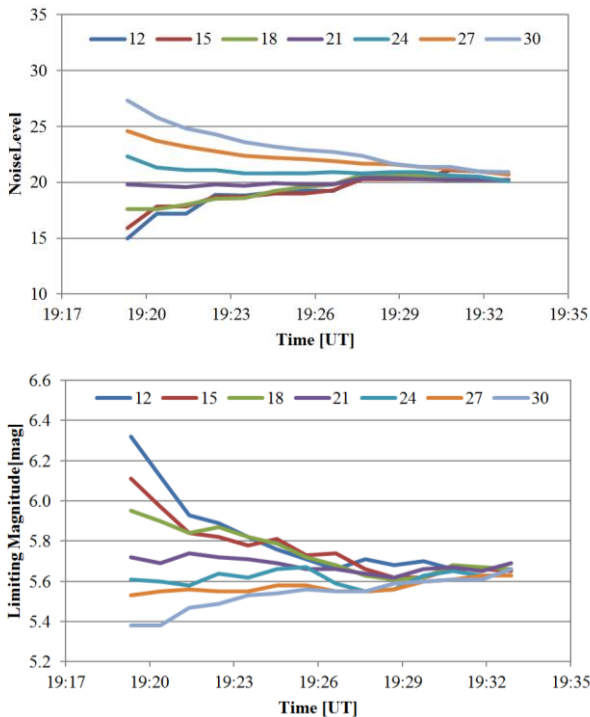


Figure 18 – Convergence of the *NoiseLevel* segmentation threshold (top) and the corresponding stellar limiting magnitude (bottom) with a fixed percentage of false detections and an asymmetric update function.

As can be clearly seen in *Figure 18*, both the *NoiseLevel* segmentation threshold and the stellar limiting magnitude converge now much faster to a single value. The

uncertainty is smaller than 0.1 mag in the end. However, to find out if the improved settings for *NoiseLevel* will indeed reduce or remove the observed correlation with the lunar phase requires real video data collected with the new software version.

## 6 Conclusion

We have shown that the IMO Video Meteor Network provides reliable measures for flux density and population index, but some unknown systematic bias causes a clear correlation with the lunar phase. Introducing the perception coefficient for video cameras reduced the scatter in the results significantly but did not remove the correlation. Improving the limiting magnitude calculation by adjusting the update function and the target value for the *NoiseLevel* segmentation threshold is another promising step. Here we will only know from real observation using the adapted algorithm if this solves the issue with the lunar phase correlation.

## Acknowledgment

We are in great debt to all observers of the IMO Video Meteor Network, which collected over years a unique database of video meteors and provided the input for this analysis.

## References

Koschack R. and Rendtel J. (1990). “Determination of Spatial Number Density and Mass Index from Visual Meteor Observation (II)”. *WGN, Journal of the IMO*, **18**, 119–140.

Molau S. (2001). “The AKM Video Meteor Network”. In Warmbein B., editor, *Proceedings of the Meteoroids 2001 Conference*, 6-10 August 2001, Kiruna, Sweden. ESA SP-495, Noordwijk, ESA Publications Division, pages 315–318.

Molau S. (2013). “Meteor showers identified from one million video meteors”. In Gyssens M., Roggemans P. and Zoladek P., editors, *Proceedings of the International Meteor Conference*, Poznan, Poland, 22-25 August 2015. IMO, pages, pages 26–38.

Molau S., Barentsen G. and Crivello S. (2014). “Obtaining population indices from video observations of meteors”. In Rault J.-L. and Roggemans P., editors, *Proceedings of the International Meteor Conference*, Giron, France, 18-21 September 2014. IMO, pages 74–79.

# Current progress in the understanding of the physics of large bodies recorded by photographic and digital fireball networks

Manuel Moreno-Ibáñez<sup>1,2</sup>, Maria Gritsevich<sup>2,3,4</sup>, Josep Ma. Trigo-Rodríguez<sup>1</sup>  
and Esko Lyytinen<sup>4</sup>

<sup>1</sup>Institute of Space Sciences (IEEC-CSIC), Meteorites, Minor Bodies and Planetary Science Group,  
Campus UAB, Carrer de Can Magrans, s/n E-08193 Cerdanyola del Vallés, Barcelona, Spain  
mmoreno@ice.csic.es, trigo@ice.csic.es

<sup>2</sup>Finnish Geospatial Research Institute, Geodeetinrinne 2, FI-02431 Masala, Finland

<sup>3</sup>Institute of Physics and Technology, Ural Federal University, 620002 Ekaterinburg, Russia  
gritsevich@list.ru

<sup>4</sup>Finnish Fireball Network, Helsinki, Finland  
esko.lyytinen@jippii.fi

The basic equations of motion of a meteor in the atmosphere require a concise knowledge about the body physical properties, such as the bulk density, shape, mass, etc. These properties do change during the flight and they also depend on the observations' reliability and camera resolution. The usual way of tackling this problem relies on using average values which are retrieved either from previous experience or from the observations available from the astrometric reduction of each specific event. Alternatively, a different approach is suggested. Instead of using the average values as input data, all unknowns can be gathered into dimensionless parameters, retrievable from the observations with the help of inverse techniques. This methodology has already been implemented in several scientific studies. In order to demonstrate the applicability of the model, we have already used archived data from the *Meteorite Observation and Recovery Project (MORP)* operated in Canada between 1970 and 1985 as well as selected recent fireball records from the Spanish Fireball and Meteorite Recovery (SPMN) Network. Recently, a correction which accounts for real atmosphere conditions has also been successfully included in the model. Our next steps foresee fireball data processing obtained by the Finnish Fireball Network (FFN) and the SPMN.

## 1 Introduction

The study of meteoroids interacting with the Earth's atmosphere relies on both, the observations and the mathematical modelling. Current ground based observations consists of a distribution of photographic and video cameras managed by local entities or national institutions. Observations usually provide meteor atmospheric trajectory data, height and velocity ( $h, v$ ); in some cases, for equipped instrumentation, spectroscopy data is released as well. Due to weather conditions and/or individual camera resolution, the observation accuracy is affected and data pre-analysis treatment is normally required. Meteor physical properties and flight dynamic behavior can be derived from well adjusted ( $h, v$ ) data (see Ceplecha et al., 1998 for a detailed review) Initial meteor mass, terminal height, ablation, etc., are essential properties for further meteor science. Since Hoppe (1937) elaborated a strong mathematical formulation for these phenomena (known as Single body theory or classical theory), it has been extensively used in common meteor studies. This formulation relies on considering as constant a series of flight variables which cannot be known beforehand and cannot be obtained directly through observations. In addition, other input flight parameters required in the formulation are assumed to be the median values of previous studies, for instance the bulk meteor density is usually introduced in the equations of motion as a fixed value which depends on the assumed

meteor classification. Other relevant assumption is the atmospheric model required to solve the equations. An exponential atmospheric model behavior does work fairly well and leads to good results. However, the atmosphere conditions vary with time, location and height; thus, in some events this should be taken into account. Due to the large number of unknowns required by the classical theory, the resolution of the equations and the results shall be treated with care and extreme attention. Slight modifications in any parameter may lead to different results.

Alternatively, the introduction of scale laws and dimensional study in the mathematical formulation can overcome these problems. Based on this, lead Stulov et al. (1995), Stulov (1997) and Gritsevich (2007) suggested a new way of resolving the equations of motion. As we will see later on this paper, their methodology reduces the number of unknowns down to two, which still show physical meaning. These two new parameters ( $\alpha$  and  $\beta$ ) are easily retrievable from ( $h, v$ ) data in most of the cases. On top of that, recent studies have succeeded in introducing alternative atmospheric models in this new mathematical formulation.

In this paper we will take an overlook to this recent methodology and its applicability. The mathematical

formulation will be described in *Section 2*. We will show the state-of-the-arts on this methodology in *Section 3*. In *Section 4* we will discuss its capabilities and show further utilities. Finally, we will go through the main conclusions in *Section 5*.

## 2 Mathematical formulae

The equations of the meteor atmospheric motion are well known and are usually projected to the tangent and normal of the trajectory (Gritsevich, 2007):

$$M \frac{dV}{dt} = -\frac{1}{2} c_d \rho_a V^2 S \quad (1)$$

$$\frac{dh}{dt} = -V \cdot \sin \gamma \quad (2)$$

$$H^* \frac{dM}{dt} = -\frac{1}{2} c_h \rho_a V^3 S \quad (3)$$

In order to solve the system (1-3) extra equations are required. On the one hand the relationship between the instant meteor mass and dragging surface is considered:  $S/S_e = (M/M_e)^\mu$ , where  $\mu$  expresses the rotation of the meteor during the flight. On the other hand, as stated previously, the atmosphere is usually considered as isothermal:  $\rho/\rho_0 = \exp(-h/h_0)$ , where  $\rho_0$  is the atmospheric density at sea level and  $h_0 = 7.16 \times 10^3$  m is the scale height.

Introducing dimensionless variables ( $M = M_e m$ ,  $V = V_e v$ ,  $h = h_0 y$ ,  $S = S_e s$  and  $\rho_a = \rho_0 \rho$ ) and solving the resulting equations with the conditions  $y = \infty$  and  $v = 1$  (for details see Gritsevich (2007) :

$$m = \exp[-(1 - v^2)\beta/(1 - \mu)] \quad (4)$$

$$y = \ln 2\alpha + \beta - \ln \Delta,$$

$$\Delta = \bar{E}_I(\beta) - \bar{E}_I(\beta v^2) \quad (5)$$

Where  $\bar{E}_I(x) = \int_{-\infty}^x \frac{e^t}{t}$ .

The resolution of these equations depends on two new variables. The parameter  $\alpha$  is related to the drag intensity suffered by the meteor during its flight. It is called the ballistic coefficient and can be expressed as:

$$\alpha = \frac{1}{2} c_d \frac{\rho_0 h_0 S_e}{M_e s \sin \gamma} \quad (6)$$

The mass loss parameter characterizes the ablation of the meteor. It can be expressed as the fraction of the kinetic energy of the unit mass of the body that is transferred to the body in the form of heat divided by the effective destruction enthalpy:

$$\beta = (1 - \mu) \frac{c_h V_e^2}{2 c_d H^*} \quad (7)$$

The derivation of parameters  $\alpha$  and  $\beta$  is done via a least squared method which adjusts (5) with the (h,v) data

retrieved from the observations (see Gritsevich, 2007, for further details). In principle, at least three (h,v) points, including the entry velocity, are required to derive  $\alpha$  and  $\beta$ .

## 3 State-of-the-art

This methodology was first implemented by Gritsevich (2008). She used the (h,v) data for four well known meteorite recoveries in order to discuss the accuracy of the methodology. This first study did also remark that, similarly to the classical theory, this recent methodology finds difficulties when meteor fragmentation is significantly present in the atmospheric flight.

Gritsevich (2009) derived  $\alpha$  and  $\beta$  parameters for 143 objects from the *Meteor Observation and Recovery Project* (MORP, Canada) and 121 objects from the Prairie Network (PN) database. This allowed the first large classification of fireballs and meteorites using accurate parameters. As can be seen in *Figure 1*, meteorites (Innisfree, Lost City, Annama and Neuschwanstein) fall in a defined distant region of the diagram compared to the rest of fireballs. The location of the few Taurids registered in the PN database is also plotted. These carbonaceous chondrites mostly fall in another delimited area of the diagram. Thus, it seems that this methodology probes to be useful to set up a new classification based on this new accurate parameters.

Gritsevich and Koschny (2011) included this dimensionless methodology when they tried to constrain the percentage of meteor kinetic energy emitted as light. This allowed them to include the meteor mass and velocity variations avoiding further assumptions on meteor bulk density, shape and initial mass.

Later on, Moreno-Ibáñez et al. (2015) studied the efficiency of simplifications of the equations (4, 5) to describe accurately the terminal height of fireballs and meteorites. A global standard deviation of 0.75 km between observed and derived terminal heights was achieved when approximated functions were introduced in the simplified solutions.

Finally, Lyytinen and Gritsevich (2016) suggested the way to successfully incorporate different atmospheric models in the dimensionless equation of motion. Using detailed height and atmospheric pressure probes to increase accuracy. If possible, local weather station information should be used. However, for most of meteor observations these data are not available. Detailed models such as the International Standard Atmosphere (ISA) model or MSIS-E-90 could also provide good results. A revised mathematical formulation should be done when real atmospheric conditions are to be considered (see Lyytinen and Gritsevich, 2016). Otherwise, for detailed atmospheric models, the exponential atmospheric model is still valid as long as individual heights are corrected for appropriate pressure values.

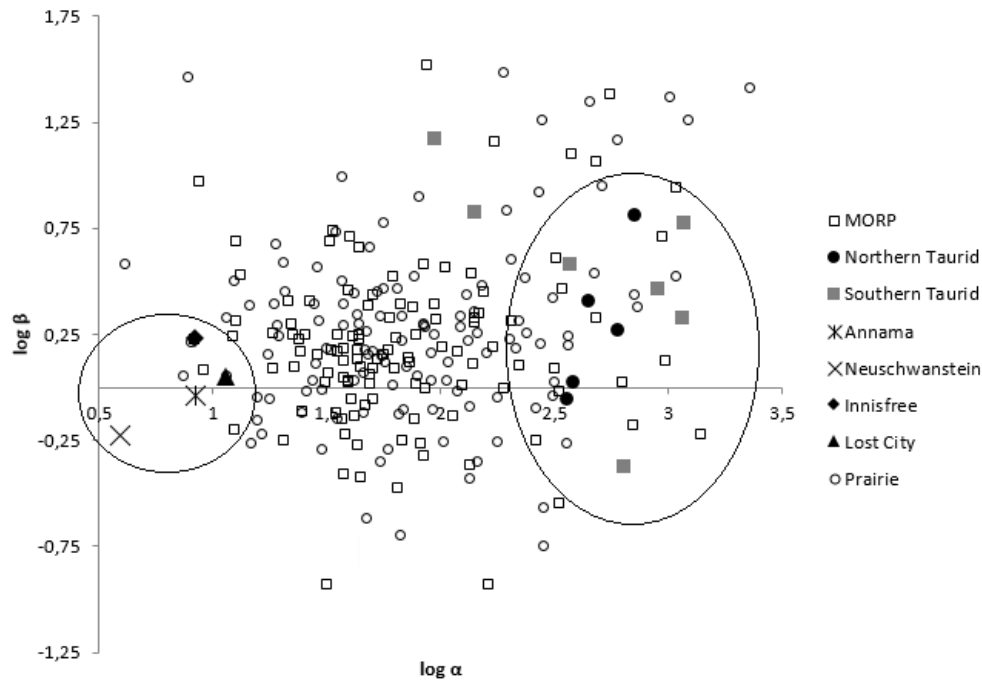


Figure 1 – Diagram showing the combination of  $\text{Log}\alpha$  and  $\text{Log}\beta$  for MORP and PN database events based on Gritsevich et al. (2012), where the few Taurids registered by the PN are marked separately. We have also printed those values for Annama, Innisfree, Neuschwanstein and Lost City meteorites. Circles mark clearly different regions on the diagram for meteorites and the Taurids shower.

#### 4 Discussion and further utilities

The use of scaling laws and dimensionless variables in the meteor equations of motion lead Stulov et al. (1995), Stulov (1997) and Gritsevich (2007) to reduce the number of unknown variables down to two parameters,  $\alpha$  and  $\beta$ . These parameters can be explained physically and, given that they are directly obtained by a least squared adjustment of the observational data, their accuracy mainly depends on that of the observations (thought the number of  $h, v$  points recorded and the part of the trajectory they represent is also relevant). This is also very convenient to set up new reliable classifications. We have printed in Figure 1 the few Taurids present within the Prairie Network data. The graphic expands results previously shown in (Gritsevich et al., 2012). In particular, it also demonstrates how the combination of  $\alpha$  and  $\beta$  parameters for the Taurids remarkably differs from those of recovered meteorites.

The inclusion of different atmosphere models is quite straightforward in this methodology compared to the single body theory, and provides more accurate results. This is quite helpful when dealing with extensive databases or particularly difficult events where atmospheric conditions could be crucial to determine further flight parameters.

Furthermore, the dimensionless methodology has proved to adequately describe individual flight parameters. The terminal height is considered a key parameter that helps understanding the deceleration suffered by the meteor. An accurate derivation of its value from the mathematical formulae not only increases chances of any suitable meteorite recovery, but it also gives the opportunity of solving the inverse problem: obtaining the  $\alpha$  and  $\beta$

parameters from complicated observations where maybe the last part of the fireball trajectory was recorded. Besides, other relevant parameters such as the ending mass or the ablation coefficient, are easily derived from  $\alpha$  and  $\beta$ .

The utilities of this new approach are various and most of them are still to be studied. For example, the time dependency of some final parameters (such as terminal height) could be used in the inverse problem to estimate the time length of the meteor flight. Systematic studies are also very convenient for these methodology, which will ultimately increase statistics and, hence, scientific knowledge. For instance, we foresee the derivation of  $\alpha$  and  $\beta$  values for the Spanish Meteor Network (SPMN) and the Finnish Fireball Network (FFN) databases.

The SPMN scans the sky of the Iberian Peninsula either at day or night. Since its official kick off in 1997 (see Trigo et al., 2004; Madiedo and Trigo-Rodríguez, 2008), the cooperation between scientists and amateurs, along with fully equipped instrumentation (CCD all sky cameras, video cameras, photographic cameras, and spectrographs) and self-developed software have led to the registration of numerous fireballs and two meteorites: Villalbeto de la Peña ordinary chondrite and Puerto Lápice eucrite (e.g. Trigo-Rodríguez et al., 2006). Similarly, FFN spreads over Finland and neighboring countries in about 400000 km<sup>2</sup> and does also rely on the co-work of amateur astronomers and scientists (Gritsevich et al., 2014). The initial operational start was in 2002 and it counts on the already mentioned instrumentation and their own software too (e.g. Lyytinen and Gritsevich, 2013). One of the latest cooperation between both networks led to the recovery, orbit

determination and parental relationship of the Annama H5 chondrite (Trigo-Rodríguez et al., 2015).

## 5 Conclusions

The methodology reviewed in this paper has proved to work efficiently and accurately. Parameters  $\alpha$  and  $\beta$  show physical meaning and are potentially the basis of a new fireball and meteorite classification.

The mathematical formulation is flexible enough so as to include different atmospheric models or real data provided by local weather stations. Besides, relevant meteor atmospheric flight parameters are easily derived from the main equations. Simplifications of the equations are also possible, and the accuracy of their results have already been checked.

Future applications and improvements of this methodology are being studied. Problems such as fragmentation will require more study to be overcome. Finally, far from being opposite, the combination of both methodologies, classical and dimensionless, would be quite helpful in some cumbersome cases.

## Acknowledgments

This study was supported, by the Spanish grant AYA 2015-67175-P, by the Academy of Finland project No 260027, by the Magnus Ehrnrooth Foundation, and by the Act 211 of the Government of the Russian Federation (agreement No 02.A03.21.0006). This study was done in the frame of a PhD. on Physics at the Autonomous University of Barcelona (UAB).

## References

- Ceplecha Z., Borovička J., Elford W. G., Revelle D. O., Hawkes R. L., Porubčan V. and Šimek M. (1998). "Meteor phenomena and bodies". *Space Sciences Reviews* **84**, 327–471.
- Gritsevich M. I. (2007). "Approximation of the observed motion of bolides by the analytical solution of equations of meteor physics". *Solar System Research*, **41**, 509–516.
- Gritsevich M. I. (2008). "The Pribram, Lost City, Innisfree, and Neuschwanstein falls: An analysis of the atmospheric trajectories". *Solar System Research*, **42**, 372–390.
- Gritsevich M. I. (2009). "Determination of parameters of meteor bodies based on flight observational data". *Advances in Space Research*, **44**, 323–334.
- Gritsevich M. and Koschny D. (2011). "Constraining the luminous efficiency of meteors". *Icarus*, **212**, 877–884.
- Gritsevich M. I., Stulov V. P. and Turchak L. I. (2012). "Consequences for collisions of natural cosmic bodies with the Earth atmosphere and surface". *Cosmic Research*, **50**, 56–64.
- Gritsevich M., Lyytinen E., Moilanen J., Kohout T., Dmitriev V., Lupovka V., Midtskogen V., Kruglikov N., Ischenko A., Yakovlev G., Grokhovsky V., Haloda J., Halodova P., Peltoniemi J., Aikkila A., Taavitsainen A., Lauanne J., Pekkola M., Kokko P., Lahtinen P. and Larionov M. (2014). "First meteorite recovery based on the observations by the Finnish Fireball Network". In Rault J.-L. and Roggemans P., editors, *Proceedings of the International Meteor Conference*, Giron, France 18–21 September 2014. IMO, pages 162–169.
- Hoppe J. (1937). "Die physikalischen Vorgänge beim Eindringen meteoritischer Körper in die Erdatmosphäre". *Astronomische Nachrichten*, **262**, 169–198.
- Lyytinen E. and Gritsevich M. (2013). "A flexible fireball entry track calculation program". In Gyssens M. and Roggemans P., editors, *Proceedings of the International Meteor Conference*, La Palma, Canary Islands, Spain, 20–23 September 2012. IMO, pages 155–167.
- Lyytinen E. and Gritsevich M. (2016). "Implications of the atmospheric density profile in the processing of fireball observations". *Planetary and Space Science*, **120**, 35–42.
- Madiedo J. M. and Trigo-Rodríguez J. M. (2008). "Multi-station video orbits of minor meteor showers". *Earth, Moon, and Planets*, **102**, 133–139.
- Moreno-Ibáñez M., Gritsevich M. and Trigo-Rodríguez J. M. (2015). "New methodology to determine the terminal height of a fireball". *Icarus*, **250**, 544–552.
- Stulov V. P. (1997). "Interactions of space bodies with the atmospheres of planets". *Applied Mechanical Review*, **50**, 671–688.
- Stulov V. P., Mirskii V. N. and Vilsyi A. I. (1995). "Aerodinamika bolidov (Aerodynamics of Bolides)". *Nauka, Moscow (in Russian)*.
- Trigo-Rodríguez J. M., Castro-Tirado A. J., Llorca J., Fabregat J., Martínez V. J., Reglero V., Jelínek M., Kubánek P., Mateo T. and De Ugarte Postigo A. (2004). "The development of the Spanish Fireball Network using a new all-sky CCD system". *Earth, Moon, and Planets*, **95**, 553–567.
- Trigo-Rodríguez J. M., Borovička J., Spurný P., Ortíz J. L., Docobo J. A., Castro-Tirado A. J. and Llorca J. (2006). "The Villalbeto de la Peña meteorite fall: II. Determination of atmospheric trajectory and orbit". *Meteoritics*, **41**, 500–517.

Trigo-Rodríguez J. M., Lyytinen E., Gritsevich M., Moreno-Ibáñez M., Bottke W. F., Williams I., Lupovka V., Dmitriev V., Kohout T. and Grokhovsky V. (2015). "Orbit and dynamic origin

of the recently recovered Annama's H5 chondrite". *Monthly Notices of the Royal Astronomical Society*, **449**, 2119–2127.



Manuel Moreno-Ibáñez and Jürgen Rendtel in discussion at the poster session.

# Large meteoroid's impact damage: review of available impact hazard simulators

Manuel Moreno-Ibáñez<sup>1,2</sup>, Maria Gritsevich<sup>2,3</sup> and Josep Ma. Trigo-Rodríguez<sup>1</sup>

<sup>1</sup>Institute of Space Sciences (IEEC-CSIC), Meteorites, Minor Bodies and Planetary Science Group,  
Campus UAB, Carrer de Can Magrans, s/n E-08193 Cerdanyola del Vallés, Barcelona, Spain  
mmoreno@ice.csic.es, trigo@ice.csic.es

<sup>2</sup>Finnish Geospatial Research Institute, Geodeetinrinne 2, FI-02431 Masala, Finland

<sup>3</sup>Institute of Physics and Technology, Ural Federal University, 620002 Ekaterinburg, Russia  
gritsevich@list.ru

The damage caused by meter-sized meteoroids encountering the Earth is expected to be severe. Meteor-sized objects in heliocentric orbits can release energies higher than  $10^8$  J either in the upper atmosphere through an energetic airblast or, if reaching the surface, their impact may create a crater, provoke an earthquake or start up a tsunami. A limited variety of cases has been observed in the recent past (e.g. Tunguska, Carancas or Chelyabinsk). Hence, our knowledge has to be constrained with the help of theoretical studies and numerical simulations. There are several simulation programs which aim to forecast the impact consequences of such events. We have tested them using the recent case of the Chelyabinsk superbolide. Particularly, Chelyabinsk belongs to the ten to hundred meter-sized objects which constitute the main source of risk to Earth given the current difficulty in detecting them in advance. Furthermore, it was a detailed documented case, thus allowing us to properly check the accuracy of the studied simulators. As we present, these open simulators provide a first approximation of the impact consequences. However, all of them fail to accurately determine the caused damage. We explain the observed discrepancies between the observed and simulated consequences with the following consideration. The large amount of unknown properties of the potential impacting meteoroid, the atmospheric conditions, the flight dynamics and the uncertainty in the impact point itself hinder any modelling task. This difficulty can be partially overcome by reducing the number of unknowns using dimensional analysis and scaling laws. Despite the description of physical processes associated with atmospheric entry could be still further improved, we conclude that such approach would significantly improve the efficiency of the simulators.

## 1 Introduction

The impact of meteoroids with the Earth is a subject of great concern nowadays, and it has been revisited after Chelyabinsk (Brown et al., 2013; Trigo-Rodríguez and Williams, 2016). Their high kinetic energy can be transferred at the Earth's continental surface (earthquake, crater, etc.) or sea (tsunami), or released during its atmospheric flight (airburst). Particularly, we are interested in possible impacts with tens-of meter size meteoroids due to its moderate size. The exact population of these objects is unknown given their small size, which also makes them difficult to be detected well in advance. However, they are big enough so as to potentially inflict severe damage. Due to the short time provided to prevent an impact with these objects planetary defense actions become complicated. Thus, we ought to be aware of their hazardous potential.

Relative recent examples like Tunguska (1908) and Chelyabinsk (2013) are the evidence of this efficient destructive power. The shock wave associated to the likely final Tunguska explosion devastated an area of 2150 km<sup>2</sup> approximately, of which, 100km<sup>2</sup> resulted with burnt trees (Chyba et al., 1993; Vasilyev, 1998). Besides, an Earthquake ranging of 4.5–5 on Richter scale was felt by the local inhabitants. All in all, the energy released by this event has been estimated in 10–50Mt (Chyba et al., 1993; Vasilyev, 1998). There was no crater and no

meteorite was recovered, so the energy was completely released by the airblast. More recently Chelyabinsk (15<sup>th</sup> February 2013, Russia) become the first largely recorded and documented hazardous event. Numerous dash car cameras recorded the atmospheric entry of the body and the damage caused (mainly broken glasses) was widely reported by local citizens of the nearby town. It was an approximately 19 m LL5 chondrite body which entered the atmosphere at 19.03 km/s with an entry angle of 18.5 grades which released an energy of about ~500 kt, (see more details in Borovička et al., 2013; Brown et al., 2013; Popova et al., 2013, Kohout et al., 2014). Chelyabinsk suffered intensive fragmentation between heights of 45 and 30 km, and only an 8 m hole on ice was found. This gives an idea of the hazardous effect of its atmospheric flight compared to the final surface impact.

The impact hazard on Earth due to these objects depends on several variables which are difficult to predict beforehand (Ceplecha et al., 1998). These variables are related to the impacting body (i.e. their size, speed, entry angle, composition, etc.), to the atmospheric conditions, and, if the fireball survives its atmospheric flight, to the exact point of impact (i.e. the sea, different types of soil, etc.). Hence, carrying on an accurate analysis of these phenomena is not easy and lots of consideration shall be taken into account. In this study we have analyzed the state-of-the-arts of impact hazard simulation tools.

Here, we have reviewed five free simulator tools available in internet. We have used Chelyabinsk registered data (Borovička et al., 2013; Brown et al., 2013; Popova et al., 2013) to test the simulation results. In *Section 2* we will briefly describe the main characteristics of each simulator. We will then apply our test case and present the results in *Section 3*. Discussion will be held in *Section 4*. Finally we summarize the main conclusions in *Section 5*.

## 2 Review of simulators

The large number of unknowns involved in the impact calculations usually constraint the development of simulation tools. Different assumptions shall be made to provide reasonable results and simplify code writing. As we will see, most of the simulators analyzed are normally designed to determine the resulting characteristics of the crater (depth and size) and the amount of energy released by the asteroid or comet. However, this energy can be released in various ways that can show different levels of destruction. An appropriate computed modelling of the energy distribution is complicated and it shall be based on theoretical models that are not still available. Hence, the limitations of the simulators are also constraint by the theoretical advances.

The five simulators we have tested are described in the following lines. We will not delve into every detail and suggested the interested reader to address directly to the source website:

1- *Impact Earth!*: developed by Gareth Collins, H. Jay Melosh and Robert Marcus at the Imperial College in London. This is a detailed scientific software which is fully described in (Collins et al., 2005). The program provides the ejecta distribution, the ground shaking, the atmospheric blast wave, and the thermal effects of an impact as well as the size of the final crater<sup>1</sup>. However, as we will discuss later, their results are not able to appropriately describe our test case.

2- *Solar System Collision*: this is a simple software that roughly estimates the consequences of an asteroid or comet impact on any planet of our solar system. The only input required are the composition of the body (ice, rock or iron), its velocity and the size (diameter). As a result the user will get the energy released, the crater size and depth, whether a quake or tsunami is provoked, and the collision likelihood of such an impact. Thus, this is a software<sup>2</sup> devoted for the use of the general public.

3- *Asteroid Impact Crater Calculator*: this is a basic JavaScript which estimates the crater main characteristics based on the assumption that the impact consequences only depend on the mass and velocity of the asteroid<sup>3</sup>. This means that the program assumes a conservative energy system. Thus, it could be useful for general public looking for a first insight of the phenomena.

4- *What if an asteroid or comet hits my town?* A very simple impact software which roughly describes the consequences of such an impact in different points of the Earth<sup>4</sup>. General input data is required and results are mainly expressed through a visual impact simulator tool which uses Google Earth.

5- *Down to Earth – Crater Impactor*: developed at the University of South Wales by Andrew Scott. The code of the software<sup>5</sup> is based on *Impact Earth!* Thus, this is a proficient scientific software. However, nor the density of the asteroid nor its size (diameter) can be input as detailed data. The outcome is large and, among other results, we remark the crater details, the energy released and the impact frequency.

It is worth noting that none of these simulators take into account further complex phenomena such as thermal effects or fragmentation. Thus, the scientific retrieval is expected to be scarce. Nonetheless, they could serve as a first approximation of the impact consequences.

## 3 Test case: Chelyabinsk

As we have stated, we are particularly interested in meter of size bodies. Fortunately, we have enough documented data of such a body, Chelyabinsk. The large number of cameras and visual witnesses that reported this event provided us with enough information to describe the phenomena with reliable accuracy. Consequently, this makes Chelyabinsk a suitable candidate to test whether the simulator tools reviewed in the previous section are reliable or not.

Testing the different simulator is not easy. Most of them only accept rough input parameters, i.e. instead of the exact asteroid bulk density sometimes we will have to choose between rock, ice or iron density. Hence, direct comparison of the final results against Chelyabinsk reported data should be done with care. Nonetheless, it is still possible to state whether the assumptions adopted by the simulators could lead to reasonable results that may eventually provide a first insight of the impact consequences and the points to be improved in each simulator.

In *Table 1* we summarize the main input variables required by each program. Since the variety in required input variables is large and it depends on each software, we have not shown those input variables required by just one simulator. Last row indicates their corresponding Chelyabinsk value (and the reference from which the value was taken). Note that this input value is merely referential as the simulator input requirements and their accuracy may vary from one to another owing to the designer criteria (i.e. real asteroid bulk density vs rock, ice or iron density).

<sup>1</sup> <http://www.impact.ese.ic.ac.uk>

<sup>2</sup> <https://janus.astro.umd.edu/astro/impact/>

<sup>3</sup> [http://www.convertalot.com/asteroid\\_impact\\_calculator.html](http://www.convertalot.com/asteroid_impact_calculator.html)

<sup>4</sup> <http://www.killerasteroids.org/impact.php>

<sup>5</sup> <http://www.simulator.down2earth.eu>

*Table 1* – Input data required by the five simulators. The term “Approx.” refers to that input where only a rough value is accepted. Last row shows the corresponding reported values for Chelyabinsk. References: (1) Borovička et al., 2013; (2) Brown et al., 2013; (3) Popova et al., 2013.

Simulator	Man initial data				
	Speed	Impact angle	Density	Bulk composition	Size (Diam.)
Impact: Earth!	Yes	Yes	Yes	No	Yes
Solar System Collision	Yes	No	No	Yes	Yes
Asteroid Impact Crater Calculator	Yes	Yes	Yes	No	Yes
What if an asteroid or comet hits my town?	No	No	No	Approx.	Approx.
Down 2 Earth - Crater Impact	Yes	Yes	Yes	Yes	Approx.
Observed Values	19.03 Km/s (1)	18.5° (1)	3300 kg/m <sup>3</sup> (3)	Dense Rock	19 m (2)

*Table 2* – Main results obtained for the five simulators using Chelyabinsk data (reported values shown in the last row). References: (1) Borovička et al., 2013; (2) Brown et al., 2013; (3) Popova et al., 2013; (4) Boslough, 2015.

Simulator	Some results for Chelyabinsk			
	Crater Diameter / Depth (m)	Energy Released (Mt)	Frequency (years)	Over Pressure (Kpa)
Impact: Earth!	No crater	0.20	...	0.656
Solar System Collision	...	0.369	17	...
Asteroid Impact Crater Calculator	159.52 / 39.88	0.511	...	...
What if an asteroid or comet hits my town?	...	...	~ 1000	...
Down 2 Earth - Crater Impact	625 / 133	57	2826	...
Observed Values	Diam.:7 m (3) or 8m (1)	0.5 (1, 2)	50 years (4)	3.2±0.6 KPa (1) / > 0.5 KPa (3)

In addition, in *Table 2* we express the main and most common results. Other individual values are retrieved but for the sake of simplicity we just show those values that are provided by at least two simulators. Chelyabinsk values and references are again written in the last row.

## 4 Discussion

The use of these five simulators is quite straightforward because most of them are user friendly and intuitive. This is probably the reason why the possibility of input more detailed values is normally constraint. Some of these simulators are designed to be useful and illustrating for the general public. Therefore, they assume that no prior knowledge shall be required and they often suggest three or four alternatives for each input variable (i.e.: ice, rock or iron for the asteroid bulk density). This also explains why some simulators do not input values of some key variables.

As for *Impact: Earth!* (Collins et al., 2005), despite of being a scientific software, the assumptions and simplifications considered in the code limit the validity of the results. Particularly, fragmentation is not included in

the code, but it is often common in the aerodynamic flight of large bolides like e.g. Chelyabinsk. However, the inclusion of fragmentation is difficult and theoretical models still find difficulties to accurately undertake it.

Regarding the results, again *Impact: Earth!* shows the better fit. *Table 2* only shows some of the results obtained, however, we can state that most of the available impact simulators fail to accurately determine the resulting damage for the Chelyabinsk event.

The observed discrepancies between the observed and simulated consequences are now explained having in mind the following consideration. As already mentioned, the large amount of unknowns in the impacting meteoroid, the atmospheric conditions, the flight dynamics, and in the uncertainty in the impact point itself hinder any modelling task. This difficulty can be partially overcome by tackling the problem in a different way. In order to improve further modelling the use of dimensional analysis and scaling laws may help reducing the number of unknowns. This recent methodology (Stulov et al., 1995; Stulov, 1997; Gritsevich, 2008, 2009; Moreno-Ibáñez et al., 2015) gathers all atmospheric

flight unknowns down to two. These two new parameters (namely the mass loss parameter and the ballistic coefficient) are easily retrievable from observations and prove to clearly show different values according to the nature of the meteoroid (see Gritsevich, 2012, 2013), thus we could assume their values from previous events (like Chelyabinsk) or proceed to further analysis based on different values of them. Furthermore, these parameters have physical meaning. An adequate combination of these two new variables with some studied orbital data (see e.g. Dmitriev et al., 2015) may simplify the equations involved and improve the accuracy of the results.

## 5 Conclusion

The scope of this study is not to enumerate the lacks and virtues of the programs tested, but to set evidence of the necessity of investing more time on this subject in order to get a more proficient prediction software. Further improvements should focus on describing with detail asteroid impact consequences and, thus, help in developing planetary defense systems. Large discrepancies obtained for a potential hazardous tens-of-meter meteoroid (Chelyabinsk) urges to develop more reliable tools soon.

The use of scaling laws and dimensionless methodologies could facilitate dealing with all the unknown impact variables. Besides, it could be easily implemented during code writing and may provide more accurate results.

## Acknowledgments

This study was supported, by the Spanish grant AYA 2015-67175-P, by the Academy of Finland project No 260027, by the Magnus Ehrnrooth Foundation, and by the Act 211 of the Government of the Russian Federation (agreement No 02.A03.21.0006). This study was done in the frame of a PhD. on Physics at the Autonomous University of Barcelona (UAB).

## References

- Borovička J., Spurný P., Brown P., Wiegert P., Kalenda P., Clark D. and Shrbený L. (2013). “The trajectory, structure and origin of the Chelyabinsk asteroidal impactor”. *Nature*, **503**, 235–237.
- Boslough M. B. (2015). “Asteroid Airbursts: Risks Assessment and Reduction”. AGU Fall Meeting 2015.
- Brown P., Assink J. D., Astiz A., Blaauw R., Boslough M. B., Borovička J., Brachet N., Brown D., Campbell-Brown M., Ceranna L., Cooke W., de Groot-Hedlin C., Drob D. P., Edwards W., Evers L. G., Garces M., Gill J., Hedlin M., Kingery A., Laske G., Le Pichon A., Mialle P., Moser D. E., Saffer A., Silber E., Smets P., Spalding R. E., Spurný P., Tagliaferri E., Uren D., Weryk R. J., Whitaker R. and Krzeminski Z. (2013). “A 500-kiloton airburst over Chelyabinsk and an enhanced hazard from small impactors”. *Nature*, **503**, 238–241.
- Cepelch Z., Borovička J., Elford W. G., Revelle D. O., Hawkes R. L., Porubčan V. and Šimek M. (1998). “Meteor Phenomena and Bodies”. *Space Science Reviews*, **84**, 327–471.
- Chyba F. C., Paul J. T. and Zahnle K. J. (1993). “The 1908 Tunguska explosion: atmospheric disruption of a stony asteroid”. *Nature*, **361**, 40–44.
- Collins G. S., Melosh H. J. and Marcus R. A. (2005). “Earth Impact Effects Program: A Web-based computer program for calculating the regional environmental consequences of a meteoroid impact on Earth”. *Meteoritics and Planetary Science*, **40**, 817–840.
- Dmitriev V., Lupovka V. and Gritsevich M. (2015). “Orbit determination based on meteor observations using numerical integration of equations of motion”. *Planetary and Space Science*, **117**, 223–235.
- Gritsevich M. I. (2008). “The Pribram, Lost City, Innisfree, and Neuschwanstein falls: An analysis of the atmospheric trajectories”. *Solar System Research*, **42**, 372–390.
- Gritsevich M. I. (2009). “Determination of Parameters of Meteor Bodies Based on Flight Observational Data”. *Advances in Space Research*, **44**, 323–334.
- Gritsevich M. I., Stulov V. P. and Turchak L. I. (2012). “Consequences for collisions of natural cosmic bodies with the Earth atmosphere and surface”. *Cosmic Research*, **50**, 56–64.
- Gritsevich M. I., Stulov V. P. and Turchak L. I. (2013). “Formation of Large Craters on the Earth as a Result of Impacts of Natural Cosmic Bodies”. *Doklady Physics*, **58**, 37–39.
- Kohout T., Gritsevich M., Grokhovsky V., Yakovlev G., Haloda J., Halodova P., Michallik R., Penttilä A. and Muinonen K. (2014). “Mineralogy, reflectance spectra, and physical properties of the Chelyabinsk LL5 chondrite - Insight into shock-induced changes in asteroid regoliths”. *Icarus*, **228**, 78–85.
- Moreno-Ibáñez M., Gritsevich M. and Trigo-Rodríguez J. M. (2015). “New methodology to determine the terminal height of a fireball”. *Icarus*, **250**, 544–552.
- Popova O. P., Jenniskens P., Emel'yanenko V., Kartashova A., Biryukov E., Khaibrakhmanov S., Shuvalov V., Rybnov Y., Dudorov A., Grokhovsky V. I., Badyukov D. D., Yin Q.-Z., Gural P. S., Albers J., Granvik M., Evers L. G., Kuiper J., Kharlamov V., Solovyov A.,

- Rusakov Y. S., Korotkiy S., Serdyuk I., Korochantsev A. V., Larionov M. Y., Glazachev D., Mayer A. E., Gisler G., Gladkovsky S. V., Wimpenny J., Sanborn M. E., Yamakawa A., Verosub K. L., Rowland D. J., Roeske S., Botto N. W., Friedrich J. M., Zolensky M. E., Le L., Ross D., Ziegler K., Nakamura T., Ahn I., Lee J. I., Zhou Q., Li X.-H., Li Q.-L., Liu Y., Tang G.-Q., Hiroi T., Sears D., Weinstein I. A., Vokhmintsev A. S., Ishchenko A. V., Schmitt-Kopplin P., Hertkorn N., Nagao K., Haba M. K., Komatsu M. and Mikouchi T. (2013). “Chelyabinsk Airburst, Damage Assessment, Meteorite Recovery, and Characterization”. *Science*, **342**, 1069–1073.
- Stulov V. P. (1997). “Interactions of space bodies with the atmospheres of planets”. *Applied Mechanical Review*, **50**, 671–688.
- Stulov V. P., Mirskii V. N. and Vilsyi A. I. (1995). “Aerodinamika bolidov (Aerodynamics of Bolides)”. Nauka, Moscow (*in Russian*).
- Trigo-Rodríguez J. M. and Williams I. P. (2016). “Dynamic sources of contemporary hazard from meteoroids and small asteroids”. In Trigo-Rodríguez J. M., Gritsevich M. and Palme H., editors, *Assessment and Mitigation of Asteroid Impact Hazards*. Springer New York, in press.
- Vasilyev N. V. (1998). “The Tunguska Meteorite problem today”. *Planetary and Space Science*, **46**, 129–150.



Malcolm Currie and Gillian Weatherley make their choice in the IMO bookshop.

# Measurements of CCD optical linearity for magnitude determination during meteor observations

Andrey Murtazov and Alexander Efimov

Astronomical Observatory, Ryazan State University, 46, Svobody St., Russia, 390000

a.murtazov@rsu.edu.ru, a.efimov@rsu.edu.ru

The results of investigating the dependency “light flux - magnitude” are presented. This dependency is used to determine the meteor brightness on CCD frames. This dependency is shown to be linear with the signal-to-noise ratio exceeding 10 dB. However, with low signal-to-noise ratio it is non-linear. This should be taken into account while measuring the faint meteors on single frames.

## 1 Introduction

The precise determination of meteor and bolide brightness is quite a relevant objective. According to some researchers, there are no precise methods of determining bolide brightness to date (Barentsen, 2012). However, measuring the brightness of faint meteors which are observable at the light sensitivity limit also necessitates careful recording of different disturbances.

These problems are generally related to the dynamic optical range which CCDs have and, in the long run, to the linearity of their optical characteristics.

In this respect, we have investigated the linearity of the “light flux – magnitude” dependency for stars on single frames and a stacked frame resulting from UFO (SonotoCo) meteor observations.

## 2 Methodology and measurements

CCDs, like any other light receiver, are sufficiently linear (Howell, 2006; Mullikin et al., 1994). In other words, according to Stoletov’s first photoelectric effect law, the number of photoelectrons appearing in pixel is proportional to the number of photons falling to the CCD.

This means that a certain (dynamic) range should maintain the ratio expressed by Pogson’s formula:  $m=2.5 \lg F$ , where  $F$  – the light flux falling on the matrix from the observed object, and  $m$  – the object magnitude.

Practically, the CCD dynamic range is determined according to the observation results of the image of comparison stars which can be found on a CCD frame.

For instance, magnitudes of variable stars and asteroids are determined relative to comparison stars, most often using the light accumulation effect on the receiving matrix.

Moreover, there are certain requirements to the comparison stars:

- comparison stars should have quite accurately measured standard magnitudes, except that the measurements should be repeated, in order to avoid

both possible errors during photoelectric measurements, and possible star variability;

- standards should have a wide range of color indices;
- standards should be located near the observed object;
- standards should be observed several times during the night;
- the night should be photometric (i.e. have quite a stable and good transparency).

In meteor CCD photometry these requirements are for the most part not met which causes the loss of accuracy in measuring meteor brightness.

In CCD methods the meteor brightness is traditionally determined on single frames from *avi-files* relative to the standard stars available on them.

The specifics of meteor magnitude measurements:

- high angular velocity of meteors gives no way for photons accumulation;
- CCD images of bright objects may be supersaturated and their brightness cannot be a linear function for the brightness of real celestial objects.

Thus, the non-availability of CCD linearity in the region of large light fluxes is the main hindrance for accurate bolide brightness measurements. The hindrance for determining the brightness of extremely faint meteors can be instrument noise.

We measured the brightness of comparison stars using the data of UFO Capture Perseids – 2015 observations (the Watec-902H camera and Computar HG0808AFCS lens with FOV 45X34 arc degrees – Murtazov, et al., 2013).

The brightness of comparison stars was measured by means of an *IRIS* aperture photometry (Buil, 2010)<sup>1</sup>. Comparison star magnitudes in *IRIS* were taken from HD (The *Henry Draper Extension Charts: A catalogue of accurate positions, proper motions, magnitudes and spectral types of 86933 stars. Centre de Donnees astronomiques de Strasbourg Reference – III/182*).

<sup>1</sup>IRIS–Astronomical image processing software. <http://www.astrosurf.com/buil/us/iris/iris.htm>.

The atmospheric extinction was determined for every frame from the *avi*-files.

Figure 1 shows a single frame with a meteor at the brightness maximum and a stacked frame output from UFO Capture based on 38 frames.

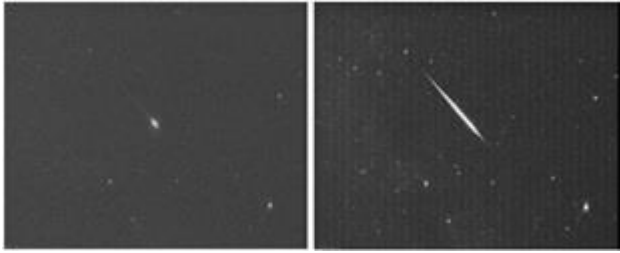


Figure 1 – Single frame (a) and added picture (b) built by UFO Capture SonotoCo.

The analysis of the comparison star images on CCD frames shows that:

- there are not so many photometric comparison stars on wide-angle CCD-frames to carry out photometric measurements;
- zenith angles of comparison stars are very much different which impairs the precision of photometric measurements because of the big light absorption difference;
- the quality of star images on each frame very strongly depends on:
  1. the state of the atmosphere and
  2. the instrumental noises for CCDs that have no cooling system.

Due to the latter factor, the errors in measuring star brightness grow while it decreases and approaches the background brightness.

Figure 2 shows the errors in measuring the brightness of different stars on the chosen 38 frames (the limiting magnitude for these frames is 4.5m). In the main part of the range from 0 to 4m the average quadratic error  $\Delta m$  at brightness measurement does not exceed 0.1m. In the region close to the limiting magnitude the error rises sharply forming for the  $SNR \approx 0$  level values tending to 1<sup>m</sup>.

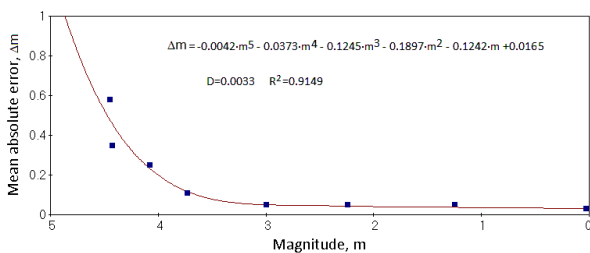


Figure 2 – Average error of comparison star brightness measurements for 38 CCD frames.

### 3 Results

#### Single frames

Figures 3–5 show the results of calculating the signal-to-noise (SNR) according to IRIS measurements versus the comparison star magnitudes on single frames. Figure 6 illustrates a similar dependency “SNR–magnitude” which is based on a stacked frame output from UFO Capture composed of 38 frames.

SNR was calculated as (Nakamura, 2006)

$$SNR = 20 \cdot \log \frac{I_{s+n}}{I_n}, \text{ dB}$$

where  $I_{s+n}$  – star brightness + background measured on a CCD frame,

and  $I_n$  – background brightness on a CCD frame.

The results of measurements were smoothed by polynomials of different degrees. Their analytical expressions, as well as root-mean-square deviations  $\sigma$  and Pearson’s correlation coefficients  $R^2$  are shown in the figures for every obtained dependency.

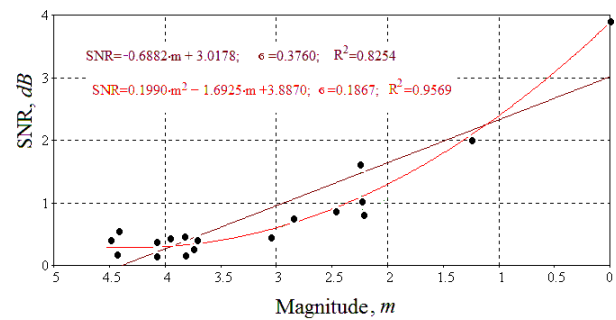


Figure 3 – Relationship between SNR and magnitude for all comparison stars on single frames.

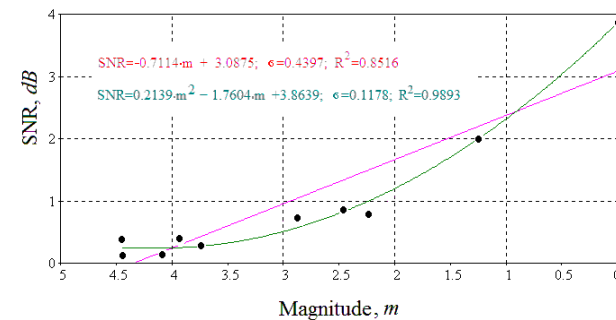


Figure 4 – Relationship between SNR and magnitude for O-F stars on single frames.

The analysis of dependencies in Figures 3–5 shows that the “SNR- magnitude” relationship for faint comparison stars that are close to limiting comparison stars is not linear. The obtained ratios are best approximated by quadratic dependencies. This is maintained both for all measured stars (Figure 3), and for the stars of the early (Figure 4) and late spectral types (Figure 5).

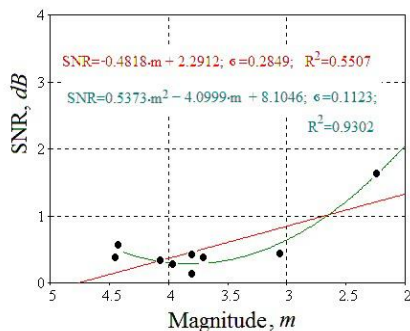


Figure 5 – Relationship between SNR and magnitude for G-M stars on single frames.

Interesting is the discrepancy between SNR data and the brightness of stars near the limiting magnitude for single frames ( $m_{lim} \approx 4.5$ ). This can be explained by the picture instability in the region of the star limiting visibility where the signal is close to the background (Signal  $\approx$  Noise).

According to the data obtained, we can determine meteor magnitude on a single frame.

A meteor’s SNR on a single frame (Figure 1a) according to the comparison star brightness IRIS measurement data is 7.2636.

Thereupon, according to the quadratic regression equation shown in Figure 3 the meteor brightness on this frame can be defined as  $m = -1.67^m \pm 0.19^m$ .

**Stacked frames**

Figure 6 shows the relationships between SNR and comparison star magnitudes on a stacked frame output from UFO Capture composed of 38 frames.

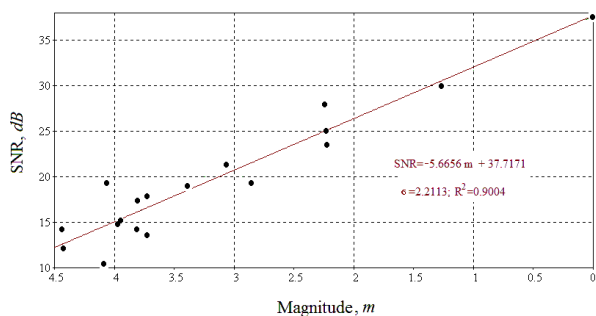


Figure 6 – Relationship between SNR and magnitude for all comparison stars in stacked frame.

For stacked frames, the brightness of star images grows in proportion to the number of added frames, n, and the brightness of the background grows in proportion to  $n^{0.5}$ . Consequently, the difference between the brightness of stars and the background noise increases and the fainter stars become visible. Consequently SNR become much higher than on single frames. With Vega, for example,

SNR increases to  $\sim 40$ . Note that the operating range of CCDs, according to their manufacturers, begins with SNR=50.

In contrast to single frames, the “SNR-magnitude” dependency for this combined frame is very well approximated by a line throughout the range of comparison star magnitudes. Thus, the dynamic range here begins from limiting apparent stars and extends to at least 0<sup>m</sup>.

According to the author’s previous data (Murtazov, 2011), the linearity of the “SNR-magnitude” feature (its upper limit) roughly extends to brightness  $m = -3$ , which corresponds to Jupiter’s brightness at the average opposition.

**4 Conclusions**

With extremely low light fluxes the SNR has a non-linear relationship to magnitude and therefore can be more accurately correlated quadratically.

With SNR above 10 this dependence becomes linear and is realized for bright star magnitude measurements.

**References**

Barentsen G. (2013). “How to measure the flux of large meteoroids”. In Gyssens M. and Roggemans P., editors, *Proceedings of the International Meteor Conference*, La Palma, Spain, 20–23 September 2012. IMO, pages 136–139.

Howell S. B. (2006). *Handbook of CCD astronomy*. Cambridge University Press.

Mullikin J. C., van Vliet L. J., Netten H., Boddeke F. R., van der Feltz G., Young I. T. (1994). “Methods for CCD camera characterization”. In Titus H. C. and Waks A., editors, *Proceedings of SPIE*, vol. 2173, “Image Acquisition and Scientific Imaging Systems”, pages 73–84.

Murtazov A. (2011). “Arrangement of integrated meteor TV-observations at the Ryazan State University Astronomical Observatory”. *Vestnik of the Siberian State Aerospace University*, n39, pages 109–113.

Murtazov A., Efimov A. and Titov P. (2013). “Double-Station Meteor Observations in Ryazan, Russia”. In Gyssens M. and Roggemans P., editors, *Proceedings of the International Meteor Conference*, La Palma, Spain, 20–23 September 2012. IMO, pages 192–195.

# Astronomy through the microscope: A workshop during the opening night of the 2016 IMC

Gert Jan Netjes and Sebastiaan de Vet

Meteor Section, Royal Netherlands Association for Meteorology and Astronomy

G.J.Netjes@inter.nl.net, Sebastiaandevet@gmail.com

During the IMC workshop meteoritical thin sections were shown live with a microscope connected to the beamer. This article will provide a background to thin sections, what we can learn from them and the tour through the solar system we can take with them.

## 1 Introduction

Is it possible to discover the solar system through the microscope? Sure, by studying thin slices of meteorite rock it is possible to see the elementary composition of the solar system. The minerals in the rock not only have an aesthetic value but also provide a valuable insight in the geological diversity of the celestial bodies not visible through a telescope.

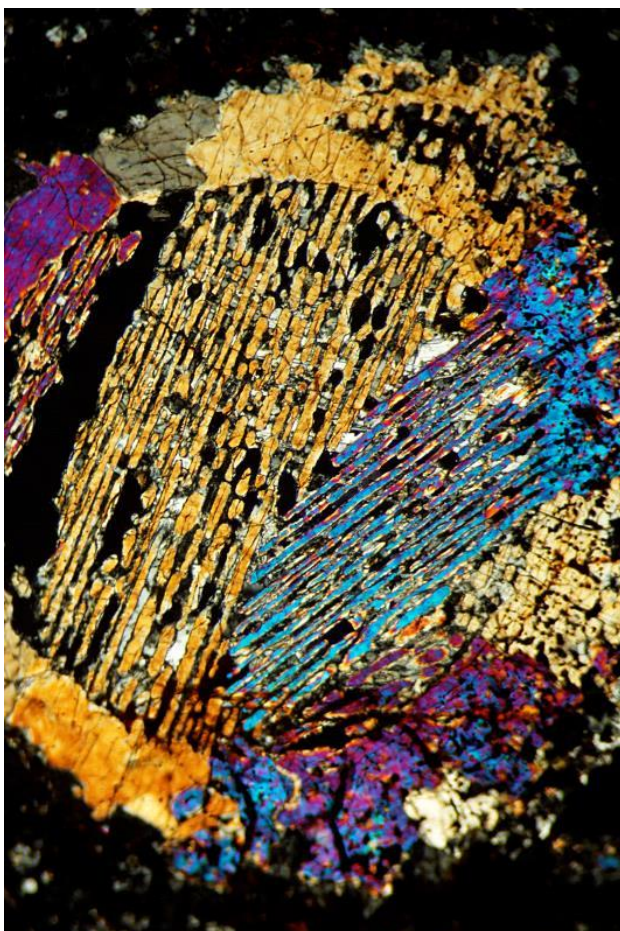


Figure 1 – Barred Olive Chondrule with beginning metamorphosis (Carbonaceous chondrite NWA 7265). Actual size 1.12 mm by 0.75 mm.

The way to study the diversity of all the different meteorite classes is by means of an petrological microscope. Pieces of meteorites will be grind to thin transparent slices and glued onto glass, the so called thin sections (Figure 2). If polarized light pass through the

thin section the white light will be influenced by the minerals and gives a kaleidoscope of colors which help to determine which mineral it is. From the overall colorful image one can with some luck determine where the meteorite came from. So by using multiple meteorites one can make voyage along the rocky planets.



Figure 2 – Thin section example, 46 x 26 mm in size.

## 2 The geological family tree of our solar system

In the past, the classification of meteorites was made on the basis of the appearance of the meteorite; stony, stony-iron and iron meteorites. This classification soon presented confusion; Stony meteorites contain iron, iron meteorites also contain stone, and stony-iron meteorites contain both. When the amount of meteorites rose and analytical methods became better, they moved to a classification scheme based on the changes the meteorites have undergone over the 4.567 billion years since their formation.

Meteorites that have remained unchanged since the birth of our solar system are called undifferentiated. These have only undergone some changes as a result of water or heat but were never completely melted. These are the most pristine meteorites that we have and they contain the first solids formed during the cooling of the gaseous nebula. The characteristic features of these meteorites are the chondrules. These round inclusions in the rock also gave the name to this group, the chondrites. Meteorites of this group come from asteroids smaller than 300 km.

If the asteroids grew larger than 300 km during their development the gravity and radioactive decay caused the temperature to rise above the melting point of the minerals. The result was that under the influence of gravity elements having a higher density (metal) moved toward the lower core and the lighter elements (silicates) went more to the surface. This created the familiar round planet shape with a metallic core and a rocky mantle. The group of meteorites that derived from these asteroids was named by the process they have undergone, differentiated. Differentiated stone meteorites are also called achondrites (since they do not contain chondrules). Iron meteorites, mesosiderites and pallasites (formerly called stony-iron meteorites) fall under the differentiated meteorites as well.

When dividing meteorites into two groups some are sure to fall outside these boundaries. So we also have meteorites with features of both groups. These are meteorites that have not been completely melted but have become so hot that the crystal structure and mineral composition has changed. These meteorites are called primitive achondrites.

### 3 Undifferentiated meteorites, the chondrites

The chondrites are the first, still preserved pages of the history of our Solar System. They mainly consist of the metals iron and nickel and some minerals. In chondrites the first condensates from the solar nebula are visible, the calcium aluminum inclusions (CAI, see *Figure 3*). These CAI's contain minerals with the highest melting point, making this the first solids which condensed from the solar nebula. They also contain chondrules (*Figure 4*), which are the largest constituents of these meteorites, about 40 to 80%. These chondrules are spherical crystal forms which took shape before the sun ignited. Chondrules have an average size of 1 mm (0.1 – 6 mm) and there are only seven different types of known. For the formation of these chondrules are several theories. According to the most accepted theory, they were ejected by the hot jets from a T Tauri Sun after which they solidified and “rained down” on the rotating nebula and accreted into the rock of the first asteroids. Other theories involve lightning or electromagnetic heating in order to quickly melt the minerals and rapidly cool them. The CAIs and the chondrules are easily recognizable under the microscope which provides us with a first determination step of a meteorite.

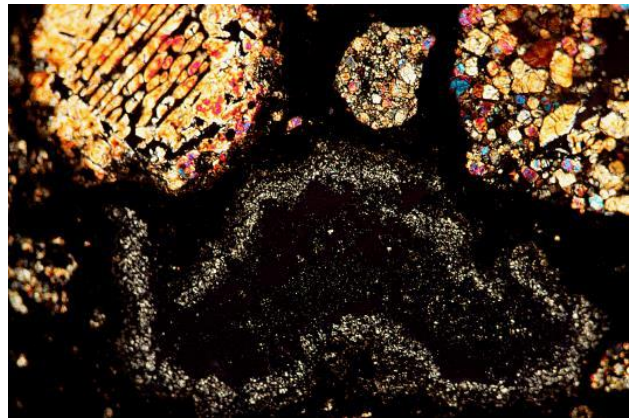


*Figure 3* – Bared olivine chondrule and two porphyritic chondrules along a CAI in the carbonaceous chondrite Allende. Actual dimensions 2.25 mm by 1.5 mm.

The chondrites are divided into sixteen classes; each class materialized at a certain distance from the sun and probably was part of one celestial body. Currently there are five classes of ordinary chondrites known; three classes of enstatite chondrites, five classes of carbonaceous chondrites and the R, K and F classes.

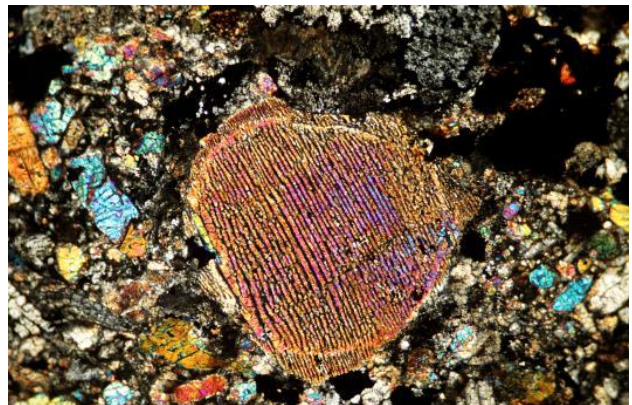


*Figure 4* – A fine Barred Olivine Chondrule in an ordinary chondrite; the Tamdaght. Actual dimensions 2.25 mm by 1.5 mm.

Within those classes the degree of metamorphism (the change of minerals by heat or contact with water) is indicated with a number. The numbers form an odd scale of 1 to 7, wherein 3 is the base. The 3 indicates that the meteorites have not undergone any influence of heat or water and are therefore the most pristine meteorites. The 1 and 2 indicate the degree of metamorphism caused by water, and 4 to 7 the metamorphism caused by heat, wherein the 7 has undergone most of the metamorphism. 3 to 7 come from different parts of the same asteroid, wherein the 3 was more on the outside and the 7 more close to core, because there the force of gravity and radioactivity provided the most heat.

Metamorphism to a chondrule is easy to see under the microscope (see *Figure 1*). Metamorphism by water will often lead to changes in the mineral composition and heat caused the crystal structure to change (*Figure 1*).

Not all subtypes within each class are currently known, but among the many meteorites coming from the north of

Africa there will undoubtedly be some missing subtypes among them. The vast majority of meteorites found are chondrites, about 86%.

## 4 Differentiated meteorites

### Primitive achondrites

Primitive achondrites are more difficult to recognize under the microscope than the chondrites, because the clearly recognizable identification characteristics, such as the chondrules are missing. The composition of minerals in the rock is still very limited, and the trained eye will find mainly minerals olivine, pyroxene and feldspar in them. Because these meteorites have been largely melted, the composition is relatively homogeneous, and the crystals often make a mutual angle of  $120^\circ$  (so-called “triple junctions” (see *Figure 5*). Primitive achondrites are divided into four classes; ureilitites, acapucoites / lodranites, brachinites and winonaites. The latter have a relationship with a class of iron meteorites. Only 0.4% of the meteorites that are classified fall into the primitive achondrites group.

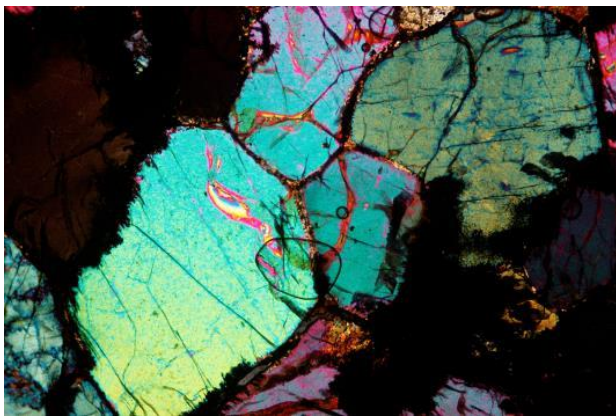


*Figure 5* – Characteristic  $120^\circ$  angles between the crystals, the so-called “triple junctions”. In ureilite NWA 5391. Actual dimensions 2.25mm by 1.5 mm.

### Achondrites

The group of differentiated meteorites also includes iron meteorites. These do not pass light and it is therefore impossible to investigate them under a petrological microscope. However, in most iron meteorites there are mineral inclusions, and these may well be viewed with the aid of a thin section and microscope. These minerals are related to the achondrites and they illustrate the relationship between these meteorites and the internal structure of a differentiated asteroid.

The achondrites (differentiated stony meteorites) are a group of meteorites that have undergone a more complex geological history. This group does not only consist of bits of large asteroids, but there are also meteorites which are derived from even larger celestial bodies. In those meteorites minerals are found that are derived from volcanic activity. Achondrite thin sections are very recognizable for terrestrial geologists because they resemble basalt, plutonic rocks and various minerals

which indicate geological processes similar to those on Earth. Generally speaking the crystals are often larger. This indicates that the rock has cooled slowly, which also points again at an origin on a larger celestial body.

There are now about seventeen classes of achondrites known, accounting for about 4.5% of all meteorites that fell on Earth. A major goal of meteorite study is to find out what class relates to what celestial body. For the ten classes of iron meteorites this is not possible. These are remnants of the core of an asteroid. This means that the planet or planetoid is no longer an intact object that exists somewhere in the asteroid belt. For the other seven classes we are already quite successful in linking the meteorites to a possible celestial body in our solar system. Meteorites have been found which are derived from the moon. They provide a broader view of the moon because the stones brought back the the Apollo program only cover a few (landing) sites and meteorites are randomly launched of the surface. Under the microscope the moon meteorites are quite homogeneous and consist of a large proportion (50-90%) of plagioclase feldspars (*Figure 6D*).

Another group of achondrites are the Mars meteorites. These are a lot more difficult to link to the red planet, as there is no real reference, such as the stones brought back from the moon. However, researchers found a solution. The gas bubbles in some Mars meteorites were found to have the same composition as the Mars atmosphere.

There are three different types of Mars meteorites, which under the microscope are very different. Basaltic structures, fine structures and shocked glass: due to the complex geology of Mars the Mars rocks under the microscope look very similar to terrestrial rocks (see *Figure 6C*).

Another impressive achondrite group is that of the HED meteorites; howardites, eucrites and diogenites are merged together. Howardites are a mixture (in various proportions) of eucrites and diogenites and thus it became clear that these three meteorites have a relation to each other. It is believed that they are from the asteroid Vesta. This was long suspected based on Hubble observations of crater Rheasilvia and spectral observations and has been largely confirmed by the spacecraft Dawn. However, nature again didn't like to be grouped. Eucrites can be divided into five types, and it is not certain whether all five do originate from Vesta. Furthermore, there is a mineralogical relation between eucrites and the mesosiderites, which cannot yet be explained on the basis of the observations of Vesta with telescopes or spacecraft. We hope that this mystery can be solved by the large flow of new meteorites from Africa and Antarctica.

Under the microscope the HED are more easily recognizable meteorites, thanks to the large crystals of the diogenites (see *Figure 6B*), fine (basalt) needles of eucrites (see *Figure 6A*) and breccia structure (the mix of fragmented rocky fragments) from the howardites.

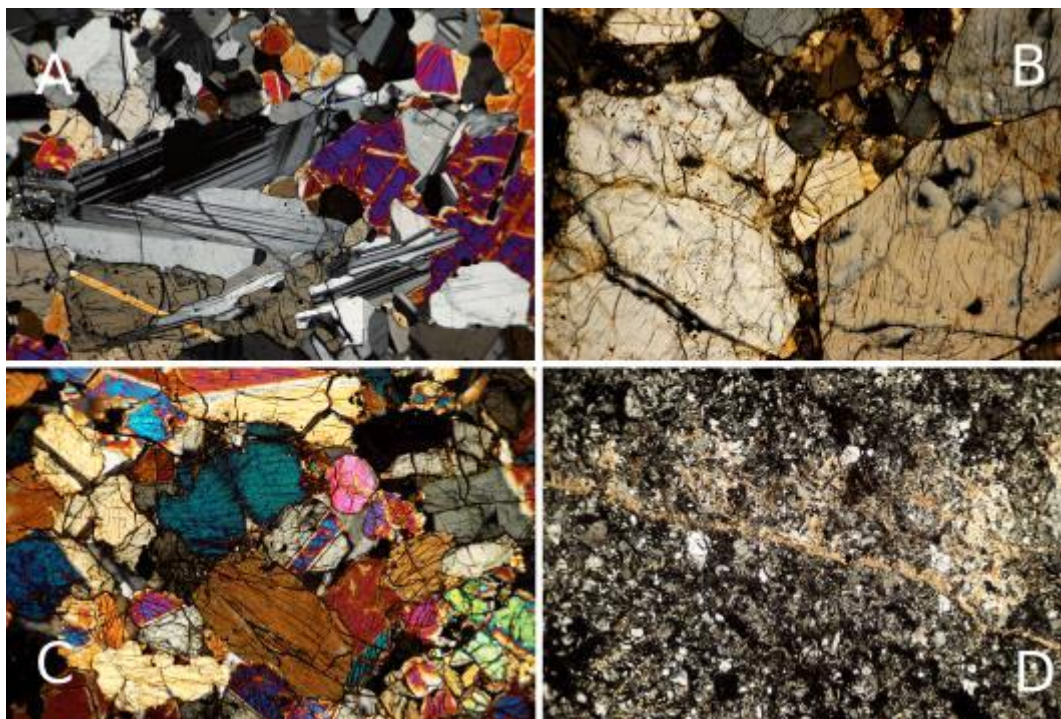


Figure 5 – Overview of achondrites. (A) Eucliet with needle-like plagioclase crystals (Tirhert), (B) Large pyroxene crystals of a Diogenite (NWA 4034), (C) pyroxenes (augite) and olivine crystals in a Mars meteorite (NWA 998), (D) plagioclase (anorthosite) and melt vein in a Moon meteorite (NWA 482). Actual dimensions (each picture) 2.25mm by 1.5 mm.

The outdated taxonomic group of stony-iron meteorites consisted of mesosiderites and pallasites. Both classes fall under the achondrites now and are also easily recognizable under the microscope. Pallasites consist almost half-and-half of metals (Fe, Ni), and olivine, this olivine forms very large, mm to cm size, crystals. When pallasites have a large terrestrial age the metals are often converted into the mineral hematite. Mesosiderites also consist half-and-half of silicates and metals, but the metal is often finer and distributed in-millimeter-sized fragments. The silicates consist of the well-known minerals olivine, pyroxene and feldspar.

## 5 Opportunities for amateurs

The meteorite research seems strongly based on the taxonomic approach of the science of the eighteenth century in some ways. It's about collecting, identifying, characterizing and see where a meteorite fits into the bigger story. This presents opportunities for amateurs into meteorite research. Thin sections are only a few square centimeters and thus each thin section can expose a completely new view of the meteorite. A thin section of the same meteorite can reveal lots of new features of that meteorite.

In addition, new meteorite falls are occurring regularly and meteorites from remote areas (think of North West Africa) go more often than not through life without proper classification. This is a niche where amateur research on classifications is possible. For example, the not yet detected subclasses of the chondrites, should be out there somewhere. And there are examples of amateurs who thus contribute to the meteorite research. In 2010, the French amateur Fabien Kuntz came across a strange

meteorite. After years of study it proved to be an entirely new class of chondrite, an F-chondrite, which had been predicted in 1977 in a model for the origin and evolution of the solar system.

It is possible to convert a (biological) microscope into a simple petrological microscope. This may be done with two filters from 3D cinema glasses, one that you place in front of the lamp and the other in front of the eyepiece. If you want to immerse yourself deeper in this field, investing in a petrological microscope is crucial. Their prices are similar to those a telescope, ranging from a few hundred euros to well into the thousands.

Making your own thin sections requires a lot of experience and practice, but they can easily be found on the Internet. Depending on the type of meteorite they are available from 50 euros onwards. If you want to delve into the theory and use of the petrological microscope you can go to petrological groups studying thin sections of terrestrial rocks, most geological societies will have these. With this gained knowledge, it is then easy to turn the earthy techniques to extraterrestrial rocks.

The solar system seen through a petrological microscope is also a nice crossover of geology and astronomy.

## Acknowledgments

I would like to thank Felix Bettonvil and Sebastiaan de Vet for their invitation to present this workshop during the 2016 IMC. This was a new audience for me and I was pleasantly surprised by the large turnout that evening. It was also very educational for me to have a talk with lots of you during the sessions in the bar. Thanks to all!

# PaDe - The particle detection program

Theresa Ott<sup>1</sup>, Esther Drolshagen<sup>1</sup>, Detlef Koschny<sup>2,3</sup> and Bjoern Poppe<sup>1</sup>

<sup>1</sup>University of Oldenburg, Germany

Theresa.ott@uni-oldenburg.de

<sup>2</sup>ESA/ESTEC, Noordwijk, The Netherlands

<sup>3</sup>Chair of Astronautics, TU Munich, Germany

This paper introduces the Particle Detection program PaDe. Its aim is to analyze dust particles in the coma of the Jupiter-family comet 67P/Churyumov-Gerasimenko which were recorded by the two OSIRIS (Optical, Spectroscopic, and Infrared Remote Imaging System) cameras onboard the ESA spacecraft Rosetta, see e.g. Keller et al. (2007). In addition to working with the Rosetta data, the code was modified to work with images from meteors. It was tested with data recorded by the ICCs (Intensified CCD Cameras) of the CILBO-System (Canary Island Long-Baseline Observatory) on the Canary Islands; compare Koschny et al. (2013). This paper presents a new method for the position determination of the observed meteors.

The PaDe program was written in *Python 3.4*. Its original intent is to find the trails of dust particles in space from the OSIRIS images. For that it determines the positions where the trail starts and ends. They were found using a fit following the so-called error function (Andrews, 1998) for the two edges of the profiles. The positions where the intensities fall to the half maximum were found to be the beginning and end of the particle. In the case of meteors, this method can be applied to find the leading edge of the meteor. The proposed method has the potential to increase the accuracy of the position determination of meteors dramatically. Other than the standard method of finding the photometric center, our method is not influenced by any trails or wakes behind the meteor. This paper presents first results of this ongoing work.

## 1 Introduction

The *Particle Detection Program* (PaDe) is written in *Python 3.4* and its main aim is to analyze images including a meteor or a trail of a dust particle in space. It determines where the trail starts and ends. The beginning and the end are both found to be the point where the intensity profile of the trail has fallen to half its maximum.

The program was initially developed for and is optimized to investigate the data of the OSIRIS (Optical, Spectroscopic, and Infrared Remote Imaging System) cameras onboard ESA's Rosetta spacecraft, for details about OSIRIS compare e.g. Keller et al. (2007). This and the underlying theory of the applied meteor position measurement are explained in detail in Drolshagen et al. (in press, 2017, PSS). The focus of this paper is to show this measurement technique using example images taken by the CILBO (Canary Island Long-Baseline Observatory) ICCs (Intensified CCD Cameras) on the Canary Islands (Koschny et al., 2013). In this case the data includes meteors which were found by the Meteor Detection Program MetRec (Molau, 1998).

The advantage of this method is that it determines the leading point of a meteor. Other software typically determines the photometric center of a meteor in a single video frame. As we will show, if a meteor develops a tail or wake during its flight, the photometric center will be shifted backwards and introduce errors. This shift can be avoided by using the proposed 'leading edge detection' algorithm. This idea goes back to a recommendation

during the Meteor Orbit Determination Workshop #03 (Koschny and Mc Auliffe, 2006).

In *Section 2* the profile of a theoretical constructed problem of a dust particle signal in space is shown. Then, in *Section 3*, the operating principle of PaDe is explained on the example of a CILBO meteor. In *Section 4* single frames will be analyzed and a shift between the photometric center of the meteor's signal and its 'real front' is found. This work presents the first results of ongoing work.

## 2 Leading edge detection using a theoretical profile

The following Section shows the intensity profile of theoretical signals of dust particles. CILBO uses video cameras to record meteors. In a single video frame, point sources (like stars) have a Gaussian-shaped signal. However, the dust particle is not fixed on the CCD and moves relative to the stars. The particle is visible as an elongated trail.

### 2.1 The intensity profile

At first, when the camera starts the exposure, the dust particle is a Gaussian-shaped point on the CCD, similar to the signal of stars. As the particle moves on it is recorded at each infinitesimal small time point.

To find the start and end of the particle the profile of the signal has to be investigated. *Figure 1* shows the profile of the created theoretical signal. For trails which are long, and for which the brightness of the moving object is

constant, there will be a plateau with constant brightness in the center part (compare *Figure 1*). As we cannot assume meteors to be of constant brightness, we use the OSIRIS dust particle trails as an example.

For the creation of the theoretical signals the start and end positions of the particle are fixed. The problem is constructed for a moving particle. In the first moment of the exposure time of the image, the Gaussian-shaped signal of the particle has its center at  $(0,0)$ . In the last moment of the exposure this center has moved to  $(N,0)$ . The positions where the intensity of the profile of the whole exposed signal has fallen to half its maximum value are exactly the positions the particle is at the beginning respectively at the end of the exposure ( $(0,0)$  and  $(N,0)$ ).

Consequently, the start and end positions of any particle can be found by finding the particle profile and determining the half-maximum points of both flanks. A theoretical description of this problem can be found in Drolshagen et al. (in press, 2017, PSS).

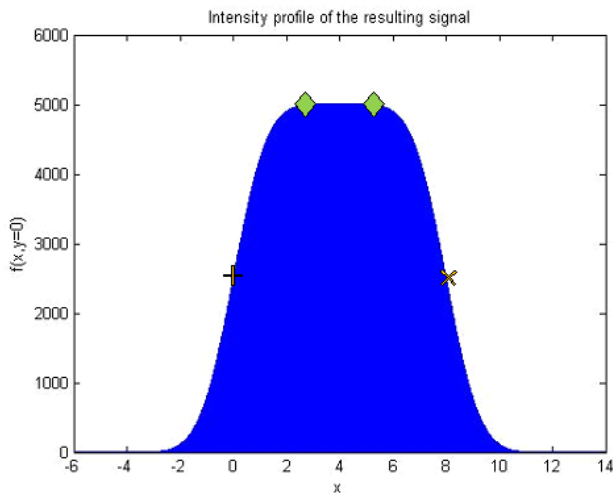


*Figure 1* – The intensity profile along the x-axis of the resulting signal. The maximum is located at the center of the profile and the beginning and end of the plateau are highlighted with green diamonds. The defined start and end of the particle are marked in orange with a plus and a cross respectively (at  $x=0$  and  $x=8$ ). These are the points where the intensity has fallen to half its maximum value.

### 3 The code

The program is optimized to analyze data including ideally one trail. The *Python* routine reads in the image data. For this, the bitmap images which were created by *MetRec* were used. These pictures contain the date and time when the meteor is detected in the lower right corner, compare *Figure 2* showing the original picture taken on the 02.01.2016 at about  $21^{\text{h}}08^{\text{m}}27^{\text{s}}$ . Because the date and time is part of each image, the lower right corner is masked by giving it the mean intensity value of the image.

Following, a *Canny algorithm* is utilized to detect the edges in the image. It is a multistage algorithm to detect edges developed by John Canny, see Canny (1986). We

use the library function in *Python* called *cv2.Canny()*, taken from the book of Bradski and Kaehler (2008). The result is presented in white in *Figure 3*. Subsequently, a *Hough Transformation* is applied to the binary image data resulting from the *Canny edge detection*. The *Hough Transformation* in general is a method for finding simple forms in an image, as lines or circles. The original *Hough Transform* was developed by Paul V. C. Hough (1959) and the use of the transformation in vision was introduced by Duda and Hart (1971). The used *Python* function is *cv2.HoughLinesP()* (Bradski and Kaehler, 2008). The lines that the *Hough Transformation* finds are on both sides of the particle. A linear fit is used to find a line that goes through the particle. The result is shown in *Figure 3* as a red dotted line.

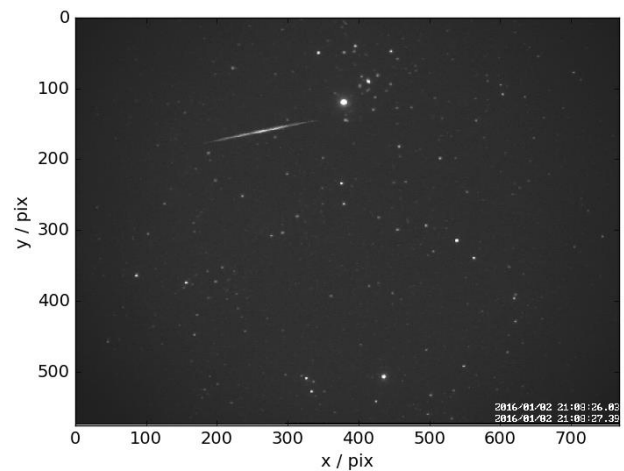


*Figure 2* – A Meteor recorded by the CILBO camera ICC7 on the 02.01.2016 at  $21^{\text{h}}08^{\text{m}}27^{\text{s}}$ . The image is the summed up image as found by *MetRec*.

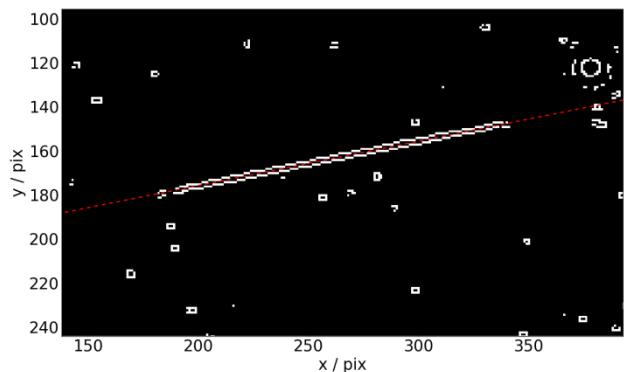


*Figure 3* – Enlarged part of *Figure 2*, with the edges found with the *Canny algorithm* in white and the line found afterwards with the *Hough transformation* as a red dotted line.

To improve the results *PaDe* searches for the maxima positions of the image. Afterwards, outliers are excluded by looking for the largest cluster and proximity to the *Hough transform* line. Following, a linear fit is performed through the found maxima values.

Next, the perpendicular lines which go through one of the points of the fit are analyzed, see e.g. the yellow line of *Figure 4*. For all perpendicular lines a Gaussian fit is attempted. If this fit was successful, the maximum of the Gaussian distribution will be utilized as the maximum point of the perpendicular line. Otherwise the point of the

highest value of the perpendicular line is used as the maximum value, compare the red dot at the intersection of the meteor and the yellow perpendicular line in *Figure 4*. Consequently, the maxima can be on a subpixel scale. Following, the maxima values found this way are checked again and outliers are ignored. Afterwards, a new linear fit through the so found maxima is performed.

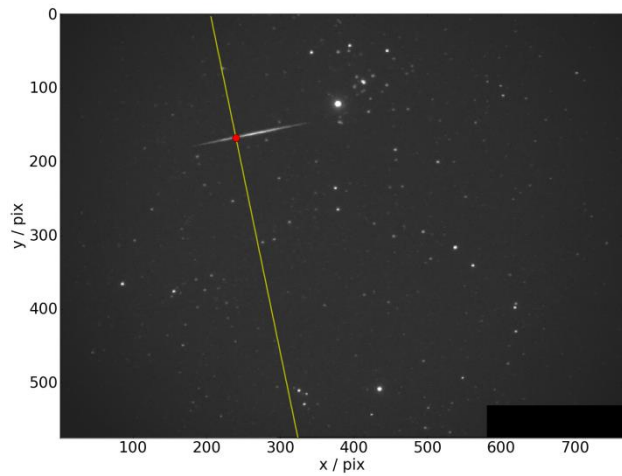


*Figure 4* – Same image as in *Figure 2* with an exemplary perpendicular line in yellow and the so found maximum position as red dot at the intersection of the meteor and the line.

Then, the profile of the signal along the fit line is created. This fit was adjusted to the single frames of the meteor, compare *Figure 8*. The corresponding intensity profile is shown in *Figure 7*. To do so, the border areas were considered as noise. The program searches for a '10 -  $\sigma$ ' deviation from this noise to define where the particle's signal starts. Afterwards, *PaDe* declares the 10 % largest intensity values as positions of a plateau and tries to find the amount that yields the best and most horizontal fit. Then, the program searches for the first and the last maxima of the plateau. The positions where the intensity values have fallen to the half maximum intensity values are declared the start and end of the particle. In the case of a meteor only the leading edge is of interest to us.

#### 4 Single frames

*Figure 2* shows a summed up image as found by *MetRec*. However, for the position determination the single frames have to be analyzed. The meteor in *Figure 2* was detected on 35 single frames, from which *MetRec* used 29 for the computations (the first three and the last three frames were excluded). *Figure 5* and *Figure 6* show enlarged parts of two example frames. The signal recorded on *Figure 5* is nearly Gauss symmetric. It is the 9<sup>th</sup> frame of the meteor's phenomena. In this case the photometric center of the signal is in the middle of the signal and this position corresponds to the position where the meteoroid really is in this frame. *Figure 6* presents the 30<sup>th</sup> frame. It is the last frame for which *PaDe* works. This signal shows a tail. In this case the photometric center (blue cross in *Figure 6*) is shifted to the right with respect to the leading edge (red plus in *Figure 6*) as found by *PaDe* by utilizing the half maximum position of the intensity

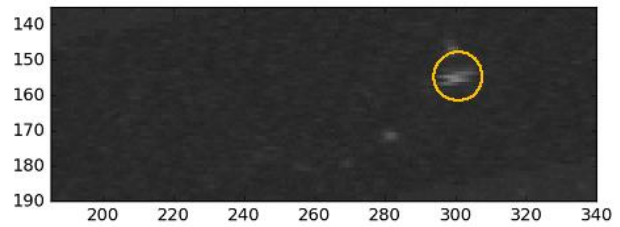


*Figure 5* – Part of the 9<sup>th</sup> frame of the summed up image shown in *Figure 2*. The meteor's signal is nearly Gaussian symmetric and highlighted in yellow.

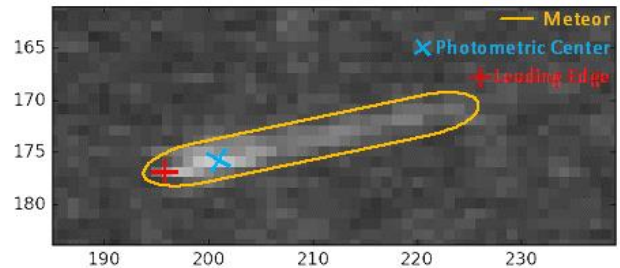


*Figure 6* – Part of the 30<sup>th</sup> frame of the summed up image shown in *Figure 2*. The meteor's signal which shows a tail in this frame is highlighted in yellow. The photometric center is indicated with the blue 'x' and the leading edge with the red '+'.

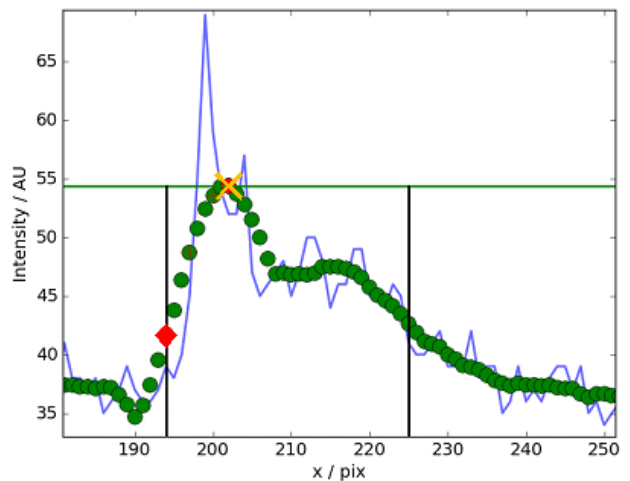


*Figure 7* – Part of the profile along the linear fit through the meteor presented in *Figure 6* as found by *PaDe*. The original profile is presented as a blue line, the smoothed profile as green dots and the found maxima plateau is highlighted with an orange 'x' which also indicates the photometric center. The positions where the intensity has fallen to half its maximum are marked by the black vertical lines and the leading edge by a red diamond. It can be seen that the detected photometric center does not represent the real end of the meteor.

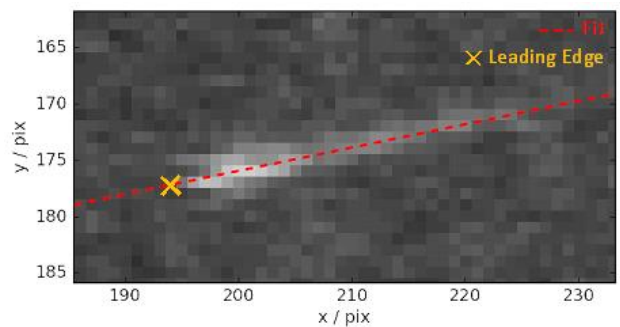


*Figure 8*– Enlarged part of *Figure 6* with the fit through the particle as a red dashed line and the leading edge found by *PaDe* as a yellow cross.

profile, compare *Figure 7*. As the linear fit through the signal the one found for the summed up image was used. This shows that a wake or tail in the meteor's signal can shift the photometric center. For this reason, the center will not be used as the position but rather the leading edge of the meteor, see *Figure 8*.

## 5 Conclusion

In this work the Particle Detection Program *PaDe* is presented, it was developed to analyze images including a meteor or a trail of a dust particle in space. The program analyzes the intensity profile of the recorded signal and detects the position of the start and end of the trail. These positions are both found to be the point where the intensity profile of the trail has fallen to half its maximum.

The program was initially developed for investigating the data of the OSIRIS cameras onboard ESA's Rosetta spacecraft. In this paper the underlying theory was explained and the applicability to measuring meteor positions was shown. This was accomplished by using example images with meteors taken by the CILBO Cameras on the Canary Islands.

The advantage of the method explained herein is the determination of the leading edge of a meteor, unlike other software which typically determines the photometric center of a meteor in a single video frame. It was shown that if a meteor develops a tail or wake during its flight, the photometric center will be shifted backwards. This introduces errors but can be avoided by using our 'leading edge detection' algorithm.

Nonetheless, the program has to be optimized to also work with very faint or noisy meteors so that the real last frame can be investigated and used for further analysis. Moreover, the statistics have to be enhanced by analyzing more meteors and their single image frames. The CILBO station has detected over 10000 double station meteors (Albin et al., 2017, in press, PSS) for which the differences of the leading edge and the photometric center can be investigated. Furthermore, meteors do not necessarily have to follow straight lines. All-sky cameras for example, record them as a curved signal due to the curvature of their field. For this case *PaDe* has to be adjusted by using the *Hough transformation* for curved forms and a profile through the curved line.

## References

- Albin T., Koschny D., Soja R., Srama R. and Poppe B. (2017). "The CILBO meteor orbit database". *Meteoroids 2016*, Proceedings of the Conference 2016. ESTEC, Noordwijk, in press.
- Andrews L. C. (1998). "Special Functions of Mathematics for Engineers". s.l.:SPIE Press; Auflage: 2.
- Bradski G. and Kaehler A. (2008). Learning OpenCV. 1005 Gravenstein Highway North, Sebastopol, CA 95472: O'Reilly Media Inc..
- Canny J. (1986). "A Computational Approach to Edge Detection". *IEEE Transactions Pattern Analysis and Machine Intelligence*, **8**, 679–698.
- Drolshagen E., Ott T., Koschny D., Guettler C., Tubiana C., Agarwal J., Sierks H., Barbieri C., Lamy P. I., Rodrigo R., Rickman H., A'Hearn M. F., Barucci M. A., Berteaux J.-L., Bertini I., Cremonese G., Da Deppo V., Davidsson B., Debei S., De Cecco M., Deller J., Fornasier S., Fulle M., Groussin O., Gutiérrez P. J., Hofmann M., Hviid S. F., Ip W.-H., Jorda L., Keller H. U., Knollenberg J., Kramm J. R., Kühr E., Küppers M., Lara L. M., Lazzarin M., Lopez Moreno J. J., Marzari F., Naletto G., Oklay N., Shi X., Thomas N., Vincent J.-B. and Poppe B. (2017). "Distance Determination Method of Dust Particles using Rosetta OSIRIS NAC and WAC Data". *Planetary and Space Science*, in press.
- Duda R. O. and Hart P. E. (1971). "Use of the Hough Transformation to Detect Lines and Curves in Pictures". *Artificial Intelligence Center*. Technical note 36.
- Hough P. V. C. (1959). "Machine Analysis of Bubble Chamber Pictures". *Proc. Int. Conf. High Energy Accelerators and Instrumentation*.
- Keller H. U., Barbieri C., Lamy P., Rickman H., Rodrigo R., Wenzel K.-P., Sierks H., A'Hearn M. F., Angrilli F., Angulo M., Bailey M. E., Barthol P., Barucci M. A., Berteaux J.-L., Bianchini G., Boit J.-L., Brown V., Burns J. A., Büttner I., Castro J. M., Cremonese G., Curdt W., Da Deppo V., Debei S., De Cecco M., Dohlen K., Fornasier S., Fulle M., Germerott D., Gliem F., Guizzo G. P., Hviid S. F., Ip W.-H., Jorda L., Koschny D., Kramm J. R., Kühr E., Küppers M., Lara L. M., Llebaria A., López A., López-Jimenez A., López-Moreno J., Meller R., Michalik H., Michelena M. D., Müller R., Naletto G., Origné A., Parzianello G., Pertile M., Quintana C., Ragazzoni R., Ramous P., Reiche K.-U., Reina M., Rodriguez J., Rousset G., Sabau L., Sanz A., Sivan J.-P., Stöckner K., Tabero J., Telljohann U., Thomas N., Timon V., Tomasch G., Wittrock T. and Zaccariotto M. (2007). "OSIRIS - The Scientific Camera System Onboard Rosetta". *Space Science Reviews*, **128**, 433–506.
- Koschny D., Bettonvil F., Licandro J., v.d. Lujt C., Mc Auliffe J., Smit H., Svedhem H., de Wit F., Witasse O. and Zender J. (2013). "A double-station meteor camera setup in the Canary Islands

– CILBO”. *Geoscientific Instrumentation Methods and Data Systems*, **2**, 339–348.

Koschny D. and Mc Auliffe J. (2006). “Meteor orbit determination - points to be considered”. In Koschny D. and Mc Auliffe J., editors, *Proceedings of the first Europlanet workshop on meteor orbit determination*, Roden, The Netherlands September 11<sup>th</sup> – 13<sup>th</sup>, pages 85–94.

Magrin S., La Forgia F., Da Deppo V., Lazzarin M., Bertini I., Ferri F., Pajola M., Barbieri M., Naletto G., Barbieri C., Tubiana C., Küppers M.,

Fornasier S., Jorda L. and Sierks H. (2015). “Pre-hibernation performances of the OSIRIS cameras onboard the Rosetta spacecraft”. *Astronomy and Astrophysics*, **574**, id Ad123, 13 pages.

Molau S. (1998). “The Meteor Detection Software MetRec”. In Baggaley W.J. and Porubcan V., editors, *Proceedings of the International Conference, Meteoroids 1998*, held at Tatranska Lomnica, Slovakia, August 17-21, 1998. Astronomical Institute of the Slovak Academy of Sciences, pages 131–134.



David Asher and Juraj Toth.

# Evaluating video digitizer errors

Chris Peterson

Denver Museum of Nature and Science, Denver, USA

clp@alumni.caltech.edu

Analog output video cameras remain popular for recording meteor data. Although these cameras uniformly employ electronic detectors with fixed pixel arrays, the digitization process requires resampling the horizontal lines as they are output in order to reconstruct the pixel data, usually resulting in a new data array of different horizontal dimensions than the native sensor. Pixel timing is not provided by the camera, and must be reconstructed based on line sync information embedded in the analog video signal. Using a technique based on hot pixels, I present evidence that jitter, sync detection, and other timing errors introduce both position and intensity errors which are not present in cameras which internally digitize their sensors and output the digital data directly.

## 1 Introduction

Video signal formats were developed in support of analog video hardware which outputs discrete rows, but non-discrete columns. Such signal formats are not ideal for outputting data from modern image sensors consisting of arrays of photosensors, but remain in common use, particularly in devices utilized to record meteor trails.

Modern electronic cameras employing CCD or CMOS sensor arrays typically digitize the value of each pixel internally and then export that value digitally, allowing an external data array to be populated with values that correspond directly with the sensor array pixels. However, there remain many cameras which utilize modern sensors, but continue to output an analog video signal. Such cameras are frequently very inexpensive, have good light sensitivity, and are utilized for CCTV and direct viewing applications. When used for meteor capture, the analog signal must be externally digitized for storage and analysis. Timing errors in both the camera and the external digitizer introduce position errors when calculating meteor positions on frames, which may be significant in some applications.

## 2 Measurement accuracy

Most meteor detection applications perform a centroid calculation on the meteor image in order to determine position to sub-pixel precision. The measurement accuracy is primarily determined by signal-to-noise considerations. Using numerical simulations, we can determine the best possible accuracy under different scenarios. For a best case example of a meteor image with a FWHM of 3 pixels and a mean intensity 45 dB above the readout noise floor, it is possible to determine the centroid to a precision of 0.1 pixels. This is typical performance for a high quality analog video camera and an 8-bit digitizer.

Photometric accuracy is less likely to be impacted, as the usual processing involves summing all the pixels in an aperture much larger than the pixel position error range. It is possible however that photometric errors are introduced if the digitizer pixel sample windows have

gaps between them, such that some integrated signal goes unmeasured.

## 3 Video format

Unlike digital output cameras, analog video depends upon a strictly defined timing sequence, where the output signal is synchronous with the readout of the sensor. While the row a pixel lies on is unambiguously determined, there is no mechanism in the analog video signal to accurately determine the location of a pixel's column, or to identify individual pixels at all. A horizontal pixel position is assumed based on the amount of time since a horizontal sync pulse was detected (*Figure 1*). The charge from a row of pixels is simply dumped to a filtered output, providing a signal which is non-discrete in both amplitude and time.

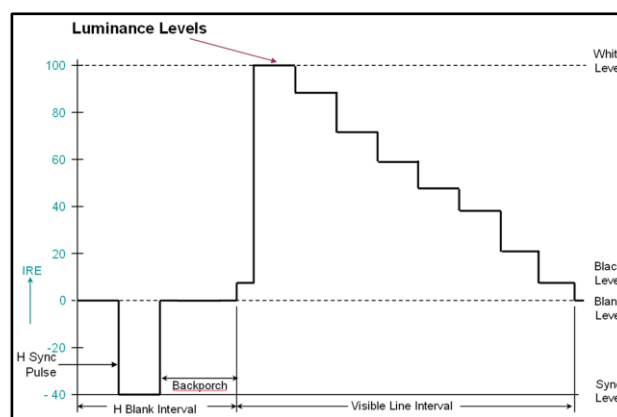


Figure 1 – Simplified video timing.

## 4 The impact of timing errors

When an analog video line is captured, it is discretely sampled at regular intervals. In the absence of perfect timing, each pixel in the output array consists of signal from more than one physical sensor pixel. Additionally, timing jitter makes the relative contribution of each physical pixel vary from line to line and frame to frame. This can result in an increase in the position error when performing a centroid measurement on the image data array.

Timing errors have two sources: timing in the camera itself and timing in the video digitizer. Most analog video cameras target the CCTV market, designed for direct viewing on monitors or recording on devices which are very tolerant of deviations from timing standards. They typically derive their internal timing from inexpensive crystals or ceramic resonators which introduce approximately 200 ps of peak-to-peak jitter on the nominally 70 nm pixel clock. Assuming an 8-bit system, this is on the order of one bit, which is probably not significant. However, with 10-bit systems this error may represent a significant percentage of the camera readout noise.

A generally more problematic source of timing errors lies in the video digitizer. Because the camera provides no reference clock, the digitizer is forced to synthesize a clock using only the horizontal sync pulses of the video signal. The digitizer is subject to similar clock jitter issues as the camera itself, but frequently relies on phase locking or on digital synthesis techniques to accommodate the wide range of possible camera timing, which can increase the jitter at the point of sampling by an order of magnitude or more. This study focuses on analyzing digitizer errors, recognizing that the results are slightly convolved with camera timing errors.

### 5 Test method

This work follows from a previous analysis (Peterson, 2011) that utilized an optical point source to simulate a meteor image. That approach demonstrated that digitizer timing errors are significant, but also introduced systemic errors that are difficult to correct for. The new methodology takes advantage of warm pixels on the camera sensor. These are pixels with fixed, unsaturated charges in the absence of any light. This produces a video output where all of the signal comes from a single physical pixel, with no shift of charge between pixels possible, and no other components except for readout noise and Poisson (shot) noise (Figure 2). The result is a near ideal test platform for digitizers.

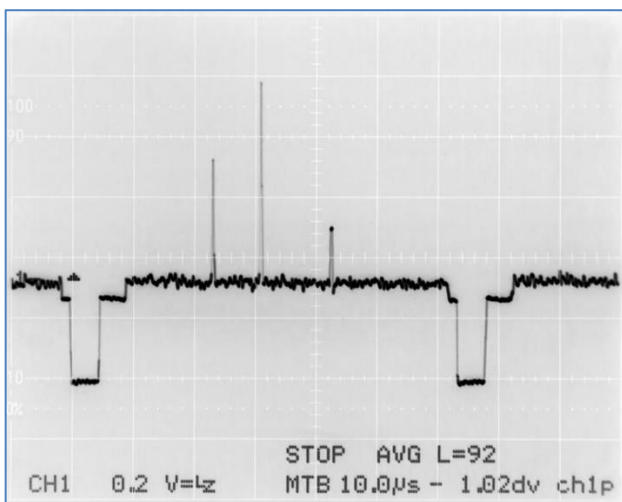


Figure 2 – Three warm pixels on a single video line.

The test procedure utilized a Watec 902H camera (Sony ICX249 AL CCD, active array size 752 x 582 pixels). Sony HAD sensors tend to accumulate warm pixels over time due to cosmic ray damage; old cameras usually have many warm and hot pixels. The camera was connected to the digitizer under evaluation, and 1000 uncompressed video dark frames were captured at a resolution of 640 x 480. The frames were de-interlaced by field duplication. An isolated warm pixel was identified, and the centroid of the pixel calculated for each frame using the IRAF *imcntr* centroid algorithm (Tody, 1993). The warm pixel was selected such that its mean amplitude was 40 dB above the noise floor. The horizontal and vertical centroid means and standard deviations were calculated, as well as the peak-to-peak variation. Two digitizers were evaluated: a Matrox Meteor II (PCI bus) and a KWorld VS-USB2800D (USB 2 bus). Video was recorded using Debut Video Capture (NCH Software) running under Windows 10. Frames were also analyzed from a control camera with a direct USB interface (Imaging Source DMK 21AU04.AS, Sony ICX098 BL CCD) utilizing a warm pixel also 40 dB above the noise floor.

### 6 Experimental results

Table 1 summarizes the 1000-sample runs with the two test digitizers and with the control camera. Note also the non-integer values of the x-axis centroids due to timing error and pixel remapping.

The actual centroid values for each test are presented as scatterplots (Figures 3–5).

Table 1 – Digitizer centroid performance.

Digitizer	Mean Centroid	SD	P-P
Meteor II	302.03 , 112.00	0.71 , 0.07	4.23 , 0.44
2800D	306.14 , 112.00	0.67, 0.08	4.43 , 0.49
DMK 21	481.00 , 110.00	0.07 , 0.07	0.40 , 0.50

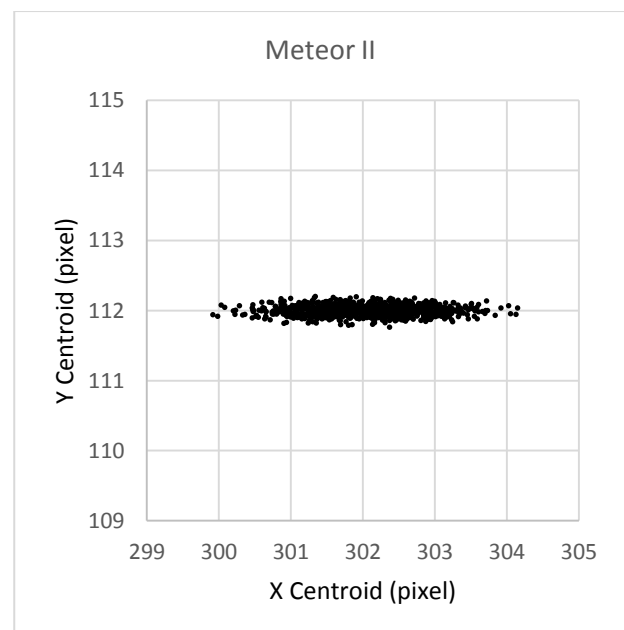


Figure 3 – Matrox Meteor II centroid scatter.

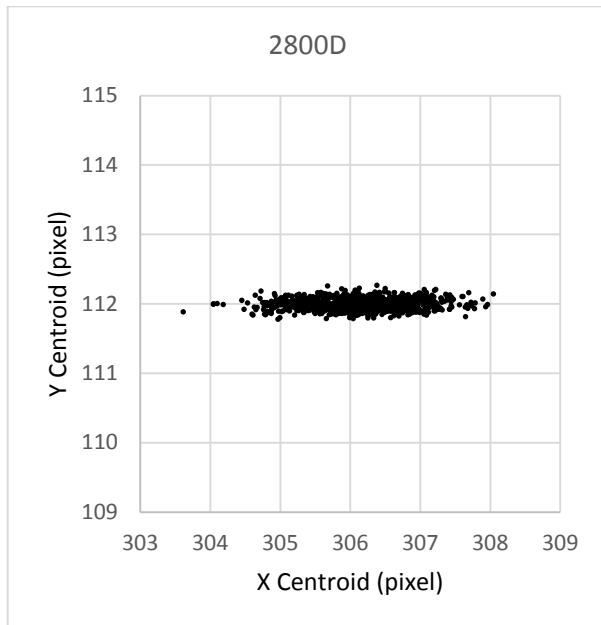


Figure 4 – KWorld VS-USB2800D centroid scatter.

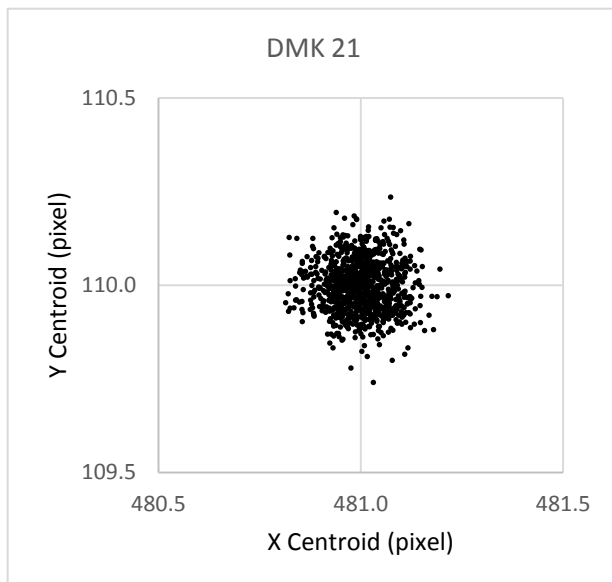


Figure 5 – Imaging Source DMK 21AU04.AS centroid scatter.

## 7 Analysis

While this testing method does not completely disentangle all possible sources of digitization error: clock jitter in both the camera and the digitizer, variable

delay between the horizontal sync pulse and the acquisition window, aliasing between the pixel sample windows and the physical pixels, variable sampling aperture, and others, it clearly demonstrates that at least some popular camera and digitizer combinations introduce significant x-axis errors- approximately an order of magnitude greater than the errors observed on the y-axis. Y-axis errors, and errors on both axes of the digital output camera, are near their theoretical minimums.

## 8 Conclusion

These errors are inherent in analog camera/video capture systems. Meteor researchers seeking to maximize their data quality should explore converting their systems to digital output cameras. Where that is not possible, formal error analysis should include the asymmetry between the horizontal and vertical axes. Cameras and digitizers are easily characterized using this technique.

Photometric algorithms that utilize peak intensities should be avoided.

We have observed some apparent improvement in orbit calculation accuracy (using known shower members as references) simply by rotating some network cameras so that stations are aligned more nearly along the camera y-axes.

## References

- Peterson C. (2011). "A comparison of the impact of jitter and timing errors on the accuracy of several popular video capture devices". NASA Workshop: Meteor Video Observations and Analysis, PARI, 2011 Aug 4-5. 16 pages.
- Tody D. (1993). "IRAF in the Nineties". In Hanisch R. J., Brissenden R. J. V. and Barnes J., editors, *Astronomical Data Analysis Software and Systems II*, A.S.P. Conference Ser., **52**, 173–183.

# Sungrazing comets and meteoroids

Eduard Pittich<sup>1</sup> and Nina Solovaya<sup>2</sup>

<sup>1</sup>Slovak Academy of Sciences, Bratislava, Slovak Republic

pittich@savba.sk

<sup>2</sup>Lomonosov Moscow University, Moscow, Russia

solov@sai.msu.ru

We studied the dynamical behavior of meteoroids ejected from sungrazing comets upon their arrival to the central part of the solar system. In order to get a clear insight into the geometry and detectability of such meteoroids, some model computations have been performed. It is assumed that dust particles emitted from the comets by low-velocity are affected by the gravitational forces of the Sun and planets, the Poynting-Robertson effect, and the pressure of the solar wind. Some of these particles come to the vicinity of the Earth, crossing its orbit, and can be candidates for collisions. Mean value of the orbital elements of the Kreutz sungrazers were applied for model computations.

## 1 Introduction

Sungrazers are quite a mysterious group of cometary population in the solar system. They are defined as comets with the perihelion distance about 2 solar radii, or less. From the historical point of view, the first sungrazer, which astronomers knew, was the comet C/1680 VI. It is the first comet, whose orbit was computed by the new Newton theory of gravitation. After this comet several later comets with similar orbits, C/1826 V, C/1843 D1, C/1880 C1, C/1882 K1, C/1882 R1, and C/1887 B1 were discovered. Kreutz (1888) turned his attention to these comets as being one group of cometary population. From this time the group of these comets is called Kreutz' group.

The number of sungrazers' discoveries has started growing rapidly thanks to the launch of coronagraphic telescopes on space probes, including Solwind, SMM, SOHO, and STEREO satellites. Especially, the SOHO program is very successful. On September 13, 2015 SOHO coronagraphs detected their 3000<sup>th</sup> comet (Fox, 2016)<sup>1</sup>.

Known sungrazers are divided into four groups according to their orbital elements (see e. g. Marsden and Williams, 2008; Minor Planet Circulars issued from July 2008<sup>2</sup>). About 83% of sungrazers are members of the Kreutz group. The other 17% belongs to some sporadic sungrazers and to the next three groups: Krach, Marsden, and Meyer. The mean values of the orbital elements for each group are listed in *Table 1* (Guliyev, 2010).

Several sungrazers, as the Great March Comet 1843 (C/1843 D1), the Great Comet 1882 (C/1882 R1), Ikeya-Seki (C/1965 S1), Lovejoy (C/2011 W3), were comets with the large tail, briefly bright to be visible in the daytime. To this group of comets belongs the comet

ISON (C/2012 S1), too. Unfortunately, it disintegrated shortly before its perihelion passage. The comet 96P Machholz is related with meteor showers. Comets from the Marsden and Krach groups are linked to several meteor streams, too. Thus particles ejected at least from several sungrazers crossed the Earth's orbit. They are detected as members of a particular meteor stream.

Some of the SOHO sungrazers display tails, which are characteristic of their dust-production histories. Unfortunately, many of the SOHO comets did not survive their perihelion passage. Sekanina (2000) showed from the analysis of 11 SOHO sungrazers that, other than solar gravity, solar radiation pressure is the only force that perceptibly affects the motion of microscopic dust in their tails. Particle ejection velocities do not broaden appreciably the tails' outlines. Electrostatic potentials to which grains are charged are so low that no Lorentz force is detected in spite of the strong magnetic fields present in the corona and the ejecta's high velocities relative to the solar wind. Analysis of Sekhar and Asher (2014) shows that for meteoroids ejected from all known sungrazing groups during recent epochs, only the Marsden family produces meteor phenomena. Such a process required ejection velocities of some hundreds of  $\text{m s}^{-1}$ .

Given the above, the aim of our work is the study of the orbital behavior of dust particles ejected with zero velocity from sungrazers of the Kreutz type. To find out whether they can reach an orbit with the nodes close to the Earth's orbit, and for which conditions components, incorporating the following applicable criteria.

## 2 Model computations

In order to get a clear insight into the geometry and detectability of sungrazer dust tails, some model computations have been performed by the authors. The figures in this paper show the orbital evolution of dust particles produced by low-velocity emissions from a sungrazing comet of the Kreutz group. For this purpose

<sup>1</sup>“ESA/NASA Solar Observatory Discovers Its 3,000th Comet”. Web page: [nasa.gov/feature/goddard/esa-nasa-solar-observatory-discovers-its-3000th-comet](http://nasa.gov/feature/goddard/esa-nasa-solar-observatory-discovers-its-3000th-comet)

<sup>2</sup>[http://www.minorplanetcenter.net/iau/ECS/MPCArchive/MPCArchive\\_TBL.html](http://www.minorplanetcenter.net/iau/ECS/MPCArchive/MPCArchive_TBL.html)

we used mean values of the orbital elements of the model sungrazer from *Table 1*.

The comet with mass  $M = 2 \times 10^{-12}$  kg is moving in a parabolic orbit of perihelion distance  $q = 0.006$  au, argument of perihelion  $\omega = 80^\circ$ , longitude of the ascending node  $\Omega = 0^\circ$ , orbital inclination  $i = 144^\circ$ , and perihelion passage  $T = 2015$  June 1 UT.

*Table 1* – Mean values of orbital elements of sungrazer groups:  $e$  – eccentricity,  $q$  – perihelion distance,  $\omega$  – argument of perihelion,  $\Omega$  – longitude of ascending node,  $i$  – inclination.

Group	$e$	$q$ au	$\omega$ °	$\Omega$ °	$i$ °
<b>Kraft</b>	0.98	0.045	59	44	13
<b>Kreutz</b>	1	0.006	80	0	144
<b>Meyer</b>	1	0.036	57	73	73
<b>Marsden</b>	0.98	0.050	24	79	27

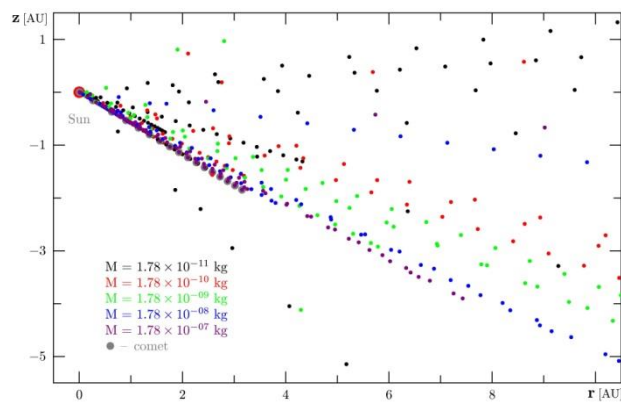


*Figure 1* – Ecliptic altitude  $z$  versus heliocentric distance  $r$  of the particles with the mass  $M$  ejected from the comet with zero velocity within the pre-perihelion interval of  $-175^\circ \leq \nu \leq +175^\circ$ . The orbital elements of the comet are average orbital elements of the Kreutz group.

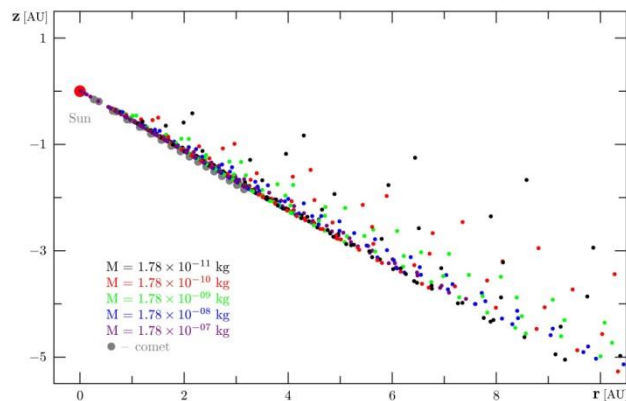


*Figure 2* – Ecliptic altitude  $z$  versus heliocentric distance  $r$  of the particles with the mass  $M$  ejected from the comet with zero velocity within the post-perihelion interval of  $-175^\circ \leq \nu \leq +175^\circ$ . The orbital elements of the comet are average orbital elements of the Kreutz group.

The colored dots in *Figures 1–2* indicate the positions of the comet and dust particles emitted from the comet by zero velocity started in the true anomaly of the comet  $\nu = -175^\circ$  until  $\nu = -150^\circ$ , with the step  $\Delta\nu = +5^\circ$ , in  $\nu = -150^\circ$  until  $\nu = +150^\circ$ , with the step  $\Delta\nu = +30^\circ$ , and in  $\nu = +150^\circ$  until  $\nu = +175^\circ$ , with the step  $\Delta\nu = +5^\circ$

again. The different steps were selected depending on the orbital velocity of the comet for a given true anomaly. The heliocentric distance of the comet is  $r = 3.15$  au for  $\nu = \pm 175^\circ$ .

The positions of the comet and dust particles correspond to their movement affected by the gravitational forces of the Sun and planets, the Poynting-Robertson effect, and the pressure of the solar wind (see e. g. Klačka and Pittich, 1994). For every value of  $\nu$  the comet and particle positions are plotted with the step of 10 days. The lower boundary of the particles mass  $M = 1.78 \times 10^{11}$  kg. Each following particle has the mass one order of magnitude higher, up to  $10^4$  times the first value.

*Figures 3–6* are similar as previous two. The comet and particle positions are plotted for a selected true anomaly with the step of 0.2 day. *Figures 3–5* show the orbital evolution of the particles with the mass, *Figure 6* – the orbital velocity, of one particle is changed so that the heliocentric distance of the particle's ascending node is equal to one AU.

For our model we adopted Verniani's (1973) value of the particle density,  $\rho = 800$  kg m $^{-3}$ , obtained for faint radio meteors. This value, assuming spherical shape of a particle, corresponds to the particle's radius  $s = 1.744 \times 10^{-5}$  m for  $M = 1.78 \times 10^{-11}$  kg,  $s = 3.758 \times 10^{-5}$  m for  $M = 1.78 \times 10^{-10}$  kg,  $s = 8.095 \times 10^{-5}$  m for  $M = 1.78 \times 10^{-9}$  kg,  $s = 1.744 \times 10^{-4}$  m for  $M = 1.78 \times 10^{-8}$  kg, and  $s = 3.758 \times 10^{-4}$  m for  $M = 1.78 \times 10^{-7}$  kg.

We traced orbital evolution of the comets and ejected particles using our numerical integration code with the integrator RA15 (Everhart, 1985). The masses and rectangular ecliptic coordinates and velocities of the planets for the numerical integrations of the equations of motion were taken from the JPL Horizons System (Giorgini et al., 1996) on the date of June 1, 2015.

### 3 Results of orbital integration

The results obtained by numerical integration for the dust particles considered in our model of a cometary orbit with the perihelion passage  $T = \text{June 1, 2015}$  are the dynamical evolution of particles ejected from the comet with zero velocity within the interval of  $-150^\circ \leq \nu \leq +150^\circ$ . In one case, the particle's ejection velocity was modified to  $15$  km s $^{-1}$ .

*Figure 1* displays the ecliptic altitude  $z$  of the particles versus their heliocentric distances  $r$  within the pre-perihelion investigated interval of the true anomaly  $\nu$  at which their ejection took place. In the first approximation, we can look at this figure as on the dispersion of particles toward the comet in its orbital plane. The dispersion of most particles is no more than 6 au at the heliocentric distance of 10 au. Some of them are moving above the ecliptic plane in a heliocentric distance greater than 2 au.

Figure 2 is similar as the previous one. It displays the orbital positions of the particles within the post-perihelion investigated interval of the true anomaly  $\nu$  at which their ejection happened. The orbital evolution of the particles ejected from the comet after its perihelion passage is quite different than those, which were ejected from the comet on its pre-perihelion orbit. The dispersion of the particles is no more than 3 au at the heliocentric distance of 10 au. Unlike the particles ejected within the pre-perihelion interval, all particles ejected after the perihelion passage of the comet move under the ecliptic plane.

The difference between the width of the dispersion of particles' position in the pre- and the post-perihelion cases is mainly due to the different length of their orbital evolution. At the post-perihelion case the time interval of the orbital evolution of particles is twice as less than in the case of their pre-perihelion evolution.

Given the character of the cometary orbit, the momentum of the particles is very little disturbed by planetary perturbations and non-gravitational forces within the investigated interval of  $\nu$ . Therefore orbital inclinations of model particles are similar to the comet's inclination.

Data plotted on Figures 1–2 suggest that some particles can reach the Earth's orbit in the case, if suitable conditions of their ejection's time and velocity are met. We computed following four examples for such cases.

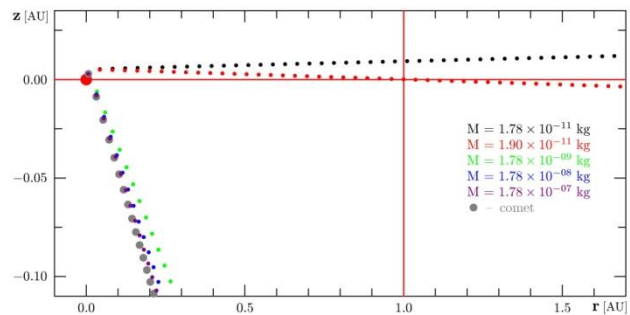


Figure 3 – Ecliptic altitude  $z$  versus heliocentric distance  $r$  of the particles with the mass  $M$  ejected from the comet with zero velocity within the interval of  $-30^\circ \leq \nu \leq +175^\circ$ . The orbital elements of the comet are average orbital elements of the Kreutz group. The red particle with mass  $M = 1.90 \times 10^{-11}$  kg crossed the Earth's orbit at 2015 June 6.3.

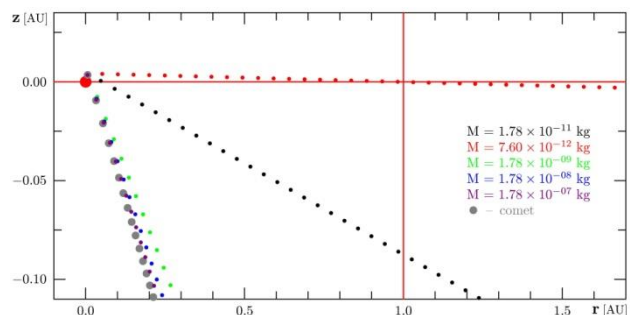


Figure 4 – Ecliptic altitude  $z$  versus heliocentric distance  $r$  of the particles with the mass  $M$  ejected from the comet with the zero velocity within the interval of  $0^\circ \leq \nu \leq +175^\circ$ . The orbital elements of the comet are average orbital elements of the Kreutz group. The red particle with mass  $M = 7.60 \times 10^{-12}$  kg crossed the Earth's orbit at 2015 June 6.3.

Figure 3 displays the ecliptic altitude  $z$  of the particles ejected at the true anomaly  $\nu = -30^\circ$  versus their heliocentric distances  $r$  within the time interval around the comet's perihelion passage. The step between each two particle's positions is 0.2 day. If the mass of the red particle was changed from our original model value  $M = 1.78 \times 10^{-11}$  kg to  $M = 1.90 \times 10^{-11}$  kg the particle's ascending node was moved to the Earth' orbit. The red particle crossed the Earth's orbit at 2015 June 6.3 UT, five days after the comet's perihelion passage.

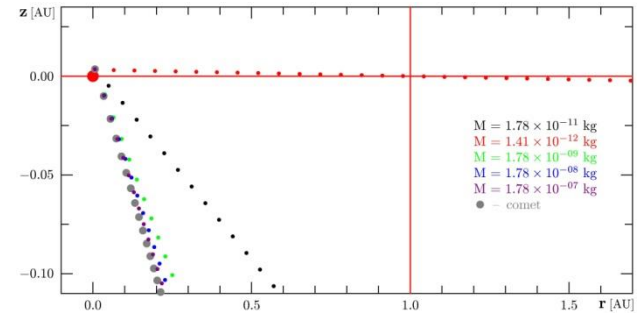


Figure 5 – Ecliptic altitude  $z$  versus heliocentric distance  $r$  of the particles with the mass  $M$  ejected from the comet with zero velocity within the interval of  $+30^\circ \leq \nu \leq +175^\circ$ . The orbital elements of the comet are average orbital elements of the Kreutz group. The red particle with mass  $M = 1.41 \times 10^{-12}$  kg crossed the Earth's orbit at 2015 June 6.3.

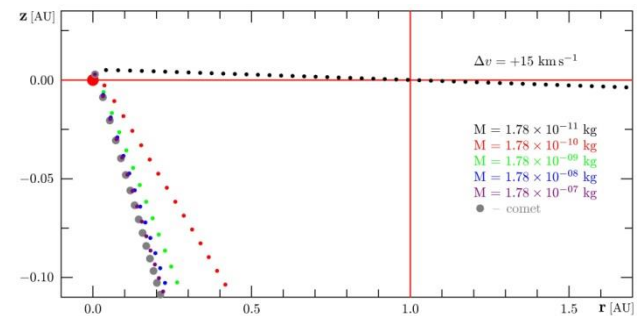


Figure 6 – Ecliptic altitude  $z$  versus heliocentric distance  $r$  of the particles with the mass  $M$  ejected from the comet with zero velocity within the interval of  $-30^\circ \leq \nu \leq +175^\circ$ . The orbital elements of the comet are average orbital elements of the Kreutz group. The black particle was ejected from the comet with velocity  $15 \text{ km s}^{-1}$  in the direction of the x-component of the heliocentric ecliptic rectangular coordinate system. It crossed the Earth' orbit at 2015 June 6.5.

Figures 4 and 5 show similar results for the ejection of particles at the true anomaly  $\nu = 0^\circ$  and  $\nu = +30^\circ$ , respectively. In the first case the original model mass of the red particle  $M = 1.78 \times 10^{-11}$  kg was changed to  $M = 7.60 \times 10^{-12}$  kg, in the second case to  $M = 1.41 \times 10^{-12}$  kg. In both cases the red particle reached the Earth's orbit after the comet's perihelion passage, at 2015 June 5.1 and 6.3, respectively.

The orbital evolution of a particle with the non-zero ejection velocity is showed in Figure 6. In this case the ejection of particles occurred at the true anomaly  $\nu = -30^\circ$ . If the black particle reaches the Earth's orbit, the ejection velocity of the particle would have to be  $15 \text{ km s}^{-1}$  in the direction of the x-component of the heliocentric ecliptic rectangular coordinate. It crossed the

Earth' orbit at 2015 June 6.5, after the comet's perihelion passage, again. Mass of the black particle was not changed. Its value is equal to our model mass  $M = 1.78 \times 10^{-11}$  kg.

The examples showed that the considered non-gravitational forces can guide an ejected particle from the Kreutz sungrazers to the Earth's crosser orbit. This process is more sensitive to the mass of a particle than to its ejection velocity. To receive an Earth crossing particle from a comet belonging to the Kreutz group a high ejection velocity is needed. The ejection velocity in our example,  $15 \text{ km s}^{-1}$ , is higher than the supposed ejection velocity of  $0.6\text{--}1 \text{ km s}^{-1}$  derived from observations of the Perseids by Harris et al. (1995) and Wu and Williams (1996) or the significantly higher values according to Williams (1996).

#### 4 Conclusion

The spatial distribution of model particles ejected with zero velocity from the comet with mean orbital elements of the Kreutz group can be used for the estimation of the possibility for such source of Earth crossing particles. Orbital elements of comets from the Kreutz group are not very different. Therefore, the structure of hyperbolic and near parabolic dust streams of the Kreutz comets at their apparition near the Sun must be very similar. The width and length of such streams depends on the activity of a parent comet and its perihelion distance. We can conclude that the resulting distribution of the investigated particles is more or less common for all comets of this group.

In spite of a number of simplifications involved, some interesting inferences are possible. Since the dust tail occupied a thin layer around the plane of a cometary orbit, the point of crossing by a detector determines uniquely the size and time release of the particles encountered. Essentially most of the dust released from comets belonging to the Kreutz sungrazers leaves the solar system on near-parabolic or hyperbolic orbits, because the radiation pressure limit is high.

A particle with favorable mass, ejection time, and velocity can cross the Earth's orbit. Due to the orbit of a parent comet, with very small perihelion distance, the probability for an Earth crossing particle is higher for the pre-perihelion ejections than for those, after the perihelion. Time interval for post-perihelion ejections is very short and does not exceed several days.

Generally, to obtain the Earth crossing particle at a given mass and ejection time, a very high ejection velocity, of several  $\text{km s}^{-1}$  is needed. On the other hand, if a particle has a suitable mass, the Earth crossing orbit of the particle is created with zero or a very small ejection velocity. Therefore, comets belonging to the Kreutz sungrazers may be considered as a source of the Earth-crossing small dust particles.

#### Acknowledgment

The authors thank the Local and Scientific organizing committee of the IMC 2016 for the conference in Egmond and its Proceedings 2016.

#### References

- Everhart E. (1985). "An efficient integrator that used Gauss-Radau spacing". In Carusi A. and Valsecchi G. B., editors, *Dynamic of Comets, their Origin and Evolution*. Reidel, Dordrecht, pages 185–202.
- Giorgini J. D., Yeomans D. K., Chamberlin A. B., Chodas P. W., Jacobson R. A., Keesey M. S., Lieske J. H., Ostro S. J., Standish E. M. and Wimberly R. N. (1996). "CJPL's on-line solar system data service". *Bull. Am. Astron. Soc.*, **28**, 1158.
- Guliyev A. C. (2010). "Origin of short-period comets". Baku, 1–151.
- Harris N. W., Yau K. K. C. and Hughes D. W. (1995). "The true extent of the nodal distribution of the Perseid meteoroid stream". *Monthly Notices of the Royal Astronomical Society*, **273**, 999–1015.
- Klačka J. and Pittich E. M. (1994). "Long-term orbital evolution of dust particles ejected from comet Encke". *Planetary and Space Science*, **42**, 109–112.
- Kreutz H. C. F. (1888). "Untersuchungen Über das Cometensystem 1843 I, 1880 I und 1882 II". Publication der Sternwarte in Kiel, Druck von C. Schaidt, C. F. Mohr, 3, 111.
- Marsden G. B. and Williams I. P. (2008). "Catalogue of Cometary Orbits". 17<sup>th</sup> ed. Minor Planet Center/Central Bureau for Astronomical Telegrams, Cambridge, MA.
- Sekanina Z. (2000). "Solar and Heliospheric Observatory Sungrazing Comets with Prominent Tails: Evidence on Dust-Production Peculiarities". *The Astrophysical Journal*, **545**, L69–L72.
- Sekhar A. and Asher D. J. (2014). "Meteor showers on Earth from sungrazing comets". *Monthly Notices of the Royal Astronomical Society*, **437**, L71–L75.
- Verniani F. (1973). "An Analysis of the Physical Parameters of 5759 Faint Radio Meteors". *Journal of Geophysical Research*, **78**, 8429–8462.
- Williams I. P. (1996). "What Can Meteoroid Streams Tell Us about the Ejection Velocities of Dust from Comets". *Earth, Moon, and Planets*, **72**, 321–326.
- Wu Z. and Williams I. P. (1996). "Leonid meteor storms". *Monthly Notices of the Royal Astronomical Society*, **280**, 1210–1218.



Yasunori Fujiwara, Jiri Borovicka and Pete Gural.



In the evening there was time for workshops. Here the workshop by Kristina Veljkovic on software for the analysis of visual meteor data.

# Werkgroep Meteoren – 70 Years and counting

Urijan Poerink<sup>1,2</sup> and Sebastiaan J. de Vet<sup>1</sup>

<sup>1</sup> Meteor Section, Royal Netherlands Association for Meteorology and Astronomy

<sup>2</sup> Esdoornlaan 12, NL-5263 GE Vught, The Netherlands

poerinku@planet.nl

In 2016 the Meteor Section of the Royal Netherlands Association for Meteorology and Astronomy celebrated its 70 year jubilee. In this paper we provide a brief historical narrative that incorporates the main developments and events of the Meteor Section, spanning seven decades of meteor observations in The Netherlands.

## 1 Introduction

Dutch amateur astronomy has a long tradition in meteor observations. Meteor research in The Netherlands truly began the 1860's, just like in other countries. The spectacular Leonid storms of 1833 and the years 1866-1868 have had a major effect on the development of the scientific study of meteors, which had previously been thought to be atmospheric phenomena. In 1866 observers counted hundreds of Leonids per minute/a few thousand per hour in Europe.



Figure 1 – Perseids, August 1906. Dr. Jan van der Bilt (r.) and Dr. Adriaan van Maanen and their big black sphere, on which they chalked the meteors (Sonnenborgh Observatory, Utrecht).

In 1943, during World War II, three young amateur astronomers, Hugo van Woerden, Sidney van den Bergh and Lammert Huizing established the Astroclub, the predecessor of the present-day Meteor Section. Their club of meteor observers comprised brothers, friends, mathematic teachers and other amateur observers and grew steadily in 1943–1944 to a group of about 35 members. They set up a national network of meteor

observers and organized observing campaigns. In their first steps in meteor observations they experienced many practical difficulties. One of those difficulties was related to the ongoing war time conditions; during World War II the occupying force confiscated most radio sets and therefore the observers could not receive time signals in order to correct their clockworks. The members of the Astroclub edited the monthly magazine 'De Meteor', which in 1946 would become the section's astronomical magazine. Observers publish their reports and results of their observations in 'De Meteor' and the monthly magazines of the Netherlands Association for Meteorology and Astronomy ('Hemel en Dampkring' and later in 'Zenit'). After WWII in August 1946, the 'Werkgroep Meteoren van de Nederlandse Vereniging voor Weer- en Sterrenkunde (NVWS)' was formally founded at the suggestion of Dr J.J. Raimond Jr., the President of the NVWS. Internationally the group became known as the Meteor Section of the Netherlands Association for Meteorology and Astronomy.

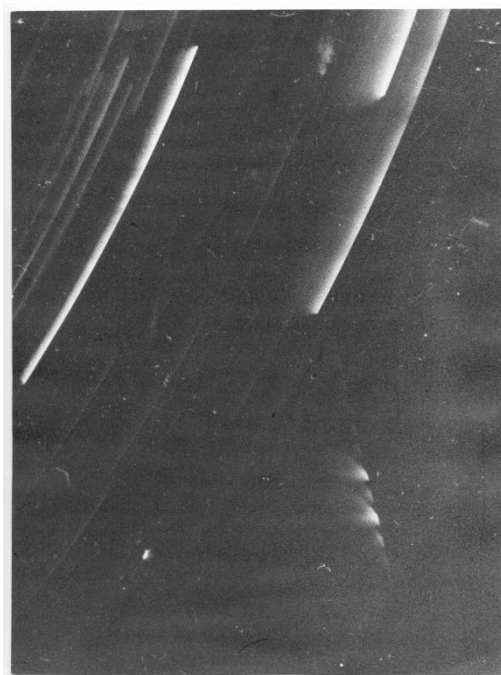


Figure 2 – First 'Dutch' meteor photograph was taken on 7 August 7 1953 during a Perseid observation campaign by amateur-astronomer Mr. M. Alberts.

## 2 Highlights from 70 years of the Meteor Section

### The 1950's

On 7 August 1953, during the Perseid Campaign, amateur astronomer Mr. Machiel Alberts obtained a very first photograph of a 'Dutch' meteor (see *Figure 2*).

### The 1960's

- In the 1960's amateurs made photographic plates of meteors with large cameras originally intended for aerial photography. ('upside-down aerial photography', *Figure 3*).
- The Meteor Section presented a catalogue, containing observations of anomalous sounds for fireballs from 1947-1958.

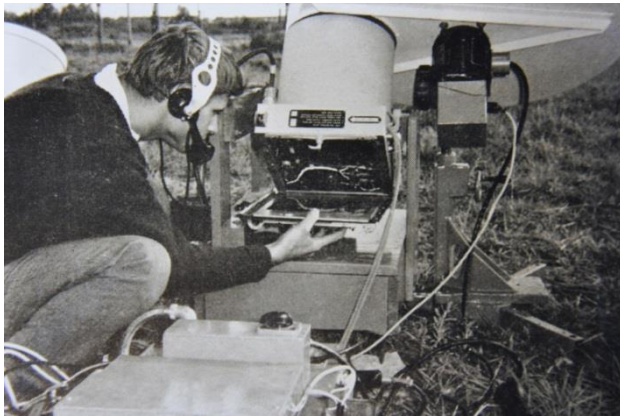


*Figure 3* – Amateurs make photographic plates of meteors with cameras originally intended for aerial photography.

- In 1966 amateurs photographed the spectrum obtained of a Lyrid meteor (*Figure 4*) and in 1967 they observed radar echoes of the Leonid outburst, using the transmitter of a radar station at the University of Eindhoven (*Figure 5*).

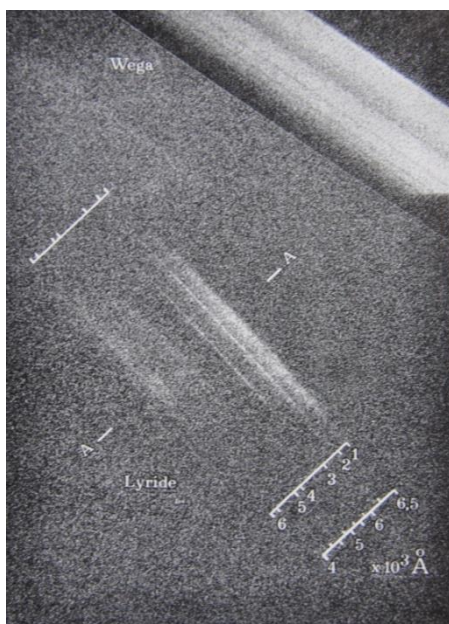


*Figure 4* – Spectrum of a Lyrid meteor taken in the skies above The Netherlands in 1966.



*Figure 5* – Member of the Meteor Section listening to the echoes of meteors via radio meteor scatter. the radio waves, reflected by the meteor, on paper. A Yagi antenna “catches” the radio signal reflected from a meteor ionization trail and a pen recorder captures it on paper.

- In 1969 amateurs used spectrographs for the imaging of meteors with a glass prism to simultaneously obtain the meteor's spectrum (*Figure 6*).

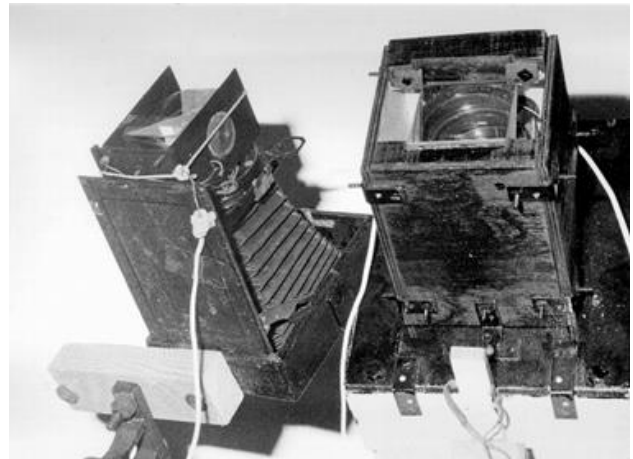


*Figure 6* – Meteor spectrographs, used by members of the Meteor Section in the late 1960s.



*Figure 7* – A Perseid campaign in the '90's. On the front the first all sky camera of Felix Bettonvil.

### The 80's and early-90's

- During annual meteor campaigns amateurs made visual and photographic observations using batteries

of two or more cameras and increasingly sophisticated equipment (*Figure 8*).



*Figure 8* – Photo batteries of six and eight single-lens reflex cameras (MECAT's), built by Felix Bettonvil (1980's, 1990's). MECAT is the acronym of 'MEteor CATcher'.

- A successful Perseid observation campaign in 1993 took a large group of members to observation sites in The Netherlands and France, where they witnessed a ZHR of more than 300 during the outburst on 11–12 August 1993 (*Figure 10*).
- Batteries of six and eight single-lens reflex cameras (MECAT = MEteor CATcher), built by Felix Bettonvil, were used extensively for all-sky meteor observations in the 1980's and 1990's (*Figure 7*).

#### The 90's and -2000's

- The Meteor Section carried out various successful international observations, e.g. to monitor the Leonid outbursts of 1998, 1999, 2001 and 2002. Members travelled to observation sites in The Netherlands, Jordan, South Korea, China, Denmark, Spain, France and Portugal. They photographed thousands of Leonids.
- The Meteor Section and its members introduced more and more meteor observing methods and developed sophisticated photographic and video equipment. A growing number of all-sky cameras cover the Dutch airspace and thanks to that, searching for meteorites takes on a new dimension. In 2013 and 2015 two fireballs led to search campaigns for meteorites. Meteorite events were organized for local inhabitants, alas with no recovery of new meteorites.
- The Meteor Section continues to expand digitally; the website and social media are used to collect fireball reports and an effective public outreach program takes place via popular social media.

### 3 Involvement in the recovery of 'Dutch' meteorites

Several meteorites have fallen in The Netherlands. On 12 June 1840, a big stone fell in front a group of peat cutters near the Dutch village of Uden. Not long thereafter on 2 June 1843, this meteorite impact was followed by the fall of two masses near the city of Utrecht. Years later those stones were recognized as meteorites. No meteorite falls have been documented in The Netherlands in the period predating 1840, with the exception perhaps of an event that took place in the city Dordrecht. On 6 August 1650, a glowing stone was strewn down "with the lightning" and broke the windows and burned the woodwork of the Mayor's house in the city of Dordrecht. In 1807 this stone was lost in the explosion of a ship stocked with gunpowder in the city Leiden, and was lost without being studied in detail to establish its nature.

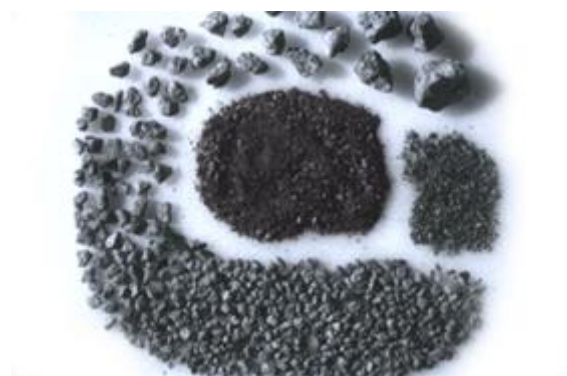


*Figure 9* – All fragments of the Glanerbrug meteorite which hit a house on 7 April 1990.

The Meteor Section played a notable role in the recovery of the Glanerbrug meteorite. In the evening of 7 April 1990 a meteorite crashed through the roof of a house in the Dutch village of Glanerbrug, near the German border (*Figure 9*). The Meteor Section and other Dutch and German astronomical and meteorological observatories and institutes received hundreds of reports of the fireball. A team of researchers of the Meteor Section and the Dutch Meteor Society interviewed witnesses and managed to reconstruct the trajectory. The fall of the Glanerbrug (LL4-6, 855 g) and the subsequent investigations and research, plus its publication, mark one of the highlights in the 70 years history of the Meteor Section.

In 2012 a meteorite (CM2-an, 65g) was rediscovered with the help from Meteor Section members. Historical research showed that on 27 October 1873 a farmer witnessed the fall of the meteorite in his field near the village of Diepenveen.

The Uden (1840), Utrecht (1843), Diepenveen (1873), Ellemeet (1925) and Glanerbrug (1990) are currently the only meteorites recovered in The Netherlands. They are considered to be items of natural historical heritage and fragments are curated in various national and international university and museum collections.



Figure 10 – The Perseid Campaign in August 1993 in Southern France. Members of the Meteor Section and other Dutch amateur astronomers witnessed the Leonid outbursts in several countries (e.g.. The Netherlands, Jordan, South Korea, China, Denmark, Spain, France, Portugal). They photographed thousands of Leonids in November 1998, 1999, 2001 and 2002

#### 4 International Meteor Conferences in the Netherlands



Figure 11 – The first IMC in The Netherlands, May 1983.

As part of its international outlook on meteor observations, the Meteor Section has continuously invested itself in organizing international events, such as the International Meteor Conferences (IMC's) of the International Meteor Organization (IMO). Since the 1980's the Meteor Section and the International Meteor Organization have organized four International Meteor Conferences in The Netherlands, which include:

- *Lattrop, Brecklenkamp, May 1983*: 24 amateurs from Belgium, Germany and the Netherlands, organized the 4<sup>th</sup> International Meteor Weekend (Figure 11).
- *De Lutte (Oldenzaal), March 1988*: 65 amateurs and professionals from 9 countries participated in the 7<sup>th</sup> International Meteor Conference (Figure 12).

- *Apeldoorn, September 1996*: The Meteor Section hosted the 15<sup>th</sup> International Meteor Conference with 61 participants from 12 countries in Apeldoorn (Figure 13).
- *Roden, September 2006*: The Meteor Section hosted the 25<sup>th</sup> International Meteor Conference with 68 participants from 16 different countries. The participants paid a visit to the Westerbork Synthese Radio Telescope and LOFAR (Low-Frequency ARray) (Figure 14).
- *Egmond, June 2016*: 157 participants from 30 countries from five continents gathered at this 35<sup>th</sup> meeting. It was the first time that so many professionals and amateurs came together at an IMC.



Figure 12 – The second IMC in The Netherlands, March 1988, with Dr. Bertil Lindblad giving his lecture.



Figure 13 – Hugo Van Woerden, one of the founding members of the Meteor Section during his talk at the 1996 IMC in Apeldoorn.

## 5 Awards for members of the Meteor Section

In recognition of their contribution to the field of meteor science, several members of the Meteor Section have been laureate for their efforts in the advancement of the field of meteor science. The most notable award is

bestowed by the Royal Netherlands Association for Meteorology and Astronomy (KNVWS). This award – named after the Dutch astronomer Dr. Jan van der Bilt (1876–1962) – was established in 1944 to honor amateurs who either contributed significantly to the popularization of astronomy, or as an amateur contributed to astronomy on a professional level. The ten Meteor Section members are recipients of the ‘Van der Bilt Prize’ include Thomas van Dijk (1957), Johan Degewij (1966), Ben Apeldoorn (1971), Machiel Albers (1974), Felix Bettonvil en Urijan Poerink (1991), Simon van Leverink (1995), Herman ten Haaf (2000) and Koen Miskotte and Casper ter Kuile (2008).

## 6 Conclusion

Meteor and meteorite research in The Netherlands has evolved and diversified significantly during the seventy years gone by since the founding of the Meteor Section. While many meteor observers are currently involved in high-tech forms of meteor observations, using all-sky cameras or automated camera systems, others are involved in computational aspects of orbits, dark flights and strewn fields; the study meteorites; or just enjoy themselves observing meteors with the unaided eye. Even after 70 years, meteor observations in The Netherlands are still a flourishing activity with dozens of active amateurs and professionals.



Figure 14 – The 2006 IMC participants on excursion at Westerbork.

# Novel methods for 3D numerical simulation of meteor radar reflections

Jukka Rabinä<sup>1</sup>, Sanna Mönkölä<sup>1</sup>, Tuomo Rossi<sup>1</sup>, Johannes Markkanen<sup>2</sup>,  
Maria Gritsevich<sup>3,4,5</sup> and Karri Muinonen<sup>2,3</sup>

<sup>1</sup>University of Jyväskylä, Department of Mathematical Information Technology,  
P.O.Box 35 (Agora), FI-40014 University of Jyväskylä, Finland

<sup>2</sup>Department of Physics, P.O. Box 64, FI-00014 University of Helsinki, Finland

<sup>3</sup>Finnish Geospatial Research Institute, P.O. Box 15, FI-02431 Masala, Finland

<sup>4</sup>Dorodnicyn Computing Centre, Federal Research Center “Computer Science and Control”  
of the Russian Academy of Sciences, 119333 Moscow, Russia

<sup>5</sup>Institute of Physics and Technology, Ural Federal University, 620002 Ekaterinburg, Russia

We use two novel methods for numerical simulation of meteor radar reflections. The one is based on the discrete exterior calculus, time-dependent simulations, and a control-based approach for accelerating the time evolution. The other is implemented as a time-harmonic solver based on the volume integral equation method for electric current. Despite the different framework, both methods give the solution in frequency domain. We model the radar reflections in a three-dimensional space as time-harmonic electromagnetic scattering from plasmatic obstacles. This makes our study different from the more conventional numerical simulations concerning scattering by a solid obstacle without a plasma model.

## 1 Introduction

The meteor head echo feature has been studied by high power large aperture (HPLA) radars since 1960's (Evans, 1965). Based on the observations conducted by the different radar systems and post-processing techniques, there exist several models for the meteor head echo simulations. One reason for this is the characteristics of the radar system, e.g., in terms of frequency and antenna geometry (Kero et al., 2012). It is also worth mentioning that there are differences in the meteor sizes. According to the observations reported by, e.g., Vertatschitsch et al. (2011) and Wannberg et al. (2011), the head echo can be modeled as overdense scatter from a plasma layer, surrounding the meteor, with a certain density distribution. In these models, the plasmatic object is assumed to be a conducting spherical object, and the electromagnetic phenomenon can be presented by partial differential equations coupling the electric and magnetic fields. The traditional way of solving electromagnetic problems, presented in the space-time domain as partial differential equations, is to use the Yee's finite difference time domain (FDTD) method (Yee, 1966). In this study, we use more generalized finite differences by applying the discrete exterior calculus (DEC) for the numerical simulation of meteor radar reflections. We also compare the method with another recently introduced efficient method that is based on the volume integral equation method for the electric current (J-VIE).

## 2 Numerical models and simulation methods

With numerical techniques, it is possible to test how changes in the atmospheric conditions affect the meteor

radar reflections and explain unexpected results in the measurements. To get reliable simulation outputs, the appropriate models, methods and input information all need to be defined. We apply the partial differential equation model, in which the source of the scatter is presented as a plasmatic obstacle, and the dielectric tensor is derived from the equation of motion presenting charged, non-magnetized cold plasma (Nickisch and Franke, 1992). Numerical simulations based on the model are presented with the FDTD for 2D layers by Dyrud et al. (2008) and for 3D domains by Yu and Simpson (2010). The recent method development and enhanced computational resources provide possibilities to improve the accuracy of the numerical simulations or solve more demanding problems. We present two numerical methods that have recently shown to be efficient for 3D simulations.

## 3 Discrete exterior calculus

The properties and calculus of differential forms is provided in a natural way at the discretization stage. Hence, with the discrete exterior calculus (DEC), constructed with discrete differential forms, we associate the degrees of freedom of the electric and magnetic fields to the primal and dual mesh structures, respectively. The connection between the primal and dual forms is obtained by the discrete Hodge operator, the quality of which depends on the mesh construction. Our generalized formulation of the DEC for Maxwell's equations (Pauly and Rossi, 2011) works on unstructured grids, and it covers both the classical Yee's FDTD scheme and the Bossavit-Kettunen approach (Bossavit and Kettunen, 1999). The method has shown to give promising results with time-dependent problems (Rabinä et al., 2015).

## 4 Accelerated convergence for time simulation

The time-harmonic solution can be reached by asymptotic time simulation. However, the method is computationally inefficient, especially for scattering problems with non-convex or inhomogeneous obstacles. We improve the method by accelerating the convergence of the time-domain simulation to the steady-state solution. The concept is earlier applied and compared to other methods in acoustics (Airaksinen and Mönkölä, 2010), elastodynamics (Mönkölä et al., 2008), and electromagnetics (Räbinä et al., 2014). With the DEC space discretization, only matrix-vector multiplications are needed for explicit time-stepping which provides efficient time evolution. The first results considering three-dimensional electromagnetics coupled with the meteor plasma dynamics are presented by Räbinä et al. (2016).

## 5 Volume integral equation method for the electric current

In the volume integral equation method for the electric current (J-VIE), the unknown equivalent electric current density is expanded with piecewise constant basis functions (Markkanen et al., 2012). The resulting system is solved iteratively by the generalized minimal residual method restarted after every 50 iterations (GMRES(50)). The matrix-vector multiplication in each iteration step is accelerated by the pre-corrected-FFT algorithm.

## 6 Conclusions

For both methods, only sparse matrices are stored. With the DEC, most of the matrices are diagonal, and the solution procedure is realized by the conjugate gradient method. Only the current and previous gradient and search vectors and scalar-valued weights must be stored at each iteration. For the VIE-based method, a large but sparse pre-correction matrix for the FFT is assembled, and the solution method (GMRES) uses the results of the earlier iterations. The DEC-based controlled time integration is found to be more efficient, and its performance is not sensitive to the level of discretization and the values of the material parameters.

## Acknowledgments

This project has been funded by the Academy of Finland, grants 259925, 257966, 260027, and 260076, the ERC Advanced Grant No 320773, "Scattering and Absorption of Electromagnetic Waves in Particulate Media" (SAEMPL), and the Act 211 of the Government of the Russian Federation, agreement No 02.A03.21.0006. The authors acknowledge being a part of the network supported by the COST Action MP1104 "Polarization as a tool to study the Solar System and beyond" and by the COST Action TD1403 "Big Data Era in Sky and Earth Observation".

## References

- Airaksinen T. and Mönkölä S. (2010). "Comparison between the shifted-Laplacian preconditioning and the controllability methods for computational acoustics". *Journal of computational and applied mathematics*, **234**, 1796–1802.
- Bossavit A. and Kettunen L. (1999). "Yee-like schemes on a tetrahedral mesh, with diagonal lumping". *International Journal of Numerical Modelling*, **12**, 129–142.
- Dyrud L., Wilson D., Boerve S., Trulsen J., Pecseli H., Close S., Chen C. and Lee Y. (2008). "Plasma and Electromagnetic Simulations of Meteor Head Echo Radar Reflections". *Advances in Meteoroid and Meteor Science*. Springer New York, pages 383–394.
- Evans J. V. (1965). "Radio-echo studies of meteors at 68-centimeter wavelength". *Journal of Geophysical Research*, **70**, 5395–5416.
- Kero J., Szasz C., Nakamura T., Terasawa T., Miyamoto H. and Nishimura K. (2012). "A meteor head echo analysis algorithm for the lower VHF band". *Annales Geophysicae*, **30**, 639–659.
- Markkanen J., Ylä-Oijala P. and Sihvola A. (2012). "Discretization of volume integral equation formulations for extremely anisotropic materials". *IEEE Trans. Ant. and Propag.* **60**, 5195–5202.
- Mönkölä S., Heikkola E., Pennanen A. and Rossi T. (2008). "Time-harmonic elasticity with controllability and higher-order discretization methods". *Journal of Computational Physics*, **227**, 5513–5534.
- Nickisch L. J. and Franke P. M. (1992). "Finite-difference time-domain solution of Maxwell's equations for the dispersive ionosphere". *IEEE Antennas and Propagation* **34**, 33–39.
- Pauly D. and Rossi T. (2011). "Theoretical considerations on the computation of generalized time-periodic waves". *Advances in Mathematical Sciences and Applications*, **21**, 105–131.
- Räbinä J., Mönkölä S. and Rossi T. (2015). "Efficient time integration of Maxwell's equations by generalized finite differences". *SIAM Journal on Scientific Computing*, **37**, B834–B854.
- Räbinä J., Mönkölä S., Rossi T., Markkanen J., Gritsevich M. and Muinonen K. (2016). "Controlled time integration for the numerical simulation of meteor radar reflections". *Journal of Quantitative Spectroscopy and Radiative Transfer*, **178**, 295–305.

Räbinä J., Mönkölä S., Rossi T., Penttilä A. and Muinonen K. (2014). “Comparison of discrete exterior calculus and discrete-dipole approximation for electromagnetic scattering”. *Journal of Quantitative Spectroscopy and Radiative Transfer*, **146**, 417–423.

Vertatschitsch L. E., Sahr J. D., Colestock P. and Close S. (2011). “Meteoroid head echo polarization features studied by numerical electromagnetics modeling”. *Radio Science*, **46**, RS6016.

Wannberg G., Westman A. and Pellinen-Wannberg A. (2011). “Meteor head echo polarization at 930

MHz studied with the EISCAT UHF HPLA radar”. *Annales Geophysicae*, **29**, 1197–1208.

Yee K. S. (1966). “Numerical solution of initial boundary value problems involving Maxwell’s equations in isotropic media”. *IEEE Transactions on antennas and propagation*, **14**, 302–307.

Yu Y. and Simpson J. J. (2010). “An EJ collocated 3-D FDTD model of electromagnetic wave propagation in magnetized cold plasma”. *IEEE Transactions on Antennas and Propagation*, **58**, 469–478.



Also kind of a tradition nowadays: table soccer. Dušan Pavlovic, Uroš and Dušan Bettonvil versus Ljubica Grašić and Javor Kac, with Snežana Todorović as supporter.

# Meteor detections at the Metsähovi Fundamental Geodetic Research Station (Finland)

Arttu Raja-Halli<sup>1</sup>, Maria Gritsevich<sup>1,2,4</sup>, Jyri Näränen<sup>1</sup>, Manuel Moreno-Ibáñez<sup>1,3</sup>, Esko Lyytinen<sup>4</sup>, Jenni Virtanen<sup>1</sup>, Nataliya Zubko<sup>1</sup>, Jouni Peltoniemi<sup>1,5</sup> and Markku Poutanen<sup>1</sup>

<sup>1</sup> Finnish Geospatial Research Institute (FGI), Masala, Finland

firstname.lastname@nls.fi

<sup>2</sup> Institute of Physics and Technology, Ural Federal University, Ekaterinburg, Russia

gritsevich@list.ru

<sup>3</sup> Institute of Space Sciences (IEEC-CSIC), Barcelona, Spain

mmoreno@ice.csic.es

<sup>4</sup> Finnish Fireball Network, Helsinki, Finland

esko.lyytinen@jippii.fi

<sup>5</sup> University of Helsinki, Helsinki, Finland

jouni.peltoniemi@helsinki.fi

We provide an overview and present some spectacular examples of the recent meteor observations at the Metsähovi Geodetic Research Station. In conjunction with the Finnish Fireball Network the all-sky images are used to reconstruct atmospheric trajectories and to calculate the pre-impact meteor orbits in the Solar System. In addition, intensive collaborative work is pursued with the meteor research groups worldwide. We foresee great potential of this activity also for educational and outreach purposes.

## 1 Introduction

The Metsähovi Geodetic Research Station of the Finnish Geospatial Research Institute (FGI) of the National Land Survey of Finland (NLS) (before 1.1.2015 Finnish Geodetic Institute) is one of the Global Geodetic Observation System (GGOS) core sites and is equipped with all the fundamental space geodetic techniques (e.g., satellite laser ranging – SLR and Global Navigation Satellite System – GNSS) together with superconducting and absolute gravimeters. Satellite laser ranging is a space geodetic technique where the flight time of short laser pulses to, e.g., Earth orbiting satellites is used to range the objects with an accuracy that is a couple of mm for low Earth orbit targets. SLR can be used, e.g., to calculate the orbits of satellites, to study the changes in the low harmonics of Earth's gravity field, and to determine the movement of the Earth's center of mass. There are currently approximately 50 operational SLR-stations worldwide. Metsähovi is one of the northernmost SLR stations of the International Laser Ranging Service (ILRS). First SLR observations in Finland were made at the Metsähovi research station already in 1978. To enrich efficiency of the station, recently we have acquired a modern kHz-capable SLR system, as well as auxiliary instrumentation like the Vaisala weather station and an Alcor OMEA 2Mpx all-sky camera devoted to continuous observations. The later enables us an efficient collaboration with the Finnish Fireball Network (FFN) and the Spanish Meteor Network (SPMN<sup>1</sup>), both in terms of meteor registrations and subsequent data analysis (Gritsevich et al., 2014; Trigo-Rodríguez et al., 2015;

Lyytinen and Gritsevich, 2016; Dmitriev et al., 2015; Moreno-Ibáñez et al., 2015; Moreno-Ibáñez et al., 2016; Blanch et al., 2016; Trigo-Rodríguez et al., 2016; Kohout et al., 2015).

## 2 Observatory building

To establish a new and modern SLR station the first SLR building in Metsähovi, erected in 1975, was torn down in 2014 and a new observatory was built. The observatory building was designed to house all the sensitive electronics of the SLR system in an almost clean-room environment on the first floor. Also the temperature of the electronics room is kept stable within one degree. An operator controls everything remotely from a second room to keep the temperature stable in the electronics room and to avoid dust entering the room. The SLR-telescope system stands on a concrete pillar in the center of the building, which is anchored to bedrock and separated from the building to avoid all vibrations. The pillar is 3.5 m high and hollow to allow the laser to be guided from the electronics room downstairs to the transmitting telescope (Coudé path). The telescope is shielded from weather conditions by a 5.3 m fast-moving slit-type dome manufactured by *Baader Planetarium GmbH*.

Externally, we have installed a high-end Vaisala weather station<sup>2</sup> equipped with temperature, humidity, pressure, wind, precipitation, global radiation and snow height sensors. In addition the dome has its own humidity and precipitation sensor for automatic closing at raining

<sup>1</sup> <http://www.spmn.uji.es>

<sup>2</sup> [www.vaisala.com](http://www.vaisala.com)

conditions. In order to image the whole sky we have installed an all-sky camera (Näränen et al., 2014), which allows cloud and meteor detections. Together with the camera we have two ADS-B antennas which register the velocity and position information broadcasted by airplanes.



Figure 1 – The new SLR observatory of the Metsähovi Fundamental Geodetic Research Station: on the left the mast with two ADS-B antennas and the 2Mpx all-sky camera for meteor observation.

### 3 Instrumentation of the SLR Station

The Metsähovi station is equipped with key items needed in an SLR system: a telescope for transmitting and receiving laser pulses; a time interval counter / event timer for timing the flight time; a detector for receiving the laser pulse; a time reference; a laser with a stable repetition rate (Hz-kHz), energy level and pulse length (few picoseconds). The main instruments of the SLR system of Metsähovi consist of: a very fast and accurately tracking ( $> 10\text{deg/s}$ ,  $< 1''$ ) *Cybioms/OMI* 50cm SLR telescope with a separate 10 cm telescope for transmitting the laser, and a 15 cm telescope for visual observations; a *HighQ GmbH* laser, capable of 2kHz repetition rate with a 0.8 W average power and a few picosecond pulse length, and a Single Photon Avalanche Diode – detector (*C-SPAD*). For more details on the SLR system see: Näränen et al., 2014; Raja-Halli et al., 2014; Raja-Halli et al., 2015.

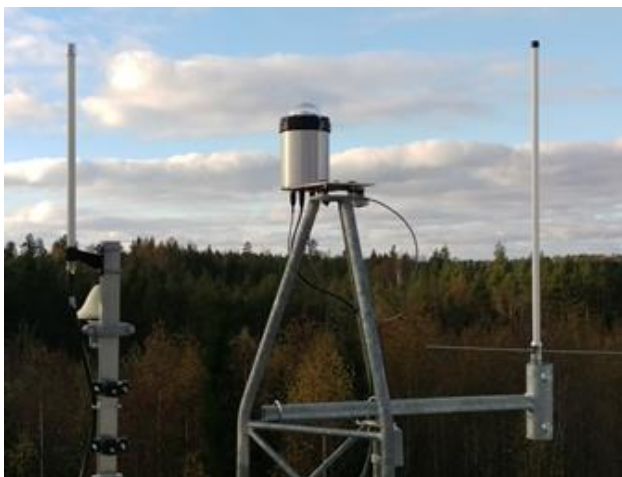


Figure 2 – Meteor detection system: 2Mpx all sky camera and ADS-B antennas.

For visualizing the sky during SLR observations we have

installed an *Alcor OMEA 2Mpx* all-sky camera on a 6 m height mast. The camera has a field of view of  $185^\circ \times 185^\circ$  and the wavelength range is 350 – 750 nm. It has an automatic iris with maximum aperture F1.8 and an automatic exposure control with exposure times ranging from 0.1 ms to one hour, which allows correcting exposure at any time. In addition, a library of dark images and a hot pixel list is created to remove noise from the images. The camera dome is provided with a heating system to remove any water condensation and ice formation; this allows us imaging even during winter nights when frosting is likely to happen. During daytime we take images every five minutes to visualize clouds. During night the camera takes the next exposure immediately as it has readout the last one. Therefore the deadtime of the camera remains small, usually less than few seconds between exposures.



Figure 3 – The new SLR telescope. The 15cm refractor is not shown in the image.

### 4 Meteor detection

From the images taken by the camera we have detected multiple aurora borealis events as well as a number of meteors. In *Figures 4 and 5* we present some examples of the recent Metsähovi all-sky camera observations. In conjunction with the Finnish Fireball Network (FFN) the images recorded by this camera are used to reconstruct atmospheric trajectories and to calculate the pre-impact meteor orbits in the Solar System (Dmitriev et al., 2015).

The Finnish Fireball Network (FFN) was established in 2002 as a result of growing interest to continuous meteor and fireball monitoring using dedicated equipment initiated by Ilkka Yrjölä in 1998<sup>3</sup>. In the current state the network consists of the 24 active stations with permanent instrumental setup and monitors a surface over Finland and neighboring areas of about 400000 km<sup>2</sup> (Gritsevich

<sup>3</sup> <http://www.kolumbus.fi/oh5iy/>

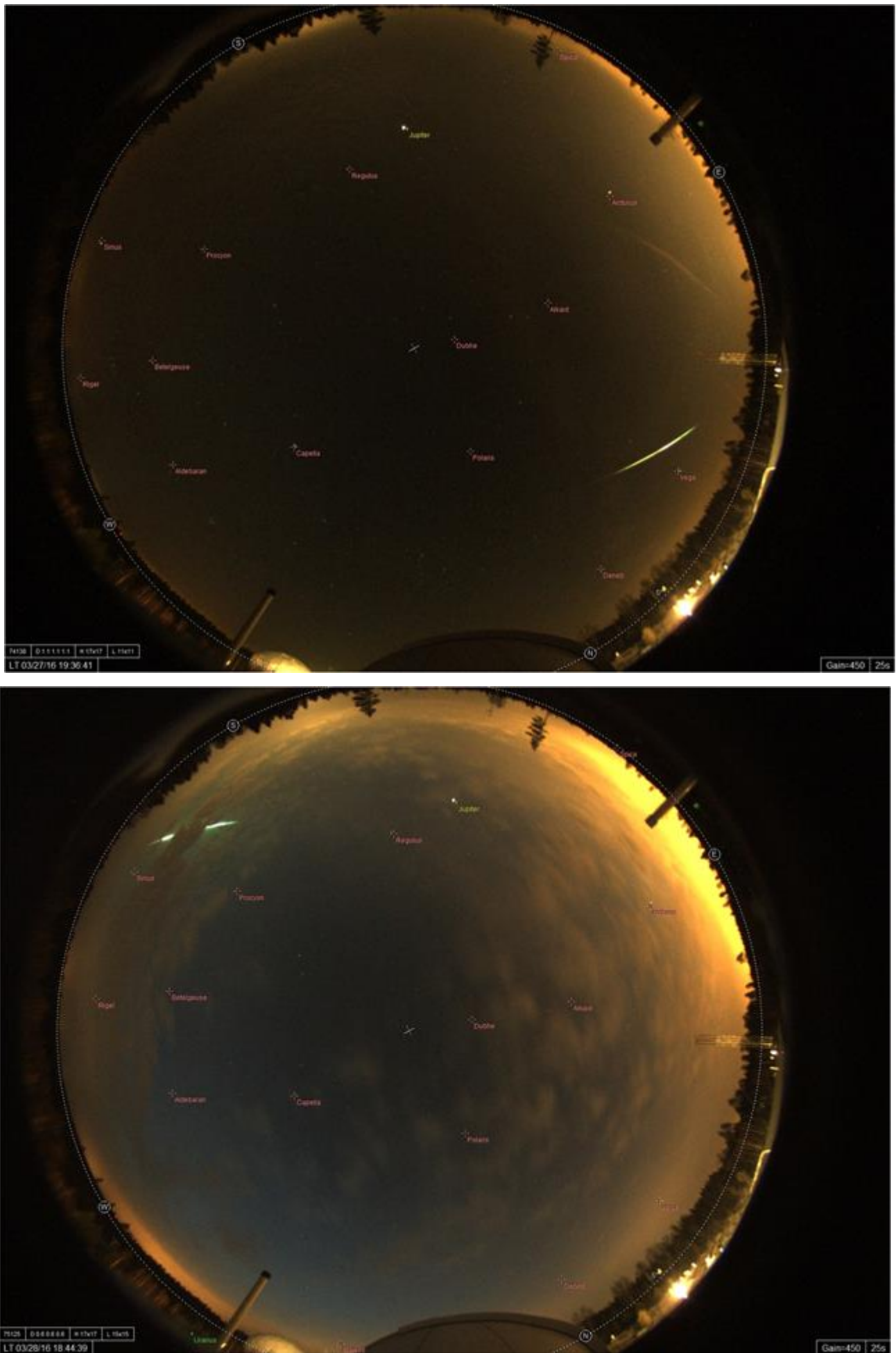


Figure 4 – Recent fireball examples recorded by the Alcor OMEA 2Mpx all-sky camera at the Metsähovi Geodetic Research Station.

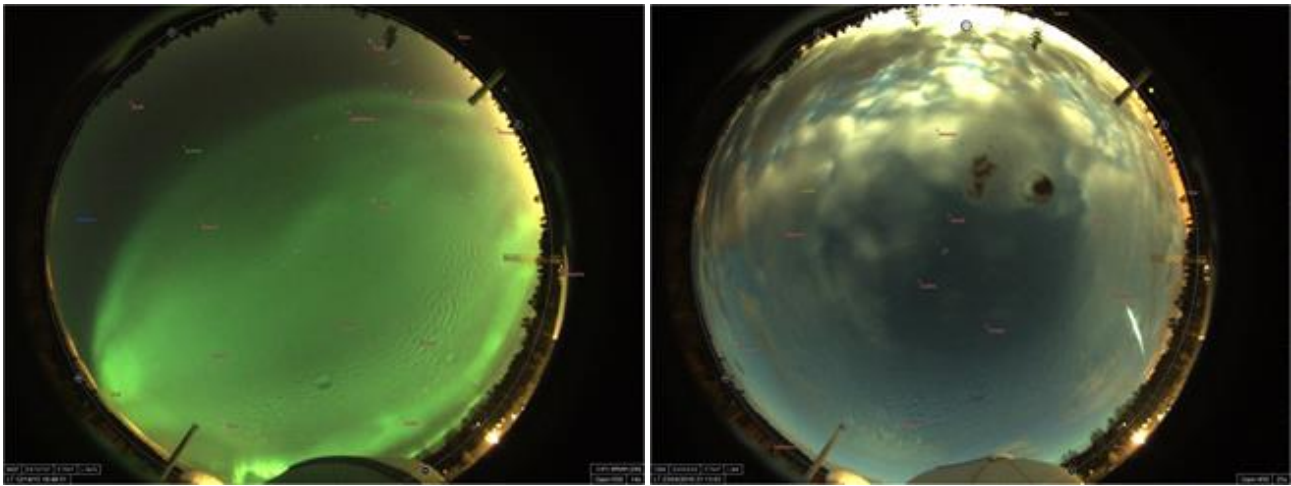


Figure 5 – Aurora borealis and recent fireball examples recorded by the *Alcor OMEA 2Mpx* all-sky camera at the Metsähovi Geodetic Research Station.

et al., 2014; Trigo-Rodríguez et al., 2015; Lyytinen and Gritsevich, 2016). Most of the active stations are run by amateur astronomers. A majority of interesting events are reduced the following days after the registration and the atmospheric trajectories corresponding to the visual path of fireballs are reproduced using the *fb\_entry program* (Lyytinen and Gritsevich, 2013). The program uses atmospheric trajectory parametrization described in (Gritsevich 2007, 2009; Gritsevich and Koschny, 2011; Bouquet et al., 2014). Selected cases – e.g. the ones matching meteorite-producing criteria introduced in (Gritsevich et al., 2012; Turchak and Gritsevich, 2014) – are studied more thoroughly including mass computation, dark flight simulations, and pre-impact orbit estimate with account for the real atmospheric conditions corresponding to the time and location of a fireball (Lyytinen and Gritsevich, 2016).

The all-sky camera installation at the Metsähovi Geodetic Research Station and the ongoing meteor work were largely inspired by the recovery of the Annama meteorite (Gritsevich et al., 2014; Trigo-Rodríguez et al., 2015; Dmitriev et al., 2015; Kohout et al., 2015; Lyytinen and Gritsevich, 2016). This was the first meteorite recovered by the FFN. The data recorded provided enough information to determine its atmospheric trajectory which allowed to eventually simulate its dark flight and enabled prompt meteorite recovery. Furthermore, the accuracy of the data available permitted the derivation of its orbital parameters and parental relationship (Trigo-Rodríguez et al., 2015; Dmitriev et al., 2015).

## 5 Conclusion and future prospects

The Metsähovi Fundamental Geodetic Research Station is adequately equipped with all the necessary instrumentation for detailed meteor detection. Thus, its use for further cooperation with fireball networks is suitable and it would largely help in meteor observation campaigns.

There is increasing interest in using SLR systems to observe also non-cooperative targets (i.e., objects with no

reflectors such as space debris (Virtanen et al., 2016) in low orbits. Recently, our team has investigated the new Metsähovi system's feasibility for space debris observations in a *MATINE*-funded research project.

The new SLR system is designed from the beginning as a flexible platform for future development. This will ensure that the Metsähovi SLR system is easily upgraded in the future and also that it can be modified to participate in state-of-the-art research such as space-debris tracking and time transfer over optical satellite link.

## Acknowledgments

Our work has been supported by the Finnish Ministry of Agriculture and Forestry, the European Space Agency (ESA), the Academy of Finland (project 260027), the Finnish Scientific Advisory Board for Defence (*MATINE*), and by the Magnus Ehrnrooth Foundation.

## References

- Blanch E., Trigo-Rodríguez J. M., Madiedo J. M., Lyytinen E., Moreno-Ibáñez M., Gritsevich M., and Altadill D. (2016). "Detection of nocturnal and daylight bolides from Ebre Observatory in the framework of the SPMN fireball network". In Trigo-Rodríguez J. M., Gritsevich M. and Palme H., editors, *Assessment and Mitigation of Asteroid Impact Hazards*, Springer, New York. In print.
- Bouquet A., Baratoux D., Vaubaillon J., Gritsevich M. I., Mimoun D., Mousis O. and Bouley S. (2014). "Simulation of the capabilities of an orbiter for monitoring the entry of interplanetary matter into the terrestrial atmosphere". *Planetary and Space Science*, **103**, 238–249  
<http://dx.doi.org/10.1016/j.pss.2014.09.001>.
- Dmitriev V., Lupovka V. and Gritsevich M. (2015). "Orbit determination based on meteor observations using numerical integration of equations of motion". *Planetary and Space*

- Science*, **117**, 223–235,  
<http://dx.doi.org/10.1016/j.pss.2015.06.015>
- Gritsevich M. and Koschny D. (2011). “Constraining the luminous efficiency of meteors”. *Icarus*, **212**, 877–884.  
<http://dx.doi.org/10.1016/j.icarus.2011.01.033>.
- Gritsevich M., Lyytinen E., Moilanen J., Kohout T., Dmitriev V., Lupovka V., Midtskogen V., Kruglikov N., Ischenko A., Yakovlev G., Grokhovsky V., Haloda J., Halodova P., Peltoniemi J., Aikkila A., Taavitsainen A., Lauanne J., Pekkola M., Kokko P., Lahtinen P. and Larionov M. (2014). “First meteorite recovery based on observations by the Finnish Fireball Network”. In Rault J.-L. and Roggemans P., editors, *Proceedings of the International Meteor Conference*, Giron, France, 18-21 September 2014. IMO, pages 162–169.
- Gritsevich M. I. (2007). “Approximation of the Observed Motion of Bolides by the Analytical Solution of the Equations of Meteor Physics”. *Solar System Research*, **41**, 509–514.  
<http://dx.doi.org/10.1134/S003809460706007X>.
- Gritsevich M. I. (2009). “Determination of Parameters of Meteor Bodies Based on Flight Observational Data”. *Advances in Space Research*, **44**, 323–334.  
<http://dx.doi.org/10.1016/j.asr.2009.03.030>.
- Gritsevich M. I., Stulov V. P. and Turchak L. I. (2012). “Consequences for Collisions of Natural Cosmic Bodies with the Earth Atmosphere and Surface”. *Cosmic Research*, **50**, 56–64.  
<http://dx.doi.org/10.1134/S0010952512010017>.
- Kohout T., Gritsevich M., Lyytinen E., Moilanen J., Trigo-Rodríguez J. M., Kruglikov N., Ishchenko A., Yakovlev G., Grokhovsky V., Haloda J., Halodova P., Meier M. M. M., Laubenstein M., Dimitrev V. and Lupovka V. (2015). “Annama H5 Meteorite Fall. Orbit, Trajectory, Recovery, Petrology, Noble Gases, and Cosmogenic Radionuclides”. *Meteoritics and Planetary Science*, **50**, MetSoc 2015 special issue, # 5209.
- Lyytinen E. and Gritsevich M. (2013). “A flexible fireball entry track calculation program”. In Gyssens M. and Roggemans P., editors, *Proceedings of the International Meteor Conference*, La Palma, Canary Islands, 20-23 September 2012. IMO, pages 155–167.
- Lyytinen E. and Gritsevich M. (2016). “Implications of the atmospheric density profile in the processing of fireball observations”. *Planetary and Space Science*, **120**, 35–42.  
<http://dx.doi.org/10.1016/j.pss.2015.10.012>.
- Moreno-Ibáñez M., Gritsevich M. and Trigo-Rodríguez J. M. (2015). “New methodology to determine the terminal height of a fireball”. *Icarus*, **250**, 544–552.  
<http://dx.doi.org/10.1016/j.icarus.2014.12.027>.
- Moreno-Ibáñez M., Gritsevich M. and Trigo-Rodríguez J. M. (2016). “Measuring the terminal heights of bolides to understand the atmospheric flight of large asteroidal fragments”. In Trigo-Rodríguez J. M., Gritsevich M. and Palme H., editors, *Assessment and Mitigation of Asteroid Impact Hazards*, Springer, New York. In print.
- Näränen J., Lankinen J. and Raja-Halli A. (2014). “A New Toolset for Passive Monitoring of Air Traffic and Sky Conditions at Metsähovi Station, Finland (3073)”. *Proceedings of the 19<sup>th</sup> International Workshop on Laser Ranging*, Annapolis MD, Oct. 27-31, 2014.
- Raja-Halli A., Näränen J., Poutanen M., Kloth A. and Steinborn J. (2014). “Progress Report on the New SLR System of GGOS'S Core Site Metsähovi, Finland (3090)”. *Proceedings of the 19<sup>th</sup> International Workshop on Laser Ranging*, Annapolis MD, Oct. 27-31, 2014.
- Raja-Halli A. and Näränen J. (2015). “Progress report on the new satellite laser ranging system of Metsähovi Geodetic Research Station”. *Conference abstract book of the XXVII Geophysics Days at the University of Oulu on 26-27 May, 2015*, pages 60–62.
- Trigo-Rodríguez J. M., Lyytinen E., Gritsevich M., Moreno-Ibáñez M., Bottke W. F., Williams I., Lupovka V., Dmitriev V., Kohout T. and Grokhovsky V. (2015). “Orbit and dynamic origin of the recently recovered Annama's H5 chondrite”. *Monthly Notices of the Royal Astronomical Society*, **449**, 2119–2127.  
<http://dx.doi.org/10.1093/mnras/stv378>.
- Trigo-Rodríguez J. M., Palme H. and Gritsevich M. (2016). “Barcelona Asteroid Day 2015: revisiting the threat by asteroid and comet impact”. In Trigo-Rodríguez J. M., Gritsevich M. and Palme H., editors, *Assessment and Mitigation of Asteroid Impact Hazards*, Springer, New York. In print.
- Turchak L. I. and Gritsevich M. I. (2014). “Meteoroids Interaction with the Earth Atmosphere”. *Journal of Theoretical and Applied Mechanics*, **44**, 15–28.  
<http://dx.doi.org/10.2478/jtam-2014-0020>.
- Virtanen J., Poikonen J., Säntti T., Komulainen T., Torppa J., Granvik M., Muinonen K., Pentikäinen H., Martikainen J., Näränen J., Lehti J. and Flohrer T. (2016). “Streak detection and analysis pipeline for space-debris optical images”. *Advances in Space Research*, **57**, 1607–1623. doi:10.1016/j.asr.2015.09.024.

# An attempt to explain VLF propagation perturbations associated with single meteors

Jean-Louis Rault<sup>1</sup> and Jean-Jacques Delcourt Dr. Sc.<sup>2</sup>

<sup>1</sup>IMO Radio Commission, 16, rue de la Vallée, Epinay sur Orge, France

f6agr@orange.fr

<sup>2</sup>ionosphere.d23@skynet.be

A first evidence of sudden changes in the amplitude of distant VLF radio transmissions related to single meteors was found during GEM 2010 meteor shower radio observations. Based on many similar observations gathered during different meteor showers, this paper is dedicated to the corresponding physical phenomena involved at the level of the D layer of the Earth ionosphere.

## 1 Introduction

Various phenomena such as UV and X rays bursts radiated by the Sun,  $\gamma$  rays radiated by distant stars, electrons precipitations induced by wave-particle interactions within the magnetosphere, nuclear explosions, etc., create transient VLF propagation disturbances by modifying the electron content of the D layer of the ionosphere (Barr, 2000).

A first evidence for sudden amplitude changes induced by single meteors on signals received from distant VLF transmitters was found during a Geminids 2010 observation campaign (Rault, 2013).

This paper is aimed to clarify the causes of such VLF propagation modifications induced by meteors.

## 2 Observations

In the frame of studies related to interactions between meteors and Earth ionosphere, 29 meteor showers (Perseids, Geminids, Draconids, Leonids, Quadrantids,  $\eta$ -Aquariids and Lyrids) and some sporadic activity have been observed simultaneously on VHF and VLF radio frequencies since 2008. A dedicated autonomous portable radio setup was developed for that purpose and used in several remote and radio electrically quiet areas.

During each observation campaign, the ELF/VLF band and the VHF forward scatter echoes produced by the meteors illuminated by the French military radar GRAVES meteors were recorded 24h a day.

A first VLF propagation disturbance associated to a single meteor was discovered in 2010 on the amplitudes of the FTA and DHO38 transmissions (see *Figure 2*).

## 3 Instrumentation and data reduction

### Observation setup

The setup (see *Figure 3*) consists in a Zoom H4N digital stereo audio recorder connected to the output of an AOR AR5000+3 communication receiver tuned on 143.050

MHz (frequency of the Graves radar) and to a wide band E-field ELF/VLF preamplifier (5 Hz to 24 kHz bandwidth). The VHF aerial consists in a  $5/8^{\text{th}}$  lambda vertical whip and the ELF/VLF sensor is made of a 1.5 m high vertical mesh cylinder (diameter: 50 mm). A 12 V car battery and a 16 gigabytes SD memory card allow the system to run remotely and continuously for more than 24h (Rault, 2010).



*Figure 1* – Locations of some of the observation sites and of the radio transmitters used for simultaneous VLF and VHF observation campaigns.

VLF transmitters: ● GBZ 19,6 kHz & GQD 22,1 kHz ■ DHO38 23,4 kHz ▲ FTA 20,9 kHz ■ HWU 21,75 kHz ○ ICV 20,27 kHz.

VHF radar used for meteor scatter detection: GRV

Observation locations: ■ Baraque de l'Air (Lozère) ★ Pic du Midi observatory.

### Data processing

The stereo audio records allow searching for possible correlations between any ELF/VLF events and the meteor forward scatter VHF echoes.

The data reduction consists in performing a spectral analysis (thanks to Fast Fourier Transformations) of the two data channels and in searching visually for any correlated events.

The VLF transmitters use a MSK (Minimum Shift Keying) modulation scheme, so the amplitude of their transmissions is measured and plotted by performing an average of the power delivered by each of the bins of the FFT output, which is centred on the mean transmission frequency of each transmitter under study.

The FFT analysis and plotting are performed thanks to the Spectrum Lab software developed by Wolfgang Büscher<sup>1</sup> (Büscher, 2016).

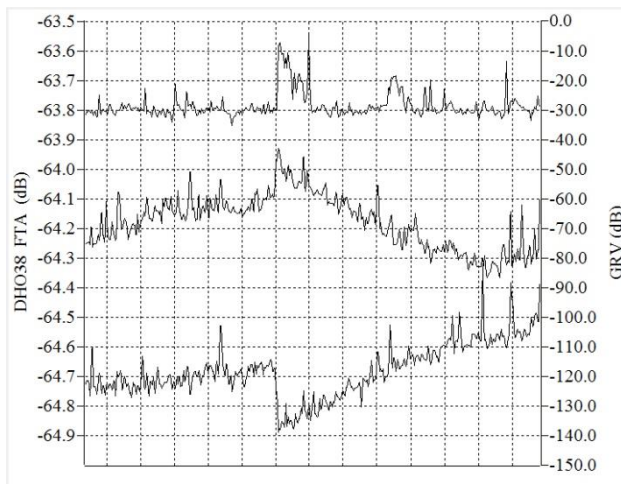


Figure 2 – First observation at Pic du Midi observatory of a constructive interference on FTA (middle trace) and of a destructive interference on DHO38 (lower trace) triggered by a single meteor (meteor VHF echo on upper trace). Time scale: 10s/square.

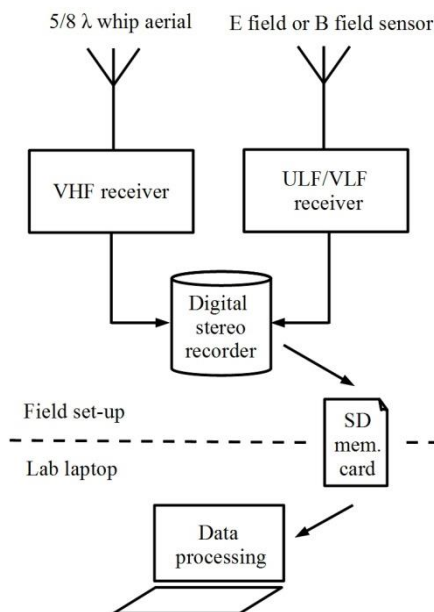


Figure 3 – Diagram of the radio VHF and ELF/VLF setup.

The original stereo data are sampled at 48 kHz by the digital recorder, but are processed at 384 kHz during the

data reduction phase. Fooling the analysis software in such a way allows processing the data 8 times faster than the real time, thus saving a lot of time during analysis.

## 4 Discussion

### Interference patterns

In this chapter are successively examined: the geometry of the VLF radio paths (see *Figure 1*), the reasons why a meteor can induce VLF constructive or destructive interferences at the observation location and the duration of the events.

### VLF transmitter-receiver radio paths

Regarding the VLF paths, we must consider three different channels: the ground wave, the sky wave (Delcourt)<sup>2</sup> and the *reflected* wave from the meteor trail (*Figure 4*). In fact, there are no *reflected* waves, neither for the ionospheric D layer circuit, nor for the *pseudo reflection* on the trail. The D region is not a sharp boundary layer but a graded index medium. There is no singularity at the virtual height of reflection ( $V$ ) but a bended path, which is an ionospheric mirage around the actual refracting height ( $R$ ). The beam is thus always transmitted but never reflected and the Fresnel's coefficients exhibit no phase opposition between the incident and the transmitted waves. The interference figure at the receiving site depends only on three parameters: wave length, length of ground path and length of virtual sky path. The real wave and the virtual wave are in phase when leaving the D layer. The difference in length for the real and virtual paths is balanced by the real and virtual propagation velocities which are linked through the refractive index.

The Transmitter-Receiver ground / sky distances difference is described as follows (see *Figure 5*):

$$d_c - d_s = 2 \sqrt{2R [R + h] \left[ 1 - \cos \frac{d_s}{2R} \right] + h^2} - d_s \quad (1)$$

$$\varepsilon = \frac{2 \sqrt{2R [R + h] \left[ 1 - \cos \frac{d_s}{2R} \right] + h^2} - d_s}{\lambda} = f_{[h, d_s, \lambda]}$$

where  $d_s$  is the ground wave path length,  $d_c$  is the sky path length,  $h$  the virtual height of reflection,  $\lambda$  the wavelength and  $R$  the Earth radius which is equal to 6378 km. The interference pattern is described as:

$$I = \cos(2\pi \cdot \varepsilon) \quad (2)$$

As shown on *Figure 6*, aerial airborne measurements known as *Hollingworth's pattern* (Hollingworth, 1926) give results consistent with the equation (2).

<sup>1</sup><http://www.qsl.net/dl4yh/spectra1.html>

<sup>2</sup>“Basse ionosphère, région D. Les fondamentaux”. (2015) <http://www.coucheD.be>

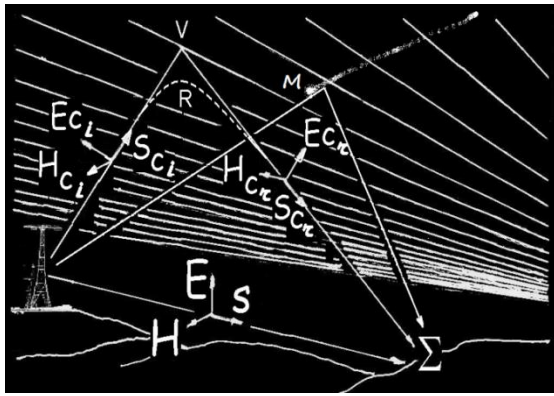


Figure 4 – VLF interference components. E and H are the electric and magnetic field vectors, S is the Pointing vector, “i” and “r” mean incident and reflected.

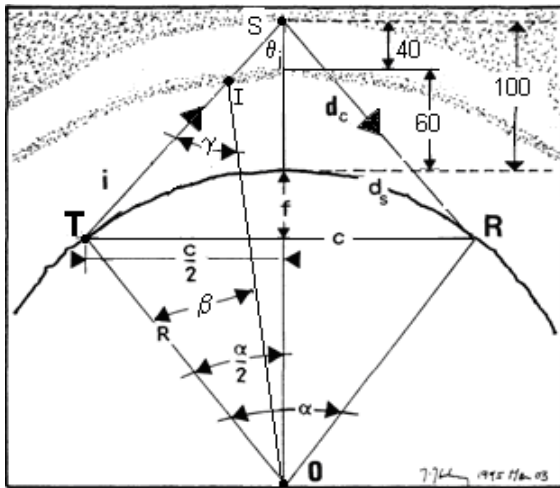


Figure 5 – Geometry of a VLF circuit involving the D layer.

The evolution of the ionosphere ionization vs altitude depends on the sun illumination in the UV and X rays wavelengths, and thus with solar time. During day time, the “reflection” altitude, in the range 60 – 70 km, is lower than the meteor trails average altitude, therefore restricting the recordings to night time when the D layer altitude reaches 90 to 100 km, which, in first approximation, is the range of altitudes area of most of the meteor trails (Figure 7).

The wavelengths of the signals radiated by the VLF transmitters are around 15 km, a value which is comparable to the length of the meteor trails. The diameter of a trail can reach 10 to 20 m, making any VLF specular reflection not possible. If we translate this in the visible domain, this would be similar to an attempt to visualize a 0.5 μm long and 5 atoms large wire with a microscope. So another explanation has to be found. After midafternoon, the D layer bottom climbs up to the mesopause region, inducing an interference pattern evolution. The concentration of electrons increases with the altitude. The localized enhancement of the electron content within a meteor trail – 10<sup>14</sup> m<sup>-3</sup> instead of 10<sup>9</sup> – (Belkovich, 2005) should counterfeit an altitude increase, and therefore a modification of the amplitude of the received signal. This modification depends on the phase φ between the ground wave and the sky wave, as follows:

- higher signal level if  $-\pi/2 < \phi < +\pi/2$  rd

- lower signal level if  $+\pi/2 < \phi < +3\pi/2$  rd

But the trail is a closed medium presenting a small ohmic resistance in the range of a few tens of ohms, so the Maxwell laws apply.

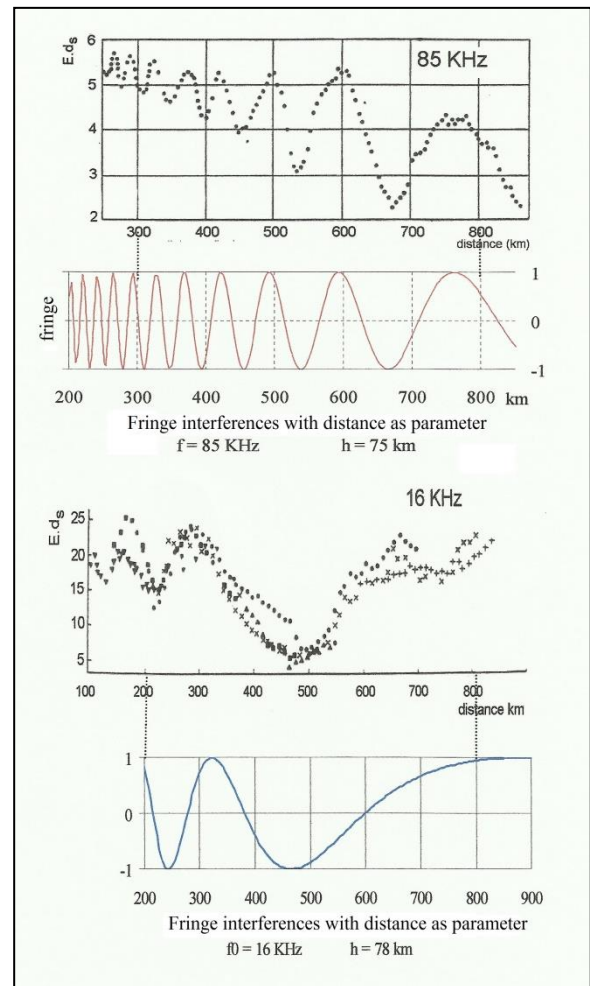


Figure 6 – Interference evolution pattern depending on d<sub>s</sub>.

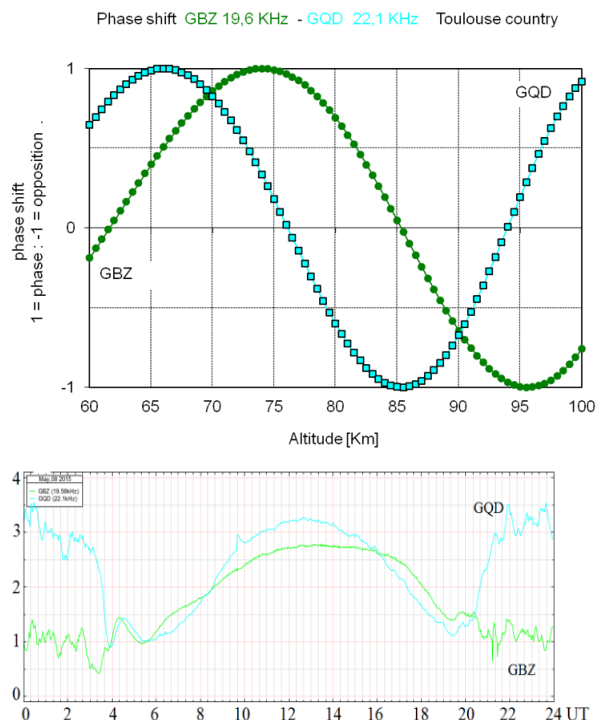


Figure 7 – Interference pattern of UK VLF transmissions due to ionospheric D layer altitude changes, as seen from Toulouse.

The local induced electric field is therefore opposed to the incident electric field, implying the following variations on the received signal:

- lower signal level if  $-\pi/2 < \varphi < +\pi/2$  rd
- higher signal level if  $+\pi/2 < \varphi < +3\pi/2$  rd

A similar result can be obtained thanks to a more general law which is applicable in the propagation plane: the incident sky wave induces an electron motion in the meteor trail population, which is thus developing a work (i.e. force x displacement). The most important part of this work is lost in collisions as heat, and after “penetrating” in the meteor trail, the sky wave Poynting vector becomes smaller than before the interaction. So the influence of the sky wave in the interference pattern becomes lower during the meteor trail expansion and diffusion.

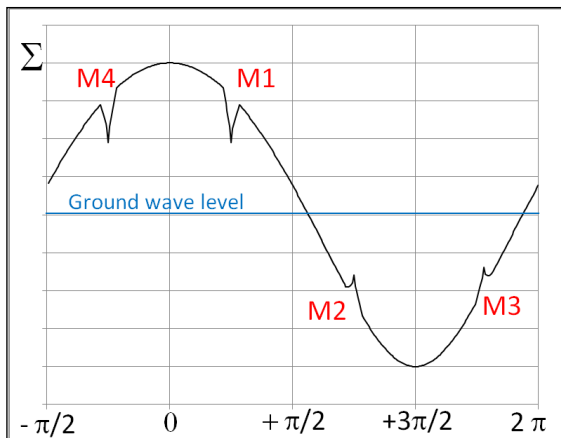
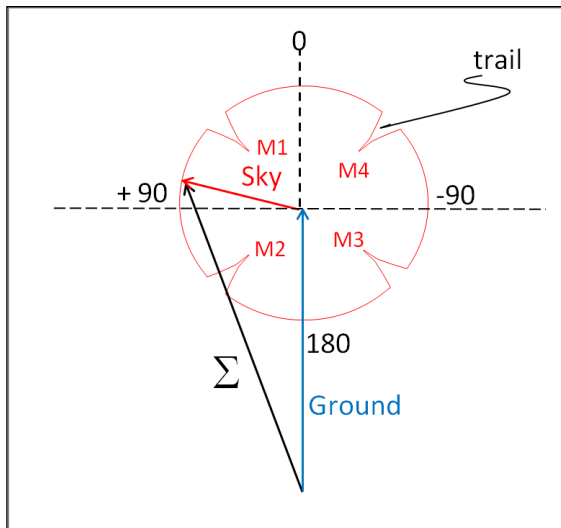


Figure 8 – Evolution of the reception level  $\Sigma$  with phase . M1 to M4 are the trail effect . The sky wave is assumed to be constant in amplitude except during trail effect. The reading can be done in the two directions counterclockwise or clockwise, from left to right or inverse.

A question arises: are these interactions a fortunate combination of circumstances? In fact, the 2D (2 dimensional) sky wave paths shown on Figures 4 and 5 are over simplified. In the real world, many different sky paths are possible, all of them being included inside an

ellipsoidal cavity which is more or less overlapping the D layer, and all of them are converging in the receiver area.

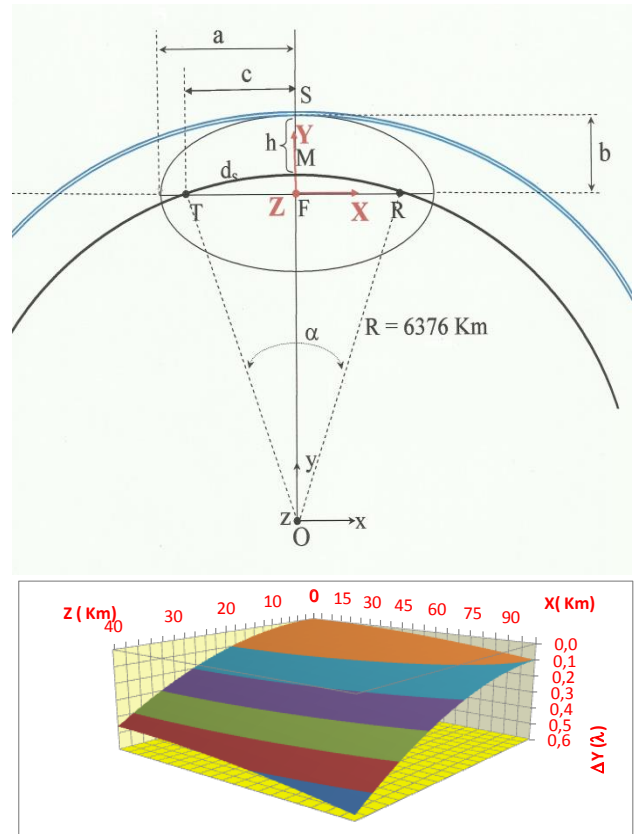


Figure 9 – Geometry of the overlapping of the ellipsoidal cavity insuring a multipath skywave with the D region at night.

Let's have the following configuration shown on Figure 9:

- transmitter – receiver distance:  $d_s = 1000$  km
- night ionospheric D layer altitude : 100 km
- Earth radius : 6376 km
- $\lambda : 15$  km
- $\alpha/2 = 0.078$  rd
- $FM = 19.594$  km
- $TR = 998.975$  km
- $a$  (semi major axis) = 513.605 km
- $b$  (semi minor axis) = 119.594 km
- translation of Earth  $\rightarrow$  ellipse axis system:

$$x = \mathbf{X}$$

$$y = \mathbf{Y} + (6376 - 19.594)$$

$$z = \mathbf{Z}$$

The Cartesian equation of the D layer at 100 km altitude is:

$$x^2 + y^2 = (6376 + 100)^2$$

The Cartesian ellipse equation is:

$$\frac{x^2}{a^2} + \frac{y^2}{b^2} = 1$$

For a deviation  $\Delta X$  of 10 km, with  $S$  being the discordance,  $\Delta Y$  between the ellipse of propagation and the D layer is 15m or  $0.001 \lambda$ ,  $0.025 \lambda$  for  $\Delta X = 50$  km,  $0.1 \lambda$  for  $\Delta X = 100$  km and  $0.42 \lambda$  for  $\Delta X = 200$  km.

So, beyond 100 km, the *reflected* beam creates a diffraction pattern on the reception site.

The problem is more crucial on the plane which is orthogonal to the propagation plane. At a distance of 100 km and for a lateral deviation of 20 km, the gap between the D layer and the ellipsoid is a little bit more than 3 km or  $0.2 \lambda$ . However the ellipsoid influences only the focalization on the receiver site and not the energy exchanged between the incident beam and the meteor trail in the 90 – 100 km altitude range.

If we accept the criteria of  $\Delta Y \leq \lambda/10$  for a reasonable diffraction pattern on the site of reception for  $d_s = 1000$  km and for a few millimeters large meteor, we can expect a meteor VLF signature if the meteor decay occurs in a volume of the ionosphere 200 km long, 40 km wide ( $S = 8000 \text{ km}^2$ ), 20 km wide and 10 km thick and centered on the virtual point of reflection the meteor.

**Analysis of the events durations**

If we consider a siderite meteor having a 1 mm diameter and a velocity of 40 km/s, the electron concentration in its trail is a function of time and distance of the trail heart according to equation (3):

$$[N_{d,t}] = \frac{[N_t]}{\pi [R_0^2 + 4 D t]} \cdot e^{-\frac{d^2}{R_0^2 + 4 D t}} = \frac{[N_t]}{\pi R_t^2} \cdot e^{-\frac{d^2}{R_t^2}} \quad (3)$$

where  $[N_t]$  is the linear electrons concentration,  $d$  the coaxial distance,  $R_0$  the initial radius of the trail,  $D$  the ambipolar diffusion coefficient and  $R_t$  the radius at which the electron concentration is the part  $e^{-1}$  of the initial concentration, and  $t$  is time (see *Figure 10*).

The trail consists of concentric quasi neutral layers of electrons and ions which are coming either from the ionized mesosphere or from the ionization of the meteor core. The mesospheric electrons and ions diffuse more promptly than those of meteoritic origin but are at least ten times less numerous (Lebedinec and Sosnova, 1967).

After 60 s which is the average duration observed for the VLF meteor signatures, the electron density of mesospheric origin is around  $2 \cdot 10^9 \text{ m}^{-3}$ , i.e. the same as the mesospheric background, while the meteoritic free electron density is in the range of  $2 \cdot 10^{10}$ , thus always discernible by the incident VLF wave.

**Geminids 2010 (from Pic du Midi Observatory)**

**Analysis of some VLF meteor events**

Many VLF propagation perturbations correlated with single meteors have been identified among the 1.5 terabytes of data collected during 29 observation campaigns. It is worth noting that no VLF meteor disturbances at all were observed during day time.

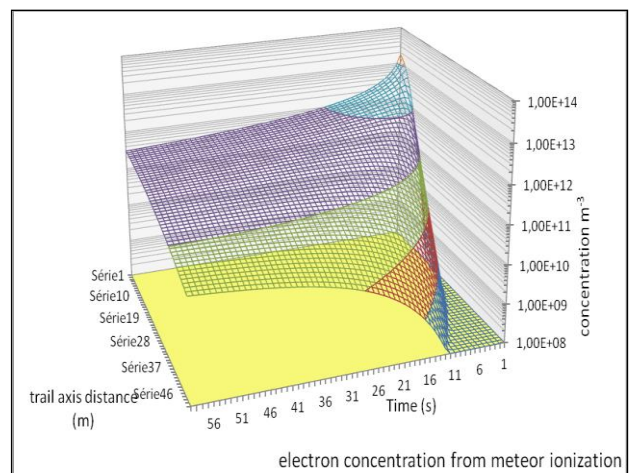
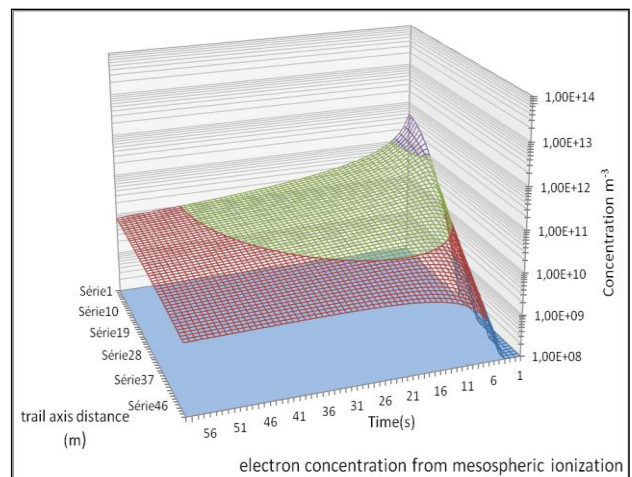


*Figure 10* – Evolution of the mesospheric and meteoric and electron concentrations vs time and distance computed from  $R_0$ .

This is explained by the fact that when the Sun is illuminating the upper atmosphere, the altitude of the ionosphere D layer decreases and its free electrons density increases dramatically, thus masking any influence of the meteor trails on the VLF propagation.

A sample of 4 night events is described below. The distances (in km) between the VLF transmitters and the observation location were as follows:

	FTA	HWU	DHO38
GEM 2010	651	429	1256
LYR 2013	466	316	1006
GEM 2014	466	316	1006

The event occurred around midnight (see *Figure 2*). The D layer bottom was at an altitude of about 95 to 100 km. The phase pattern evolution is shown by the coloured rectangle on the right of *Figure 11*. The reception level of DHO38 was on the rise while that of FTA was on the decline. On the graph we are moving from the left to the right. In accordance with what was explained above, the DHO38 level should drop and that of FTA should increase with a meteor decay at  $h > 95$  Km, which was the case.

**Lyrids 2013 (from Baraque de l’Air, Lozère)**

The date of the observing records is important. We are one month after the equinox and during night, the ceiling of the D layer is lower than in december at Le Pic du Midi Observatory.

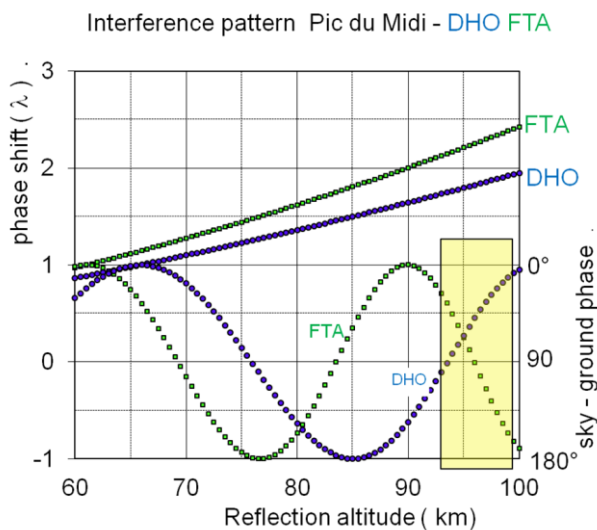


Figure 11 – Evolution of the interference fringes with altitude at Pic du Midi Observatory.

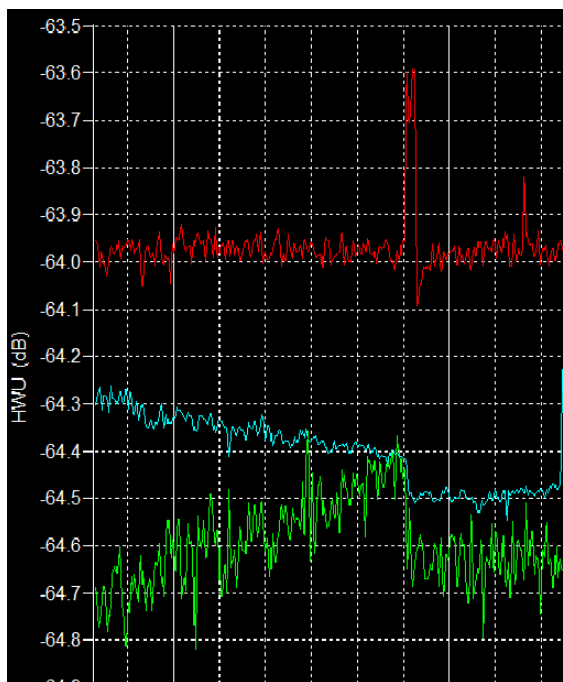


Figure 12 – Top in red: Graves radar signal. In blue: DHO38, in green HWU. Recorded at Baraque de l’Air / Lozère on 2013 April 21, 23<sup>h</sup>24<sup>m</sup>54<sup>s</sup>UTC.

The evolution of the interference figure is from left to right at rise for both DHO38 and HWU, which finally leads to a dip on the reception level (*Figures 12 and 13*). In the present case,  $h$  is greater than 93 km.

*Figure 14* shows the record of a trail appearing 4 ½ hours later, with an amplitude peak instead of a dip.

At 04<sup>h</sup> UTC, at the ionospheric mid *reflective* point we are just in the middle of the sunrise phase at the level of the mesopause. Within ten minutes, all the D layer is wholly illuminated and in an half hour the D layer floor has collapsed down to an altitude of 70 km. Thus the declining HWU interference pattern is followed from right to left, producing an amplitude peak for HWU.

**Geminids 2014 (from Baraque de l’Air, Lozère)**

During this December campaign, the receiving site was the same as in April 2013.

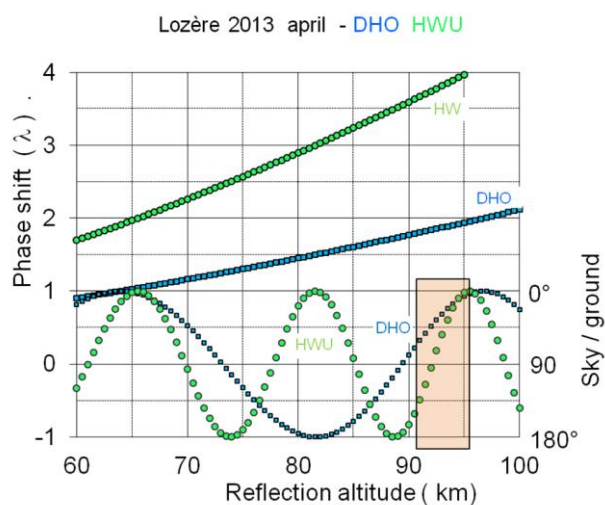


Figure 13 – Evolution of the interference fringes with altitude at Baraque de l’Air / Lozère.

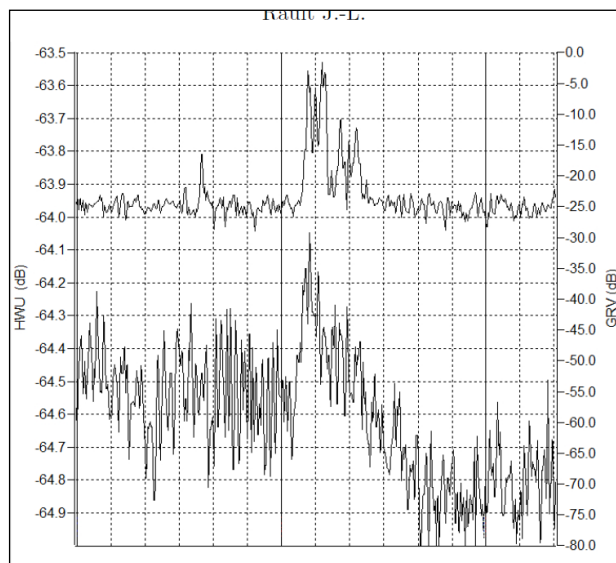


Figure 14 – Top: Graves radar echo, bottom: HWU amplitude recorded at Baraque de l’Air / Lozère on 2013 April 22, 04<sup>h</sup>03<sup>m</sup>29<sup>s</sup> UTC, 10s/div.

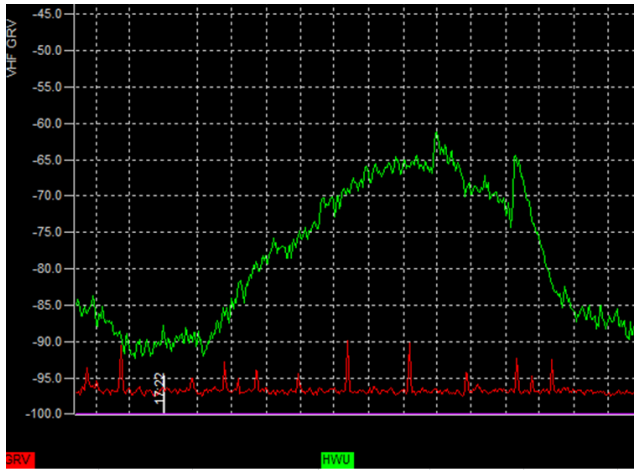


Figure 15 – HWU amplitude (green) and Graves signal (red). 0,1 dB<sub>(V)</sub> / vertical division, 32 s / horizontal division. Recorded at Baraque de l’Air / Lozère.

During night the reception level is not totally erratic and we can observe fluctuating trends moving up or down with a period of a few minutes to a half hour (see Figure 15). The reception levels are the result of a wandering along the interference pattern. In the middle of the winter nights, the cause is exclusively aeronomic and even meteorological. The fluctuations in the interference figure are approximately 6 minutes long, including two meteor interference events probably of the M3 type (see Figure 8) at an altitude of  $90 \text{ km} < h < 93 \text{ km}$ .

## 5 Conclusion

Hundred hours of observation of various meteor showers and sporadic meteor activity and manual analysis have led to the evidence of multiple VLF amplitude disturbances directly correlated with single meteors during night time. A coherent theoretical explanation of these observations has been elaborated in this paper. In the next future, a statistical study of the shapes,

amplitudes and durations of a large batch of VLF meteor events should allow to improve the detailed understanding of these phenomena.

## References

- Barr R., Jones D. L. and Rodgers C. J. (2000). “ELF and VLF radio waves”. *Journal of Atmospheric and Solar-Terrestrial Physics*, **62**, 1689–1718.
- Bel’Kovich O. I. (2005). “The physics of meteoroid ablation and the formation of ionized meteor trails”. In Verbeeck C. and Wislez J.M, editors, *Proceedings of the Radio Meteor School*, Oostmalle, Belgium, 10–14 September 2005. IMO, pages 21–26.
- Büscher W. (2016). Spectrum Laboratory software.
- Hollingworth J. (1926). “The propagation of radio waves”. *IEE Journal*, **64**, 579–589.
- Lebedinec V. N. and Sosnova A. K. (1967). “Radio reflections from meteor trails”. In Kresak L. and Millman P. M, editors, *Physics and dynamics of meteors IAU symposium n°33*, Tatranska Lomnica, Czechoslovakia, 4–9 september 1967, pages 27–44.
- Rault J. L. (2013). “Evidence for VLF propagation perturbations associated with single meteors”. In Gysens M., Roggemans P. and Zoladek P., editors, *Proceedings of the International Meteor Conference*, Poznan, Poland, 22-25 August 2013. IMO, pages 345–351.
- Rault J. L. (2010). “Searching for ELF/VLF meteor signatures”. *WGN, Journal of the IMO*, **38**, 67–75.

# 65 years of meteor radar research at Adelaide

Iain M. Reid<sup>1,2</sup> and Joel Younger<sup>1,2</sup>

<sup>1</sup> ATRAD Pty Ltd, Adelaide, Australia, 5031

ireid@atrad.com.au

<sup>2</sup> School of Chemistry and Physics, University of Adelaide, Australia, 5005

Over 65 years of radar research using meteor radar at Adelaide University in Australia is very briefly reviewed.

## 1 Early days

Radio studies of meteors began at Adelaide in 1949, and like many radio and radar based research efforts of that era, grew out of wartime radar research. Lenard Huxley arrived at Adelaide University from the University of Birmingham in 1948 to take the Elder Chair of Physics, and began revitalizing the Department, and establishing a number of research areas (Crompton, 2007)<sup>1</sup>. He was supported in this by the new Vice Chancellor, A.P. Rowe. Both Rowe and Huxley had been at the Telecommunications Research Establishment (TRE) during the Second World War. Rowe had been Chief Superintendent, and Huxley had established and headed the radar training school for both civilian and service personnel in the TRE. In another interesting connection to wartime research, Adelaide graduate Sir Mark Oliphant had drawn Huxley's attention to the advertisement for the position (Blake, 2010)<sup>2</sup>.

One of the new research areas to be initiated in physics was radar meteor astronomy, and Huxley asked Graham Elford to pursue this topic. After the first measurements of upper atmosphere winds inferred by the drift of meteor trails were reported by Manning et al. (1950) at Stanford, the Adelaide effort was broadened out to include the study of the upper atmosphere. This became Graham Elford's main research area. In 1950, two Honors students, Des Liddy and Alan Weiss, joined the group, followed by PhD student David Robertson at the beginning in 1951. Robertson had previously worked with Oliphant at Birmingham, and brought considerable technical expertise to the group (Blake, 2010)<sup>2</sup>.

Robertson was an amateur radio ham, and it was his personal 500W transmitter located at his home at Mount Lofty, together with receivers in Adelaide, Burra and Kulpara, that was used to make the first observations of meteor trails by the group in 1951. Subsequently, he developed the Adelaide meteor wind radar together with Elford and Liddy, the basic design concepts of which continued to be used at Adelaide until the mid-1970's, and which were also used later for the meteor radar at Atlanta by Bob Roper (Roper, 1984). This system

operated at 27 MHz and used a 240 W continuous wave (CW) approach. Robertson submitted his PhD thesis on 'Reflection of radio waves from meteor trails, with applications to the measurement of upper atmosphere winds', in August 1953. Graham Elford followed late in 1954 with his thesis on the investigation of winds in the upper atmosphere. Robertson and Elford (1953) published the first



Figure 1 – the Upper Atmosphere Group 1962. Back row: R. Roper, J. Welsby, C. Nilsson, A. Bastian, B. Stone. Front row: Dr. E. Murray, Miss J. Allister, Miss M. Chapman, Dr. G. Elford.

observations of upper atmosphere winds using the meteor technique after those of Manning et al. (1950). In March 1955, this version of the Adelaide Meteor wind radar was decommissioned.

Beginning in early 1954, with funding from the Australian Antarctic Division, effort was directed to the development of a new radar to measure upper atmosphere winds in the Antarctic. The new pulsed radar system for this work (see Figure 2) was developed by Eric Murray. In December 1956, Carl Nilsson, a very recent BSc graduate, took the equipment to Mawson Base and operated it there during the International Geophysical year. Murray analyzed the data for his PhD thesis.

The work on meteor astronomy continued along with the upper atmosphere winds work. Nilsson later completed a PhD on meteor orbits which used some of the Mawson radar data. With support in the form of radar equipment

<sup>1</sup> <http://adb.anu.edu.au/biography/huxley-sir-leonard-george-holden-516/text22851>

<sup>2</sup> <https://physsci.adelaide.edu.au/about/physics/history/document/s/physics-in-adelaide-the-1950s.pdf>

provided by Sir Bernard Lovell at the University of Manchester, Alan Weiss set up an independent radar system to study meteor showers. This work formed part of his PhD thesis, which he submitted in May 1954. He published his work on the distribution of the orbits of sporadic meteors in Weiss (1957).

## 2 New field sites

### St Kilda

The Mawson meteor radar was very difficult to maintain, and it was decommissioned in 1959. Effort had shifted to

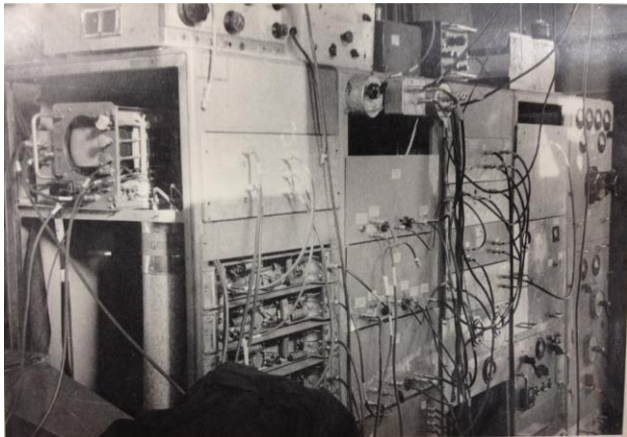


Figure 2 – The Mawson meteor radar. The first upper atmosphere wind measurements on the Antarctic Continent were made using this equipment.

the development of a new dedicated field site at St Kilda, north of Adelaide, and a new radar, with the transmitter located in Adelaide, and the main receiving station at St Kilda was completed in 1958. The arrangement is shown in Figure 3, and one of the remote receiving sites is shown in Figure 5. The Upper Atmosphere Group in 1962 is shown in Figure 1.

Highlights of the work produced using this radar included the determination of meteor orbits, measurements of ‘turbulence’ intensity, and long term measurements of upper atmosphere winds. Nilsson’s work (Nilsson, 1964) resulted in the first set of measurements of meteor orbits in the southern hemisphere (2200 in total). Most orbits were found to lie close to the plane of the ecliptic. Bob Roper was the first person to measure upper atmosphere variability at small scales (< 2 km). His measurements were interpreted as being related to the turbulent dissipation rate at 93 km, but are more likely due to small scale wave motions rather than actual turbulence. Nevertheless, they were a valuable contribution to better understanding the dynamics of this region. Interferometric measurements of the mean wind field (see

Figure 4 and Figure 6) continued using this radar until the mid-1970’s, although it was run in campaign mode after 1972. Work at the St Kilda field site ceased in the mid-1970’s and was relocated to the nearby Buckland Park field site.

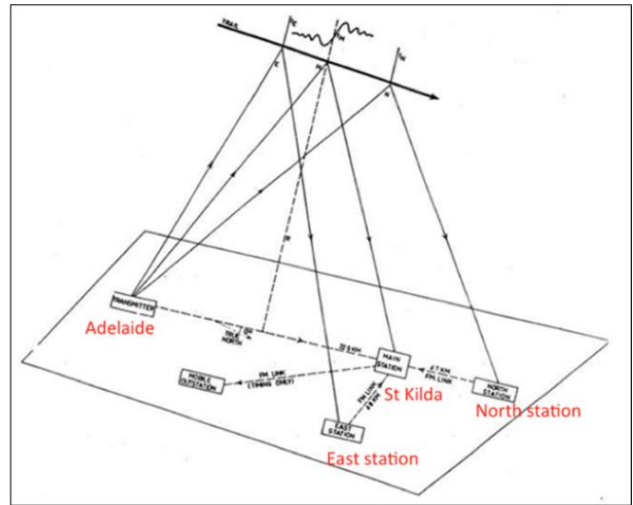


Figure 3 – The multi-station system in 1958. The receiving main site at St Kilda had two supplementary receiving sites about 5 km East and North and the data were sent to the main station via FM links.

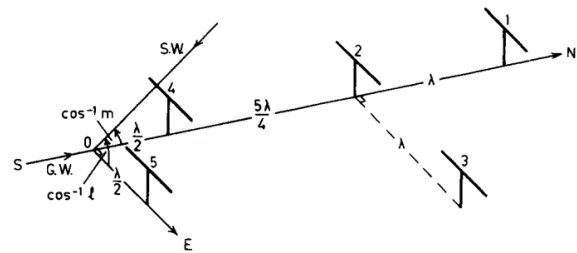


Figure 4 – The interferometer used for wind measurements at the St Kilda field site. Each antenna was a half-wave dipole and the direction cosines of the sky wave were deduced from the relative phases on the five antennas.

### Buckland Park

Basil Briggs joined the Department in 1962. He had been a Junior Scientific Officer at the TRE between 1942 and 1946 before joining the Radio Research Group at the Cavendish Laboratory, Cambridge, where he worked from 1946 to 1961. Together with Graham Elford, he developed the large MF/HF radar array at Buckland Park (Briggs et al., 1969). This versatile array was used for investigations of the ionosphere, the neutral atmosphere and of meteors observed at both 2 and 6 MHz. Examples of the latter work include observations of 2 MHz meteor echoes (Brown, 1976), their height distribution (Olsson-Steel and Elford, 1987), and the measurements of winds using 2 MHz meteor trails (Tsutsumi et al., 1999).

### 3 Decline and rebirth of meteor wind radars



Figure 5 – Bob Roper and Carl Nilsson with receiving equipment at one of the St Kilda remote receiving sites.

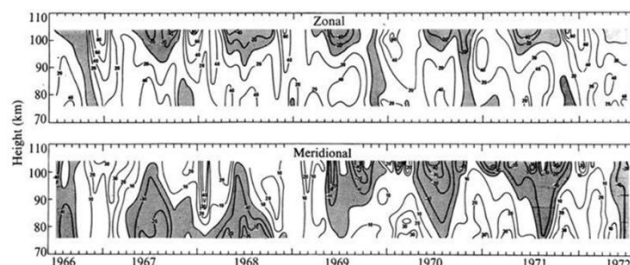


Figure 6 – Six years of upper atmosphere winds measured using the St Kilda radar.

#### Decline of meteor wind radars

The closure of the St Kilda site and the dedicated meteor radar in the mid-1970's was typical of a general decline of radar meteor upper atmosphere wind research around the world, and the measurement of upper atmosphere winds became more common by using partial reflection radars (see e.g., Reid, 2015). But some new meteor radars were developed in this period. For example, in the early 1970's, the Soviet VETA radars were developed by the Kharkov Institute of Radio Electronics. These formed the basis of an extensive network, albeit one with no height information. This is briefly discussed by Roper (1984). A new meteor radar was also developed in Kyoto by Aso et al. (1979), but generally the technique fell from favor until the late 1990's.

#### Rebirth of meteor wind radars

Increased interest in using meteor trails for the measurements of upper atmosphere winds came

following the advent of ST and MST radars. These powerful radars operating in the lower VHF band were designed to measure winds using the Doppler technique in the Stratosphere and Troposphere (ST), and for the most powerful radars, the Mesosphere (M) as well. By piggybacking a dedicated data acquisition system onto these pulsed radars, their narrow beams could be used for meteor studies. One such system, MEDAC, was developed at the University of Colorado (e.g., Valentic et al., 1996) and used with a number of ST radars.

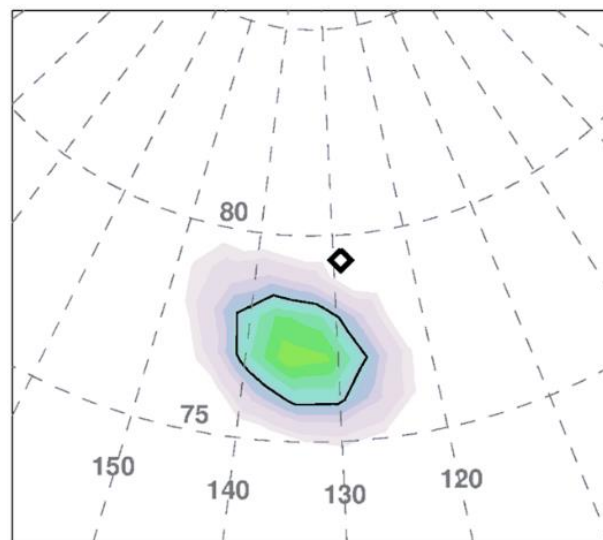


Figure 7 – The Camelopardalids 2014 Activity Map. The diamond is the pre-infall radiant, the solid contour is the full width half maximum (further details in Younger et al., 2015a).

One issue with this approach is that because most meteor trails occur low in the sky, most meteor trails are detected in the radar sidelobes, and without interferometry, their actual location is indeterminate. At Adelaide, the main beam of the radar was directed at  $60^\circ$  off-zenith, successfully avoiding this issue (e.g., Cervera and Reid, 1995).

A variation of this approach using an additional receiving only interferometer together with an MST radar was pioneered on the MU MST radar in Japan (e.g., Tsutsumi et al., 1994). This was followed by the development of a new class of dedicated all-sky meteor radars using an interferometric approach and producing real-time winds in the late early 1990's (e.g., Holdsworth et al., 2004). This development was made possible by the ready availability of cheap powerful computers, and development of solid state transmitters and better data acquisition systems. These radars have now largely displaced the previously more common partial reflection radars used for measuring upper atmosphere winds.

### 4 Recent work

The 21<sup>st</sup> century has seen meteor radar become a standard tool for the routine measurement of upper atmospheric winds, with radars developed by ATRAD achieving detection rates in excess of 30000 meteors per day. Ongoing wind observations continue to provide deep insights into the structure and dynamics of the

atmosphere and how the motions of air masses are coupled between the upper and lower atmosphere (Bossert et al., 2015). The ability to measure atmospheric conditions in the meteor region at higher temporal resolutions has facilitated the studies of mesospheric meteorology, exotic plasma behaviours, and detailed astronomical observations. A substantial breakthrough has been the implementation of the Fresnel transform technique, which provides high-accuracy meteoroid speeds, in addition to producing images of radar reflectivity along meteor trails (Elford, 2004; Holdsworth et al., 2007).

Astronomy has followed a similar path to atmospheric observations, as broad surveys of shower activity (Younger et al., 2009) have given way to detailed investigations of individual showers. Individual showers have enabled the performance of radar techniques to be tested with known populations, further refining established practices (Younger et al., 2012). The unprecedented detection of the Camelopardalids shower of 2014 (Younger et al., 2015b) was the first time that a new shower had been predicted prior to its first occurrence and demonstrated the ability of meteor radar data to be rapidly analysed in response to unusual events (see also Younger et al., 2016).

New fields of research have been opened, as old assumptions have given way to a better understanding of meteor trail plasma. Meteor radar echo durations have been found to be strongly affected by plasma neutralization at lower altitudes (Lee et al., 2013; Younger et al., 2014), which allows observation of the chemistry of the D-region of the ionosphere. Inconsistent temperature estimates can now be explained (Cervera and Reid, 2000; Holdsworth et al., 2006), and new methods of using meteor radar to measure atmospheric density have been developed (Younger et al., 2015a).

Moving forward, the future of meteor radar lies in the establishment of networks of radars to observe not just the conditions above a single site, but the motions of the atmosphere across large areas. Together with Chinese colleagues, the utility of small meteor radars to investigate non-specular echoes and some aspects of plasma irregularities has been explored (Li et al., 2013). Advances in radar sensitivity and echo interpretation are allowing meteor radars to also be used to study the lower portion of the ionosphere, including sporadic E layers. The use of remote receiving sites, such as those used in the St Kilda radar is being reinvestigated using GPS locking, and is a promising new development for the measurement of wind fields over large regions. Astronomical applications will also benefit, as complete coverage of the celestial sphere is achieved, with the observations of multiple sites being assimilated into large-scale virtual observatories.

## 5 Conclusion

We have very briefly reported on more than 65 years of meteor radar research at Adelaide University. A feature

of the work has been observations both in Australia and Antarctica over that period, and of continuing innovation. The group is continuing to exploit the observations for measurements of temperature, density and scale heights in the upper atmosphere, and the use of remote GPS-locked receiving sites. The Adelaide all-sky meteor radars have been commercialized, and there are an increasing number of meteor radars in China.

## Acknowledgments

We have relied in part on notes made and conversations with Graham Elford to form part of the background to this work. Graham is the authority and any errors are of course ours.

## References

- Aso T., Tsuda T. and Kato S., (1979). "Meteor radar observations at Kyoto University". *Journal of Atmospheric and Terrestrial Physics*, **41**, 517–525.
- Blake A. (2010). "Physics at Adelaide, the 1950's – A decade of Change". 22 pages.
- Bossert K., Fritts D. C., Pautet P. D., Williams B. P., Taylor M. J., Kaifler B., Dörnbrack A., Reid I. M., Murphy D. J., Spargo A. J. and MacKinnon A. D. (2015). "Momentum flux estimates accompanying multiscale gravity waves over Mount Cook, New Zealand, on 13 July 2014 during the DEEPWAVE campaign". *Journal of Geophysical Research: Atmospheres*, **120**, 9323–9337.
- Briggs B. H., Elford W. G., Felgate D. G., Golley M. G., Rossiter D. E. and Smith J. W. (1969). "Buckland Park aerial array". *Nature*, **223**, 1321–1325.
- Brown N. (1976). "Radio echoes from meteor trains at a radio frequency of 1.98 MHz". *Journal of Atmospheric and Terrestrial Physics*, **38**, 83–87.
- Crompton R. W. (2007). "Huxley, Sir Leonard George Holden (1902–1988)". *Australian Dictionary of Biography*, National Centre of Biography, Australian National University.
- Cervera M. A. and Reid I. M. (1995). "Comparison of simultaneous wind measurements using colocated VHF meteor radar and MF spaced antenna radar systems". *Radio Science*, **30**, 1245–1261.
- Cervera M. A. and I. M. Reid (2000). "Comparison of atmospheric parameters derived from meteor observations with CIRA". *Radio Science*, **35**, 833–843.
- Elford W. G. and Robertson D. S. (1953). "Measurements of winds in the upper atmosphere by means of drifting meteor trails II". *Journal of Atmospheric and Terrestrial Physics*, **4**, 271–284.

- Elford W. G. (2004). "Radar observations of meteor trails, and their interpretation using Fresnel holography: a new tool in meteor science". *Atmospheric Chemistry and Physics*, **4**, 911–921.
- Holdsworth D., Elford W., Vincent R., Reid I., Murphy D. and Singer W. (2007). "All-sky interferometric meteor radar meteoroid speed estimation using the Fresnel transform". *Annales Geophysicae*, **25**, 385–398.
- Holdsworth D. A., Reid I. M. and Cervera M. A. (2004). "Buckland Park all-sky interferometric meteor radar". *Radio science*, **39** (5), 12 pages.
- Holdsworth D. A., Morris R. J., Murphy D. J., Reid I. M., Burns G. B. and French W. J. R. (2006). "Antarctic mesospheric temperature estimation using the Davis mesosphere-stratosphere-troposphere radar". *Journal of Geophysical Research: Atmospheres*, **111**(D5), DOI 10.1029/2005JD006589.
- Lee C. S., Younger J. P., Reid I. M., Kim Y. H. and Kim J. H. (2013). "The effect of recombination and attachment on meteor radar diffusion coefficient profiles". *Journal of Geophysical Research: Atmospheres*, **118**(7), 3037–3043.
- Li G., Ning B., Hu L., Chu Y. H., Reid I. M. and Dolman B. K. (2012). "A comparison of lower thermospheric winds derived from range spread and specular meteor trail echoes". *Journal of Geophysical Research: Space Physics*, **117**(A3), DOI 10.1029/2011JA016847.
- Manning L. A., Villard Jr O. G. and Peterson A. M. (1950). "Meteoric echo study of upper atmosphere winds". *Proceedings of the IRE*, **38**, 877–883.
- Nilsson C. S. (1964). "A Southern Hemisphere radio survey of meteor streams". *Australian Journal of Physics*, **17**, 205–256.
- Olsson-Steel D. and Elford W. G. (1987). "The height distribution of radio meteors: observations at 2 MHz". *Journal of Atmospheric and Terrestrial Physics*, **49**, 243–258.
- Reid I. M. (2015). "MF and HF radar techniques for investigating the dynamics and structure of the 50 to 110 km height region: a review". *Progress in Earth and Planetary Science*, **2**, 1–34.
- Roper R. G. (1984). "MWR, Meteor Wind Radars". In International Council of Scientific Unions Middle Atmosphere Handbook, **13**, 124–134 (SEE N85-17452 08-46).
- Tsutsumi M., Tsuda T., Nakamura T. and Fukao S. (1994). "Temperature fluctuations near the mesopause inferred from meteor observations with the middle and upper atmosphere radar". *Radio Science*, **29**, 599–610.
- Tsutsumi M., Holdsworth D., Nakamura T. and Reid I. (1999). "Meteor observations with an MF radar". *Earth Planets Space*, **51**, 691–699.
- Valentic T. A., Avery J. P., Avery S. K., Cervera M. A., Elford W. G., Vincent R. A. and Reid I. M. (1996). "A comparison of meteor radar systems at Buckland Park". *Radio Science*, **31**, 1313–1329.
- Weiss A. A. (1957). "The incidence of meteor particles upon the earth". *Australian Journal of Physics*, **10**, 77–102.
- Younger J. P., Reid I. M., Vincent R. A., Holdsworth D. A. and Murphy D. J. (2009). "A southern hemisphere survey of meteor shower radiants and associated stream orbits using single station radar observations". *Monthly Notices of the Royal Astronomical Society*, **398**, 350–356.
- Younger J. P., Reid I. M., Vincent R. A. and Murphy D. J. (2012). "Meteor shower velocity estimates from single-station meteor radar: accuracy and precision". *Monthly Notices of the Royal Astronomical Society*, **425**, 1473–1478.
- Younger J. P., Lee C. S., Reid I. M., Vincent R. A., Kim Y. H. and Murphy D. J. (2014). "The effects of deionization processes on meteor radar diffusion coefficients below 90 km". *Journal of Geophysical Research: Atmospheres*, **119**, 10027–10043. Doi:10.1002/2014JD021787.
- Younger J. P., Reid I. M., Vincent R. A. and Murphy D. J. (2015a). "A method for estimating the height of a mesospheric density level using meteor radar". *Geophysical Research Letters*, **42**, 6106–6111.
- Younger J. P., Reid I. M., Li G., Ning B. and Hu L. (2015b). "Observations of the new Camelopardalids meteor shower using a 38.9 MHz radar at Mohe, China". *Icarus*, **253**, 25–30.
- Younger J. P., Reid I. M. and Murphy D. J. (2016). "Radar Observations of the Volantids Meteor Shower". In Roggemans A. and Roggemans P., editors, *Proceedings of the International Meteor Conference*, Egmond, the Netherlands, 2-5 June 2016. Pages 352–357.

# Minor meteor shower activity

Jürgen Rendtel

Leibniz-Institut für Astrophysik Potsdam, An der Sternwarte 16, 14482 Potsdam, Germany

International Meteor Organization, Eschenweg 16, 14476 Potsdam, Germany

jrendtel@web.de

Video meteor observations provide us with data to analyze structures in minor meteor showers or weak features in flux profiles. Samples obtained independently by other techniques allow to calibrate the data sets and to improve the confidence of results as demonstrated with a few results. Both, the confirmation of events predicted by model calculation and the input of observational data to improve the modelling results may help to better understand meteoroid stream evolution processes. Furthermore, calibrated data series can be used for studies of the long-term evolution of meteor shower activity.

## 1 Introduction

Over the recent years, a substantial number of minor meteor showers have been detected using video meteor data. Most of the new entries to the IAU meteor shower database have been found from orbital data obtained by multiple station observations. The data also allow deriving physical parameters such as the flux or particle size distribution for weak sources. In this paper we discuss optical observations. Radio techniques can contribute to several of the raised points as well.

A large sample is expected to include a sufficient number of meteors from weak sources and thus allows us to deal with details of low activity showers. Nevertheless, at some point the question of the reliability of short-term or weak features in ZHR or flux profiles arises. In such cases it is useful to have an independent data sample at hand.

Over the previous decades, a huge amount of data has been collected by other techniques, mainly visual observations. In some cases, additional activity information can be retrieved from publications which give sufficient details back over decades. This allows investigating long-term evolution of meteor shower activity, particularly for major and well established showers such as the Geminids (Rendtel, 2004) or the Orionids (Rendtel, 2008). It has also been shown that in case of a large continuous sample, minor features in rate profiles can be resolved, for example a short pre-maximum peak of the Orionids in 1993 (Rendtel and Betlem, 1993).

Currently, observational data obtained with different methods is available for the activity periods of many meteor showers. By combining these data it is possible to detect and confirm weak features and to be more confident with the results. Furthermore, such dual samples allow calibrating data sets obtained by different methods. This way it is possible to later combine old visual and recent video data to extend the covered period for long-term studies.

## 2 Some results

In order to check the possibilities for detection of weak features in minor showers, we may first look at details in major shower activity profiles which are usually well covered by observations obtained with different techniques. In a next step, we can then analyze data of minor showers in the same way.

The Quadrantid (010 QUA) maximum 2016 was expected around January 4, 8<sup>h</sup> UT. A possible rate enhancement between 22<sup>h</sup> UT and 2<sup>h</sup> UT (corresponding to  $\lambda_{\odot}$  282.74° and 282.91°) was suggested from calculations of Vaubaillon given in the IMO Meteor Shower Calendar for 2016. Both, the video and visual data show a slight enhancement at  $\lambda_{\odot} = 282.88^{\circ}$  (Figure 1). The coincidence in position and level as well as the slightly later occurring dip at 282.94° provide confidence that the features are real.

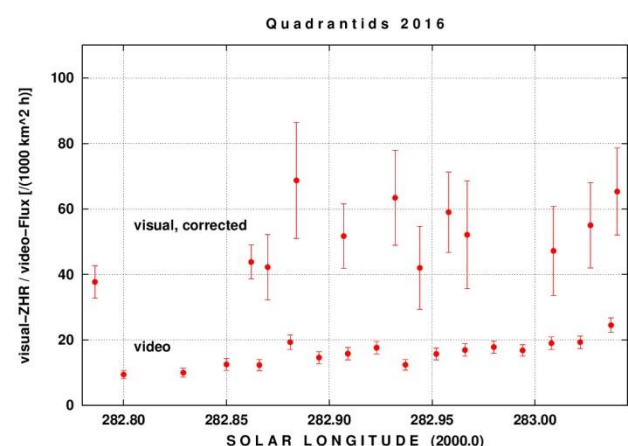


Figure 1 – Detail from the ascending branch of the 2016 Quadrantids observed visually (ZHR) and by video (flux). Two minor features can be found in both data samples: a minor peak at  $\lambda_{\odot} = 282.88^{\circ}$  and an also very minor dip at  $\lambda_{\odot} = 282.94^{\circ}$ . Each data set alone would not provide confidence that this may be a real structure in the stream.

A similar short peak was found in the Perseid (007 PER) ZHR and flux profiles of 2015 obtained by visual and video observers (see Figure 8 in Molau et al., 2015a). As

the peak occurs just in one data bin, a single data set would have left a large uncertainty about the reliability. Detecting the short peak in coinciding bins of independent samples obtained by different techniques increases the confidence significantly.

In the case of most minor showers the amount of data is much smaller than for near-maximum periods. So it may happen that different samples provide us with no conclusive information about the activity profiles. The information about a possible activity of the kappa-Cepheids (751 KCE) on 2015 September 21 was scarce (Segon et al., 2015) and the activity derived from a very small visual meteor sample (Rendtel, 2015) is not confirmed by video data (Molau et al., 2016).

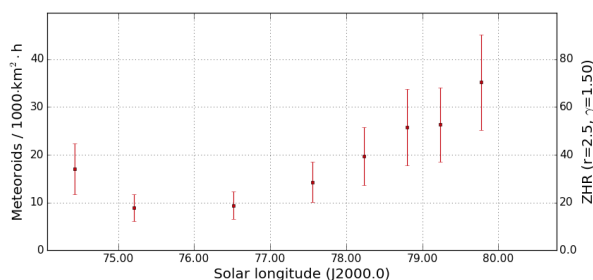


Figure 2 – Flux of the 171 ARI calculated from video data of the IMO VMN from 2011 to 2015 using the tool provided by meteorflux.io on the net. (Parameters: minimum sample 10 shower meteors per bin, minimum radiant elevation 5°.) The activity is well detectable, but no profile with a maximum occurs.

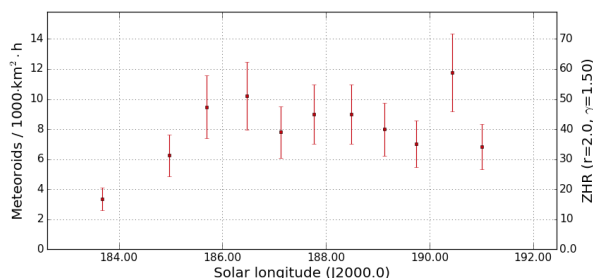


Figure 3 – Flux of the 221 DSX calculated from video data of the IMO VMN from 2011 to 2015. The profile shows slightly higher flux values around the middle of the period, but no clear maximum. (Parameters: minimum sample 20 shower meteors per bin, minimum radiant elevation 5°.)

Extending the observing period into the twilight, some attempts are made to collect data of the Daytime Arietids (171 ARI) in early June and the Daytime Sextantids (221 DSX) around end of September. Certainly, radio and radar data would be best to establish flux profiles, these are not yet available. Both showers can easily be found in video data, but do not allow deriving a reliable flux profile yet. The observing conditions are close to the limits particularly for the Arietids (Figure 2) due to the twilight at northern locations but are slightly better for the Sextantids near the autumnal equinox (Figure 3). Currently we find that the

fluxes increase only after the listed maximum positions at 77° and 184°, respectively. In both cases the corrections due to rapidly changing radiant elevation and observing conditions need to be improved – likely a case for combining radio and video data.

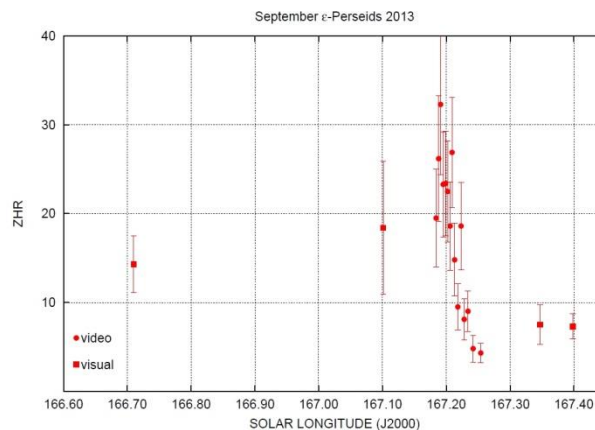


Figure 4 – The combination of visual and video observations around the peak of the September epsilon-Perseids in 2013 allows to complete the profile and to calibrate the values obtained by the different methods.

The situation was much better in the case of the September epsilon-Perseids 2013. Here the data of the visual and video observations can be perfectly used to complete the information about the ZHR/flux and the population index (Figure 4, from Rendtel et al., 2014).

Extending the length of data series is not only possible for major or medium level showers as mentioned in the Introduction. It can also be applied to minor showers, provided that the radiant position used for the shower association remained consistent over the period under study. This, for example, is the case for the northern radiant of the kappa-Cygnids. Its position is far away from other active radiants at the same time and their velocity is obviously low. This allowed searching for suspected periodicities in rate enhancements back over 41 years. A wavelet analysis was applied to the data set to check whether there are signs of periodicities within the 41 years covered by the data (Figure 5). The available data includes no hints at periods lower than 20 years in the kappa-Cygnid appearance (for details refer to Rendtel and Arlt, 2016).

### 3 Conclusions

Improved technical equipment and collaboration allow us to detect and analyze minor showers and weak features in the flux profiles.

Almost complete coverage of the observable time with video meteor networks seems to make visual observation obsolete. But there are several good reasons to continue using various techniques.

Independent samples of one target are useful to calibrate the data and to obtain better information about the reliability of observed features and quantities in flux

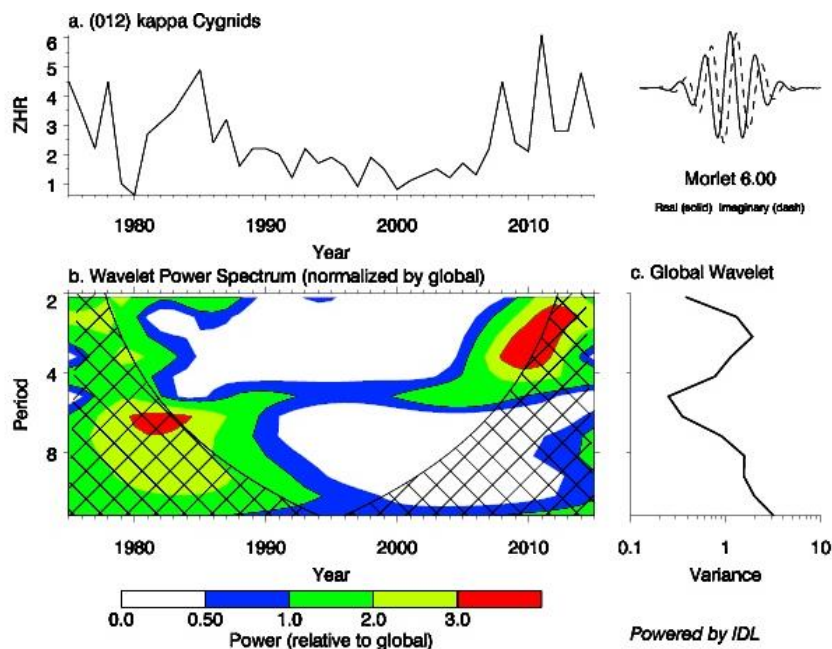


Figure 5 – Wavelet analysis of the kappa Cygnid ZHR data from 41 years. Panel (a) shows the ZHR, (b) the wavelet power spectrum. The cross-hatched region is the cone of influence and (c) gives the global wavelet power spectrum. Details are given in (Rendtel and Arlt, 2016).

profiles. Since visual observers often concentrate to major shower activity periods, it is worth to alert them in periods with possible meteors from usually weak or unknown sources. This is one purpose of the annual IMO Meteor Shower Calendar.

Activity of meteor showers may vary considerably from one return to the next. Therefore, in many cases an average activity profile of a given shower does not provide appropriate information about the meteoroid stream. Well calibrated video and visual data may be used to establish long time series. So we may for example look for a pattern in the occurrence of the high northern showers in September-October (Rendtel and Molau, 2010). The currently very weak delta-Aurigids (224 DAU) might have been more prominent in the past since Drummond (1982) referred to photographic data.

Another important field is the interaction between observers and authors of model calculations which should optimally work in both directions: observers check the periods with predicted possible rate anomalies, but provide information which may help to improve the models, eventually understanding the meteoroid release processes from their parent better.

## References

Drummond J. (1982). “A note on the Delta Aurigid meteor stream”. *Icarus*, **51**, 655–659.

Molau S., Crivello S., Goncalves R., Saraiva C., Stomeo E. and Kac J. (2015). “Results of the IMO Video Meteor Network - August 2015”. *WGN, Journal of the IMO*, **43**, 188–194.

Molau S., Crivello S., Goncalves R., Saraiva C., Stomeo E. and Kac J. (2016). “Results of the IMO

Video Meteor Network - September 2015”. *WGN, Journal of the IMO*, **44**, 21–26.

Rendtel J. (2004). “Evolution of the Geminids observed over 60 years”. *Earth, Moon, and Planets*, **95**, 27–32.

Rendtel J. (2008). “The Orionid meteor shower observed over 70 years”. *Earth, Moon, and Planets*, **102**, 103–110.

Rendtel J. (2015). “Minor kappa-Cepheid (751 KCE) activity on 2015 September 21”. *WGN, Journal of the IMO*, **43**, 177–178.

Rendtel J. and Arlt R. (2016). “Kappa Cygnid rate variations over 41 years”. *WGN, Journal of the IMO*, **44**, 62–66.

Rendtel J. and Betlem H. (1993). “Orionid meteor activity on October 18, 1993”. *WGN, Journal of the IMO*, **21**, 264–268.

Rendtel J., Lyytinen E., Molau S. and Barentsen G. (2014). “Peculiar activity of the September epsilon-Perseids on 2013 September 9”. *WGN, Journal of the IMO*, **42**, 40–47.

Rendtel J. and Molau S. (2010). “Meteor activity from the Perseus-Auriga region in September and October”. *WGN, Journal of the IMO*, **38**, 161–166.

Šegon D., Andreić Ž., Korlević K. and Vida D. (2015). “Croatian meteor network: ongoing work 2014–2015”. In Rault J.-L. and Roggemans P., editors, *Proceedings of the International Meteor Conference*, Mistelbach, Austria, 27–30 August 2015. IMO, pages 51–57.

# The radio meteor signal path from transmitter to spectrogram: an overview

Tom Roelandts

Impulse Response, Beerse, Belgium

tom@impulseresponse.eu

In this paper, we present an overview of the radio meteor signal path, from the sinusoidal carrier wave that is initially transmitted, to the spectrogram that is typically used as the final result in the receiving chain. We describe the amplitude modulation and Doppler shift that is caused by the meteor, the combination of the reflected with the directly received signal at the antenna, the down conversion in the receiver, the sampling, and the down sampling in software. A simulation of the complete process results in detailed plots at each of these steps.

## 1 Introduction

The results of the *Belgian Radio Meteor Stations (BRAMS)* network (Calders and Lamy, 2011), (Ranvier et al., 2015) are often analyzed through *spectrograms*. In this paper, we provide an overview of the complete radio meteor signal path that leads to these spectrograms at the very end of the receiving chain.

Starting from the knowledge that the transmitted signal is a simple sinusoidal carrier wave, the conceptual picture is clear. A BRAMS spectrogram represents the reflection of that carrier off a number of meteor trails, together with a relatively low amplitude directly received signal (and plane echoes, which we ignore in this paper). However, in practice, several things happen to the signal in addition to it being reflected off the meteor trail.

In this paper, we describe all the major effects that the signal encounters before it is finally plotted as a spectrogram. Additionally, we have implemented a simulation of the complete signal path, which allows showing detailed plots at each step. Both the description and the simulation are meant to demonstrate the major effects that happen, without necessarily capturing every last detail of each process.

## 2 Signal path

### Overview

*Figure 1* shows an overview of the signal path. The initial carrier is modified by the interaction with the meteor trail, by being combined with the directly received signal at the antenna, by being down converted in the receiver, by being sampled, and by being down sampled in software. In the remainder of this paper, each of these steps is described in more detail.

The different effects are illustrated by plots that were generated through a simulation of the complete signal path. This simulation was performed at a radio frequency (RF) of 100 kHz. This is equivalent to using the true RF, since the down conversion step is independent of that RF.

### Transmitter

The transmitter produces a simple sinusoidal carrier wave at a frequency of  $f_T = 49970000$  Hz. Hence, the carrier wave can be defined as

$$\sin(2\pi f_T t),$$

where  $t$  is the time in seconds.

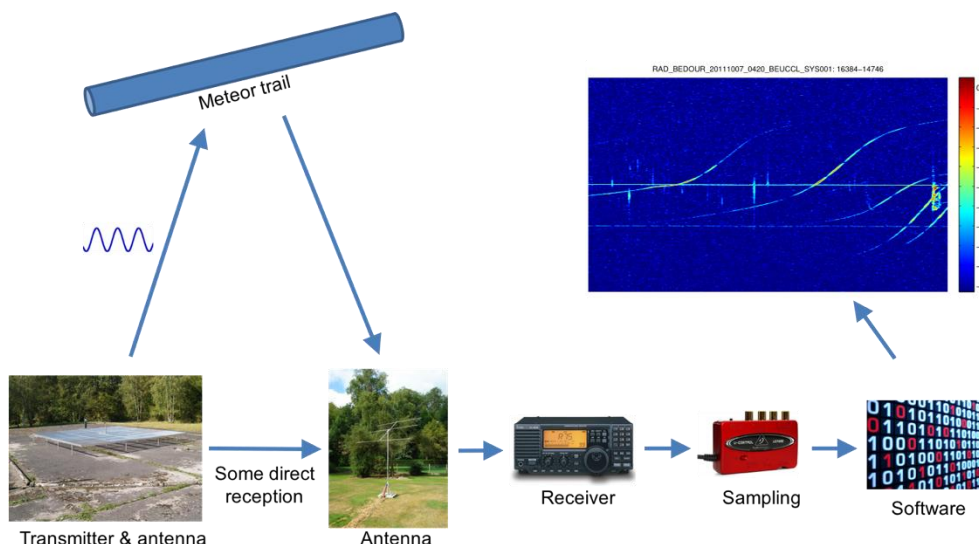


Figure 1 – Overview of the signal path.

### Meteor trail

If a meteor trail with a geometrically favorable orientation is present, it will reflect the carrier wave towards the antenna. The effect of this reflection is a modulation of the *amplitude* of the carrier. In the simulation, a simple meteor amplitude profile was used, consisting of a fast linear rise followed by an exponential decay (*Figure 2*). We write this amplitude profile as  $A(t)$ . The fast linear rise models the quick formation of the trail, while the exponential decay models its diffusion.

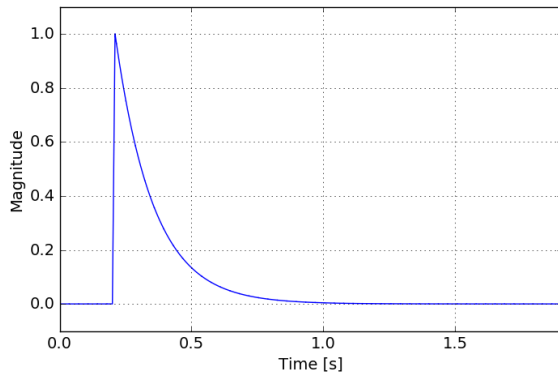


Figure 2 – Meteor amplitude profile.

In addition to the amplitude modulation, the reflection off the trail also causes a Doppler shift of the carrier frequency, if the trail is moving due to high altitude winds. Such a Doppler shift is observed very often in practice. If the reflection off the trail causes a Doppler shift of  $f_D$  Hz, then the received frequency will be  $f_T + f_D$  Hz.

Combining the amplitude profile of the meteor with the Doppler shift, the reflected wave that is received by the antenna is

$$A(t) \sin(2\pi(f_T + f_D)t).$$

This amplitude-modulated carrier is illustrated in *Figure 3*. The graph is solid blue because of the very high frequency of the carrier.

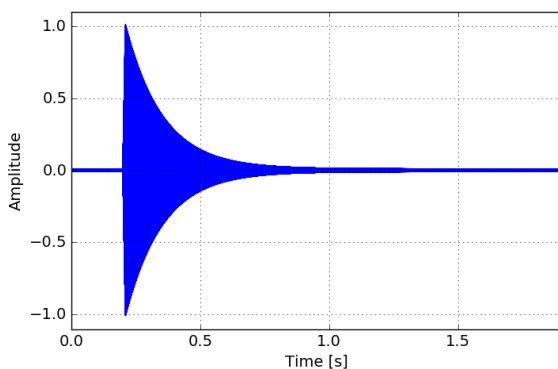


Figure 3 – Amplitude-modulated carrier after reflection off the meteor trail.

### Receiver Antenna

At most of the BRAMS stations, the antenna picks up a low-amplitude signal directly from the transmitter. When a meteor appears, its signal is combined with it. The directly received signal has a much lower amplitude than

many of the meteor reflections. However, this does not imply that it can be ignored. In the simulation, we have set the amplitude of the directly received signal to 1% of the maximum level of the simulated meteor.

Due to the Doppler shift that the reflected signal contains, the two signals that are combined at the antenna have a different frequency. At a direct reception level of  $D$ , the combined signal can be written as

$$D \sin(2\pi f_T t) + A(t) \sin(2\pi(f_T + f_D)t).$$

Summing two sinusoids with a slightly different frequency produces *beats*, which are variations in the amplitude of the signal due to alternating constructive and destructive interference. In the simulation, we have used a Doppler rate of 25 Hz. *Figure 4* shows how the resulting beats are superimposed on the received amplitude profile as small “bumps”. The frequency of 25 Hz can be recognized in the period of the amplitude variations.

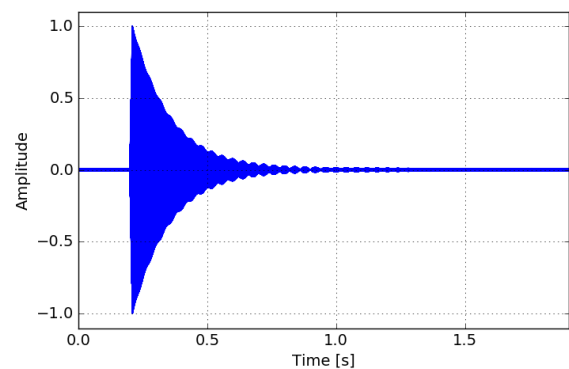


Figure 4 – The combined reflected and directly received signal at the antenna.

The corresponding power profile, which is simply the signal of *Figure 4* squared, is shown in *Figure 5*.

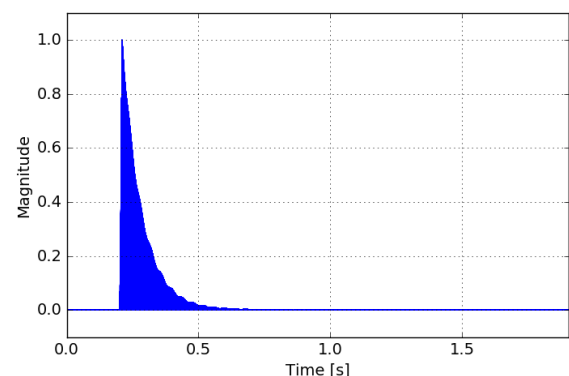


Figure 5 – Power profile of the received signal.

Although the Doppler shift of the reflection might be deduced from the period of these beats, it can easily be determined more directly from a spectrum or a spectrogram. Hence, it might be better to remove the directly received signal from the data, and avoid these beats altogether, since they might be obscuring the properties of the reflection itself. Removing the directly

received signal is relatively easy, since the received carrier is quite constant, both in frequency and in power.

### Receiver

The signal of *Figure 4* is the input to the receiver. This implies that the received spectrum can now be computed. *Figure 6* shows a part of the complete spectrum, centered at the original carrier frequency of, in the simulation, 100 kHz. There is a small peak at 100 kHz and the larger peak of the meteor reflection at an offset of 25 Hz (the Doppler offset).

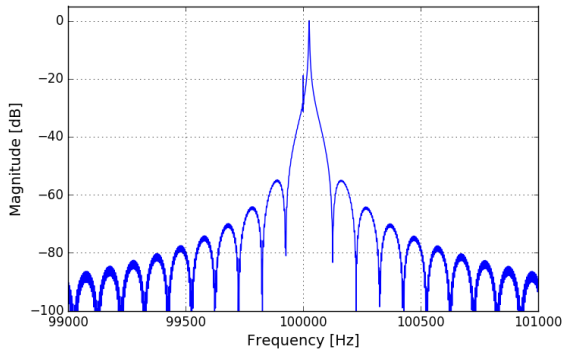


*Figure 6* – The spectrum that is received at the receiver.

At the receiver, this signal is *mixed*, i.e., *multiplied*, with a local oscillator (LO) at a small frequency offset of 1 kHz. This is done simply by tuning the receiver to a frequency of 49969000 Hz instead of the exact value of  $f_T$ . Note that this multiplication of signals is completely different from what happens at the antenna, where two signals are *added*. Moreover, the offset of the LO is on purpose. The effect of mixing the received signal with an LO that is offset is that the frequency contents of the meteor reflection is *down converted*, i.e., its frequencies are *shifted* from its original RF frequencies around  $f_T + f_D$  to a range of frequencies around 1 kHz.

When sinusoids at two frequencies  $f_1$  and  $f_2$  are multiplied, we have that

$$\sin(f_1) \sin(f_2) = \cos(f_1 - f_2) - \cos(f_1 + f_2),$$

from the well-known *product-to-sum* trigonometric identities. This means that, for an ideal mixer, the result of mixing is a first frequency component at the difference  $f_1 - f_2$  and a second frequency component at the sum  $f_1 + f_2$  of the original frequencies.

With the LO frequency  $f_{LO} = f_T - 1$  kHz, the two components of the directly received signal will be at  $f_T - f_{LO} = 1$  kHz and at  $f_T + f_{LO} = 2f_T - 1$  kHz. The two components of the meteor reflection, with its additional Doppler shift, will be at  $f_T + f_D - f_{LO} = f_D + 1$  kHz and at  $f_T + f_D + f_{LO} = 2f_T + f_D - 1$  kHz. The complete spectrum is shown in *Figure 7*. In that figure, there is clearly a first peak at 1 kHz and a second one just below 200 kHz (again, the simulation uses 100 kHz instead of  $f_T$ ). To illustrate that these peaks are indeed two copies of the original spectrum, compare the detailed

version of the spectrum that shows the component at 1 kHz (*Figure 8*) with *Figure 6*.

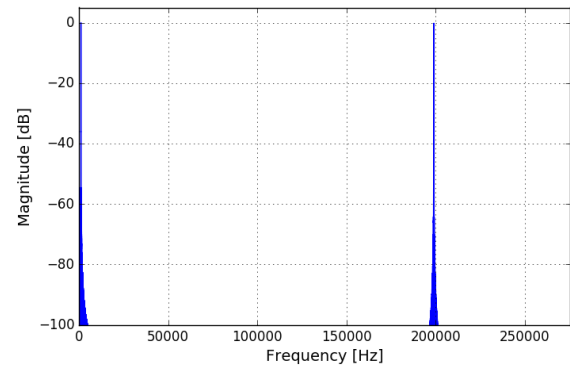


*Figure 7* – The full spectrum of the input signal mixed with the local oscillator.

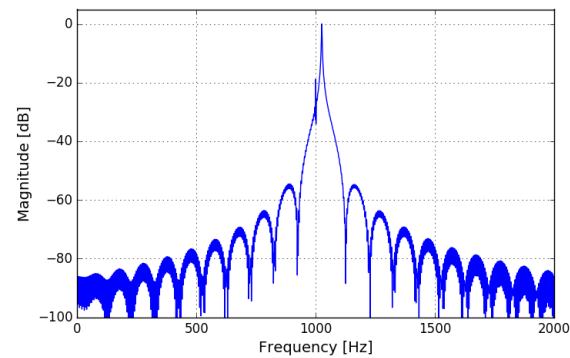


*Figure 8* – The spectrum of the input signal mixed with the local oscillator, centered at 1 kHz.

Because of this frequency shift, the signal can be sampled at much lower sampling rates than would be necessary to sample directly at the RF.

### Sampling

The Behringer UCA222 sampling device is programmed to sample the down converted signal at 22050 Hz. As is to be expected, the CODEC chip in the sampling device correctly low-pass filters the incoming signal, i.e., it removes frequencies above 11025 Hz, which is half the sampling rate (Texas Instruments, 2008).

The sampling process is the only place where the simulation is not exactly like the real setup. In the simulation, the complete signal path is digital, so there is no actual sampling step at this point. However, that step is replaced with a *down sampling* step that takes the sampling rate of the simulation, which is 551200 Hz, and reduces it to 5512 Hz. A proper low-pass filter with a cutoff frequency of 2756 Hz is included. The spectrum of the down sampled signal is shown in *Figure 9*.

### Software

The two operations in the software that are relevant for the signal path are a further down sampling from 22050 Hz to 5512 Hz and the generation of the spectrogram itself. For the down sampling, an additional low-pass filter is included, to remove the frequency contents between 11025 Hz to 2756 Hz. This makes the

output of the simulation equivalent to the output of the software.

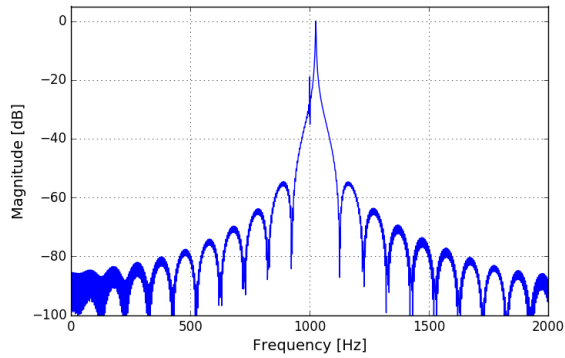


Figure 9 – Spectrum of the sampled signal.

**Comparison with the original spectrum**

The spectrum at the final sampling rate of 5512 Hz (Figure 9) is very close to the originally received spectrum of Figure 8. Moreover, it is also quite close to the *bandpass* spectrum of Figure 6, confirming that down converting and down sampling the received signal is a valid methodology.

To further explore this, we can also compare the spectrum of Figure 9 with the spectrum of the original meteor profile. A *two-sided* spectrum, i.e., with 0 Hz in the middle, corresponding to the profile of Figure 2, is shown in Figure 10. Typically, a spectrum such as this would be shown *one-sided*, i.e., with a frequency range between 0 Hz and some appropriate maximum, since it is symmetrical. However, for easier comparison with the spectrum of Figure 9, we have chosen to plot it two-sided here.

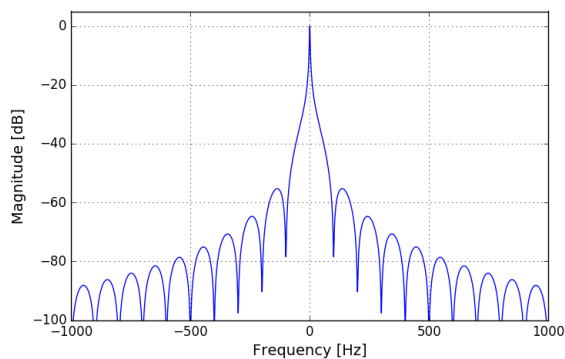


Figure 10 – Spectrum of meteor profile.

The main differences between Figure 9 and Figure 10 are the Doppler shift and the small secondary peak caused by the directly received carrier. However, apart from these small changes, both spectra are quite similar.

**Spectrogram**

Although spectra are a very insightful way to compare the signal at the different stages of processing, they do not provide insight in the time component of the received signal. For that, a spectrogram is generated (Figure 11).

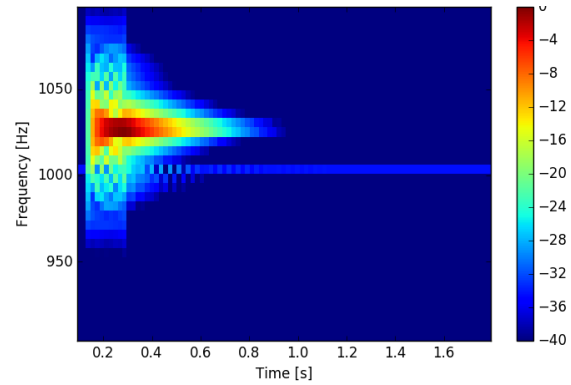


Figure 11 – Spectrogram of the sampled signal.

For comparison with the spectrograms as they are usually presented for BRAMS, Figure 12 shows the same spectrogram as Figure 11, but then for the usual time period of 5 minutes.

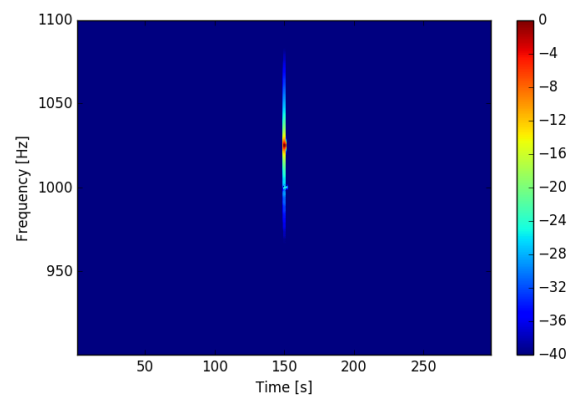


Figure 12 – Spectrogram of the sampled signal, rescaled to a time axis of 5 minutes.

The reflection in Figure 12 is close to a typical short meteor in an actual BRAMS spectrogram.

**3 Conclusion**

We have provided an overview of the complete signal path of a radio meteor, from the transmitter to the spectrogram as it is typically generated by a BRAMS station.

**References**

Calders S. and Lamy H. (2011). “Brams : status of the network and preliminary results”. In Gyssens M. and Roggemans P., editors, *Proceedings International Meteor Conference*, 15-18 September 2011, Sibiu, Romania. IMO, pages 73–76.

Ranvier S., Lamy H., Anciaux M., Calderys S., Gamby E. and De Keyser J. (2015). “Instrumentation of the Belgian Radio Meteor Stations (BRAMS)”. *International Conference on Electromagnetics in Advanced Applications (ICEAA)*, Turin, Italy, 7-11 September 2015, pages 1345–1348.

Texas Instruments (2008). “PCM2902 Stereo Audio CODEC w/USB Interface” datasheet.

# Status of the CAMS-BeNeLux network

Paul Roggemans<sup>1</sup>, Carl Johannink<sup>2</sup> and Martin Breukers<sup>2</sup>

<sup>1</sup>MeteorNews.org, Pijnboomstraat 25, 2800 Mechelen, Belgium

paul.roggemans@gmail.com

<sup>2</sup>Dutch Meteor Society & KNVWS Werkgroep meteoren, the Netherlands

c.johannink@t-online.de, breukers@wxns.nl

An overview is being given of the further expansion of the CAMS@BeNeLux network since previous IMC, July 2015 until May 2016. The weather proved less favorable than in the year before, but thanks to a number of new cameras and extra observing stations, the overall performance of the network remained at the same level in spite of the often poor weather circumstances.

This paper compares the Kappa-Cygnids performance of 2015 with the analyses made for the 2014 data, following the same methodology. In 2015 the Kappa Cygnids were remarkable absent which confirms the periodic nature of the abundant Kappa-Cygnids display in 2014.

The CAMS@BeNeLux network was the first to draw attention to enhanced activity of the newly discovered Chi Cygnids meteor shower with 5 accurate orbits in the night of 14–15 September 2015. A search through a selection of all orbits of September 2015 yield 71 possible Chi Cygnid orbits of which 18 were selected to calculate the average orbital elements.

## 1 Introduction

CAMS or *Cameras for All Sky Meteor Surveillance*<sup>1</sup> is a project financed by NASA, coordinated by Peter Jenniskens. The purpose of the project is to validate the IAU Working List of Meteor Showers<sup>2</sup>. CAMS uses small field of view optics covering the complete sky as a mosaic, and this since end 2010 from three different observing sites in California, US. The concept has been applied by amateur astronomers since 2012 in the Netherlands and since 2014 in Florida and at the Mid Atlantic coast. A complete professional system has been installed at two stations in New Zealand since 2014 and another one is being installed in the United Arab Emirates in 2016. The build-up of the CAMS network has been described in detail in different publications (Bettonvil et al., 2014; Gural 2011; Jenniskens et al., 2011; Roggemans et al., 2014, 2015).

## 2 Evolution of the CAMS@BeNeLux

At the previous IMC end of August 2015 the status of the CAMS@BeNeLux network was described until June 2015. Between July 2015 and April 2016, 8 new cameras became operational, 4 of these at the new CAMS stations Gent, Uccle and Dourbes in Belgium (*Figure 1*). The station Lieshout (NL) has suspended its participation due to lack of time by the operator, Paul Lindsay. The extra cameras and stations permitted to increase the density of the network and to expand the collection area in the atmosphere with two new regions over the West of Belgium and the North of France (*Figure 2*).

Regardless the number of available cameras, the rather unfavorable climate offers no more than about a couple of clear nights per month throughout the year in the North West of Europe. Most of the nights during which our

network collects orbits are just partial clear nights with a very variable cloud cover at each CAMS-station. Overall we can say that the past 10 months were monitored under less favorable weather circumstances than previous year, with exceptions for the period from end July, August, September October 2015 and first half of May 2016 which had better weather circumstances compared to these months in a year before.



*Figure 1* – The positions of the 15 cameras at 7 stations in Belgium, the 34 cameras at 9 stations in the Netherlands and the 7 cameras at one station in Germany.

<sup>1</sup> <http://cams.seti.org/>

<sup>2</sup> <http://www.astro.amu.edu.pl/~jopek/MDC2007/index.php>

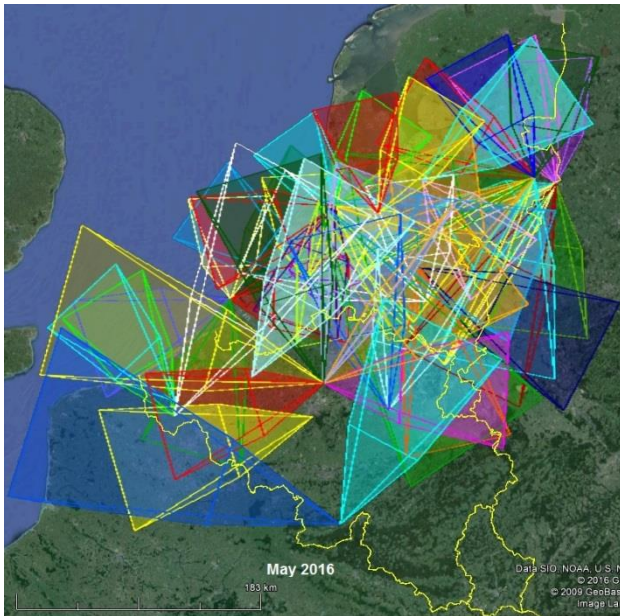


Figure 2 – The coverage of the atmosphere of all operational cameras, intersected at 90 km elevation.

The rather poor weather could be compensated to a large extent by the installation of Auto-CAMS at several stations. Auto-CAMS has been adapted and tested for Europe by Steve Rau and assures that the cameras run each night as long as the Sun is 8° below the horizon. This way no unexpected periods with clear skies are lost during the nights while manual CAMS operators may decide not to run their cameras because of a too bad weather forecast. The general poorer weather circumstances of past 10 months explain why the average number of cameras with successfully collected orbits per month (red line in Figure 3) did not increase with the increasing number of active cameras (green line in Figure 3). The number of clear or partial clear nights with orbits improved slightly (blue bars in Figure 3).

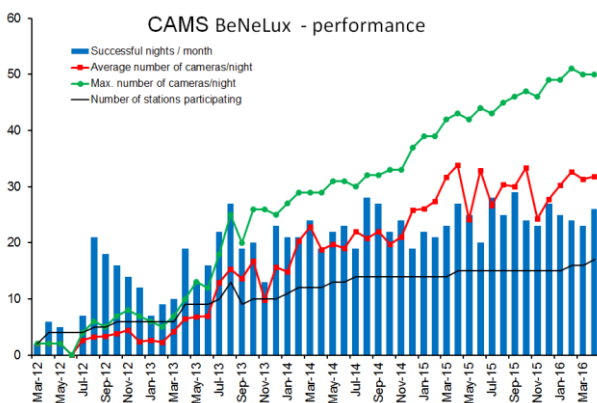


Figure 3 – The performance of the CAMS@BeNeLux network.

Figure 4 shows the monthly yield in orbits while Figure 5 displays the growth of the database of collected orbits. On 25–26 May 2016, the 40000<sup>th</sup> orbit was obtained. August, September and October 2015 added significant numbers of orbits. 4 years after the start of our CAMS network only 4 nights of the calendar year remain without any orbits. Figure 6 shows a significant progress made in past 10 months with as many as 140 nights with 100 or more orbits available per night. Datasets with over 100

orbits per night should allow for shower association searches. Since the CAMS@BeNeLux results are only a subset of the global CAMS dataset of orbits, significant larger numbers of orbits are available for global CAMS shower searches.

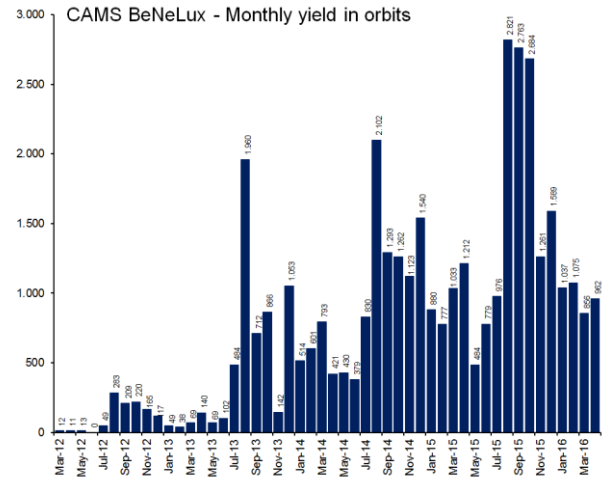


Figure 4 – Monthly distribution of the heliocentric orbits obtained by the CAMS@BeNeLux-network.

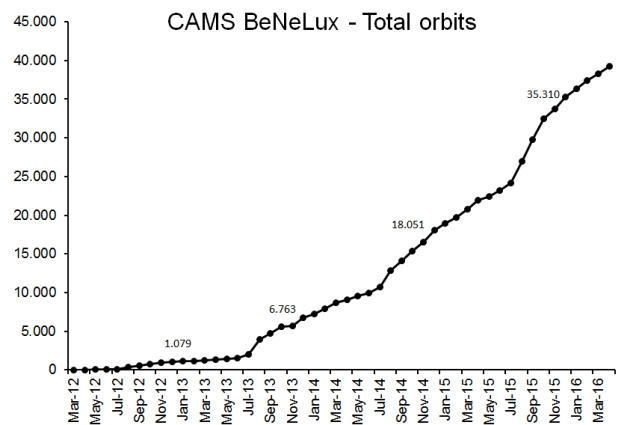


Figure 5 – The evolution of the total number of heliocentric orbits accumulated by the CAMS – BNL network.

TOTAL	2010	2011	2012	2013	2014	2015	2016
January	2	53	493	97	65	130	21
February	68	138	90	92	65	134	60
March	28	45	147	122	89	80	178
April	58	35	7	64	68	128	38
May	14	33	63	34	65	16	34
June	25	29	64	60	60	86	64
July	115	23	92	18	97	111	42
August	350	308	96	311	367	282	156
September	1354	260	140	119	137	29	60
October	337	335	337	348	27	138	62
November	203	197	115	50	34	84	39
December	2	40	146	109	113	129	183

Figure 6 – Total number of orbits per calendar date (~1° in Solar Longitude) accumulated 2012–2016 (until April 2016).

The CAMS@BeNeLux network is operated by a team of motivated amateurs. The success of each station depends a lot on the commitment of the other stations to run their cameras in order to enable simultaneous registrations of meteors at different stations. Running one up to 8 cameras per station during successive nights all year round and calibrating, confirming and reporting the data on a day-by-day bases without any problematic delays, altogether represents a lot of work. The CAMS team is

running with a mixture of new and veteran meteor observers, all very dedicated to assure the continuity and efficiency of the network.

### 3 Highlights July 2015 – May 2016

The rather average weather in July 2015 produced only few 100% clear nights for the network. Weather improved in August and although that 11–12 August was overcast without any orbits, 12–13 August produced as many as 713 orbits in a single night! After a poor last week of August, September was blessed with more than usual clear nights with over 200 orbits per night. The Chi Cygnids displayed enhanced activity on 14–15 September and were first reported by the CAMS network and later confirmed by other networks.

October still counted a fair number of clear nights although most of the Orionid activity period was lost due to cloudy weather. November confirmed its reputation to be rather unfavorable for astronomical observations in the Low Lands of North Western Europe. No winter weather in December but also rather few clear nights and no luck with the best Geminid nights.

2016 started with poor circumstances for the Quadrantids, but overall January 2016 was just a normal month as were February and March with less clear nights than in 2015 when these months were doing better than usual for the winter season. April was again a normal month with a good coverage of the Lyrid activity. The exceptional series of clear nights in the first part of May allowed monitoring the Eta Aquariids, but the second half of May was again rather poor.

### 4 What about the $\kappa$ -Cygnids in 2015?

A selection of 149 orbits was made with a radiant position within the range  $\alpha \approx [220^\circ \text{ to } 310^\circ]$  and  $\delta \approx [+39^\circ \text{ to } +74^\circ]$ , the geocentric velocity  $V_g \approx [12 \text{ to } 34 \text{ km/s}]$ , with as inclination  $i \approx [16^\circ \text{ to } 46^\circ]$  and as argument of perihelion  $\omega \approx [150^\circ - 216^\circ]$  for the period  $\lambda_\odot [115^\circ - 158^\circ]$  (*Figure 7*). These criteria were chosen on bases of the known information available on the  $\kappa$ -Cygnids and related showers. For a single station visual observer each of these meteors, regardless where these would be spotted at the sky, would fulfil the criteria available for visual observers to identify a meteor as a  $\kappa$ -Cygnid.

In 2014 as many as 250 possible Kappa Cygnids were listed, while 2015 produced only 149 such meteors. We applied the same method as for the 2014 Kappa Cygnid analyses. Each orbit was compared to the reference orbits of the Kappa Cygnids (12 KCG) and four meteor showers associated with the Kappa Cygnids: the  $\gamma$ -Draconids (184 GDR), the  $\iota$ -Draconids (703 IOD), the August Draconids (197 AUD) and the August  $\mu$ -Draconids (470 AMD) (*Table 1*). The shower association was done using the D criterion according to Drummond (1981), indicated as  $D'$ . Some of the orbits fulfil the criteria for more than one of the reference showers.

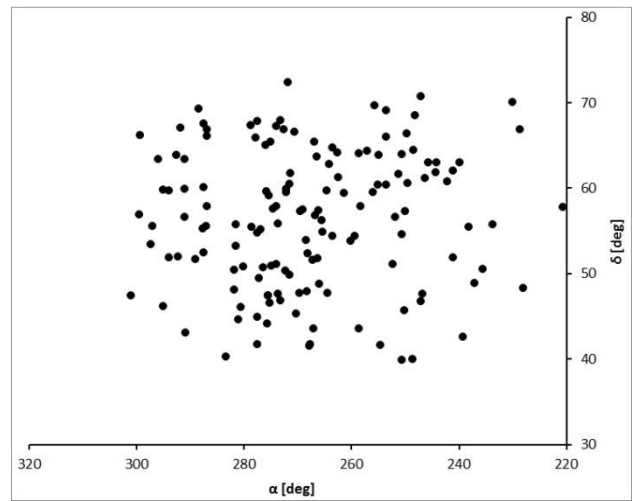


*Figure 7* – Radiant plot of selected ‘possible’  $\kappa$ -Cygnid orbits.

If the same orbit fulfilled the criteria for two or more of the reference orbits, the orbit was associated with the reference orbit which produced the best fit. The procedure was followed for both the results using the criterion according to Drummond and according to Southworth & Hawkins. As threshold we took as upper limit  $D' < 0.105$  for Drummond and  $D_{SH} < 0.25$  for Southworth and Hawkins. For most associations this results in the same association, but not for all. The orbits are all somehow related and question is how to determine the right association?

In *Figure 8a* we reproduce the plot of the 2014 radiants in ecliptic coordinates and in *Figure 8b* we do the same for the 2015 radiants. It is very obvious that the Kappa Cygnids which were very abundant in *Figure 8a* do not appear at all in *Figure 8b*. Only 69 out of the 149 possible Kappa Cygnid meteors qualify for shower association according to the D-criterion of Drummond and only 53 according to Southworth and Hawkins. In 2014, 189 orbits out of the 250 candidates fulfilled the  $D'$  criterion, among as many as 131 orbits confirmed as Kappa Cygnids. In 2015 only 6 orbits were identified as Kappa Cygnids based on  $D'$  (also 6 if we use  $D_{SH}$  as criterion).

For the 2014 analyses we had removed all the radiants that did not associate with any of the reference orbits, for 2015 we included these as orange dots in *Figure 8b*. Only 2 associate with the  $\gamma$ -Draconids (10 in 2014), 20 with the  $\iota$ -Draconids (6 in 2014), 28 with the August Draconids (22 in 2014) and 7 with the August  $\mu$ -Draconids (20 in 2014).

The distinguishing between associations of a single orbit with multiple candidate reference orbits is rather confusing and not at all well determined. Either another methodology is required to distinguish between different related sources, or the relevance of the existence of the various related showers should be questioned. Does it make sense to consider closely related concentrations within a rather dispersed complex? The Kappa Cygnids and its associated showers are probably comparable with the Taurid complex.

Table 1 – Reference orbits obtained by CAMS (Jenniskens et al., 2016a, 2016b, 2016c and 2016d) used to identify the possible Kappa Cygnids with the D criterion of Drummond and the D-criterion according to Southworth and Hawkins.

Shower	N	RA <sub>geo</sub>	DEC <sub>geo</sub>	V <sub>geo</sub>	q	a	e	i	ω	Ω
	Orbits	(°)	(°)	km/sec	AU	AU		(°)	(°)	(°)
184 GDR	40	280.1	50.3	27.5	0.977	16.42	0.967	40.3	202.5	124.7
703 IOD	12	232.3	53.3	17.8	0.990	2.93	0.664	26.1	161.5	157.2
12 KCG	25	277.5	52.8	20.9	0.995	2.95	0.662	32.5	196.9	140.0
197 AUD	17	271.7	58.9	21.1	1.008	2.82	0.644	33.8	188.7	142.6
470 AMD	53	256.4	62.5	21.3	1.009	2.87	0.648	33.8	175.5	149.5

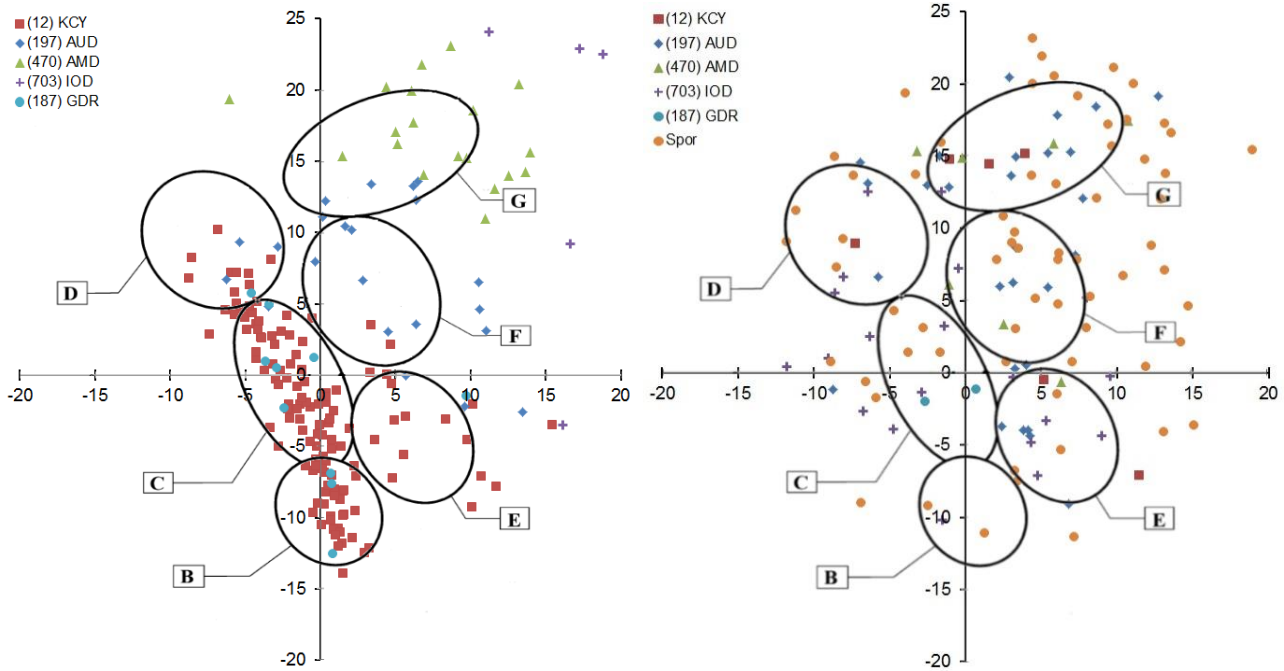


Figure 8a – The radiant plot in ecliptic coordinates according to the D criterion of Drummond ( $D' < 0.105$ ) in 2014. Figure 8b – The radiant plot in ecliptic coordinates according to the D criterion of Drummond ( $D' < 0.105$ ) in 2015. The shapes in both figures refer to the radiant associations as described in a previous paper (Roggemans et al., 2015) in order to compare with an analyses of Masahiro Koseki (2014).

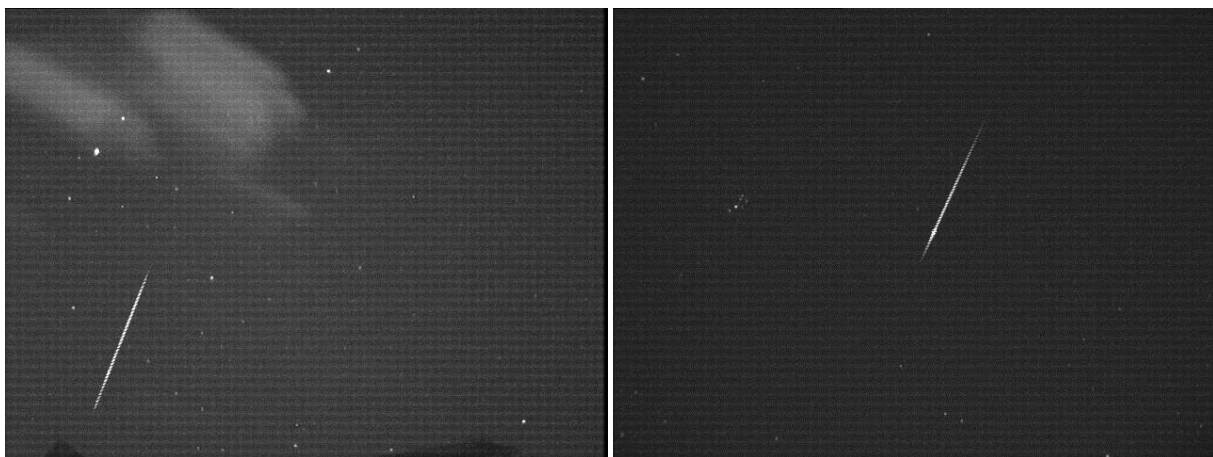


Figure 9a – (left) Chi-Cygnid recorded by Martin Breukers (CAMS 321) at 14 Sep. 2015, 19<sup>h</sup>50<sup>m</sup>08.51<sup>s</sup> UT.

Figure 9b – (left) Chi-Cygnid recorded by Hans Betlem (CAMS 372) at 15 Sep. 2015, 00<sup>h</sup>05<sup>m</sup>31.76<sup>s</sup> UT.

## 5 Discovery of the $\chi$ -Cygnids (757 CCY)

During the night of 14–15 September 2015, visual observers Koen Miskotte and Michel Vandeputte suspected some activity from a radiant region in Cygnus. Martin Breukers could confirm this very quickly from the CAMS-data of this night and also Peter Jenniskens could add a few more orbits obtained by CAMS California. On September 17 Daniel Green issued CBAT 4144 (2015) to announce the ‘new’ meteor shower.

Yasuo Shiba verified the records of the SonotaCo network and found 5 similar orbits recorded between 13 and 21 September 2015. Four more orbits were found in the 2010 dataset of SonotaCo (Shiba, 2015). Jakub Koukal checked the EDMOND database and selected 16 orbits for the period 8–17 September (Koukal et al., 2016). He also could select 49 orbits from the entire EDMOND database with the earliest orbits for the Chi Cygnids found in 2007.

After the initial discovery of the shower, Martin Breukers and Carl Johannink selected 450 orbits from the 2763 orbits collected in September 2015 for further investigation. The D criterion according to Drummond (Drummond, 1981) was applied and 71 orbits collected between 1 and 29 September fulfilled the criterion  $D' < 0.1$ . The nature of this shower with its very low

velocity produces a very large scattered radiant. To eliminate suspected outliers an additional filter was applied with  $\alpha \approx [296^\circ \text{ to } 306^\circ]$ ,  $\delta \approx [+27.6^\circ \text{ to } +37.6^\circ]$  and the geocentric velocity  $V_g \approx [12.5 \text{ to } 17.5 \text{ km/s}]$ . This selection left 21 orbits to fit all the selection criteria during a period from 10 to 28 September. Considering the radiant plot, there is no trace of any radiant drift (*Figure 10*).

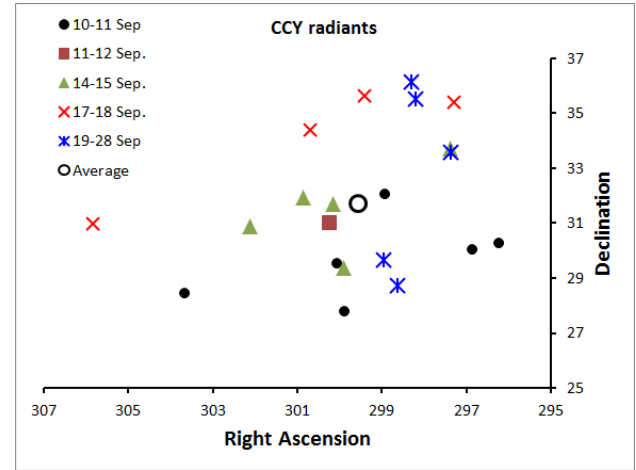


Figure 10 – Radiant plot of the orbits associated with the Chi Cygnids (757 CCY), for different dates: no trace of a radiant drift can be seen in this plot.

Table 2 – The final 21 orbits which fulfil the D criterion of Drummond ( $D'_{EDM}$ ) using the orbit obtained from EDMOND data as reference and the D criterion of Drummond ( $D'_{CAMS}$ ) using the initial orbit obtained by CAMS as reference.

Observed	Beg Time	$\alpha_{geo}$	$\delta_{geo}$	$V_{geo}$	q	a	e	i	$\omega$	$\Omega$	$D'_{EDM}$	$D'_{CAMS}$
10/09/2015	19:11:36.67	303.7	+28.4	14.2	0.9347	2.39	0.609	16.5	215.87	167.56	<b>0.05</b>	<b>0.06</b>
10/09/2015	19:31:04.40	296.8	+30.0	14.6	0.95651	2.85	0.664	17.4	209.01	167.57	<b>0.04</b>	<b>0.03</b>
10/09/2015	20:27:53.48	296.2	+30.3	13.8	0.95989	2.53	0.621	16.7	208.59	167.61	<b>0.04</b>	<b>0.05</b>
10/09/2015	20:50:57.82	300.1	+29.5	14.4	0.94697	2.61	0.637	17.1	212.12	167.62	<b>0.01</b>	<b>0.02</b>
10/09/2015	20:55:49.90	298.9	+32.0	14.6	0.95124	2.56	0.628	18.0	211.07	167.62	<b>0.02</b>	<b>0.03</b>
10/09/2015	23:47:35.13	299.9	+27.8	13.8	0.94848	2.52	0.624	16.0	211.90	167.74	<b>0.03</b>	<b>0.04</b>
11/09/2015	22:02:34.86	300.2	+31.0	14.9	0.94781	2.77	0.658	18.0	211.49	168.64	<b>0.03</b>	<b>0.02</b>
14/09/2015	21:18:22.83	302.1	+30.9	14.2	0.94883	2.55	0.627	17.1	211.48	171.53	<b>0.02</b>	<b>0.03</b>
14/09/2015	21:21:19.62	300.9	+31.9	14.7	0.95192	2.74	0.653	17.9	210.22	171.53	<b>0.02</b>	<b>0.01</b>
14/09/2015	21:21:59.04	297.4	+33.7	14.9	0.96206	2.88	0.666	18.6	207.01	171.53	<b>0.04</b>	<b>0.03</b>
14/09/2015	22:23:21.14	299.9	+29.4	13.4	0.95672	2.47	0.612	15.9	209.39	171.58	<b>0.05</b>	<b>0.06</b>
15/09/2015	00:05:31.76	300.2	+31.7	13.9	0.95573	2.48	0.614	17.0	209.66	171.65	<b>0.04</b>	<b>0.05</b>
17/09/2015	19:27:51.74	297.3	+35.4	14.6	0.96705	2.72	0.644	18.6	205.39	174.38	<b>0.02</b>	<b>0.01</b>
18/09/2015	00:30:10.44	299.4	+35.6	15.6	0.96064	3.11	0.692	19.7	206.88	174.59	<b>0.08</b>	<b>0.07</b>
18/09/2015	00:43:21.81	300.7	+34.4	14.8	0.95807	2.74	0.650	18.5	208.20	174.60	<b>0.02</b>	<b>0.01</b>
18/09/2015	01:35:19.02	305.8	+31.0	15.4	0.94028	3.07	0.694	18.0	212.57	174.63	<b>0.08</b>	<b>0.07</b>
19/09/2015	23:30:26.49	298.3	+36.1	14.6	0.96746	2.71	0.643	18.7	205.07	176.50	<b>0.02</b>	<b>0.02</b>
20/09/2015	22:38:34.19	298.6	+28.7	13.2	0.96896	2.77	0.651	15.2	204.37	177.44	<b>0.03</b>	<b>0.02</b>
24/09/2015	21:06:26.01	298.9	+29.6	13.9	0.97225	3.29	0.704	15.9	202.24	181.29	<b>0.10</b>	<b>0.09</b>
27/09/2015	20:27:52.87	297.4	+33.6	14.2	0.97819	3.29	0.703	17.3	199.64	184.20	<b>0.09</b>	<b>0.09</b>
28/09/2015	02:15:15.57	298.2	+35.5	13.5	0.97753	2.63	0.628	17.1	200.57	184.44	<b>0.04</b>	<b>0.04</b>

Table 3 – Comparing the first released orbit (CAMS) with EDMOND 2015, EDMOND 2007–2015 and this analysis.

	$\alpha_{\text{geo}}$	$\delta_{\text{geo}}$	$V_{\text{geo}}$	q	a	e	i	$\omega$	$\Omega$
CBET	301.0±2.2	32.6±1.6	15.1±0.9	0.949±0.003	2.75±0.40	0.655±0.041	18.6±1.6	209.9±1.9	171.64±0.23
E-2015	300.5±2.1	31.7±2.3	14.2±0.6	0.953±0.009	2.56±0.25	0.627±0.036	17.4±1.0	210.1±2.9	171.43±2.11
EDMOND	300.6±2.9	31.5±3.1	14.5±0.8	0.951±0.011	2.64±0.24	0.640±0.032	17.6±1.4	210.6±3.2	170.71±2.44
This (18)	299.8±2.3	31.5±2.5	14.4±0.6	0.955±0.009	2.69±0.20	0.644±0.024	17.5±1.1	209.5±2.9	171.35±3.30

Table 2 Lists all 21 orbits that fulfilled all criteria. Note that most of the 50 eliminated orbits are very likely related to this shower but the current methodology does not allow an unambiguous identification.

In Table 3 the initial orbit obtained from the first CAMS data is compared to the data obtained from the EDMOND database, the 2015 EDMOND data and the long term EDMOND data. The average orbit for CAMS@BeNeLux has been considered for the 18 orbits in the range of 10 to 20 September. The  $\chi$ -Cygids (757 CCY) displayed enhanced activity in 2015 but the display wasn't short lived but covering at least a couple of weeks. Orbits from this meteor shower can be detected at least during two weeks. It may be too early to draw any conclusions about any periodicity in the occurrence of enhanced activity, but the shower probably displayed enhanced activity in 2010 too, which was not detected by any network as far as we know. The very slow velocity and large scatter on the radiant area may explain why the shower escaped from the attention of meteor surveys before.

## 6 Meteorite hunt for fireball 2015 March 25, 23<sup>h</sup>00<sup>m</sup>45<sup>s</sup> UT

In May 2016 several CAMS operators participated in field searches for meteorites dropped by the fireball of 25 March 2015. This fireball passed close to the fields of view of several cameras of our network but managed to slip in between the camera fields, illustrating the need for an even more dense coverage by cameras.



Figure 11 – The ongoing field searches in May 2016 here with Adriana Roggemans, Paul Roggemans and Tim Polfliet.

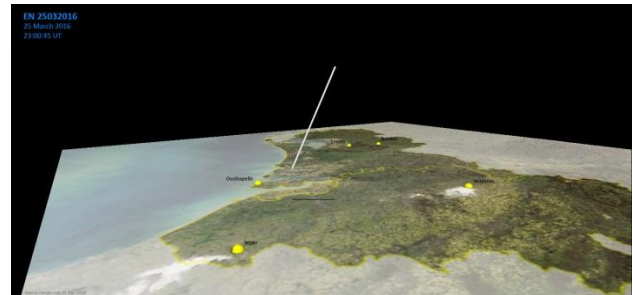


Figure 12 – The 2015 March 25, 23<sup>h</sup>00<sup>m</sup>45<sup>s</sup> UT fireball that managed to slip in between the coverage of our CAMS network without being captured (Credit Marco Langbroek).

## 7 Conclusions

The CAMS@BeNeLux network expanded further since the last IMC, with extra cameras, extra stations and more volume in the atmosphere being covered. Since the last IMC more than 17000 orbits were collected and the total number of orbits obtained by the network reached over 40000 orbits since 25–26 May 2016. The weather in general was less favorable during the considered period than the year before.

The Kappa Cygnids were remarkable absent in 2015 after their abundant display in 2014. CAMS@BeNeLux was the first to draw attention to the enhanced activity of the Chi Cygnids with a sample of 5 accurate orbits obtained in the night of 14–15 September 2016, after a hint from visual observers Koen Miskotte and Michel Vandeputte. In this paper we could list 21 orbits associated with the new shower 757 CCY.

## Acknowledgment

The authors wish to thank all participants for their efforts and discipline to submit the CAMS data shortly after each observing night. We also emphasize that all the efforts of the CAMS@BeNeLux team are done as volunteers and that all equipment is being financed privately by each participant without any kind of subsidies. The current (May 2016) CAMS@BeNeLux team:

*Hans Betlem* (Leiden, operating CAMS 371, 372 and 373), *Felix Bettonvil* (Utrecht, operating CAMS 376 and 377), *Jean-Marie Biets* (Wilderen, operating CAMS 381 and 382), *BISA – Hervé Lamy* (Dourbes, operating CAMS 394 and 395, Uccle, operating CAMS 393), *Martin Breukers* (Hengelo, assistant coordinator and

operating CAMS 320, 321, 322, 323, 324, 325, 326 and 327), *Franky Dubois* (Langemark, operating CAMS 386), *Luc Gobin* (Mechelen, operating CAMS 390 and 391), *Robert Haas* (Alphen aan de Rijn, operating CAMS 360, 361, 362, 363, 364 and 365), *Klaas Jobse* (Oostkapelle, operating CAMS 331, 332, 337, 338 and 339), *Carl Johannink* (Gronau, coordinator and operating CAMS 311, 312, 313, 314, 315 and 316), *Paul Lindsay* (Lieshout, operating CAMS 356 and 357), *Koen Miskotte* (Ermelo, operating CAMS 351 and 352), *Piet Neels* (Ooltgenplaat, operating CAMS 341, 342, 343 and 344), *Tim Polfliet* (Gent, operating CAMS 396), *Steve Rau* (Zillebeke, operating CAMS 385 and 387), *Paul Roggemans* (Mechelen, operating CAMS 383, 384, 388 and 389) and *Erwin Van Ballegoij* (Heesch, operating CAMS 347 and 348).

The authors also wish to thank *Pete Gural*, *Peter Jenniskens* and *Denis Vida* for their continuous support with CAMS related questions, software solutions and updates.

## References

- Bettonvil F., Johannink C. and Breukers M. (2014). "CAMS BeNeLux". In Rault J.-L., and Roggemans P., editors, *Proceedings of the International Meteor Conference*, Giron, France, 18–21 September 2014. IMO, pages 55–58.
- Drummond J. D. (1981). "A test of comet and meteor shower associations". *Icarus*, **45**, 545–553.
- Green D. W. E. (2015). "New chi Cygnids meteor shower". Central Bureau Electronic Telegram No. 4144.
- Gural P. S. (2011). "The California All-sky Meteor Surveillance (CAMS) System". In Asher D. J., Christou A. A., Atreya P. and Barentsen G., editors, *Proceedings of the International Meteor Conference*, Armagh, Northern Ireland, 16–19 September 2010. IMO, pages 28–31.
- Jenniskens P., Gural P. S., Dynneson L., Grigsby B. J., Newman K. E., Borden M., Koop M. and Holman D. (2011). "CAMS: Cameras for Allsky Meteor Surveillance to establish minor meteor showers". *Icarus*, **216**, 40–61.
- Jenniskens P., Nénon Q., Albers J., Gural P. S., Haberman B., Holman D., Morales R., Grigsby B. J., Samuels D. and Johannink C. (2016a). "The established meteor showers as observed by CAMS". *Icarus*, **266**, 331–354.
- Jenniskens P., Nénon Q., Gural P. S., Albers J., Haberman B., Johnson B., Holman D., Morales R., Grigsby B. J., Samuels D. and Johannink C. (2016b). "CAMS confirmation of previously reported meteor showers". *Icarus*, **266**, 355–370.
- Jenniskens P. and Nénon Q. (2016c). "CAMS verification of single-linked high-threshold D-criterion detected meteor showers". *Icarus*, **266**, 371–383.
- Jenniskens P., Nénon Q., Gural P. S., Albers J., Haberman B., Johnson B., Holman D., Morales R., Grigsby B. J., Samuels D. and Johannink C. (2016d). "CAMS newly detected meteor showers and the sporadic background". *Icarus*, **266**, 384–409.
- Koseki M. (2014). "Various meteor scenes II: Cygnid-Draconid Complex ( $\kappa$ -Cygnids)". *WGN, Journal of the IMO*, **42**, 181–197.
- Koukal J., Srba J. and Toth J. (2016). "Confirmation of the  $\chi$  Cygnids (CCY, IAU#757)". *WGN, Journal of the IMO*, **44**, 5–9.
- Roggemans P., Betlem H., Bettonvil F., Biets J. M., Breukers M., Haas R., Jobse K., Johannink C., Langbroek M., Miskotte K., Neels P., Nijland J. and ter Kuile C. (2014). "The Benelux CAMS Network – status July 2013". In Gyssens M., Roggemans P. and Zoladek P., editors, *Proceedings of the International Meteor Conference*, Poznan, Poland, 22–25 August 2013. IMO, pages 173–175.
- Roggemans P., Breukers M. and Johannink C. (2015). "Status of the CAMS-BeNeLux network". In Rault J.-L. and Roggemans P., editors, *Proceedings of the International Meteor Conference*, Mistelbach, Austria, 27–30 August 2015. IMO, pages 41–50.
- Shiba Y. (2015). " $\chi$  Cygnids observation in Japan". *WGN, Journal of the IMO*, **43**, 179–180.
- Southworth R. R. and Hawkins G. S. (1963). "Statistics of meteor streams". *Smithsonian Contributions to Astrophysics*, **7**, 261–286.

# eMeteorNews: website and PDF journal

Paul Roggemans<sup>1</sup>, Richard Kacerek<sup>2</sup>, Jakub Koukal<sup>3</sup>, Koen Miskotte<sup>4</sup> and Roman Piffel<sup>5</sup>

<sup>1</sup> Pijnboomstraat 25, 2800 Mechelen, Belgium

paul.roggemans@gmail.com

<sup>2</sup> 19 Comet Close, Ash Vale, Surrey, GU125SG, United Kingdom

rickzkm@gmail.com

<sup>3</sup> Valašské Meziříčí Observatory, Vsetínská 78, 75701 Valašské Meziříčí, Czech Republic

j.koukal@post.cz

<sup>4</sup> De la Reystraat 92, 3851 BK Ermelo, the Netherlands

k.miskotte@upcmail.nl

<sup>5</sup> astrofoto.sk, Azalková 28, 90042 Dunajská Lužná, Slovakia

ceres@global.sk

Amateur meteor workers have always been interested to exchange information and experience. In the past this was only possible via personal contacts by letter or by specialized journals. With internet a much faster medium became available and plenty of websites, mailing lists, Facebook groups, etc., have been created in order to communicate about meteors. Today there is a wealth of meteor data circulating on internet, but the information is very scattered and not directly available to everyone. The authors have been considering how to organize an easy access to the many different meteor related publications. The best solution for the current needs of amateur meteor observers proved to be a dedicated website combined with a PDF journal, both being free available without any subscription fee or registration requirement. The authors decided to start with this project and in March 2016 the website meteornews.org has been created. A first issue of eMeteorNews was prepared in April 2016. The year 2016 will be a test period for this project. The mission statement of this project is: “Minimizing overhead and editorial constraints to assure a swift exchange of information dedicated to all fields of active amateur meteor work.”

## 1 Introduction

Amateur meteor work is booming since video meteor observing became easily accessible for a large number of amateurs. However it is very difficult to follow all the developments as there are too many different sources to check. Some journals impose time-consuming editing procedures and require a semiprofessional level. Most amateurs don't have the time for that and therefore seek alternatives in social media such as Facebook and Twitter, various online Newsgroups and blogs. So far internet and social media in particular prove to be a jungle of information and it became impossible to keep track of all interesting news. The traditional media like specialized journals serve mainly as reference source for ongoing research. These journals are not suitable for amateurs who just wish some 'easy reading' information about the meteor community. Something is missing and the question is if and how amateurs can improve the situation.

## 2 Meteor publication history

Amateur meteor astronomy has been for a long time a marginal domain within astronomy compared to planetary, variable or double star observing. The first attempts for a methodologic approach of meteor observations were made by professional astronomers and explorers as a kind of hobby in the first part of the 19<sup>th</sup> century. Systematic meteor observing by amateur astronomers started around mid-19<sup>th</sup> century and has been

marked by ups and downs. Meteor astronomy has been sadly neglected by professional astronomers for a long time as astrophysics offered better career options. Who could be interested to spend a professional career to deal with no more than just the dust in our solar system? In the first half of the 20<sup>th</sup> century, the domain has been left over to a large extent to amateur astronomers with only a few exceptions of professional astronomers dealing with meteor work. The options to publish about meteor observations were limited to a few popular astronomy journals. A few amateur meteor observers centralized observing reports and published these. Thanks to their efforts we have some information about meteor stream activity in the late 19<sup>th</sup> and early 20<sup>th</sup> century. People like F. Denning in the UK, C.P. Olivier in the USA and C. Hoffmeister in Germany left a treasure of observational data with their regular meteor reports.

Things improved around mid-20<sup>th</sup> century with a new generation of astronomy students and future professional astronomers who caught interest in meteor observing. The development of radio and radar observations offered a complete new tool while the upcoming research for aerospace triggered important investments in risk assessment for spaceflights in the 1950s. Publications about meteor research boomed and amateur meteor work flourished. Unfortunately, once the risk assessments proved save for spaceflights, major meteor research programs were shut down. The popularity of amateur meteor observers got a nasty blow begin 1960's and

professional meteor research remained limited to a few specialized institutes across the globe.



Figure 1 – Frederick William Denning, one of the most productive authors of meteor reports and news ever.

End 60ies, early 70ies the moon landings and space exploration inspired many young amateur astronomers. Meteor observing didn't require any expensive equipment and proved an ideal activity for clubs to explore the constellations and to enjoy the ever surprising meteor phenomena. Some young amateurs got fascinated by the poorly known nature of the major meteor showers and specialized into meteor observing. This new generation of meteor observers was confronted with one major drawback: lack of information. The books "*Meteor astronomy*" (Lovell, 1954) and "*Meteor Science and engineering*" (McKinley, 1961) were sold out and only available at some libraries. Research papers published in professional journals remained inaccessible for most young amateurs. The gap in the market was solved with a number of amateur meteor journals and newsletters: "Meteor News" (quarterly, USA), "Meteoros" (quarterly, UK), "NVWS Bulletin" (bi-monthly, Netherlands), "Meteor" (monthly, Hungary), "Radiant" (bi-monthly, Netherlands), "Werkgroepnieuws" (monthly, Belgium), etc. These homemade journals helped amateurs to read about each other's results and experiences and inspired for more international cooperation. The content covered easy reading reports about visual observing campaigns, basic analyses of data, fireball descriptions, some peculiar meteor phenomena, etc. Although these journals were very basic in lay out and quality, active observers looked forward to read about each other's work.

Typically amateur achievements often depend on the work and commitment of one or few volunteers. Most of the popular journals of the 70ies and 80ies disappeared. To save printing and mailing costs the journal Radiant of the Dutch Meteor Society became "eRadiant" and still continues as popular reading in PDF format among Dutch speaking amateurs. WGN published meteor work from amateurs worldwide and became the Journal of the IMO in 1988. WGN evolved into a semiprofessional journal which is very valuable as source for references for future research. Originally WGN was distributed as a newsletter free of charge. When printing and mailing costs increased a modest subscription fee was charged, for instance in 1981 the annual subscription fee to WGN was 2 Euro. The cheap price was possible thanks to the efforts of volunteers to avoid all sources of costs. Also in that time any content was edited and published within two months after receipt of a contribution. The subscription fee increased when the printing wasn't done any longer by volunteers, but by a commercial service and also other overhead costs had to be covered by the subscription fee.

### 3 Back to the roots?

The success of most amateur meteor newsletters was due to the rapid publication of observing reports at a very low fee if it was not just for free. Too complicated editing procedures and or too high subscription fees may explain why active meteor observers decide not to subscribe or to quit their subscription. Amateurs got plenty of alternatives to exchange their observing experiences via internet, such as on Facebook, Twitter, News Groups, blogs, etc. Internet offers the possibility to share meteor news without any costs, which was the purpose in the 1970's and 1980's.

It is obvious that there is a gap between the swift publication on line and the advanced paper publications. Could a new meteor platform fill the gap in the market? eRadiant as online journal in PDF is still very popular among Dutch speaking amateurs. Would it be useful to set up something similar for the international community of amateur meteor observers? Discussions with several leading amateur meteor workers in recent months proved very positive. The idea was suggested to consider a new online publication with as name eMeteorNews which is straightforward for what it stands for. The first idea was to produce an online journal as PDF, inspired by eRadiant. But another brilliant idea was to set up a dedicated website to publish meteor news as soon as possible when it becomes available. The main purpose is to share meteor news, quickly and easy, with a minimum of editing constraints. Thanks to the new technology we can get rid of overhead costs and get back at the working conditions of over 30 years ago: rapid sharing of information free of charge. The authors very quickly reached a consensus to set up the MeteorNews project.

## 4 A new project: MeteorNews

Combining the advantages of a Meteor News website with these of a PDF journal, we can ‘eat from two bags of food’ and have something as fast as social media, combined with a PDF journal for archiving and reference purposes. Some of the advantages would be:

- Free of charge as the production would require zero costs;
- No membership and no registration required being independent from any society;
- Fast publication on the website;
- Flexibility in volume and periodicity for the PDF journal;
- Archiving as PDF for storage with the ADS Abstract service;
- Ease of use with no editing constraints to submit content;
- Printable as PDF format ready for local printing;
- Searchable content on both the website and in the PDF archive;
- Full color publication on the website and in the PDF;
- Boost outreach in this field being unlimited free available to anyone interested.

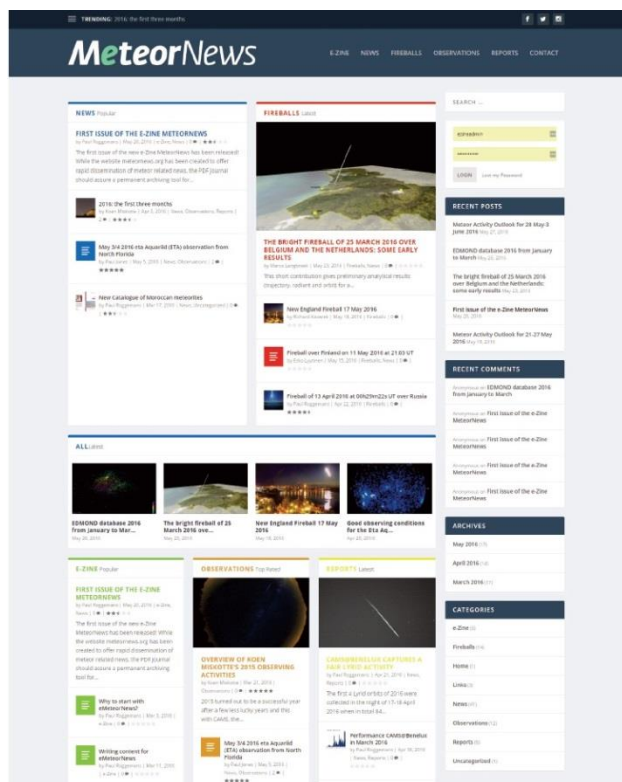


Figure 2 – The MeteorNews.org website with the layout designed by the website administrator, Roman Piffel, has been created and put online in just a few days.

With eMeteorNews we hope to bring the essential information together accessible from a single source. The new eMeteorNews should be complementary and not compete with any existing publications. There is no restriction to the type of content but it should remain dedicated to the active amateur meteor workers for quick

and efficient dissemination of meteor news without any bureaucratic overhead.

The mission statement of this project is: “*Minimizing overhead and editorial constraints to assure a swift exchange of information dedicated to all fields of active amateur meteor work.*”

## 5 Practical aspects

Who will take care of this? Beyond the authors of this paper some more people volunteered to become MN-editor. Meteor workers interested to join the editorial board are welcome to join the current editorial board:

- Salvador Aguirre (*Mexico*)
- Karl Antier (*France*)
- François Colas (*France*)
- Antal Igaz (*Hungary*)
- Paul Jones (*USA*)
- Richard Kacerek (*U.K.*)
- Jakub Koukal (*Czech Republic*)
- Marco Langbroek (*Netherlands*)
- Bob Lunsford (*USA*)
- Jose Maria Madiedo (*Spain*)
- Koen Miskotte (*Netherlands*)
- Roman Piffel (*Slovakia*)
- Paul Roggemans (*Belgium*)
- Your name here?

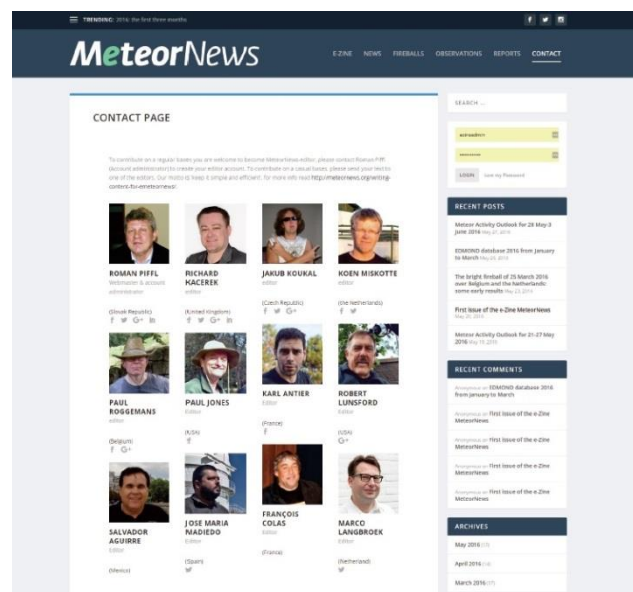


Figure 3 – The MeteorNews editorial board.

When? Discussions about this project started begin of 2016. The response to the idea was very positive. Several people offered to help and are interested to participate. Since we start from scratch, we’ll work out a prototype as experiment and use the rest of 2016 as a test period. We hope to collect news on the website meteornews.org and to compile a few online issues in PDF format. If the test period proves successful we’ll register an ISSN number and start archiving with ADS abstract service in 2017.

*What to publish?* We welcome input from all meteor workers: reports on visual observations, reports from camera networks, reports on radio observations, fireball and particular meteor sightings, anything related to meteor work. The content should focus on practical aspects, the style should be informal easy reading text.



Figure 4 – The first issue of the eZine appeared in May 2016.

*How to submit content?* Send your text and pictures by mail to one of the MeteorNews.org editors. Short announcements can be published easily in WordPress without any layout requirements. To keep MeteorNews.org easy reading, submit the following as text without bothering about editing aspects:

- A short title (mandatory);
- Name(s) of author(s) (mandatory);
- Contact address(es) of the author(s) (optional);
- Abstract (optional for news but recommended for articles);
- Body text (mandatory);
- Pictures (optional, but if pictures are submitted a caption is mandatory);
- References (optional).

If you have a relative long and elaborated contribution it may be worth the effort to prepare this as a Word document. In such case we recommend to use the Word template which can be downloaded from MeteorNews.org. Save this dotx file on your computer. In Word you find under 'File' – 'Options' – 'Add ins', here at the bottom you see 'Manage' select 'Templates' and click 'Go' in the tab 'Templates browse to select the eMeteorNews dotx file. Make sure to mark 'Automatically update document styles'.

## 6 Publication policy

As soon as some content is received by an editor, it will be published as soon as possible on the MeteorNews.org website.

Every now and then a selection of articles collected on the website will be assembled as a journal in PDF which will be reported and archived with the ADS abstract service (from 2017 onwards). All papers published in MeteorNews.org and its PDF journal eMeteorNews will be archived for consultation and reference purposes.

The website will include short news flashes which refer to other publications and these items will not be included in the PDF Journal for the simple reason that these are being published elsewhere. The PDF version of eMeteorNews will certainly cover all original and elaborated submissions from the MeteorNews website. In particular observing reports from visual observers and activity reports from camera networks will be included in the PDF Journal.

# An overview of the CILBO spectral observation program

Regina Rudawska, Joe Zender and Detlef Koschny

European Space Agency, Noordwijk, the Netherlands

`rrudawska@cosmos.esa.int`

The video equipment can be easily adopted with a spectral grating to obtain spectral information from meteors. Therefore, in recent years spectroscopic observations of meteors have become quite popular. The Meteor Research Group (MRG) of the European Space Agency has been working on upgrading the analysis of meteor spectra as well, operating image-intensified camera with objective grating (ICC8). ICC8 is located on Tenerife station of the double-station camera setup CILBO (Canary Island Long-Baseline Observatory). The pipeline software processes data with the standard calibration procedure (dark current, flat field, lens distortion corrections). While using the position of a meteor recorded by ICC7 camera (zero order), the position of the 1st order spectrum as a function of wavelength is computed. Moreover, thanks to the double meteor observations carried by ICC7 (Tenerife) and ICC9 (La Palma), trajectory of a meteor and its orbit is determined. Which merged with simultaneously measurement of meteor spectrum from ICC8, allow us to identify the source of the meteoroid. Here, we report on preliminary results from a sample of meteor spectra collected by CILBO-ICC8 camera since 2012.



J r mie Vaubailon and Regina Rudawska.

# ESA/ESTEC Meteor Research Group – behind the scenes

**Regina Rudawska**

**European Space Agency, Noordwijk, The Netherlands**

`rrudawska@cosmos.esa.int`

The ESA/ESTEC Meteor Research Group consists of a team people with one goal: understand the effects of meteoric phenomena on planetary atmospheres and surfaces, as well as on spacecraft. The team carries out observational and theoretical studies in order to increase our knowledge of the small particle complex in the solar system. This talk addresses a number of tasks within the group seen from a perspective of a research fellow.



Joost Hartman, spotted in the back office, early in the morning.

# Meteor reporting made easy- The Fireballs in the Sky smartphone app

Eleanor Sansom<sup>1</sup>, Jay Ridgewell<sup>2</sup>, Phil Bland<sup>1</sup> and Jonathan Paxman<sup>3</sup>

<sup>1</sup>Dept. Applied Geology, Curtin University, Perth, Australia  
eleanor.sansom@postgrad.curtin.edu.au

<sup>2</sup>Science Outreach, School of Science, Curtin University, Perth, Australia

<sup>3</sup>Dept. Mechanical Engineering, Curtin University, Perth, Australia

Using smartphone technology, the award-winning 'Fireballs in the Sky' app provides a new approach to public meteor reporting. Using the internal GPS and sensors of a smartphone, a user can record the start and end position of a meteor sighting with a background star field as reference. Animations are used to visualize the duration and characteristics of the meteor. The intuitive application can be used in situ, providing a more accurate eye witness account than after-the-fact reports (although reports may also be made through a website interface). Since its launch in 2013, the app has received over 2000 submissions, including 73 events which were reported by multiple users. The app database is linked to the Desert Fireball Network in Australia (DFN), meaning app reports can be confirmed by DFN observatories. Supporting features include an integrated meteor shower tool that provides updates on active showers, their visibility based on moon phase, as well as a tool to point the user toward the radiant. The locations of reports are also now shown on a live map on the Fireballs in the Sky webpage.

## 1 Introduction

The International Meteor Organization received 19082 reports of fireballs via their web-form between Jun 01, 2015 and May 31, 2016 (IMO, 2016). In order to use eyewitness reports to reconstruct meteor/fireball trajectories, the key elements required are the position of the observer and the start and end direction (both altitude and azimuth) of the event. The duration, brightness, color, fragmentation events and any associated sounds (sonic booms) are additional useful information. Accurately estimating start and end directions, in particular the altitude, can be difficult. The Fireballs in the Sky smartphone app, developed by *Thoughtworks Inc.*, in collaboration with Curtin University, uses the technology of smartphones to allow users to report on the spot. Updated features include an integrated meteor shower tool that provides updates on active showers, their visibility based on moon phase, as well as a tool to point the user toward the radiant. This app is freely available through Google Play and the iTunes App stores.

## 2 Reporting made easy

To submit a report of either a meteor or a fireball, users will be guided through the following steps (illustrated in *Figure 1, 2, 3 and 4*):

1. Note whether any sonic booms were heard. This can be modified if a delayed boom was later heard.
2. Aim phone at location where fireball started, aided by a background star field to more accurately report orientation (*Figure 2*).
3. Aim phone at location where fireball ended, again using reference star background (*Figure 3*).
4. Describe additional details such as duration, brightness, color and any flare/fragmentations (as well as number of fragments seen). The responsive

animation allows the user to adjust the simulation to accurately reflect their sighting (*Figure 4*).

5. Report summary is presented and additional notes, including contact details in case of further investigation, may be provided.

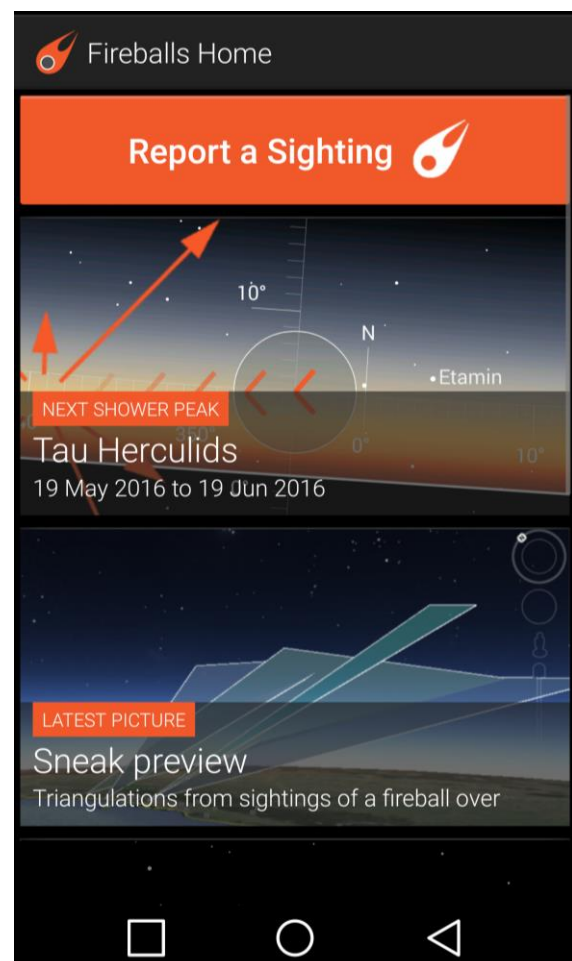


*Figure 1* – Screenshots of the Fireballs in the sky reporting procedure. a) homepage- report a sighting, or checkout meteor shower tool.

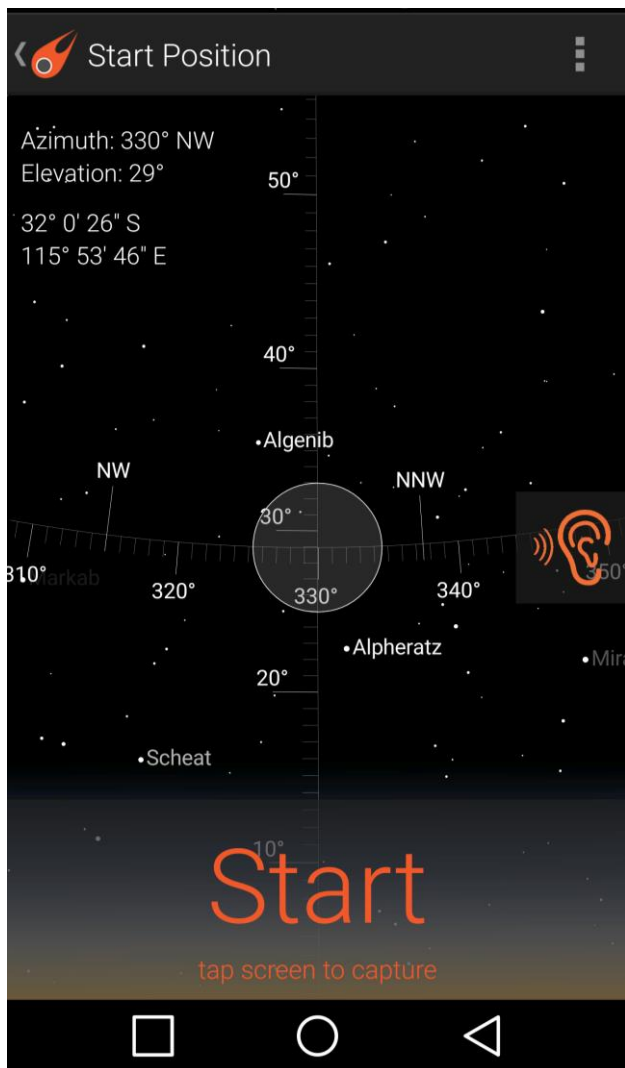


Figure 2 – Screenshots of the Fireballs in the sky reporting procedure. b) step 2- record where fireball started.

The app uses the internal GPS, accelerometers, magnetometers and gyroscopes to record the orientation of the phone when reporting a fireball. When a report is submitted, it will include the GPS location of the observer, the altitude and azimuth of both start and end points recorded by the internal phone sensors, as well as all the other fireball information. If phone signal is unavailable at the time of submission, as long as the phone GPS is still active, the report will be saved until the user returns to an area with network coverage. Users can also report a fireball at a later time on the webpage<sup>1</sup>. Report locations can be seen on the Fireballs in the Sky webpage<sup>2</sup>. Reports made within close proximity at similar times are automatically grouped and users will receive a message saying their sighting has been “corroborated”. Reports that have been verified by photographic records are marked as “confirmed”. Reporting via the app is simple and accessible to all members of the public to report an event, even children.

The app database is linked to the Desert Fireball Network in Australia (DFN), meaning app reports can be confirmed by DFN observatories. Corroborated reports

<sup>1</sup> <http://fireballsinthesky.com>

<sup>2</sup> <http://fireballsinthesky.com.au/maps/app-sightings/>

are automatically triangulated, using a straight line trajectory assumption, in a similar workflow to that used by the DFN. When app users report an event that is observed by multiple DFN observatories, an assessment of app report reliability can be made. Since its launch in 2013, the app has received over 2000 submissions, including 73 events which were reported by multiple users. Some reports are for daytime events which are unable to be captured by DFN observatories that run only during the night. App reports are therefore able to provide data on fireballs that may not otherwise be recorded.

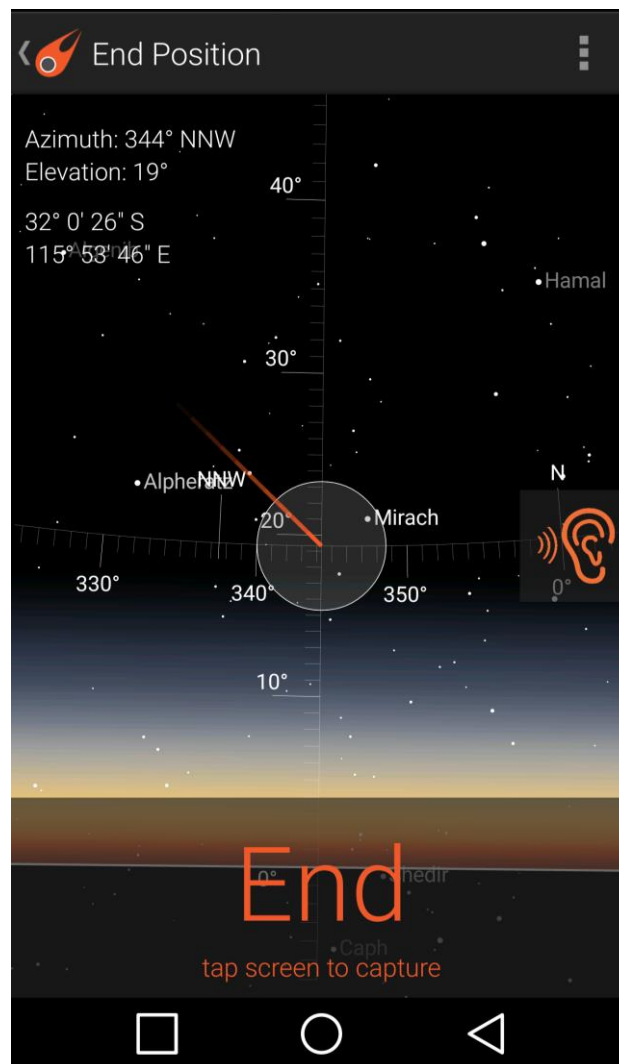


Figure 3 – Screenshots of the Fireballs in the sky reporting procedure. c) step 3- record where fireball ended.

### Improved error estimation

Eyewitness reports can provide fireball trajectories, though errors in both altitude and azimuth can be greater than 30° (Tatum, 1998). The use of smartphone sensors can increase the accuracy of reported observations, aided by the star background and fireball animation for user reference. As the report is made on-the-spot this will help improve the quality of the report while it is fresh in the observer's mind.

### 3 Meteor shower tool

A recent addition to the app is a meteor shower information tool. The next shower peak will appear on the home screen. 69 showers are separated into major and

minor depending on zenithal hourly rate. Their peak day is given along with their expected viewing dates. After selecting a shower, an introduction is given, including the viewing conditions based on the phase of the moon during shower peak. The tool also points the user toward the radiant.

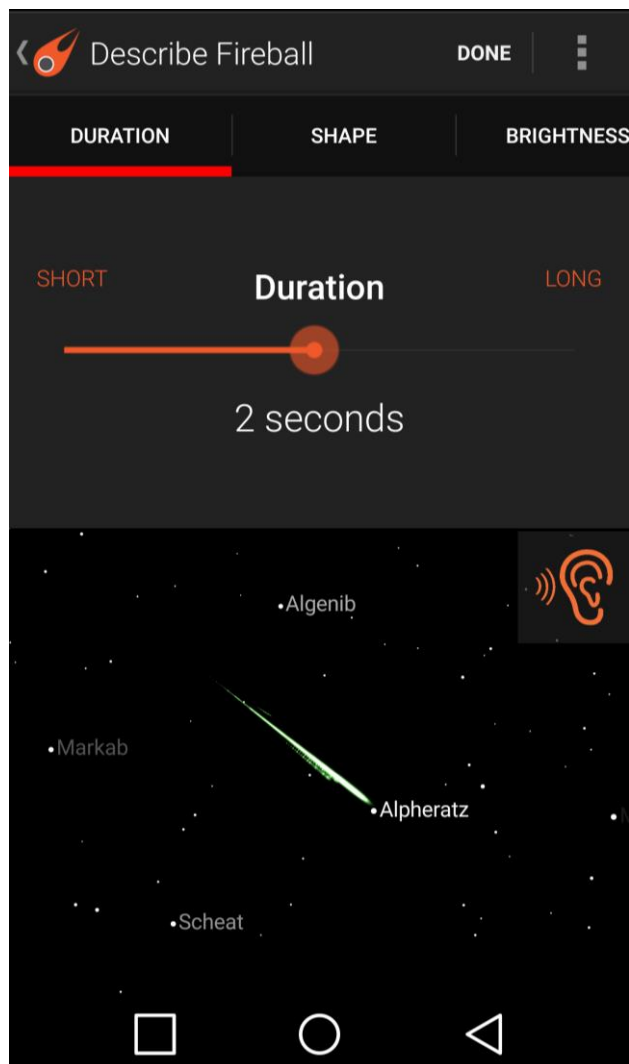


Figure 4 – Screenshots of the Fireballs in the sky reporting procedure. d) describe characteristics with help of fireball animation.

## 4 Conclusion

The easy-to-use Fireballs in the Sky smartphone app encourages and enables users around the world to report scientifically useful fireballs on the spot. The use of smartphone technology and animations aims to increase the accuracy of meteor and fireball reports. Through the app, users can also access an interactive meteor shower finder with an augmented reality radiant indicator, information on current and upcoming meteor showers and their estimated visibility.

## Acknowledgments

The app was conceived as part of the Fireballs in the Sky outreach project, funded by *Inspiring Australia* and developed by *Thoughtworks Inc.*

## References

- IMO (2016). “Fireball Reports”. URL: [fireballs.imo.net](http://fireballs.imo.net) accessed: 13 June 2016.
- Tatum J. B. (1998). “Tracking a fireball from eyewitness accounts with reference to the west coast event of 1995 December 22”. *Journal of the Royal Astronomical Society of Canada*, **92**, 78–82.

# Croatian Meteor Network: Ongoing work 2015 – 2016

Damir Šegon<sup>1</sup>, Denis Vida<sup>2</sup>, Korado Korlević<sup>3</sup> and Željko Andreić<sup>4</sup>

<sup>1</sup> Astronomical Society Istra Pula, Park Monte Zaro 2, 52100 Pula, Croatia  
Višnjan Science and Education Center, Istarska 5, 51463 Višnjan, Croatia  
damir.segon@pu.htnet.hr

<sup>2</sup> Astronomical Society “Anonymus”, B. Radića 34, 31550 Valpovo, Croatia  
Faculty of Electrical Engineering, University of Osijek, KnezaTrpimira 2B, 31000 Osijek, Croatia  
denis.vida@gmail.com

<sup>3</sup> Višnjan Science and Education Center, Istarska 5, 51463 Višnjan, Croatia  
korado@astro.hr

<sup>4</sup> University of Zagreb, Faculty of Mining, Geology and Petroleum Engineering, Pierottijeva 6, 10000 Zagreb  
zeljko.andreic@oblaak.rgn.hr

Ongoing work of the Croatian Meteor Network (CMN) between the 2015 and 2016 International Meteor Conferences is presented. The current sky coverage is considered, software updates and updates of orbit catalogues are described. Furthermore, the work done on meteor shower searches, international collaborations as well as new fields of research are discussed. Finally, the educational efforts made by the CMN are described.

## 1 Introduction

In this paper we present the ongoing work of the Croatian Meteor Network (CMN) between the 2015 and 2016 IMCs, as well as the results from previous years' analysis. Topics covered by this paper contain information on the current sky coverage of CMN cameras, improvements done on CMN software, status of the CMN orbit catalogues, results from international collaborations, a brief overview of new fields of research and efforts made on educating young people interested in meteor astronomy.

## 2 CMN sky coverage

During the period between the two IMCs, the number of active cameras has remained at 22. As pointed out in our 2015 IMC proceedings paper (Šegon et al., 2015), there is a significantly smaller coverage over the southern part of Croatia. However, we managed out to reinstall one camera (CMN Čiovo) and regain at least partial coverage over that part of Croatia. The sky coverage at 100 km height can be seen in *Figure 1*.

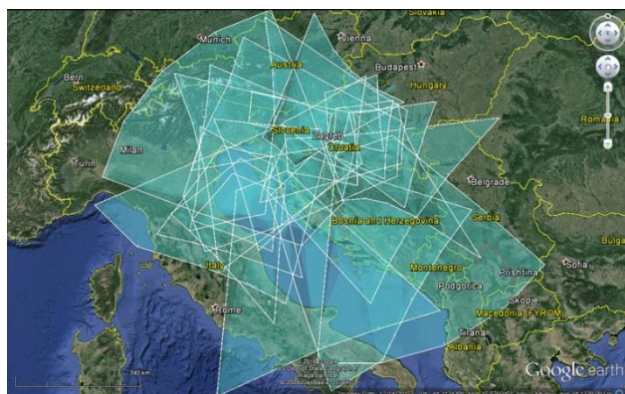


Figure 1 – CMN sky coverage at the height of 100 km.

As far as the coverage at 20 km height is concerned, a significant part of the sky in the mid-Adriatic coastal part of Croatia has been regained again thanks to the Čiovo camera. Our intention is to have a complete coverage over Croatia at 20 km height, by at least by one camera. This is of the highest importance for recording meteorite-dropping fireballs and estimating their terminal point dynamics, which combined with other trajectory dynamics and light curve data should provide information about a possible meteorite fall.



Figure 2 – CMN sky coverage at the height of 20 km.

## 3 CMN orbit catalogues and software updates

All data up to 2016 has been processed and it is ready for final review and orbit catalogue production. Only three stations remained in an unautomated processing mode, due to hardware limitations and unavailability of internet connection at those locations.

Since 2014, most of the CMN stations operate in an almost completely automatic mode (Vida et al., 2014), meaning almost no manual effort is needed to reduce the

data. As such, all incoming data are ready for orbit pairing. However, prior to the introduction of the automation procedures, up to the year 2014, there was still a considerable number of stations which required some degree of manual data reduction. That is the reason why only one catalogue, the one for 2013, has been published between the two IMCs. The catalogues for 2014 and 2015 should be completed and published during this year as their preparation is mostly complete.

Furthermore, significant improvements were done on the *CMN\_BinViewer* software (Vida et al., 2014) which allowed many CMN and CAMS camera operators to recheck and visualize their observations in a more convenient way. As noted by the software's users, the Confirmation feature used by CAMS camera operators proved to be most useful and timesaving.

#### 4 International collaboration and results

In the paper published in WGN43:5 we presented our last results from the 2013 CMN shower search which used the SonotaCo and CMN meteor orbit databases, presenting the last four candidate meteor showers possibly connected to four asteroidal parent bodies (Šegon et al., 2015). Jérémie Vaubaillon did the dynamical modeling for all potential meteor shower associations to parent bodies, results of which are being analyzed in a paper to be published soon.

At the last year's IMC at Mistelbach, we announced the possibility of an enhanced activity by Kappa Cepheids on September 21<sup>st</sup>. This activity had been only observed visually by Jürgen Rendtel (Rendtel, 2015) observing from the island of La Palma in Spain. However, there are no confirmations from video or radar observations up to this date about any enhanced activity of the shower. We do not have any announcements for 2016, according to the modeling done by Jérémie Vaubaillon there are no predicted direct intersections of meteoroid orbits with the Earth's orbit in 2016 for that shower.

A very strong Taurid activity has been observed during 2015 by the CMN as well as by other meteor observers (Molau, 2016). One very interesting event recorded by the CMN was a Taurid fireball which produced a long lasting meteor train (more than 45 minutes). The fireball itself has been observed by three CMN video cameras, as well as four Slovenian Meteor Network all-sky and DSLR cameras. Thanks to members of the Slovenian Meteor Network, the propagation of the train is currently being investigated from combined observations, and will be presented in a separate paper.

#### 5 New technology and fields of research

##### Low-cost radiometer – an improved version

The low-cost radiometer project presented at the 2015 IMC (Vida et al., 2015) has been continued and an improved version has been developed. While the first version used a single operational amplifier and only one

*BPW34* photodiode, the new version uses a quad operational amplifier and a total of 9 photodiodes. Groups of 3 *BPW34* photodiodes have their signal summed and fed into one of the channels of the amplifier. The amplified signal of all 3 groups is summed. There is an option to feed the resulting signal into the fourth channel of the amplifier for additional amplification. This approach resulted in a larger signal to noise ratio. The encountered issue was a ~50 Hz noise caused by the light pollution in urban areas, thus it was decided to develop a standalone system powered by the *Raspberry Pi* single-board computer which can run on batteries charged by a solar panel and be installed in a remote location.

The system has been tested from several urban locations. The recordings were found to be very noisy because of the present light pollution. A simple noise filtering procedure was implemented, but it was discovered the system is also sensitive to the very slight frequency drift ( $\pm 0.01$  Hz) present in the electrical grid. This frequency drift causes issues during filtering as one cannot assume a constant frequency during the observed time. Thus a more advanced procedure has been developed which models the noise on a short segment of the recording during which it assumes a linear frequency drift. The noise model is then subtracted from the raw data to obtain a clean signal. This approach is limited as the frequency drift is a stochastic process which can sometimes cause a bad model fit. We continue the work to solve this issue. As the system was not directly paired to a video camera and we encountered issues with keeping a proper time on the *Raspberry Pi*, we cannot confidently claim that the system recorded any meteors or fireballs yet. There are many candidates in the recorded data but no direct correlation can be made at this moment. Nevertheless, many fireworks were recorded during the New Year's celebration in Pula, Croatia. The total cost of the system (not counting the *Raspberry Pi 2* computer) is about 10€. Next steps are to install the system in a non-light polluted location, paired with an all-sky camera running on the same *Raspberry Pi* computer. This combination is possible as the radiometer recording procedures are not computationally intensive, while the meteor capture and detection software for the *RPi* exists. (Vida et al., 2015; 2016).

##### Open-source low-cost meteor station

During last year's IMC, (Zubović et al., 2015) presented a low-cost video meteor station. This year, (Vida et al., 2016) provided an update on this project. In summary, a complete solution for video meteor capture and detection has been developed for a price of about 150 USD. Some minor work on testing and documentation still needs to be done, but the system is close to being fully functional. The developed system is compatible with CAMS standards and represents an opportunity for a cheap way to create new and expand existing meteor networks. Furthermore, the price of the system makes it suitable for educational purposes – one of the long term goals of the CMN is to give high school and university students an opportunity to have their own meteor station at home and

to learn about astronomy, computer and data science with their own equipment and data.

### Telescopic meteors

One of the most common issues when dealing with video meteor orbit data is the lack of astrometrical precision. The work of (Skokić et al., 2016) has shown that even most reliable video orbits made by CAMS software show significant dispersion in D-criteria.

Initial tests done by the Slovak Video Meteor Network (Koukal et al., 2015), Sirko Molau (Molau, 2015) and the CMN during 2014 have shown that telescopic meteors are not elusive. We have conducted parallel tests using a 55mm F/1.0 *Kowa* lens and a 4mm F/1.2 lens during the night of December 12–13, the pre-maximum night of the 2014 Geminids. The moderate field of view lens (4mm) yielded a total of 118 meteors, while the 55mm *Kowa* lens yielded 42 meteors. Regarding the *Kowa* lens, due to its significantly longer focal length and a significantly higher on-chip meteor velocity, we have concluded that the camera's geometry (FOV center in respect to radiant position) plays an important role in terms of the number of recorded meteors.

As the initial results in regard to the number of recorded meteors were encouraging, it was decided to pursue the matter further. To maximize the number of recorded telescopic meteors, a system of 8 *Kowa* lenses in a 4x2 configuration was built. 8 *Sony ICX672 (NTSC Exview HAD II)* NTSC board cameras are used for imaging with the lenses. The developed system covers a FOV of about  $15.6^\circ \times 10.4^\circ$  and records a live video with stars visible down to magnitude 10. A second such system is being built and both will be operational in the near future.

Questions which we want to discuss here are how many meteors would such setup record compared to a moderate FOV lens, and could the system be useful for flux and ZHR estimations? Thus, in order to have a grasp of the numbers involved, Peter Gural performed simulations using the *MeteorSim* software (Gural, 2001), and the results are presented below.

As the used lenses have a much higher focal length than moderate FOV systems, ground separation of the stations can be much closer due to a higher astrometrical precision. A smaller distance between the stations thus means a higher sky volume overlap between the stations, which in turn could yield a higher number of recorded common events. These events could therefore be of similar apparent magnitudes as the distance between meteors and the stations is much larger than the distance between the stations themselves.

Fainter limiting magnitude should allow capturing more sporadic meteors as the population index for sporadic sources is about 3 or more (Rendtel, 2004). All these factors can be accounted for in the simulation. Furthermore, one important point to consider are weather conditions for both stations as it rarely occurs they are ideal. In the case of the telescopic setup, weather

conditions should be more or less the same for both due to their proximity to each other.

*MeteorSim* simulations were done using three entrance velocities, paired with population indices: 72 km/s ( $r = 2.5$ ), 35 km/s ( $r = 2.5$ ) and 12.5 km/s ( $r = 3.0$ ). Two types of output were analyzed: meteor limiting magnitude and meteor count, for different radiant distances (i.e. the distance between the center of the FOV and the radiant). The resulting graphs are shown in *Figures 3 and 4*. From *Figure 3* can be noticed that meteor counts strongly depend on the radiant distance, but this dependence is less pronounced for slower meteors.

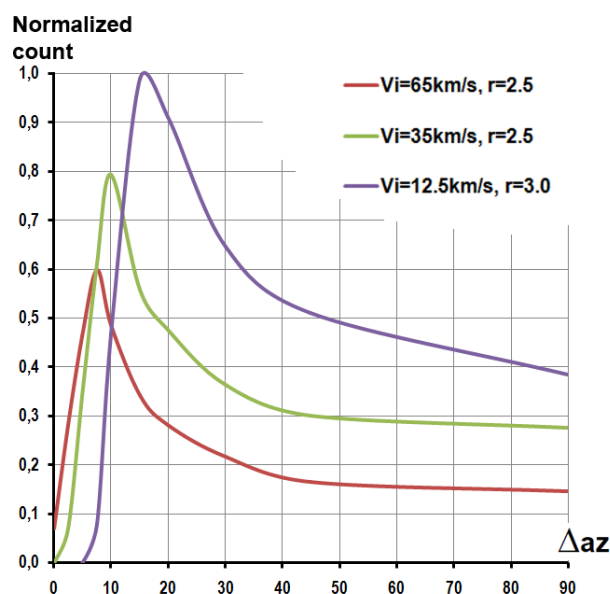


Figure 3 – CMN Normalized meteor counts versus radiant distance for three entrance velocities: 72, 35 and 12.5 km/s, according to *MeteorSim* results.

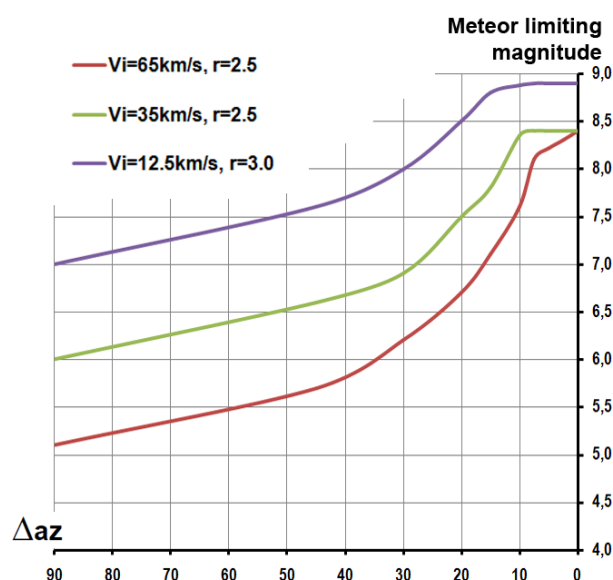


Figure 4 – CMN Limiting meteor magnitude versus radiant distance for three entrance velocities: 72, 35 and 12.5 km/s, according to *MeteorSim* results.

Figure 4 shows that regardless the entrance velocity, the setup should be able to detect all meteors down to the 5<sup>th</sup> magnitude, and all meteors down to magnitude 6 for meteors with the entrance velocity of 35 km/s. These

results mean that the system should have acceptable ZHR estimations for e.g. Geminids, regardless of the radiant distance.

One of the primary goals of this project is to obtain high-precision deceleration data of the recorded meteors which would yield very precise orbits. Furthermore, as the meteor's on-chip velocity is large and the frame rate of the used camera is not all that high (60 Hz per field with the NTSC camera after deinterlacing, i.e. ~16.7 ms per field), meteors appear as streaks on individual fields. During the testing we have found many meteors that have streaks longer than 50 pixels per one field. If one looks at the profile of each streak and extracts its light curve with 1 pixel steps, that process would allow converting spatial information of meteor's brightness to temporal information. Effectively, that would mean that the light curve of a telescopic meteor could be sampled with thousands of samples per second.

Finally, the data generated by this system could be used for other purposes, such as analysis of star scintillations and occultations.

## 6 Education

From the very beginnings of the Croatian Meteor Network, one of our main goals is education of students, ranging from elementary school to university students.

One of the students' groups at the Višnjan School of Astronomy (which takes place for more than 25 years) is always dedicated to meteor work. Each group has about 4 to 5 students who are led by a mentor. Such approach allows for a higher individuality and a deeper concentration on the matter, but still requires much teamwork. Most importantly, students are being introduced to the scientific method through original (very often their own) observations which adds value to their work.

During the 2015/16 academic year, the CMN deepened contacts with teachers interested in astronomy and provided data for Croatian astronomy contests and other educational projects. Two of the new CMN cameras are situated on schools in Koprivnica and Rovinj. Our goal is to spread this collaboration further and deploy more meteor stations on schools.

Workshops and lectures about the CMN and meteor astronomy in general were held at the Physics Department of the University of Osijek and at the Fran Galović high school in Koprivnica.

## 7 Conclusion

Ongoing work of the Croatian Meteor Network between the two IMCs has been presented. The current status of the network was described, results of scientific endeavors were discussed, and the status of ongoing projects was given.

The discussed projects have enough material to be elaborated in separate papers, as this was done for a chosen set of projects. The others were described here in a shorter format to minimize the required time for their description, while still providing some information about them. Any reader interested in a particular project is encouraged to contact the authors for more information.

## Acknowledgments

Our acknowledgments go to all members of the Croatian Meteor Network, in alphabetical order (by first name): Alan Pevec, Aleksandar Borojević, Aleksandar Merlak, Alen Žizak, Dalibor Brdarić, Damir Matković, Dario Klarić, Dario Zubović, Dejan Kalebić, Denis Štogl, Dorian Božičević, Filip Lolić, Filip Novoselnik, Gloryan Grabner, Goran Ljaljić, Ivan Gašparić, Ivica Ćiković, Janko Mravik, Josip Belas, Krunoslav Vardijan, Luka Osokruš, Maja Crnić, Mark Sylvester, Mirjana Malarić, Reiner Stoos, Saša Švigelj, Sonja Janeković, Tomislav Sorić, Zvonko Prihoda, Željko Arnautović, Željko Krulić and most of all, Peter Gural. This work was partially supported by the Faculty of Mining, Geology and Petroleum Engineering, University of Zagreb, Višnjan Science and Education Center and by private funds of CMN members.

## References

- Gural P. (2002). "Meteor Observation Simulation Tool". In Triglav M., Knöfel A. and Trayner C., editors, *Proceedings of the International Meteor Conference*, Cerkno, Slovenia, 20-23 September 2001. IMO, pages 29–35.
- Koukal J., Srba J. and Gorková S. (2015). "NFC - Narrow Field Camera". In Rault J.-L. and Roggemans P., editors, *Proceedings of the International Meteor Conference*, Mistelbach, Austria, 27-30 August 2015. IMO, pages 91–93.
- Molau S., Kac J., Crivello S., Stomeo E., Barentsen G., Goncalves R., Saraiva C., Maciejewski M. and Maslov M. (2015). "Results of the IMO Video Meteor Network – October 2014". *WGN, Journal of the IMO*, **43**, 33–38.
- Molau S., Crivello S., Goncalves R., Saraiva C., Stomeo E. and Kac J. (2016). "Results of the IMO Video Meteor Network – November 2015". *WGN, Journal of the IMO*, **44**, 46–50.
- Šegon D., Andreić Ž., Korlević K. and Vida D. (2015). "Croatian Meteor Network: ongoing work 2014 – 2015". In Rault J.-L. and Roggemans P., editors, *Proceedings of the International Meteor Conference*, Mistelbach, Austria, 27-30 August 2015. IMO, pages 51–57.
- Šegon D., Gural P., Andreić Ž., Vida D., Skokić I. and Novoselnik F. (2015). "Four possible new high-declination showers". *WGN, Journal of the IMO*, **43**, 147–150.

- Rendtel J. (2004). “The population index of sporadic meteors”. In Triglav-Čekada M. and Trayner C., editors, *Proceedings of the International Meteor Conference*, Bollmannsruh, Germany, 19-21 September 2003. IMO, pages 114–122.
- Rendtel J. (2015). “Minor kappa-Cepheid (751 KCE) activity on 2015 September 21”. *WGN, Journal of the IMO*, **43**, 177–178.
- Skokić I., Šegon D. and Kurtović G. (2016). “On the accuracy of orbits from video meteor observations”. In Roggemans A. and Roggemans P., editors, *Proceedings of the International Meteor Conference*, Egmond, the Netherlands, 2-5 June 2016. Pages 280–283.
- Vida D., Turčinov R., Šegon D. and Silađi E. (2015). “Low-cost meteor radiometer”. In Rault J.-L. and Roggemans P., editors, *Proceedings of the International Meteor Conference*, Mistelbach, Austria, 27-30 August 2015. IMO, pages 180–184.
- Vida D., Šegon D., Gural P. S., Martinović G. and Skokić I. (2014). “CMN\_ADAPT and CMN\_binViewer software”. In Rault J.-L. and Roggemans P., editors, *Proceedings of the International Meteor Conference*, Giron, France, 18-21 September 2014. IMO, pages 59–63.
- Vida D., Zubović D., Šegon D., Gural P. and Cupec R. (2016). “Open-source meteor detection software for low-cost single-board computers”. In Roggemans A. and Roggemans P., editors, *Proceedings of the International Meteor Conference*, Egmond, the Netherlands, 2-5 June 2016. Pages 307–318.
- Zubović D., Vida D., Gural P. and Šegon D. (2015). “Advances in the development of a low-cost video meteor station”. In Rault J.-L. and Roggemans P., editors, *Proceedings of the International Meteor Conference*, Mistelbach, Austria, 27-30 August 2015. IMO, pages 94–97.



Damir Šegon.

# Fireballs from Australian Desert Fireball Network – search for similar orbits

Lukáš Shrbený<sup>1</sup>, Pavel Spurný<sup>1</sup> and Phil A. Bland<sup>2</sup>

<sup>1</sup>Interplanetary matter department, Astronomical Institute of the Czech Academy of Sciences, Ondřejov, Czech Republic  
shrbeny@asu.cas.cz

<sup>2</sup>Department of Applied Geology, Curtin University, Perth, Australia

We studied the fireball activity from the Desert Fireball Network records from 2006 to 2014 and identified a couple of time periods with increased number of fireballs. We searched for orbital similarities among the fireballs in these time periods and have found members of 10 individual meteor showers and two groups of similar orbits that do not correspond to any known meteor shower.

## 1 Introduction

The multi-station photographic observation of fireballs using fireball networks represents a very efficient and precise method of recording the atmospheric interactions of larger meteoroids. During the short moment of meteoroid ablation we can determine its atmospheric trajectory, orbit, light curve and basic physical properties. The only one photographic fireball network in the Southern Hemisphere is the *Desert Fireball Network* (DN) in Australia. The DN was designed to recover number of meteorites with accurate orbits, and thus bright fireballs with possibility of meteorite fall were processed preferentially. The published data cover two successful recoveries of Bunburra Rockhole and Mason Gully meteorites (e.g. Bland et al., 2009; Spurný et al., 2011; 2012; Welten et al., 2012), observation of the HAYABUSA spacecraft reentry (Borovička et al., 2011), and atmospheric trajectories and orbits of other 30 bright fireballs presented at Asteroids, Comets, Meteors 2008 conference in Baltimore (Bland et al., 2008).

We used already measured fireballs to search for similarities in their radiant positions and heliocentric orbits with meteor showers or with other DN fireballs. We present five time periods during a year of increased fireball activity, fireballs belonging to five individual meteor showers from the IAU MDC working list of meteor showers, and two groups of similar orbits that do not correspond to any known meteor shower.

## 2 Instrumentation, observations and data processing

One of the most advanced fireball networks was the Desert Fireball Network (Bland et al., 2004), where each station was equipped with a modern and sophisticated Autonomous Fireball Observatory (AFO) (Spurný et al., 2007). The AFO imaging system consists of a Zeiss Distagon fish-eye objective ( $f/3.5$ ,  $f = 30$  mm) and a large-format sheet film ( $9 \times 12$  cm emulsion ILFORD FP4 125 with panchromatic spectral sensitivity approximately between 360 and 650 nm). All AFOs are

equipped with a rotating shutter close to the focal plane to determine the fireball velocity. Each AFO also includes an all-sky brightness sensor (radiometer) with a sampling rate of 500 measurements per second. Therefore, along with an accurate time of the fireball passage and duration, we also obtain a very detailed light curve. The multi-station operation of the network started in December 2005 and the last film was exposed in April 2015. Altogether, more than 260 multi-station fireballs were recorded. The network has been changed in last few years and the number of cameras has increased to 30 digital fireball observatories (ADFO) equipped by Nikon D800 still cameras and Watec 902H video cameras (Bland et al., 2014; Towner et al., 2015). Over the next few months, the DN should establish over 50 new ADFOs (Sansom et al., 2015).

We predominantly search for shower fireballs in time intervals with increased fireball activity. Only about 90 fireballs were measured and calculated so far so it is very probable that other meteor shower members will be identified after processing of the whole DN data set.

All the presented fireballs were measured and processed using our standard procedures (Borovička et al., 1995; Ceplecha, 1987). The Fishscan software, created by Dr. Jiří Borovička, serves for positional and photometric measuring of fireballs on scanned copies of films. Therefore, all the fireballs here, along with precise atmospheric trajectories, also have precise Fishscan photometry (for details see Shrbený, 2009 or Shrbený and Spurný, 2009).

## 3 Activity of DN fireballs and proposed shower membership

### Fireball activity

After developing and processing of all the DN films we were interested if there are time periods during a year with increased fireball activity. We took dates of 853 fireball occurrences (single-station events also included) of nine complete years from 2006 to 2014 and plotted the

histogram with 9–11 days bins (depending on the month length, 3 bins per month). The number of fireballs was corrected to 10 days for all the bins (*Figure 1*). The average value of fireballs observed per 10 days is 23. Five most prominent activity periods and meteor showers active in these periods are the beginning of March ( $\sigma$ -Hydriids,  $\gamma$ -Normiids), end of May ( $\alpha$ -Scorpiids, S  $\omega$ -Scorpiids), end of July/beginning of August (Piscis Austriniids, S  $\delta$ -Aquiriids,  $\alpha$ -Capricorniids, S  $\iota$ -Aquiriids,  $\eta$ -Eridaniids), end of October/beginning of November (S and N Tauriids), and beginning of December (Phoeniciids, December Monocerotiids, N  $\chi$ -Orionids,  $\gamma$ -Puppids, Geminiids).

### Working list of meteor showers

Seven fireballs belonging to five individual meteor showers from the IAU MDC working list of meteor showers were identified. The meteor showers are N  $\mu$ -Sagittariids, June  $\varepsilon$ -Ophiuchiids,  $\kappa$ -Aquiriids, N  $\chi$ -Orionids, and  $\gamma$ -Puppids. Atmospheric trajectories of the fireballs are presented in *Table 1*, physical data in *Table 2*, and orbital elements in *Table 3*.

The dynamic pressures,  $p$ , in *Table 2* are determined from the high resolution light curves from AFO radiometers and correspond to the first significant outburst. If we assume that these significant outbursts correspond to fragmentation points, the dynamic pressures in *Table 2* are the highest ones reached without fragmentation. Thus a comparison with the tensile strength of the material can be made. The dynamic pressures are a function of the velocity,  $v$ , and the air density,  $\rho$ , at the fragmentation point ( $p = \rho v^2$ ).

N  $\mu$ -Sagittariid fireballs are according to the PE criterion the most fragile and probably of cometary origin. The orbital association of DN210606A and DN240606 with the shower is not very confident, since the  $D_H$  criterion (Jopek, 1993) between the fireballs and fireballs and the mean shower orbit is 0.1. The shower is also part of the antihelion source so the orbital similarities could be incidental.

The atmospheric trajectory and the dynamics of DN120907 were determined with accuracy high enough to apply the fragmentation model of Ceplecha et al., 1993 and determine precise values of initial velocity, ablation coefficient, and product  $Km^{-1/3}$ . The terminal height of 50 km was reached by this meteor with a terminal velocity of only 6 km/s and with an absolute brightness of  $-1.8 \pm 0.8$  mag, which corresponds to an almost completely decelerated object. The model provides a solution with one fragmentation point at a height of 56.5 km, and the ablation coefficient of  $0.110 \text{ s}^2/\text{km}^2$ . This corresponds to a velocity of 15.3 km/s and a dynamic pressure of 0.118 MPa. The results of the model can also help to constrain the meteoroid bulk density,  $\rho_d$ . We can separate  $\rho_d$  from the definition of the shape-density coefficient,  $K$ , if we know  $m_{inf}$  and the value of product  $\Gamma A$ . The same procedure was applied on one Leonid fireball (Spurný et al., 2000), and in our case ( $m_{inf} = 58 \text{ g}$  and assuming  $\Gamma A = 1.1$ ) this provides an estimate of bulk

density of  $3.2 \text{ g/cm}^3$ . A couple of significant outbursts of the brightness of the DN120907 are visible in its light curve. The outbursts correspond to heights of 60 and 52.5 km, or to dynamic pressures of 0.082 and 0.146 MPa respectively, which is in good agreement with the fragmentation model. According to the PE criterion (Ceplecha and McCrosky, 1976) the DN120907 is of type II, which is between the classifications based on the ablation coefficient and the bulk density. However, if we take the unknown shape of the body ( $\Gamma A$ ) and the accuracy of  $m_{inf}$  into account the spread of possible bulk densities is large: from 1.9 to  $3.5 \text{ g/cm}^3$ .

The second fireball with the fragmentation model solution is DN061207A. The model provides a solution without fragmentation. The results of the model can also provide an estimate of the meteoroid bulk density. If we apply the same procedure as described above and use  $m_{inf} = 40 \text{ g}$ , we arrive at a bulk density of  $0.6 \text{ g/cm}^3$ . No significant outbursts of the brightness of DN061207A are visible in its light curve. This is in good agreement with a no-fragmentation solution of the fragmentation model.

*Table 1* – Atmospheric trajectories of the fireballs belonging to the working list of meteor showers.  $H$  is the height above sea level, the subscript “ $B$ ” denotes values at the beginning point of the atmospheric trajectory, the subscript “ $E$ ” at the end point.

Fireball name	Time (UT)	$H_B$ (km)	$H_E$ (km)	IAU No. and code
DN210606A	17:17:40	81.23	64.60	067 NSA
DN240606	15:10:24	88.75	76.02	067 NSA
DN210606B	12:21:41	78.93	68.47	459 JEO
DN120907	14:32:11	74.38	50.00	076 KAQ
DN021207	14:56:25	87.07	73.51	256 ORN
DN071205B	12:17:36	93.38	80.50	301 PUP
DN061207A	18:09:55	92.00	61.74	301 PUP

*Table 2* – Physical data on the fireballs belonging to the working list of meteor showers.  $ZD_E$  is the zenith distance of the radiant at the end point of the atmospheric trajectory,  $v_{inf}$  is the initial velocity,  $M_{max}$  is the maximum absolute magnitude,  $m_{inf}$  is the initial photometric mass, the  $PE$  coefficient describes the empirical end height criterion and designates the type of fireball (Ceplecha and McCrosky, 1976), and  $p$  is the dynamic pressure at the height of the first fragmentation (high resolution light curve is not available for DN071205B due to Moon that was brighter than the fireball).

Fireball name	$ZD_E$ (deg)	$v_{inf}$ (km/s)	$M_{max}$ (mag)	$m_{inf}$ (g)	PE type	$p$ (MPa)
DN210606A	28.9	25.39	-8.8	250	IIIA	0.055
DN240606	15.7	26.32	-5.8	30	IIIB	0.008
DN210606B	28.65	17.96	-8.2	420	IIIB	0.023
DN120907	17.68	16.49	-4.3	58	II	0.082
DN021207	60.01	30.76	-5.9	27	II/IIIA	0.044
DN071205B	73.95	43.53	-5.4	10	II	-
DN061207A	21.67	44.06	-7.8	40	II	0.117

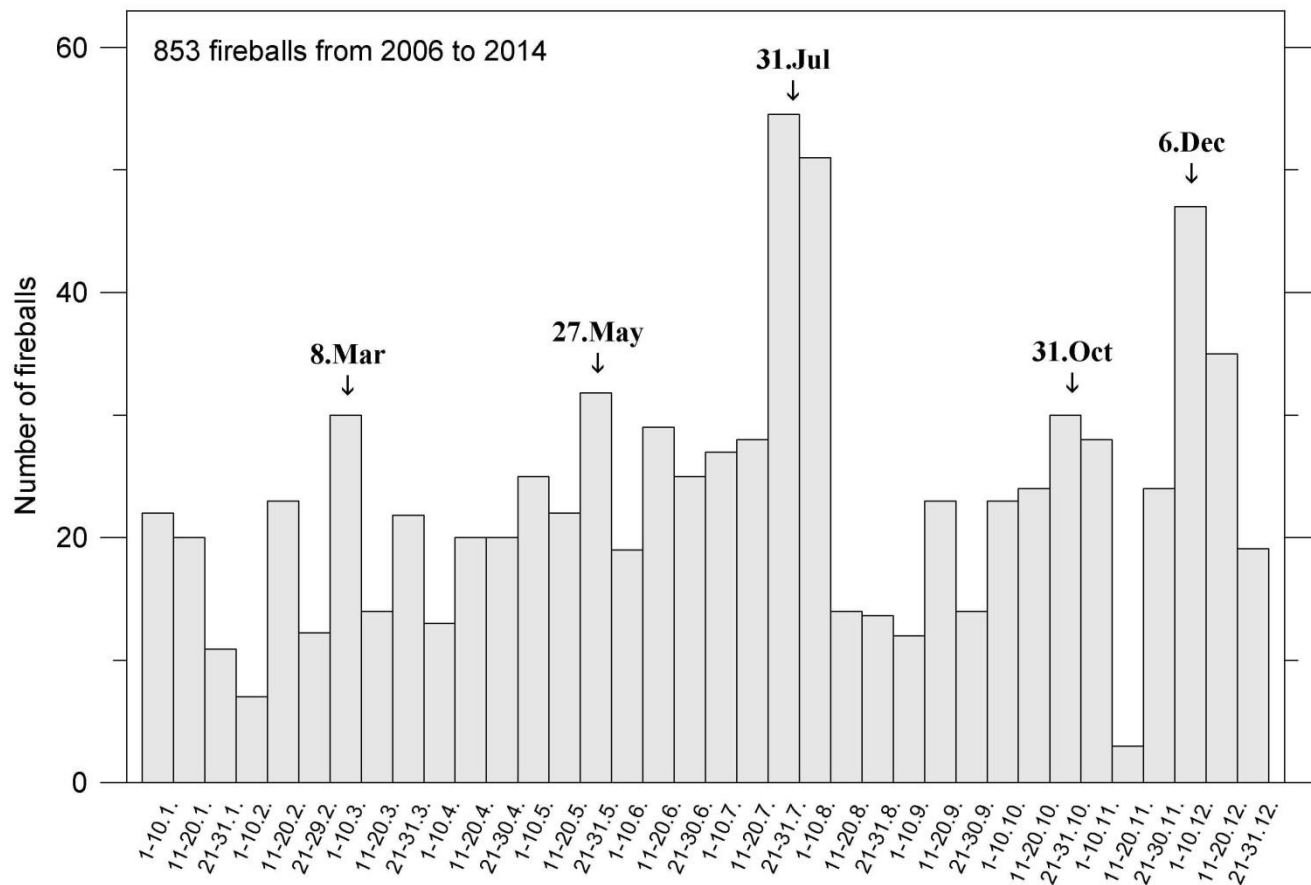


Figure 1 – Activity of DN fireballs from 2006 to 2014. The five most prominent activity periods are marked.

Table 3 – Radiants and orbital elements (J2000.0) of the presented fireballs. ( $\alpha_G$ ,  $\delta_G$ ) is the geocentric radiant and  $v_G$  is geocentric mean velocity without atmospheric drag (not measurable on our records).

Fireball name	$\alpha_G$ (deg)	$\delta_G$ (deg)	$v_G$ (km/s)	a (AU)	e	q (AU)	$\omega$ (deg)	$\Omega$ (deg)	i (deg)	IAU No. and code
DN210606A	267.39	-12.0	22.8	2.87	0.789	0.615	264.1	90.1143	8.5	067 NSA
DN240606	271.46	-16.67	23.83	3.09	0.8121	0.5805	267.52	92.8962	5.35	067 NSA
DN210606B	245.27	-8.44	14.11	2.54	0.655	0.8750	229.53	89.9219	5.11	459 JEO
DN120907	319.55	-15.96	12.30	2.64	0.6582	0.9012	42.63	349.287	0.08	076 KAQ
DN021207	82.03	26.86	28.55	2.002	0.8292	0.3419	296.17	249.9206	4.33	256 ORN
DN071205B	129.76	-47.62	41.81	2.88	0.661	0.97741	11.39	75.4213	73.60	301 PUP
DN061207A	131.79	-47.15	42.55	2.78	0.647	0.98169	7.83	74.1286	75.44	301 PUP
DN220506	259.33	-22.80	35.64	2.79	0.931	0.191	312.90	61.36	0.55	-
DN270506	264.21	-25.62	35.78	2.98	0.935	0.195	132.22	246.1525	4.54	-
DN240509	263.7	-15.1	35.14	2.33	0.915	0.197	313.2	63.5607	16	-
DN200606B	294.9	-16.7	39.97	3.14	0.968	0.099	326.5	88.9844	14	-
DN230606	296.88	-21.27	35.17	1.96	0.924	0.149	141.13	271.98	0.3	-

Only two minor outbursts are presented and correspond to heights of 79 and 72 km, or to dynamic pressures of 0.042 and 0.118 MPa respectively. According to the *PE* criterion both the  $\gamma$ -Puppids are of type II, which is not in good agreement with the estimate of the bulk density. This discrepancy can be only partially explained by the unknown shape of the body and the accuracy of  $m_{inf}$ . In all the cases, the bulk density is no higher than 1 g/cm<sup>3</sup>, and such an overestimation of  $m_{inf}$  to increase the density is not probable ( $m_{inf}$  of 3 g gives 2.2 g/cm<sup>3</sup>).

We are aware that any association of a small number of orbits with any meteor shower is doubtful without modelling of the dynamical evolution of the orbits, which would confirm the shower membership. To prove the proposed associations this kind of modelling is needed.

**Similarities without any shower membership**

Two groups of similar orbits that do not correspond to any known meteor shower were identified among DN fireballs using the  $D_H$  criterion (Jopek, 1993). Their

radiants and orbital elements are in *Table 3* and we can see that both groups belong to the antihelion source, which increase the probability that the orbital similarities are incidental. Atmospheric trajectories of the fireballs are presented in *Table 4* and physical data in *Table 5*.

*Table 4* – Atmospheric trajectories of the fireballs not belonging to known meteor showers.  $H$  is the height above sea level, the subscript “ $B$ ” denotes values at the beginning point of the atmospheric trajectory, the subscript “ $E$ ” at the end point.

Fireball name	Time (UT)	$H_B$ (km)	$H_E$ (km)
DN220506	14:34:26	94.66	80.36
DN270506	16:28:13	96.08	67.65
DN240509	17:49:27	83.29	48.58
DN200606B	12:56:39	78.26	42.58
DN230606	20:51:10	76.34	49.48

*Table 5* – Physical data on the fireballs not belonging to known meteor showers.  $ZD_E$  is the zenith distance of the radiant at the end point of the atmospheric trajectory,  $v_{inf}$  is the initial velocity,  $M_{max}$  is the maximum absolute magnitude,  $m_{inf}$  is the initial photometric mass,  $PE$  coefficient describes the empirical end height criterion and designates the type of fireball (Ceplecha and McCrosky, 1976), and  $p$  is the dynamic pressure at the height of the first fragmentation.

Fireball name	$ZD_E$ (deg)	$v_{inf}$ (km/s)	$M_{max}$ (mag)	$m_{inf}$ (g)	PE type	$p$ (MPa)
DN220506	30.90	37.33	-6.5	6	IIIA/IIIB	0.011
DN270506	5.95	37.50	-8.6	50	II/IIIA	0.026
DN240509	22.2	36.85	-10.5	1300	II	1.045
DN200606B	57.4	41.48	-11.6	1600	I	1.68
DN230606	49.14	36.88	-8.1	120	I	0.44

The first group was observed in the end of May. There were three fireballs observed with similar radiant position and shape of heliocentric orbit (especially the two ones in 2006). These fireballs belong to the antihelion source, so the orbital similarities may be incidental. Also the distinct atmospheric behavior of these fireballs prefers rather an incidental connection than a common origin. PE types differ from type II to IIIB and also the dynamic pressures cover a wide range from 0.01 to 1.0 MPa. A heterogeneous nature of a possible parent object is not impossible but incidental orbital similarities are more probable.

The second group was observed in the end of June. There were two fireballs with similar radiant position and shape of heliocentric orbit, especially a small perihelion distance. Both the fireballs performed similar atmospheric behavior, both showed significant deceleration, a small value of the ablation coefficient (0.001 and 0.003 s<sup>2</sup>/km<sup>2</sup>), and both penetrated deep into the atmosphere (PE type I). The orbital similarity can be incidental also in this case. A very similar atmospheric behavior can be caused by a close approach to the Sun where a change of the material nature takes place due to thermal desorption of Na (Čapek and Borovička, 2009).

Na is almost lost when  $q \leq 0.2$  AU and the meteoroid is smaller than 10 cm.

## 4 Conclusion

We have searched for orbital similarities among DN fireballs and meteor showers in time periods during a year with increased fireball activity. We have identified fireball members of five individual meteor showers from the IAU MDC working list of meteor showers. We have also identified two groups of similar orbits that do not correspond to any known meteor shower. On the basis of their radiant positions, heliocentric orbits, and atmospheric behavior it is probable that these associations are incidental.

External sources of shower elements are needed to identify shower members in DN fireballs due to the small number of fireballs in our data set belonging to one shower. Once identified, DN fireballs can provide precise data on meteor showers, since the majority of DN fireballs have a precise atmospheric trajectory and heliocentric orbit, detailed light curve, dynamic pressure in the first fragmentation point and modelling of some of them can provide ablation coefficient and bulk density.

## Acknowledgment

This work was supported in part by Preamium Academiae from the Czech Academy of Sciences and by the institutional project RVO:67985815.

## References

- Bland P. A. (2004). “Fireball cameras: The Desert Fireball Network”. *Astronomy and Geophysics*, **45**, 5.20–5.23.
- Bland P. A., Spurný P., Shrbený L., Borovička J., Bevan A. W. R., Towner M. C., McClafferty T., Vaughan D. and Deacon G. (2008). “The Desert Fireball Network: First Results of Two Years Systematic Monitoring of Fireballs over the Nullarbor Desert of South Western Australia”. *Asteroids, Comets, Meteors 2008. LPI Contribution No. 1405*, id. 8246.
- Bland P. A., Spurný P., Towner M. C., Bevan A. W. R., Singleton A. T., Bottke W. F., Greenwood R. C., Chesley S. R., Shrbený L., Borovička J., Ceplecha Z., McClafferty T. P., Vaughan D., Benedix G. K., Deacon G., Howard K. T., Franchi I. A. and Hough R. M. (2009). “An Anomalous Basaltic Meteorite from the Innermost Main Belt”. *Science*, **325**, 1525–1527.
- Bland P. A., Towner M. C., Paxman J. P., Howie R. M., Sansom E. K., Cupak M., Benedix G. K., Tingay S. J., Harrison J. A., Dyl K. A., Bevan A. W. R. and Galloway M. J. (2014). “Digital Expansion of the Desert Fireball Network”. *LPI Contribution No. 1800*, id.5287.

- Borovička J., Spurný P. and Keclíková J. (1995). "A new positional astrometric method for all-sky cameras". *Astronomy and Astrophysics Supplement*, **112**, 173–178.
- Borovička J., Abe S., Shrbený L., Spurný P. and Bland P. A. (2011). "Photographic and Radiometric Observations of the HAYABUSA Re-Entry". *Publications of the Astronomical Society of Japan*, **63**, 1003–1009.
- Ceplecha Z. (1987). "Geometric, dynamic, orbital and photometric data on meteoroids from photographic fireball networks". *Bulletin of the Astronomical Institutes of Czechoslovakia*, **38**, 222–234.
- Ceplecha Z. and McCrosky R. E. (1976). "Fireball end heights - A diagnostic for the structure of meteoric material". *Journal of Geophysical Research*, **81**, 6257–6275.
- Ceplecha Z., Spurný P., Borovička J. and Keclíková J. (1993). "Atmospheric fragmentation of meteoroids". *Astronomy and Astrophysics*, **279**, 615–626.
- Čapek D. and Borovička J. (2009). "Quantitative model of the release of sodium from meteoroids in the vicinity of the Sun: Application to Geminids". *Icarus*, **202**, 361–370.
- Jopek T. J. (1993). "Remarks on the meteor orbital similarity D-criterion". *Icarus*, **106**, 603–607.
- Sansom E. K., Bland P. A., Paxman J. A. and Towner M. (2015). "A novel approach to fireball modeling: The observable and the calculated". *Meteoritics and Planetary Science*, **50**, 1423–1435.
- Shrbený L. (2009). "Meteor Shower Fireballs". PhD thesis.
- Shrbený L. and Spurný P. (2009). "Precise data on Leonid fireballs from all-sky photographic records". *Astronomy and Astrophysics*, **506**, 1445–1454.
- Spurný P., Betlem H., van't Leven J. and Jenniskens P. (2000). "Atmospheric behavior and extreme beginning heights of the thirteen brightest photographic Leonid meteors from the ground-based expedition to China". *Meteoritics and Planetary Science*, **35**, 243–249.
- Spurný P., Borovička J. and Shrbený L. (2007). "Automation of the Czech part of the European fireball network: equipment, methods and first results". In Valsecchi G. B., Vokrouhlický D. and Milani A., editors, *Near Earth Objects, our Celestial Neighbors: Opportunity and Risk*, Proceedings of IAU Symposium 236. Cambridge: Cambridge University Press, pages 121–130.
- Spurný P., Bland P. A., Shrbený L., Towner M. C., Borovička J., Bevan A. W. R. and Vaughan D. (2011). "The Mason Gully Meteorite Fall in SW Australia: Fireball Trajectory and Orbit from Photographic Records". 74th Annual Meeting of the Meteoritical Society. Published in *Meteoritics and Planetary Science Supplement*, id.5101.
- Spurný P., Bland P. A., Shrbený L., Borovička J., Ceplecha Z., Singelton A., Bevan A. W. R., Vaughan D., Towner M. C., McClafferty T. P., Toumi R. and Deacon G. (2012). "The Bunburra Rockhole meteorite fall in SW Australia: fireball trajectory, luminosity, dynamics, orbit, and impact position from photographic and photoelectric records". *Meteoritics and Planetary Science*, **47**, 163–185.
- Towner M. C., Bland P. A., Cupak M. C., Howie R. M., Sansom E. K., Paxman J. P., Inie M., Galloway M., Deacon G., Dyl K. A., Benedix G. K., Tingay S. J., Harrison J. A. and Bevan A. W. R. (2015). "Initial Results from the Desert Fireball Network". *LPI Contribution No. 1832*, 1693.
- Welten K. C., Meier M. M. M., Caffee M. W., Laubenstein M., Nishizumi K., Wieler R., Bland P. A., Towner M. C. and Spurný P. (2012). "Cosmic-ray exposure age and preatmospheric size of the Bunburra Rockhole achondrite". *Meteoritics and Planetary Science*, **47**, 186–196.

# On the accuracy of orbits from video meteor observations

Ivica Skokić<sup>1</sup>, Damir Šegon<sup>2</sup> and Goran Kurtović<sup>1,3</sup>

<sup>1</sup> **Astronomical Society “Anonymus”, B. Radića 34, 31550 Valpovo, Croatia**  
ivica.skokic@gmail.com

<sup>2</sup> **Astronomical Society Istra Pula, Park Monte Zaro 2, 52100 Pula, Croatia**  
damir.segon@pu.htnet.hr

<sup>3</sup> **Faculty of Electrical Engineering, University of Osijek, Kneza Trpimira 2B, 31000 Osijek, Croatia**  
goran.kurtovic@gmail.com

The velocity limits of the meteor shower’s geocentric velocity distribution from the CAMS meteoroid database were determined and used to calculate perturbed orbits. These were compared with the mean stream orbit using the  $D_{SH}$  dissimilarity criterion. It was found that for the slow meteor showers (Alpha Capricornids and Geminids), the resulting orbits are within the generally accepted cutoff values for stream associations, while for the faster showers (Perseids, Orionids and Quadrantids) the resulting orbits differ significantly from their mean stream orbit.

## 1 Introduction

In recent years we witnessed a fast growth and development of video meteor networks providing accurate multi-station measurements of atmospheric meteoroid trajectories and determination of their heliocentric orbits. As a result, several video meteor databases have been compiled, e.g. CAMS, Cameras for Allsky Meteor Surveillance (Jenniskens et al., 2016), SonotaCo (SonotaCo, 2009), EDMOND, European Video Meteor Network Database (Kornoš et al., 2013) and CMN, the Croatian Meteor Network database (Korlević et al., 2013). The wealth of data in these databases improved parameters of established meteor showers and enabled discoveries of many new possible showers.

Several different methods are used to determine error propagation from the measured meteor path to the calculated radiant and heliocentric orbit parameters. Ceplecha (1987) used a convergence angle between the intersecting planes containing the meteor as observed from two or more stations, as a measure of quality of the determined orbit. Better error estimation is achieved by least-squares fitting and a covariance matrix calculation (e.g. Borovička, 1990; Gural, 2012; Dmitriev et al., 2015), by Monte Carlo type simulations (e.g. SonotaCo, 2016) or a combination of the two (e.g. Bettonvil, 2006). These methods assume that observational errors are well known, which is mostly the case for positional measurements, but might not be true for velocity measurements, which are very important for the pre-atmospheric orbit determination. Among other factors that may influence the velocity measurement, we mention the frame rate of the video systems (Albin et al., 2016) and the meteor deceleration profile.

In this paper, as our first step in the analysis of the accuracy of video meteoroid orbits, we check how the

spread in velocity distribution affects the mean orbit, for a given meteor shower.

## 2 Method and data

We used the CAMS v2.0 meteoroid database (Jenniskens et al., 2016), which contains more than 110000 orbits from the period 2010–2013 with detailed information about atmospheric and pre-atmospheric orbits and even shower associations. The speed accuracy of the catalog data is stated to be <10% (median 0.9%).

First, a geocentric velocity ( $V_g$ ) distribution of all meteoroids of a particular shower is plotted and the mean velocity and velocity spread are estimated. This is done visually to account for a possible asymmetry in the distribution. Next, the mean geocentric velocity of the shower is perturbed by the velocity range determined earlier, and the resulting orbit is compared with the mean shower orbit.

For the comparison of orbits we used an orbit dissimilarity criterion, a numerical value which tells us by how much two orbits differ from each other. Several criteria have been proposed and all have their strengths and weaknesses (Moorhead, 2016). Different authors give or use slightly different cutoff values for the criteria, for the two orbits to represent the same meteoroid stream (e.g. Galligan, 2001; Rudawska et al., 2012). Here we use the  $D_{SH}$  criterion, introduced by Southworth and Hawkins (1963), with a typically used cutoff value of 0.15.

## 3 Results

We performed an analysis of the five established meteor showers, Alpha Capricornids (CAP), Geminids (GEM), Quadrantids (QUA), Perseids (PER) and Orionids (ORI), that were selected on the basis of the increasing geocentric velocity and large number of recorded

meteors. The shower details and calculation results are presented in *Table 1*.

**Alpha Capricornids**

This is a shower with slow meteors whose geocentric velocity distribution shows a range between 20–27 km s<sup>-1</sup> with a typical velocity around 23 km s<sup>-1</sup> (*Figure 1*). As can be seen from *Table 1*, the orbits of the minimum and maximum V<sub>g</sub> are indeed within our D<sub>SH</sub> < 0.15 limit for association with the mean orbit of this shower.

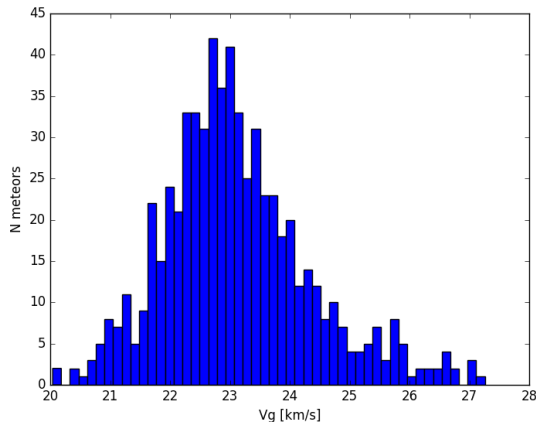


*Figure 1* – Alpha Capricornids V<sub>g</sub> distribution.

**Geminids**

A well-known slow shower originating from the asteroid 3200 Phaethon shows a typical geocentric velocity of 34 km s<sup>-1</sup> (*Figure 2*). Most Geminid meteors have a velocity between 30–40 km s<sup>-1</sup> with a small number of fast meteors going up to 45 km s<sup>-1</sup>. Nevertheless, all of them have a strong orbit similarity with D<sub>SH</sub> ~0.07. The calculation shows that to reach the limiting D<sub>SH</sub> = 0.15 value, mean V<sub>g</sub> can be perturbed by -8 up to +16 km s<sup>-1</sup>.

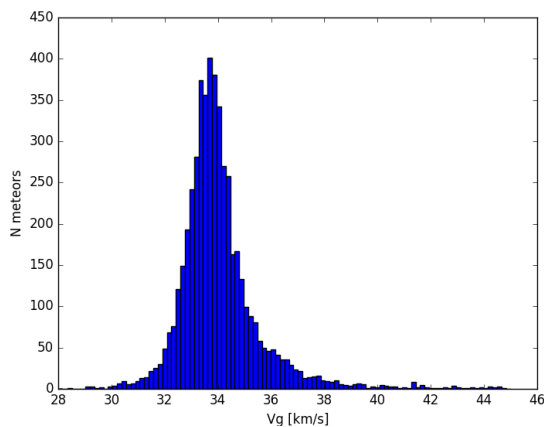


*Figure 1* – Geminids V<sub>g</sub> distribution.

**Quadrantids**

Quadrantids are somewhat faster than Geminids with a typical velocity of 41 km s<sup>-1</sup> and range of 37–48 km s<sup>-1</sup> with several meteors even going down to 35 and up to 50 km s<sup>-1</sup> (*Figure 3*). These slower and faster than mean meteors have a high D<sub>SH</sub> of 0.2–0.5, well over the limit of 0.15 as cutoff value for shower association. To be within this D<sub>SH</sub> value, QUA meteors should fall in the 39–43 km s<sup>-1</sup> V<sub>g</sub> range.

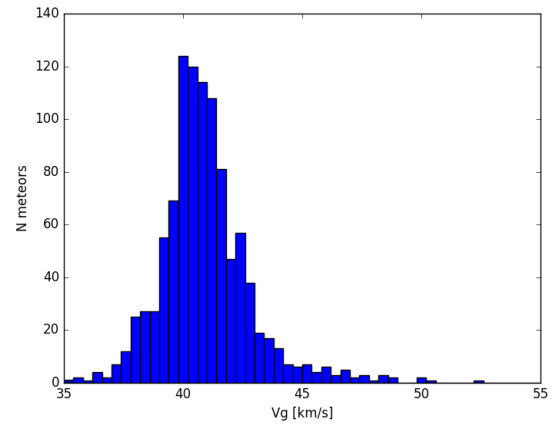


*Figure 3* – Quadrantids V<sub>g</sub> distribution.

**Perseids**

Perseids are fast meteors with a mean V<sub>g</sub> of 59 km s<sup>-1</sup> (*Figure 4*). Most PER meteors have velocities within ±4 km s<sup>-1</sup> from the mean, but there is a hint of a small bump in the 65–70 km s<sup>-1</sup> range. These V<sub>g</sub> values result in high D<sub>SH</sub> = 0.6 – 1.0 indicating that they might not be members of PER shower.

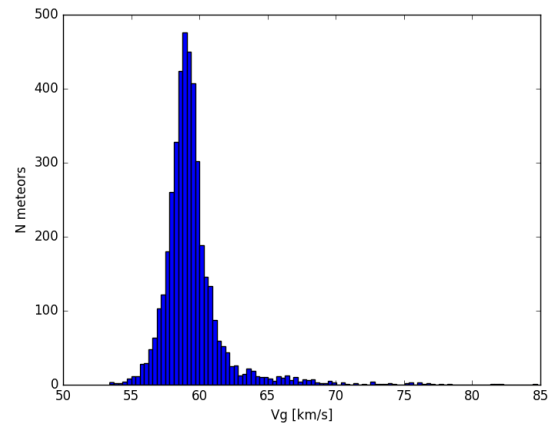


*Figure 4* – Perseids V<sub>g</sub> distribution.

*Table 1* – Shower V<sub>g</sub> values and resulting D<sub>SH</sub>

Shower	N	V <sub>g</sub> [km s <sup>-1</sup> ]	V <sub>g</sub> (min–max) [km s <sup>-1</sup> ]	D <sub>SH</sub> (min–max)	ΔV <sub>g</sub> (D <sub>SH</sub> = 0.15) [km s <sup>-1</sup> ]
CAP	640	23	20-27	0.11-0.14	±4
GEM	5064	34	30-40	0.06-0.07	-8 +16
QUA	1028	41	37-48	0.22-0.48	±2.5
PER	4258	59	55-70	0.62-1.01	±2
ORI	3002	66	62-75	0.18-0.62	±3

## Orionids

The final and fastest shower in this analysis, Orionids, has a typical  $V_g$  of  $66 \text{ km s}^{-1}$  with most meteors in  $62\text{--}75 \text{ km s}^{-1}$  range (Figure 5). Almost all slower meteors satisfy the  $D_{SH}$  0.15 limit, but faster meteors do not. There is even a small number of meteors between the  $76\text{--}80 \text{ km s}^{-1}$  range which might not at all be part of this shower. The  $D_{SH}$  limit of 0.15 gives a velocity range  $63\text{--}69 \text{ km s}^{-1}$ , so all meteors faster than  $70 \text{ km s}^{-1}$  possibly do not belong to the Orionids.

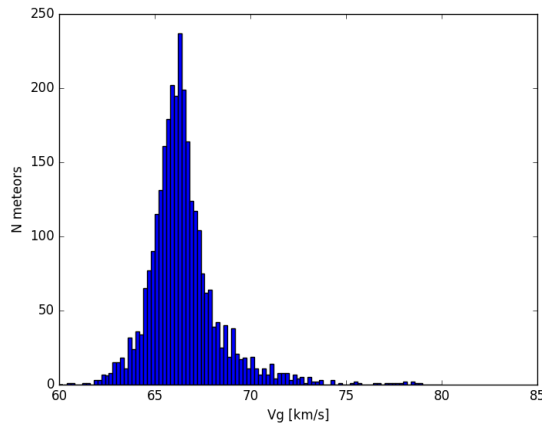


Figure 5 – Orionids  $V_g$  distribution.

## 4 Discussion and conclusions

All showers show an asymmetric geocentric velocity distribution with an excess of higher velocity meteoroids. The meteors from the  $V_g$  distribution tail show a good similarity with the mean orbit for slow showers (CAP and GEM) and can be reliably associated with the shower, but for faster showers (QUA, PER and ORI), this is not the case. The  $D_{SH} = 0.15$  condition limits the  $V_g$  to within  $2\text{--}3 \text{ km s}^{-1}$  of the mean value for these faster showers, and yet they all display a much larger velocity spread. If these meteors from the distribution tail belong to the same shower is hard to tell without detailed dynamical analysis. It may be that the large  $D_{SH}$  value in some of these cases is not due to the  $V_g$  spread, but linked to some other parameter influencing the result. For example, it is known that the orbit inclination has an effect on the  $D$  criteria limits (Galligan, 2001). Due to the small statistical sample of only five analyzed showers, it is impossible to tell if this is the case here and it will be a topic of further investigation.

The meteors in the tails of  $V_g$  distribution might also just be outliers due to the method used to associate them with the certain shower. One possible explanation is that the velocity fit of the observational data is sensitive to small perturbations and can result in these outliers (Jenniskens, personal communication; Albin et al., 2016). Another possibility might be the fact that  $D$  criteria do not have a single fixed threshold value that fits all the cases (Rudawska et al., 2012).

This paper is only a preliminary first step in a more detailed analysis in preparation. The plan is to check the influence of measurement errors on different parameters,

such as errors in the radiant position, velocity and meteoroid orbits. Also, we plan to check more showers, use all available meteoroid databases, other  $D$  criteria and extensive simulations with a final goal of quantifying the accuracy of meteoroid orbits determined from video observations.

## Acknowledgment

We thank the CAMS network for publishing the CAMS v2.0 meteoroid orbit database. We also thank Denis Vida (CMN) for his constructive comments and Paul Roggemans for his patience while preparing this paper.

## References

- Albin T., Koschny D., Soja R., Srama R. and Poppe B. (2016). “A Monte-Carlo based extension of the Meteor Orbit and Trajectory Software (MOTS) for computations of orbital elements”. In Roggemans A. and Roggemans P., editors, *Proceedings of the International Meteor Conference*, Egmond, Netherlands, 02–05 June 2016. Pages 20–25.
- Bettonvil E. J. A. (2006). “Least squares estimation of a meteor trajectory and radiant with a Gauss-Markov model”. In Bastiaens L., Verbert J., Wislez J.-M. and Verbeeck C., editors, *Proceedings of the International Meteor Conference*, Oostmalle, Belgium, 15–18 September 2005. IMO, pages 63–73.
- Borovička J. (1990). “The comparison of two methods of determining meteor trajectories from photographs”. *Bulletin Astronomical Institutes of Czechoslovakia*, **41**, 391–396.
- Ceplecha Z. (1987). “Geometric, dynamic, orbital and photometric data on meteoroids from photographic fireball networks”. *Bulletin Astronomical Institutes of Czechoslovakia*, **38**, 222–234.
- Dmitriev V., Lupovka V. and Gritsevich M. (2015). “Orbit determination based on meteor observations using numerical integration of equations of motion”. *Planetary and Space Science*, **117**, 223–235.
- Galligan D. P. (2001). “Performance of the  $D$ -criteria in recovery of meteoroid stream orbits in a radar data set”. *Monthly Notices of the Royal Astronomical Society*, **327**, 623–628.
- Gural P. S. (2012). “A new method of meteor trajectory determination applied to multiple unsynchronized video cameras”. *Meteoritics and Planetary Science*, **47**, 1405–1418.
- Jenniskens P., Nénon Q., Albers J., Gural P. S., Haberman B., Holman D., Morales R., Grigsby B. J., Samuels D. and Johannink C.

- (2015). “The established meteor showers as observed by CAMS”. *Icarus*, **266**, 331–354.
- Korlević K., Šegon D., Andreić Ž., Novoselnik F., Vida D. and Skokić I. (2013). “Croatian Meteor Network Catalogues of Orbits for 2008 and 2009”. *WGN, Journal of the IMO*, **41**, 48–51.
- Kornoš L., Koukal J., Piffil R. and Toth J. (2013). “Database of meteoroid orbits from several European video networks”. In Gyssens M. and Roggemans P., editors, *Proceedings of the International Meteor Conference*, La Palma, Canary Islands, Spain, 20–23 September 2012. IMO, pages 21–25.
- Moorhead A. V. (2016). “Performance of D-criteria in isolating meteor showers from the sporadic background in an optical data set”. *Monthly Notices of the Royal Astronomical Society*, **455**, 4329–4338.
- Rudawska R., Vaubaillon J. and Atreya P. (2012). “Association of individual meteors with their parent bodies”. *Astronomy and Astrophysics*, **541**, A2, 1–5.
- SonotaCo (2009). “A meteor shower catalog based on video observations in 2007-2008”. *WGN, Journal of the IMO*, **37**, 55–62.
- SonotaCo (2016). “Observation error propagation on video meteor orbit determination”. *WGN, Journal of the IMO*, **44**, 42–45.
- Southworth R. B. and Hawkins G. S. (1963). “Statistics of meteor streams”. *Smithsonian Contributions to Astrophysics*, **7**, 261–285.



Robert Haas and Mirel Birlan.

# Collisional lifetimes of meteoroids

Rachel Halina Soja<sup>1</sup>, G. J. Schwarzkopf<sup>1</sup>, Maximilian Sommer<sup>1</sup>, Jérémie Vaubaillon<sup>3</sup>,  
Thomas Albin<sup>1,4</sup>, Jens Rodmann<sup>2</sup>, Eberhard Grün<sup>5</sup> and Ralf Srama<sup>1</sup>

<sup>1</sup>Institute of Space Systems, University of Stuttgart, Pfaffenwaldring 29, 70569 Stuttgart, Germany  
soja@irs.uni-stuttgart.de

<sup>2</sup>Institute for Astrophysics, University of Göttingen, Germany

<sup>3</sup>IMCEE, Paris, France

<sup>4</sup>Universitätssternwarte Oldenburg, Carl von Ossietzky University, Oldenburg, Germany

<sup>5</sup>Max Planck Institute for Nuclear Physics (MPIK), Saupfercheckweg 1, 69117 Heidelberg, Germany

Collisions of meteoroids with interplanetary dust grain fragments particles, dispersing larger particles amongst lower mass intervals. Here we use the method of Grün et al. (1985) and the IMEM interplanetary dust model to calculate the collisional lifetimes for different orbits, and for particles in different meteor showers. The timescales are usually long – of order  $10^4$  years for 1mm grains on Jupiter-family and Hally-type comet orbits. However, near-sun orbits particles suffer more frequent collisions and therefore have much shorter lifetimes. We discuss factors that affect the accuracy of these calculations.

## 1 Introduction

Meteoroids ejected from their parent bodies are dispersed from their original orbits by various gravitational and non-gravitational forces, including the gravity of the Sun and planets, radiation pressure and Poynting-Robertson effect. The very smallest sub-micron particles are blown out of the solar system by radiation forces. Other small grains spiral into the sun as a result of the Poynting-Robertson drag force. However, the dynamics of larger visual-meteor-forming particles are not strongly affected by these processes. It is therefore likely that their lifetimes are dominated by collisions with other particles in the interplanetary dust cloud (Grün et al., 1985) or by other processes.

Understanding the timescale on which a given meteoroid is likely to be destructed by a collision is important for understanding the evolution of streams and the sporadic background. Currently available estimations of the collisional lifetime of meteoroids rely on old models of the interplanetary dust flux and velocity distribution (Tokhtas'ev, 1982; Grün et al., 1985; Steel and Elford, 1986). Here we use ESA's Interplanetary Meteoroid Environment Model (IMEM) (Dikarev et al., 2005) to recalculate the collisional lifetimes, and discuss consequences for meteor showers resulting from low-perihelion parent bodies.

## 2 Calculation of collisional lifetimes

Here we describe the calculation of the collisional lifetimes for meteoroids in interplanetary space. This is dependent on the number of impactor particles (the interplanetary dust cloud), and the size and properties of the meteoroid, which determines how often it is hit, and what energy is required to disrupt the particle. The relative velocity of the collision is also necessary, in order to determine the energy of the collision.

The lifetime is not a fixed quantity, because the collisional probability varies along the orbit of the particle – nearer the Sun, the flux of interplanetary particles is higher, and the probability of impact increases. It will also vary as the orbit of the particle changes due to gravitational perturbations and Poynting-Robertson drag. We therefore evaluate the collisional probability at 100 points along one orbit of the meteoroid, and sum the contributions. This provides us with the collisional lifetime for a particular type of orbit. It describes the collisional lifetime of a specific object only when the orbit is stable.

We calculate the rate of catastrophic collisions – those for which the largest fragment is half the size of the original mass. We assume that the meteoroid is disrupted by the smallest size of particle able to do so. We then require (1) a formalism to describe the size of this projectile, and (2) a model to describe the flux of particles of this size.

A target particle with mass  $m_1$  is catastrophically disrupted by a projectile of mass  $m_2$  when  $m_1 \leq \Gamma m_2$ . Here  $\Gamma$  depends on particle properties (target particle density  $\rho$  ( $\text{g/cm}^3$ ) and unconfined compressive strength  $S_c$  (kbar)) and the impact speed  $v$  (km/s). As derived from results of Gault (1973) and Hörz et al. (1975), and given by Grün et al. (1985):

$$\Gamma = 9.76 \times 10^2 S_c^{-0.45} (m_1 / \rho_1)^{0.075} v^2$$

These equations are used to calculate the mass of a particle that can cause catastrophic disruption for a given impact velocity. The collisional probability is calculated by determining the number of particles with this mass that impact the meteoroid. Grün et al. (1985) use fluxes at 1 AU derived from Pegasus and HEOS-2 measurements, and assumes an impact velocity of 20 km/s at 1 AU, applying a factor  $(r/r_0)^{-1}$  to account for the speed dependent with heliocentric distance  $r$  (AU).

We take projectile particle fluxes and impact velocities from IMEM. The number of impacts is the sum of the flux of particles from six different impact directions and five different impactor populations (two cometary, two asteroidal, and interstellar dust) (Dikarev et al., 2005). This allows us to calculate the collisional lifetime along any orbit in the inner solar system.

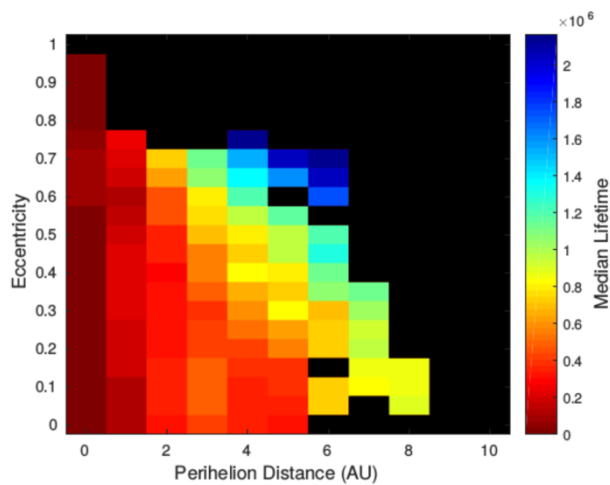


Figure 1 – Median collisional lifetime for particles with a radius of  $100\mu\text{m}$  and a bulk density of  $2000\text{ kg/m}^3$ , as a function of perihelion distance and eccentricity, for a sample of 4000 solar system objects.

The collisional lifetimes at Earth orbit agree with the results of Grün et al. (1985), as expected. We then calculate the lifetimes along the current orbits of more than 4000 solar system bodies: asteroids, comets, and planets, and evaluate the median lifetime for prograde orbits for each combination of perihelion distance and eccentricity (Figure 1). This demonstrates that lifetimes are longest for orbits with high perihelion distance and eccentricity, and shortest for low perihelion orbits.

### 3 Results for meteor showers

In Figure 2 we show the collisional lifetime as a function of mass for different meteor shower parent bodies, for a bulk density of  $2000\text{ kg/m}^3$ . The collisional lifetimes of visual-meteor-sized ( $\sim 1\text{--}10\text{mm}$ ) meteoroids are generally long ( $10^4$  or  $10^5$  years). In addition, meteoroids from Jupiter family comets can survive longer because their orbits are frequently altered by Jupiter. However, for some comets with low perihelion and low-moderate eccentricity, the collisional lifetimes can be short (Figure 2). These lifetimes are also dependent on the bulk density and the compressive strength of the particles. These calculations find that Geminid meteoroids of size  $5\text{ mm}$  ( $10^{-3}\text{ kg}$ ) survive 500–1000 years, for densities  $1000\text{--}3500\text{ kg/m}^3$ , respectively.  $100\mu\text{m}$  particles survive roughly 10 times longer. Thus, large particles in the Geminids and other near-sun streams might be removed by collisions on timescales shorter than the expected lifetimes of the shower particles.

These results are dependent on the accuracy of the IMEM interplanetary dust model and our collisional model. The equations given in Section 2 arise from experiments made

with a narrow range of materials that may not well describe the composition, structure or velocities of meteoroids.

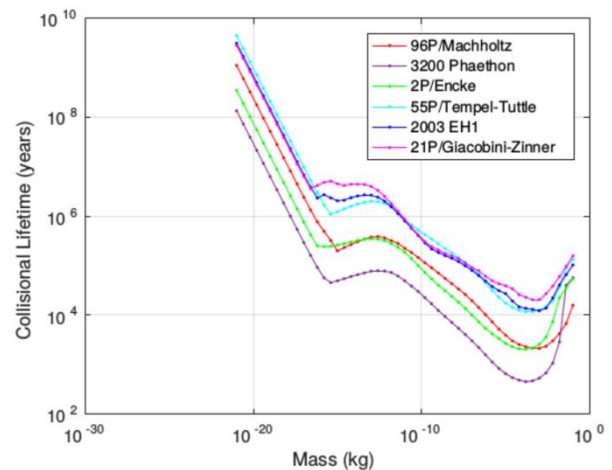


Figure 2 – Collisional lifetime as a function of mass for six probable meteor shower parent objects, for meteoroids with a bulk density of  $2000\text{ kg/m}^3$ .

Meteor shower studies and other investigations of the dust cloud might provide additional constraints to the model. For instance, no lack of large particles was found in the mass distribution of the Geminids, which might be indicative of short lifetimes, and dynamical models indicate that this meteor shower is unlikely to be able to form over only a few hundred years (Ryabova, 1999). Ryabova (1999) also estimates the age of the Geminids at about 2000 years. Additionally, other authors find meteoroid modeling requires higher collisional lifetimes, at least for some particle sizes, than those given by the model of Grün et al. (1985) (Nesvorný et al., 2012; Pokorný et al., 2014).

### 4 Conclusion

We present calculations of the collisional lifetimes of meteoroids using the formalism of Grün et al. (1985) and meteoroid fluxes and velocities from the IMEM model. We find low lifetimes for meteoroid streams with low perihelion distances.

However, further work is required to define the collisional lifetimes of large meteoroids. The lifetime depends strongly on the physical parameters of the meteoroid, including the bulk density and compressive strength. It also depends on the definition of the  $\Gamma$  parameter. Existing experimental results may not well describe the materials and impact velocities of meteoroids in interplanetary space. We are therefore investigating if the results of simulations of collisions of interplanetary particles can be used to constrain this parameter, and provide more relevant lifetime estimates.

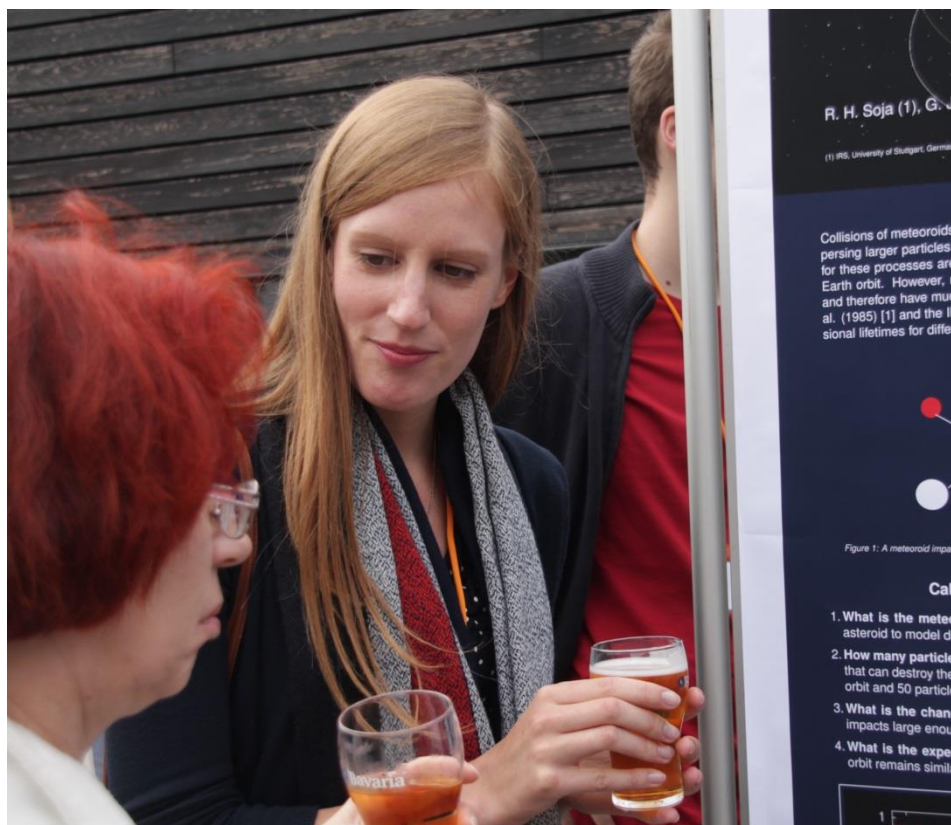
It has also been suggested that additional mechanisms may cause large grains to break up on very short timescales (Jenniskens, 2015). It is clear that questions remain about the dominant mechanisms for removing interplanetary meteoroids as a function of size.

## Acknowledgments

This work is funded under ESA contract 4000114513/15/NL/HK.

## References

- Dikarev V., Grün E., Baggaley J., Galligan D., Landgraf M. and Jehn R. (2005). "The new ESA meteoroid model". *Advances in Space Research*, **35**, 1282–1289.
- Giese R. H. and Grün E. (1976). "The compatibility of recent micrometeoroid flux curves with observations and models of the zodiacal light". *Interplanetary Dust and Zodiacal Light*, **48**, 135–139.
- Grün E., Zook H. A., Fechtig H. and Giese R. H. (1985). "Collisional balance of the meteoritic complex". *Icarus*, **62**, 244–272.
- Hörz F., Schneider E., Gault D. E., Hartung J. B. and Brownlee D. E. (1975). "Catastrophic rupture of lunar rocks - A Monte Carlo simulation". *The Moon*, **13**, 235–258.
- Jenniskens P. (2015). "Meteoroid Streams and the Zodiacal Cloud". In Michel P., DeMeo F. E. and Bottke W. F., editors, *Asteroids IV*. University of Arizona Press, Tucson, pages 281–295.
- Nesvorný D., Jenniskens P., Levison H. F., Bottke W. F., Vokrouhlický D. and Gounelle M. (2010). "Cometary Origin of the Zodiacal Cloud and Carbonaceous Micrometeorites. Implications for Hot Debris Disks". *The Astrophysical Journal*, **713**, 816–836.
- Pokorný P., Vokrouhlický D., Nesvorný D., Campbell-Brown M. and Brown P. (2014). "Dynamical Model for the Toroidal Sporadic Meteors". *The Astrophysical Journal*, **789**, id. 25, 20 pages.
- Ryabova G. O. (1999). "Age of the Geminid Meteor Stream (Review)". *Solar System Research*, **33**, 224–238.
- Tokhtas'ev V. S. (1982). "Influence of collisions of meteor bodies on the evolution rate of meteoroid streams". (Russian Title: Влияние столкновений между телами на скорость эволюции метеорных потоков), *Meteor matter in the interplanetary space*, In Bel'kovich O. I., Babadzhyanov P. B., Bronshten V. A. and Sulejmanov N. I., editors, Proceedings of the All-USSR symposium held in Kazan, USSR, Sept. 9–11, 1980. Moskow-Kazan, pages. 162–174.



Galina Ryabova and Rachel Halina Soja.

# EN091214 Zdar – one of the most precisely documented meteorite fall

Pavel Spurny, Jiri Borovicka, Jakub Haloda, Lukas Shrbeny and Tomas Zikmund

Astronomical Institute of the Czech Academy of Sciences, 251 65 Ondřejov, Czech Republic  
pavel.spurny@asu.cas.cz

This contribution will provide an overview of the current status of fireball observations conducted by the Astronomical Institute of the Czech Academy of Sciences in Ondřejov and will bring a detailed analysis of the Zdar nad Sazavou meteorite fall in the Czech Republic on 9 December 2014, which is one of the most precisely determined and predicted meteorite fall in history.



Pavel Spurny giving his lecture.

# The Swedish Allsky Meteor Network: first results

Eric Stempels<sup>1</sup> and Johan Kero<sup>2</sup>

<sup>1</sup>Department of Physics & Astronomy, Uppsala University, Sweden

Eric.Stempels@physics.uu.se

<sup>2</sup>Swedish Institute of Space Physics, Kiruna, Sweden

kero@irf.se

The Swedish Allsky Meteor Network started operations with two cameras in early 2014 and has since grown steadily. Currently, seven stations are active and several more will come online in the near future. The network to a large degree relies on low-cost stations run by private individuals or small societies of amateur astronomers. Originally based on the Danish meteor network Stjernes kud, the central node of Uppsala University provides the network with the necessary infrastructure, such as a continually updated software distribution and automatic processing of data from all stations. Although covering a very large land mass with relatively low resources is challenging, there have up to now been several well-observed events, often in collaboration with observations from neighboring countries. We give a short overview of the network's current status, chosen technical solutions, and some results.

## 1 Introduction

The Swedish Allsky Meteor Network was initiated as a response to the need of objective and empirical references for (often exaggerated) reports of meteors and meteorites in popular media. It has since grown to a fully integrated network of self-reporting all-sky camera stations that deliver data for in-depth analysis of meteors and fireballs.

Starting from a single camera at Uppsala University in early 2014, the network currently consists of seven active stations, of which four are run by amateur astronomers. Another four stations are expected to come online during 2016, and a few more stations are in an early planning stage. See also *Figure 1*.

Very similar networks have been implemented in Denmark<sup>1</sup> (currently eight cameras) and Norway<sup>2</sup> (three cameras). There is a close collaboration among these networks, and we have established a common data format for easy exchange of observations.

Detailed information on activities and results of the Swedish Allsky Meteor Network can be found online<sup>3</sup> (albeit in Swedish).

## 2 Implementation

In terms of surface area Sweden is the third largest country in Europe (after France and Spain), but has a relatively small population mainly concentrated in urban areas in the south and east. It is therefore challenging to plan for a dense network with small baselines. Instead, the network is constructed as a “citizen science” project, where interested individuals, schools and amateur astronomer societies can contribute. Central support to the network is offered by Uppsala University, providing central computing resources, software development and

webpages. Because of this format, the chosen implementations for software and hardware are deliberately kept simple, flexible and at low cost. A typical station costs €500 – €1000, depending on the exact choice of components, and there is hardly any maintenance required.

### Hardware solutions

A dedicated software package has been developed for this project. This package only requires a moderately fast CPU, and is able to run on recycled computers or small card-based Linux devices (ODROID, Raspberry Pi2 or better). The software implements the *Video4Linux (V4L)* library and therefore supports any V4L video device. While typical webcams cannot provide the sensitivity necessary for capturing meteors, V4L also supports framegrabbers, which makes it possible to combine these with high-sensitivity analog video cameras such as the popular WATEC 902H2 Ultimate (ca 0.4 Mpix) video camera. Currently four out of seven active stations use this solution, together with small f/2 180-degree fisheye lenses.

Recently, several affordable digital camera chips with fast readout have become available through the ZWO ASI brand of cameras, for which also a Linux-based API is available. Experiments with a 1/3” ASI120MC (1.2 Mpix) and the low-noise 1/1.9” ASI185MC (2.3 Mpix) led us to add support for these cameras to our software. With these new cameras routine detection of meteors down to ca  $V = 1^m$  is possible, gaining about 1–2 magnitudes compared to a WATEC 902H2 Ultimate, as well as a strong improvement in the astrometric solution due to the increased resolution. ZWO ASI cameras will be implemented in at least two stations during 2016.

### Software solutions

Software for all stations is distributed by Uppsala University through the *Subversion* version control package. Each station monitors the sky at a rate of

<sup>1</sup>“Stjernes kud”, see <http://www.stjernes kud.info>

<sup>2</sup>“Norsk Meteornettverk”, see <http://norskmeteornettverk.no>

<sup>3</sup><http://www.astro.uu.se/meteorwiki>

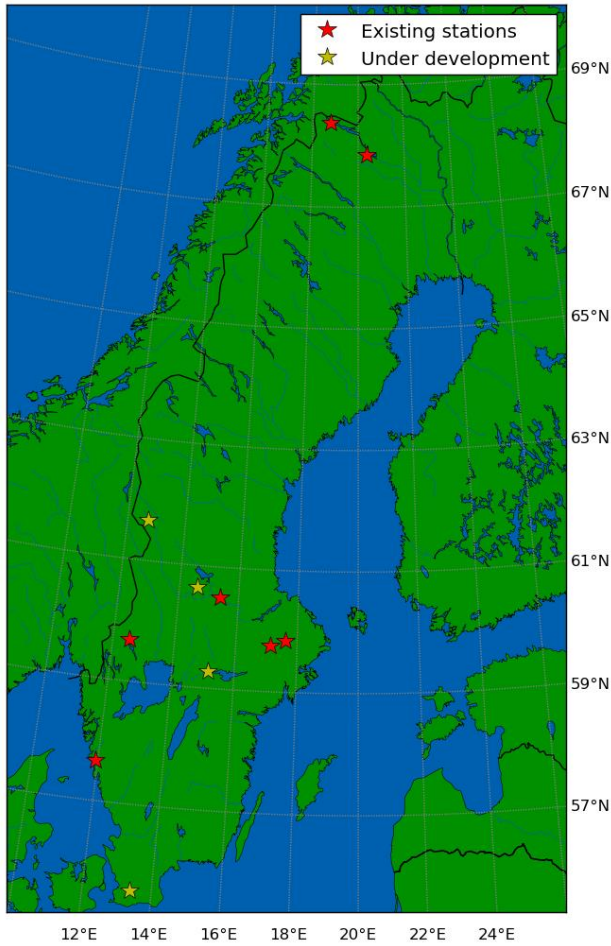


Figure 1 – An overview of the current extent of the Swedish Allsky Meteor Network.

10–25 fps, and performs on-line motion analysis and only saves video data when significant meteor-like events are detected. In addition, each node archives one-minute stacked frames for future reference. Data from each station is available on a webpage in near real-time.

Recorded events are processed at each station, calculating an astrometric solution for the observed trajectory at the sky. Events are then handed over to the central node in Uppsala, where an automatic triangulation and speed analysis of common events is performed. Events with deep atmospheric penetration are analyzed in further detail with a dark-flight code developed in Uppsala, based on the formulation of Pecina and Ceplecha (1983) and Ceplecha and Revelle (2005 – single body solution), including wind shift. The code is able to reproduce the dark flight and impact locations of other well-studied meteor falls, such as Neuschwanstein (2002), Benešov (1991) and Maribo (2009).

### 3 Results

During two years of operation the Swedish Allsky Meteor Network has detected a wide range of events. During prominent meteor showers, such as the Perseids or the Geminids, several hundreds of meteors were recorded. For about half of these events triangulated trajectories are available. Sporadic and bright fireballs that require dark-flight modelling are detected at a rate of about once to

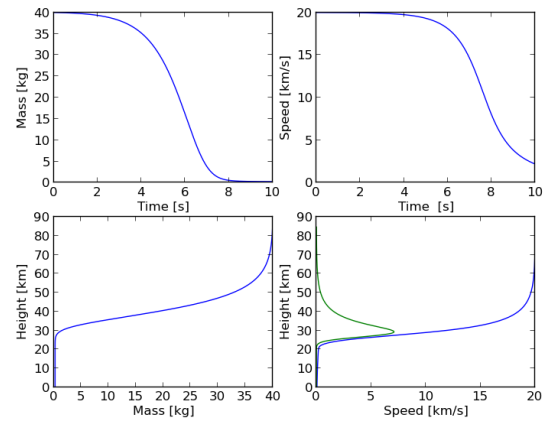


Figure 2 – Four graphs showing the simulated evolution of the meteoroid body of the August 13, 2015 fireball. The green line on the bottom right shows the deceleration of the meteoroid in  $\text{km s}^{-2}$ .

twice per month. Any bright event that might trigger public interest is published online through the network’s homepage.

A good example of what the network can achieve is the potentially meteorite-dropping fireball that was observed in the early morning of August 13, 2015. Since the fireball occurred on the same night as the Perseid meteor shower, many casual observers witnessed this event, and some even caught the luminous trail on camera. The event itself is not related to the Perseids, as is evident from its reconstructed infall trajectory.

The fireball was about as luminous as the full moon (at a distance of about 100 km), and was visible for more than 7 seconds. Five automated stations recorded the fireball, two near Uppsala, one almost below the track in Arvika, as well as two stations of the Norwegian network. The combined video data suggest an infall velocity of 20.0 km/sec, and the meteoroid appears to have come from an Aten-type orbit. As can be seen from the infall and dark-flight simulation in Figure 2 the body most likely fragmented at a height of about 35–40 km, when the meteoroid experienced a large deceleration, corresponding to a dynamic pressure of about 1 MPa. The final mass of the meteoroid fragment that reached the ground is estimated to be about 0.5 kg. Although the luminous path of the fireball is completely within Swedish territory, the predicted fall area is 10 km into Norway, close to the town of Aremark. Searches for meteorites have been conducted in this area, but no finds have been reported. These results are in agreement with independently calculated solutions by the Finnish URSA Fireball Network (Lyytinen, priv. comm.).

Another notable event detected by the Swedish network was an explosive and very luminous and slow fireball south of Stockholm in the early evening of October 23, 2015. Although simulations indicate a very high probability for this event to generate meteorites the impact area was over the Baltic Sea.

Although central Sweden now is reaching an adequate coverage of stations with baselines of 300–400 km, several fireballs were detected at great distances. Currently, the most distant events detected were recorded from Uppsala, at 650 km (Copenhagen) and 700 km (St Petersburg). Even though the accuracy of detections at such distances is not very large, these observations make it possible to confirm or deny that fireballs occurred, thereby providing valuable feedback to local media.

#### 4 Future plans

Apart from integrating new camera models in software, most development efforts are currently in improving the collaboration with neighboring countries, if possible through automatic exchange of data. In addition, we plan to continue the expansion of the Swedish network in terms of a “citizen science” project. While this is likely to improve coverage in central and southern Sweden, it will be more challenging to monitor northern Sweden, with a relatively low population density. Depending on the

available funding, we are therefore also considering to design “packaged” stations, where a prospective user only needs to assemble the station and make it available online.

#### Acknowledgments

We acknowledge support from the *Märta and Erik Holmberg endowment*, which financed the first allsky meteor camera in Sweden.

#### References

- Pecina P. and Cepelch Z. (1983). “New aspects in single-body meteor physics”. *Bulletin of the Astronomical Institutes of Czechoslovakia*, **34**, 102–121.
- Cepelch Z. and Revelle D. O. (2005). “Fragmentation model of meteoroid motion, mass loss, and radiation in the atmosphere”. *Meteoritics and Planetary Science*, **40**, 35–54.



Reception manned by Dragana Okolić and Dušan Bettonvil.

# No sign of the 2015 Daytime Sextantids through combined radio observations

Giancarlo Tomezzoli<sup>1</sup> and Lorenzo Barbieri<sup>2</sup>

<sup>1</sup> EurAstro Association, Zeppelinstrasse 43, D-81669 Munich, Germany  
gt@gmx.de

<sup>2</sup> Associazione Astrofili Bolognesi, Via Sebastiano Serlio 25/2, c/o Parco DLF, I-40100 Bologna, Italy  
barbieriofiuco@gmail.com

To investigate the presence or absence of the daytime Sextantids in the year 2015, the EurAstro Radio Station (EARS) in Munich (DE) performed a combined radio observation campaign together with the Radio Astronomy and Meteor Bologna (RAMBO) radio station located in Bologna (IT). The combined radio observations of EARS and RAMBO are in mutual agreement and confirm that, as in the year 2014, also in the year 2015 no evidence has existed of a meteor activity due the 2015 daytime Sextantids.

## 1 Introduction

DSX 221<sup>1</sup> also indicated as Sextantids is a daytime meteor shower having features not well-known. It was discovered by Weiss in September 1957, who recorded 30 meteors per hour. No more Sextantids were reported until 1961. The next shower was observed in 1969, so the hypothesis has been advanced that DSX 221 is a four year periodic meteor shower.

Following the invitation made by Rendtel at the IMC 2014 in Giron, France (Rendtel, 2014) to observe DSX 221 in the period 30 September – 05 October 2014 by any possible means, the EurAstro Radio Station (EARS) in Munich, Germany (48°07'58,0"N, 11°34'47.3"E) performed radio observation of DSX 221 in the recording period 30/09/2014, 07h00m UT – 05/10/2014, 16h00m UT (Tomezzoli and Verbeeck, 2015). The conclusion was that the meteor activity of DSX 221, if present at all, was at a much lower level than the sporadic meteor activity.

In order to investigate the presence or absence of the daytime Sextantids in the year 2015, EARS performed a combined radio observation campaign together with the Radio Astronomy and Meteor Bologna (RAMBO) radio station located in Bologna, Italy (44°30'28,9"N, 11°21'12,0"E).

## 2 EARS and RAMBO combined radio observation

EARS, based on the forward scattering principle and operated by Giancarlo Tomezzoli, adopted the same observation configuration adopted in the year 2014: radio beacon from the GRAVES radar (emitter at Broysès-lès-Pesmes, 47°20'51.72"N, 05°30'58.68"E, about 500 km from Munich), vertical antenna J-Pole 144, receiver ICOM 1500 (USB mode, 143.049 MHz), computer Pavillion dv6 (processor Intel Core Duo T2500) and SpecLab V26 b10 as recording software. The EARS radio observation in the recording period from 27/09/2015,

08h15m UT – 03/10/2015, 07h30m UT proceeded smoothly without problems. Meteor radio echoes were counted visually by Giancarlo Tomezzoli by looking at the JPG images recorded by SpecLab every 5 minutes.

RAMBO, based on the forward scattering principle and operated by Lorenzo Barbieri and others, adopted the following observation configuration: radio beacon from the GRAVES radar (about 500 km from Bologna), Yagi 7 elements antenna, Yaesu 897 receiver, Arduino microcontroller and homemade recording software. The RAMBO radio observation in the recording period from 28/09/2015, 00h00m UT – 04/10/2015, 00h00m UT proceeded smoothly without problems. Meteor radio echoes were counted by an ad hoc developed RAMBO software and plotted in graphic form by using Gnuplot<sup>2</sup>.

The EARS observed hourly meteor radio echo rates in the EARS observing period are summarized in the diagrams of *Figure 1*. Evidently the meteors of DSX 221, if any, were superposed on the ever present sporadic meteors. To better characterize the meteor radio echoes in the recording period, an underdense radio echo from the images recorded by EARS was assumed as underdense reference radio echo to distinguish between recorded underdense strong and faint radio echoes. The results of

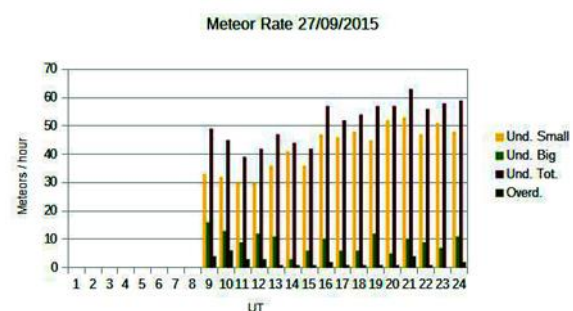


Figure 1a – EARS observed hourly meteor radio echo rates during the EARS recording period: 27 September 2015.

<sup>1</sup> <http://www.bbc.co.uk/dna/ptop/plain/A40721212>

<sup>2</sup> <http://www.gnuplot.info/>

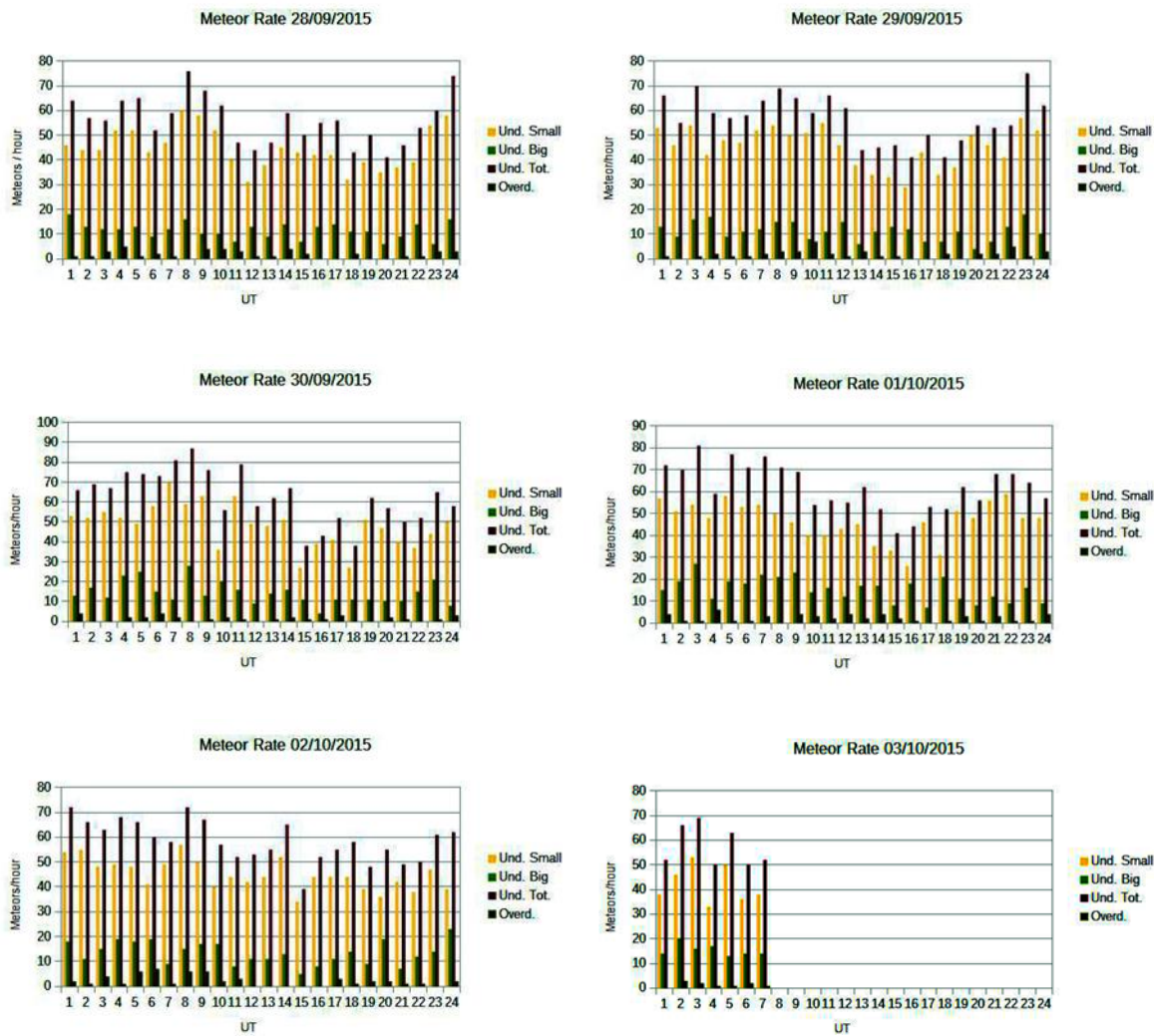


Figure 1b, 1c, 1d, 1e, 1f, 1g – EARS observed hourly meteor radio echo rates during the EARS recording period: 28 September – 3 October 2015.

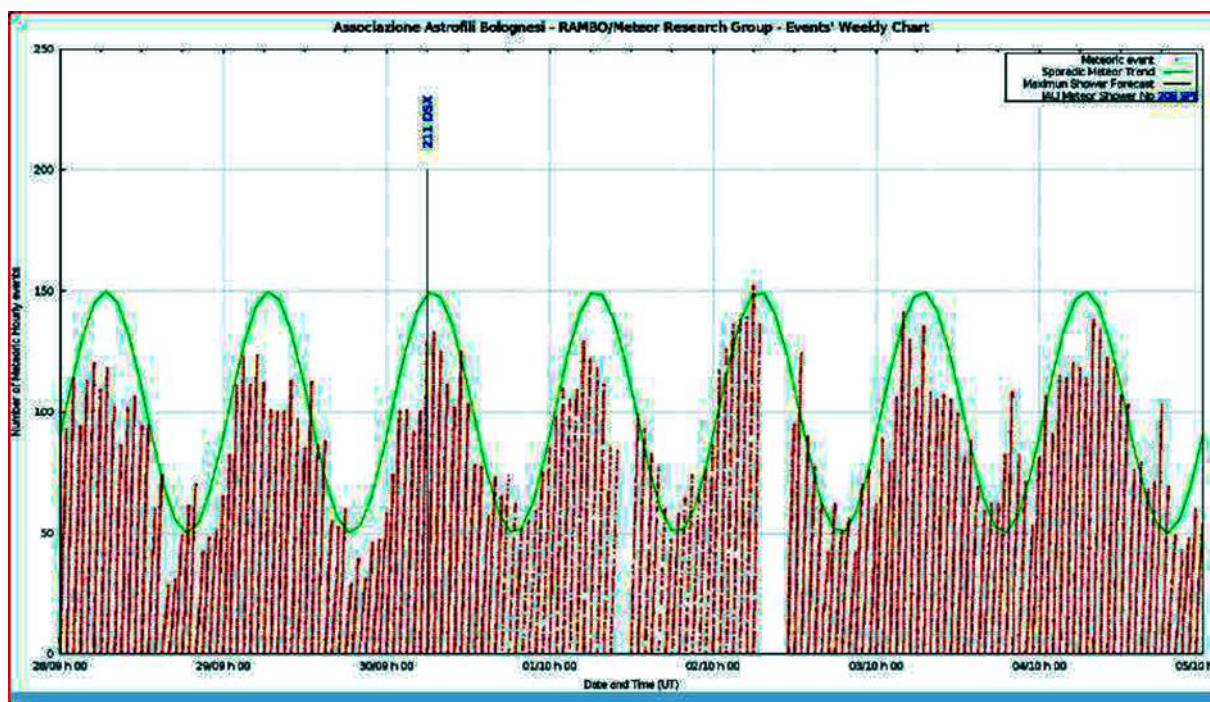


Figure 2 – RAMBO observed hourly meteor radio echo rates during the RAMBO recording period – the position of the expected maximum of DSX 221 is indicated.

the comparison are shown in *Figure 1*. Looking at the diagrams in *Figure 1*, it is possible to recognize that during the EARS recording period no maximum attributable to DSX 221 was detected.

The RAMBO observed hourly meteor radio echo rates in the RAMBO observing period are summarized in the diagram of *Figure 2*. Looking at the diagram in *Figure 2*, it is possible to recognize that during the RAMBO recording period no maximum attributable to DSX 221 was detected.

### 3 Conclusions

The combined radio observations of EARS and RAMBO are in mutual agreement and confirm that, as in the year 2014, also in the year 2015 no evidence has existed of a meteor activity due the 2015 daytime Sextantids.

### References

- Rendtel J. (2014). “Daytime meteor showers”. In Rault J.-L. and Roggemans P., editors, *Proceedings of the International Meteor Conference*, Giron, France, 18-21 September 2014. IMO, pages 93–97.
- Tomezzoli G., Verbeeck C. (2015). “No sign of the 2014 Daytime Sextantids and mass indexes determination from radio observations”. In Rault J.-L. and Roggemans P., editors, *Proceedings of the International Meteor Conference*, Mistelbach, Austria, 27-30 August 2015. IMO, pages 165–170.



Mirel Birlan and Tudor Georgescu in a silent corner in the restaurant.

# AMOS - trajectory and orbital data from SVMN and Canary Islands

Juraj Tóth<sup>1</sup>, Leonard Kornoš<sup>1</sup>, František Ďuriš<sup>1</sup>, Pavol Zigo<sup>1</sup>, Štefan Gajdoš<sup>1</sup>, Dušan Kalmančok<sup>1</sup>, Jozef Világi<sup>1</sup>, Jaroslav Šimon<sup>1</sup>, Marek Buček<sup>1</sup>, Jaroslav Šimon<sup>1</sup>, Miquel Serra-Ricart<sup>2</sup>, Juan Carlos Perez<sup>2</sup>, Javier Licandro<sup>2</sup>, Ovidiu Vaduvescu<sup>2</sup> and Jürgen Rendtel<sup>3</sup>

<sup>1</sup> Dept. of Astronomy, Physics of the Earth and Meteorology, Faculty of Mathematics, Physics and Informatics, Comenius University in Bratislava, Slovak Republic  
toth@fmph.uniba.sk

<sup>2</sup> Instituto de Astrofísica de Canarias, Canary Islands, Spain

<sup>3</sup> International Meteor Organization

The Slovak Video Meteor Network based on four stations from October 2013 (double station from 2009) and two cameras on the Canary Islands from March 2015 have recorded several tens of thousands meteors by the end of 2015. Naturally, only a part (about 20%) was observed simultaneously. Using precise all-sky astrometry (Borovička, 1995) and our own trajectory and orbit program based on Ceplecha (1987), we gained the reliable video meteors database for further meteor studies.

## 1 Introduction

Observations are performed every clear night, even in partly cloudy sky and during all Moon phases. The optical system is identical in all four Slovakian stations (camera resolution 1280 × 960 pixels, 15 frames per second, Tóth et al., 2011; Zigo et al., 2013). The only difference with the Canary Islands and Atacama Desert stations in Chile is the camera resolution 1600 × 1200 pixels, 20 frames per second (Tóth et al., 2015). All together from March 2016, 8 AMOS cameras are working from both hemispheres.

Currently, the UFOAnalyzer software (SonotaCo) provides us the identification of stars and meteors on individual frames. Astrometry from the all-sky reduction method of Borovička (1995) is used for special events following the atmospheric trajectory and orbit calculation by our own program MT 2.4 based on Ceplecha (1987). Automatization and more precise photometric reduction of data reduction will be done in the near future.

The database will be publicly available with all atmospheric and orbital parameters including uncertainties from the Monte Carlo error propagation (Kornoš et al., 2015).

## 2 Conclusion

We have successfully developed, tested and installed AMOS cameras in Slovakia, on the Canary Islands and in the Atacama Desert in Chile. The data will be available soon.

## Acknowledgment

This work was supported by APVV-0517-12, and VEGA 1/0225/14.

## References

- Borovička J., Spurný P. and Keclikova J. (1995). “A new positional astrometric method for all-sky cameras”. *Astronomy and Astrophysics Supplement*, **112**, 173–178.
- Ceplecha Z. (1987). “Geometric, dynamic, orbital and photometric data on meteoroids from photographic fireball networks”. *Bulletin of the Astronomical Institutes of Czechoslovakia*, **38**, 222–234.
- Kornoš L., Ďuriš F. and Tóth J. (2015). “Astrometric precision and orbit determination by AMOS”. In Rault J.-L. and Roggemans P., editors, *Proceedings of the International Meteor Conference*, Mistelbach, Austria, 27-30 August 2015. IMO, pages 101–104.
- Tóth J., Kornoš L., Vereš P., Šilha J., Kalmančok D., Zigo P. and Világi J. (2011). “All-Sky Video Orbits of Lyrids 2009”. *Publications of the Astronomical Society of Japan*, **63**, 331–334.
- Tóth J., Zigo P., Kalmančok D., Simon J., Kornos L., Világi J., Rudawska R., Serra-Ricart M., Perez J. C. and Licandro J. (2015). “5 months of AMOS on the Canary Islands”. In Rault J.-L. and Roggemans P., editors, *Proceedings of the International Meteor Conference*, Mistelbach, Austria, 27-30 August 2015. IMO, pages 63–65.
- Zigo P., Tóth J. and Kalmančok D. (2013). “All-Sky Meteor Orbit System (AMOS)”. In Gyssens M. and Roggemans P., editors, *Proceedings of the International Meteor Conference*, La Palma, Canary Islands, Spain, 20-23 September 2012. IMO, pages 18–20.

# Expedition Atacama - project AMOS in Chile

Juraj Tóth<sup>1</sup> and Stanislav Kaniansky<sup>2</sup>

<sup>1</sup> Dept. of Astronomy, Physics of the Earth and Meteorology, Faculty of Mathematics, Physics and Informatics, Comenius University in Bratislava, Slovak Republic  
toth@fmph.uniba.sk

<sup>2</sup> Hvezdáreň v Banskej Bystrici, organizačná súčasť Krajskej hvezdárne a planetária  
M. Hella v Žiari nad Hronom

The Slovak Video Meteor Network operates since 2009 (Tóth et al., 2011). It currently consists of four semi-automated all-sky video cameras, developed at the Astronomical Observatory in Modra, Comenius University in Bratislava, Slovakia. Two new generations of AMOS (All-sky Meteor Orbit System) cameras operate fully automatically at the Canary Islands, Tenerife and La Palma, since March 2015 (Tóth et al., 2015). As a logical step, we plan to cover the southern hemisphere from Chile. We present observational experiences in meteor astronomy from the Atacama Desert and other astronomical sites in Chile. This summary of the observations lists meteor spectra records (26) between Nov.5–13, 2015 mostly Taurid meteors, single and double station meteors as well as the first light from the permanent AMOS stations in Chile.

## 1 Introduction

The main aim of the expedition was to select two sites for the new AMOS cameras in Chile. Sites need to have a local infrastructure and good observing condition. Moreover, the responsible persons need to agree with such installation.

## 2 Sites selection and installation

In this paper, we present observational experiences in meteor astronomy from the Atacama Desert and other astronomical sites in Chile. The summary of the observations lists meteor spectra records (26) between Nov. 5–13, 2015 mostly from Taurid meteors (*Figure 2*). We also present fish-eye views from selected sites with ideal astronomical conditions as well as sky brightness observations. We measured the mean sky background at SpaceObs (*Figure 1*) of 21.75 mag./sq.arsec influenced by strong airglow emission.

Finally, we have selected two sites for location and installation of the AMOS cameras at SpaceObs near San Pedro de Atacama and Paniri Caur observatory near Calama. The distance between these two stations is 83.5 km and is ideal for trajectory and orbit calculations depending on the meteor plane with respect to both stations. The small private observatory Paniri Caur is situated in the village Chiu-Chiu 30 km North-East from Calama city. The altitude of the observatory is at 2533 m above sea level. The second site was selected after the agreement with Alain Maury in SpaceObs, which is 6 km South of San Pedro de Atacama at 2400 m altitude.

The installation of the two AMOS systems was performed successfully in March 2016 by Pavol Zigo and Jaroslav Šimon.

## 3 Conclusion

We have successfully selected and installed AMOS cameras in the Atacama Desert in Chile. The cameras are working fine in the desert conditions.

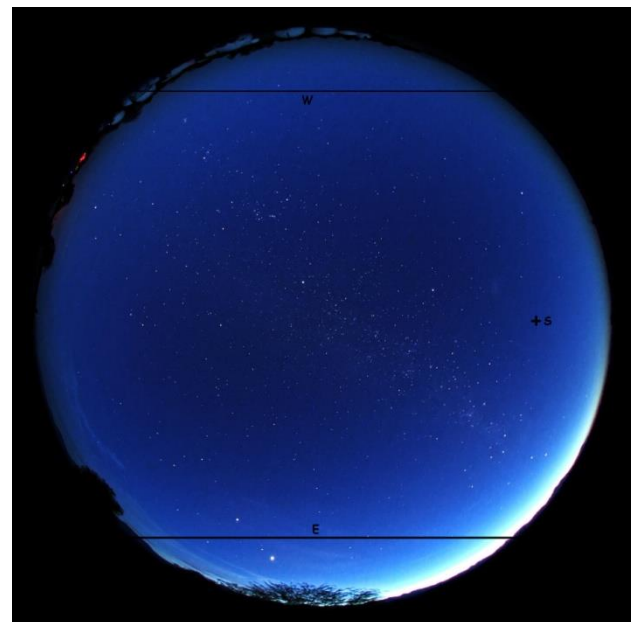


*Figure 1* – Fish-eye view of the sky from San Pedro de Atacama (SpaceObs). The actual field of view of AMOS is depicted by black lines on the West and East side.

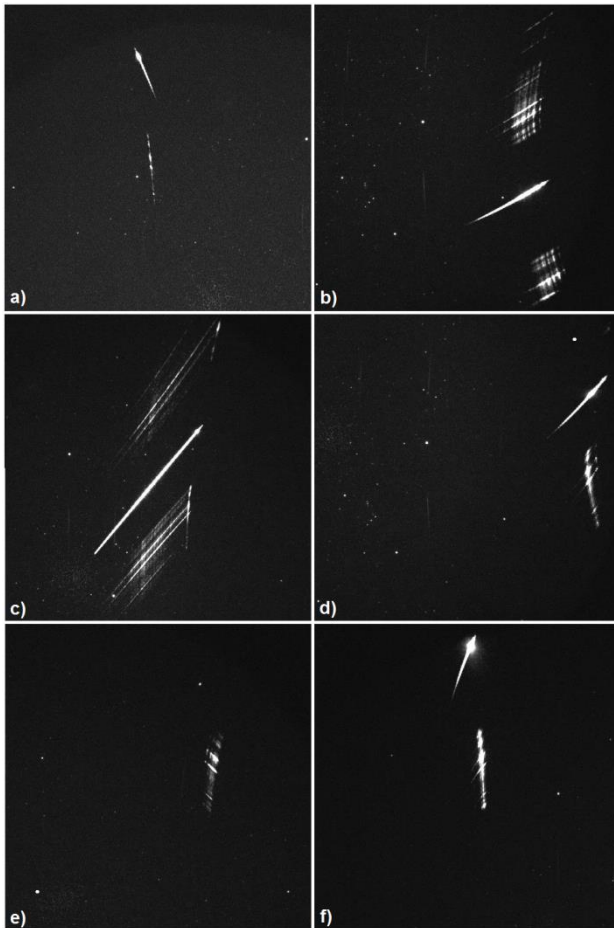


Figure 2 – Meteor spectra of Taurids by the AMOS camera with 500 lp/mm gratings. The observation was performed from San Pedro de Atacama on November 5–12, 2015.

## Acknowledgment

This work was supported by APVV-0517-12, and VEGA 1/0225/14. We would like to thank Ján Mäsiar, R. Piffli, I. Majchrovič for the photographic techniques we used during the expedition and the local staff in SpaceObs, Paniri Caur and Pangué Observatory.

## References

- Tóth J., Kornoš L., Vereš P., Šilha J., Kalmančok D., Zigo P. and Világi J. (2011). “All-Sky Video Orbits of Lyrids 2009”. *Publications of the Astronomical Society of Japan*, **63**, 331–334.
- Tóth J., Zigo P., Kalmančok D., Simon J., Kornos L., Világi J., Rudawska R., Serra-Ricart M., Perez J. C. and Licandro J. (2015). “5 months of AMOS on the Canary Islands”. In Rault J.-L. and Roggemans P., editors, *Proceedings of the International Meteor Conference*, Mistelbach, Austria, 27-30 August 2015. IMO, pages 63–65.

# AMOS-Spec - meteor spectra from Modra Observatory

Juraj Tóth<sup>1</sup>, Pavol Matlovič<sup>1</sup>, Regina Rudawska<sup>2</sup>, Pavol Zigo<sup>1</sup> and Dušan Kalmančok<sup>1</sup>

<sup>1</sup>Dept. of Astronomy, Physics of the Earth and Meteorology, Faculty of Mathematics,  
Physics and Informatics, Comenius University in Bratislava, Slovak Republic  
toth@fmph.uniba.sk

<sup>2</sup>ESA/ ESTEC, Noordwijk, the Netherlands

We present results from the meteor spectra program at Modra observatory, Slovakia (Comenius University in Bratislava) in the period November 2013 – April 2016. The advantage of the program is the presence of the Slovak Video Meteor Network and close collaboration with the European Fireball Network and CEMENT and EDMOND networks which provide trajectory and orbital data for almost all observed meteor spectra.

## 1 Introduction

The primary aims of our research are focused on determining the spectral and physical differences between cometary and asteroidal bodies, the role of sodium abundance in meteoroids, and the spectral characteristics of different shower and sporadic meteors. We utilize the observations of the spectral All-sky Meteor Orbit System (AMOS-Spec), which provides a systematic survey of meteor spectra since November 2013. The system is installed at the Modra observatory with the setup based on the standard AMOS system (Tóth et al., 2011) equipped with a 30 mm f/3.5 lens (FOV  $\sim 140^\circ \times 100^\circ$ ), and 1000 grooves/mm grating yielding a spectral resolution of  $\sim 1.3$  nm/pix. The absolute limiting magnitude of a meteor with spectrum is around -2.

First results (Rudawska et al., 2016) demonstrated the capability of the system and showed promise in pursuing our scientific goals. Here, we report the results of 131 meteor spectra collected during 11/2013 – 04/2016.

The analyzed spectral events were corrected for dark current, flat-fielded, and divided by the spectral response curve of the system. Before evaluating the relative intensities of studied emission lines of the meteoroid atoms and ions, the continuum radiation and atmospheric lines were subtracted from the spectrum.

## 2 Conclusion

The presence of the Slovak Video Meteor Network (SVMN) consisting of 4 additional AMOS stations in Slovakia enabled multi-station observations of studied meteors. Additional observations were kindly provided by Pavel Spurný (European Fireball Network) and Jakub Koukal (Central European Meteor Network). Of the 131 meteors captured with spectra, 103 were observed by multiple stations, which allows us to determine heliocentric orbits and additional physical properties of

meteoroids such as the photometric mass, material strength parameters Kb and PE (Ceplecha, 1988) and dynamical pressure causing the meteoroid fragmentation (Popova et al., 2011). Results will be available in another publication.

## Acknowledgment

This work was supported by APVV-0517-12, and VEGA 1/0225/14.

## References

- Borovička J., Koten P., Spurný P., Boček J. and Štork R. (1995). “A survey of meteor spectra and orbits: evidence for three populations of Na-free meteoroids”. *Icarus*, **174**, 15–30.
- Ceplecha Z. (1988). “Earth's influx of different populations of sporadic meteoroids from photographic and television data”. *Bulletin of the Astronomical Institutes of Czechoslovakia*, **39**, 221–236.
- Rudawska R., Tóth J., Kalmančok D., Zigo P. and Matlovič P. (2016). “Meteor spectra from AMOS video system”. *Planetary and Space Science*, **123**, 25–32.
- Tóth J., Kornoš L., Vereš P., Šilha J., Kalmančok D., Zigo P. and Világi J. (2011). “All-Sky Video Orbits of Lyrids 2009”. *Publications of the Astronomical Society of Japan*, **63**, 331–334.
- Popova O., Borovička J., Hartmann W. K., Spurný P., Gnos E., Nemtchinov I. and Trigo-Rodríguez J. M. (2011). “Very low strengths of interplanetary meteoroids and small asteroids”. *Meteoritics and Planetary Science*, **46**, 1525–1550.

# Rediscovery of Polish meteorites

Zbigniew Tymiński<sup>1,2</sup>, Marcin Stolarz<sup>1</sup>, Przemysław Żołądek<sup>1</sup>,  
Mariusz Wiśniewski<sup>1</sup> and Arkadiusz Olech<sup>1,3</sup>

<sup>1</sup> Polish Fireball Network, Comets and Meteors Workshop, ul. Bartycka 18, 00-716 Warszawa, Poland  
pkim.inbox@gmail.com

<sup>2</sup> National Centre for Nuclear Research RC POLATOM, ul. Sołtana 7, 05-400 Otwock, Poland  
Zbyszek.tyminski@gmail.com

<sup>3</sup> Copernicus Astronomical Center, Polish Academy of Sciences, ul. Bartycka 18, 00-716 Warszawa, Poland  
olech@camk.edu.pl

The total number of Polish registered meteorites (by July 2016) including the meteoritical artifacts as Czestochowa Raków I and II is 22. Most of them are described by the pioneer of Polish Meteoritics Jerzy Pokrzywnicki who also identified the meteorite fall locations. In recent years prospectors found impressive specimens of known Polish meteorites such as Morasko: 34 kg, 50 kg, 164 kg, 174 kg and 261 kg or Pultusk: 1578 g, 1576 g, 1510 g, 610 g and 580 g expanding and determining precisely the known meteorite strewn fields.

## 1 Introduction

The history of meteoritics in Poland dates back to the early nineteenth century due to Vilnius Log (Dziennik Wileński) which was the only science bulletin at that time in Polish language publishing the information about the meteorites especially about the falls. The large historical meteorite drops such as Białystok (1827) and Pultusk (1868) didn't allow the scientists to leave this extraordinary subject. In 1894 Ernest F. Chladni, German physicist, published a groundbreaking essay about falling rocks from space but decades earlier in 1825, Feliks Drzewiński presented in Polish the article "Of meteoritic stones and the reasons that could create them", unfortunately with the explanation out of truth. During today's the keen interest in the subject continues but it seems that is more by amateurs than by scientists. A very large group of Polish enthusiasts dealing with meteorites but people associated with meteorites professionally forms a small community. The phenomenon of a sizeable group of meteorite hunters in our country is supported also by the law which fortunately does not prohibits to collect meteorites (but one needs the permission of the Environment Ministry for abroad transportation), unlike archaeological sites, where searching with a metal detector can lead to serious consequences not only in Poland.

## 2 Most famous meteorite falls

### Pultusk, chondrite fall 1868

The largest meteorite fall observed in the modern history, before February 2013 when the superbolide Chelyabinsk appeared, was the Pultusk meteorite. In Chelyabinsk, the bolide dropped a huge number of meteorites from which a large part is still lying in the fields around the village of Pervomaisky. The fall of Pultusk was similar and both falls are classic examples of "meteorites shower". Pieces from the Pultusk meteoroid (type H4/5) felt at least in the area of the village Obryte to St. Rosalie and Rzewnie (15

km long) forming a strewn field divided into two relatively equal parts by the Narew river. Around this river prospectors try their luck hunting for meteorites with a much better effect than the lottery win. Because the area was flooded in the time of the fall, some meteorites have not been picked up there. Nowadays the fact that the riverbed of the Narew is shifted and the drainage was done in the fields it gives high chances to find meteorites. Today seekers equipped with specialized detectors (for stony meteorites type VLF is recommended) bring a few to several new meteorites each year from fields in Pultusk. The biggest masses of finds during last years were 1578 g (Bingoraj, 2008), 1510 g (Smuła, 2009), 580g (Stolarz, 2010), and 1576 g (Kosmowski, 2015). The biggest pieces discovered just after the fall were about 9 kg and two pieces of about 8 kg (one meteorite is kept by the Earth Museum of the Polish Academy of Sciences and the others are in the Natural History Museums in London and in Berlin). Pultusk is also known from many small meteorites called "pultusk peas" – the total number was estimated to 70000 pieces (Samsonowicz, 1952). The main supplier of this meteorite for Europe was German mineral dealer F. Krantz (he sold about 7000 pieces). Thanks to him the Pultusk meteorites are in all the famous museum collections in the world. They are also in many private collections.

### Białystok, eucrite fall 1827

The second famous meteorite in Poland is Białystok because of its observed fall in a time when people didn't believe that stones can originate from the "sky". The prove was about 4 kg of meteorites collected after the loudly fall event that scared many people. There are also reports of meteorites, which were kept in the homes till the 60's of the last century. In Poland, there are few specimens of the meteorite – only one sample (4 grams) is in the collection of Museum of Earth in Warsaw, the others are just a few but with not really known origin.



Figure 1 – The map of strewn field of Pultusk taken from the pamphlet published by Central School in Warsaw few years after the fall.



Figure 2 – The Pultusk 580g-specimen just after it was dug out from the soil (photo by M. Stolarz).

The meteorite is part of the Vesta asteroid group as eucrite. The Białystok strewn field is a place to which one would be happy to come back. Some people are convinced that meteorites can still be found around the Supraśl river but the effort of meteorite hunters didn't bring any positive results yet.

### **Łowicz, mesosiderite fall 1935**

Mesosiderites, the type of meteorites that contains a similar amount of achondritic material rock and iron, most of them come from Vesta. Isotopic studies indicate their impact origin and indeed the results of the analysis made by the DAWN mission confirmed this assumption (as revealed the presence of diogenites, eucrites and howardites in the mantle of this asteroid). These are widely recognized among the Polish collectors of meteorites due to the rarity of their occurrence, and probably also due to the Łowicz meteorite, which is the representative of this group. In contrast to Białystok this meteorite is commonly known in the site of fall. The systematic search led to the discovery of 49 kg from an estimated 110 kg – two biggest were 10 and 8 kg and the searchers noticed some craters produced by impacts. There are also documented meteorites held by the local people long after the World War II. For this reason the area of the Łowicz meteorite fall is visited by meteorite hunters and apparently even one specimen was found after years of searching. Unfortunately nothing more about this find is known.

## **3 Most famous meteorite finds**

### **Świecie, IIIAB iron meteorite, 1850**

The meteorite Schwetz (Świecie) has been excavated in 1850 on the left bank of the Wda river during the works on the construction of the railway line leading to East Prussia. Information from some sources mentions that 21.5 kg meteorite has been excavated at the flattening of the hill-top for the railway line from the depth of 3–4 feet and that it broke up into three parts after excavation. There is ambiguous information about the location of the meteorite find – one report describes the excavation close to the bridge girders, another one says a meteorite was found next to the Konopat town. A couple of searching campaigns were organized in this area but due to the unknown location of this find they failed.

### **Przelazy, iron IAB-MG iron meteorite**

In the middle of the seventeenth century a local farmer in the village of Przelazy (Seeläsgen) found a lump of iron while digging a trench – it weighted 102 kg. In 1847 the stone was recognized as a meteorite and taken to Wrocław. In 1852, Clark Smith described the meteorite as an oval body covered by a thin layer of weathered iron (0.5–1.5 mm). There were no signs of fragmentation and the meteorite was covered with regmaglypts. Today, a number of attempts were made to find any remaining fragments. Some specimens were found on the eastern side of the lake by Mr. Henryk Nowacki. There are more explorations planned to confirm the findings.

### **Morasko, IAB-MG iron meteorite, 1914**

The Morasko represents one of the biggest iron meteorite falls in Europe. The strewn field was discovered by World War I soldiers, digging trenches in 1914 near Poznań. A mass of rock weighing approximately 77.5 kg was first extracted. Then more masses were discovered in 1936, 1956, 1992, 1995 and up to 2015 totaling about 1 ton of known meteorites. The meteorite is classified as an octahedrite IAB-MG – the most popular iron type but is distinctive from the other meteorites by the low iridium while gallium content is high. Among the Polish meteorites the Morasko is the easiest to find. It can be done using the simplest type of metal detector. There is a group of depressions associated with the fall. They were found by Jerzy Pokrzywnicki as craters. In recent years, prospectors found near them an impressive specimen of Morasko, as big as: 164 kg (Socha, 2006), 261 kg (Smuła and Skirzewska, 2012), 174 kg (Owczarzak and Nebelski, 2015).

### **Zakłodzie, enstatite achondrite-ungrouped**

At the end of September 1998 Mr Stanisław Jachymek - collector of minerals found a “strange”, heavy and rusty stone. The stone was lying on the road near the forest between the villages “Zakłodzie Dół” and “Zakłodzie Góra”. After examining the find it turned out to be a rare specimen of a meteorite, weighing 8.68 kg. Further research (noble gases) showed that the meteorite (despite weathering) is a relatively fresh fall. Under the layer of the weathering a fusion crust is visible. It has been discovered that most probably the meteorite fell in April 1898 (one hundred years earlier). At this time a very bright fireball was seen from the south-east of Poland and this was described in local newspapers. Unfortunately, further explorations by Mr Jachymek and other meteorite hunters were unsuccessful.

## **4 Unclassified meteorite**

### **Siewierz meteorite**

The last Polish find is meteorite Siewierz, not registered yet. The meteorite sparked debate in the Polish meteorite world, because is shrouded in mystery since the story of its discovery is unknown. Meteorite Paris was recorded in 2010. It probably does not come from Paris, but was rediscovered in 2001 in a box with various objects belonging to a mining engineer working in the French Colonies. These items, together with the meteorite were purchased on sale in Paris, hence the name of the meteorite. The meteorite was registered as “unknown location”. We have now a similar case – a meteorite, Siewierz, was recognized in the collectibles of the grandfather of the finder, deceased 20 years ago. A photo of the specimen and later a fragment was handed over to check by some jeweler and collector of meteorites, who confirmed its cosmic origin. In this way the finders proved this as suspicion and we have a chance for a 23<sup>th</sup> Polish meteorite. There are some investigators trying to find out the history of the meteorite either in libraries searching local archives or by scientific research.

## 5 Conclusion

There are relatively few meteorites discovered in Poland (22). Most of them are described by the pioneer of Polish Meteoritics Jerzy Pokrzywnicki who identified also the meteorite fall locations. Those known meteorite strewn fields can be still successfully exploited. The fields where meteorites dropped from huge bolides such as Pułtusk or Morasko can still bring additional material for research and for collections. For this reason many prospectors try to find meteorites there. In recent years meteorite hunters found impressive specimens of meteorites in Morasko: 34 kg, 50 kg, 164 kg, 174 kg and 261 kg. The pieces found last years in Pułtusk field were still smaller than known museum specimens, weighting: 1578 g, 1576 g, 1510 g, 610 g and 580 g.

The classification and description of Polish meteorites can be found on the Meteoritical Bulletin site<sup>1</sup>.

## Acknowledgment

We are thankful to the NCN for research funds – Grant no. 2013/09/B/ST9/02168.

## References

- Borovička J., Spurný P., Brown P., Wiegert P., Kalenda P., Clark D. and Shrubny L. (2013). “The trajectory, structure and origin of the Chelyabinsk asteroidal impactor”. *Nature*, **503**, 235–237.
- Buchwald V. F. (1975). “Handbook of Iron Meteorites. Their History”. Distribution, Composition, and Structure, University of California Press, Berkeley.
- Hanczke T. (1995). “Meteority i tektyty w zbiorach Muzeum Ziemi. Katalog”. Muzeum Ziemi, Warszawa (in Polish).
- Kosiński J. and Kamińska E. (2011). “The Fall and Distribution of Fragments Pułtusk Meteorite”. *Acta Societatis Meteoriticae Polonorum*, **2**, 57–66 (in Polish).
- Krzesińska A. and Fritz J. (2014). “Weakly shocked and deformed CM microxenoliths in the Pułtusk H chondrite”. *Meteoritics and Planetary Science*, **49**, 595–610.
- Krzesińska A., Gattacceca J., Friedrich J. M. and Rochette P. (2015). “Impact-related noncoaxial deformation in the Pułtusk H chondrite inferred from petrofabric analysis”. *Meteoritics and Planetary Science*, **50**, 401–417.
- Lang B. and Kowalski M. (1971). “On possible number and mass of fragments from Pułtusk meteorite shower”. *Meteoritics*, **6**, 149–158.
- Lang B. (1972). “On the mass distribution of fragments from Lowicz meteorite shower 1935”. *Earth and Planetary Science Letters*, **14**, 245–248.
- Norton O. R. (2002). “The Cambridge Encyclopedia of Meteorites”. Cambridge.
- Norton O. R. and Chitwood L. (2008). “Field Guide to Meteors and Meteorites”. Cambridge.
- Pokrzywnicki J. (1964). “I. Meteority Polski. II. Katalog meteorytów w zbiorach polskich”. *Studia Geologica Polonica*, **XV**, 114–115.
- Pilski Andrzej S. (1995). “The Białystok meteorite shower”. *Meteoritel*, **1**, 22–23.
- Pilski A. S. (1999). “Nieziemskie skarby, Prószyński i S-ka”. Warszawa (in Polish).
- Pilski A. S., Wasson J. T., Muszyński A., Kryza R., Karwowski Ł. and Nowak M. (2013). “Low-Ir IAB irons from Morasko and other locations in central Europe: One fall, possibly distinct from IAB-MG”. *Meteoritics and Planetary Science*, **48**, 2531–2541.
- Przylibski T. A., Zagożdżon P., Kryza R. and Pilski A. S. (2005). “The Zakłodzie enstatite meteorite: Mineralogy, petrology, origin and classification”. *Meteoritics and Planetary Science*, **40**, 185–200.
- Rose G. (1852). “On the Meteoric mass discovered at Schwetz”. *American Journal of Science and Arts*, **13**, 142.
- Rose G. (1863). “Systematisches Verzeichniss der Meteoriten in dem mineralogischen Museum der Universität zu Berlin”. *Annalen der Physik*, **118**, 419–423.
- Samsonowicz J. (1952). “The age, origin, presumed number and mass of Pułtusk meteorite”. *Wiadomości Muzeum Ziemi*, **VI**, 57–68 (in Polish).
- Stankowski W. (2001). “The geology and morphology of the natural reserve ‘Meteoryt Morasko’”. *Planetary and Space Science*, **49**, 749–753.
- Tymiński Z. and Brachaniec T. (2015). “Łowicz Meteorite - Mesosiderite from Vesta”. *Meteoritics and Planetary Science*, **49**, 5426.
- Tymiński Z., Stolarz M., Żołądek P., Wiśniewski M., Olech A., Kubalczak T., Zaręba P., Myszkiwicz M., Polakowski K. and Kosiński J. W. (2015). “Meteorite search campaigns of the Polish Fireball Network”. In Rault J.-L. and Roggemans P., editors, *Proceedings of the International Meteor Conference*, Mistelbach, Austria, 27-30 August 2015. IMO, pages 143–146.

<sup>1</sup> <http://www.lpi.usra.edu/meteor> and furthermore at: <http://wiki.meteoritica.pl> (in Polish).

# A (revised) confidence index for the forecasting of meteor showers

Jeremie Vaubaillon

IMCCE, Paris Observatory, univ-PSL, Paris, France

vaubaill@imcce.fr

A confidence index for the forecasting of meteor showers is presented. The goal is to provide users with information regarding the way the forecasting is performed, so several degrees of confidence is achieved. This paper presents the meaning of the index coding system.

## 1 Introduction

The prediction of meteor showers has seen great success (McNaught and Asher, 1999), as well as deep disappointment in the past (Vaubaillon et al., 2014). Every year IMO publishes the calendar of the coming meteor showers, on the basis of forecasting performed by several authors. Comments included in the text allow one to decide whether or not such and such shower is worth travelling to the end of the world to observe. I believe every shower is worth observation, but of course in a practical sense everyone needs to choose how much effort to put in a given event. For this reason, the goal of this paper is to provide the meteor community with an explanation of the confidence index presented during the IMC.

## 2 The confidence index

### How the index is built

The confidence index is basically a code providing information on how the ephemeris of a given meteor shower was performed.

The *first* letter informs us with the trail(s) the Earth (or any planet) is encountering. An encounter with a single trail is noted “**S**” (as in single), whereas an encounter with several trails is labelled “**G**” (as in global). Usually, single trail encounters are more accurate than multiple (Global) trails.

The *second* letter tells us about the year the forecasting is performed. Most of the time the prediction is made by taking into account only the simulated particles crossing the planet at a given year. In this case we label it “**Y**” (as in year). In other cases, there are not enough particles to really compute the location of the stream. As a consequence, we take into account all the particles crossing the planet concatenated over several years. In such a case we label it “**B**” (as in background).

The *third* element of the index tells how many perihelion passage of the parent body were observed, as well as how

many passages were simulated. In short, the more observations, the better the confidence. The index is this built as: “O no/ns” with no: number of observed passages and ns: number of simulated passages.

The *fourth* element provides information regarding the stability of the orbit of the parent body. Orbits are usually best perturbed by close encounters with giant planets. The effect of such an encounter can be measured thanks to the mass of the planet, the distance of closest encounter and the velocity at the minimum distance. The index is the sum of all the contributions of the close encounters of a given trail (or sum of trails). The higher this number the less confident the forecasting can be, unless the parent body was observed before and after the encounter. If a single trail is considered the label starts with “**CE**” (as in close encounter), otherwise with “**CU**” (as in cumulative close encounters). Then the number (3 digits or more) of the sum of the close encounters is provided.

## 3 Example of confidence index

*LEO in 2001*: SYO0/ICE0.00 => single trail, single year, and passage not observed, no close encounter.

*PER in 2017*: GYO3/17CU0.00 => global trail, single year, 3 passages observed out of 17 simulated, no close encounter whatsoever during the whole duration of the simulations.

*209P in 2014*: GYO3/75CU46 => global trail, single year, 3 passages observed out of 75 simulated, cumulative encounter sum up to 46, which is quite a big number.

*QUA in 2017*: GYO1/57CU1500 => global trail, single year, one passage observed out of 75 simulated, cumulative encounter sum up to 1500, suggesting that the exact origin is unknown and the forecasting provides only statistical results. Note: my forecasting of the QUA is systematically offset by a few hours. In other words, the close encounter index tells us that one should not really rely on such a forecasting.

## 4 Conclusion

This confidence index is certainly not perfect, but it is better than nothing.

## Acknowledgment

I am thankful to the IMC2016 team for such a terrific conference, as well as to G. Valsecchi for insights regarding the close encounters.

## References

- McNaught R. and Asher D. (1999). “Leonid Dust Trails and Meteor Storms”. *WGN, Journal of the IMO*, **27**, 85–102.
- Vaubailion J., Maquet L. and Soja R. (2014). “Meteor hurricane at Mars on 2014 October 19 from comet C/2013”. *Monthly Notices of the Royal Astronomical Society*, **439**, 3294–3299.



Nagatoshi Nogami and Eva Bojurova on the boat to the Waddenzee.

# Software for Analysis of Visual Meteor Data: R package *MetFns* – Workshop report

Kristina Veljković

Petnica Meteor Group, Valjevo, Serbia

mackikac@gmail.com

New version of the package *MetFns* for analysis of visual meteor data, written in statistical software R, was presented on the workshop.

## 1 Introduction

New version of the package *MetFns* for analysis of visual meteor data (Veljković and Ivanović, 2014; 2015), written in statistical software R, was presented on the workshop. At the beginning, we downloaded the newest version of R from the site<sup>1</sup>. After that, a short introduction to R was made containing its history, advantages, few words about *GUI* (graphical user interface), text editors. We talked about types of objects, in R, giving more attention to vectors, factors, data frames and functions, necessary for better understanding and using the functions from the package. Note that both the package *MetFns* and statistical software R are open source and free.

## 2 Topics discussed and examples covered

We downloaded the package from the site<sup>2</sup>. In order to understand how its functions can be used, we checked the manual, which can be downloaded<sup>3</sup>.

An overview of the package was made. It contains visual meteor data (yearly rate data, yearly magnitude data and accompanying data) and functions for data manipulation. In the current version, only data for selected years are part of the package, due to the limitation of the package capacity. But, there is also a possibility to read yearly rate or magnitude data directly from the IMO web site using provided functions. Package *MetFns* consists of 12 filter functions for data selection: by shower code, by period of days or months, by IMO observer code, by observer's first and last name, by geographical coordinates of observing site, by name of the observing site, by country, by solar longitudes, by correction factor(s) for field-of-view obstruction, by limiting magnitude(s), by radiant elevation(s) and by total correction factor. Also, there is a global filter function that combines previously mentioned filters in order to perform data selection by more than given in the manual, to the R command line. Then, we discussed the following functions for data calculations, provided in the package:

- function for calculation of solar longitude;
- function for calculation of calendar date and time corresponding to given value of solar longitude;
- function for calculation of the table and graphical representation of the summarized magnitude distribution of the meteor shower;
- function for calculation and graphical representation of the population index based on the method of linear regression that incorporates the probabilities of meteor perception;
- function for calculation and graphical representation of population index based on the method of the average distance from the limiting magnitude which uses an adaptive-bin size algorithm;
- function for calculation of the zenithal hourly rate of a meteor shower that uses an adaptive-bin size algorithm, with a population index being constant or calculated from the magnitude data.

Again, we copied the examples given in the manual to R, to illustrate how to use previously mentioned functions. Also, we made some changes to the parameter values of the functions, in order to show how the user can make adjustments for performing different analyses.

## 3 Conclusion

Participants of the workshop gave a lot of comments and suggestions, what to add and change in the package *MetFns*. All of these will lead to the new package version which is expected in the near future.

## Reference

- Veljković K. and Ivanović I. (2014). "Software for analysis of visual meteor data". In Rault J.-L. and Roggemans P., editors, *Proceedings of the International Meteor Conference*, Giron, France, 18-21 September 2014. IMO, pages 104–108.
- Veljković K. and Ivanović I. (2015). "Improvement of software for analysis of visual meteor data". In Rault J.-L. and Roggemans P., editors, *Proceedings of the International Meteor Conference*, Mistelbach, Austria, 27-30 August 2015. IMO, pages 27–29.

<sup>1</sup> <https://cran.r-project.org/>

<sup>2</sup> <https://cran.r-project.org/web/packages/MetFns/>

<sup>3</sup> <https://cran.r-project.org/web/packages/MetFns/MetFns.pdf>

# Summary of the Open Session at the IMC 2016

Cis Verbeeck<sup>1</sup>, Megan Argo<sup>2</sup>, Peter Brown<sup>3</sup>, Sirko Molau<sup>4</sup>,  
Jürgen Rendtel<sup>5</sup> and Antonio Martínez Picar<sup>6</sup>

<sup>1</sup>Royal Observatory of Belgium, Avenue Circulaire 3, 1180 Uccle, Belgium  
cis.verbeeck@oma.be

<sup>2</sup>Jodrell Bank Centre for Astrophysics, School of Physics and Astronomy,  
The University of Manchester, Oxford Road, Manchester, M13 9PL, U.K.  
megan.argo@gmail.com

<sup>3</sup>Dept. of Physics and Astronomy, University of Western Ontario, London, Ontario, N6A 3K7, Canada  
pbrown@uwo.ca

<sup>4</sup>Abenstalstr. 13b, 84072 Seysdorf, Germany  
sirko@molau.de

<sup>5</sup>Leibniz-Institut für Astrophysik Potsdam (AIP) An der Sternwarte 16, 14482 Potsdam, Germany  
jrendtel@web.de

<sup>6</sup>Solar–Terrestrial Centre of Excellence – Royal Observatory of Belgium, Brussels, Belgium  
antonio.martinez@observatory.be

The Open Session at the IMC 2016 took place on Friday, June 3<sup>rd</sup> 2016 evening (21:30-22:30) and was intended to accommodate beginners' questions about meteor astronomy. Megan Argo moderated a panel of experts, consisting of Peter Brown, Sirko Molau, Jürgen Rendtel, and Antonio Martínez Picar.

## 1 Introduction

15 persons attended the Open Session. With only two questions received via the IMC 2016 website, the Open Session did not take the format of Q&A for beginners. Instead, the moderator asked the panel where and how amateurs can help meteor science best. The answers from the panel drew several comments from the audience, yielding a lively discussion. Here, we describe the basic recommendations from the experts.

## 2 Fireball shock waves

*Peter Brown* encourages amateurs to observe fireball shock waves with infrasound systems (a few hundred Hz to 0.01 Hz). It is easy to build a system but you need a lot of space. You can buy a system for a few hundred dollars, and it is recommended to add water hoses to protect against noise. By looking at the period of the sound, you get an idea of the energy. If you've got many microphones, you can do more. Software is typically included.

## 3 High resolution video

*Sirko Molau* points out that it is most interesting to go for new techniques like high resolution video and lunar impacts (which should be possible e.g., with a C8 telescope).

Sirko would start with a Watec camera if he would start now as a video observer. If you are hunting for fireballs, you use a large field of view (FOV). If you are going for good meteor statistics, you go for an intermediate FOV.

You can then observe the visual showers which you cannot observe by radar.

There are a lot of geographical regions which are underrepresented in video observations, e.g., the Southern hemisphere, the large Asiatic region between Europe and China/Japan, and Hawaii.

## 4 Radio meteor astronomy

*Sumio Nakane* asks how amateurs can contribute to radio meteor astronomy. *Antonio Martínez Picar* is convinced that simplest is best. The continuous wave technique exists for many years, and is still his recommendation since it is simpler than other techniques.

*Gaetano Brando* asks which kind of antenna to use for meteor astronomy: a directional one or a dipole? Antonio suggests that a simple dipole may be best, unless your transmitter is so distant that you need a high (directional) gain to detect the signal. Also, he prefers a zenithal direction for the antenna since then you know the geometry better. The CMOR radar in London, Ontario also has a rather broad, zenithal gain pattern, and has about half of its maximal gain at 45 degrees zenith distance.

## 5 Visual observations

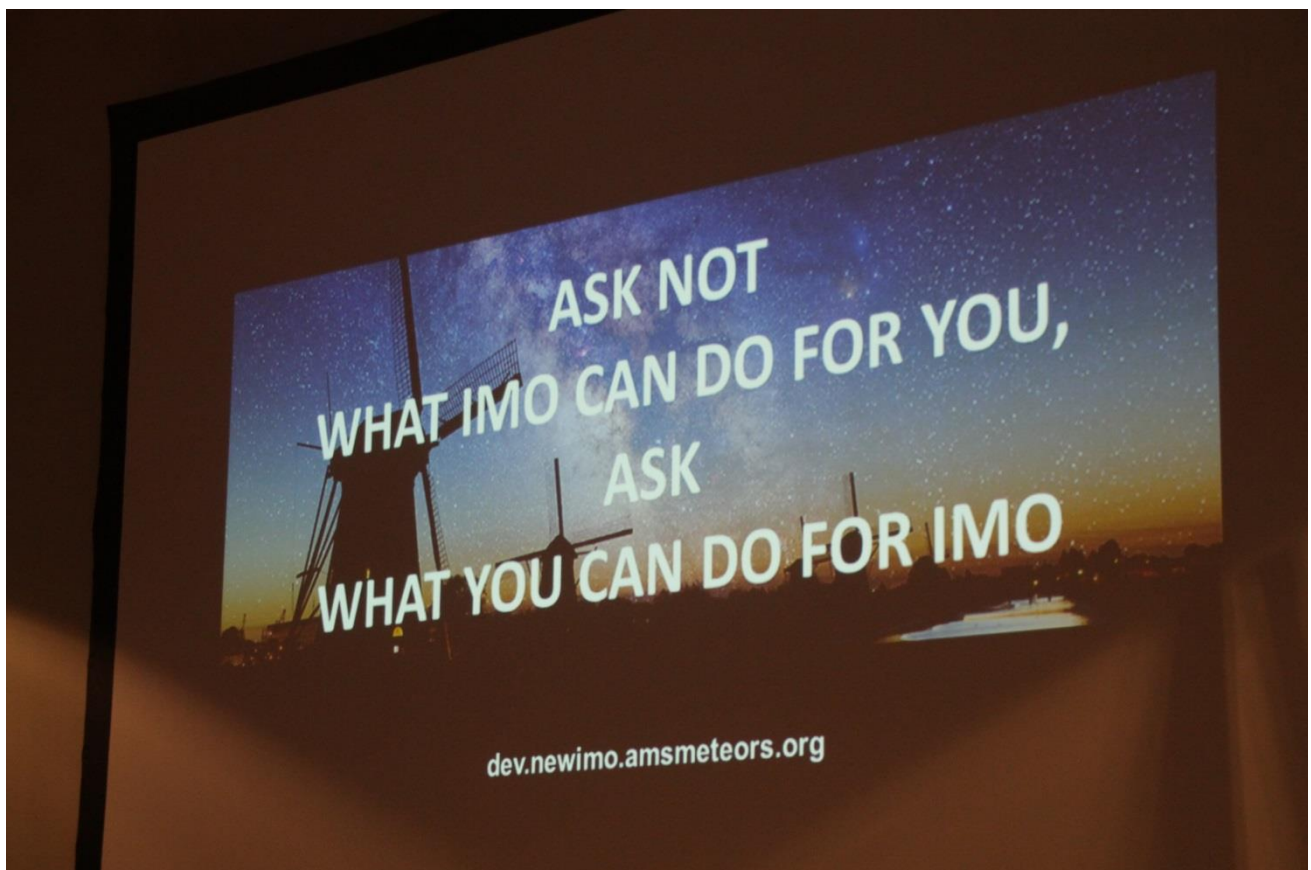
What can visual observers do? Visual observations are still important and complement video and radio observations. Visual observations provide first hand experiential impressions, rather than just looking at data on your screen. Observing together creates collaboration

between individuals, and IMO was created because of the ensuing collaboration between groups.

There are still really old and reliable visual datasets, which means that visual observations enable long term studies. For instance when the resonance in the Orionids 2006-2007 was found, *Jürgen Rendtel* went back to old observations back to 1913-1914 and did find a periodicity. Visual observations have a low threshold for beginners.

Sirko remarks that a good video observer should first do some visual observations for a better understanding about what meteors are all about.

*Alejandro Sánchez de Miguel* suggests developing an app to record visual observations, but the screen should not be too bright.



Presentation of the new IMO website: help with the IMO website is much appreciated!

# Open-source meteor detection software for low-cost single-board computers

Denis Vida<sup>1</sup>, Dario Zubović<sup>2</sup>, Damir Šegon<sup>3</sup>, Peter Gural<sup>4</sup> and Robert Cupec<sup>5</sup>

<sup>1</sup> Astronomical Society “Anonymus”, B. Radić 34, 31550 Valpovo, Croatia  
Faculty of Electrical Engineering, University of Osijek, Kneza Trpimira 2B, 31000 Osijek, Croatia  
denis.vida@gmail.com

<sup>2</sup> Croatian Meteor Network  
dario@zubovic.email

<sup>3</sup> Astronomical Society Istra Pula, Park Monte Zaro 2, 52100 Pula, Croatia  
damir.segon@pu.htnet.hr

<sup>4</sup> Gural Software Development, 351 Samantha Drive, Sterling, Virginia, USA 20164  
peter.s.gural@leidos.com

<sup>5</sup> Faculty of Electrical Engineering, University of Osijek, Kneza Trpimira 2B, 31000 Osijek, Croatia  
rcupec@etfos.hr

This work aims to overcome the current price threshold of meteor stations which can sometimes deter meteor enthusiasts from owning one. In recent years small card-sized computers became widely available and are used for numerous applications. To utilize such computers for meteor work, software which can run on them is needed. In this paper we present a detailed description of newly-developed open-source software for fireball and meteor detection optimized for running on low-cost single board computers. Furthermore, an update on the development of automated open-source software which will handle video capture, fireball and meteor detection, astrometry and photometry is given.

## 1 Introduction

With the advent of low-cost sensitive video security cameras, amateur meteor enthusiasts quickly embraced this technology and noted its potential for meteor surveillance (Gural and Šegon, 2009). The technology has proven capable of delivering quality data, such that a meteorite recovery was possible based on an amateur meteor network (Borovička et al., 2015) using such cameras. As the price of these cameras has continued to decline, falling below 50 USD (Samuels et al., 2014), the main price component of a meteor station became the computer for recording and processing the data. As the computer’s price is an order of magnitude larger than that of a single camera, the question of replacing it with a cheaper alternative naturally arises. The possible candidates were found in the form of low-cost single-board computers. A set of these computers were tested in (Zubović et al., 2015) and it was concluded that a viable alternative exists, namely the *Raspberry Pi 2* device which seemed affordable and powerful enough to serve the purpose. Furthermore, it was concluded that a low-cost meteor station using the *Raspberry Pi 2* computer could be built for about 150 USD, including all components. While the hardware is not the main topic of this paper, it is worth mentioning that a new generation of the *Raspberry Pi* has recently been released, the *Raspberry Pi 3* which offers up to 50% more computing power<sup>1</sup> than the previous generation. Although the hardware options are plentiful, there were no software

solutions capable of running on such devices. Their ARM CPU architecture and the Unix-based operating system create a unique problem, where to successfully compile and use meteor processing pipeline software, one needs to obtain its source code and adapt it to run under such a system configuration. The work in (Zubović et al., 2015) presented software which works on *Raspberry Pi 2* devices, records video from the camera, compresses it into the CAMS FTP format (Gural, 2011) and performs a rudimentary real-time fireball detection.

In this paper new and improved algorithms are presented which include complete procedures for real-time fireball detection, meteor detection, star extraction and data calibration. All software is open-source and available on the project’s GitHub page<sup>2</sup>. The authors believe that meteor surveillance is a matter of great importance, and as such it should be available to all. By making the software open-source, anyone can use the code, contribute to it and more experienced contributors can improve it significantly. The *Python* programming language was chosen as the main development language, while the computationally intensive parts of the code are written in C++. The choice of this combination of programming languages is common for astronomical purposes<sup>3</sup> in the recent years.

<sup>1</sup> <https://www.raspberrypi.org/magpi/raspberry-pi-3-specs-benchmarks/>

<sup>2</sup> <https://github.com/CroatianMeteorNetwork/RMS>

<sup>3</sup> <http://python-in-astronomy.github.io/>

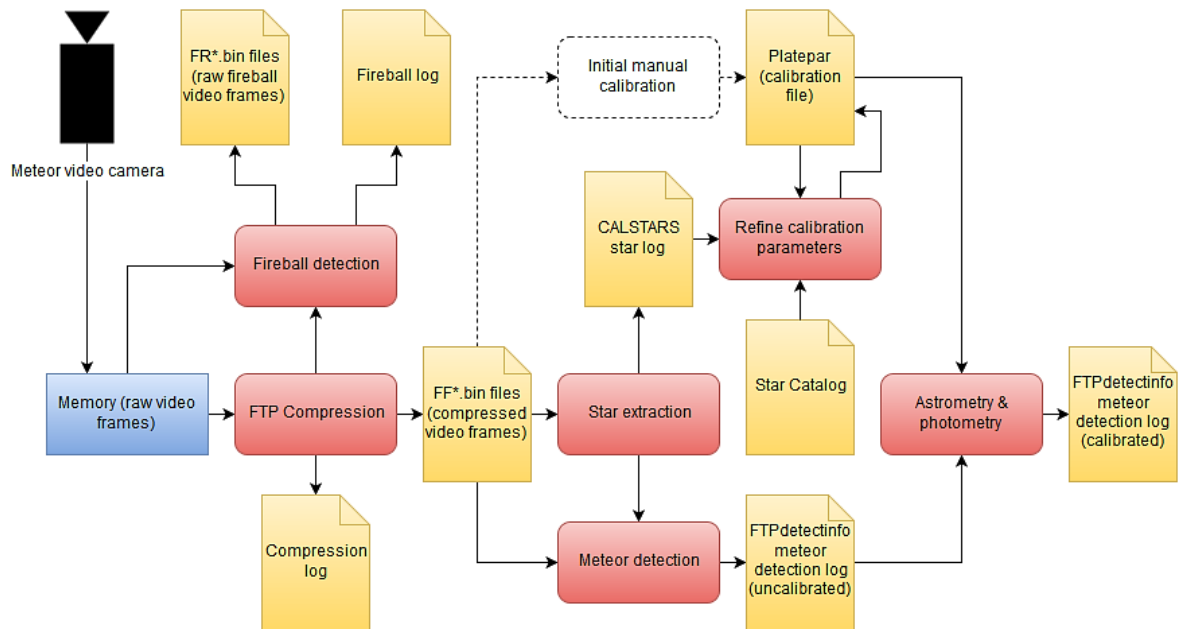


Figure 1 – A block diagram of the developed software.

## 2 Software overview

An overview of the developed software is shown on *Figure 1*.

The raw frames from the grabber are compressed in the CAMS FTP compression format (Gural, 2011). The compression procedure compresses 256 raw video frames into 4 images: maximum pixel value image (maxpixel), average pixel value image excluding the maximum (avepixel), standard deviation pixel value image excluding the maximum (stdpixel) and an image which tracks the time of the occurrence of the maximum pixel value (maxframe). The time, i.e. the frame number of the maximum pixel value is encoded as a byte valued image level. If a certain pixel has several maximum values occurring at different frames, the frame number which is stored in the maxframe image is randomly chosen to distribute noise peaks uniformly in time.

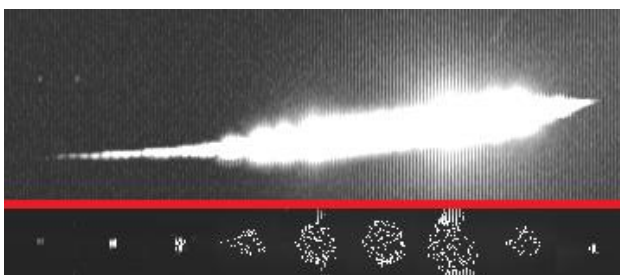


Figure 2 – Fireball maxpixel image (top) and several reconstructed frames showing compression artifacts (below).

While the aforementioned compression procedure works sufficiently enough to preserve meteors of moderate brightness, certain problems can occur with very bright fireballs. As the fireball saturates the CCD sensor and leaves a path of saturated values along its track, the compression algorithm only takes a single saturated value encoded in time. The effect of this is visible in *Figure 2*. The top of the figure shows the maxpixel image, while

the bottom shows several reconstructed video frames. It can be seen that the reconstructed frames suffer from compression artifacts which can impair the precision of the centroid determination as information about the real position of the fireball is lost.

To counter this problem a real-time fireball detector was developed to enable saving the raw video frames while they are still in the temporary memory buffer. Fireballs have orders of magnitude higher signal-to-noise ratio in respect to the background than meteors of moderate brightness, and thus the authors believe that a dedicated fireball detector provides more consistent results than a combined approach. Furthermore, a fireball detection algorithm is simpler and faster, thus satisfying the real-time requirement. Fainter and moderate brightness meteors are detected on the compressed data with more elaborated methods offline, as they generally do not suffer from compression artifacts.

Besides fireball detection, to make a low-cost meteor station competitive with the existing solutions, an option to detect fainter meteors is highly desirable. As there are constraints on the computing power, the algorithm needs to be fast, reasonably robust and sensitive enough to detect meteors not detected by the fireball detector. To consider how fast the algorithm actually must be, Worst Case Execution Time and the maximum average time which can be spent per each image for meteor detection must be calculated.

To use the full power of the *RPi* computer, all 4 of its cores are employed. The capturing process has the highest priority and it needs to run in real-time, thus one core is completely dedicated to this task. Two cores are dedicated to video compression and real-time fireball detection. The compression and fireball detection process is serial, meaning that fireball detection is run after the compression. Thus each of these two cores run the same serial process, but the input data stream is alternated

between the two, to double the available processing time per single serial procedure. The one remaining core runs star extraction and meteor detection. Once the capture process is finished, all 4 cores run star extraction and meteor detection procedures. Finally, after the detection procedures finishes, astrometry and photometry procedures are performed.

With the core utilization laid out, the total available processing time for star extraction and meteor detection can be calculated. The longest night of the year at latitude  $50^\circ$  north is about 16 hours, which translates into 5625 CAMS format FF files at 25FPS and 256 frames per file. With the proposed core utilization, during the longest night the algorithm will have 16 hours available during the night on one core, and the remaining 8 hours on 4 cores. Thus the total computation available is 48 hours (not taking into account system housekeeping and post-processing). This translates to the maximum average time which the algorithm can spend on one FF file of about 30 seconds. Furthermore, taking into account that the *Raspberry Pi 2* is at least an order of magnitude less powerful than contemporary normal-sized computers, the average maximum time the algorithm running on a normal-sized computer can spend on each image is around 3 second. As this time is quite short, the algorithm should make an effort to reduce the number of analyzed files early on.

### 3 Fireball detector

An initial version of the fireball detection algorithm was presented in (Zubović et al., 2015). In this paper an improved version of the algorithm is presented - the algorithm was re-implemented in *Cython*<sup>4</sup> for faster execution and input parameters were fine tuned. Furthermore, the algorithm is discussed in more detail below.

The input data to the detector are the FTP compressed file and raw video frames. To detect significant rises in image intensity over the background, image thresholding is performed with the following operation:

$$\text{Threshold}(\max, \text{avg}, \text{stddev}) = \begin{cases} \text{white}, & (\max > \text{avg} + K_1 \cdot \text{stddev}) \ \& \ (\max > 40) \\ \text{black}, & \text{otherwise} \end{cases}$$

The  $K_1$  parameters determines how many standard deviations above the background level the maximum intensity must be to be considered to be part of the fireball, i.e. a white pixel. The chosen value was  $K_1 = 4$ , based on numerous experiments on fireball images. Furthermore, the minimum intensity level of the pixel must be 40. *Figure 3* shows the influence of the varying value of the  $K_1$  parameter. As it can be seen on the given figure, values of  $K_1$  below 4 produce too many white pixels. Values above 4 can produce black regions in the middle of the fireball – these are caused by the very high standard deviation values in the middle of the fireball.

When these high values are multiplied by the  $K_1$  parameter of a higher value, the  $\text{avg} + K_1 \cdot \text{stddev}$  expression can exceed the maximum digitization value of 255, thus making the maximum image value unable to pass this threshold. If one requires such a high threshold, it is possible to clip the calculated value to 254 and thus ensure saturated pixels get through. As this would introduce a slight overhead in computation time, this feature was not implemented.

Following this procedure, the image pixels are now either white (pixels of interest) or black (background). As the CAMS FTP format image contains information about the occurrence of every maximum pixel value, the thresholded image can be shown as a 3D point cloud, XY components representing the image axes, and Z component representing the time axis. The resulting 3D point cloud can be seen in inset *a*) of *Figure 4*. To further reduce the noise and reduce the total number of points of interest, a subsampling procedure is performed. The point cloud is sampled by  $16 \times 16 \times 256$  bins. A secondary thresholding is performed which is based on counting the number of points in each bin. If the number of points is less than 8, the bin is rejected. The result is shown in inset *b*) of *Figure 4*. As fireballs can often have bright flashes, an algorithm which removes the flashes (i.e. slices at the time axis which have considerably more points than average) is applied to the 3D point cloud. An example of such 3D point cloud is given on the inset *b*) of *Figure 4*, where a plane of points at frame 90 can be noticed. The flash filter looks for such planes in the data, i.e. the frames when the fireball 3D point cloud has at least 10x more points than the median number of points per frame. The frame is removed and the result is shown in inset *c*) of *Figure 4*.

After the described preprocessing, it is obvious from *Figure 4 inset c*) that the fireball is represented as a line segment in 3D space. Thus a new line segment detection algorithm has been independently developed and implemented in *Cython*. First, the points are sorted by their respective frames. Then the algorithm pairs each point with each other to hypothesize a line. Each hypothesized line is tested for the number of points in its neighborhood. The neighborhood is defined as cylinder around the hypothesized line (with a fixed radius). The algorithm evaluates each hypothesized line by the number of points and their distances from the line by producing a weighted score. The closer the point is to the line, the higher the score it has. Furthermore, if the algorithm determines that there is a discontinuity in the concentration of points, that particular hypothesized line is rejected as the goal is to find compact line segments. The line with the best cumulative score is chosen, its points are removed from the point cloud and the algorithm runs recursively until all acceptable lines are found. The pseudo code of the algorithm, as well as the description of the input parameters, are given in Code segment A. The line segment detection algorithm has a time complexity of  $O(N^3)$  in the worst case, and given

<sup>4</sup> <http://cython.org/>

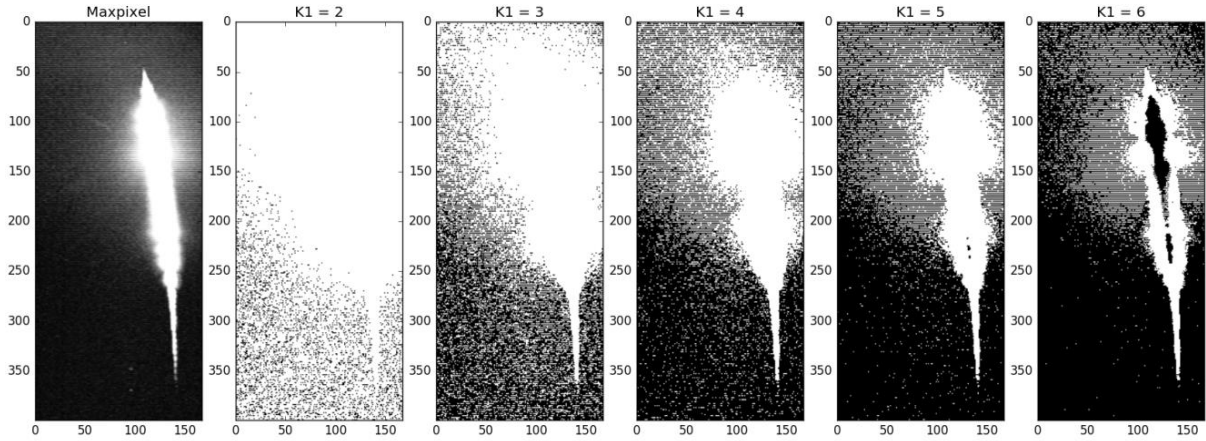


Figure 3 – Thresholding the fireball with various values of  $K_1$ .

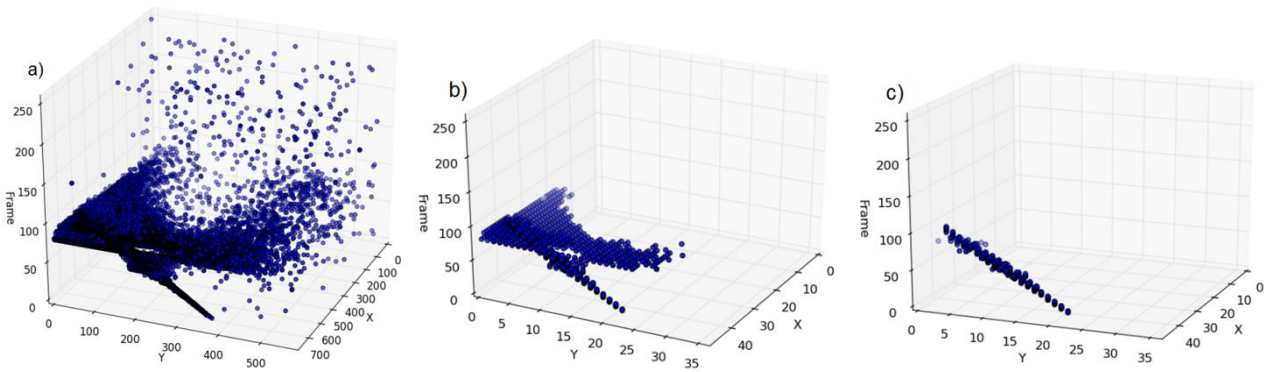


Figure 4 – Steps in the fireball detection thresholding procedure.

the restrictions on the computing time available, the total number of points which are fed into the algorithm was limited to 1000. If the point cloud contains more points, 1000 points are randomly chosen. In principle, the newly developed line segment detector is very similar to RANSAC (Fischler and Bolles, 1981), although it contains several key differences which enable it to search specifically for line segments, in contrast to unbounded lines. After the fireball is located, raw video frames containing the fireball are pulled from memory and are stored on disk for later use.

The performance of the fireball detector was evaluated on about a hundred examples of fireball images from the Croatian Meteor Network archives. The brightness of successfully detected events ranges from fireballs which saturated half the image, to 0<sup>th</sup> magnitude meteors. After examining the results, the authors have concluded that the fireball detector is robust and suitable its purpose.

#### 4 Meteor detector

To reduce the total processing time, the star extraction procedure (described in the next section) is run before meteor detection. If the number of detected stars is too low, meaning that the sky is not clear, the meteor detection algorithm will not be run at all on the given image. When the skies are clear, the processing flow will include the detection procedure.

As the CAMS compression format saves the maximum and the average value of each pixel during 256 frames, as well as its standard deviation, thresholding the image to find events brighter than the average is done by applying the following operation on the image:

$$\text{Threshold}(\max, \text{avg}, \text{stddev}) = \begin{cases} \text{white}, & \max > \text{avg} + K_1 \cdot \text{stddev} + J_1 \\ \text{black}, & \text{otherwise} \end{cases}$$

$K_1$  is a scaling factor which determines how many standard deviations above average the event should be, while  $J_1$  is an absolute factor which adds to the total level threshold by adding a minimum background level. The combination of factors  $K_1 = 1.7$ ,  $J_1 = 9$  proved to be optimal for discriminating meteors from the background noise.

After the image is thresholded, the algorithm checks the ratio between the thresholded and the total area of the image. If the thresholded part covers more than 5% of the image, the image is rejected. The reason for this is that moonlit clouds can often cause many above average pixel exceedances, which in turn slows down the algorithm.

As one compressed image contains information of about 256 frames, this allows reconstructing the whole video from the compressed file. To reduce noise, the whole 256-frame block is not analyzed at once, but only a 64 frame “window” is reconstructed from the FF file. The

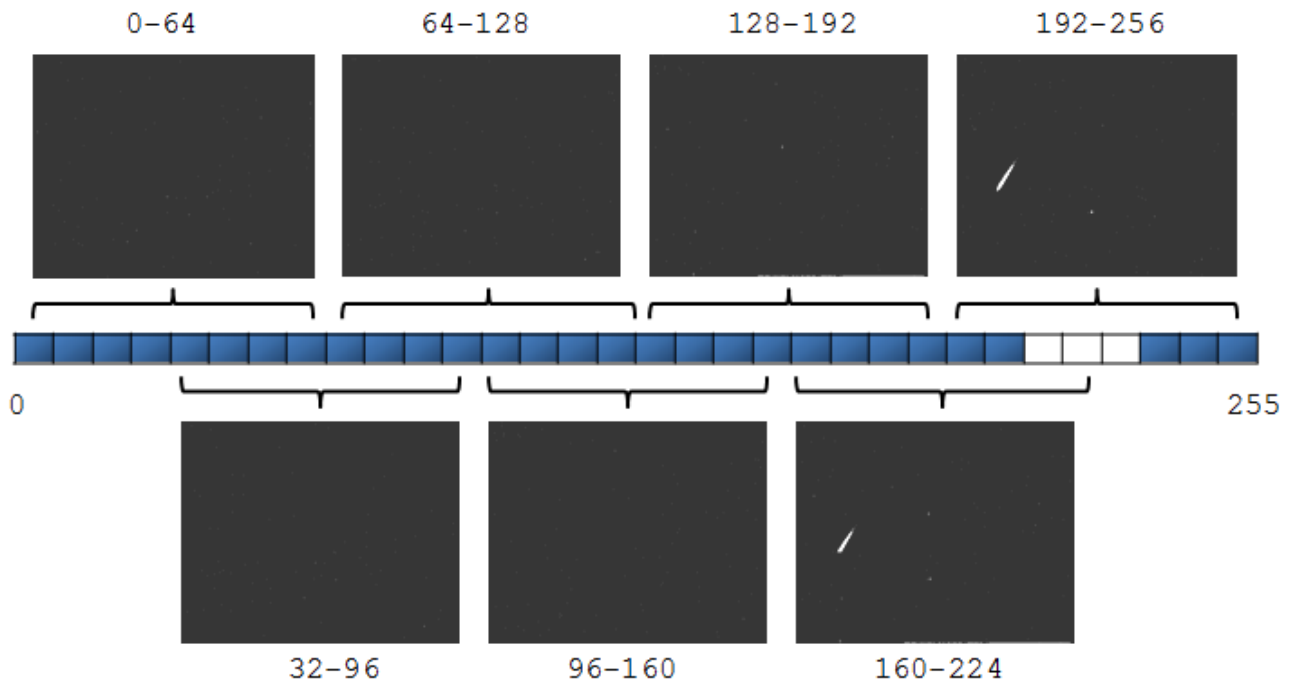


Figure 5 – Frame reconstruction and frame “windows”. The meteor appears on frames from 211 to 228.

starting frame of each reconstructed window is shifted by 32 frames, producing 7 such windows covering frame ranges of 1–64, 32–96, 64–128, 96–160, 128–192, 160–224, and 192–256, thus the windows are overlapped in time to avoid “leakage” of meteors spanning processing windows. The mentioned “window” is not a set of 64 actual frames, but the maxpixel of the short window block. Figure 5 illustrates the described procedure and shows individual frame “windows”.

On each such window a set of image morphological operations (Gonzales and Woods, 2008) is performed. First, morphological cleaning is performed; a process which removes isolated pixels. This operation removes most of the noise on the image. Figure 6 illustrates the described procedure.

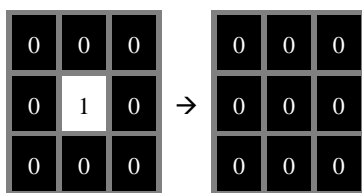


Figure 6 – Morphological cleaning.

Then a morphological bridging operation is performed which connects pixels which are on the opposite sides and all other pixels are 0. This operation helps to connect disconnected features on the image, such as broken lines. Figure 7 illustrates the described procedure for 1 of 4 possible pixel orientations.

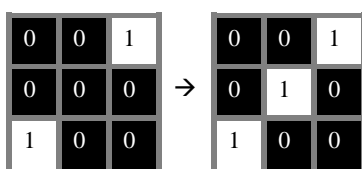


Figure 7 – Morphological bridging.

After that, a morphological closing is performed. Closing is a structured filling in of hollow image features which consists of two sub-operations: morphological dilation followed by erosion, using the same structuring element for both operations. This operation helps to fill in all the possible gaps in the thresholded meteor.

To prepare the image for line identification, all possible lines must be as thin as possible. Thus a *Zhan-Suen thinning algorithm* (Zhang and Suen, 1984) is applied to the image which skeletonizes the image i.e. makes all possible meteors on the image to appear as long thin lines.

Finally, a morphological cleaning is performed again to remove all noise on the image remaining after thinning. Now the image is ready to run the line detection algorithm. Figure 8 shows an example of the maxpixel image (left), the image after thresholding (middle) and the image after the complete pre-processing procedure (right).

The image pre-processing procedure was implemented due to the peculiar operation of the chosen line finding algorithm. After a period of experimentation, it was decided to settle on the *Kernel-Based Hough Transform (KHT)* (Fernandes and Oliveira, 2008) due to its superior speed and performance, which was necessary due to the low computation power of single board computers. The authors of the *KHT* made it open-source which perfectly aligned with our needs and software development philosophy. The preprocessed images are fed into the algorithm and it returns all line candidates on the image.

After all lines have been retrieved on all 64-frame “windows”, similar lines are identified using the *Discrete*

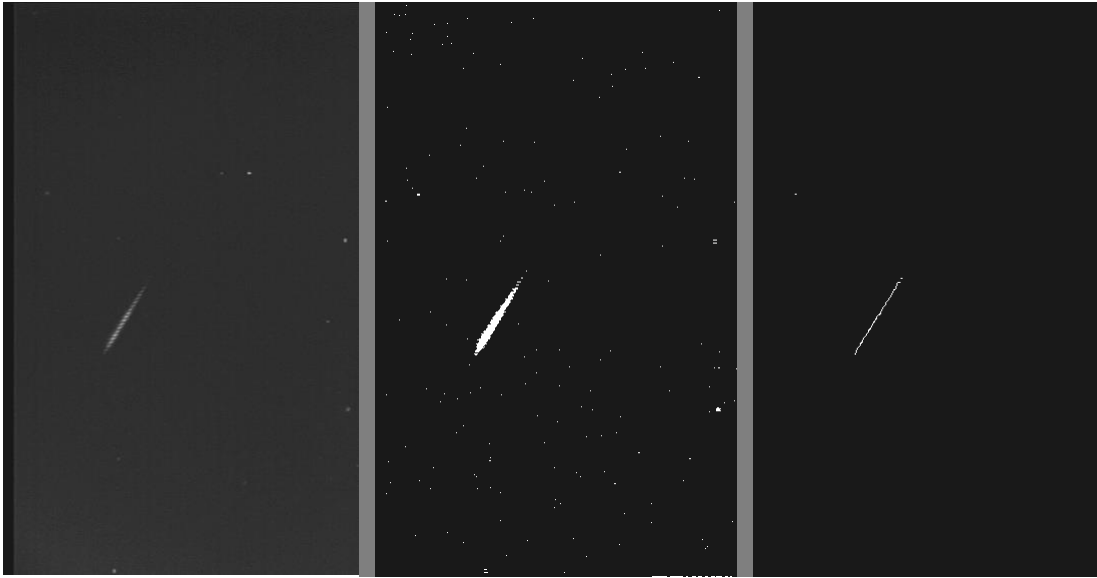


Figure 8 – Maxpixel image of a meteor (left), thresholded image (middle), image after preprocessing (right).

*Fréchet distance* (Eiter and Mannila, 1994) as the similarity measure and are averaged. During the line segment merging, the exact “windows” on which the line appears are tracked, thus the approximate time of the line appearance is known. In this point the algorithm has a list of candidate lines which need to be confirmed as meteors. If this list is empty, meaning no lines satisfying the given parameters were found, the procedure is aborted and the image is rejected and it is considered to not contain any meteors. On the other hand, if there are lines in the list, the algorithm proceeds to confirm that the found lines could be meteors.

The next phase of the algorithm determines if the candidate line contains a possible meteor by determining if the line propagates through time. First, as the approximate time of the line appearance is known as a range of frames between which the candidate line appeared, this fact is used to reconstruct the “window” image using the given frame range. Then a strip of about 50 pixels in width is extracted around the line. In CAMS FTP format, each pixel has an assigned time component of its maximum value during the 256 frame period, meaning that each pixel in the strip is given a time component. Thus a 3D point cloud is obtained - a line propagating through time should be a compact line in this point cloud, thus the same algorithm as the one in fireball detection is used, although with a different set of parameters to allow for smaller lines to be detected. The algorithm determines the exact starting and ending frames of the propagating line, as well as the true orientation of the line. Any event shorter than 4 frames (i.e. 0.16 seconds at 25 frames per second) is rejected due to a large number of such short events detected during cloudy weather, which can considerably slow down the algorithm. This also means that all meteors shorter than 4 frames are not detected. In the case of future improvements in available computational power, this restriction can be easily lifted.

After the algorithm determines the exact duration (i.e. the beginning and ending frames) of the event, centroiding is performed by reconstructing each frame of the event and again extracting a strip around the event. A center-of-mass calculation is performed, using pixel intensities as weights (Berry and Burnell, 2005). As the video camera employed produces an interlaced signal, a deinterlacing procedure is performed beforehand – centroiding is done separately on odd and even image rows, thus giving a half-frame time resolution. Finally, the obtained centroids are filtered by rejecting those which considerably deviate from the fitted trend line. Figure 9 shows the marked centroids of the meteor shown on Figure 8. The results of the detection procedure are written out as a CAMS *FTPdetectinfo* file format, so that the results can be processed with the existing (although proprietary) CAMS procedures.

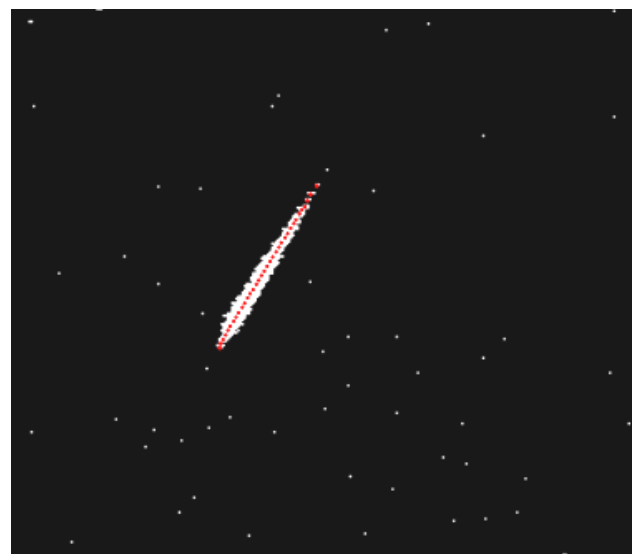


Figure 9 – A detected meteor with marked centroids.

The performance of the meteor detector was evaluated on about a hundred carefully chosen meteor images. The

Table 1 – Comparison of meteor detection performance between the new detector and the CAMS detector.

Type	Night ID	No. files	Total proc. time (sec)	Time per file (sec)	Meteors detected		False positives	
					New	CAMS	New	CAMS
1	VIB_20160419	3211	29390	9.15	14	11	53	18
2	OSE_20160417	3269	7770	2.37	0	2	9	61
3	VID_20160417	3263	37100	11.36	0	0	1679	304
4	OSO_20160419	3233	9430	2.91	2	4	36	2941
5	OSE_20160501	2950	2590	0.87	0	0	0	318
TOTAL					16	17	1777	3642

goal was to sample a wide variety of meteors of varying brightness, duration and velocity to test the algorithm's detection performance. The algorithm's parameters were tuned until all chosen meteors were successfully detected.

Furthermore, the detector was tested on 5 full nights, each containing about 3000 individual image files. The night types were chosen to be representative of the conditions encountered during the year:

1. A clear and Moonless night with several meteors;
2. A cloudy night with the presence of the Moon with very few meteors;
3. A night with fast moving clouds with the presence of the Moon;
4. A rainy night in a light polluted environment, resulting in visible falling raindrops;
5. A cloudy and stormy night with the presence of lightning.

The goal of these data was to test the algorithms robustness and false positive rate. The results were compared to those obtained by the *MeteorScan detector* employed as a part of the CAMS processing pipeline (Jenniskens et al., 2011) in *FTP\_CaptureAndDetect version 1.6* software. The results of comparison for full nights are given in Table 1.

Compared to the CAMS detector, the total number of false positives was considerably smaller. It was discovered that this was caused by the condition that the detection procedure is run only when a minimum number of stars is present on the image, thus eliminating most of the detections on clouds and during daytime. On the other hand, the new detector produced lots of false positives when part of the image contained fast moving moonlit clouds while the other part was clear. This behavior will be addressed in the future by introducing cloud mitigation techniques.

The total number of detected meteors was also smaller. After careful comparison, it was determined that the missing detections are those meteors shorter than 4 frames in duration (which are automatically rejected by the new detector) and meteors between the clouds. On the other hand, during clear nights the new detector performed similar to the CAMS detector. Real differences cannot be determined without a detailed comparison, but it is worth mentioning that in several

cases the new detector detected more meteors than the CAMS detector (with the detection parameters used by the Croatian Meteor Network). Furthermore, on all tested data the algorithm never exceeded the maximum average processing time per image. The maximum average processing time per image for the tested nights on the *Raspberry Pi 2* device was about 11.5 seconds, including both the star extraction and meteor detection.

Although the detection rate was similar to the CAMS detection procedure, further analysis is needed. But based on these early results, it can be concluded that under the circumstances and the given computational power the newly developed detector is performing satisfactory for the needs of an amateur meteor enthusiast. Room for improvement still exists and it is hoped that a more successful algorithm will be implemented in the future, most probably the one given in (Gural, 2016). Furthermore, the algorithm should be tested on even more data to confirm its performance.

As the system is fully automated by design, a manual meteor confirmation procedure is not a part of the processing pipeline. False meteor detections will be rejected during orbit estimation as they will not form realizable orbit solutions. Nevertheless, as the results are CAMS compatible, it is possible to perform manual confirmation using the available software solutions, such as the *CMN\_binViewer* (Vida et al., 2014).

## 5 Star extraction

To astrometrically calibrate the intrinsic (field distortion) and extrinsic (coordinate transformations) parameters of the camera, a set of stars from each recorded image is needed. Thus a robust algorithm for detecting stars on the recorded FF files was developed. The algorithm takes the "average pixel" image from the FF file and first calculates the mean intensity of the image. To quickly check if the algorithm should proceed at all, the mean image value is compared to a predefined threshold. If the image is too bright (e.g. an image recorded during the day), it is rejected. If the image passes this test, the inverse hyperbolic sine function is applied to all pixels on the image to adjust levels of the image so that the stars become more prominent. The maximum image filter (i.e. morphological erosion) is applied to the image; while on a copy of the original image a minimum image filter (i.e. morphological dilation) is applied. The difference of the 2

images thresholded by a fixed threshold value leaves only the areas of the image which are considerably brighter than their background. These peaks are detected and the center of mass is calculated for each on the original average pixel image, giving the approximate coordinates of the candidate stars.

To refine the results, and to better determine if the candidate is really a star or not, *point spread function (PSF) fitting* is performed by fitting a 2D Gaussian function to an area of  $9 \times 9$  pixels centered around each candidate star using the least squares regression. The authors are aware that a 2D Gaussian does not perfectly represent the real *PSF* of the star, but for the purposes in video meteors which have a lower photometric resolution, a pure Gaussian *PSF* is assumed. Initial *PSF* parameters are approximated beforehand so that real stars converge quickly to a solution. Thus if the fitting does not converge in a limited number of iterations, the candidate is rejected. This procedure has proven to be a good discriminator between real stars and spurious detections. Furthermore, if the *PSF* fitting procedure is completed successfully, the covariance matrix of the *PSF* is evaluated. If the *PSF* is too narrow, the candidate star is rejected as a hot pixel (i.e. bright dot defect). Finally, as a consequence of fitting the *PSF*, the location of each star is known very accurately and its precision is on a subpixel level. The intensity of each star is calculated as a volume under the fitted *PSF*.

Finally, the stars found are written in the CAMS *CALSTARS* format, so that the calibration procedure can be done using CAMS-compatible procedures if needed.

The results of the new algorithm were compared to the results of the *CAMS FTP\_CalStarExtractor* software. It was concluded that the newly developed algorithm yields very little false positives, only about 5%, while the *FTP\_CalStarExtractor* often detects more false positives than real stars. Furthermore, the proposed algorithm yields virtually no detections during cloudy weather, thus its results can be used to determine weather conditions in the time of recording. When comparing the number of true positives between the two algorithms, the new algorithm detects about 90% of stars present in the CAMS data. The average number of detected stars per image during the periods of clear skies in the sample moderate field of view data was about 30. Combining frames from the same camera over the course of the night yields an average total number of detected stars in the tens of thousands.

## 6 Astrometry and photometry procedures

To transform the image coordinates of the meteor detection to celestial coordinates, an astrometric plate solution of the associated camera is needed. The initial plate constants (field center, scale, field distortion parameters) are first manually estimated by knowing the pointing direction of the camera and its optical properties. To further refine the plate constants, the detected stars

need to be matched with stars from a star catalog. For this purpose, the Yale Bright Star Catalog<sup>5</sup> is used. To have a better quality of the solution and to cover a larger part of the focal plane, stars detected on images all throughout the night are used. As the total number of all stars in a single night can be in the tens of thousands, which can be hazardous for the computational time needed to calculate an astrometric solution, a random sample of images is taken where images with more stars have a greater probability of being chosen. At least 500 stars are needed to continue with the calibration, the number being chosen on the basis of findings in (Šegon, 2009).

The image coordinates of the chosen stars are transformed to celestial coordinates using the initial calibration parameters. The transformed coordinates are then matched to their nearest neighbors among the catalog values in celestial coordinates, but only if the coordinates are closer than a predefined angular distance threshold. The distance and the direction of the shift between each of the matched stars are recorded, the median values are calculated and the correction is applied to the plate constants. The procedure is repeated by reducing the angular distance threshold during each iteration, until the desired match is achieved. The matching metric is evaluated as a quotient of the standard deviation of the shift between the detected and catalog stars and the total number of matched stars. Thus a better solution is one that yields a smaller value.

Once the initial parameter refinement is complete, a more elaborate refining of the field center position is performed using the *Nelder-Mead method* (Nelder and Mead, 1965). Right ascension and declination of the center is adjusted until the algorithm converges to a stable solution – the same evaluation method is used as in the initial refinement procedure. Next, the distortion parameters are also refined using the same above-mentioned procedures. The image distortion is estimated by 3<sup>rd</sup> order polynomials with 2 extra “radial distortion” terms in both *X* and *Y* directions, albeit with different coefficient values:

$$f_x(x, y) = x + a_1 + a_2x + a_3y + a_4x^2 + a_5xy + a_6y^2 + a_7x^3 + a_8x^2y + a_9xy^2 + a_{10}y^3 + a_{11}x\sqrt{x^2 + y^2} + a_{12}y\sqrt{x^2 + y^2}$$

$$f_y(x, y) = y + b_1 + b_2x + b_3y + b_4x^2 + b_5xy + b_6y^2 + b_7x^3 + b_8x^2y + b_9xy^2 + b_{10}y^3 + b_{11}x\sqrt{x^2 + y^2} + b_{12}y\sqrt{x^2 + y^2}$$

The extra terms in the polynomials were first used as a part of the Croatian Meteor Network calibration procedures, but have been unpublished until now. During the initial development of the CMN procedures it was found that the modified polynomials produce smaller residuals compared to the ordinary 3<sup>rd</sup> order polynomials. This hypothesis has been tested again before the final implementation in this software and it was found that the

<sup>5</sup> <http://tdc-www.harvard.edu/catalogs/bsc5.html>

proposed equations produce significantly smaller standard deviations in the fitted star positions than the ordinary third order polynomials. The theoretical background behind the reasons of such behavior was not explored, that will be a topic of some future work.

After the astrometry parameter estimation is done and if the calibration was successful, a photometric calibration procedure is performed. Instrumental intensities of matched stars are compared to the apparent visual magnitude catalog values of said stars. A regression procedure is performed to fit the well-known intensity vs. magnitude function (Berry and Burnell, 2005):

$$m_1 = -2.5 \log_{10} C_1 + 2.5 \log_{10} C_2 + m_2$$

where  $m_1$  is the calculated magnitude,  $C_1$  is the input intensity, while  $C_2$  and  $m_2$  parameters are fitted from the abovementioned data. It is worth noting that the photometric procedures are very basic and with no regard to spectral sensitivity of the camera. Furthermore, no correction for saturated pixel values is performed. This part of the calibration procedure requires further work and improvement, which is hoped to be done in the future. Finally, meteor detections are converted from the image plane coordinates to celestial coordinates using the estimated plate constants and intensities are converted to apparent magnitudes.

The results of the proposed astrometric calibration procedure were compared to the results of the existing CMN calibration procedure. The new algorithm produced an order of magnitude better results, although results of the subsequent runs on the same dataset varied slightly because of the random sampling of the images from which the stars are used.

## 7 Discussion

The authors believe it is worth discussing the benefits that an automated low-cost meteor station could provide. Lowering the starting price of a meteor surveillance system would mean that existing networks could be easily expanded, as the human resources and a certain level of expertise exists among already organized groups. Furthermore, new networks could be easily formed with very little financial investment, meaning that meteor science would be available to a wider audience, especially in less than well-off nations. The total effect would be a considerable rise in the atmospheric collecting area and longitudinal coverage. An educational aspect should also be considered – students could be introduced to astronomy, computer and data science by installing such a system on their school and make them involved in every step of its operation. Moreover, scientists from other fields could recognize the practicality of a self-contained system with a video camera and repurpose it for their needs, such as bird watching or monitoring atmospheric phenomena.

If the project is favorably seen by a larger audience willing to set up a network of such systems, the authors believe that data produced by this hypothetical network using open-source software should be publically available. The usual arguments for keeping the data closed, such as the cost of the developed system, no longer justifies not publishing detailed data in this case, and no time is spent on manual processing as the system is fully automated. A similar open database exists in the form of the IMO Fireball Report (Hankey and Perlerin, 2014) and the authors hope that in the future more video meteor data will be open and the methods of its generation will become more transparent.

Finally, the benefits of a wide-spread meteor network to actual meteor science could be immense. Most meter-scale impactors are not observed optically, as the existing fireball and meteor networks cover only a fraction of the sky and most are only detected with non-optical methods which lack astrometric precision and show certain biases towards faster objects (Brown et al., 2016). In the recent years there have been reports of short meteor shower outbursts which were observed only by one or two meteor networks, namely the February Eta Draconids (Jenniskens and Gural, 2011) and April alpha Capricornids (SonotaCo et al., 2014). These occurrences lead to the question whether some meteor shower outbursts were not noticed due to overcast weather or the nonexistence of a meteor network beneath the skies where the outburst was visible.

## 8 Conclusion

A complete open-source software solution for video meteor capture and detection on the *RaspberryPi 2* single-board computer has been developed and described in detail. First, a set of requirements were set which such a station should meet. Next, real-time compression to CAMS FTP format and a fireball detection algorithm were described. Also, a newly-developed meteor detection algorithm was described and evaluated with the conclusion that it suits the needs of a low-cost meteor station. The pseudo code of a line segment detector in a 3D point cloud used by both fireball and meteor detectors was given. Furthermore, a star extraction algorithm which uses a Gaussian *PSF* fitting to stars was developed and tested with very positive results. Finally, the astrometry and photometry procedures were implemented and discussed.

While the individual segments of software described in this paper performed within the requirements on sample data, system tests during an actual night of meteor recording still need to be performed. Also, the software needs to be made more user-friendly and the documentation is to be expanded. It is the hope of the authors that the number of contributors to this project will rise in the future and that the developed system will find its place among meteor enthusiasts.

## References

- Berry R. and Burnell J. (2005). "The Handbook of Astronomical Image Processing", Willmann-Bell, 2nd edition.
- Borovička J., Spurný P., Šegon D., Andreić Ž., Kac J., Korlević K., Atanackov J., Kladnik G., Mucke H., Vida D. and Novoselnik F. (2015). "The instrumentally recorded fall of the Križevci meteorite, Croatia, February 4, 2011". *Meteoritics and Planetary Science*, **50**, 1244–1259.
- Brown P., Wiegert P., Clark D. and Tagliaferri E. (2016). "Orbital and physical characteristics of meter-scale impactors from airburst observations". *Icarus*, **266**, 96–111.
- Eiter T. and Mannila H. (1994). "Computing discrete Fréchet distance". Technical Report CD-TR 94/64, Christian Doppler Laboratory for Expert Systems, TU Vienna, Austria.
- Fernandes L. A. F. and Oliveira M. M. (2008). "Real-time line detection through an improved Hough transform voting scheme". *Pattern Recognition (PR)*, Elsevier, 41:1, 2008. Pages 299–314.
- Fischler M. A. and Bolles R. C. (1981). "Random Sample Consensus: A Paradigm for Model Fitting with Applications to Image Analysis and Automated Cartography". *Communications of the ACM*, **24**, 381–395.
- Gonzalez R. and Woods R. (2008). "Digital Image Processing". Pearson, Third Edition, pages 627–676.
- Gural P. S. (2011). "The California All-sky Meteor Surveillance (CAMS) System". In Asher D. J., Christou A. A., Atreya P. and Barentsen G., editors, *Proceedings of the International Meteor Conference*, Armagh, Northern Ireland, 16-19 September, 2010. IMO, pages 28–31.
- Gural P. (2016). "A Fast Meteor Detection Algorithm". In Roggemans A. and Roggemans P., editors, *Proceedings of the International Meteor Conference*, Egmond, the Netherlands, 2-5 June 2016. Pages 96–104.
- Gural P. and Šegon D. (2009). "A new meteor detection processing approach for observations collected by the Croatian Meteor Network (CMN)". *WGN, Journal of the IMO*, **37**, 28–32.
- Hankey M. and Perlerin V. (2014). "IMO Fireball Reports". In Rault J.-L. and Roggemans P., editors, *Proceedings of the International Meteor Conference*, Giron, France, 18-21 September 2014. IMO, pages 160–162.
- Jenniskens P., Gural P. S., Dynneson L., Grigsby B. J., Newman K. E., Borden M., Koop M. and Holman D. (2011). "CAMS: Cameras for Allsky Meteor Surveillance to establish minor meteor showers". *Icarus*, **216**, 40–61.
- Jenniskens P. and Gural P. S. (2011). "Discovery of the February Eta Draconids (FED, IAU#427): the dust trail of a potentially hazardous long-period comet". *WGN, Journal of the IMO*, **39**, 93–97.
- Nelder J. A. and Mead R. (1965). "A simplex method for function minimization". *Computer Journal*, **7**, 308–313.
- Samuels D., Wray J., Gural P. S. and Jenniskens P. (2014). "Performance of new low-cost 1/3" security cameras for meteor surveillance". In Rault J.-L. and Roggemans P., editors, *Proceedings of the International Meteor Conference*, Giron, France, 18-21 September 2014. IMO, pages 66–73.
- Šegon D. (2009). "How many stars are needed for a good camera calibration?". *WGN, The Journal of the IMO*, **37**, 80–83.
- SonotaCo, Shimoda C., Inoue H., Masuzawa T. and Sato M. (2014). "Observation of April alpha Capricornids (IAU#752 AAC)". *WGN, Journal of the IMO*, **42**, 222–226.
- Vida D., Šegon D., Gural P. S., Martinović G. and Skokić I. (2014). "CMN\_ADAPT and CMN\_binViewer software". In Rault J.-L. and Roggemans P., editors, *Proceedings of the International Meteor Conference*, Giron, France, 18-21 September 2014. IMO, pages 59–63.
- Zhang T. Y. and Suen C. Y., (1984). "A Fast Parallel Algorithm for Thinning Digital Patterns". *Communications of the ACM*, **27**, 236–239.
- Zubović D., Vida D., Gural P. and Šegon D. (2015). "Advances in the development of a low-cost video meteor station". In Rault J.-L. and Roggemans P., editors, *Proceedings of the International Meteor Conference*, Mistelbach, Austria, 27-30 August 2015. IMO, pages 94–97.

**Code segment A. 3D line detector pseudo code**


---

```

Function FindLines(Point_cloud, Lines_found){

    // Check if the previously found lines exceed the maximum number of lines to be found
    If (Length(Lines_found) >= Max_lines){
        Return Lines_found;
    }

    Results_list = [];

    For each point P1 in Point_cloud{
        For each point P2 in Point_cloud{
            Line = Line defined by P1 and P2;
            Distance_sum = 0;
            Point_counter = 0;
            Previous_P3 = P1;

            For each point P3 in Point_cloud{
                // Check if the point is close enough to the line
                If (Distance(Line, P3) < Distance_threshold){

                    // Check if the point is too far away from the previous point
                    If (Distance(Previous_P3, P3) > Gap_threshold){
                        // Reject the hypothesized line if the previous point
                        // was too far away from the second point that defines the line
                        If (Distance(Previous_P3, P2) > Gap_threshold){
                            Point_counter = 0;
                        }
                    }
                    Break loop;
                }
                Point_counter++;
                Distance_sum += Distance(Line, P3);
                Previous_P3 = P3;
            }
        }

        // Reject the hypothesized line if it envelops too few points
        If (Point_counter < Minimum_points)
            Continue loop;

        Average_distance = Distance_sum / Point_counter;
        Quality = Point_counter - Distance_weight * Average_distance;

        Add Line in Results_list;
    }
}

// Choose the best hypothesized line
Best_line = Line with the largest Quality in Results_list;
Point_ratio = (Number of points in Best_line) / (Number of points in Point_cloud);

// Remove the points of the best line from the point cloud
Point_cloud = Point_cloud \ Points(Best_line);

// Add the best line to results only if it covers a minimum number of frames
If (Frame_range(Best_line) >= Minimum_frame_range)
    Add Best_line in Lines_found;

// Iteratively find lines on the point cloud until most of points
// in the cloud have been covered, the remaining number of points is not too low,
// and the flag for returning just one line was not set
If ((Point_ratio < Ratio_threshold) & (Number of points in Point_cloud > 10)
    & NOT Return_one_line)
    FindLines(Point_cloud, Lines_found);

Return Lines_found;

```

---

Table 2 – 3D line segment detector input parameters.

Name	Data type	Description
Point_cloud	list	a list of points in the point cloud, each point is defined by the (X, Y, Z) tuple
Max_lines	integer	the maximum number of lines which the algorithm should find
Distance_threshold	float	the radius of the cylinder around the hypothesized line
Gap_threshold	float	the maximum distance between subsequent points which make the line
Minimum_points	integer	the minimum number of points a line should have to be accepted
Distance_weight	float	the weight by which the point-line distance will be multiplied, a larger value of the parameter yields compact lines with a smaller amount of points, while a smaller value yields dispersed lines with more points
Minimum_frame_range	integer	minimum length of the Z axis component, i.e. the minimum number of frames the line segment covers
Ratio_threshold	float	minimum ratio between the found and the total points in the point cloud until the algorithm is stopped, e.g. if the ratio is 0.7, the algorithm will run until at least 70% of points are joined to a certain line, or no line satisfies the minimum requirements to be accepted
Return_one_line	boolean	if True, the algorithm will not do an iterative search, but return only one line

Table 3 – 3D line segment detector output description.

Name	Data type	Description
Lines_found	list	a list of lines found in the point cloud



Queuing to get some speaking time with Korado Korlević (left). Sirko Molau waiting for Denis Vida to finish...

# Big data era in meteor science

Dejan Vinković<sup>1,2</sup>, Maria Gritsevich<sup>3,4,5</sup>, Vladimir Srećković<sup>6</sup>, Bojan Pečnik<sup>7</sup>, Gyula Szabó<sup>8,9</sup>, Victor Debattista<sup>10</sup>, Petr Škoda<sup>11</sup>, Ashish Mahabal<sup>12</sup>, Jouni Peltoniemi<sup>3,13</sup>, Sanna Mönkölä<sup>14</sup>, Areg Mickaelian<sup>15</sup>, Esa Turunen<sup>16</sup>, Jakub Kákona<sup>17</sup>, Jarkko Koskinen<sup>3</sup> and Victor Grokhovsky<sup>4</sup>

<sup>1</sup> Physics Department, University of Split, Nikole Tesle 12, 21000 Split, Croatia  
dejan@iszd.hr

<sup>2</sup> Science and Society Synergy Institute, Bana J. Jelacica 22, 40000 Cakovec, Croatia

<sup>3</sup> Finnish Geospatial Research Institute (FGI), Geodeetinrinne 2, FI-02430 Masala, Finland  
maria.gritsevich@nls.fi

<sup>4</sup> Institute of Physics and Technology, Ural Federal University, Mira street 19,  
620002 Ekaterinburg, Russia

<sup>5</sup> Extraterrestrial Laboratory (MExLab), Moscow State University of Geodesy and  
Cartography (MIIGAiK), Gorokhovsky pereulok 4, 105064 Moscow, Russia

<sup>6</sup> Institute of Physics, University of Belgrade, P.O. Box 57, 11001 Belgrade, Serbia  
vlada@ipb.ac.rs

<sup>7</sup> HiperSfera Ltd. Ilica 36, Zagreb, Croatia  
bpecnik@hipersfera.hr

<sup>8</sup> ELTE Gothard Astrophysical Observatory, H-9704, Szombathely, Szent Imre herceg út 112  
szgy@gothard.hu

<sup>9</sup> Konkoly Observatory, Research Centre for Astronomy and Earth Sciences, Hungarian  
Academy of Sciences, H- 1121 Budapest, Konkoly Thege Miklós út 15-17, Hungary

<sup>10</sup> Jeremiah Horrocks Institute, University of Central Lancashire, Preston, PR1 2HE, UK  
vpdebattista@uclan.ac.uk

<sup>11</sup> Astronomical Institute of the Czech Academy of Sciences, Fričova 298,  
Ondřejov, 25165 Czech Republic  
skoda@sunstel.asu.cas.cz

<sup>12</sup> California Institute of Technology, 1200 E California Bl., Pasadena, CA 91125, USA  
aam@astro.caltech.edu

<sup>13</sup> Department of Physics, P.O. Box 64, FI-00014 University of Helsinki, Finland  
jouni.peltoniemi@helsinki.fi

<sup>14</sup> Department of Mathematical Information Technology, P.O. Box 35,  
FI-40014 University of Jyväskylä, Finland  
sanna.monkola@jyu.fi

<sup>15</sup> Byurakan Astrophysical Observatory (BAO), Byurakan 0213, Aragatzotn Province, Armenia  
aregmick@yahoo.com

<sup>16</sup> Sodankylä Geophysical Observatory, University of Oulu, Tähteläntie 62, FI-99600 Sodankylä  
esa.turunen@sgo.fi

<sup>17</sup> Czech Institute of Informatics, Robotics and Cybernetics, Czech Technical University,  
Prague, Czech Republic  
kakonjak@fel.cvut.cz

Over the last couple of decades technological advancements in observational techniques in meteor science have yielded drastic improvements in the quality, quantity and diversity of meteor data, while even more ambitious instruments are about to become operational. This empowers meteor science to boost its experimental and theoretical horizons and seek more advanced science goals. We review some of the developments that push meteor science into the big data era that requires more complex methodological approaches through interdisciplinary collaborations with other branches of physics and computer science. We argue that meteor science should become an integral part of large surveys in astronomy, aeronomy and space physics, and tackle the complexity of micro-physics of meteor plasma and its interaction with the atmosphere.

## 1 Introduction

Exploration of meteor physics and meteor related phenomena has reached the level of complexity that requires new experimental and theoretical advancements. There is a clear demand on more reliable data on meteor plasma and meteor-atmosphere interaction, as our current understanding of these physics is not comprehensive. The recent increased interest in meteor science triggered by the Chelyabinsk airburst (Borovička et al., 2013; Brown et al., 2013; Popova et al., 2013; Proud, 2013; Antolik et al., 2014; Kohout et al., 2014) helps in building the case for technologically and logistically more ambitious meteor projects. This requires developing new methodological approaches in meteor research, with Big Data science and close collaboration between geoscience and astronomy as critical elements. We discuss possibilities for improvements and promote an opportunity for collaboration in meteor science within the BigSkyEarth<sup>1</sup> network.

## 2 Big Data I

High-resolution and high-sensitivity meteor detections with high-precision photometry exist on images from big telescopes that resolve the meteors. For example, Iye et al. (2007) used the 8.2 meter Subaru telescope's 80 megapixel SuprimeCam camera and observed 13 faint meteors in 5 days. This proves that meteors are quite common stochastic feature in such images, but they are treated as a noise and stay untouched and unexplored. Finding them requires an automatic search for meteors in large astronomical databases. A recent example is an ongoing search for meteors in the SDSS database<sup>2</sup> (Beketešević, 2015), which required a development of a new machine recognition procedure for linear feature detection (Beketešević et al., 2016). Many other databases can be targeted by that approach, but this requires techniques in the domain of Big Data methodologies, where a small number of events has to be detected within terabytes or petabytes of imaging data. The upcoming big surveys covering the time domain in addition to large sky coverage will also have a daily stream of transient events alerts (e.g., LSST). Many current surveys too have such streams, either public (e.g. CRTS) or private (e.g. iPTF and Pan-STARRS). In fact searches on PTF data have been carried out to look for comets (using extendedness, Waszczack et al., 2013), and similar searches are on for asteroids (using streakiness), and a program has begun to get the missed ones using machine-learning. The meteor science community could be actively involved in these big sky survey collaborations and make an effort to put meteor detection into the surveys' automatic image recognition pipeline.

## 3 Big Data II

A recent discovery of MHz emission from meteors in the VHF radio band (Obenberger, 2014) demonstrates the need for monitoring possible meteor signals in sky surveys outside the traditional visual bands and comfort zone of meteor astronomers. The nature of this emission is not understood, but it shows the richness of meteor plasma physics. The ongoing and upcoming radio sky surveys will produce petabytes and soon exabytes of data (LOFAR, SKA). The meteor science community could pursue projects that combine meteor detection with different types of sensors simultaneously to extract more complex science from the data and to obtain precise timing of meteor appearance required for extracting data from big sky survey databases.

## 4 Big Data III

A search for dark energy and large-scale structure of the Universe as well as investigation of Galactic structure has motivated the development of specialized massively multi-object spectrographs equipped with several thousands of rapidly fixable fibres or Integral Field Unit spectrographs (IFUs). While some of them have very small field of view (e.g. 1 arcmin for ESO MUSE), other have several degrees, e.g. LAMOST<sup>3</sup> survey contains 4000 fibres of over 5°, the planned HETDEX survey even 33600 spectra in 22 arcmin (Adams et al., 2011). Those systems are running wide-field spectroscopic surveys with an exposure time of tens of minutes to several hours. As the observation is continuously running for months or years, there is a high probability that many meteoric spectra were registered by them, which are, however hidden in the noise. Serendipitous observations of meteors with such instruments are of a great value, since the individual spectra can reveal differences in emission from various parts of the resolved defocused meteor image.

The spectra are reduced by automatic pipelines, with automatic matching of significant features like strong emission (for redshift estimation) and/or global matching with a library of templates (for stellar classification), but always individually, one spectrum independently of others. As the targets are usually faint, the signal-to-noise ratios are low and so the meteoric spectrum will be hidden in the noise. However, the potential of the astroinformatics approach is in finding the correlations in intensity of noise among all fibre spectra exposed during the same exposure, which are in addition correlated with position of fibres on the sky. So the data have a character of a sparse data cube – looking like an image, where every point contains a whole spectrum (the spatial coverage is regular grid in case of IFUs).

Finding such correlations is a challenge for advanced statistics and big data processing. The probability of such a detection requires analyzing of an enormous amount of data (of the order of hundreds of TB), which must have a

<sup>1</sup> <http://bigskyearth.eu/>

<sup>2</sup> [http://vinkovic.org/Projects/MindExercises/radnje/2015\\_Dino.pdf](http://vinkovic.org/Projects/MindExercises/radnje/2015_Dino.pdf)

<sup>3</sup> <http://www.lamost.org/public/?locale=en>

unified metadata description. The great advantage of such a novel approach is in the possibility of observing changes of spectra of the meteor along the orbit while passing over different fibres or IFU elements.

This type of meteor astronomy requires new algorithms for meteor detection and analysis of their multispectral data as well as involvement of experts on advanced statistics and informatics understanding scientific Big Data processing.

Enormous potential, yet unexploited, presents the cross-matching of all such surveys in a global manner, with an aim to find observations of the same regions of the sky at the same time with different instruments, namely at the moment of a bright meteor detection in the wide field surveys. This may be feasible, if all the surveys follow the standards of the International Virtual Observatory Alliance (IVOA), namely the Table Access Protocol (Nandrekar-Heinis et al., 2014) operating on Observation Data Model Core Components (Louys et al., 2011) designed for temporal, spectral and spatial description of virtually all types of astronomical data.

We also suggest considering dedicated observation projects with middle class telescopes, with the telescope focus set onto the meteors. From SDSS statistics we see that the distribution diverges from the prediction from major meteor storms. I.e., there are a number of telescopic meteor storms with a small size distribution, which can dominate the optical groups in the telescopic magnitude range. The optimal strategy might be to make predictions from sky surveys and other detections, and to allocate the telescope time to the peaks of telescopic meteors. Even with a Schmidt telescope with 180 cm focal length, the sharp picture of a meteor at 110 km distance is 3 millimeters behind the sharp images of stars, leading to a blurred image by approximately 3 arcsec. The blurring keeps worsening heavily with the increasing focal length. A well-focused telescope can, on the other hand, reach a few 10 cm resolution, which is a solid observational basis for studying the plasma trail.

## 5 New meteor plasma physics

There is mounting evidence that our understanding of the meteor plasma physics is not adequate to explain various meteor related phenomena. High altitude meteors at about 130 km altitude have been explained by sputtering (Popova et al., 2007; Vinković, 2007), but some images show jets and structures that require additional explanations (Spurný, 2000). Similar fast jets have been detected at lower altitudes too (LeBlanc et al., 2000), and a complex plasma dynamics in the rarefied magnetized ionospheric environment might be the reason. Maybe this physics has some connection to the phenomenon of electrophonic sounds, which had been detected instrumentally, but their explanation is still missing (Zgrablić et al., 2002). The main problem is that this sound seems to originate from strong electric fields on the ground, but created at ionospheric altitudes. However, such strong quasi-electrostatic disturbances should not be

able to propagate to the ground. Also, fragmentation above 100 km altitude can explain some radar or imaging data, but there is no explanation for detected high speed fragments at these altitudes (Stokan and Campbell-Brown, 2014). Similarly, fast (millisecond) high-amplitude flickering of light curves (Spurný and Cepelcha, 2008) and stationary oscillations of radar cross section (Kero et al., 2008) are still not explained. A large halo around a meteor detected in a high-speed recording (Stenbaek-Nielsen and Jenniskens, 2004) is probably connected to the same type of physics. A new theoretical model (Šiljić et al., 2016) seeks explanation for many of these phenomena in electromagnetic coupling between meteors and their surrounding ionosphere, where the Earth's magnetic field plays an important role.

The most up-to-date papers detailing radiation physics of meteors are still the works by Öpik (1933, 1955), though of course there exist many studies, where not yet well-known processes are simply modelled using a heavily increased number of free parameters. The use of scaling laws to formulate a well-posed inverse problem helps in finding some key meteor parameters (Gritsevich, 2009; Gritsevich and Koschny, 2011), but there is still room for improvement. The meteor trails are also a complex topic.

The magnetization of trail electrons results in their faster drift along the direction of the magnetic field, which has been detected by radars and simulated recently in 3D (Oppenheim and Dimant, 2015). Theory also shows that strong electric fields could be induced with the trail, which can drastically increase the complexity of meteor plasma dynamics (Dimant et al., 2009). Such a long list of unexplained meteor related phenomena suggests that our understanding of meteor plasma and hypervelocity shock physics in rarefied partially ionized and partially magnetized ionospheric plasma is not complete. The variety of detection techniques required for measuring these phenomena argues for a highly interdisciplinary approach with a combination of astronomical and geophysical techniques.

## 6 Numerical simulations

The recent development of numerical simulation methods and enhanced computational resources provide possibilities to forecast the meteor plasma dynamics and to test how changes in the atmospheric conditions affect the meteor radar reflections and explain unexpected results in the observations. Computer simulations, built by using modern and computationally efficient methods (see, e.g., Marshall and Close, 2015; Sansom et al., 2015; Rabinä et al., 2016), are reasonable tools to test new meteor plasma models and consider, e.g., the fragmentation of a meteoroid into smaller pieces (e.g. Kero et al., 2008; Zhu et al., 2016). However, when it comes to simulations of hypersonic meteor flight, numerical simulations are often scarce and simplified. These simulations can reveal details of the meteor non-equilibrium plasma formation and its properties and composition, but it is a highly complex problem. The meteor plasma physics includes a plethora of phenomena

– collisional processes between various charged and neutral plasma species; processes of atomic and molecular excitation, dissociation, ionization and recombination; evaporation (ablation) of the meteoroid surface; thermal radiative processes and transfer; chemical and charge exchange reactions; dusty plasma effects; etc. – and all that coupled with internal and external electric and magnetic field dynamics that influence election and ion mobility in different ways, depending on the ratio between their collision and cyclotron frequency. Not surprisingly, the meteor hypersonic flight simulations have been simplified to include only basic kinetics of atmospheric and meteor vapor species (Boyd, 2000; Vinković, 2007; Dyrud et al., 2008) or, in its most advanced version, a radiative gas dynamic model of physically and chemically non-equilibrium flow at lower meteor heights (70 km) where the atmosphere is dense enough to fulfil conditions for ignoring external electric and magnetic fields and for applying simulation methods developed for modelling the re-entry of space vehicles (Surzhikov, 2014). Hence, we still do not have numerical simulations that can address the issues of meteor plasma at typical heights between 70 and 130km, where: the flow is in a transition regime from free-molecule to continuous flow (Popova et al., 2000); electrons react to the external magnetic field while the ion mobility is still collisional dominated; we expect a self-induced electric field within the meteor's diffuse shock front (Farbar and Boyd, 2010). These new simulation frontiers are required to test the latest theoretical attempts of exploring the impact of the ionospheric electric and magnetic field on the meteor plasma dynamics (Dimant et al., 2009; Šiljić et al., 2016).

## 7 Complex connection with other atmospheric phenomena

Although the majority of meteors are sub-millimeter in size, they still have a great importance for the Earth's atmosphere. They are the main source of metallic ions for the ionospheric Sporadic E layers — thin layers of metallic ion plasma which form mostly between 100 and 125 km (Haldoupis, 2012). Meteor airbursts create a plethora of large scale atmospheric and ionospheric disturbances. Meteor storms can significantly disturb the ionosphere and its ionization levels (e.g. Baumann et al., 2013; Pellinen-Wannberg et al., 2014). Nanometer size smoke particles from meteor ablation influence ion chemistry at altitudes from 80 to 120 km and are most likely nucleation sites for ice particles that make up noctilucent clouds (Hervig et al., 2012). It is also confirmed now that meteors can trigger sprites (large-scale electrical discharges high above thunderstorms), although the exact physical mechanism enabling this phenomenon is not understood (Qin et al., 2014). These examples demonstrate the complexity of the meteor-atmosphere interaction that goes far beyond meteor ablation physics.

## 8 Three dimensional radar observations

Radars play a critical role in the exploration of meteor plasma properties – from meteor head to meteor trails. A new dimension of meteor plasma exploration has been reached with a simultaneous usage of three radars. The potential observing capabilities of a radar system are evaluated by McCrea et al. (2015), McKay-Bukowski et al. (2015) and Pellinen-Wannberg et al. (2016). The authors address an important topic of improving the estimates for the flux of extraterrestrial matter to the Earth based on the data obtained using a high-power radar system. EISCAT\_3D (Europe's Next-Generation Radar for Atmospheric and Geospace Science) is incoherent scatter radar and it is expected to be one of the most advanced instruments to investigate plasma physics phenomena in the terrestrial atmosphere. The multi-beaming capability makes it possible to perform three or more tri-static observations at different heights simultaneously, while the lower operating frequency makes head echoes observable at heights up to 115 km.

## 9 Meteorite fall location using weather radar imagery

This is a recently proven approach to locate fresh meteorite fall (Fries and Fries, 2010; Fries et al., 2014). Weather radars are operated by national weather bureaus worldwide and have assisted in the recovery of several meteorites in the United States within the past years, including the Sutter's Mill and Battle Mountain meteorites. Up to now the search for the specific signatures within the data acquired by weather radar has been performed manually and was initiated due to the existence of the other fireball records indicating a possible meteorite fall (i.e. by having the time and tentative location constrains available from the other observation means). However dedicated automatic software may be developed to recognize the 'meteorite signature' in the whole set of weather radar data and to calculate timely the locations and create immediate alerts for detected meteorite falls.

## 10 Emission and/or scattering of VLF

Very low frequency (VLF) radio waves have been occasionally explored in relation to meteors. The interest for this topic initially emerged from theoretical predictions of VLF being the cause of electrophonic sounds. However, their relation to meteors has not been firmly established and they have not been detected concurrently with electrophonic sounds. Instead, even lower radio frequencies (in the range of quasi-electrostatic fields) are suspected as the source of these sounds (Zgrablić et al., 2002). Two types of possible correlations between VLF and meteors have been implied: meteors emitting VLF waves (*case a*) or their perturbed surrounding simply scatter the atmospheric VLF waves (*case b*) producing the variations of amplitudes and a phase of kHz VLF signals. With a VLF receiver or network of receivers (Šulić et al., 2016) we

can continuously monitor and later analyze these meteors correlated VLF radio waves.

**Case a**

First we consider the electromagnetic detection of meteors. Recently, it was reported that a meteor shower produces ELF/VLF waves which propagate and reach the ground. It has been shown that 35% of observed meteors and corresponding VLF events are in correlations. However, more data with a statistical approach and further investigations are needed to confirm the statement that the process of possible detecting meteors with the help of an electromagnetic spectrum has potential to become a widely useful tool. In spite that it is at a very noisy frequency band (lot of EM waves produced in this band by other sources like lightning, electrical circuits, power supplies) this possible technique would have the advantage over the visual detection because it can be applicable at any time day/night and in almost all weather conditions. A dynamic VLF spectrum with broadband data is shown in *Figure 1*. With the help of this spectrum we can get all frequencies between 5 kHz and 13 kHz (possible emitted by meteors) compare and process them. This kind of data, i.e. a large volume of spectral images with spectral wavelengths, takes up a few GB per hour and requires complex processing and analysis.

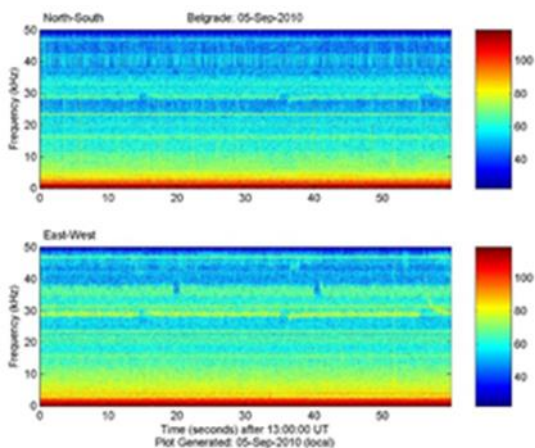


*Figure 1* – Broadband data includes information at all frequencies between the systems cutoffs (few Hz – 47 kHz) recorded at receiver site.

**Case b**

Possible detection of meteors can be done by simply taking the amplitude and phase, separately (of a single narrow frequency range, specified in the software, and usually corresponding to the frequency of a VLF transmitter which can be seen from the map in *Figure 2*) and compared to the non-perturbed level. This can be quite improved with a simultaneous usage of different transmitters i.e. the usage of signals from different directions (path dependent) in order to really collect correlation between signal perturbation and meteor detection.

The physical explanation-mechanism for case b demonstrates the complexity of the meteor-atmosphere interaction (meteor plasma, ionization, triggering sprites, etc.). Meteor particles, due to collisions and perturbation

of the surrounding ionosphere (neutral molecules), pass the kinetic energy and convert into potential energy of ionization with the production of extra ionization in the ionosphere. Meteors and this extra ionization produced by them during their passage through the lower ionosphere may have been the cause of high variation of signal level of amplitudes /phase of VLF signals in the Earth-ionosphere waveguide (recorded after their journey through a long distance), which is few times its normal value (De et al., 2012).



*Figure 2* – Worldwide VLF transmitters.

It would be very useful for VLF researchers to make effort and implement some new solutions which are already used in other fields of astro- and geoscience, such as events alerts (e.g., CRTS). It was with the Palomar-QUEST, and CRTS that the VOEvent protocol was developed and implemented under the aegis of the US Virtual Observatory (NVO, VAO). The VOEvent (Williams and Seaman, 2006) is a simple and small packet describing the what/where/when/how/why of an event and can be conveyed as a variety of inter-transferable structured data-formats such that humans as well as machines that can make decisions and automated telescopes can receive them. CRTS, for instance, has made extensive use of it (Drake et al., 2009; Djorgovski et al., 2011; Mahabal et al., 2011). Recent systems like Gaia are using variations on the theme, and LSST plans to use an extended version to also include small image cutouts. We propose to the meteor science community more networked VLF observatories for a better understanding of this phenomenon and we propose a highly interdisciplinary approach utilizing the infrastructural developments in optical astronomy as mentioned above. The VLF event alerts can be combined with alerts of meteor detection coming from meteor networks. Such networks of video cameras are now established in many countries and often operated by amateur astronomers. The networks detect meteors and their trajectories and provide invaluable data for meteor activity and their origin exploration. But they can be further utilized as targets of meteor VLF events. A network observing the sky on the path of VLF signals from transmitters can feed the VLF observer with meteor detection alerts. In case ionization from a meteor shower or from bright individual meteors creates disturbances in the VLF signal, the cross-correlation between meteor and VLF alerts would reveal details of the physics behind this connection. However, such a coordinated work is not

challenging only from logistical point of view, but also from a Big Data perspective.

There is also an active radio observation of meteors ongoing in the VHF range using the French military satellite tracking radar system GRAVES at 143.05 MHz. An example of such VHF activity is the Czech radio meteor detection network Bolidozor (Pinter et al., 2013; Kákona et al., 2015). The primary goal of this network is calculation of meteor trajectories from multi-station meteor radio echoes. Bolidozor stations' and receivers' configuration is shown on *Figure 3a and 3b*.

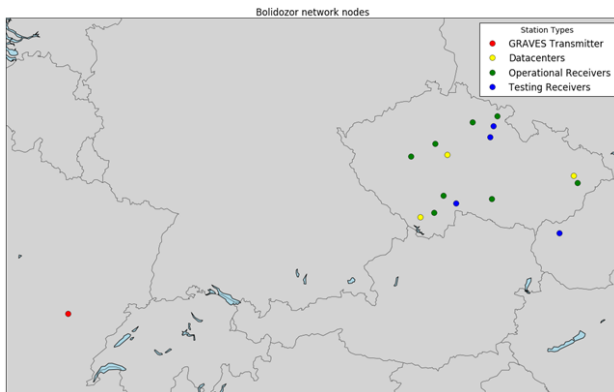


*Figure 3a* – Czech VHF meteor detection network Bolidozor. The red dot in France is the VHF transmitter GRAVES.

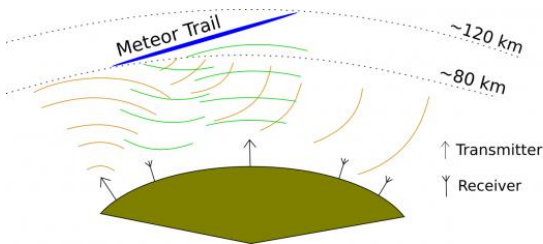


*Figure 3b* – The core of the system is made of a network of meteor radio detectors that are gradually upgraded and extended to contain new measurement methods.

The network is technically limited mainly by signal processing algorithm implementation because the multi-static systems require numerically demanding statistical calculations, which are furthermore being done in real-time and with a signal containing a high proportion of interference. Each station currently generates 1GB of pre-filtered data per day. The data are accumulated in a central data server located at the Ondřejov observatory. In order to effectively use the multi-static signal, there have to exist algorithms able to detect objects covered by interference and using the data from multiple stations, but the data processing complexity requires a high amount of computing power which is usually in the form of distributed computing power in modern scientific experiments, e.g. BOINC<sup>4</sup>. Such computing methods require data distribution on multiple nodes, which means the distributed storage of a big data amount, is necessary for such system. One of the promising, less computationally demanding methods seems to be an application of artificial neural networks (Roman and Buiu, 2014). However the research is just at the

<sup>4</sup> <http://boinc.berkeley.edu>

beginning and therefore there are many tasks open from the informatics point of view.

## 11 Solar migration

The study of meteors can also help inform the study of the Galaxy we live in. There is a growing consensus that the Milky Way has experienced significant levels of stellar radial migration, with stars having changed their orbital radius within the Milky Way significantly while retaining nearly circular orbits (Roskar et al., 2008; Hayden et al., 2015; Loebman et al., 2016). However the exact extent to which stars have migrated, particularly in the Solar neighborhood, is not well known. In much the same way as stars migrate, interstellar meteoroids will also have. A small, but not negligible, fraction of meteors reaching the Earth will originate from across the Milky Way, giving us direct access to conditions across the Milky Way. Properties, such as the relative abundance of alpha-elements (for instance, carbon, oxygen, magnesium, and calcium) compared with iron-peak elements, vary across the Milky Way, providing a means by which the origin within the Milky Way of meteors can be recognized. Such meteors at the Earth are therefore particularly useful for helping to constrain the extent to which migration has been taking place in the solar neighborhood.

## 12 Detection of meteors from orbit and stratosphere

Certain aspects of meteor science require observations outside the atmosphere, or at least above the majority of the atmosphere (Bouquet et al., 2014; Vaubaillon et al., 2015). For example, observations from satellites enable detection of meteor UV spectra and infrared signatures (Rambaux et al., 2014). In comparison with existing ground-based observations, a space-based optical system for meteor detection would escape dependency on weather and atmospheric conditions, critical not only for detectability, but also for subsequent data analysis (Lyytinen and Gritsevich, 2016). It is also the easiest way to set up meteor observations on other planets (Christou et al., 2012, 2014). Bouquet et al. (2014) recently evaluated potential performance by such systems as a function of observation parameters (optical system capabilities, orbital parameters) and considering a reasonable range of meteoroid properties (mass, velocity, composition) determining their luminosity. The authors developed a numerical tool called SWARMS (Simulator for Wide Area Recording of Meteors from Space) and calculated optimistic meteor detection rates for two different systems: the SPOSH (Smart Panoramic Optical Sensor Head) camera optimized for the observation of transient luminous events (Oberst et al., 2011; Christou et al., 2012), and the JEM-EUSO (Japanese Experiment Module – Extreme Universe Space Observatory) experiment on the International Space Station (ISS).

We also propose the creation of a stratospheric platform for meteor observations put on an autonomous unmanned airship. This would enable observations in a rarefied

atmosphere, above the majority of water vapor. Under such conditions meteors can be observed close to the horizon and with infrared detectors. Airborne meteor observations have a long history (Clifton, 1971; Millman, 1976), but it was the NASA MAC campaigns targeting Leonid showers that transformed airborne meteor science into a mainstream science (Jenniskens and Butow, 1999). This campaign has expanded in its scope and it is now using various types of aircraft<sup>5</sup> for observing meteor showers and it recently helped organize the first European airborne meteor observation campaign (Vaubailon et al., 2015). The airborne platforms have an advantage of avoiding clouds and have access to a reduced air-mass of water vapor. This enables sampling of a large volume of atmosphere in search for meteors closer to the horizon. It also enables observations of meteor light-curves and spectra in wavelength regions typically inaccessible due to atmospheric water vapor.

A stratospheric airship would provide an entirely new direction in airborne meteor observations. Unlike airplane campaigns that last for a few days, such an airship would provide a continuous service over the year. It would also reach higher altitudes, nominally about 20 km above the sea level. And it would be much cheaper to operate it and maintain. Its science case would not be just meteor observations, but also a multitude of other topics in astronomy (e.g. infrared astronomy, where the need is already demonstrated by the SOFIA airborne telescope (Gehrz et al., 2009)), aeronomy (e.g. transient light phenomena above thunderclouds), Earth observation and remote sensing (e.g. continuous high resolution ground monitoring of about 4000 km<sup>2</sup> not possible with the current drone, airplane or satellite observations) and meteorology (e.g. continuous measurements of atmospheric conditions at high altitudes and during landing/rising maneuver). Such a stratospheric platform would be also ideal for testing various new technologies/instruments aimed for future deployment on satellites.

The key technical characteristics of the proposed airship are already provided by Hipersfera Ltd.<sup>6</sup>, a company uniquely specialized for this type of autonomous unmanned aerial vehicles. The airship would host a stable payload platform for about 12 hours (during night time in case of astronomical observations), followed by a landing maneuver and just a few hours for maintenance, repair and overhaul procedures. This makes the airship ready for a new mission every day. The payload capacity would be 100 kg, with 5 kW of continuous and 7-10 kW peak electric power supply. The airship design allows mounting of useful payload either on the bottom or on the top side of the airship. Instruments of a small weight (simple sensors) can be attached on a side. The airship has a rigid structure with attached vectored thrust for attitude and position control. The stabilized payload platform (e.g. designed as a Stewart platform) is connected to the airship through passive vibration

isolation, which improves on the default 0.2–0.5 deg/s stability achieved with the vector thrust. The vibration isolation can be further improved on request (e.g. with 3- or 5-axial gimbal). The airship design is scalable, which means that a larger payload can be achieved simply by scaling up the airship volume.

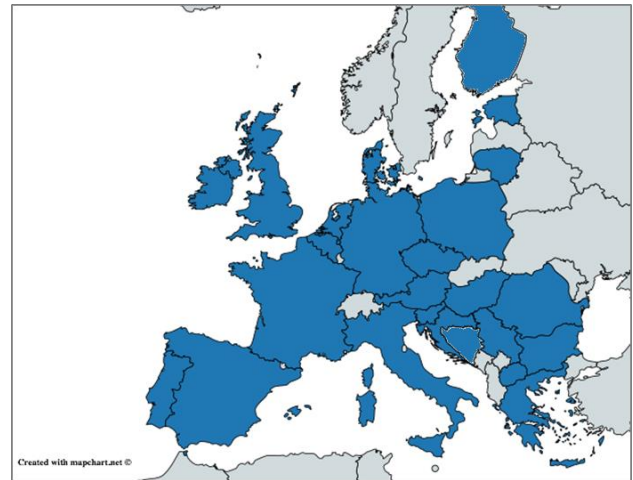


Figure 4 – The map showing COST member countries participating in the COST Action BigSkyEarth (as of June 2016). Further information on BigSkyEarth and its activities are given at <http://bigskyeearth.eu/>.

The TD COST Action TD1403 “Big Data Era in Sky and Earth Observation” (BigSkyEarth, Figure 4) network offers an excellent platform to develop the stated big ideas for possible future advances in meteor science, as well as it provides suitable environment for efficient collaboration and joint research studies.

## Acknowledgment

This review article is based upon a collaborative work from the COST Action TD1403 “Big Data Era in Sky and Earth Observation”, supported by the COST (European Cooperation in Science and Technology, <http://www.cost.eu/>).



<sup>5</sup> <http://airborne.seti.org>

<sup>6</sup> <http://www.hipersfera.hr>

## References

- Adams J. J., Blanc G. A., Hill G. J., Gebhardt K., Drory N., Hao L., Bender R., Byun J., Ciardullo R., Cornell M. E., Finkelstein S. L., Fry A., Gawiser E., Gronwall C., Hopp U., Jeong D., Kelz A., Kelzenberg R., Komatsu E., MacQueen P. J., Murphy J., Odoms P. S., Roth M., Schneider D. P., Tufts J. R. and Wilkinson C. P. (2011). "The HETDEX Pilot Survey. I. Survey Design, Performance, and Catalog of Emission-line Galaxies". *The Astrophysical Journal Supplement*, **192**, id 5, 34 pages.
- Antolik M., Ichinose G., Creasey J. and Clauter D. (2014). "Seismic and Infrasonic Analysis of the Major Bolide Event of 15 February 2013". *Seismological Research Letters*, **85**, 334–343.
- Baumann C., Rapp M., Kero A. and Enell C.-F. (2013). "Meteor smoke influences on the D-region charge balance - review of recent in situ measurements and one-dimensional model results". *Annales Geophysicae*, **31**, 2049–2062.
- Bekkešević D. (2015). "Linear feature detection in SDSS images". Master Thesis, University of Split.
- Bekkešević D., Cikota S., Jevremović D. and Vinković D. (2016). "Linear feature detection algorithm for astronomical surveys II. Parameter optimization". In preparation.
- Borovička J., Spurný P., Brown P., Wiegert P., Kalenda P., Clark D. and Shrbený L. (2013). "The trajectory, structure and origin of the Chelyabinsk asteroidal impactor". *Nature*, **503**, 235–237.
- Bouquet A., Baratoux D., Vaubaillon J., Gritsevich M. I., Mimoun D., Mosis O. and Bouley S. (2014). "Simulation of the capabilities of an orbiter for monitoring the entry of interplanetary matter into the terrestrial atmosphere". *Planetary and Space Science*, **103**, 238–249. doi: 10.1016/j.pss.2014.09.001.
- Boyd I. D. (2000). "Computation of Atmospheric Entry Flow about a Leonid Meteoroid". *Earth, Moon, and Planets*, **82/83**, 93–108.
- Brown P., Assink J. D., Astiz A., Blaauw R., Boslough M. B., Borovička J., Brachet N., Brown D., Campbell-Brown M., Ceranna L., Cooke W., de Groot-Hedlin C., Drob D. P., Edwards W., Evers L. G., Garces M., Gill J., Hedlin M., Kingery A., Laske G., Le Pichon A., Mialle P., Moser D. E., Saffer A., Silber E., Smets P., Spalding R. E., Spurný P., Tagliaferri E., Uren D., Weryk R. J., Whitaker R. and Krzeminski Z. (2013). "A 500-kiloton airburst over Chelyabinsk and an enhanced hazard from small impactors". *Nature*, **503**, 238–241.
- Christou A. A., Oberst J., Elgner S., Flohrer J., Margonis A., McAuliffe J. P. and Koschny D. (2012). "Orbital observations of meteors in the Martian atmosphere using the SPOSH camera". *Planetary and Space Science*, **60**, 229–235.
- Christou A. A., Oberst J., Lupovka V., Dmitriev V. and Gritsevich M. (2014). "The meteoroid environment and impacts on Phobos". *Planetary and Space Science*, **102**, 164–170.
- Clifton K. S. (1971). "Airborne meteor observations at high latitudes". *NASA Technical Note D-6303*.
- De S. S., Bandyopadhyay B., Barui S., Paul S., Haldar D. K., De D., De B. K., Chattopadhyay S. and Kundu A. K. (2012). "Studies on the Effects of 2009 Leonid Meteor Shower on Subionospheric Transmitted VLF Signals and Vertical Electric Potential Gradient". *Earth, Moon, and Planets*, **108**, 111–121.
- Dimant Y. S., Oppenheim M. M. and Milikh G. M. (2009). "Meteor plasma trails: effects of external electric field". *Annales Geophysicae*, **27**, 279–296.
- Djorgovski S. G., Drake A. J., Mahabal A. A., Graham M. J., Donalek C., Williams R., Beshore E. C., Larson S. M., Prieto J., Catelan M., Christensen E. and McNaught R. H. (2011). "The Catalina Real-Time Transient Survey (CRTS)". arXiv:1102.5004.
- Drake A. J., Djorgovski S. G., Mahabal A., Beshore E., Larson S., Graham M. J., Williams R., Christensen E., Catelan M., Boattini A., Gibbs A., Hill R. and Kowalski R. (2009). "First Results from the Catalina Real-Time Transient Survey". *The Astrophysical Journal*, **696**, 870–884.
- Dyrud L., Wilson D., Boerve S., Trulsen J., Pecseli H., Close S., Chen C. and Lee Y. (2008). "Plasma and electromagnetic wave simulations of meteors". *Advances in Space Research*, **42**, 136–142.
- Farbar E. D. and Boyd I. D. (2010). "Modeling of the plasma generated in a rarefied hypersonic shock layer". *Physics of Fluids*, **22**, 106101–106101–12.
- Fries M. and Fries J. (2010). "Doppler weather radar as a meteorite recovery tool". *Meteoritics and Planetary Science*, **45**, 1476–1487.
- Fries M., Le Corre L., Hankey M., Fries J., Matson R., Schaefer J. and Reddy V. (2014). "Detection and rapid recovery of the Sutter's Mill meteorite fall as a model for future recoveries worldwide". *Meteoritics and Planetary Science*, **49**, 1989–1996.
- Gehrz R. D., Becklin E. E., de Pater I., Lester D. F., Roellig T. L. and Woodward C. E. (2009). "A new window on the cosmos: The Stratospheric

- Observatory for Infrared Astronomy (SOFIA)". *Advances in Space Research*, **44**, 413–432.
- Gritsevich M. and Koschny D. (2011). "Constraining the luminous efficiency of meteors". *Icarus*, **212**, 877–884. doi: 10.1016/j.icarus.2011.01.033.
- Gritsevich M. I. (2009). "Determination of parameters of meteor bodies based on flight observational data". *Advances in Space Research*, **44**, 323–334. doi: 10.1016/j.asr.2009.03.030.
- Haldoupis C. (2012). "Midlatitude Sporadic E. A Typical Paradigm of Atmosphere-Ionosphere Coupling". *Space Science Reviews*, **168**, 441–461.
- Hayden M. R., Bovy J., Holtzman J. A., Nidever D. L., Bird J. C., Weinberg D. H., Andrews B. H., Majewski S. R., Allende Prieto C., Anders F., Beers T. C., Bizyaev D., Chiappini C., Cunha K., Frinchaboy P., García-Hernández D. A., García Pérez A. E., Girardi L., Harding P., Hearty F. R., Johnson J. A., Mészáros S., Minchev I., O'Connell R., Pan K., Robin A. C., Schiavon R. P., Schneider D. P., Schultheis M., Shetrone M., Skrutskie M., Steinmetz M., Smith V., Wilson J. C., Zamora O. and Zasowski G. (2015). "Chemical Cartography with APOGEE: Metallicity Distribution Functions and the Chemical Structure of the Milky Way Disk". *The Astrophysical Journal*, **808**, 132.
- Hervig M. E., Deaver L. E., Bardeen C. G., Russell J. M., Bailey S. M. and Gordley L. L. (2012). "The content and composition of meteoric smoke in mesospheric ice particles from SOFIE observations". *Journal of Atmospheric and Solar-Terrestrial Physics*, **84**, 1–6.
- Iye M., Tanaka M., Yanagisawa M., Ebizuka N., Ohnishi K., Hirose C., Asami N., Komiyama Y. and Furusawa H. (2007). "SuprimeCam Observation of Sporadic Meteors during Perseids 2004". *Publications of the Astronomical Society of Japan*, **59**, 841–855.
- Jenniskens P. and Butow S. J. (1999). "The 1998 Leonid multi-instrument aircraft campaign – an early review". *Meteoritics and Planetary Science*, **34**, 933–943.
- Kákona J., Kákona M., Povišer M., Milík J., Dvořák R., Štrobl J., Kovář P., Szylar J., Bednář P., Křivský L. and Chroust J. (2015). "Bolidozor radio meteor detection network". In Rault J.-L. and Roggemans P., editors, *Proceedings of the International Meteor Conference*, Mistelbach, Austria, 27-30 August 2015. IMO, pages 157–160.
- Kero J., Szasz C., Pellinen-Wannberg A., Wannberg G., Westman A. and Meisel D. D. (2008). "Three-dimensional radar observation of a submillimeter meteoroid fragmentation". *Geophysical Research Letters*, **35**, CiteID L04101.
- Kohout T., Gritsevich M., Grokhovsky V., Yakovlev G., Haloda J., Halodova P., Michallik R., Penttilä A. and Muinonen K. (2014). "Mineralogy, reflectance spectra, and physical properties of the Chelyabinsk LL5 chondrite – Insight into shock-induced changes in asteroid regoliths". *Icarus*, **228**, 78–85. doi: 10.1016/j.icarus.2013.09.027.
- LeBlanc A. G., Murray I. S., Hawkes R. L., Worden P., Campbell M. D., Brown P., Jenniskens P., Correll R. R., Montague T. and Babcock D. D. (2000). "Evidence for transverse spread in Leonid meteors". *Monthly Notices of the Royal Astronomical Society*, **313**, L9–L13.
- Loebman S. R., Debattista V. P., Nidever D. L., Hayden M. R., Holtzman J. A., Clarke A. J., Roskar R. and Valluri M. (2016). "Imprints of Radial Migration on the Milky Way's Metallicity Distribution Functions". *The Astrophysical Journal Letters*, **818**, L6.
- Louys M., Bonnarel F., Schade D., Dowler P., Micol A., Durand D., Tody D., Michel L., Salgado J., Chilingarian I., Rino B., Santander-Vela J. D. and Škoda P. (2011). "IVOA Recommendation: Observation data model core components and its implementation in the table access protocol version 1.0". arXiv: 1111.1758.
- Lyytinen E. and Gritsevich M. (2016). "Implications of the atmospheric density profile in the processing of fireball observations". *Planetary and Space Science*, **120**, 35–42. doi: 10.1016/j.pss.2015.10.012.
- Mahabal A. A., Djorgovski S. G., Drake A. J., Donalek C., Graham M. J., Williams R. D., Chen Y., Moghaddam B., Turmon M., Beshore E. and Larson S. (2011). "Discovery, classification, and scientific exploration of transient events from the Catalina Real-time Transient Survey". *Bulletin of the Astronomical Society of India*, **39**, 387–408. <http://arxiv.org/pdf/1111.0313.pdf>
- Marshall R. A. and Close S. (2015). "An FDTD model of scattering from meteor head plasma". *Journal of Geophysical Research*, **120**, 5931–5942.
- McCrea I., Aikio A., Alfonsi L., Belova E., Buchert S., Clilverd M., Engler N., Gustavsson B., Heinselman C., Kero J., Kosch M., Lamy H., Leyser T., Ogawa Y., Oksavik K., Pellinen-Wannberg A., Pitout F., Rapp M., Stanislawska I. and Vierinen J. (2015). "The science case for the EISCAT\_3D radar". *Progress in Earth and Planetary Science*, **1**, 1–63.
- McKay-Bukowski D., Vierinen J., Virtanen I. I., Fallows R., Postila M., Ulich T., Wucknitz O.,

- Brentjens M., Ebbendorf N., Enell C.-F., Gerbers M., Grit T., Gruppen P., Kero A., Iinatti T., Lehtinen M., Meulman H., Norden M., Orispää M., Raita T., de Reijer J. P., Roininen L., Schoenmakers A., Stuurwold K. and Turunen E. (2015). “KAIRA: The Kilpisjärvi Atmospheric Imaging Receiver Array-System Overview and First Results”. *IEEE Transactions on Geoscience and Remote Sensing*, **53**, 1440–1451.
- Millman P. M. (1976). “Quadrantid meteors from 41,000 feet”. *Sky and Telescope*, **51**, 225–228.
- Nandrekar-Heinis D., Michel L., Louys M. and Bonnarel F. (2014). “The Table Access Protocol: Providing standard access to astronomical data”. *Astronomy and Computing*, **7–8**, 37–44.
- Obenberger K. S., Taylor G. B., Lin C. S., Dowell J., Schinzel F. K. and Stovall K. (2015). “Dynamic radio spectra from two fireballs”. *Journal of Geophysical Research: Space Physics*, **120**, 9916–9928. doi:10.1002/2015JA021229.
- Oberst J., Flohrer J., Elgner S., Maue T., Margonis A., Schrödter R., Tost W., Buhl M., Ehrich J., Christou A. and Koschny D. (2011). “The smart panoramic optical sensor head (SPOSH) – A camera for observations of transient luminous events on planetary night sides”. *Planetary and Space Science*, **59**, 1–9.
- Öpik E. J. (1933). “Atomic Collisions and Radiation of Meteors”. *Harvard Reprint Series*, **100**, Is. 100, 1–39.
- Öpik E. J. (1955). “Meteor Radiation, Ionization and Atomic Luminous Efficiency”. *Proceedings of the Royal Society of London. Series A, Mathematical and Physical Sciences*, **230**, Is. 1183, 463–501.
- Oppenheim M. M. and Dimant Y. S. (2015). “First 3-D simulations of meteor plasma dynamics and turbulence”. *Geophysical Research Letters*, **42**, 681–687.
- Pellinen-Wannberg A., Häggström I., Carrillo Sánchez J. D., Plane J. M. C. and Westman A. (2014). “Strong E region ionization caused by the 1767 trail during the 2002 Leonids”. *Journal of Geophysical Research*, **119**, 7880–7888.
- Pellinen-Wannberg A., Kero J., Häggström I., Mann I. and Tjulin A. (2016). “The forthcoming EISCAT\_3D as an extra-terrestrial matter monitor”. *Planetary and Space Science*, **123**, 33–40. <http://dx.doi.org/10.1016/j.pss.2015.10.009>.
- Pinter T., Kákona J., Kákona M. and Křivský L. (2013). “Radio meteor scattering with Software Defined Radio based on Open Hardware”. In Gyssens M. and Roggemans P., editors, *Proceedings of the International Meteor Conference*, La Palma, Canary Islands, 20–23 September 2012. IMO, pages 213–217. doi: 10.5281/zenodo.53085.
- Popova O. P., Sidneva S. N., Shuvalov V. V. and Strelkov A. S. (2000). “Screening of Meteoroids by Ablation Vapor in High-Velocity Meteors”. *Earth, Moon, and Planets*, **82/83**, 109–128.
- Popova O. P., Strelkov A. S. and Sidneva S. N. (2007). “Sputtering of fast meteoroids’ surface”. *Advances in Space Research*, **39**, 567–573.
- Popova O. P., Jenniskens P., Emel’yanenko V., Kartashova A., Biryukov E., Khaibrakhamanov S., Shuvalov V., Rybnov Y., Dudorov A., Grokhovsky V. I., Badyukov D. D., Yin Q.-Z., Gural P. S., Albers J., Granvik M., Evers L. G., Kuiper J., Kharlamov V., Solovyov A., Rusakov Y. S., Korotkiy S., Serdyuk I., Korochantsev A. V., Larionov M., Y., Glazachev D., Mayer A. E., Gisler G., Gladkovsky S. V., Wimpenny J., Sanborn M. E., Yamakawa A., Verosub K. L., Rowland D. J., Roeske S., Botto N. W., Friedrich J. M., Zolensky M. E., Le L., Ross D., Ziegler K., Nakamura T., Ahn I., Lee J. I., Zhou Q., Li X.-H., Li Q.-L., Liu Y., Tang G.-Q., Hiroi T., Sears D., Weinstein I. A., Vokhmintsev A. S., Ishchenko A. V., Schmitt-Kopplin P., Hertkorn N., Nagao K., Haba M. K., Komatsu M. and Mikouchi T. (2013). “Chelyabinsk Airburst, Damage Assessment, Meteorite Recovery, and Characterization”. *Science*, **342**, 1069–1073.
- Proud S. R. (2013). “Reconstructing the orbit of the Chelyabinsk meteor using satellite observations”. *Geophysical Research Letters*, **40**, 3351–3355. doi:10.1002/grl.50660.
- Qin J., Pasko V. P., McHarg M. G. and Stenbaek-Nielsen H. C. (2014). “Plasma irregularities in the D-region ionosphere in association with sprite streamer initiation”. *Nature Communications*, **5**, id. 3740.
- Räbinä J., Mönkölä S., Rossi T., Markkanen J., Gritsevich M. and Muinonen K. (2016). “Controlled time integration for the numerical simulation of meteor radar reflections”. *Journal of Quantitative Spectroscopy and Radiative Transfer*, **178**, 295–305.
- Rambaux N., Galayko D., Mariscal J. F., Breton M. A., Vaubaillon J., Birlan M., Colas F. and Fouchet T. (2014). “Detection of spectral UV from meteors by a nanosatellite”. In Rault J.-L. and Roggemans P., editors, *Proceedings of the International Meteor Conference*, Giron, France, 18–21 September 2014. IMO, pages 182–184.
- Roman V. S. and Buiu C. (2014). “Automatic detection of meteors using artificial neural networks”. In Rault J.-L. and Roggemans P., editors,

- Proceedings of the International Meteor Conference*, Giron, France, 18-21 September 2014. IMO, pages 122–125.
- Roskar R., Debattista V. P., Quinn T. R., Stinson G. S. and Wadsley J. (2008). "Riding the Spiral Waves: Implications of Stellar Migration for the Properties of Galactic Disks". *The Astrophysical Journal*, **684**, L79.
- Sansom E. K., Bland P., Paxman J. and Towner M. (2015). "A novel approach to fireball modeling: The observable and the calculated". *Meteoritics and Planetary Science*, **50**, 1423–1435. doi: 10.1111/maps.12478.
- Šiljić A., Lunić F., Teklić J. and Vinković D. (2016). "Proton-induced halo formation in charged meteors". In preparation.
- Spurný P., Betlem H., Jobse K., Koteš P. and van't Leven J. (2000). "New type of radiation of bright Leonid meteors above 130 km". *Meteoritics and Planetary Science*, **35**, 1109–1115.
- Spurný P. and Ceplecha Z. (2008). "Is electric charge separation the main process for kinetic energy transformation into the meteor phenomenon?". *Astronomy and Astrophysics*, **489**, 449–454.
- Stenbaek-Nielsen H. C. and Jenniskens P. (2004). "A "shocking" Leonid meteor at 1000 fps". *Advances in Space Research*, **33**, 1459–1465.
- Stokan E. and Campbell-Brown M. D. (2014). "Transverse motion of fragmenting faint meteors observed with the Canadian Automated Meteor Observatory". *Icarus*, **232**, 1–12.
- Šulić D. M., Srećković V. A. and Mihajlov A. A. (2016). "A study of VLF signals variations associated with the changes of ionization level in the D-region in consequence of solar conditions". *Advances in Space Research*, **57**, 1029–1043.
- Surzhikov S. T. (2014). "Non-Equilibrium Radiative Gas Dynamics of Small Meteor". 44th AIAA Fluid Dynamics Conference, AIAA Aviation, 16-20 June 2014, Atlanta, AIAA 2014-2636.
- Vaubailion J., Koteš P., Margonis A., Toth J., Rudawska R., Gritsevich M., Zender J., McAuliffe J., Pautet P. D., Jenniskens P., Koschny D., Colas F., Bouley S., Maquet L., Leroy A., Lecacheux J., Borovicka J., Watanabe J. and Oberst J. (2015). "The 2011 Draconids: the first European airborne meteor observation campaign". *Earth, Moon, and Planets*, **114**, 137–157. doi: 10.1007/s11038-014-9455-5.
- Vinković D. (2007). "Thermalization of sputtered particles as the source of diffuse radiation from high altitude meteors". *Advances in Space Research*, **39**, 574–582.
- Waszczak A., Ofek E. O., Aharonson O., Kulkarni S. R., Polishook D., Bauer J. M., Levitan D., Sesar B., Laher R., Surace J., and the PTF Team (2013). "Main-belt comets in the Palomar Transient Factory survey – I. The search for extendedness". *Monthly Notices of the Royal Astronomical Society*, **433**, 3115–3132.
- Williams R. and Seaman R. (2006). "VOEvent: Information Infrastructure for Real-Time Astronomy". *Astronomical Data Analysis Software and Systems XV ASP Conference Series*. Proceedings of the Conference Held 2-5 October 2005 in San Lorenzo de El Escorial, Spain. Edited by Carlos Gabriel, Christophe Arviset, Daniel Ponz, and Enrique Solano. San Francisco: Astronomical Society of the Pacific, 2006. **351**, 637–640.
- Zgrablić G., Vinković D., Gradečak S., Kovačić D., Biliškov N., Grbac N., Andreić Ž. and Garaj S. (2002). "Instrumental recording of electrophonic sounds from Leonid fireballs". *Journal of Geophysical Research*, **107**, SIA 11-1–SIA 11-9. DOI: 10.1029/2001JA000310.
- Zhu Q., Dinsmore R., Gao B. and Mathews J. D. (2016). "High-resolution radar observations of meteoroid fragmentation and flaring at the Jicamarca Radio Observatory". *Monthly Notices of the Royal Astronomical Society*, **457**, 1759–1769.

# Statistical approach to meteoroid shape estimation

Vladimir Vinnikov<sup>1</sup>, Maria Gritsevich<sup>1,2,3</sup>, Daria Kuznetsova<sup>1,4</sup>,  
Olga Krivonosova<sup>5</sup>, Dmitry Zhilenko<sup>5</sup> and Leonid Turchak<sup>1</sup>

<sup>1</sup>Dorodnicyn Computing Centre, Federal Research Center “Computer Science and Control”  
of the Russian Academy of Sciences, 119333 Moscow, Russia  
vinnikov@ccas.ru

<sup>2</sup>Finnish Geospatial Research Institute, Department of Geodesy and Geodynamics, FI-02431 Masala, Finland  
maria.gritsevich@nls.fi

<sup>3</sup>Ural Federal University, Institute of Physics and Technology, 620002 Ekaterinburg, Russia  
gritsevich@list.ru

<sup>4</sup>Laboratoire d’Aérodynamique, Observatoire Midi-Pyrénées, 14 av. Edouard Belin, 31400 Toulouse, France  
daria.kuznetsova@aero.obs-mip.fr

<sup>5</sup>Institute of Mechanics, Lomonosov Moscow State University, Michyrinskiy prospect 1, 119192 Moscow, Russia  
olga@imec.msu.ru

This paper describes a statistically-based technique for meteoroid shape estimation. The idea to obtain the pre-entry shape from a distribution of fragment masses is derived from the experiments on brittle fracturing, that produce multiple fragments of sizes less than or equal to the least dimension of the body. The fragment masses determine the number of fragments as a power law with exponential cutoff. The initial form of the fragmented body is essentially indicated by the value of this scaling exponent.

## 1 Introduction to the mathematical model

We explore the possibility of determining the proportions of a pre-fragmented meteoroid for the cases with large number of recovered meteorite fragments. The method follows the concepts proposed in (Oddershede et al., 1993; 1998; Vinnikov et al., 2015; 2016) and it is based on the following assumptions:

- The meteoroid material is assumed to be brittle. The common definition of brittleness involves the practical absence of plastic deformation prior to fracturing. We also assume that the crack propagation speed is comparable to the speed of sound through a brittle media and is at least one order higher than the acoustic speed of the surrounding environment. However, we do not completely address the issue of supersonic fracture (Buehler et al., 2003);
- The masses of the fragments recovered within one meteorite fall can be fitted via the power law (which is a special case of a *Weibull* distribution) with relatively small least squares error;
- A complementary cumulative distribution function (CCDF) can be constrained by the scaling exponent  $B_0$ , which accounts for the largest recovered fragment mass via an exponential cutoff:

$$F_c(m) = Cm^{-B_0} e^{-\frac{m}{m_U}}, \quad (1)$$

- For the value of  $B_0^*$  obtained by fitting *Equation 1* to the masses of recovered fragments, we can estimate a dimensionless shape parameter,  $d$  (its definition is based on size proportions  $a_x$ ,  $a_y$ ,  $a_z$ ) from the empirical equation

$$0.13d^2 - 0.21d + (1.1 - B_0^*) = 0 \quad (2)$$

In formula (1)  $C$  is a normalization constant,  $m_U > m_L$  is the upper cutoff fragment mass,  $m_U$  corresponds to the threshold where the exponential decay starts to dominate over the power law, and  $m_L > 0$  is an arbitrary lower mass limit acting as an additional constraint for undersampled tiny unrecoverable particles resulting from the fragmentation. These mass constraints are also among the sought parameters.

We have applied the technique of the described scaling analysis to the empirical data on the mass distributions for the *Košice*, *Sutter’s Mill* and *Bassikounou* meteorites. Each studied meteorite sample consists of  $N$  fragments ranging in mass from  $m_0$  to  $m_{N-1}$ . In our analysis we arrange the fragment masses  $m_i$  in the ascending order and the values  $m_L$  and  $m_U$  are intermediate in the initial range. If two or more fragments possess equal masses, then we add a small value corresponding to the fragment mass measurement error (e.g. 0.001 g) to one of them, to disambiguate the masses. The fragment mass distribution for the *Košice* meteorite was additionally studied in further detail (Gritsevich et al., 2014; 2016). These mass distributions manifest undersampling for small fragments and an exponential cutoff due to a finite size effect. We apply methods of numerical optimization to estimate the best-fit values for the scaling exponent, the lower and upper constraints as well as the dimensionless shape parameter. Next, the shape parameter is converted into the triad of relative sizes along respective Cartesian axes. Therefore, the obtained triad yields one of the three distinct options of the estimated shape: rod-like, plate-like and sphere-like.

## 2 Results and discussion

The obtained power-law fits to the empirical fragment mass distributions of the considered meteoroids are presented on *Figure 1*.

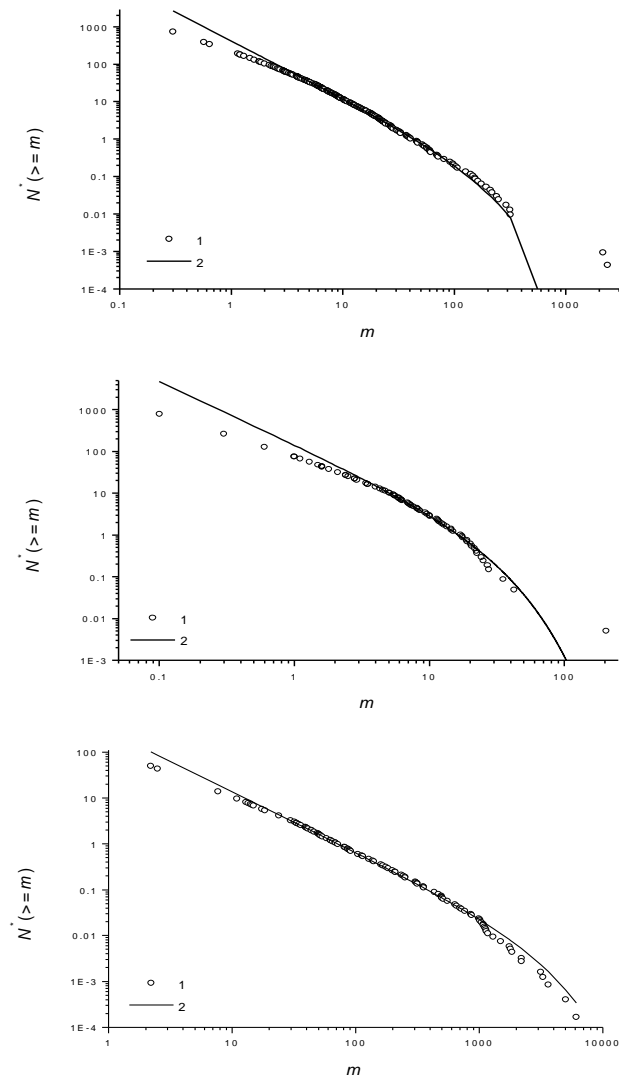


*Figure 1* – Complementary cumulative number of fragments  $N^*(\geq m)$  vs  $m$ . 1 – Observed data, 2 – Power law distribution with exponential cutoff.

### Košice (*Figure 1 Top*)

$$B_0 = 1.53, \quad m_L = 5.64, \quad m_U = 155.17, \quad d = 2.8, \\ (a : b : c) = (2.0 : 1.69 : 1.0);$$

### Sutter's Mill (*Figure 1 Middle*)

$$B_0 = 1.51, \quad m_L = 5.0, \quad m_U = 21.0, \quad d = 2.76, \\ (a : b : c) = (2.13 : 1.58 : 1.0);$$

### Bassikounou (*Figure 1 Bottom*)

$$B_0 = 1.32, \quad m_L = 29.9, \quad m_U = 2839.42, \quad d = 2.34, \\ (a : b : c) = (2.98 : 1.13 : 1.0);$$

$a, b, c$  are the linear dimensions of the fragment.

We emphasize that the applicability of the described meteoroid shape estimation technique is limited to non-prestrained homogeneous brittle solids. The prestrained

solids respond differently to the external load due to the stress points with concentrated internal energy and their fragments do not comply to a power law mass distribution. However, we consider that the scaling analysis is suitable for the shape estimation, since the mass distribution of the asteroid belt formed by multiple fragmentations follows a power law (Hughes et al., 1994).

The scaling analysis of Oddershede et al. (1993) is subjected to criticism by Meibom and Balslev (1996), who performed fragmentation experiments with thick plates of dry clay. The experiments revealed different exponents for fragments larger and smaller than the plate thickness, so Meibom made implications denying scale and material invariance and expressed the opinion that “*the measured mass distribution tells little about the mechanisms of the fragmentation process*”. On the second thought, this reasoning can be ruled out by the following facts. The speed of sound for clay is about 1–2.8 km/s, in contrast the respective values for gypsum are 2.3 km/s for transverse S-waves and 5 km/s for longitudinal P-waves. In comparison, the speed of sound for chondrites is about 3.5 km/s as stated by Rivkin and Bottke (1996). This leads to the question if the clay really exhibits brittle behavior. Indeed, the universal scaling was not observed for thick large plates of dry clay, but the masses of these plates (540–920 g) were an order of magnitude greater than those of small gypsum plates (58–77 g). We believe that the experiments with thick clay plates failed to provide energy sufficient for brittle fracture conditions. The brittle fracture is a dissipative process, which disperses locally supplied energy over the whole bulk via crack propagation. When all initially channeled energy dissipates, then in absence of internal strains the cracks cease to spread further. The results of experiments with small thin clay plates (237–393 g) by Meibom and Balslev (1996) exactly confirm the ideas and results of Oddershede et al. (1993). There is a theory of an additional fracturing mechanism for thin plates as stated in Linna et al. (2005). However, recent studies by Renshaw et al. (2001) and by Aström (2009) cast a doubt on the existence of the separate scaling law fragmentation models for thin plates and volumetric bodies. Anyway, for meteoroid applications the buildup of energy flux from the atmosphere drag (via ram pressure) is usually sufficient for fragmentation at all scales (with the exception of the top heaviest iron meteorites).

Recent studies provide increasing evidence to support the theory of power law distributions for fragment masses. For example, papers of Sotolongo-Costa et al. (2000; 2007) assume that high energy experiments with violent fragmentation processes produce power law distributions. On the contrary, low energy processes generate classical statistical functions like *log-normal* or *Rosin-Ramler*. The direct experiment on the Murchison CM2 chondrite with a high velocity impactor also yields a simple power law distribution (Flynn et al., 2007). Computational experiments considered in Domokos et al. (2015) show that the calculated mass distribution is best fitted by a

power law with an exponential cutoff. In addition, the transition from low energy distributions to a high energy power law is studied numerically in a paper of Hernández (2001) via a *random stopping mathematical model* as well as in a paper of Spahn et al. (2014) via a *random-walk model*. Considering these findings, we assume that meteoroid shapes can be estimated from the value of a power law exponent.

### 3 Conclusions

In the outcome of the study we obtained the following conclusions. The number of meteorite fragments depends on the fragment masses as a power law with an exponential cutoff. The scaling exponent essentially indicates the initial form of the fragmented body. The application of the scaling analysis to the meteorite cases with a large number of recovered fragments is feasible and can form a solid basis for future theoretical and experimental studies on this subject.

### Acknowledgments

This work was supported by the Russian Foundation for Basic Research, project Nos 14-08-00204, 16-05-00004 and 16-07-01072.

### References

- Aström J. A. (2009). “Difference between fracture of thin brittle sheets and two-dimensional fracture”. *Physical Review E*, **80** (4 Pt 2), 046113.
- Buehler M. J., Abraham F. F. and Gao H. (2003). “Hyperelasticity governs dynamic fracture at a critical length scale”. *Nature*, **426**, 141–146.
- Domokos G., Kun F., Sipos A. Á. and Szabó T. (2015). “Universality of fragment shapes”. *Scientific reports*, **5**, 9147.
- Flynn G. J., Durda D. D., Kreft J. W., Sitnitsky I. and Strait M. (2007). “Catastrophic disruption experiments on the murchison hydrous meteorite”. *Lunar and Planetary Science Conference*, **38**, 1744.
- Gritsevich M., Dmitriev V., Vinnikov V., Kuznetsova D., Lupovka V., Peltoniemi J., Mönkölä S., Brower J. and Pupyrev Y. (2016). “Constraining the pre-atmospheric parameters of large meteoroids: Košice, a case study”. *Assessment and Mitigation of Asteroid Impact Hazards*, Springer, New York. In print.
- Gritsevich M., Vinnikov V., Kohout T., Tóth J., Peltoniemi J., Turchak L. and Virtanen J. (2014). “A comprehensive study of distribution laws for the fragments of Košice meteorite”. *Meteoritics and planetary science*, **49**, 328–345.
- Hernández G. (2001). “Discrete model for fragmentation with random stopping”. *Physica A: Statistical*

*Mechanics and its Applications*, **300**, issues 1-2, 13–24.

- Hughes D. W. and Harris N. W. (1994). “The distribution of asteroid sizes and its significance”. *Planetary and space science*, **42**, 291–295.
- Linna R. P., Åström J. A. and Timonen J. (2005). “Dimensional effects in dynamic fragmentation of brittle materials”. *Physical Review E*, **72**, 015601(R).
- Meibom A. and Balslev I. (1996). “Composite power laws in shock fragmentation”. *Physical Review Letters*, **76**, 2492.
- Oddershede L., Dimon P. and Bohr J. (1993). “Self-organized criticality in fragmenting”. *Physical Review Letters*, **71**, 3107–3110.
- Oddershede L., Meibom A. and Bohr J. (1998). “Scaling analysis of meteorite shower mass distributions”. *Europhysics Letters*, **43**, 598–604.
- Renshaw C. E. and Schulson E. M. (2001). “Universal behaviour in compressive failure of brittle materials”. *Nature*, **412**, 897–900.
- Rivkin A. S. and Bottke W. F. (1996). “Hypovelocity impacts in the asteroid belt”. *Lunar and Planetary Science*, **27**, 1077–1078.
- Sotolongo-Costa O., Gamez R., Luzon F., Posadas A. and Weigandt Beckmann P. (2007). “Non Extensivity in Meteor Showers”. <http://arxiv.org/abs/0710.4963>.
- Sotolongo-Costa O., Rodriguez A. H. and Rodgers G. J. (2000). “Tsallis entropy and the transition to scaling in fragmentation”. *Entropy*, **2**, 172–177.
- Spahn F., Vieira Neto E., Guimaraes A. H. F., Gorban A. N. and Brilliantov N. V. (2014). “A statistical model of aggregate fragmentation”. *New Journal of Physics*, **16**, 013031.
- Vinnikov V. V., Gritsevich M. I., Kuznetsova D. V. and Turchak L. I. (2016). “Estimation of the initial shape of meteoroids based on statistical distributions of fragment masses”. *Doklady Physics*, **61**, 305–308. DOI:10.1134/S1028335816060021
- Vinnikov V., Gritsevich M. and Turchak L. (2015). “Shape estimation for Košice, Almahata Sitta and Bassikounou meteoroids”. In Heavens A. F., Starck J.-L. and Krone-Martins A., editors, *Proceedings of the International Astronomical Union (Cambridge Journals UK)*, Symposium S306, May 2014, volume 10, pages 394–396. <http://dx.doi.org/10.1017/S1743921314013519>

# Catalogue of representative meteor spectra

Vlastimil Vojáček<sup>1,2</sup>, Jiří Borovička<sup>2</sup>, Pavel Koten<sup>2</sup>, Pavel Spurný<sup>2</sup> and Rostislav Štork<sup>2</sup>

<sup>1</sup> **Astronomical Institute of the CAS, Ondřejov, Fričova 298, Czech Republic**

vojacek@asu.cas.cz, borovicka@asu.cas.cz

<sup>2</sup> **Astronomical Institute of the Charles University in Prague, V Holešovičkách 2, Czech Republic**

We present a library of low-resolution meteor spectra that includes sporadic meteors, members of minor meteor showers, and major meteor showers. These meteors are in the magnitude range from +2 to −3, corresponding to meteoroid sizes from 1 mm to 10 mm. This catalogue is available online at the CDS for those interested in video meteor spectra.

## 1 Introduction

Despite the long history of meteor spectroscopy, very few general surveys of meteor spectra have been presented. Harvey (Harvey, 1973) published statistics of visual inspection of 500 photographic meteor spectra. Borovička et al. (Borovička et al., 2005) presented a survey of 97 spectra of mainly sporadic meteors mostly in the magnitude range from +3 to 0. Because of increasing popularity of the meteor spectra video observations, we present a catalogue of 84 video spectra of both sporadic and shower meteors. The catalogue of representative meteor spectra intends to serve as a reference work for future spectral surveys of meteors.

The full catalogue can be found in Vojáček et al. (2015).

## 2 Instruments and observations

All meteors were captured by our sensitive video technique. Double station observations were performed during the periods of activity of major meteor showers between the years 2006 and 2012.

Each station was equipped with S-VHS-C camcorders with the second-generation image intensifiers *Mullard XXI332*. One direct camera and one spectral camera were operated from one station and one direct camera was operated from the other station.

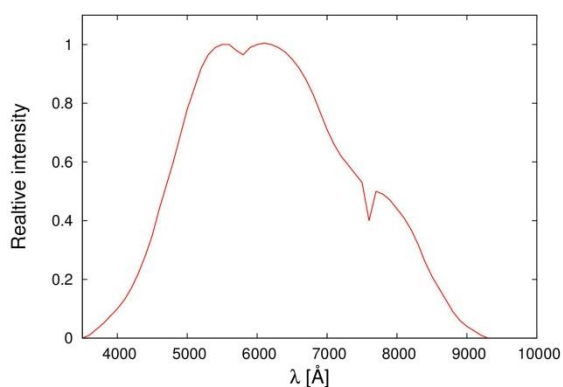


Figure 1 – Sensitivity curve of the system.

The uncompressed AVI files from cameras have a resolution of  $768 \times 576$  pixels  $\times$  8 bit.

The spectral grating with 600 grooves/mm and the *Arsat 1.4/50 mm* lens was used for most spectral observations. The resulting dispersion was  $30 \text{ \AA pixel}^{-1}$  for the *Arsat* lens. The spectral sensitivity extends from  $3800 \text{ \AA}$  to  $9000 \text{ \AA}$ . The sensitivity curve for the whole system (camera, image intensifier, and lens) is given in *Figure 1*.

## 3 Description and classification of the spectra

### Description of the spectra

The observed spectrum usually consists of the continuum, the emission from the heated atmosphere (specifically the oxygen and nitrogen lines and the nitrogen molecular bands) and the emission that originated in the evaporated material of the meteoroid: the meteoritic lines.

The low-temperature lines of this three meteoric elements can be recognized in the video spectrum:

- Mg I :  $5182 \text{ \AA}$
- Na I :  $5892 \text{ \AA}$
- Fe I :  $5269 - 5449 \text{ \AA}$

Another group is formed by the lines from the meteor wake emitted just behind the meteoroid. In the last group, there is only one line, the forbidden green oxygen line at  $5577 \text{ \AA}$ .

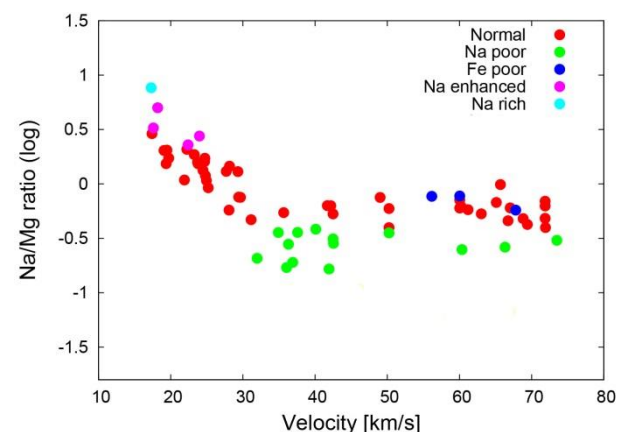
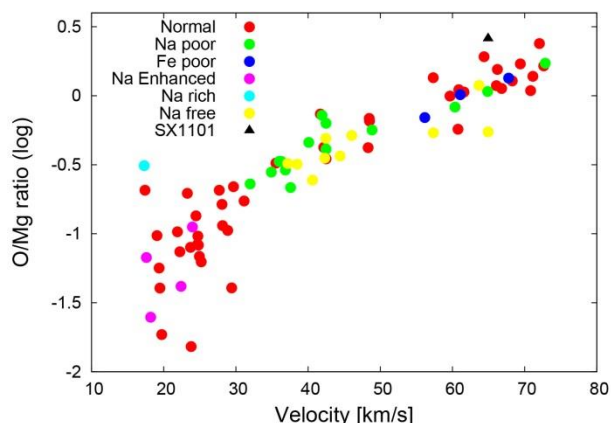


Figure 2 – Intensity ratio of the Na/Mg lines in meteor spectra as a function of the meteor speed.

The appearance of the spectrum can depend on the

velocity of the meteor (*Figure 2*). We observed that the dependence of the Na/Mg ratio on the velocity is valid for speeds below  $\approx 35$  km/s. The excitation and the evaporation temperatures are lower for smaller velocities and therefore the more volatile sodium has a brighter line for the given speed. There is no velocity dependence for speeds higher than  $\approx 35$  km/s.

In *Figure 3* we show the O/Mg ratio as a function of the velocity. The ratio of the O to Mg line intensities increases with the velocity. Fast meteors are characterized by more dominant atmospheric lines. For speeds below  $30 \text{ km s}^{-1}$  the scatter is large, mainly due to the faintness of the O line.



*Figure 3* – Intensity ratio of the O/Mg lines in meteor spectra as a function of the meteor speed.

### Classification of spectra

The contributions of individual multiplets were summed along the meteor path, so we worked with total line intensities. To visualize the spectral classification we used the Mg-Na-Fe ternary diagram (*Figures 4 and 5*) and the diagram of the dependence of the Mg/Na ratio on the velocity (*Figure 2*).

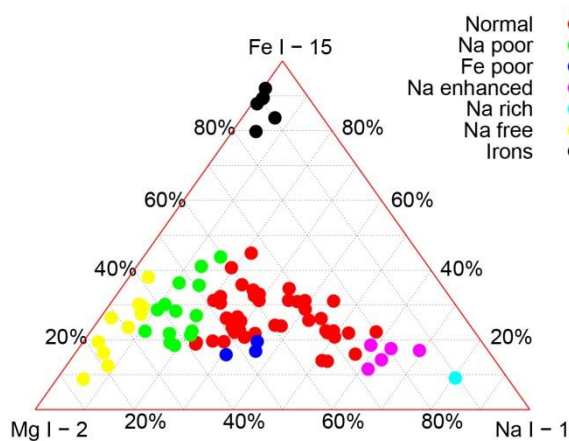


*Figure 4* – Classification of spectra. Relative intensities of lines Mg I, Na I, Fe I.

We used the spectral classification of meteor populations suggested by Borovička et al. (2005). The meteoroids were divided as follows:

- Iron meteoroids;
- Na-free meteoroids;

- Na-rich meteoroids;
- Mainstream meteoroids;
  - Normal meteoroids;
  - Na-poor meteoroids;
  - Na-enhanced meteoroids;
- Fe-poor meteoroids.

The approach for the classification of spectra that we use was developed only for small meteoroids in the 1–10 mm size range.

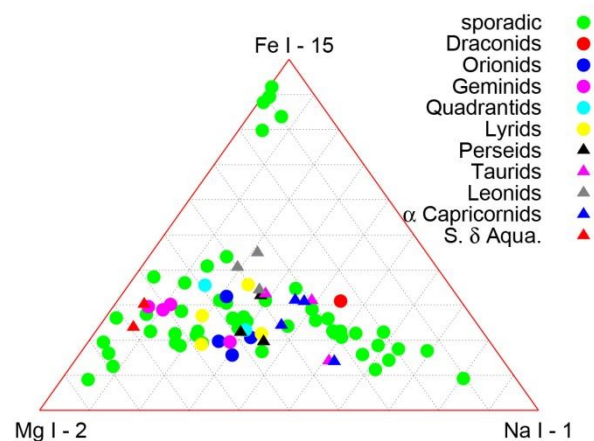


*Figure 5* – Classification of spectra: meteor showers positions.

*Figure 5* shows the Na-Mg-Fe ternary graph as well, but symbols of individual meteors represent the association with the shower. Most of the major shower meteoroids have been classified as normal. The only exceptions are the Geminids and two Southern  $\delta$  Aquariids. Both Southern  $\delta$  Aquariids meteoroids were classified as Na-free.

The Geminids have members of the Na-free, Na-poor, and normal spectral groups. The reason of Na depletion in both showers is solar heating at low perihelion distances (Čapek and Borovička, 2009). The perihelion distance of Geminids is somewhat larger and the degree of Na depletion probably depends on the meteoroid size and structure, especially porosity (Borovička, 2010).

The intensities of the spectral lines correspond to different meteoroid compositions (with the speed dependence taken into account). It is well known that different strength categories of meteoroids in the millimeter-size range have different beginnings of the meteor luminous path (Ceplecha, 1988). For a given speed, a meteoroid composed of stronger material has a lower beginning height than the meteoroid formed by weaker material. As we can see in *Figure 6*, the iron meteoroids and the Na-free meteoroids started to ablate at lower heights compared to most meteoroids, while the Fe-poor meteoroids started higher.

## 4 Meteoroid orbits

The heliocentric orbits are known for all 84 meteors from double-station observations. The catalogue has a representative sample of orbits with a wide variety of orbital elements.

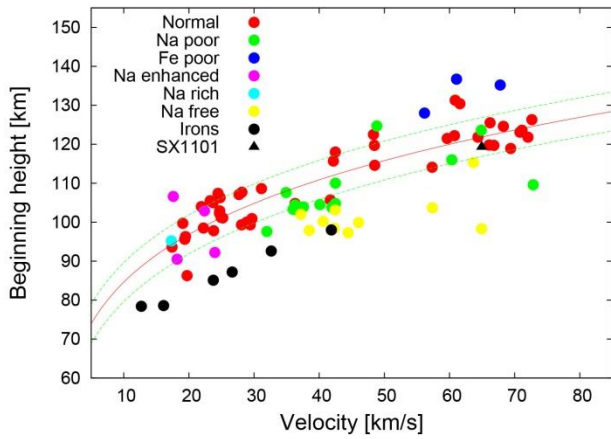


Figure 6 – Beginning height of meteor as a function of speed.

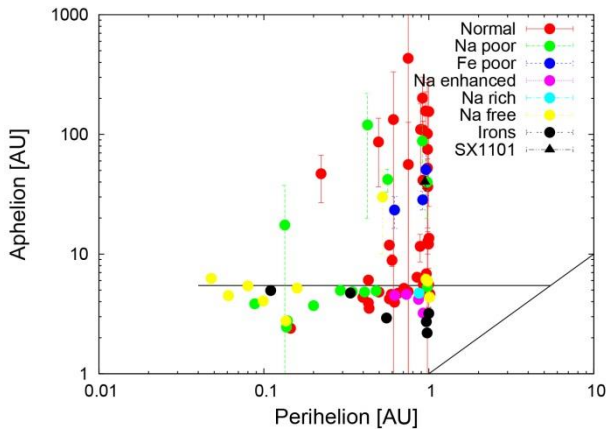


Figure 7– Aphelion and perihelion of meteoroids from the catalogue.

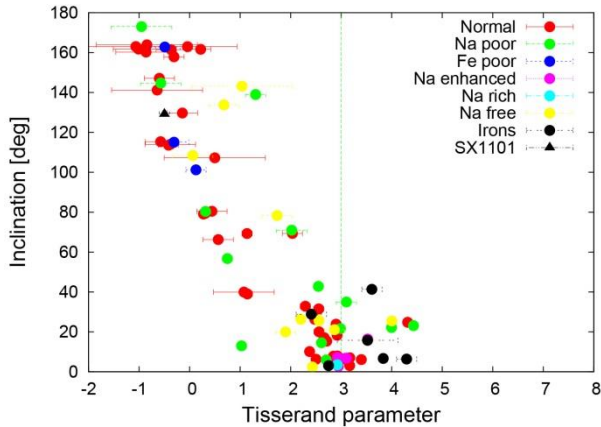


Figure 8– Tisserand parameter relative to Jupiter and the inclination of orbits for meteoroids from the catalogue.

#### 4.1 Relation of meteor orbit to spectral classification

Five classes of meteoroid orbits were defined by Borovička et al. (2005):

- (SA) Sun-approaching orbits:  $q < 0.2$  AU. Orbits with small perihelion distances are defined as a separate class.
- (ES) Ecliptic shower orbits: Members of ecliptical meteor showers. For example, the Taurid meteors derived from the comet 2P/Encke.
- (HT) Halley-type orbits:  $TJ < 2$  or  $2 < TJ < 3$  and  $i > 45^\circ$ .
- (JF) Jupiter-family orbits:  $2 < TJ < 3$  and  $i < 45^\circ$  and  $Q > 4.5$  AU.

- (A-C) Asteroidal-chondritic orbits:  $TJ > 3$  or  $Q < 4.5$  AU.

Spectral classes of meteoroids from the catalogue and their positions within the orbit classification schemes are shown in Figures 7 and 8.

#### 4.2. Iron meteoroids

Six meteors were classified as iron meteoroids. The orbits of four of them satisfy the condition for the asteroidal-chondritic class. One meteoroid with a perihelion of only 0.11 AU can be classified as a Sun-approaching meteoroid. The orbit of one meteoroid can be classified as a Jupiter-family orbit, but asteroidal origin cannot be excluded, since the inclination is only 3 degrees and the aphelion of 4.7 AU is not particularly large.

#### 4.3. Na-free meteoroids

We can clearly distinguish two different populations in the Na-free-meteoroids: the Sun-approaching population with small perihelia and the Halley-type population with high inclinations.

##### 4.3.1. Sun-approaching meteoroids

Most of meteoroids with a perihelion distance  $q < 0.2$  are Na-free or Na-poor.

The material of Na-free meteoroids also tends to have a greater strength (see Figure 6).

##### 4.3.2. Cometary Na-free meteoroids

The close approach to the Sun is not the only process that causes depletion of Na in meteoroids. In our sample we have three meteoroids without a Na line in their spectra, but their orbits are different from those of Sun approaching meteoroids. Their perihelion distances are closer to 1 AU, and they have high inclinations or even retrograde orbits.

These orbits are of Halley type. According to Borovička et al. (2005), the reason for Na depletion in these types of orbits might be the long exposure to cosmic rays on the comet surface during their residence in the Oort cloud. This process can lead to the formation of a Na free refractory crust. The gradual or sudden disintegration of the crust during the cometary passage through the inner solar system then produces millimeter-sized compact Na free meteoroids.

#### 4.4. Na-rich meteoroids

There is only one Na-rich meteoroid in our catalogue. The body has a Jupiter-family orbit.

#### 4.5. Normal meteoroids

Both cometary and asteroidal orbits are found among meteoroids classified as normal. But only a part of these meteoroids have a typically chondritic composition, many of them show somewhat fainter Fe lines. The sample of meteoroids classified as normal is a mixture of normal chondritic material and cometary material similar to the

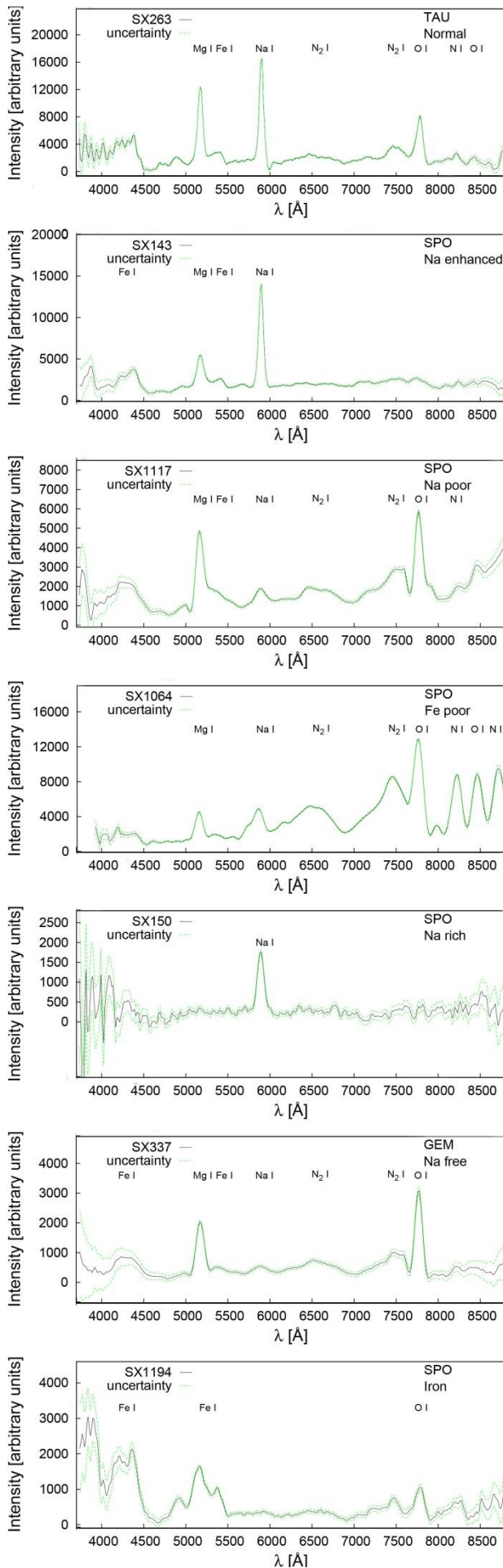


Figure 9 – Examples of typical spectrum for each spectral class.

Leonids. Three Taurid meteors with ecliptic shower orbits have a normal composition.

#### 4.6. Fe-poor meteoroids

Three of the meteoroids in the catalogue were classified as Fe-poor. The iron lines were too faint to classify the meteoroids as normal, although the boundary is somewhat arbitrary. All of the Fe-poor meteoroids have cometary Halley-type orbits. Fe-poor meteoroids have low material strength, their beginning heights of ablation are usually high (see *Figure 6*).

#### 4.7. Na-poor meteoroids

Na-poor meteoroids are the transition between normal and Na-free meteoroids. Like the Na-free meteoroids, some of them have low perihelia, others have cometary orbits. Thus they probably have the same two origins as the Na-free meteoroids.

#### 4.8. Enhanced-Na meteoroids

Five meteoroids were classified as enhanced-Na meteoroids. One has a typical asteroidal-chondritic orbit. The other four meteoroids can be classified as ecliptical or Jupiter-family meteoroids. Their orbits were similar to the Na-rich meteoroid.

## 5 The catalogue

The full catalogue was published in Vojáček et al. (2015). The atmospheric trajectories and orbital elements for all meteors of the catalogue are at the CDS. Heliocentric orbits are known for all meteors, they are also available at the CDS.

Illustrative examples of typical spectra from each class are available in *Figure 9*. Calibrated and uncalibrated spectra of all 84 meteors are available at the CDS. The total intensities of the multiplets Mg1-2, Na1-1, and Fe1-15 are given explicitly in a separate file.

The catalogue is available online at the CDS via anonymous ftp<sup>1</sup> or via the website<sup>2</sup>.

## 6 Conclusions

We presented a survey of 84 meteors in the magnitude range from +2 to −3, corresponding to meteor sizes from 1 mm to 10 mm. We also computed heliocentric orbits. We classified the meteor spectra according to the classification suggested by Borovička et al. (2005). Only a part of the meteoroids were found to have a typical chondritic composition. We found a variety of Na depletion, Fe depletion, or Na enhancement. Approximately 20% of the whole sample was found to contain no sodium in the spectra. Three populations can be distinguished among the Na free meteoroids: the iron meteoroids with an asteroidal origin, the Sun-approaching meteoroids with Na depleted by frequent approaches within  $\approx 0.2$  AU to the Sun, and the cometary Na free meteoroids with Na depletion that might be caused by

<sup>1</sup>cdsarc.u-strasbg.fr (130.79.128.5)

<sup>2</sup><http://cdsarc.u-strasbg.fr/viz-bin/qcat?J/A+A/580/A67>

long exposure to cosmic rays of the surface of comets in the Oort cloud.

Most of the major shower meteors have been classified as normal. Some members of the Geminid shower and two members of Southern  $\delta$  Aquariids were classified as Na-free.

Most of the meteoroids on the asteroidal-chondritic orbits were found to be iron meteoroids. One iron meteoroid has a typical sun-approaching orbit. Meteoroids with cometary origin had a heterogenous composition, from Na-free, Na-poor, and Fe-poor for Halley-type orbits to Na-rich and enhanced-Na for Jupiter-family orbits.

## Acknowledgments

This work was supported by grant No. P209/11/1382 from GA ČR and by the project SVV-260089 by the Charles University in Prague.

## References

Borovička J., Koten P., Spurný P., Boček J. and Štork R. (2005). "A survey of meteor spectra and orbits: evidence for three populations of Na-free meteoroids". *Icarus*, **174**, 15–30.

Borovička J., Koten P., Spurný P., Štrbený L. and Štork R. (2010). "Material properties of transition objects 3200 Phaethon and 2003 EH<sub>1</sub>". *Icy Bodies of the Solar System, Proceedings of the International Astronomical Union, IAU Symposium*, **263**, 218–222.

Čapek D. and Borovička J. (2009). "Quantitative model of the release of sodium from meteoroids in the vicinity of the Sun: Application to Geminids". *Icarus*, **202**, 361–370.

Ceplecha Z. (1988). "Earth's influx of different populations of sporadic meteoroids from photographic and television data". *Bulletin Astronomical Institutes of Czechoslovakia*, **39**, 221–236.

Harvey G. A. (1973). "Elemental abundance determinations for meteors by spectroscopy". *Journal of Geophysical Research*, **78**, 3913–3926.

Vojáček V., Borovička J., Koten P., Spurný P. and Štork R. (2015). "Catalogue of representative meteor spectra". *Astronomy and Astrophysics*, **580**, id. A67, 31 pp.



Arnold Tukkers busy with preparation of the lunchboxes for the excursion on Saturday afternoon.

# 2014 Southern $\delta$ -Aquariid observing campaign – carried out from Crete

Thomas Weiland

Ospelgasse 12-14/6/19, 1200 Wien, Austria

thomas.weiland@aon.at

With a peak ZHR of 15–20 at the end of July, the Southern  $\delta$ -Aquariids rank as a major annual shower, but observation is often neglected in favor of the much more active Perseids of August, mainly as a consequence of their southerly radiant, which makes the stream a prominent target from low latitudes and the southern hemisphere. The extended activity period of more than a month, lacking a distinctive peak, and the paucity of bright meteors does not enhance interest of most observers, either. Nevertheless, one has not to go too far south in order to monitor the stream properly to gain scientific results. The Greek island of Crete, at the southernmost tip of Europe, is such a place, offering sufficiently dark skies and a 90 % probability of clear weather in July and August. Encouraged by a New Moon on July 26<sup>th</sup> an eight-night-long visual observing campaign was carried out in 2014. As a consequence, I managed to record nearly 250 Southern  $\delta$ -Aquariids within 40 hours of effective observing time. An impression of the campaign together with a summary of the results is presented.

## 1 Why observing the Southern $\delta$ -Aquariids from Crete?

With a radiant declination of  $\delta = -16^\circ$ , the Southern  $\delta$ -Aquariid meteor shower (SDA) is best observable from low latitudes and the southern hemisphere. Nevertheless, at the southernmost tip of Europe, the Greek Island of Crete ( $\sim 35^\circ$  North), the radiant culminates at a height of  $\sim 40^\circ$ , making it a suitable place in order to monitor the stream properly and gain scientific results.

Even at sea level many parts of Crete, especially in the southwest, offer sufficiently dark skies (limiting magnitudes 6.10 to 6.50 on average) and in case of hazy weather one has only to move to the nearby mountains (500 to 1000 m altitude) to be rewarded with nearly unspoiled, pristine skies (limiting magnitudes  $> 6.20$ , but very often close to the standard sky). In addition to this, with a 90 % probability of clear weather in July and August, successful observing is almost guaranteed.

To make it short, the benefits of observing from Crete during the northern hemisphere summer months can be summarized as “African climate combined with European comfort”!

## 2 The 2014 observing campaign

With respect to New Moon on July 26<sup>th</sup> my visual observing campaign in 2014 started out on July 25<sup>th</sup>–26<sup>th</sup> and lasted until August 01<sup>st</sup>–02<sup>nd</sup> (8 nights).

As expected, the weather stayed quite cooperative. Very few isolated clouds at the end of the campaign did not hamper anyway, and transparent skies prevailed.

As a consequence, limiting magnitudes (averaged over each night) were ranging between 6.10 and 6.50 (direct view method, averted vision), averaging on 6.32 (see *Table 1*).

Finally I managed to record 242 SDA (counting method) within 40.26 hours of effective observing time (see *Table 1*).

## 3 Results

### 3.1 Magnitude distribution / Population index

From the overall magnitude distribution (see *Table 1*; *Figure 1*) it can be deduced that the SDA mainly yielded faint meteors (48 % of magnitudes +4 to +5), and only 12 % of all SDA reached at least magnitude 0, less than other major annual streams.

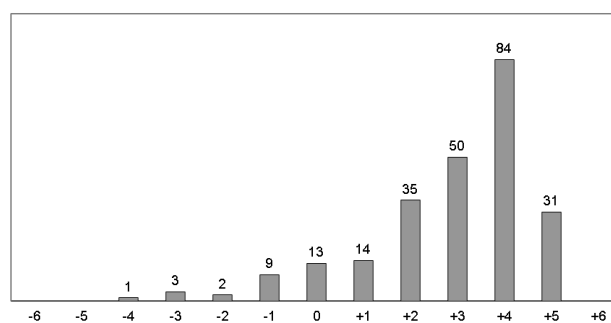


*Figure 1* – Magnitude distribution for the Southern Delta-Aquariids 2014, July 25<sup>th</sup>–26<sup>th</sup> until August 01<sup>st</sup>–02<sup>nd</sup> (242 SDA).

Fireballs ( $\geq$  magnitude  $-3$ ) were quite scarce (4 SDA), the brightest one of them matched magnitude  $-4$  (July 29<sup>th</sup>, 21<sup>h</sup>35<sup>m</sup>50<sup>s</sup> UT).

Interestingly, the number of bright SDA was increasing during the maximum and post-maximum period (Johannink and Miskotte, 2012). For comparison, the two brightest SDA ever recorded by the author (both of magnitude  $-5$ ) occurred during the post-maximum period, too (2009, August 01<sup>st</sup>, 23<sup>h</sup>48<sup>m</sup>05<sup>s</sup> UT; 2015, August 10<sup>th</sup>, 23<sup>h</sup>32<sup>m</sup>25<sup>s</sup> UT).

Table 1 – Limiting magnitudes, magnitude distribution and meteor numbers.

Shower	Date	lm	-6	-5	-4	-3	-2	-1	0	1	2	3	4	5	6	Σ
SDA	25/26	6.1	0	0	0	0	0	0	0	0	3	0	4	0	0	7
SDA	26/27	6.3	0	0	0	0	0	0	1	1	1	3	9	3	0	18
SDA	27/28	6.17	0	0	0	0	1	2	0	1	3	3	10	7	0	27
SDA	28/29	6.5	0	0	0	1	1	2	3	3	8	14	12	11	0	55
SDA	29/30	6.38	0	0	1	0	0	1	2	5	4	6	21	1	0	41
SDA	30/31	6.2	0	0	0	0	0	1	4	3	5	10	8	2	0	33
SDA	31/01	6.44	0	0	0	2	0	2	0	0	8	4	8	5	0	29
SDA	01/02	6.5	0	0	0	0	0	1	3	1	3	10	12	2	0	32
Σ			0	0	1	3	2	9	13	14	35	50	84	31	0	242
Mean	6.32															

In a further step the mean population index for the SDA was derived, using the magnitude difference between the meteors and the limiting stellar magnitude, based on table 7.2, p. 122 in the Handbook for Meteor Observers (Rendtel and Arlt, 2014).

This yielded a mean r-value of  $2.39 \pm 0.14$ , which is significantly lower than the value given by IMO ( $r = 2.8$ ; Rendtel, 2015). However, compared to the mean r obtained for the sporadic background ( $2.78 \pm 0.12$ ; based on 648 SPO), the mean population index for the SDA during the given period can be regarded as real.

**3.2 Zenithal hourly rates**

ZHR calculation followed the procedure given in the Handbook for Meteor Observers (Rendtel and Arlt, 2014). Due to the fact that limiting magnitudes were close to or even matching the standard sky of 6.50, using individual population indices would have a minor impact on ZHR calculation. Nevertheless, I took the individual r-value of 2.39 (cf. 3.1) and considered only time frames with a mean radiant height  $\geq 15^\circ$ . The zenith exponent was assumed to be  $\gamma = 1.0$ . No perception coefficient was applied.

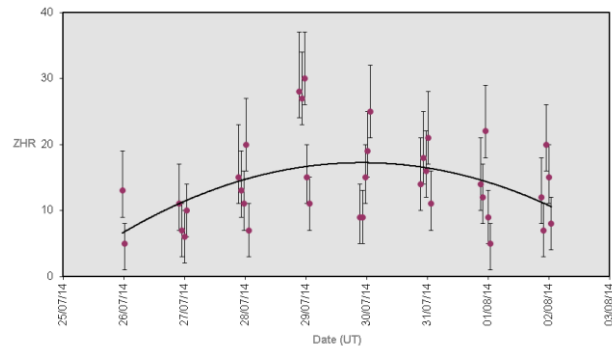


Figure 2 – ZHR profile with polynomial trend function for the Southern Delta-Aquariids 2014 ( $r = 2.39$ ).

As expected, ZHR-values show a flat, skew profile with large fluctuations (see Figure 2). They started out with  $\sim 10$  on July 25<sup>th</sup>–26<sup>th</sup> and reached their maximum ( $\sim 30$ ) on July 28<sup>th</sup>–29<sup>th</sup>. After that they were slowly declining to

$\sim 10$  on August 01<sup>st</sup>–02<sup>nd</sup> again. This is quite in agreement with the corresponding IMO live ZHR profile.

However, an Excel-generated polynomial trend function yielded a broader maximum one day later, around July 29<sup>th</sup>–30<sup>th</sup>, with a peak ZHR of  $\sim 17$ , which fits better the parameters given in the Meteor Shower Calendar (ZHR 16; maximum July 30<sup>th</sup>; Rendtel, 2015).

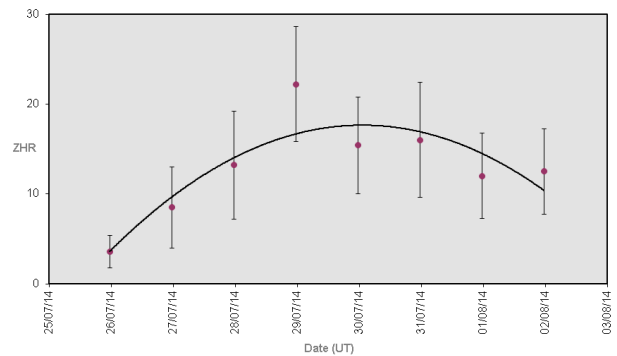


Figure 3 – Mean ZHR profile with polynomial trend function for the Southern Delta-Aquariids 2014 ( $r = 2.39$ ).

Averaging ZHR-values over each night did not affect the date of the maximum (July 28<sup>th</sup>–29<sup>th</sup>), but rather their height (peak ZHR  $22 \pm 6$ ; see Figure 3). In any case, the polynomial trend function was not altered, only becoming slightly more skew.

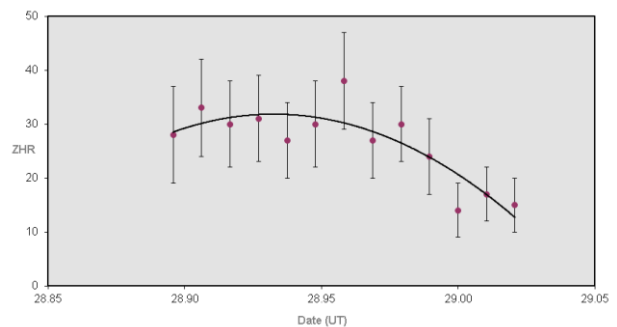


Figure 4 – ZHR profile around maximum with polynomial trend function for the Southern Delta-Aquariids 2014, Maximum July 28<sup>th</sup>–29<sup>th</sup> ( $r = 2.39$ ).

In order to smooth the profile and to get the peak out more clearly, ZHR values were averaged using a sliding mean of 5 bins per step (A5), shifted by 15 minutes. This puts the time of the maximum to July 28<sup>th</sup>, 23<sup>h</sup>00<sup>m</sup> ± 15<sup>m</sup> UT (ZHR 38 ± 9; see *Figure 4*). The polynomial trend function gives July 28<sup>th</sup>, 22<sup>h</sup>30<sup>m</sup> ± 15<sup>m</sup> UT, with a peak ZHR ~32.

### 3.3 General Appearance

A typical feature of the SDA meteors is the scarcity of trains, similar to the Geminids. According to that, only 1 % of all SDA logged showed a prominent train (+2 and +4 magnitude class) and additional 18 % produced a short one (-4 to +4 magnitude class).

Flares were not observed at all.

Color estimates yielded mainly orange and yellow hues, with white and blue tints to a much lesser extent.

### 3.4 Conclusion

The 2014 observational results can be summarized as follows:

- The mean population index found in 2014 ( $r = 2.39$ ) is significantly lower than the value given by IMO ( $r = 2.8$ ).
- A higher percentage of bright meteors during the maximum and post-maximum period indicates mass-sorting within the stream (Johannink and Miskotte, 2012).
- The peak ZHR found in 2014 (~30) is significantly higher than the value given by IMO (16).
- The (almost complete) absence of prominent trains and flares indicates a high mean bulk density and low porosity of the meteoroids (Babadzhanov and Kokhirova, 2009). Taking the extremely small perihelion distance ( $q = \sim 0.09$  AU) into account, one may assume a sintered surface of the meteoroids, similar to the Geminids.
- Despite the extremely small  $q$  the predominance of orange and yellow colors suggests an incomplete loss of volatile elements, like sodium.

## 4 Future Work

Due to the fact that there are still open questions about the observational stream parameters, visual meteor work should be focused on the following items:

- A complete r-profile over the whole activity period in order to prove mass-sorting within the stream (Johannink and Miskotte, 2012).
- Complete ZHR-profiles of moonless returns in order to prove whether peak ZHR-values are subject to variability (Johannink and Miskotte, 2012; Molau et al., 2015).

Favorable observing conditions in 2016, 2017 and 2019 offer good opportunities to follow up the performance of the stream!

## References

- Babadzhanov P. B. and Kokhirova G. I. (2009). "Densities and Porosities of Meteoroids". *Astronomy and Astrophysics*, **495**, 353–358.
- Johannink C. and Miskotte K. (2012). "Results for the Aquariid-expedition to Namibia, July 2011". *WGN, Journal of the IMO*, **40**, 65–68.
- Molau S., Crivello S., Goncalves R., Saraiva C., Stomeo E. and Kac J. (2015). "Results of the IMO Video Meteor Network – August 2015". *WGN, Journal of the IMO*, **43**, 188–191.
- Rendtel J. (editor) (2015). 2016 Meteor Shower Calendar. IMO.
- Rendtel J. and Arlt R. (editors) (2014). Handbook for Meteor Observers. International Meteor Organization, Potsdam.

# Current status of Polish Fireball Network

Mariusz Wiśniewski<sup>1,2</sup>, Przemysław Żołądek<sup>1</sup>, Arkadiusz Olech<sup>1,3</sup>, Zbigniew Tyminski<sup>1,4</sup>, Maciej Maciejewski<sup>1</sup>, Karol Fietkiewicz<sup>1</sup>, Mariusz Gozdalski<sup>1</sup>, Marcin Przemysław Gawroński<sup>1,5</sup>, Tomasz Suchodolski<sup>1,6</sup>, Maciej Myszkiwicz<sup>1</sup>, Marcin Stolarz<sup>1</sup> and Krzysztof Polakowski<sup>1</sup>

<sup>1</sup> Polish Fireball Network, Comets and Meteors Workshop, ul. Bartycka 18, 00-716 Warsaw, Poland  
brahi@op.pl, mazziek@gmail.com, parmo.pfn@gmail.com, ma.gozdalski@gmail.com,  
spammer.m@gmail.com, marcin.stolarz@gmail.com, krzysiek-pol20@o2.pl

<sup>2</sup> Central Office of Measures, ul. Elektoralna 2, 00-139 Warsaw, Poland  
marand.w@gmail.com

<sup>3</sup> Nicolaus Copernicus Astronomical Center, ul. Bartycka 18, 00-716 Warsaw, Poland  
olech@camk.edu.pl

<sup>4</sup> National Centre of Nuclear Research RC POLATOM, Soltan 7, Otwock-Świerk, Poland  
zbyszek.tyminski@gmail.com

<sup>5</sup> Faculty of Physics, Astronomy and Informatics, Nicolaus Copernicus University,  
Grudziądzka 5, 87-100 Toruń, Poland  
motylek@astro.uni.torun.pl

<sup>6</sup> Space Research Centre, Polish Academy of Sciences, ul. Bartycka 18A, 00-716 Warszawa, Poland  
tomasz.suchodolski@ptma.pl

The PFN started in March 2004. Most of its observers are amateurs, members of the Comets and Meteors Workshop. The network consists of 40 continuously working stations, where nearly 80 sensitive CCTV video and digital cameras operate. During the years 2011–2015 PFN cameras recorded 215049 single events. Using this data 34608 trajectories and orbits have been calculated.

## 1 Introduction

Since 2004 the Polish sky has been patrolled by cameras of the Polish Fireball Network (PFN). Most of PFN observers are amateurs, members of the Comets and Meteors Workshop performing observations from their homes. Some stations are located in astronomy clubs and schools. The network consists of 40 continuously working stations, where nearly 80 sensitive CCTV video and digital cameras operate (Olech et al., 2006). The PFN team published a number of papers with detailed analyzes of interesting events like the Leonids 2002 outburst (Wiśniewski et al., 2003), EN200204 “Łaskarzew” fireball (Spurny et al., 2004), PF030405a “Krzyszowice” fireball (Żołądek et al., 2007), PF191012 “Myszyniec” - highest Orionid meteor ever recorded (Olech et al., 2013), PF131010 Ciechanow fireball possible related to Near Earth Asteroids 2010 TB54 and 2010 SX11 (Olech et al., 2015).

## 2 Cameras of PFN

The network consists of 40 continuously working stations with nearly 80 cameras. The PFN cameras patrol the sky over entire Poland (see *Figure 1*). In Most stations we use low cost sensitive CCTV analog video cameras equipped with lenses with  $65.6 \times 49.2^\circ$  field of view. We use MetRec (Molau, 1999) and UFOCapture (SonotaCo, 2005)<sup>1</sup> software for meteor detection. The *UFOAnalyzer*

software is used for the astrometric reduction of video recordings.

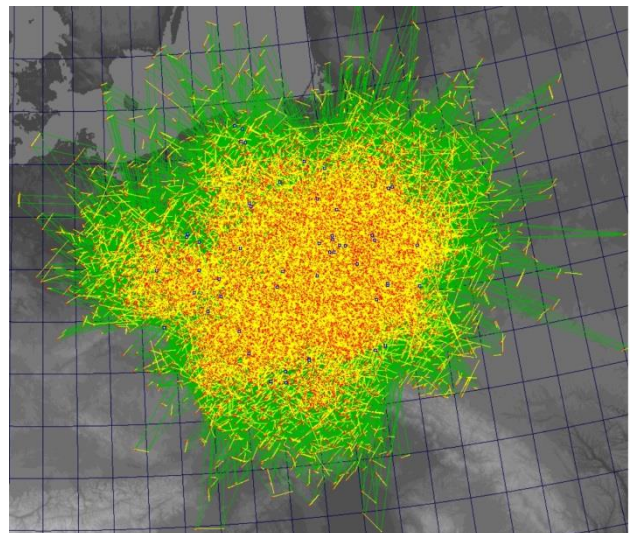


Figure 1 – Calculated trajectories of meteoroids in 2011-2015.

Part of the stations is equipped with high sensitive Mintron 12v6 cameras with fast lenses. These cameras detected up to 4 times more meteors than low cost cameras. Due to a higher sensitivity and smaller fields of view we can record a large number of fainter meteors.

New “Meteor Digital Cameras” (MDC) are based on the sensitive *DMK 33GX236*. These cameras have a

<sup>1</sup> <http://sonotaco.com/soft/UFO2/help/english/index.html>  
“UFCaptureV2 Users Manual”.

Table 1 – Types of camera working in PFN.

Parameter	Low cost setup	Sensitive setup	HD digital setup
Camera type	Tayama C3102-01A1	Mintron 12v6	DMK 33GX 236
Image resolution	480 x 576 pixels Interlaced	768 x 576 pixels Interlaced	1920 x 1200 pixels Progressive
Time resolution	25/50 fps 8 bit	25/50 fps 8 bit	50/25 fps 8/12 bit
Lens	1.2/4 mm	0,8/6 mm - 0,8/12 mm	1.2/2.4 mm
FOV	66x50 degrees	<66x50 degrees	130x80 deg
Pixel size	5'/pixel	<5'/pixel	4'/pixel

resolution of 1920 x 1200 pixels. The new cameras are working with lenses with a focal length of 2.4 mm which gives 130 x 80° field of view. The new cameras offer images with much better quality compared to analog cameras.

Detections from all PFN cameras are automatically transmitted via internet to a central server where double station events are detected, analyzed and then a trajectory and orbit is determined. All calculations are checked by manual inspection. We create the PyFN software for trajectory and orbit calculation. PyFN (Żołądek, 2012) utilizing the *Celpeha* method (Ceplecha, 1987).

Comparison of low cost setup, sensitive setup and new digital HD setup was presented in Table 1.

### 3 Results of PFN in years 2011–2015

In years 2011–2015 PFN cameras recorded 215049 single events. Using this data 34608 trajectories and orbits have been calculated. Detailed numbers of meteors were presented in Table 2. A special spike in the amount of registered meteors occurred in 2015. This was due to the launch of a number of new sets of sensitive cameras. During the next year, we are planning an extensive modernization of the PFN network, equipping it with dozens of new sensitive and digital HD cameras.

With the development of the network increases the number of registered detection of multiple stations (see Figure 2). This has a significant impact on improving the quality of the orbits.

Table 2 – Results of PFN in last 5 years.

Year	Detections	Orbits
2011	24099	3430
2012	28471	4186
2013	36347	6114
2014	46936	7351
2015	79083	13528

### Acknowledgment

This work was supported by the National Science Center (decision No. DEC-2013/09/B/ST9/02168).

Multistation detections

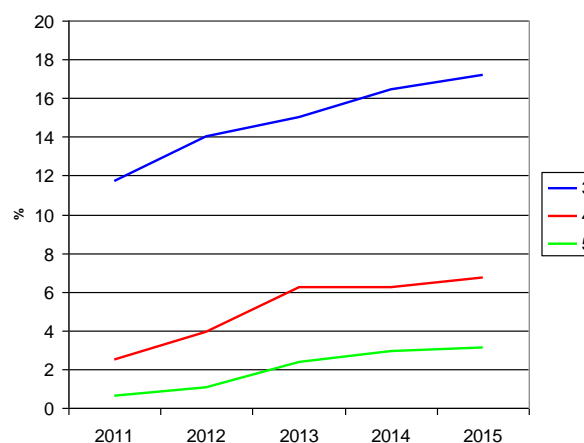


Figure 2 – Percentages of multistation detections in 2011–2015.

### References

- Ceplecha Z. (1987). “Geometric, dynamic, orbital and photometric data on meteoroids from photographic fireball networks”. *Bulletin of the Astronomical Institutes of Czechoslovakia*, **38**, 222–234.
- Molau S. (1999). “The meteor detection software MetRec”. In Baggaley W. J. and Porubcan V., editors., *Meteoroids 1998*, Proceedings of the International Conference held at Tatranska Lomnica, Slovakia, August 17-21, 1998. Astronomical Institute of the Slovak Academy of Sciences, pages 131–134.
- Olech A., Żołądek P., Wiśniewski M., Kransowski M., Kwinta M., Fajfer T., Fietkiewicz K., Dorosz D., Kowalski Ł., Olejnik J., Mularczyk K. and Złoczewski K. (2006). “Polish Fireball Network”. In Bastiaens L., Verbert J., Wislez J.-M. and Verbeeck C., editors, *Proceedings of the International Meteor Conference*, Oostmalle, Belgium, 15-18 September, 2005. IMO, pages 53–62.
- Olech A., Żołądek P., Wiśniewski M., Fietkiewicz K., Maciejewski M., Tyminski Z., Krzyzanowski T., Krasnowski M., Kwinta M., Myszkiwicz M., Polakowski K. and Zaręba P. (2013). “PF191012

Myszyniec - highest Orionid meteor ever recorded". *Astronomy and Astrophysics*, **557**, A89.

Olech A., Żołądek P., Wiśniewski M., Rudawska R., Laskowski J., Polakowski K., Maciejewski M., Kransowski M., Krzyżanowski T., Fajfer T. and Tymiński Z. (2015). "PF131010 Ciechanow fireball - the body possible related to Near Earth Asteroids 2010 TB54 and 2010 SX11". *Monthly Notices of the Royal Astronomical Society*, **454**, 2965–2971.

Spurny P., Olech A. and Kedzierski P. (2004). "Trajectory and orbit of the EN200204 Łaskarzew fireball". *WGN, Journal of the IMO*, **32**, 48–50.

Wiśniewski M., Kędzierski P., Mularczyk K. and Złoczewski K. (2003). "Polish Automated Video Observations (PAVO)". *WGN, Journal of the IMO*, **31**, 33–34.

Żołądek P., Olech A., Wiśniewski M. and Kwinta M. (2007). "The PF030405a "Krzeszowice" fireball". *Earth, Moon, and Planets*, **100**, 215–224.

Żołądek P. (2012). "PyFN - multipurpose meteor software". In Gyssens M. and Roggemans P., editors, *Proceedings of the International Meteor Conference*, Sibiu, Romania, 15-18 September, 2011. IMO, pages 53–55.



Ad-hoc LOC meeting at the reception with Arnold Tukkers, Elise Ijland, Joost Hartman: 'what do we do if we run out of drinking tokens?'.  
 IMC logo: INTERNATIONAL METEOR CONFERENCE 2016

# Space fireworks for upper atmospheric wind measurements by sounding rocket experiments

Masa-yuki Yamamoto

School of Systems Engineering, Kochi University of Technology, Kami, Japan

Yamamoto.masa-yuki@kochi-tech.ac.jp

Artificial meteor trains generated by chemical releases by using sounding rockets flown in upper atmosphere were successfully observed by multiple sites on ground and from an aircraft. We have started the rocket experiment campaign since 2007 and call it “Space fireworks” as it illuminates resonance scattering light from the released gas under sunlit/moonlit condition. By using this method, we have acquired a new technique to derive upper atmospheric wind profiles in twilight condition as well as in moonlit night and even in daytime. Magnificent artificial meteor train images with the surrounding physics and dynamics in the upper atmosphere where the meteors usually appear will be introduced by using fruitful results by the “Space firework” sounding rocket experiments in this decade.

## 1 Introduction

Meteor trains have been studied as one of luminescence events in upper atmosphere just after a large meteoroid entered into the upper atmosphere. Imaging of the meteor trains is difficult because it is a statistically rare event and has never been predicted when and where it occurs in the sky. However, just at the occasion of the maximum of the Leonids with its 33-years revolution, many meteor observers tried to figure out many unknown but principal parameters of the meteor trains with their imaging observations concentrated at a time of the maximum Leonid storm encounter (*Figure 1 – left*). Most recently, based on some fruitful results obtained during 1998–2002, morphology, details of the luminescence process, spectroscopic studies, height distributions and three-dimensional (3-D) spatial evolutions of meteor trains are studied (Higa et al., 2005; Borovicka and Koten, 2003; Abe et al., 2005; Yamamoto et al., 2003; 2005). Moreover, due to the enhancement of imaging devices of CCD and CMOS in these days, meteor train imaging with high temporal resolution has been realized, revealing the earliest stage of the meteor train process in the upper atmosphere. When we can obtain information about temporal evolution of the long-lasting faint emission of meteor trains by multiple-site observation, it can reveal the 3-D structures of meteor trains as well as a possible wind profile in the upper atmosphere within a height range of about 80 km up to 105 km by using the luminous cloud as a tracer. However, such effort for obtaining information about the neutral wind by using the natural meteor trains is limited only at an occasion of the peak period of a meteor storm which provides fireball-class bright meteors.

After becoming the space era in human history, as for the purpose of determining the neutral wind profiles in the upper atmosphere, many trials are devoted for atmospheric studies by using sounding rockets with developing so-called chemical release technique that produces artificial meteor trains in the sky at an exact

place and height range at a precise time and date on demand. Since the early date of space era in 1950’s, the chemical release technique has gradually been established, resulting in some beneficial chemical species of making long-lasting luminous trails in the sky (Davis, 1979). One luminous mechanism is the resonance-scattering illuminations of atomic metallic particles such as, Lithium, Sodium, Barium and Strontium by getting the energy of projecting light from the Sun mainly at the local time zone of twilight, namely under sunlit upper atmosphere with dark sky condition on the ground. Another mechanism is using a light-emitting chemical reaction process with releasing organo-aluminum molecules like tri-methyl-aluminum (TMA) that can effectively recombine with the oxygen and water vapor (or OH molecule) in the upper atmosphere, thus it means TMA is a kind of danger items on the ground. Luminescence of the TMA is not so bright that it has only been used for nighttime wind measurements (Larsen, 2002). The nature of daytime wind profiles in the Earth’s thermosphere has rarely been investigated before the present days because its extremely severe environment to measure with high background luminescence of the daytime blue sky, however the trials of using Lithium vapor released by sounding rockets have been carried out

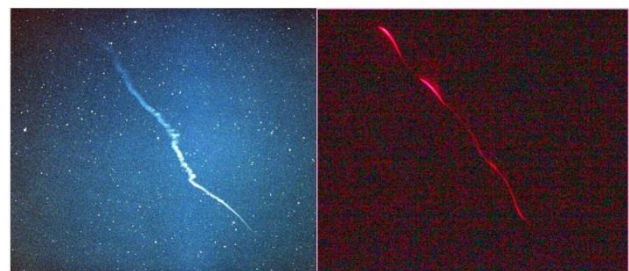


*Figure 1* – A natural meteor train (left) and an artificial Lithium trails (right). The meteor train of a Leonid in 1997 was photographed by M. Toda (Toda et al., 2004). The Lithium trails consist of three parts of chemical releases during the down-leg of the rocket (Habu et al., 2013). Height ranges of both luminescence are almost the same for each.

by some teams of atmospheric scientists since the 1960's. The technique of the Lithium release was once suspended because of the great success of TMA chemical release method established and no one continued the development after the 1980's and unfortunately it gradually disappeared in the 1990's.

## 2 Visualization of upper atmosphere by "Space Fireworks" technique

After gathering a few documents written at that time in the U.S.A., India and Japan, we decided to create a new Lithium Ejection System (LES) to restart the trials of daytime wind measurements in 2005. Then, a comprehensive observation campaign using the JAXA S-520 type sounding rocket was successfully carried out on Sep. 2, 2007 with releasing three Lithium vapor clouds in the thermosphere in the summer evening sky over the Pacific Ocean along the southern coast of Japan (Yamamoto et al., 2014). The artificial clouds that were introduced as "Space Fireworks" at that time greatly illuminated with its resonance-scattering light of 670.8 nm emission of Lithium and were successfully imaged at 4 camera sites on the southern coast simultaneously at an exact synchronized time frame continuously for at least 45 minutes after the first release. Comparison between onboard plasma measuring sensors and the 3-D triangulation results of the Lithium clouds was also established (Uemoto et al., 2010).



Figure 2 – Lithium Ejection System (LES).

The structures of LES are shown in Figure 2, where 125 g metallic Lithium was installed in each cylindrical pod in each LES canister and typical ingredients of the termite reaction were also installed at a torus-like region around the Lithium pod for a heat source required for vaporizing the metallic Lithium to the gaseous one in several seconds. The termite reaction is shown as:



Finally, the vaporized Lithium can be released by its thermal pressure (initial speed) into the space (Yamamoto et al., 2014).

As in the WINDs (Wind measurement for Ionized and Neutral atmospheric Dynamics study) campaign, we

conducted two rocket experiments in the summer evening in 2007 as well as in winter dawn in 2012. In the second experiment, 2 of 3 planned releases were not successful; however, we could measure the neutral wind profile in the twilight thermosphere within a height range between 76 km and 400 km only using three Lithium releases with 125 g for each. As for the imaging of 670.8 nm Lithium emission, we developed new optics with a tele-centric lens with a narrow band-pass-filter (BPF) in order to obtain a 12 nm limitation in passing wavelength for high S/N ratio with a wide field of view of about 100 degrees. The tele-centric optics enable us to put a BPF between the lens and an imaging sensor. Imaging devices of usual single-reflex digital cameras (Canon, EOS Kiss Digital N and EOS Kiss X4) were used with the optics but with removing their IR-cut filters on the CMOS sensors. Due to the high sensitivity of the recent digital devices, the imaging of the faint Lithium clouds was successful even in the situation of the shaded region of the lower part of the third-released cloud in the case of the 2007 experiment (Figure 3 – lower part of left image), thus suggesting the possibilities of using the technique in daytime or nighttime under Full Moon condition after the two experiments of the WINDs campaign.

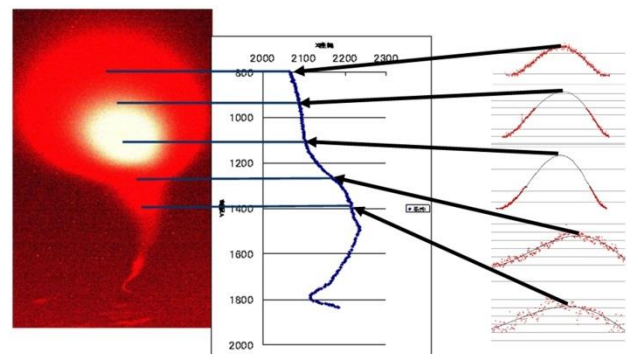


Figure 3 – Lithium clouds and image processing method to get a central position curve on diffusive fireworks. (Yamamoto et al., 2014).

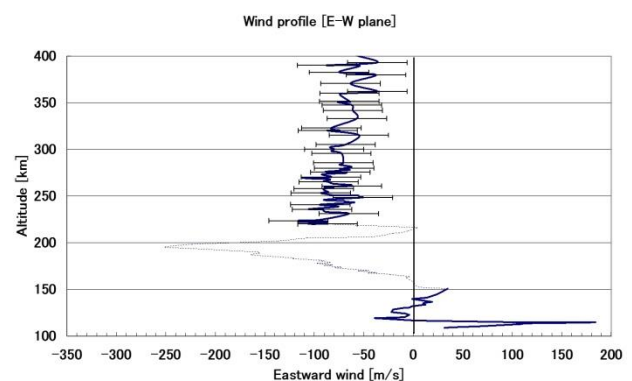


Figure 4 – Neutral wind profile on zonal plane (Yamamoto et al., 2014).

The image processing method can be used for determining the precise coordinates on each snapshot even in a case of rapid diffusion by a rarefied background atmospheric pressure level at the altitude of over about 160 km. It is noteworthy that the observed Lithium clouds showed a great diffusion feature very clearly at the middle/upper thermosphere in comparison with the lower

thermospheric case, usually seen for the natural meteor trains in an altitude range between 80 km and 105 km, whereas the artificial vapor clouds shows almost the same feature as the natural ones under the same altitude condition (*Figure 1*).

It can suggest the principal physical process of rapid diffusion in the upper atmosphere is the same although these luminous mechanisms are different from each other. It means that the error bars above 220 km shown in *Figure 4* are depending on the diffusion rate at each bin, whereas the error bars for the lower part of the profile is within the width of the plotted solid curve. A dotted curve between them shows the profile with some ambiguity because of a superimposed situation of two independent Lithium clouds at the same altitude range by rapid vertical diffusion. Wind shear structures are clearly observed in the profile at about 115 km and 200 km. The lower one is usually seen at the altitude range when we use a TMA chemical release, however the wind shear found at about 200 km might be an important feature at the environment which we usually cannot see without having the chemical release of Lithium.

The transition region of the diffusion process from a viscosity-dependent collisional region to a molecule-dependent collision-less region is usually considered as the turbo-pause height. Such environmental change in altitude might be connected with the strong wind shear regions. Thus the artificial chemical release clearly visualized the diffusion process in the upper atmosphere and it is a significant technique for calibrating some environmental parameters in the surrounding media of the Earth's atmosphere and it is almost the same region of the meteor phenomena.

### 3 Ongoing experiments for unknown fields of upper atmospheric study

After establishing the LES instrumentations onboard a sounding rocket, daytime and moonlit-midnight Lithium release experiments by using NASA/JAXA sounding rocket facilities were carried out in 2011 and 2013. As the first trial was not successful in 2011, we need to figure out the faced problems and solve them in those years, but finally, we could obtain faint images of the artificial Lithium clouds under the extremely severe S/N ratio conditions. Because of the bright blue-sky background in daytime by rayleigh scattering of the sunlight as well as the very faint moonlight source for the resonance-scattering of Lithium that is almost 1/500000 of sunlit Lithium clouds, the same brightness ratio between the Full Moon (-12.7 magnitude) and the Sun (-26.7 mag.) as well.

After the unsuccessful experiment in 2011, we conducted careful calibration of the absolute intensity of the Lithium emission as well as the background sky intensity level by using integral sphere facilities in Japan (NIPR and JAXA) for a given absolute light source in a unit of Rayleigh (R:  $10^6$  photons/m<sup>2</sup>/s/sr). The calibration was

achieved by applying image sequences of the dawn experiment in 2012, where we experienced the condition of enhancing the background sky level due to the sunrise, getting into the daytime condition. At the time of these experiments with very severe S/N ratio condition, we concluded to use an airplane to reduce the background rayleigh scattering by flying into the lower stratosphere at about 13 km in the sky reducing the background intensity into 1/10 or less than the observation on ground.

Another approach using few limited opportunities of artificial reentries of a capsule and/or spacecraft has also been carried out. In these experiments, artificial meteor trains due to the ablation and/or fragmentation process were successfully imaged (Yamamoto et al., 2011).

## 4 Conclusion

During the decade of 2005–2015, many kinds of experiments to acquire/improve the chemical release technique using sounding rockets have been carried out in Japan and the U.S. with a deep collaboration with each other, resulting in some fruitful outputs for both scientific and engineering aspects. This article is only an introduction of such a field of study for the readers of meteor science. The region of interests is almost similar, however the relationship between both fields is still limited mainly because the fields of studies are, in recent days, divided into many fractions of societies of scientific study. Human interaction between such adjacent fields looks important to open new significant studies of science we have never met before. In the near future, artificial experiments concerning the meteor and meteorite studies will be realized in some contexts in physics and technology. Such studies would probably provide us new knowledge about the interaction between the meteoroids and the Earth's atmosphere.

## Acknowledgment

Technical information was provided at the initial stage of the development by Vikram Sarabhai Space Center, ISRO. Observation of the rocket campaign was carried out with Prof. Shigeto Watanabe (Hokkaido University), Prof. Miguel Larsen (Clemson University), Dr. Takumi Abe (ISAS/JAXA), Dr. Hiroto Habu (ISAS/JAXA), Prof. Mamoru Yamamoto (RISH, Kyoto University), Dr. Robert Pfaff (GSFC/NASA), partly supported by Dr. Yuichi Otsuka (STEL, Nagoya University), Dr. Akinori Saito (Kyoto University) and Prof. Takayuki Ono (Tohoku University) and their colleagues and students. The author and his colleagues wish to express their sincere thanks to the rocket team of ISAS/JAXA as well as of WFF/NASA and Andoya Rocket Range (ARR), Norway. They are also grateful to the Aeronautical Technology Directorate of JAXA, National Institute of Polar Research (NIPR) as well as many collaborators and supporters who provided their facilities to use for the observations and calibrating experiments. The meteor train image in *Figure 1* was provided by Masayuki Toda (Nippon Meteor Society).

## References

- Abe S., Ebizuka N., Murayama H., Ohtsuka K., Sugimoto S., Yamamoto M.-Y., Yano H., Watanabe J.-I. and Borovicka J. (2005). "Video and photographic spectroscopy of 1998 and 2001 Leonid persistent trains from 300 to 930 nm". *Earth, Moon, and Planets*, **95**, 265–277.
- Borovicka J. and Koten P. (2003). "Three phases in the evolution of Leonid meteor trains". In Yano H., Abe S. and Yoshikawa M., editors, *Proceedings of the 2002 International Science Symposium on the Leonid Meteor Storms*, Inst. Space Astronaut. Sci., Sagamihara, Japan, ISAS Report SP 15, pages 165–173.
- Davis T. N. (1979). "Chemical releases in the ionosphere". *Rep. Prog. Phys.*, **42**, 1565–1595.
- Habu H., Yamamoto M.-Y., Watanabe S. and Larsen M. F. (2013). "Rocket-borne Lithium ejection system for neutral wind measurement". In Oyama K. and Cheng C. Z., editors, *An introduction to space instrumentation*. TERAPUB, 53–61.
- Higa Y., Yamamoto M.-Y., Toda M., Maeda K. and Watanabe J.-I. (2005). "Catalogue of Persistent Trains II: Images of Leonid Meteor Trains during the METRO campaign 1998-2002". *Publ. Natl. Astron. Obs. Japan*, **7**, 67–131.
- Larsen M. F. (2002). "Winds and shears in the mesosphere and lower thermosphere: Results from four decades of chemical release wind measurements". *Journal of Geophysical Research*, **107**, Issue A8, 10.1029/2001JA000218.
- Toda M., Yamamoto M.-Y., Higa Y. and Watanabe J.-I. (2004). "Catalogue of persistent trains I: Meteor train images during 1988-1997 and development of optimum observing technique". *Publ. Natl. Astron. Obs. Japan*, **7**, 53–66.
- Uemoto J., Ono T., Yamada Y., Suzuki T., Yamamoto M.-Y., Watanabe S., Kumamoto A. and Iizima M. (2010). "Impact of lithium releases on ionospheric electron density observed by impedance probe during WIND campaign". *Earth Planets Space*, **62**, 589–597.
- Yamamoto M.-Y., Toda M., Higa Y., Fujita M. and Suzuki S. (2003). "METRO campaign in Japan II: Three-dimensional structures of two Leonids meteor trains in early stage". In Yano H., Abe S. and Yoshikawa M., editors, *Proceedings of the 2002 International Science Symposium on the Leonid Meteor Storms*, Inst. Space Astronaut. Sci., Sagamihara, Japan, ISAS Report SP, 16, 237–244.
- Yamamoto M.-Y., Toda M., Higa Y., Maeda K. and Watanabe J.-I. (2005). "Altitudinal Distribution of 20 Persistent Meteor Trains: Estimates Derived from METRO Campaign Archives". *Earth, Moon, and Planets*, **95**, 279–287.
- Yamamoto M.-Y., Ishihara Y., Hiramatsu Y., Kitamura K., Ueda M., Shiba Y., Furumoto M. and Fujita K. (2011). "Detection of Acoustic/Infrasonic/Seismic Waves Generated by Hypersonic Re-Entry of the HAYABUSA Capsule and Fragmented Parts of the Spacecraft". *Publications of the Astronomical Society of Japan*, **63**, 971–978.
- Yamamoto M.-Y., Kakinami Y., Kihara D., Watanabe S., Habu H., Abe T., Yamamoto M. and Larsen M. F. (2014). "Measurement of neutral wind profile in nighttime and daytime by Lithium releases and airborne observations". *Proc. of ISAS/JAXA Atmosphere Symposium*, 4-3 (in Japanese).

# Exploring the relationship between meteor parameters based on photographic data

Yulia Yancheva<sup>1</sup>, Simona Hristova<sup>2</sup> and Eva Bojurova<sup>3</sup>

<sup>1</sup>Astroclub Canopus, Astronomical Observatory and Planetarium Nicholas Copernicus, Varna, Bulgaria  
methenarwhal@gmail.com

<sup>2</sup>High school of mathematics Baba Tonka, Ruse, Bulgaria  
simona.hristowa@abv.bg

<sup>3</sup>Astronomical observatory and Planetarium Nicholas Copernicus, Varna, Bulgaria  
eva.bojurova@gmail.com

The paper presents an attempt to investigate the relationship between the luminosity and the linear length of the meteors, based on photographic observations of the Geminid meteor shower during the night of maximum in December 2015.

## 1 Introduction

The luminosity of the meteors depends on a number of factors, including the masses and chemical composition of the meteoric particles, their linear velocities and the angles at which they enter the Earth's atmosphere. The same is true for the linear lengths of the luminous paths of the ablating meteoroids through the atmosphere. One can easily suppose that the two parameters – the luminosity of the meteors and their linear lengths – should be related in some way, i.e. the more massive meteor particles should produce brighter and longer meteors, and therefore brighter meteors should be longer. As obvious as it is, it could be still interesting to explore this relationship, bearing in mind that the masses of the meteors, which are fundamental to it, cannot be measured directly, but the luminosities and the lengths of the meteors can be derived from observations. For our investigation we use meteors belonging to one meteor shower – the Geminids. We can consider that all meteor particles from the Geminid stream have very similar linear velocities and chemical composition. Therefore the influence of these two factors on the relationship we study can be excluded. Looking to the future, a similar exploration would allow us to make an interesting comparison between the distinctive characteristics of this relationship for different meteor showers.

## 2 The observations

The photographic observations were carried out during the night of 14–15 December 2015 on the Plana Mountain near Sofia, Bulgaria. The photographer was Lyubomir Simeonov, a student in the Physics Department of Sofia University, who kindly provided the images to us. On them we found 11 Geminid meteors that were suitable for our measurements. The images were taken by a Nikon 3100 D camera with a 18-55mm lens and the exposure time for each image was 30 sec.

## 3 The linear paths of the meteors

We first used *Stellarium* software to define the angular length of every Geminid meteor in our series. The position of the meteor was found by comparing the star positions in the images with those on the *Stellarium* computer map. In this approximate method, we used the nearest stars to the beginning and to the end point of a meteor and found its angular length. We used the data shown by *Stellarium* to determine the height above the horizon of the beginning and end point of each meteor and the zenithal elongation of the shower radiant at the time of observation. We then measured the angular distance of the beginning and the end point of each meteor from the radiant.

*Table 1* – The heights  $h_b$  and  $h_e$  of the beginning and the end point of each meteor above the horizon and the distances  $\psi_b$  and  $\psi_e$  of the beginning and the end point of each meteor from the Geminid radiant.

Meteor	$h_b$	$h_e$	$\psi_b$	$\psi_e$
1	26.0°	24.2°	25.7°	29.8°
2	37.3°	36.9°	17.8°	20.9°
3	25.3°	21.6°	55.5°	61.6°
4	55.1°	53.8°	42.3°	46.8°
5	43.2°	41.8°	30.1°	34.7°
6	38.4°	36.6°	33.0°	36.6°
7	25.1°	20.4°	26.8°	32.1°
8	62.7°	62.2°	31.2°	35.2°
9	49.2°	44.8°	36.4°	44.5°
10	41.0°	39.1°	26.6°	29.2°
11	21.3°	17.5°	39.2°	43.3°

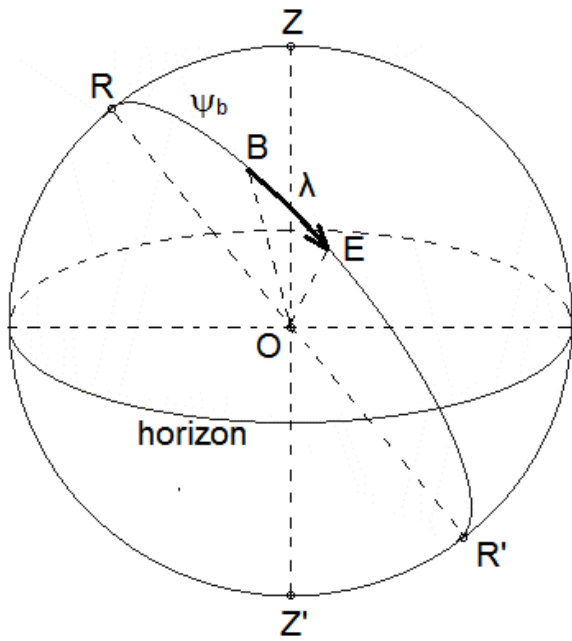


Figure 1 – The celestial sphere centered on the observer O with the positions of the radiant and anti-radiant R and R', and a shower meteor with its beginning and end points B and E.

First we calculate the angular length of the meteor:

$$\lambda = \psi_b - \psi_e$$

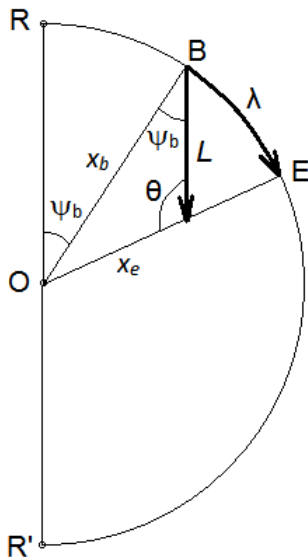


Figure 2 – The observer O, the radiant of the shower R, the angular length  $\lambda$  and the linear length L of the meteor.

In Figure 2 we can see a representation of the apparent angular length  $\lambda$  and the linear length L of the meteor which is actually parallel to the radiant direction from the observer.

We assume that the Geminid meteors start to glow at a height of  $H \approx 80$  km above the Earth's surface<sup>1</sup>. Of course the height will not be equal for all meteors and will depend on their masses and the angles at which they enter the Earth's atmosphere. That is why our

<sup>1</sup> <http://earthsky.org/space/at-what-altitude-do-meteors-become-incandescent>

investigation will be quite approximate. We then use the Earth's radius R and the sine theorem to calculate first the angles  $\alpha$  and  $\beta$ , and then the distance  $x_b$  from the observer O to the beginning point B of the meteor:

$$\alpha = \arcsin\left(\sin(180^\circ - z_b) \cdot \frac{R}{R + H}\right)$$

where  $z_b = 90^\circ - h_b$  is the zenithal distance of point B.

$$\beta = z_b - \alpha$$

$$x_b = R \cdot \frac{\sin\beta}{\sin\alpha}$$

Now we go back to Figure 2 and, once again using the sine theorem, we finally find the length L of the meteor in kilometers:

$$L = x_b \cdot \frac{\sin\lambda}{\sin\theta}$$

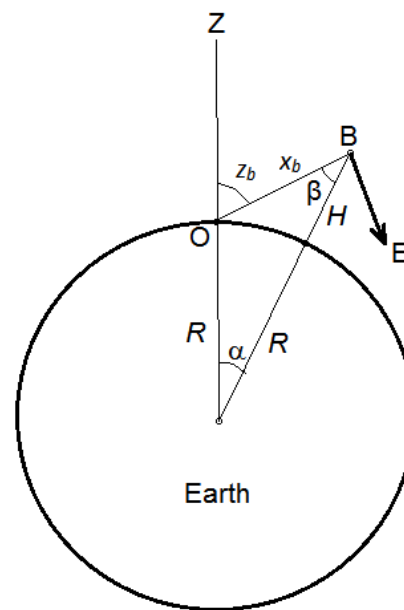


Figure 3 – The position O of the observer on the Earth and the meteor.

We calculated the linear lengths of all the meteors and then we tried to verify our results. We used the linear velocity of the Geminids  $v = 35$  km/s and determined the duration of each meteor:

$$\Delta t = \frac{L}{v}$$

Then we used the angular length of each meteor to find its apparent angular velocity:

$$\omega = \frac{\lambda}{\Delta t}$$

There is a relationship between the angular velocities of the meteors and their distances from the radiant. We compared our results with the values given in the tables about Geminids in the Handbook for Visual Meteor

Observations (Roggemans et al., 1992). We could see that there is a good agreement.

Table 2 – Apparent angular velocities of the meteors calculated using the results for their linear lengths.

Meteor	$L$ [km]	$t$ [s]	$\lambda$	$\omega$ [°/s]
1	25.6	0.73	4.13°	5.7
2	19.5	0.56	2.96°	5.3
3	22.1	0.63	6.14°	9.7
4	10.5	0.30	4.43°	14.8
5	16.4	0.47	4.38°	9.4
6	13.4	0.38	4.86°	12.67
7	31.9	0.91	5.26°	5.8
8	10.7	0.31	3.78°	12.4
9	21.12	0.60	8.07°	13.4
10	11.5	0.33	2.73°	8.3
11	22.0	0.63	4.15°	6.6

#### 4 The brightness of the meteors

In order to find the meteor's brightness, we used the IRIS software. We measured the brightness at six points on the trajectory of each meteor, subtracting the background level of illumination. We then calculated the average value for the meteor  $E$ . In addition, we had to take into account the different distance of each meteor from the observer. To eliminate this factor we determined the brightness which the meteor would have had if it had appeared in the zenith –  $E_z$ . First we found the distance of the end point of the meteor from the observer (Figure 2):

$$x_e = L \cdot \frac{\sin \psi_b}{\sin \lambda}$$

We calculated a kind of “average” distance from the observer to the meteor:

$$x = \frac{x_b + x_e}{2}$$

And after that we reduced the observed meteor brightness to a zenithal position of the meteor:

$$E_z = E \cdot \frac{x^2}{H^2}$$

#### 5 The results

Finally, we combined the two characteristics and built a graph representing the relationship between a meteor's luminosity and its linear length.

As it can be seen from the graph in Figure 4, the relationship between the two parameters is obvious as we expected. Further development of the method could improve the accuracy of the data. We applied a quite

primitive method to obtain the apparent angular parameters of the meteors, by comparison between the images and stellar maps. We could instead use the astrometric options of the IRIS software. Nevertheless, some parameters will still remain not very accurate. For instance, it is difficult to define a brightness of a meteor – it has a different brightness at each point of its trajectory. It is also difficult to determine the positions of the beginning and the end point of a meteor on a photograph because the glow of the meteor does not begin and end abruptly. A major problem is the influence of the angle at which the meteors enter the Earth's atmosphere, or in other words, the altitude of shower radiant above the horizon. This influence should be significant but taking it into account requires quite complicate modeling of the behavior of the meteor particles in the atmosphere. Another source of inaccuracy is that for those meteors more distant from the observer, less of the meteor path would be bright enough to be visible to the observer, which would lead to underestimation of the length of the meteor.

Table 3 – Brightness of the Geminids (reduced to zenithal position) and their linear length.

Meteor	$E_z$ instr. units	$L$ km
1	572.9	25.6
2	129.0	19.5
3	665.5	22.1
4	71.5	10.5
5	85.3	16.4
6	134.8	13.4
7	1715.0	31.9
8	56.4	10.7
9	192.8	21.1
10	186.4	11.5
11	811.0	22.0

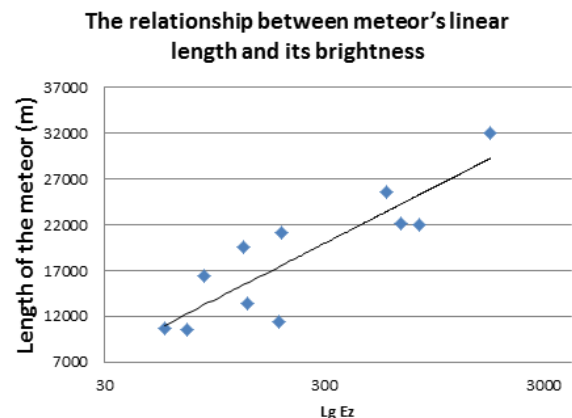


Figure 4 – Relationship between the brightness of the Geminids and their linear lengths.

## 6 Conclusions

We applied a simple and approximate method to determine the linear lengths and the brightness of a series of Geminid meteors and produced a graph showing the relationship between the two parameters.

The accuracy of the method could be increased by using more precise methods of measurement. However, there are natural limitations that ensue from the stochastic character of the meteor phenomenon itself. So another way to improve the results of this investigation would be to use a much greater amount of data so as to achieve more statistically significant results.

An interesting option for future work would be to explore the relationship between the brightness and the linear length for other meteor showers and to compare the parameters of this relationship.

## References

- Roggemans P., Gyssens M., Steyaert C. and Vanmunster T. (1992). "Handbook Visual Meteor Observations". NATURELLA, Sofia (*in Bulgarian*).



Vivid discussion between Vincent Perlerin (in the center, 'did I overlook something?'), Sirko Molau, Javor Kac and Cis Verbeeck. In the background Hans-Georg Schmidt and Bernd Gärhken.

# Radar observations of the Volantids meteor shower

Joel Younger<sup>1,2</sup>, Iain Reid<sup>1,2</sup>, Damian Murphy<sup>3</sup>

<sup>1</sup> ATRAD Pty Ltd, Thebarton, Australia

jyounger@atrad.com.au, ireid@atrad.com.au

<sup>2</sup> School of Physical Sciences, The University of Adelaide, Adelaide, Australia

<sup>3</sup> Australian Antarctic Division, Kingston, Australia

damian.murphy@aad.gov.au

A new meteor shower occurring for the first time on 31 December 2015 in the constellation Volans was identified by the CAMS meteor video network in New Zealand. Data from two VHF meteor radars located in Australia and Antarctica have been analyzed using the great circle method to search for Volantids activity. The new shower was found to be active for at least three days over the period 31 December 2015 – 2 January 2016, peaking at an apparent radiant of R.A. =  $119.3 \pm 3.7$ , dec. =  $-74.5 \pm 1.9$  on January 1<sup>st</sup>. Measurements of meteoroid velocity were made using the Fresnel transform technique, yielding a geocentric shower velocity of  $28.1 \pm 1.8$  km s<sup>-1</sup>. The orbital parameters for the parent stream are estimated to be  $a = 2.11$  AU,  $e = 0.568$ ,  $i = 47.2^\circ$ , with a perihelion distance of  $q = 0.970$  AU.

## 1 Introduction

The Camera for Allsky Meteor Surveillance (CAMS) video network in New Zealand reported the first detections of a meteor shower originating from a radiant of R.A. = 120.6, dec. = -72.0 in the constellation Volans on New Year's Eve 2015 (Jenniskens and Baggaley, 2016). A review of previous CAMS data indicated that the shower had not occurred in the previous year. In total, cameras recorded the trajectories of 21 Volantids meteors on December 31 and two on January 1, 2016, with activity peaking around 10<sup>h</sup>15<sup>m</sup> UT on 31 December. Shower meteors had a geocentric velocity of 28.4 km s<sup>-1</sup> and visual magnitudes ranging from +3 to -2 (Jenniskens et al., 2016).

Existing VHF meteor radars, which are primarily used to study winds and plasma diffusion rates in the mesosphere/lower thermosphere (MLT) region of the atmosphere, can also be applied to the detection of meteor showers, with the advantage of being able to detect meteors during daylight hours and in inclement weather. Analysis of meteor radar echoes enables meteoroid velocity to be inferred, which, combined with the radiant of a detected shower, allows for orbital parameters of meteoroid streams to be calculated. Data collected in the course of unrelated atmospheric studies by two meteor radars in Australia and Antarctica were successfully searched for evidence of the new Volantids shower.

## 2 Meteor radar

### Detection of meteor trails by radar

As a meteoroid enters Earth's atmosphere, kinetic energy is converted to thermal energy through collisions with atmospheric molecules. Once meteoroids are heated to the point of evaporation, atoms leave the meteoroid still traveling at similar geocentric velocities to the parent body. Subsequent collisions between atmospheric

constituents and evaporated meteoric material can be energetic enough to ionize one or both of the colliding particles. This results in a trail of plasma behind the ablating meteoroid, comprised of a mixture of ions and electrons embedded in a background of neutral atmospheric molecules.

Meteoric plasma scatters incident radio waves, making it possible to detect meteor trails using the reflection of transmitted signals. The motion of meteor trails as they

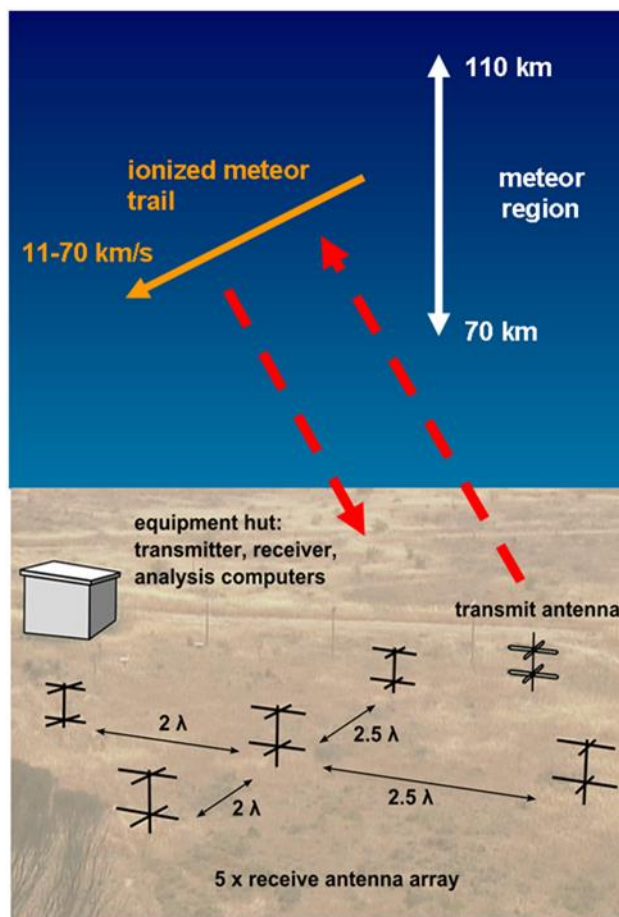


Figure 1 – Typical meteor radar configuration.

drift with background winds produces measurable Doppler shifts along the detection vector that can be combined across detections in different directions to infer the wind speed and direction in the meteor region. For small meteoroids (O(1 mm) diameter and smaller) that constitute the majority of the meteoroid flux, the meteoric plasma may be less than  $2.4 \times 10^{14}$  electrons  $m^{-1}$ , which classifies the trail as underdense (McKinley, 1961).

Radio waves can fully penetrate underdense plasmas, which produce specular echoes. Scatter from different points along the trail combines to produce the strongest echoes when the trail is perpendicular to the line of sight to the radar. Furthermore, meteoric plasma undergoes diffusion once formed, as the ions and electrons execute random walks away from the trail axis. The movement of meteoric plasma away from the trail axis reduces the intensity of observed radar backscatter through destructive interference. For underdense meteor trails, this results in a distinctive exponential decay in echo intensity over time. Hence, the duration of underdense meteor radar echoes can be used to infer the rate of plasma diffusion in the MLT, which can be used to estimate atmospheric temperature (Hocking, 1999; Cervera and Reid, 2000) and density (Younger et al., 2015a).

The radar backscatter produced during the passage of a meteoroid with a plasma trail across the field of view of a radar is analogous to a knife-edge diffraction pattern. The recording of echo phase in addition to intensity by a radar enables the diffraction pattern to be deconvolved through a process known as the Fresnel transform. The result is a profile of the scattering intensity along the trail, but an estimate of meteoroid speed is a fortunate byproduct of the process (Elford, 2004). Thus, radars can provide the three dimensional position of the perpendicular scattering point of a meteor trail and the instantaneous speed of the meteoroid as it passed that point.

### Radar configuration

VHF meteor radars are a common tool for monitoring the atmosphere at heights between 70–110 km using frequencies in the range of 30–60 MHz. Modern meteor radars generally conform to similar configurations, consisting of a single all-sky transmit antenna and a five-element receive array (Jones et al., 1998), as shown in *Figure 1*.

The five antennas of the receive array form an interferometer, arranged in a T, L, or cross shape of two baselines sharing a common antenna. Antennas along the two perpendicular baselines are spaced at 2 and 2.5 times the radar wavelength,  $\lambda$ . The direction of incident backscatter is determined by comparing the phase differences of the different antenna pairs. The combination of the 2 and 2.5  $\lambda$  allows for the construction of a virtual 0.5  $\lambda$  antenna spacing, which provides unambiguous angle of arrival estimates, in addition to a higher precision 4.5  $\lambda$  antenna pair. The minimum spacing of 2  $\lambda$  ensures that mutual coupling between antennas is minimized.

### Radars used in this study

Two ATRAD meteor radars were used for detection of Volantids shower activity in this study: a 40 kW 55 MHz radar at Buckland Park (34.6 S, 138.5 E) near Adelaide, Australia operated by The University of Adelaide and a 6.8 kW 33 MHz radar at Davis Station, Antarctica (68.6 S, 78.0 E) operated by the Australian Antarctic Division (Holdsworth et al., 2008). Both radars have a cross-shape receive array and transmit a 4-bit coded complimentary pulse at a pulse repetition frequency of 430 Hz. Signal to noise is improved using four-pulse coherent integration, which provides an effective sampling rate of 107.5 Hz. Details of meteor detection and classification criteria are given in (Holdsworth et al., 2004).

The Davis Station radar detects significantly more meteors than the Buckland Park radar. This is due in part to the polar location of the Davis Station radar and the higher radio noise in Buckland Park’s metropolitan

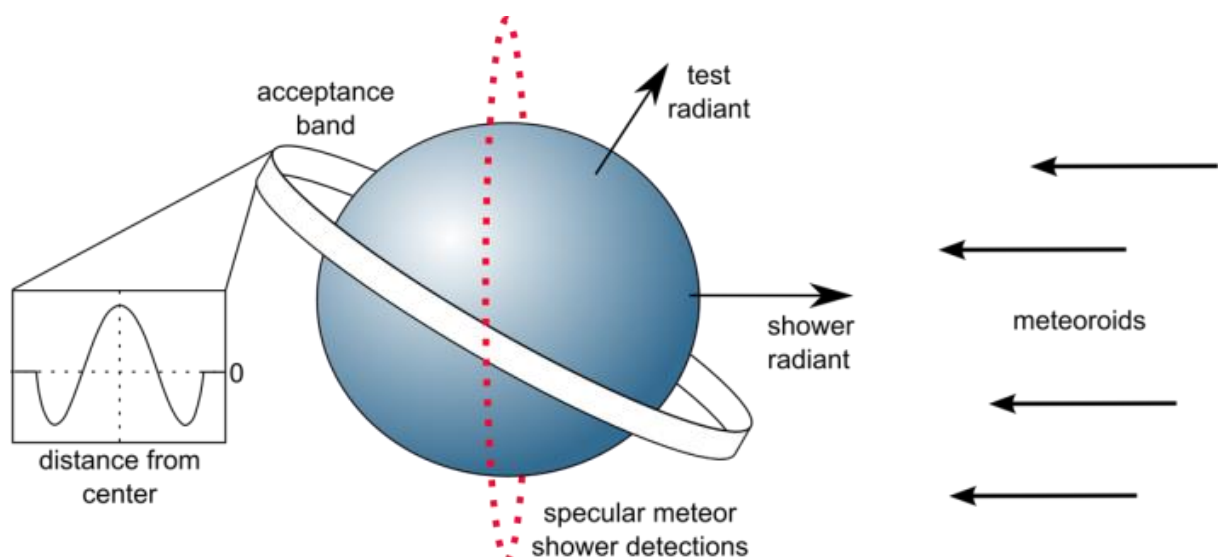


*Figure 2* – Geometry of the great circle technique used to estimate shower activity using perpendicular detections. Possible radar detections resulting from a shower incident from the right are shown as a red dotted line. Earth rotates inside of the shaded celestial sphere. The inset plot depicts the weighting function as given by (1).

environment, but also to the lower transmitting frequency. As the minimum detectable plasma density is proportional to  $\lambda^{3/2}$ , where  $\lambda$  is the wavelength of the radar (Cepelcha et al., 1998), the minimum detectable trail density for the Buckland Park radar is more than double the minimum detectable density for the Davis Station radar at the same transmitting power levels. Additionally, during the Volantids observation period, the Buckland Park radar was operated as a passive radiometer for five out of every 15 minutes as part of an unrelated astrophysics experiment, which resulted in the array being used as a radar for only 2/3 of the time. Hence, while the Davis Station radar recorded an average of approximately 14000 meteor detections per day, the Buckland Park radar only recorded an average detection

rate of about 4000 meteors per day.

### 3 Great circle method

#### General technique

The specular scatter of radio waves by underdense meteor trails produces the condition that meteors are detected when the line of sight to a meteor is perpendicular to the trail axis. This means that the trajectory of individual meteors cannot be determined by a single-station meteor radar. Thus, knowledge of the trajectory of single meteoroids is limited to a plane of ambiguity. This condition can, however, be exploited through a statistical analysis of large numbers of meteor detections.

If a well-defined filament of debris is in an orbit that

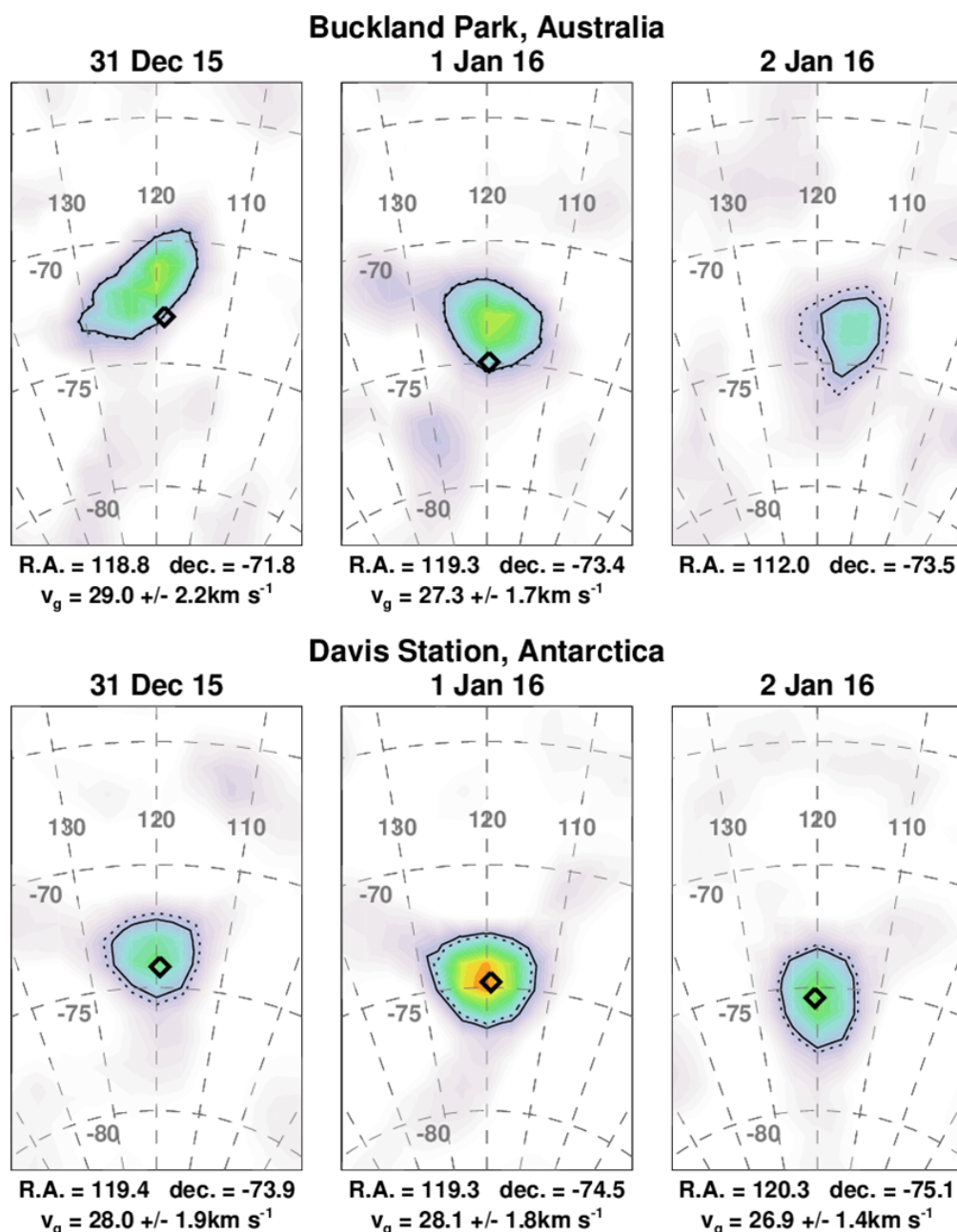


Figure 3 – Radiant activity maps showing daily detections of the Volantids shower in galactic-equatorial coordinates (J2000). Diamonds denote the position of the radiant after adjustment for zenith attraction. Dotted lines follow the full width at half maximum (FWHM) of the radiant activity peaks. Solid lines are the SNR = 5 contours used to flag possible shower activity. Data collected at Buckland Park on 2 January were insufficient to produce an estimate of shower velocity.

intersects the path of Earth, a meteor shower will occur. The perpendicular radar detections that result from a shower will lie in a ring on the celestial sphere, with the ring located perpendicular to the shower radiant, as depicted in *Figure 2*. Hence, radiants with shower activity can be found by counting the number of meteor detections in bands perpendicular to all possible radiants and searching for radiants with significantly elevated rates of perpendicular detections (Jones and Jones, 2006).

### Application to this study

The great circle method has been applied previously by the authors to meteor radar data as part of a survey of Southern hemisphere shower activity (Younger et al., 2009) and for a detailed study of the predicted Camelopardalids shower in 2014 (Younger et al., 2015). To summarize the search process, the celestial sphere is first divided into discrete test radiants, separated by approximately one degree of solid angle. Radiant activity is quantified by a weighted count of meteors perpendicular to each radiant.

To reduce the blurring of narrow showers on the radiant activity map due to the overlap of perpendicular detection rings with misaligned acceptance bands, a weighting function,

$$w(\theta) = \begin{cases} 1 - 6 \left(\frac{\theta}{\delta\theta}\right)^2 + 5 \left(\frac{\theta}{\delta\theta}\right)^4 & \text{for } |\theta| \leq \delta\theta \\ 0 & \text{for } |\theta| > \delta\theta \end{cases} \quad (1)$$

is applied, where  $\theta$  is the distance from the center of the acceptance band. The width of the weighting function,  $\delta\theta$ , is dependent on the width of showers being searched for and the angular accuracy of the radar. For this application, a value of four degrees has been found to work best.

Once activity values have been calculated for every possible radiant, an algorithm searches for discrete peaks corresponding to active showers. Radiant activity values are found to adhere to a normal distribution, so noise is defined as the standard deviation of non-zero radiant activity levels. The radiant activity map is searched for peaks that exceed the defined noise level by a factor of five. Shower activity peaks are characterized by fitting an ellipse to the noise threshold boundary on the map, which provides an estimate of the extent of the shower peak in right ascension and declination. Shower velocity is initially estimated by fitting a Gaussian curve to the velocities of meteors in a four degree wide band perpendicular to the peak centroid. Only meteors above the median detection height in the band are used to minimize the effects of deceleration (Younger et al., 2012).

Velocity distributions were further refined by subtracting an estimate of the sporadic background velocity distribution. The background velocity distribution was constructed by collecting candidate meteors from the average radiant of the detected Volantids shower in apex-centered solar coordinates on days to either side of

shower activity. The background distribution was then subtracted from the detected shower candidate velocity distribution, with the resultant peak used to infer the apparent velocity of shower meteoroids.

## 4 Volantids shower detections

### Initial detection

The great circle method as described was applied to single-day sets of meteor radar detections for each radar, peaking on January 1<sup>st</sup> at R.A. =  $119.3 \pm 3.7$ , dec. =  $-74.5 \pm 1.9$ , as seen from Davis Station. Combined estimates of the apparent radiant at each location were used to construct the background velocity distribution as described. Summaries of the daily detection SNR values are given in *Table 1* and radiants locations are listed in *Figure 3*.

*Table 1* – Daily signal to noise ratio of detections from each radar.

	signal to noise ratio	
	Buckland Park	Davis Station
31 Dec	9.7	8.3
1 Jan	9.5	11.7
2 Jan	7.3	8.8

Detailed estimates of the behavior of the detection rate over time are difficult, as the shower radiant passes close to the zenith of the Davis Station radar, which places shower trails' perpendicular reflection points on the horizon, where detection is impossible. This produces a detection distribution with a gap during what would otherwise be the time of the peak detection rate. Radiant analysis of a moving window of eight hour data subsets spaced two hours apart, shown in *Figure 4*, indicates that the Volantids shower occurred at least as early as 00<sup>h</sup>00<sup>m</sup> UT, 31 December 2015 and finished no earlier than 22<sup>h</sup>00<sup>m</sup> UT, 2 January 2016. Shower activity peaked at approximately 1300 UT, 1 January 2016. Volantids activity displays a gradual increase over the first three days, with a comparatively abrupt end. The Buckland Park radar, while more favorably located, did not achieve sufficient detection rates for a detailed analysis of radiant activity.

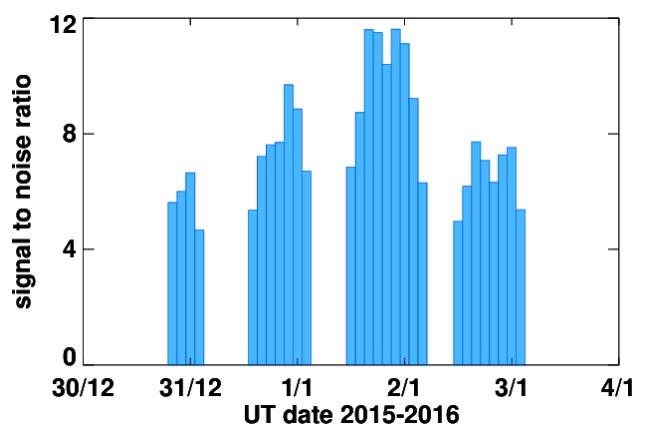


*Figure 4* – 8-hour smoothed Volantids radiant activity at Davis Station, Antarctica.

### Correction of apparent radiant

Earth's gravity affects the observed shower properties in two ways. Firstly, meteoroids are accelerated from their initial geocentric orbital velocity by the gravitational pull of Earth. Secondly, the gravitational pull towards Earth's barycenter causes meteoroid trajectories to be pulled towards the local zenith.

The geocentric velocity,  $v_g$ , of meteoroids can be calculated from the apparent velocity,  $v_a$ , that is observed on Earth via the equation

$$v_g = \sqrt{v_a^2 - \frac{GM_\oplus}{r_a}}, \quad (2)$$

Where  $G$  is the gravitational constant,  $M_\oplus$  is the mass of Earth, and  $r_a$  is the distance from the center of Earth to the meteor detections. The last term was determined by calculating the radius of Earth at each observing site using the WGS84 ellipsoid (Decker, 1986) and adding a nominal meteor detection height of 90 km.

The change in meteoroid trajectory zenith angle due to zenith attraction,  $\Delta\varphi$ , is given by

$$\Delta\varphi = 2 \tan^{-1} \left( \frac{v_a - v_g}{v_a + v_g} \tan \frac{\varphi}{2} \right), \quad (3)$$

where  $\varphi$  is the observed zenith angle. This correction was applied to the observed radiant of the Volantids to determine the radiant of the shower prior to the influence of Earth's gravity as shown as diamonds in *Figure 3*.

## 5 Orbit of the Volantid stream

The direction of the shower radiant can be combined with the speed of the shower meteoroids to estimate the orbital parameters of the parent stream (for equations, see e.g. Younger et al., 2009), the results of which are shown in *Table 2*. Uncertainties in the input variables were handled by using a Monte Carlo simulation, assuming normal statistics. 50000 calculations of orbital parameters were performed using randomized, normally distributed uncertainties centered on the measured values of right ascension, declination, and velocity. The widths of the randomized distributions were taken from the estimates of the standard deviations of the measured parameters.

### Orbital parameter statistics

Estimation of uncertainty is problematic for some of the calculated values of the orbital elements. Eccentricity, inclination, and the argument of the perihelion all maintain normal or close to normal distribution following the propagation of input Gaussian uncertainty through orbital calculations, but the distributions of the calculated values of semi-major axis and perihelion distance exhibit substantial asymmetry, as can be seen in *Figure 5*.

To provide an estimate of the most likely value of  $a$  and  $q$ , the peak values of probability were used. A proxy for the 1-sigma uncertainty in each direction was determined

by calculating the cumulative probability of the distribution moving away from the peak probability. The 1-sigma value was then assigned to the value for which the cumulative probability in each direction is equal to 0.34, which provides upper and lower uncertainty estimates for  $a$  and  $q$ .

*Table 2* – Volantids orbital parameters determined from Monte Carlo simulation.

element	symbol	estimate	uncertainty
semi-major axis	$a$	2.11 AU	+ 0.50 - 0.18
eccentricity	$e$	0.568	$\pm 0.069$
inclination	$i$	47.2°	$\pm 2.6$
ascending node	$\Omega$	100.3°	
perihelion arg.	$\omega$	343.4°	$\pm 3.4$
perihelion distance	$q$	0.970 AU	+ 0.004 - 0.009

No uncertainty is provided for the argument of the ascending node, as the shower was observed at the ascending passage of the stream. The given value of the ascending node was determined from the solar longitude of Earth at the estimated time of maximum shower activity.

### Comparison with CAMS derived orbit

The calculated values of  $a$  and  $q$  are slightly less than those given by Jenniskens and Baggaley in the initial announcement. This is likely due to the underestimation of meteoroid velocity by the radars. As meteor radars are specifically configured to detect faint meteor trails, radar detections are biased towards smaller meteoroids, which are strongly decelerated during ablation. By comparison, video detections necessarily correspond to larger meteoroids.

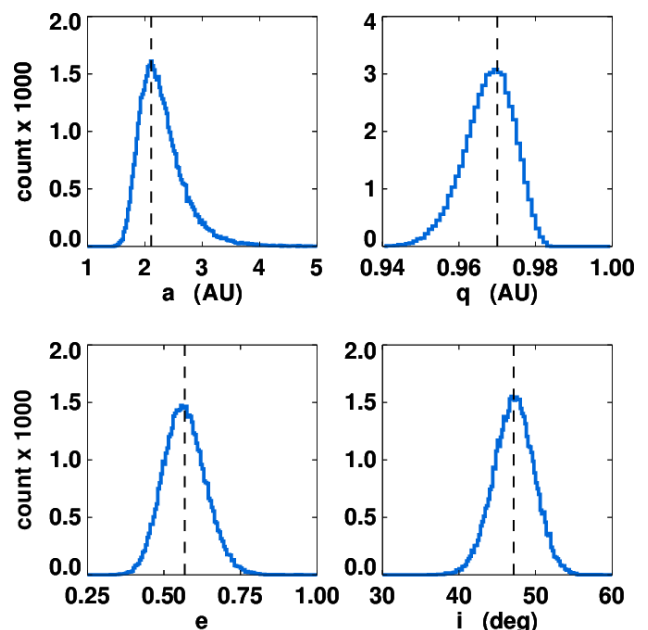


*Figure 4* – Distributions of orbital parameters calculated in Monte Carlo simulation. Dashed lines show the final values listed in *Table 2*.

## 6 Conclusion

The Volantids shower of 2015/2016 has been detected by two meteor radars in the southern hemisphere, with results in good agreement with those of the CAMS video network that provided the initial detection. The use of radar enabled the monitoring of Volantid shower activity through daylight hours and in the absence of meteoroids sufficiently large enough to produce visible trails.

This study represents the first time that the Buckland Park meteor radar was used for astronomical purposes, which was done while the receive array was being periodically occupied by other experiments. This demonstrates the ability of the great circle method to successfully detect shower activity even from modestly performing meteor radars. The source of the Volantids is still unknown, but the stream is already well characterized after a single occurrence of the shower.

## Acknowledgments

This project was made possible by generous financial support from ATRAD Pty Ltd. Radar observations were conducted with financial support from Australian Research Council grants DP0878144 and DP1096901 and ASAC grant 2325.

## References

- Cepelcha Z., Borovička J., Elford W. G., Revelle D. O., Hawkes R. L., Porubčan V. and Šimek M. (1998). “Meteor phenomena and bodies”. *Space Science Reviews.*, **84**, 327–471.
- Cervera M. A. and Reid I. M. (2000). “Comparison of atmospheric parameters derived from meteor observations with CIRA”. *Radio Science*, **35**, 833–843.
- Decker B. L. (1986). “World geodetic system 1984”. Defense Mapping Agency Aerospace Center St Louis Afs Mo.
- Elford W. G. (2004). “Radar observations of meteor trails, and their interpretation using Fresnel holography: a new tool in meteor science”. *Atmos. Chem. Phys.*, **4**, 695–729.
- Hocking W. K. (1999). “Temperatures using radar-meteor decay times”. *Geophysical Research Letters*, **26**, 3297–3300.
- Holdsworth D. A., Murphy D. J., Reid I. M. and Morris R. J. (2008). “Antarctic meteor observations using the Davis MST and meteor radars”. *Advances in Space Research*, **42**, 143–154, doi:10.1016/j.asr.2007.02.037.
- Holdsworth D. A., Reid I. M. and Cervera M. A. (2004). “Buckland Park all-sky interferometric meteor radar”. *Radio Science*, **39**, 1–12, doi:10.1029/2003RS003014.
- Jenniskens P. and Baggaley J. (2016). “Volantid meteor shower outburst on New Year’s Eve 2015”. CBET 4261, Central Bureau for Astronomical Telegrams.
- Jenniskens P., Baggaley J., Crumpton I., Aldous P., Gural P. S., Samuels D., Albers J. and Soja R. (2016). “A surprise southern hemisphere meteor shower on New-Year’s Eve 2015: the Volantids (IAU#758, VOL)”. *WGN, Journal of the IMO*, **44**, 35–41.
- Jones J. and Jones W. (2006). “Meteor radiant activity mapping using single-station radar observations”. *Monthly Notices of the Royal Astronomical Society*, **367**, 1050–1056, doi:10.1111/j.1365-2966.2006.10025.x.
- Jones J., Webster A. R. and Hocking W. K. (1998). “An improved interferometer design for use with meteor radars”. *Radio Science*, **33**, 55–65.
- McKinley D. W. R. (1961). *Meteor Science and Engineering*, McGraw-Hill, New York.
- Younger J. P., Reid I. M., Vincent R. A., Holdsworth D. A. and Murphy D. J. (2009). “A southern hemisphere survey of meteor shower radiants and associated stream orbits using single station radar observations”. *Monthly Notices of the Royal Astronomical Society*, **398**, 350–356, doi:10.1111/j.1365-2966.2009.15142.x.
- Younger J. P., Reid I. M., Vincent R. A. and Murphy D. J. (2012). “Meteor shower velocity estimates from single-station meteor radar: accuracy and precision”. *Monthly Notices of the Royal Astronomical Society*, **425**, 1473–1478, doi:10.1111/j.1365-2966.2012.21632.x.
- Younger J. P., Reid I. M., Li G., Ning B. and Hu L. (2015). “Observations of the new Camelopardalids meteor shower using a 38.9 MHz radar at Mohe, China”. *Icarus*, **253**, 25–30, doi: 10.1016/j.icarus.2015.02.021
- Younger J. P., Reid I. M., Vincent R. A. and Murphy D. J. (2015a). “A method for estimating the height of a mesospheric density level using meteor radar”. *Geophysical Research Letter.*, **42**, 1–6, doi:10.1002/2015GL065066.

# Taurids 2015

Przemysław Żołądek<sup>\*1</sup>, Arkadiusz Olech<sup>2</sup>, Mariusz Wiśniewski<sup>3,1</sup>, Regina Rudawska<sup>4</sup>,  
Marcin Bęben<sup>1</sup>, Tomasz Krzyżanowski<sup>1</sup>, Maciej Myszkiwicz<sup>8,1</sup>, Marcin Stolarz<sup>1</sup>, Marcin Gawroński<sup>5</sup>,  
Mariusz Gozdalski<sup>1</sup>, Tomasz Suchodolski<sup>6</sup>, Walburga Węgrzyk<sup>1</sup> and Zbigniew Tymiński<sup>7,1</sup>

<sup>1</sup> Comets and Meteors Workshop, ul. Bartycka 18 00-716 Warszawa, Poland

\*brahi@op.pl

<sup>2</sup> Nicolaus Copernicus Astronomical Center, Polish Academy of Science ul. Bartycka 18 00-716 Warszawa, Poland

<sup>3</sup> Central Office of Measures, ul. Elektoralna 2 00-139 Warszawa, Poland

<sup>4</sup> ESA European Space Agency Research and Technology Centre, Noordwijk, The Netherlands

<sup>5</sup> Toruń Centre for Astronomy, Faculty of Physics, Astronomy and Applied Informatics,  
Nicolaus Copernicus University, ul. Grudziądzka 5, 87-100 Toruń, Poland

<sup>6</sup> Space Research Centre, Polish Academy of Science, ul. Bartycka 18A 00-716 Warszawa, Poland

<sup>7</sup> National Centre for Nuclear Research, POLATOM, ul. Sołtana 7 05-400 Otwock, Poland

<sup>8</sup> Warsaw University Observatory, Al. Ujazdowskie 4 00-478 Warszawa, Poland

Enhanced activity of the Southern Taurids has been detected in the evening of 31 October 2015. Polish Fireball Network cameras detected several bright meteors and fireballs including extremely bright events at 18<sup>h</sup>05<sup>m</sup> UT and 23<sup>h</sup>13<sup>m</sup> UT. Trajectories and orbital elements have been calculated, the orbits of both fireballs have been compared with the NEO orbital database. Three asteroids on very similar orbits have been found – 2015TX24, 2005UR and 2015TF50. All these bodies have orbital periods close to a 7:2 resonance with Jupiter.

## 1 Introduction

The Northern and Southern Taurids are well known autumn meteor showers. Observed during several decades by visual observers and presently by modern equipment, the Taurids look to be a meteor shower with many interesting features. This is an ecliptic meteor stream divided in two branches known as the Northern Taurids (NTA) and the Southern Taurids (STA). Both Taurid streams usually produce rather low visual rates, typical activity doesn't exceed a ZHR = 5. According to the IMO visual data Northern Taurids are active from October 10 to December 20 with a barely visible maximum close to November 12. Southern Taurids are active from September 10 to November 20 with a maximum close to October 10. Both streams produce also daylight meteor showers. The Northern branch of the Taurids encounters the Earth again at the end of June producing the daytime Beta Taurids, the Southern branch meets the Earth in the beginning of June producing the daytime Zeta Perseids. Various authors described the complex structure of the Taurids which is detectable using modern observing techniques. There is a large number of streams which can be connected with comet 2P/Encke (Porubčan et al., 2006), all these streams create a widely dispersed complex of meteor showers. For most of these showers NEO asteroids on similar orbits were found.

Some data suggests that the Taurids are responsible for some unusual activity outbursts with enhanced numbers of bright fireballs observed. All these observations have been analyzed (Asher and Clube, 1993). The authors found traces of the high activity in October 1951,

November 1978, November 1981 and November 1988. There are also observations of transient lunar phenomena in June 1931 and June 1975 probably caused by meteoroids hitting the moon during daytime encounters with the stream. Authors pointed out that such activity may be connected with a Taurid filament which is in a resonance of 7:2 with Jupiter. Further possible enhancements of activity were predicted for 1995, 1998 and 2005. Higher ZHR's were observed in 1998 and 2005 (Dubietis and Arlt, 2007). Especially the 2005 maximum was spectacular, with a higher overall activity and enhanced number of very bright STA fireballs. Between 28 October and 10 November the Polish Fireball Network observed five bright Taurid fireballs, the brightest one, a -15 magnitude fireball was observed on November 4, 2005.

A new prediction of the outburst has been published after the 2005 maximum with a possible enhanced activity in 2015.

## 2 Observations

During the evening of 31 October 31 the sky over Poland was clear. Shortly after sunset video cameras of the Polish Fireball Network started to observe. It is worth to mention that this evening many amateur astronomers photographed the northern sky trying to register the 2015 TB145 asteroid visible at the same time. An extremely bright fireball appeared over Northern horizon on 18<sup>h</sup>05<sup>m</sup> UT reaching a magnitude much brighter than the Full Moon. Casual observers describe the fireball as a



Figure 1 – The “Okonek” fireball, 31 October 2015 18<sup>h</sup>05<sup>m</sup> UT. Image taken in Czernice Borowe, 80 km north of Warsaw.

moderate speed, blue-green fireball with multiple flashes which completely lightened the sky and surrounding landscape. Some observers located exactly below the trajectory reported electrophonic sounds exactly in the moment of brightest flare, they didn't notice any other sound effects. The persistent trail left by this fireball has been visible for at least 50 minutes drifting slowly to the west.

The 18<sup>h</sup>05<sup>m</sup> fireball was registered by multiple stations of the Polish Fireball Network, most of recordings were only partially usable due to strong image saturation. A very precise fireball image has been obtained by a casual photographer from Czernice Borowe (former PFN22 station), 80km north of Warsaw. The fireball trail visible on this image is almost complete and the terminal part of the trajectory is clearly visible. The same photographer also registered a very detailed image of the persistent trail.

After the fireball, during the next few hours a significant rise in the Taurids activity has been observed. Dozens of Taurids have been observed by the whole network resulting in 14 calculated trajectories and orbits. This activity was concentrated between 20<sup>h</sup> UT and 21<sup>h</sup> UT.

The second very bright fireball appeared at 23<sup>h</sup>13<sup>m</sup> UT and was not so widely noticed by casual observers. This fireball saturated cameras located in the north-western part of Poland, the more distant stations recorded quite usable video material. This event was a bit fainter and had a shorter duration than the fireball observed on

18<sup>h</sup>05<sup>m</sup> UT. The fireball appeared over the western part of Poland, and was located higher at the sky in most of the fireball stations.

During the second half of the night the Southern Taurid activity decreased and only two Southern Taurids have been observed before the sunrise.

### 3 Results

All meteors and fireballs from the 31 October 2015 night have been measured and after that the trajectories and orbital elements have been calculated using the *PyFN* software (Żołądek, 2012). Most of the coordinates used for calculations come directly from the *MetRec* software while the brightest fireballs have been measured manually due to possible errors caused by image saturation.

The fireball which occurred at 18<sup>h</sup>05<sup>m</sup> UT reached an absolute magnitude of  $-16$  over the town Okonek in north-western Poland. The east-west oriented trajectory of this fireball was located close to the cities Chojnice, Drawsko Pomorskie and Szczecinek. The fireball appeared at a height of 118 km and terminated its luminous patch at the height of 60 km after a 181 km long flight.

The second fireball reached a brightness of  $-14.5$  magnitude 82 kilometers above the town Ostrowite, 80 km east of Poznań. The trajectory was steep, with the beginning at 108 kilometers and the terminal point at 58 kilometers.

In total 64 orbits have been calculated for this particular night, among which 20 orbits belong to the Southern Taurids, 4 orbits belong to the Northern Taurids and the remaining 40 orbits are sporadics and minor showers.

The orbits of the Okonek and Ostrowite fireballs are very similar, with Drummond similarity criterion  $D' = 0.011$ . The semimajor axis of the Okonek fireball is 2.25 AU and for Ostrowite fireball 2.27 AU. The resulting orbital periods are 1234 days and 1282 days respectively while the orbital period of the 7:2 resonance stream is 1238 days. Both fireballs were caused by meteoroids orbiting the Sun close to the 7:2 resonance, this is in good agreement with model published by Asher and Clube (1993).

Orbital elements of these two meteoroids have been compared with the NEODYS database using the Drummond criterion. We found three NEO objects on similar orbits, with an orbital period close to a 7:2 resonance with Jupiter. The most similar object is 2015TX24 – this NEO asteroid orbiting the Sun on an almost identical orbit as the “Ostrowite” fireball ( $D' = 0.0056$ ), moreover this quite big, few hundred meters sized body has been discovered on 8 October 2015 and encountered the Earth on 29 October 2015, just two days before the “Okonek” and “Ostrowite” fireballs. The orbital period of 2015TX24 perfectly fits the 7:2 resonance with Jupiter (1248 days). The second body is 2005UR, with an orbital period of 1241 days and  $D' = 0.036$  (if compared to the Ostrowite fireball). It is interesting that also this body has encountered the Earth during the previous Southern Taurid maximum in 2005, the closest encounter was observed on 30 October 2005 at 13<sup>h</sup> UT. The third body is the 2005TF50 ( $D' = 0.042$  with the Ostrowite fireball). This body has an orbital period of 1251 days and is previously recognized as a body associated with one of the Taurid filaments (Porubčan et al., 2006).

## 4 Conclusion

The 2015 Taurid maximum occurred as expected, with a noticeable enhancement in stream activity. Two very

bright, spectacular fireballs appeared in the evening of 31 October 2015, both significantly brighter than the Full Moon. The orbital elements of the fireballs have been calculated and compared to the orbital elements from the NEODYS database. Three bodies orbiting the Sun on very similar orbits have been found, especially one of these asteroids – 2015TX24 orbiting the Sun on an almost identical orbit like the second observed fireball. The orbital periods of both fireballs and all three NEO asteroids are very close to the 7:2 resonance with Jupiter which is in good agreement with the existing model. These NEO objects shouldn't be treated as parent bodies of the 7:2 filament, it is more correct to treat them as the most massive remnants of the larger body fragmented in the past. It's worth to mention that larger numbers of such bodies may exist in the Southern Taurid stream creating a kind of asteroidal core of the 7:2 stream.

## Acknowledgment

This work was supported by the NCN grant number 2013/09/B/ST9/02168.

## References

- Asher D. J. and Clube S. V. M. (1993). “An Extraterrestrial Influence during the Current Glacial-Interglacial”. *Quarterly Journal of the Royal Astronomical Society*, **34**, 481–511.
- Dubietis A. and Arlt R. (2007). “Taurid resonant-swarm encounters from two decades of visual observations”. *Monthly Notices of the Royal Astronomical Society*, **376**, 890–894.
- Porubčan V., Kornoš L. and Williams I. P. (1993). “The Taurid complex meteor showers and asteroids”. *Contributions of the Astronomical Observatory Skalnaté Pleso*, **36**, 103–117.
- Żołądek P. (2012). “PyFN – multipurpose meteor software”. In Gyssens M. and Roggemans P., editors, *Proceedings of the International Meteor Conference*, Sibiu, Romania, 15-18 September 2011. IMO, pages 53–55.

# International Meteor Conference 2017 Petnica, Serbia, September 21–24, 2017

Dušan Pavlović, Snežana Todorović  
and Miroslav Živanović

Petnica Science Center, Petnica, Valjevo, Serbia

dusan.pavlovicc@gmail.com, pmg.todsn@gmail.com,  
miroslavzivanovic6@gmail.com

The International Meteor Conference 2017 will be hosted by Petnica Science Center in Petnica, a village near the city of Valjevo, Serbia, from September 21 to September 24, 2017. Here we present some basic information about this conference, as presented at the International Meteor Conference 2016 in Egmond, the Netherlands.

## 1 Introduction

In 1997 the International Meteor Conference was held in Petnica Science Center, in Serbia. At that time, one of the most interesting experiences was the fact that there was a *large number of very active young meteor observers*.

Now, exactly 20 years after the previous IMC in Serbia, Petnica Science Center will host once more an IMC in 2017.

In the meantime, Petnica Meteor Group, the group which works within the Petnica Science Center since 1993, continued to bring together meteor observers and those interested in other fields of meteor science (not only the high school students but people from all disciplines and of all professions). The Petnica Meteor Group experienced a significant boost by hosting the IMC in 1997. The visual observations were enriched by video and all-sky observations, a little bit of theoretical work and data analysis, and greatly by the School of Meteor Astronomy, a week-long seminar teaching the high school students the basics of meteor science. Those are all the reasons to bring the IMC back to Petnica next year.

## 2 Date and location

The International Meteor Conference 2017 will be hosted by Petnica Science Center from Thursday evening, September 21, till Sunday lunch time, September 24, 2017, in Petnica Science Center, near the city of Valjevo, Serbia.

The PSC is an extracurricular science education center for high school students from all countries of former Yugoslavia. It is located in Petnica, the small village near the city of Valjevo, about 100 km southwest from Belgrade.

## 3 Accommodation

The PSC campus has undergone a significant expansion since the IMC 1997. Today, the PSC has a campus with separate buildings hosting lecture halls and classrooms, a

library, laboratories, dormitories, a restaurant, etc. The IMC 2017 participants will be accommodated on-campus. Since all conference events will be hosted on-campus, there will be plenty of opportunity for the meteor community to interact at the conference, both formally and informally.



Figure 1 – The dormitory building.

There will be 14 single, 20 double and 28 triple bedrooms (138 beds in total) available in the dormitory building, which is connected to the main conference building by a covered walkway.



Figure 2 – The night sky at Petnica over the restaurant and cafe.

The talks and poster sessions will be held in the nearby main building. The talks will be presented in an amphitheater (150 seats) and the posters will be displayed



Figure 3 – A part of the Petnica Science Center campus, Petnica, Serbia.



Figure 4 – An aerial view at Petnica Science Center campus.

in the hallway and two small classrooms (50 seats per classroom) across the hall and at the lower floor of the building. Also, there is an open amphitheater with 500 seats which can be used for the evening activities.

The campus is covered by free WiFi internet and all bedrooms also have LAN connections.

The campus includes a restaurant (350 seats), a café, and a small shop. The restaurant and café open up to a nice terrace overlooking the area. Special food requirements can be arranged in advance.

#### 4 Program and social events

As usual at the IMCs, the main part of the program will consist of talks and poster sessions. The exact schedule of those activities will be determined after the end of the registration period, when we get a clear picture of the number of registered speakers and topics. There will be short talks and extended sessions, as well as workshops organized by the prominent specialists in various fields of meteor science.

All presentations, both talks and posters, will be included in the IMC 2017 Proceedings as full-length papers or abstracts.

Also, there will be a contest for the best poster and the best meteor photo.

Social events include evening activities, an excursion to points of interest in and around Valjevo and a visit to one of the local wineries in the evening after the excursion.

## 5 Registration

Registration opens in January 2017. This will be announced in the IMO journal WGN and on the IMO and IMC 2017 web sites. The early-bird registration deadline is June 30, 2017. The final deadline will be August 15, 2017, but mind that registration may have to be closed earlier if full capacity is reached before that date.

The early-bird registration fee is 130 EUR per person for accommodation in a triple bedroom, 170 EUR per person for accommodation in a double bedroom and 240 EUR for accommodation in a single bedroom. After June 30th, 2017 an extra fee of 20 EUR is charged.

The standard registration fee includes full board (accommodation, breakfast, lunch, and dinner) from Thursday evening September 21 (dinner included) till Sunday noon September 24 (lunch included), IMC lectures, coffee breaks and the excursion. Accompanying persons older than 12 years sharing a room with a participant must also register as a participant. T-shirts and printed proceedings can be purchased separately upon registering. An electronic version of the proceedings will be made available to all participants for no additional charge.

More detailed information will be announced when the registration is opened.

## 6 Travel information

As Petnica is a small village, there is no bus connection, but a shuttle will be available from the Valjevo bus and train stations located 7 km from Petnica. So, participants (if not arriving by car directly to Petnica Science Center) should come to Valjevo, from where an organized free

shuttle bus will bring them to Petnica Science Center. The GPS location of the Petnica Science Center is 44° 14' 48" N, 19° 55' 52" E.

Detailed travel information and instructions for car drivers will be published in due time on the IMC 2017 web pages. Here, we limit ourselves to some general information.

If you travel by plane, the best way is to fly to Belgrade (Airport "Nikola Tesla"), then go to the Belgrade central bus or train station, and from there to Valjevo by bus or train (there is a connection approximately every hour). You can also rent a car at the airport – you will find the car rental agencies at the arrivals terminal.

If you travel by bus or train, the best way is to go to Belgrade and from the Belgrade central bus or train station to Valjevo by bus or train (there is a connection approximately every hour).

If you travel by car, you can use the E70 and E75 Motorways connecting Zagreb, Novi Sad, Belgrade and Niš. Or simply drive to Belgrade and from Belgrade to Valjevo.

We encourage the participants to consider carpooling. The Local Organizing Committee (LOC) will provide assistance once the registration is closed. By encouraging carpooling we want to reduce the number of cars, lower the cost by sharing cars and promote socializing while traveling to the IMC.

## 7 Contact

Detailed information will be posted at the IMC 2017 web pages as they become available. (As usual, a link to these pages will be provided on the homepage of the IMO website as soon as they are active.) Meanwhile, you may contact the LOC at [imc2017@imo.net](mailto:imc2017@imo.net).

See you next year at the IMC 2017 in Petnica!

## Acknowledgments

We want to thank Vladimir Lukić, Marc Gyssens, Dragana Okolić and Branislav Savić for useful comments on this text and the presentation of the IMC 2017.

## List of participants

The alphabetical list below contains all participants of the 35<sup>th</sup> International Meteor Conference. Numbers serve to identify positions in the group photographs, if applicable. You can find the group photograph on page 369.

- |   |   |
|---|---|
| Abe Shinsuke, Japan (127)                         | Haas Robert, Netherlands (Not on the photo)     |
| Abedin Abedin, Canada (Not on the photo)          | Hajduková Mária, Slovakia (83)                  |
| Albin Thomas, Germany (118)                       | Hankey Michael, United States (32)              |
| Argo Megan, United Kingdom (124)                  | Hartman Joost, Netherlands (106)                |
| Asher David, United Kingdom (125)                 | Hillestad Eli Fugelsoe, Norway (62)             |
| Bagrov Alexander, Russia (21)                     | Hillestad Trond Erik, Norway (60)               |
| Barbieri Lorenzo, Italy (52)                      | Hristova Simona, Bulgaria (126)                 |
| Bastiaens Luc, Belgium (48)                       | Ibhi Abderrahmane, Morocco (54)                 |
| Bettonvil Uros, Netherlands ()                    | Igaz Réka, Hungary (13)                         |
| Bettonvil Dusan, Netherlands (6)                  | Igaz Antal, Hungary (12)                        |
| Bettonvil Eduard, Netherlands (53)                | IJland Elise, Netherlands (121)                 |
| Bettonvil Felix, Netherlands (71)                 | Jacobs Lars, Belgium (86)                       |
| Biondić Jakov, Croatia (109)                      | Jenniskens Peter, United States (117)           |
| Biondić Damir, Croatia (110)                      | Jobse Klaas, Netherlands (38)                   |
| Birlan Mirel, France (19)                         | Kac Javor, Slovenia (92)                        |
| Bojurova Eva, Bulgaria (41)                       | Kákona Jakub, Czech Republic (36)               |
| Bonino Donata, Italy (137)                        | Kartashova Anna, Russia (133)                   |
| Borovička Jiří, Czech Republic (141)              | Kastinen Daniel, Sweden (116)                   |
| Brando Gaetano, Italy (47)                        | Keeris Roy, Netherlands (120)                   |
| Bronikowska Malgorzata, Poland (Not on the photo) | Kero Johan, Sweden (115)                        |
| Brown Peter, Canada (1)                           | Klemt Bernd, Germany (96)                       |
| Calders Stijn, Belgium (79)                       | Knöfel André, Germany (69)                      |
| Campbell-Brown Margaret, Canada (2)               | Koelers Selma, Netherlands (101)                |
| Čapek David, Czech Republic (34)                  | Kokkeler Ben, Netherlands (Not on the photo)    |
| Colas Francois, France (93)                       | Korec Matej, Slovakia (123)                     |
| Çubuk Kerem Osman, Turkey (Not on the photo)      | Korlević Korado, Croatia (16)                   |
| Currie Malcolm, United Kingdom (51)               | Koschny Gabi, Netherlands (64)                  |
| De Queiroz José, Switzerland (Not on the photo)   | Koschny Detlef, Netherlands (66)                |
| de Vet Sebastiaan, Netherlands (3)                | Koten Pavel, Czech Republic (10)                |
| Devillepoix Hadrien, Australia (8)                | Koukal Jakub, Czech Republic (140)              |
| Dolinský Peter, Slovakia (Not on the photo)       | Kurtović Goran, Croatia (114)                   |
| Drolshagen Esther, Germany (87)                   | Lamy Hervé, Belgium (Not on the photo)          |
| Dubs Martin, Switzerland (46)                     | Lesanu Cezar, Romania (95)                      |
| Egal Auriane, France (7)                          | Maciejewski Maciej, Poland (23)                 |
| Fujiwara Yasunori, Japan (98)                     | Madkour Waleed, Japan (119)                     |
| Gährken Bernd, Germany (70)                       | Malarić Mirjana, Croatia (112)                  |
| Gardiol Daniele, Italy (90)                       | Markham Tony, United Kingdom (104)              |
| Georgescu Ana, Romania (82)                       | Marshall Robert, United States (18)             |
| Georgescu Tudor, Romania (80)                     | Martínez Picar Antonio, Belgium (14)            |
| Gostinski David, Croatia (78)                     | Mizumoto Satoshi, Japan (103)                   |
| Grašić Ljubica, Serbia (128)                      | Molau Sirko, Germany (73)                       |
| Gritsevich Maria, Finland (42)                    | Moreno-Ibáñez Manuel, Spain (22)                |
| Guliyev Ayyub, Azerbaijan (89)                    | Nakane Sumio, Japan (Not on the photo)          |
| Gural Pete, United States (5)                     | Neijts Marc, Netherlands (122)                  |
| Gyssens Marc, Belgium (58)                        | Netjes Gert Jan, Netherlands (Not on the photo) |

Nijland Jos, Netherlands (65)	Slagter Daan, Netherlands (76)
Nogami Nagatoshi, Japan (102)	Smeets Nastassia, Belgium (30)
Novoselnik Filip, Croatia (111)	Soja Rachel Halina, Germany (132)
Ocaña González Francisco, Spain (94)	Solovaya Nina, Slovakia (88)
O'Connell Michael, Ireland (75)	Spurný Pavel, Czech Republic (56)
Okolić Dragana, Netherlands (134)	Stewart Peter, United Kingdom (113)
Ott Theresa, Germany (85)	Steyaert Chris, Belgium (57)
Ozeren Ferhat Fikri, Turkey (Not on the photo)	Stolarz Marcin, Poland (20)
Pavela Debora, Serbia (29)	Sutherland Paul, United Kingdom (45)
Pavlović Dušan, Serbia (129)	ter Kuile Casper, Netherlands (Not on the photo)
Perlerin Vincent, France (31)	Theiler Laura, Germany (43)
Peterson Chris, United States (15)	Theiler Carina, Germany (72)
Pittich Eduard, Slovakia (138)	Todorović Snežana, Serbia (131)
Poerink Urijan, Netherlands (17)	Tomezzoli Giancarlo, Germany (Not on the photo)
Polakowski Krzysztof, Poland (63)	Tóth Juraj, Slovakia (139)
Polfliet Tim, Belgium (59)	Tukkers Arnold, Netherlands (11)
Popescu Miruna, United Kingdom (55)	Vaubailon Jeremie, France (24)
Rault Jean-Louis, France (25)	Veljković Kristina, Slovenia (Not on the photo)
Reid Iain, Australia (37)	Verbeeck Cis, Belgium (67)
Rendtel Juergen, Germany (33)	Verbert Jan, Belgium (81)
Roelandts Tom, Belgium (27)	Vida Denis, Croatia (107)
Roggemans Paul, Belgium (39)	Vojáček Vlastimil, Czech Republic (9)
Roggemans Adriana, Belgium (44)	Ward Bill, United Kingdom (28)
Rudawska Regina, Netherlands (135)	Weatherley Gillian, United Kingdom (50)
Ryabova Galina, Russia (Not on the photo)	Weiland Thomas, Austria (61)
Sánchez de Miguel Alejandro, Spain (49)	Wiśniewski Mariusz, Poland (100)
Sansom Eleanor, Australia (35)	Wrigley Nick, United Kingdom (130)
Schenker Jonas, Switzerland (91)	Yamamoto Masa-yuki, Japan (99)
Schmidt Irmgard, Germany (97)	Yancheva Yulia, Bulgaria (136)
Schmidt Hans-Georg, Germany (105)	Younger Joel, Australia (40)
Šegon Damir, Croatia (4)	Zender Joe, Netherlands (Not on the photo)
Shrbený Lukáš, Czech Republic (68)	Zigo Pavol, Slovakia (74)
Shuttleworth Alan, United Kingdom (Not on the photo)	Živanović Miroslav, Serbia (26)
Skokić Ivica, Croatia (108)	Żołądek Przemysław, Poland (84)
Skunca Gordan, Croatia (77)	

If you wish to locate a particular person on the group photo on the adjacent page, search for his or her name in the alphabetical list above, and find the face corresponding to the number mentioned using the key under the group photo.

Conversely, if you wish to identify a face on the group photo, find the corresponding number in the key, and find his or her name in the numerically ordered list below:

(1) Brown Peter; (2) Campbell-Brown Margaret; (3) de Vet Sebastiaan; (4) Šegon Damir; (5) Gural Pete; (6) Bettonvil Dusan; (7) Egal Auriane; (8) Devillepoix Hadrien; (9) Vojáček Vlastimil; (10) Koten Pavel; (11) Tukkers Arnold; (12) Igaz Antal; (13) Igaz Réka; (14) Martínez Picar Antonio; (15) Peterson Chris; (16) Korlević Korado; (17) Poerink Urijan; (18) Marshall Robert; (19) Birlan Mirel; (20) Stolarz Marcin; (21) Bagrov Alexander; (22) Moreno-Ibáñez Manuel; (23) Maciejewski Maciej; (24) Vaubailon Jeremie; (25) Rault Jean-Louis; (26) Živanović Miroslav; (27) Roelandts Tom; (28) Ward Bill; (29) Pavela Debora; (30) Smeets Nastassia; (31) Perlerin Vincent; (32) Hankey Michael; (33) Rendtel Juergen; (34) Čapek David; (35) Sansom Eleanor; (36) Kákona Jakub; (37) Reid Iain; (38) Jobse Klaas; (39) Roggemans Paul; (40) Younger Joel; (41) Bojurova Eva; (42) Gritsevich Maria; (43) Theiler Laura; (44) Roggemans Adriana; (45) Sutherland Paul; (46) Dubs Martin; (47) Brando Gaetano; (48) Bastiaens Luc; (49) Sánchez de Miguel Alejandro; (50) Weatherley Gillian; (51) Currie Malcolm; (52) Barbieri Lorenzo; (53) Bettonvil Eduard; (54) Ibhi Abderrahmane; (55) Popescu Miruna; (56) Spurný Pavel; (57) Steyaert Chris; (58) Gyssens Marc; (59) Polfliet Tim; (60) Hillestad Trond Erik; (61) Weiland Thomas; (62) Hillestad Eli Fugelsoe; (63) Polakowski Krzysztof; (64) Koschny Gabi; (65) Nijland

Jos; (66) Koschny Detlef; (67) Verbeeck Cis; (68) Shrbený Lukáš; (69) Knöfel André; (70) Gährken Bernd; (71) Bettonvil Felix; (72) Theiler Carina; (73) Molau Sirko; (74) Zigo Pavol; (75) O'Connell Michael; (76) Slagter Daan; (77) Skunca Gordan; (78) Gostinski David; (79) Calders Stijn; (80) Georgescu Tudor; (81) Verbert Jan; (82) Georgescu Ana; (83) Hajduková Mária; (84) Żołądek Przemysław; (85) Ott Theresa; (86) Jacobs Lars; (87) Drolshagen Esther; (88) Solovaya Nina; (89) Guliyev Ayyub; (90) Gardiol Daniele; (91) Schenker Jonas; (92) Kac Javor; (93) Colas Francois; (94) Ocaña González Francisco; (95) Lesanu Cezar; (96) Klemt Bernd; (97) Schmidt Irmgard; (98) Fujiwara Yasunori; (99) Yamamoto Masa-yuki; (100) Wiśniewski Mariusz; (101) Koelers Selma; (102) Nogami Nagatoshi; (103) Mizumoto Satoshi; (104) Markham Tony; (105) Schmidt Hans-Georg; (106) Hartman Joost; (107) Vida Denis; (108) Skokić Ivica; (109) Biondić Jakov; (110) Biondić Damir; (111) Novoselnik Filip; (112) Malarić Mirjana; (113) Stewart Peter; (114) Kurtović Goran; (115) Kero Johan; (116) Kastinen Daniel; (117) Jenniskens Peter; (118) Albin Thomas; (119) Madkour Waleed; (120) Keeris Roy; (121) IJland Elise; (122) Neijts Marc; (123) Korec Matej; (124) Argo Megan; (125) Asher David; (126) Hristova Simona; (127) Abe Shinsuke; (128) Grašić Ljubica; (129) Pavlović Dušan; (130) Wrigley Nick; (131) Todorović Snežana; (132) Soja Rachel Halina; (133) Kartashova Anna; (134) Okolić Dragana; (135) Rudawska Regina; (136) Yancheva Yulia; (137) Bonino Donata; (138) Pittich Eduard; (139) Tóth Juraj; (140) Koukal Jakub; (141) Borovička Jiří.

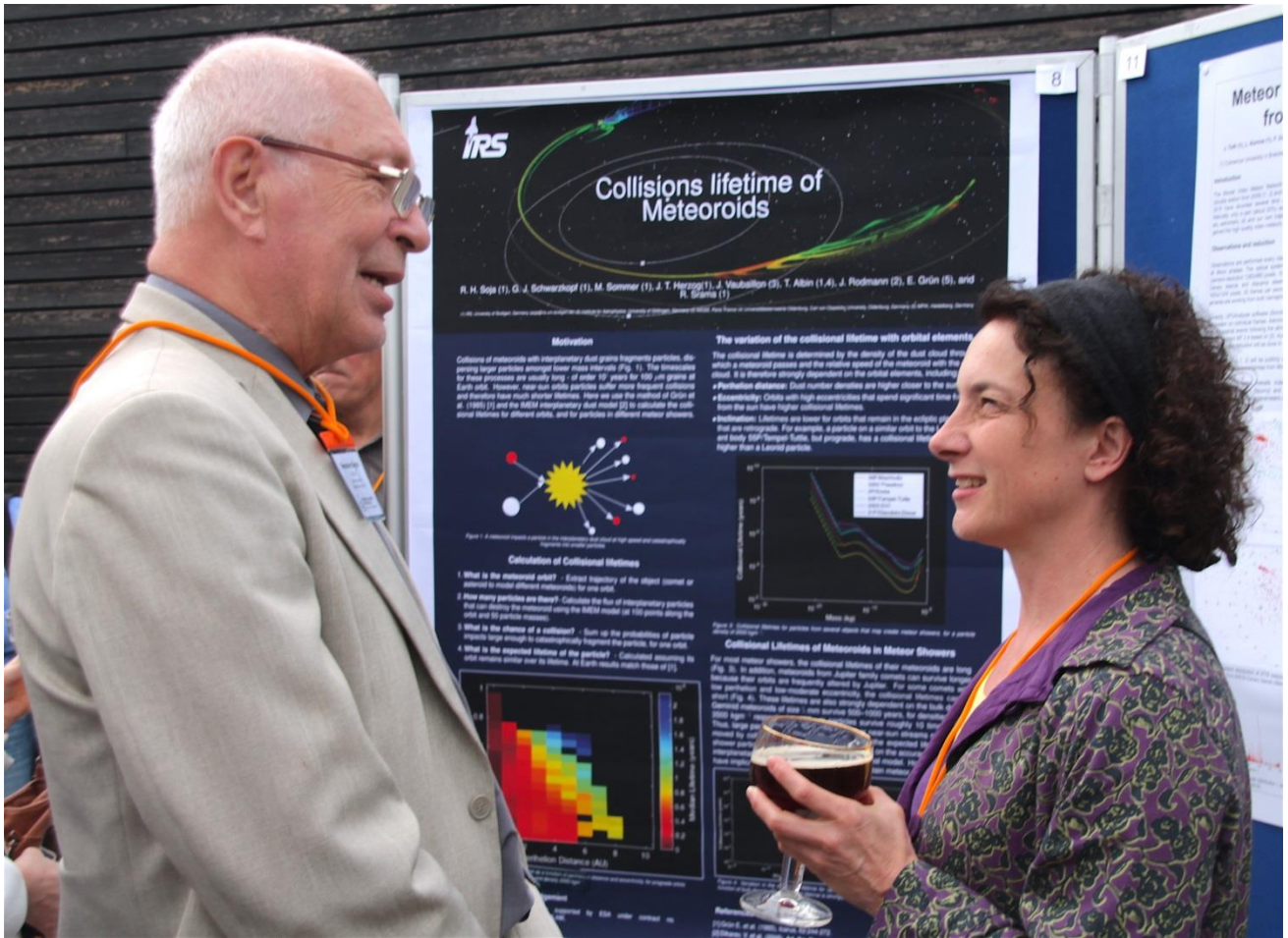
Missing in the group photo: Abedin Abedin; Bettonvil Uros; Çubuk Kerem Osman; De Queiroz José, Dolinsky Peter; Haas Robert; Kokkeler Ben; Lamy Hervé; Nakane Sumio; Netjes Gert Jan; Ozeren Ferhat Fikri; Ryabova Galina; Shuttleworth Alan; ter Kuile Casper; Tomazzoli Giancarlo; Veljković Kristina and Zender Joe.

The group photo has been made by Casper ter Kuile.

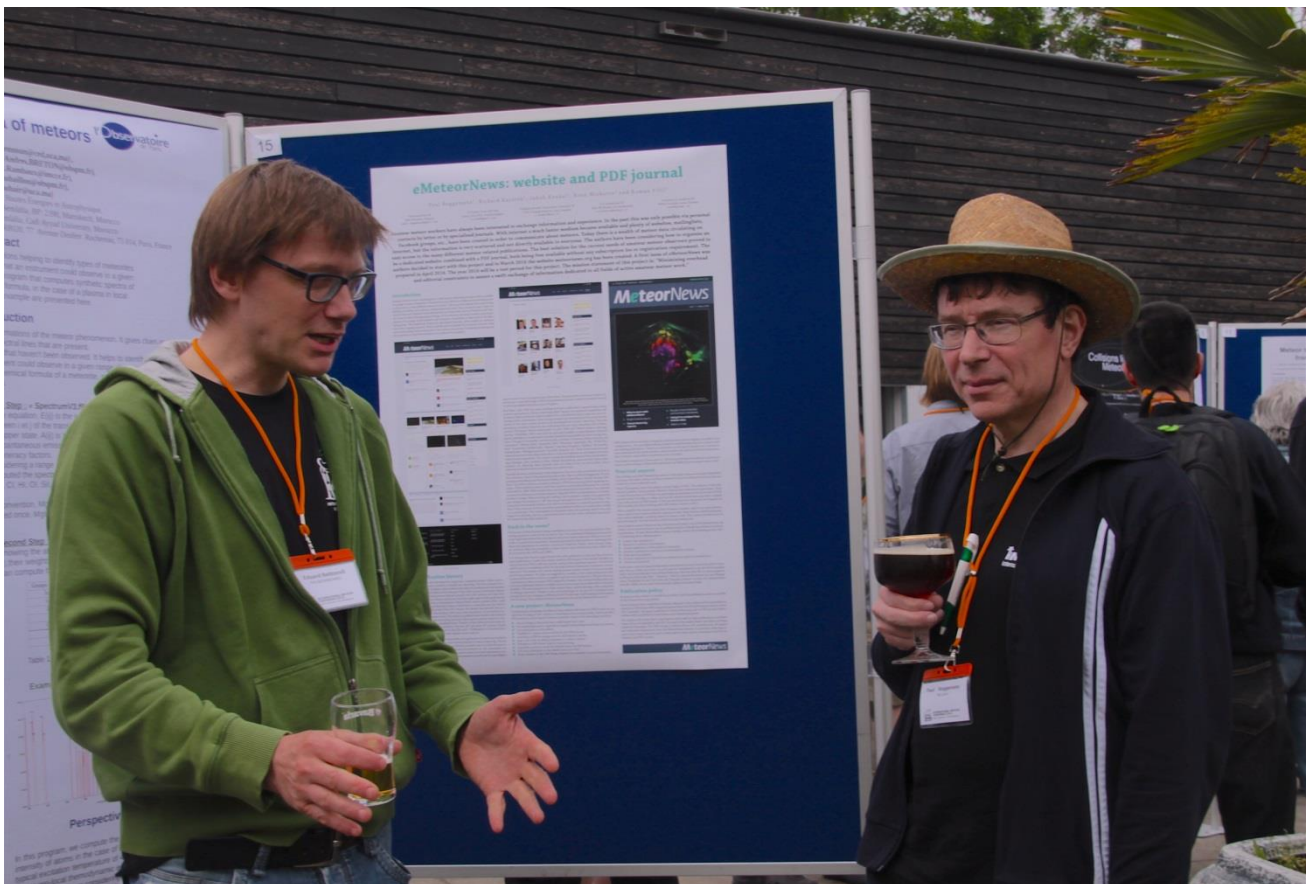
Due to a lack of identification, the names of the photographers of some of the photographs included in these Proceedings could not be mentioned with each photo. We apologize for this.



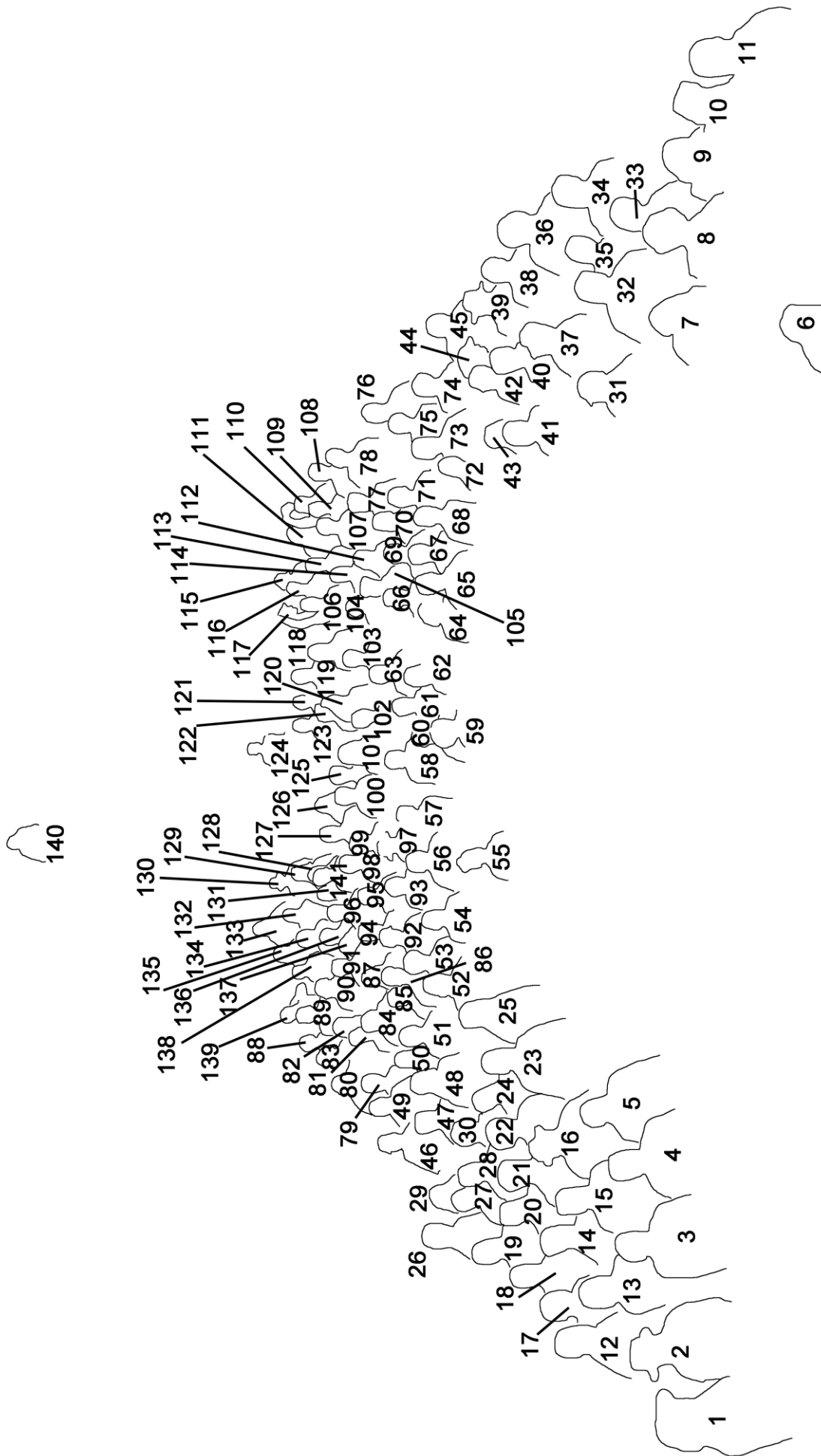
Next year the IMC will be in Petnica, Serbia!

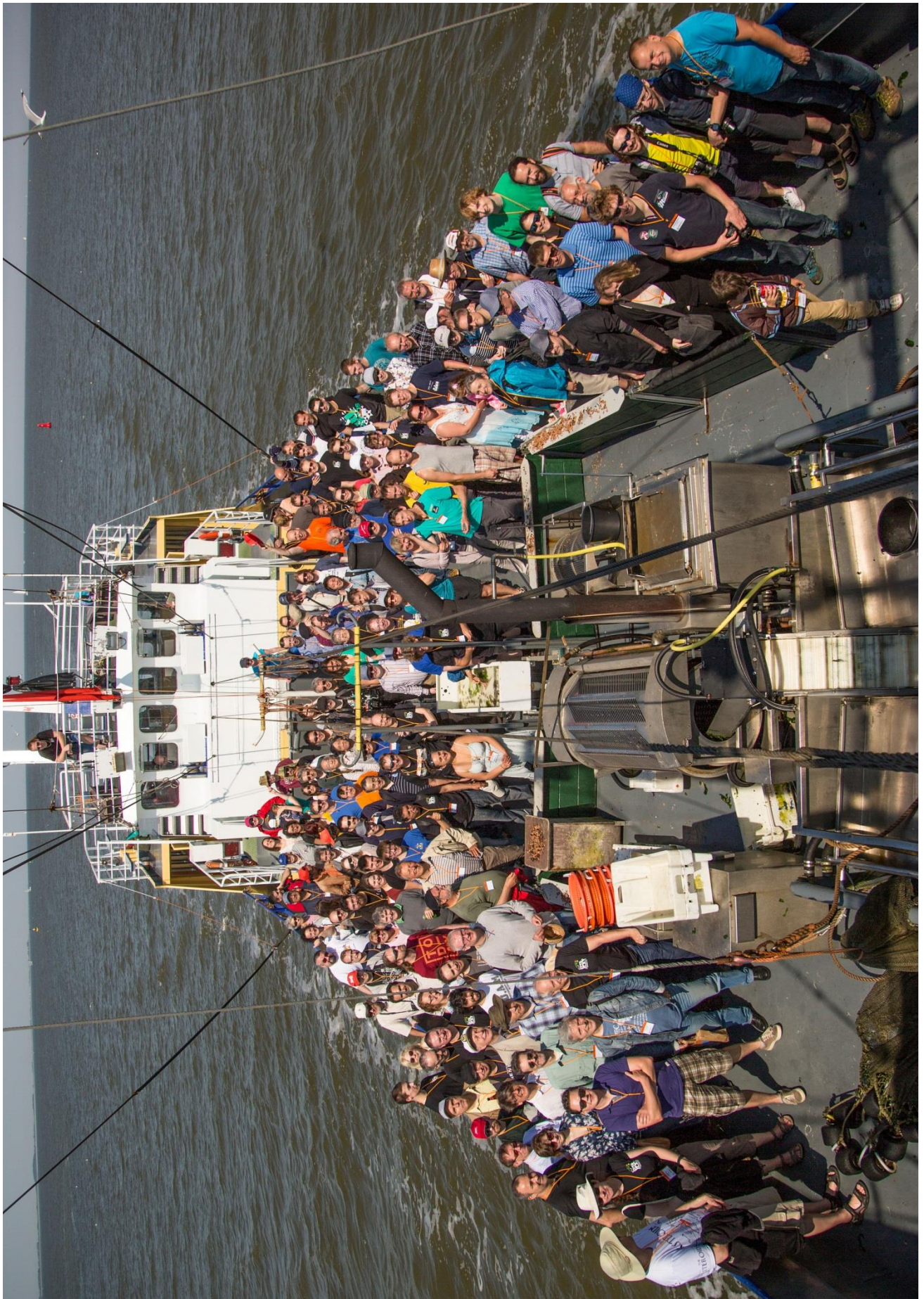


Alexander Bagrov and Maria Hajduckova at the poster session.



Eduard Bettonvil enthusiastically prizes his ideas on meteors to Paul Roggemans.







The girls from Petnica (Serbia) in a row: Ljubica Grašić, Debora Pavela, Snežana Todorović and Dragana Okolić.



Felix and Dušan Bettonvil: father and son, and as almost always both at the IMC.

## The song of the IMC – 2016

- Jérémie Vaubaillon -

*Don't ask me where is the IMC  
I can't say the name but it's close to the sea  
the crew is dressed all in orange  
as a result they are a bit strange*

*(chorus)*

*You're very welcome,  
You're very welcome to the IMC*

*At the bar I was doing so well  
but someone ring me the Dutch bell  
I had to talk about the stream  
when all I wanted was to have a shrimp*

*(Chorus)*

*You're very welcome,  
You're very welcome to the IMC*

*I was looking for the tulip  
but all I found was a big ship  
next to the bow we took a photo  
and to the seagull we throw nemo*

*(Chorus)*

*You're very welcome,  
You're very welcome to the IMC!  
You're very welcome,  
You're very welcome to the IMC!!!*

## Author index

Abe S.	17, 18	Dolinský P.	63
Abedin A.	19	Droldhagen E.	209
Albin T.	20, 284	Dubs M.	65
Anciaux M.	175	Dumitru B.A.	69
Andreic Ž.	270	Đuriš F.	294
Argo M.	305	Efimov A.	202
Audureau Y.	55	Egal A.	55, 73
Bagrov A.V.	148, 151	Ferrière L.	55
Barbieri L.	26, 291	Ferus M.	137
Bęben M.	358	Fietkiewicz K.	341
Benkhaldoun Z.	91	Fliegel K.	133
Bettonvil F.	6, 31	Fujiwara Y.	18, 167
Birlan M.	55, 69	Gajdoš S.	294
Birnbaum C.	55	Gamby E.	175
Bland P.A.	60, 267, 275	Gardiol D.	55, 76
Blanpain C.	55	Gattacceca J.	55
Bojurova E.	348	Gawroński M.P.	341, 358
Bolgova G.	120	Georgescu A.	80
Borovička J.	34, 53, 287, 333	Georgescu. T.	80
Bouley S.	55	Glazachev D.	120
Brando G.	39	Gorková S.	137
Breton M.-A.	91	Gozdalski M.	341, 358
Brown P.	19, 42, 171, 305	Grašić L.	83
Buček M.	294	Gritsevich M.	87, 159, 192, 197, 227, 230, 319, 330
Calders S.	46, 175	Grokhovsky V.	319
Camargo J.	55	Grün E.	284
Caminade S.	55	Guennoun M.	91
Campbell-Brown	50	Gulliyev A.	94
Čapek D.	53	Gural P.	96, 307
Cellino A.	55, 76	Hajdukova M. jr.	105
Civiš S.	137	Haloda J.	287
Close S.	171	Hankey M.	111
Colas F.	55, 73	Hartig B.A.D.	60
Cupák M.	60	Hashiguchi H.	18
Cupec R.	307	Howie R.M.	60
de Vet S.	56, 205, 222	Hristova S.	348
Debattista V.	319	Ibhi A.	127
Delcourt J.-J.	235	Jansen-Sturgeon T.	60
Devillepoix H.A.R.	60	Jenniskens P.	113
Di Martino M.	55, 76	Jorda L.	55
Dimant Y.	171		

Kaiserová T.	137	Mönkölä S.	227, 319
Kákona J.	114, 117	Moreno-Ibáñez M.	192, 197, 230
Kákona J.	319	Muinsonen K.	227
Kalmančok D.	294, 297	Murphy D.	352
Kaniansky S.	295	Murtazov A.	202
Kartashova A.	120	Myszkiewicz M.	341, 358
Kastinen D.	18, 123	Nakamura T.	18
Kero J.	18, 123, 288	Näränen Y.	230
Khiri F.	127	Nedelcu A.	69
Knížek A.	137	Netjes G.J.	205
Korlević K.	270	Nishizono T.	17
Kornoš L.	294	Nitschelm C.	55
Koschny D.	20, 131, 209, 265	Nojiri Y.	17
Koskinen J.	319	Okajima L.	17
Koten P.	133, 333	Olech A.	298, 341, 358
Koukal J.	137	Ott T.	209
Krivososova O.	330	Ouknine L.	127
Krzyżanowski T.	358	Páta P.	133
Kubelík P.	137	Pavlović D.	83, 361
Kurtović G.	280	Paxman J.	60, 267
Kuznetsova D.	330	Pečnik B.	319
Kwon M.-K.	55, 73	Peltoniemi J.	230, 319
Lamy H.	46, 143, 175	Perez J.C.	294
Lecubin J.	55	Perlerin V.	111
Lenža L.	137	Peterson C.	214
Leonov V.A.	148, 151	Pittich E.	217
Lesanu C.E.	80, 155	Poerink U.	222
Licandro J.	294	Pokorny P.	19
Loizeau D.	55	Polakowski K.	341
Lyytinen E.	159, 192, 230	Popescu M.	55, 69
Maciejewski M.	341	Popova O.	120
Madkour W.	164, 179	Poppe B.	20, 209
Maeda K.	65, 167	Poutanen M.	230
Mahabal A.	319	Räbinä J.	227
Malgoyre A.	55	Raja-Halli A.	230
Maquet L.	55	Rambaux N.	91
Markkanen J.	227	Ranvier S.	175
Marmo C.	55, 73	Rault J.-L.	55, 235
Marqué C.	175	Reid I.M.	242, 352
Marshall R.A.	171	Rendtel J.	247, 294, 305
Martínez Picar A.	46, 175, 305	Ridgewell J.	267
Matlovič P.	297	Rodmann J.	284
Medjkane M.	127	Roelandts T.	250
Mickaelian A.	319	Roggemans P.	8, 254, 261
Milanović N.	83	Rossi T.	227
Mizumoto S.	179	Rotaru M.	55
Molau S.	185, 305	Rudawska R.	265, 266, 297, 258

Rybnov Y.	120	Vaduvescu O.	294
Sahara H.	17	Valenzuela M.	55
Saint-Gerant T.	127	Váňa P.	137
Sansom E.K.	60, 267	Vaubailon J.	55, 73, 91, 284, 302
Schwarzkopf G.J.	284	Veljković K.	304
Šegon D.	270, 280, 307	Verbeeck C.	46, 175, 305
Serra-Ricart M.	294	Vernazza P.	55
Shrbený L.	275, 287	Vida D.	270, 307
Šimon J.	294	Világi J.	294
Škoda P.	319	Vinković D.	319
Skokić I.	280	Vinnikov V.	330
Soja R.H.	20, 284	Virtanen J.	230
Solovaya N.	217	Vítek S.	133
Sommer M.	284	Vojáček V.	333
Spurný P.	275, 287, 333	Watanabe J.	18
Srama R.	20, 284	Watanabe T.	17
Srba J.	137	Węgrzyk W.	358
Srećković V.	319	Weiland T.	338
Stempels E.	288	Wiegert P.	19
Stolarz M.	298, 341, 358	Wiśniewski M.	298, 341, 358
Štork R.	133, 333	Yamamoto M.	164, 179, 344
Suchodolski T.	341, 358	Yancheva Y.	348
Szabó G.	319	Younger J.	242, 352
Tétard C.	143, 175	Zanda B.	55
Todorović S.	361	Zender J.	265
Tomezzoli G.	291	Zhilenko D.	330
Tóth J.	294, 295, 297	Zigo P.	294, 297
Towner M.C.	60	Zikmund T.	287
Trigo-Rodríguez J.M.	192, 197	Živanović M.	361
Turchak L.	330	Żołądek P.	298, 341, 358
Turunen E.	319	Zubko N.	230
Tymiński Z.	298, 341, 358	Zubović D.	307



## ACKNOWLEDGEMENT TO SPONSORS

We are sincerely grateful to our Sponsors whose generous contributions helped greatly in organizing this IMC. The Local Organization Committee of the IMC along with the conference organizers, in particular acknowledge the following companies and organizations:



Universiteit Leiden

ASTRON



LCTEC

Thank you all!